Cell Stem Cell

Best of 2013

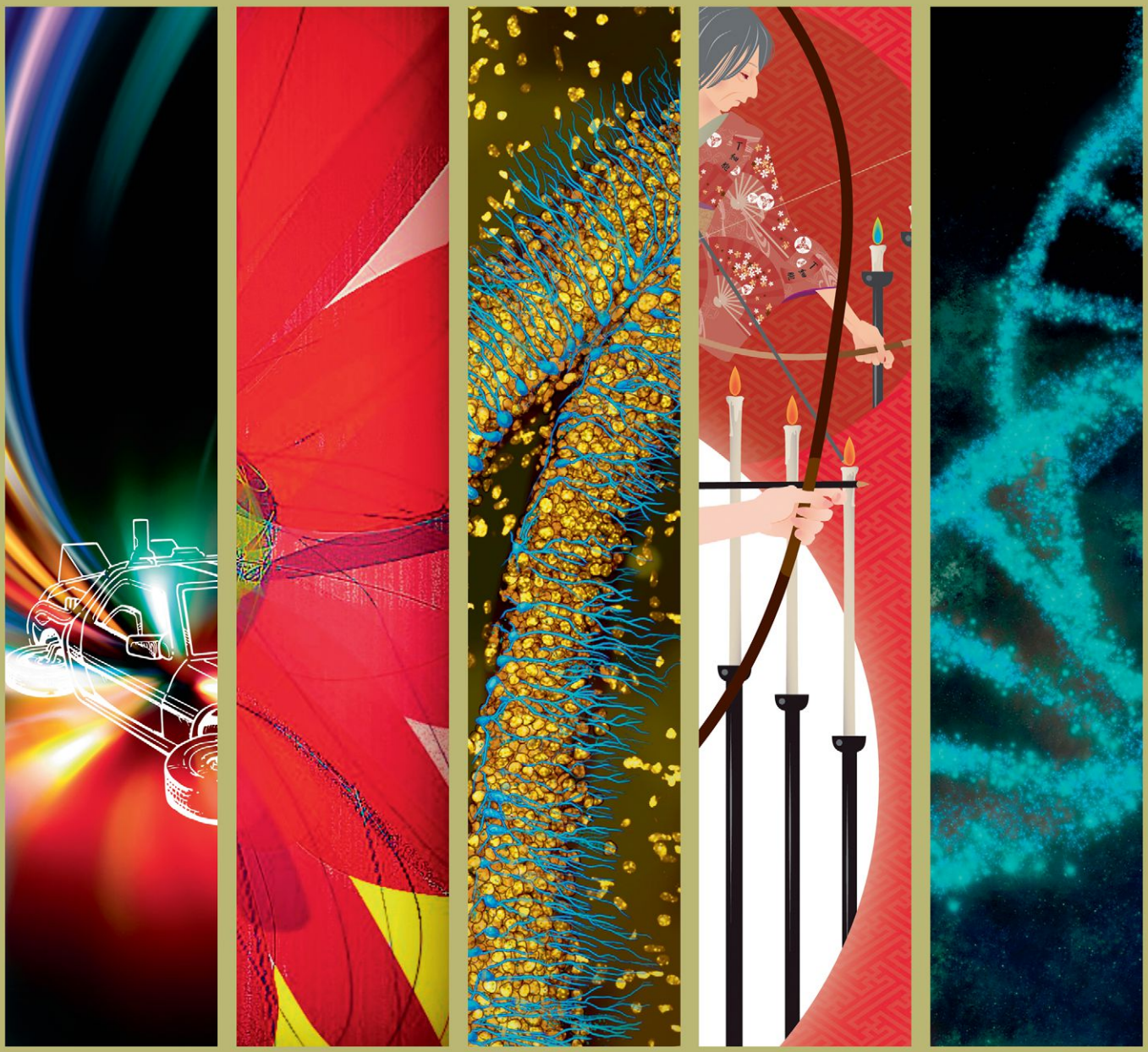

CellPress
www.cell.com

We make human cells.

We can't state it more simply: We manufacture human cells from induced pluripotent stem cells. Our highly pure iCell® and MyCell® products are consistent and reproducible from lot-to-lot, enabling you to focus on the biology . . . and what drives your research.

True Human Biology. Why use an animal or immortalized cell model as a proxy when a true human model, consistent across lots, is available? If you have a phenotype of interest, we can make iPSCs and terminal cells from your donors.

Highly Characterized. Highly Predictive. Our cells have the appropriate gene and protein expression and the relevant physiological response of the target cell type, with numerous peer-reviewed publications detailing their characterization and predictivity of human response.

MORE Cells. CDI provides more cells than other providers: 96-well capacity per vial. GUARANTEED.

Any cell type.
Any genotype.
Any quantity.

Cellular Dynamics international

You make:

safer medicines
discoveries
therapies
breakthroughs
tenure
your peers envious with a tier 1 publication

Check out the iCell community of scientists who discuss the difference iCell products have made in their research:

www.cellulardynamics.com/community

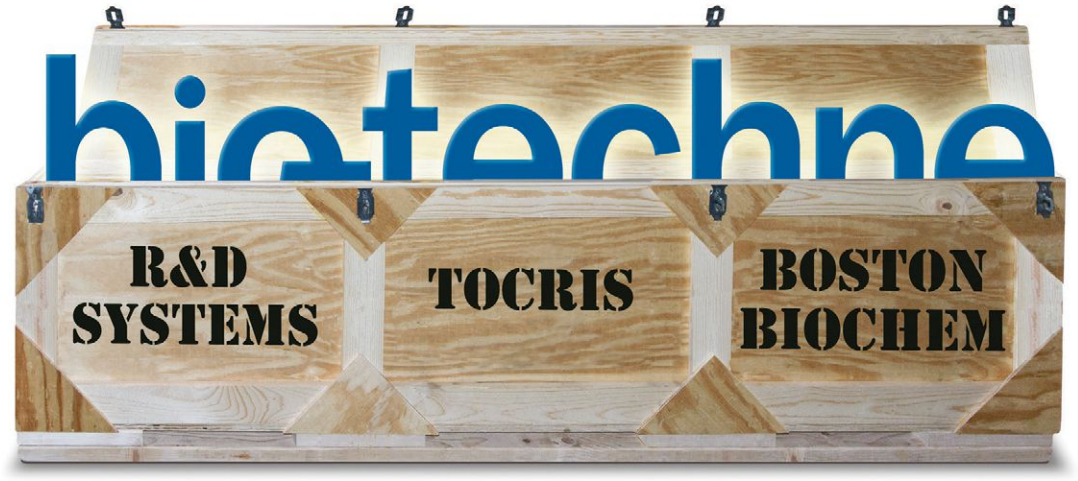

coming soon

bio-techne.com/launch

STEMGENT® | ASTERAND®

Giving scientists new ways to transform human lives.

Stemgent-Asterand is the leading supplier of stem cell reprogramming and tissue-based research products and services, providing a comprehensive portfolio of tools for cell research.

- mRNA reprogramming systems and services
- Reagents for pluripotent cell culture and differentiation
- Global supplier of human tissue and biofluids
- Target and biomarker validation services
- Compound profiling services in cell-based assays

www.stemgent.com | www.asterand.com

Please explore.

Trusted by researchers around the world.
Proudly introducing new technologies
and environments for your most
rigorous exploration.

BAKER RUSKINN

SCI-tive Hypoxia Workstation

HypoxyCOOL™

Complete closed-culture solutions designed exclusively for low-oxygen studies. Learn more on our website.

BakerRuskinn.com

Make The Right Cut With OriGene's CRISPR/Cas9 Tools

CRISPR is revolutionizing genetics, particularly mammalian genetics.

With unprecedented efficiency, CRISPR enables precise genome disruption in almost all model organisms. RNA-guided cleavage paired with donor-guided repair allows easy introduction of any desired modification in a living cell.

OriGene offers a wide selection of ready-to-use CRISPR tools. Blue Heron, OriGene's gene synthesis division, provides quick, reliable, and confidential service for any CRISPR-related constructs.

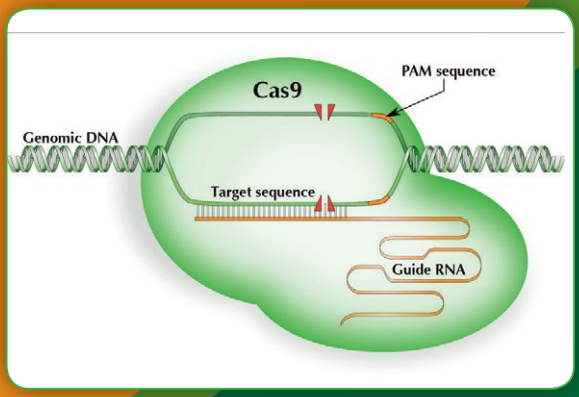

All-in-one gRNA/CAS9 vectors

gRNA cloning service

Donor cloning service

Gene knockout kits
(pre-designed gRNAs and donor)

Scan this QR code to view our 4-min in video on CRISPR

ORIGENE

www.origene.com

Foreword

Two years ago, Cell Press launched the "Best of" reprint collections across a number of our journals, including *Cell Stem Cell*. We are pleased to introduce a new "Best of" that focuses on articles published over the course of 2013. For this edition, we made our selection by looking at review and research articles with the most full-text HTML and PDF downloads since publication, which inevitably somewhat favors articles published earlier in the year. We have organized the highlighted articles in the order that you would see them in a monthly issue and hope you will enjoy browsing through them in the same way as you would browse through the journal each month.

To complement this selection approach, we have also compiled an online 2013 timeline that looks at review and research articles highlighted using a variety of different methods, and we encourage you to browse through it on our website (http://www.cell.com/cell-stem-cell/home). For the downloads section of the online feature, we focused on the first three months after publication, leading to some differences in terms of the articles that are included relative to this compiled "Best of" collection. To broaden the range of input involved, we also turned to Altmetrics, Facebook, Twitter, our editorial board, and citations to give an overview of the articles that most captured the attention of our readers.

We recognize that no one measurement can be indicative of the "best" papers over a given period of time, especially when the articles are relatively new and their true significance may still need time to be established. Nevertheless, we hope that this combination of approaches to highlighting articles will give you a snapshot of different perspectives on the studies that we published during 2013.

We hope that you will enjoy reading this special collection and that you will visit http://www.cell.com/cell-stem-cell/home to see the latest findings that we have had the privilege to publish, presented in the new website format that we launched earlier this year. While you're there, check out our regular rotation of Featured Five Reviews and free access to all Cell Press articles from 1 year after publication. If you prefer to read articles on a mobile device, you may also want to use our Journal Reader app, now available across multiple platforms from http://www.cell.com/mobile. Also, be sure to visit http://www.cell.com to find other high-quality articles published in the full collection of Cell Press journals.

Last but definitely not least, we are grateful for the generosity of our sponsors, who helped to make this reprint collection possible.

Cell Stem Cell

For information for the Best of Series, please contact:
Jonathan Christison
Program Director, Best of Cell Press
e: jchristison@cell.com
p: 617-397-2893
t: @CellPressBiz

Optimal and Innovative Solutions for Stem Cell Culture Research

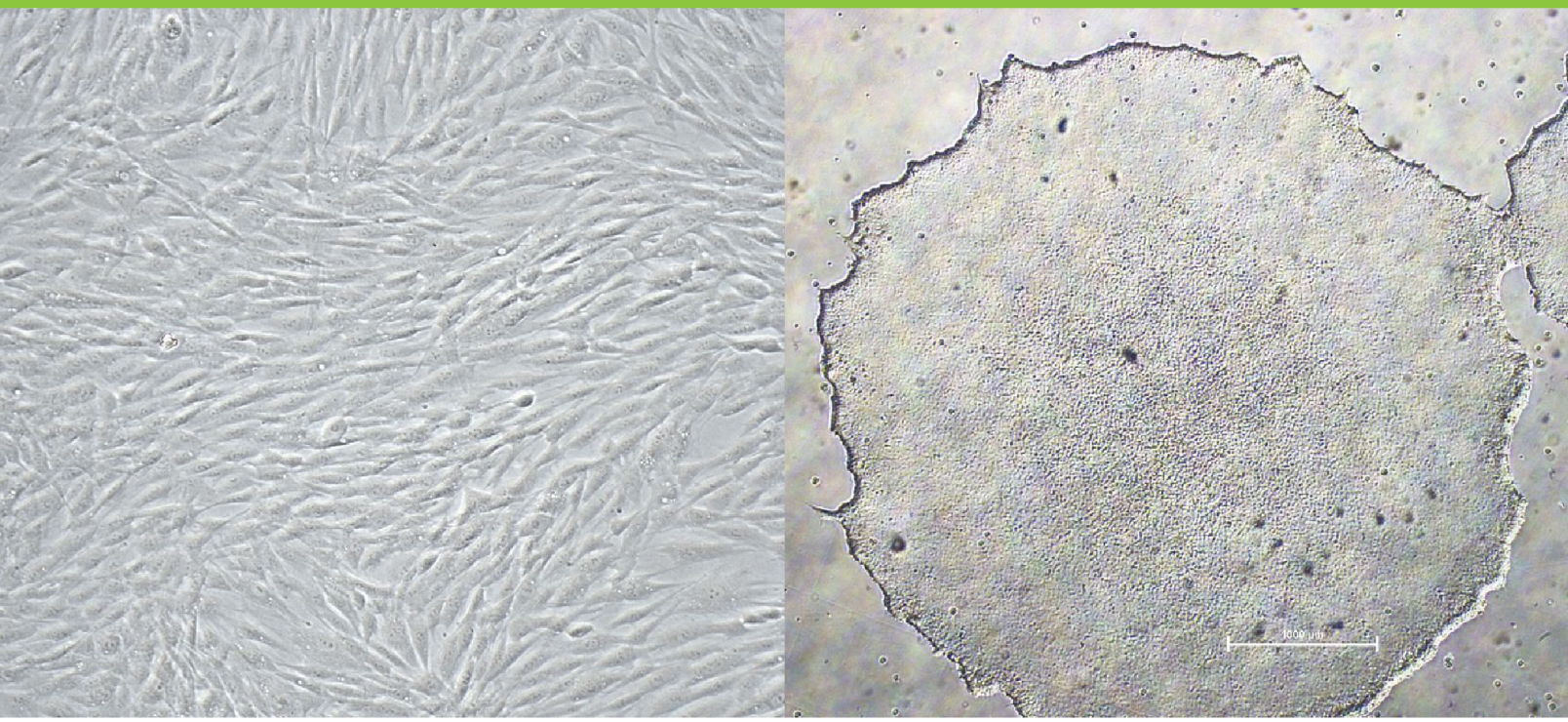

Look to Biological Industries (BI), a leading global provider of advanced products for cell and tissue culture for over 30 years.

Our NutriStem® serum-free, xeno-free stem cell culture media have become the gold standard in many laboratories, helping to advance the fields of stem cell-based therapies.

For optimal growth and expansion of human embryonic stem cells (hESC), induced pluripotent stem cells (iPS) and human mesenchymal stem cells (hMSC), chose Biological Industries.

Now available in the U.S from Rainbow Scientific, Inc.

Biological Industries' products are available in the U.S. through Rainbow Scientific, Inc. (RSI), a North American distributor of state-of-the-art products and solutions to academic, government, clinical and biotechnology laboratories for over sixteen years.

For more information or for a **free sample**, visit rainbowscientific.com or contact us at info@rainbowscientific.com.

Biological Industries products are for research use only.

Complete Product Line

- Serum-Free (SF) Media & Animal Component-Free (ACF) Culture Media
- Xeno-Free, SF, ACF Stem Cell Culture Media& Reagents
- Custom Formulations & Manufacturing
- Mycoplasma Elimination and Disinfectants
- Cell Proliferation & Viability Kits & Reagents
- Human Cytogenetics Media, Reagents & Supplements
- Classical Tissue Culture Media

BI Biological Industries
Culture of Excellence
www.bioind.com

CE CERTIFIED QMS ISO 9001 2008 CERTIFIED QMS ISO 13485 2003 cGMP Manufacturing Facility

US Distributor
Rainbow Scientific, Inc.

Rainbow Scientific, Inc. • 83 Maple Avenue, Windsor, CT 06095 USA • Tel: 860-298-8382 • Fax: 860-298-8586 • www.rainbowscientific.com

Cell Stem Cell

Best of 2013

Reviews

Brief Report

Articles

Short Articles

89 NORTH®

PhotoFluor® LM-75

World's first direct-mounted metal halide light source.

An ideal light source for fluorescence microscopy should provide strong, stable output power across the spectrum, should be extremely simple to use with no user alignment and should be priced lower than you expect.

The new PhotoFluor LM-75 from 89 North is all this and more with a wide array of features and benefits, including:

- Direct-mounting eliminates need for a liquid light guide
- As much or more usable power at the sample than a 200W metal halide light source
- Pre-aligned, user exchangeable lamp with a long lifetime
- Extremely quiet operation with minimal heat production
- Built-in ballast eliminates need for external control box, reducing the bench space needed
- Low up-front cost and lower overall cost of ownership than other fluorescence light sources

info@89north.com • 89north.com

CHROMA®

Catch the perfect (evanescent) wave.

Chroma's unique solution for two major challenges created by through-the-objective TIRF imaging:

- Eliminate spurious fluorescence signal from beyond the TIRF zone by using dichroics with surfaces flat enough to reflect TIRF lasers and produce optimal evanescent waves. With other dichroics, some laser photons will propagate into the sample, producing unwanted fluorescence. And because they're mounted in our patented metal TIRF cubes, they'll remain flat in your microscope.
- Block the extremely high levels of laser illumination returning through the objective when you use the emission filters in our TIRF sets to achieve the highest signal/noise ratios.

Chroma's complete, sputtered TIRF sets remove the guesswork so you can have confidence in your data. Our UltraFlat dichroic mirrors mounted in metal TIRF cubes provide distortion-free reflection of lasers, giving you the ability to create the perfect evanescent wave.

sales@chroma.com • chroma.com

An Unveiling of

STEM CELL INNOVATION

ISSCR 2015

ANNUAL MEETING

STOCKHOLM | SWEDEN

24-27 JUNE

Stockholmsmässan

ISSCR2015.ORG

ISSCR INTERNATIONAL SOCIETY FOR STEM CELL RESEARCH

Co-Sponsored By: WiRM

proteintech™

ANTIBODY WISH LIST

- ✓ WORKS IN ALL MY APPLICATIONS
- ✓ HIGH SENSITIVITY AND BINDING AFFINITY
- ✓ EXTENSIVELY VALIDATED IN UNMODIFIED SAMPLES
- ✓ ALL VALIDATION DATA AVAILABLE ONLINE
- ✓ SUITABLE FOR USE IN MULTIPLE SPECIES
- ✓ SATISFACTION GUARANTEED OR MY GRANT MONEY BACK
- ✓ 100% ORIGINAL PRODUCT FROM THE ORIGINAL MANUFACTURER

PROTEINTECH GROUP FULFILS EVERY SCIENTIST'S ANTIBODY WISH LIST

Find out more at ptglab.com

REGISTRATION AND ABSTRACTS OPEN JULY 7 WWW.ISSCR.ORG

NOV 5–7

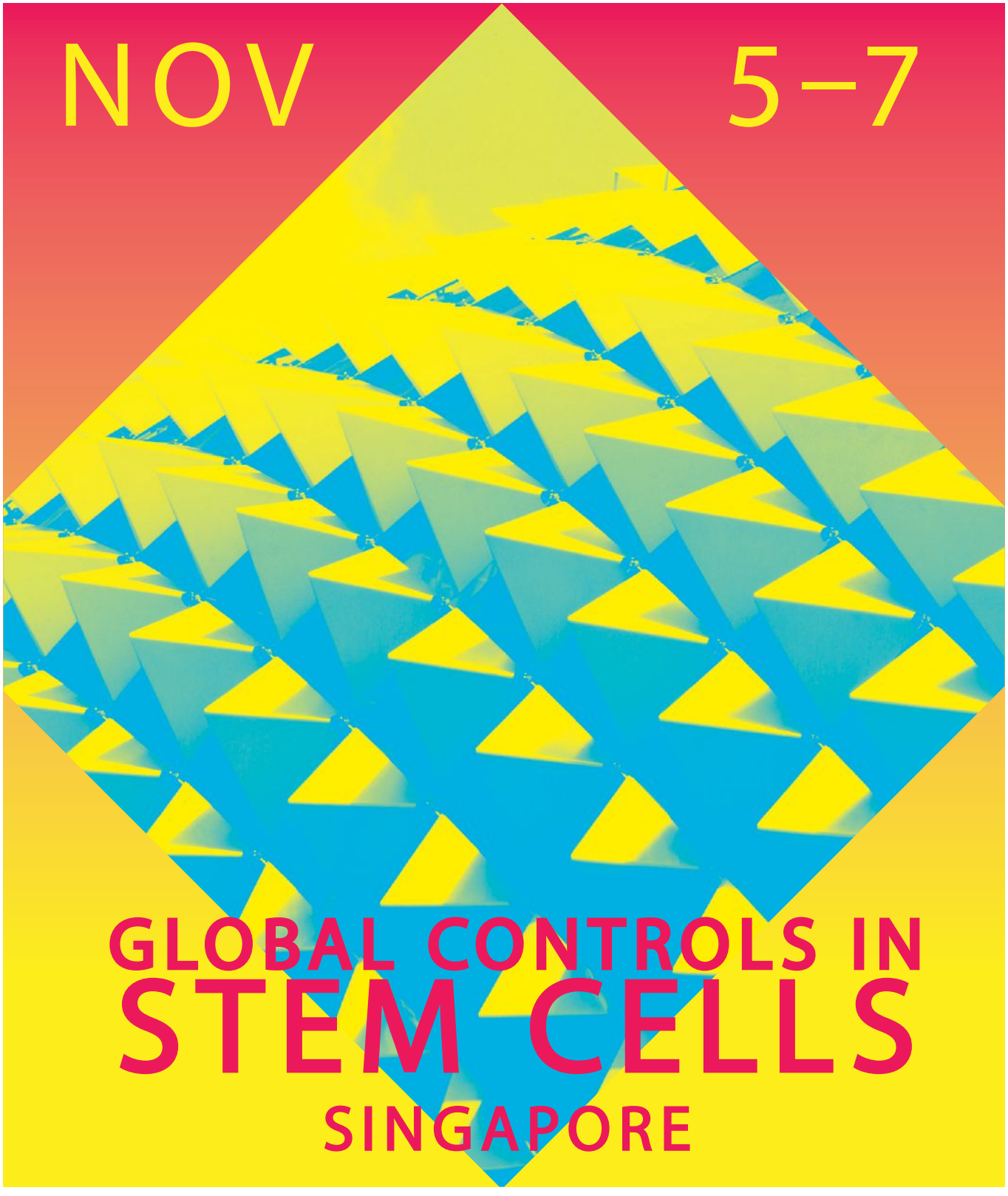

GLOBAL CONTROLS IN STEM CELLS

SINGAPORE

REGIONAL FORUM SERIES 2014

ISSCR INTERNATIONAL SOCIETY FOR STEM CELL RESEARCH

STEM CELL SOCIETY SINGAPORE

eppendorf

Impress Yourself

The new Eppendorf Cell Culture Consumables

The all new product line of Eppendorf Cell Culture Consumables will truly delight your cells. Its outstanding design, reliability and purity is based on more than 50 years of experience. Products created by experts, developed for perfectionists. Impress yourself!

> Unsurpassed quality, clarity, purity and sterility, providing reliable cell culture conditions
> Significantly improved design for more safety and consistency
> Maximum safety and confidence during storage and transportation

www.eppendorf.com/ccc

ISSCR CONNECT

Your online link to the latest stem cell research.

Our field is continually evolving, making it more important than ever to stay current with the latest discoveries, connect with colleagues and explore new collaborations. Each month, the interactive ISSCR Connect platform features scientific presentations covering advances across many topics of stem cell research.

Become an ISSCR member and gain full access to the latest data and global scientific community through ISSCR Connect.

Learn more at www.isscrconnect.org

ISSCR

INTERNATIONAL SOCIETY FOR STEM CELL RESEARCH

“WE’RE BRINGING A NEW PERSPECTIVE TO

cancer metabolism research

XF technology provides the easiest and most comprehensive assessment of cancer cell metabolism, measuring glucose and glutamine metabolism, and fatty acid oxidation of cancer cells in a microplate, in real-time!”

— David Ferrick, PhD,
CSO, Seahorse Bioscience

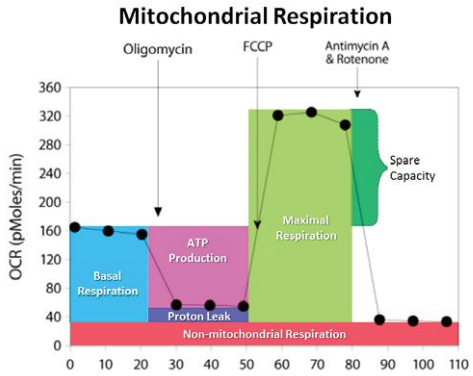

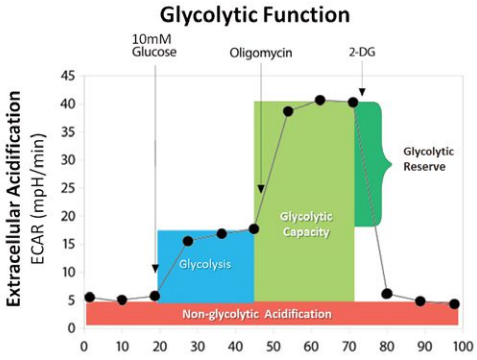

The Seahorse XF^{e} Extracellular Flux Analyzer

Measurements of cellular glycolysis are essential to understanding cancer, immune response, stem cell differentiation, aging, and cardiovascular and neurodegenerative diseases. The XF^{e} Analyzers and XF Glycolysis Stress Test Kit make it easy to measure the three key parameters of cellular glycolysis in a microplate: glycolysis, glycolytic capacity, and glycolytic reserve, revealing critical information not evident in mitochondrial respiration measurements alone.

See what’s possible.

Scan this QR code to view videos and see what the XF^{e} Analyzer can achieve.
Visit www.seahorsebio.com/cancercell for more information!

Seahorse *Bioscience*

Cell SnapShot archive

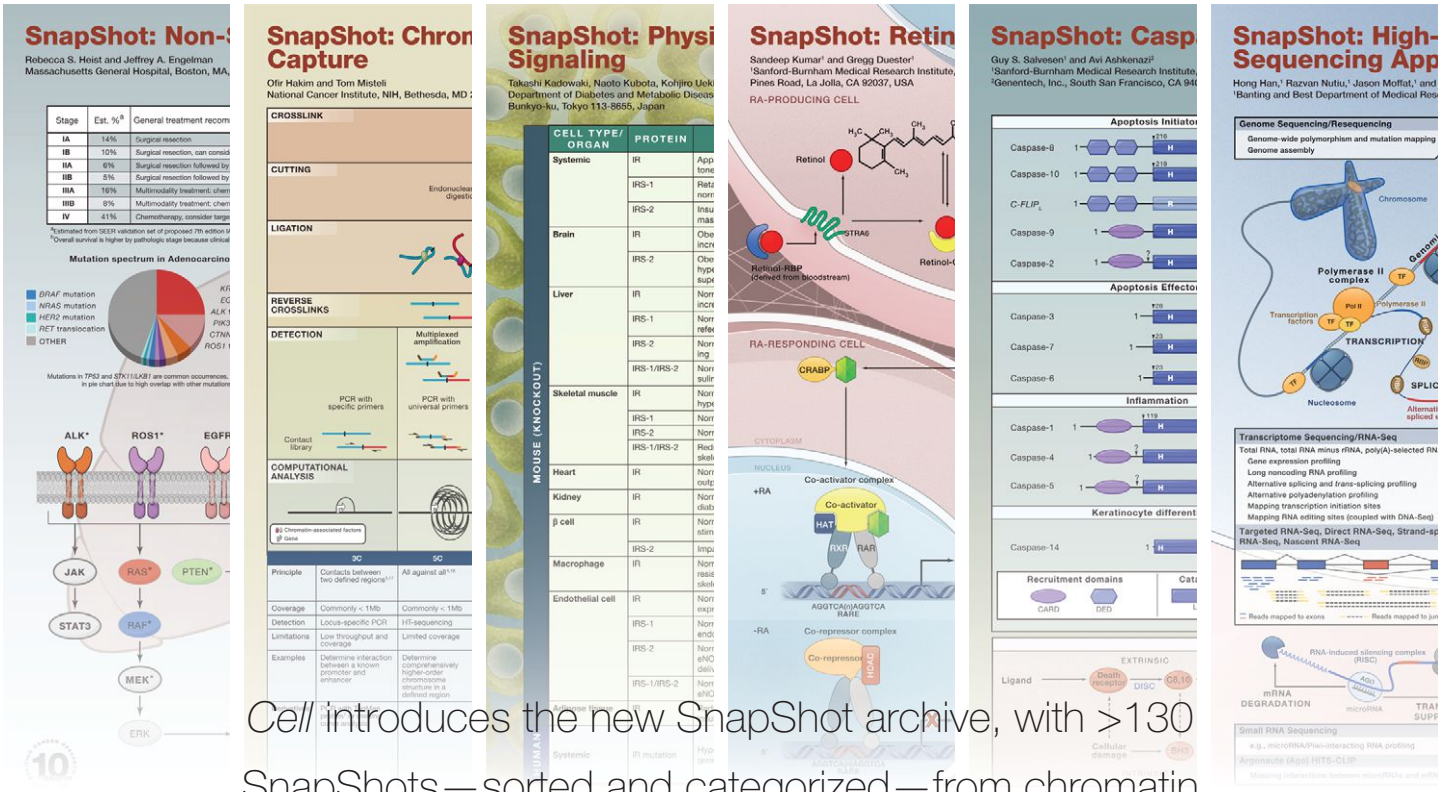

Cell introduces the new SnapShot archive, with >130 SnapShots—sorted and categorized—from chromatin remodelers and autophagy to cancer and autism. All SnapShots published from a year ago or more are open access and freely available.

view the archive

Cell PRESS

snapshots.cell.com

Next-Generation Genome Engineering Technologies & Services

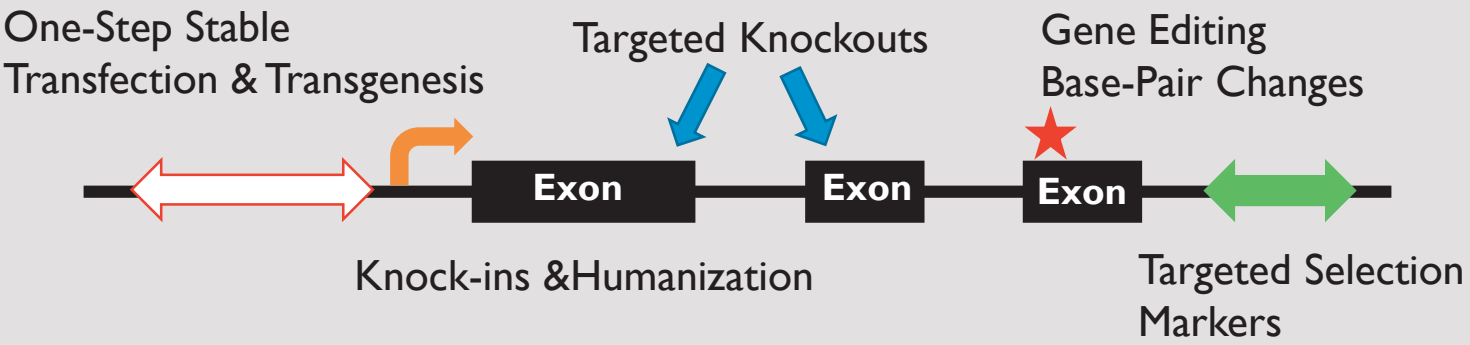

With So Many Opportunities What Are You Waiting For?

Footprint-Free™ Gene Editing

NextGEN™ CRISPR

XTN™ TALEN

Stable Transfection Kits & piggyBac™ Transposon

Cell Line & Rodent Model Engineering Services

Your Next Discovery Awaits

Transposagen
Better Models. Better Results.™

1-844-GEN-EDIT
info@transposagenbio.com
www.transposagenbio.com

NYSCF The New York Stem Cell Foundation Research Institute

NINTH ANNUAL TRANSLATIONAL STEM CELL RESEARCH CONFERENCE

OCTOBER 22-23, 2014

AT THE ROCKEFELLER UNIVERSITY, NEW YORK CITY

NYSCF CONFERENCE OVERVIEW

The NYSCF Conference is unique: it focuses on translational stem cell research, demonstrating the potential to advance cures for the major diseases of our time.

It is designed for all professionals with an interest in stem cell research, including physicians, researchers, clinical investigators, professors, government and health officials, postdoctoral fellows and graduate students. The panels on Tuesday are designed to reach a broader audience, including lay public.

CONFIRMED SPEAKERS AND PANELISTS INCLUDE

Domenico Accili, MD
Columbia University
Ali H. Brivanlou, PhD
The Rockefeller University
Moses V. Chao, PhD
Skirball Institute, NYU
Shuibing Chen, PhD
Weill Cornell Medical College
Kenneth R. Chien, MD, PhD
Karolinska Institutet
George Church, PhD
Harvard Medical School
Peter J. Coffey, DPhil
UCL – Institute of Ophthalmology
Bruce Conklin, MD
Gladstone Institute of Cardiovascular Disease
Michele De Luca, PhD
University of Modena and Reggio Emilia
Dieter Egli, PhD
The NYSCF Research Institute
Samuel E. Gandy, MD, PhD
Icahn School of Medicine at Mount Sinai
John Greally, PhD
Albert Einstein College of Medicine
Jacob Hanna, MD, PhD
Weizmann Institute of Science
Catriona Jamieson, MD, PhD
University of California, San Diego
Rudolf Jaenisch, MD
The Whitehead Institute
Ruth Lehmann, PhD
Skirball Institute, NYU
Ihor Lemischka, PhD
Icahn School of Medicine at Mount Sinai
Dan R. Littman, MD, PhD
Skirball Institute, NYU
Ravi Majeti, MD, PhD
Stanford University
Michael Milone, MD, PhD
University of Pennsylvania
Christine Mummery, PhD
Leiden University Medical Center
Chuck Murry, MD, PhD
University of Washington
Scott Noggle, PhD
The NYSCF Research Institute
Mahendra Rao, MD, PhD
The NYSCF Research Institute
Derrick Rossi, PhD
Harvard University
Jeffrey Rothstein, MD, PhD
Johns Hopkins University
Lee Rubin, PhD
Harvard University
Eric Schadt, PhD
Icahn School of Medicine at Mount Sinai
Susan L. Solomon, JD
The New York Stem Cell Foundation
Lorenz Studer, MD
Memorial Sloan-Kettering Cancer Center
Ludovic Vallier, PhD
University of Cambridge
Gordana Vunjak-Novakovic, PhD
Columbia University
Sir Ian Wilmut, FRS, FRSE
University of Edinburgh

The New York Stem Cell Foundation Research Institute is a non-profit organization dedicated to accelerating cures for the major diseases of our time through stem cell research.

To register for the conference, go to nyscf.org/conference

NYSCF
The New York Stem Cell Foundation Research Institute

Cell Stem Cell
Review

The Sox Family of Transcription Factors: Versatile Regulators of Stem and Progenitor Cell Fate

Abby Sarkar[1,2,3] and Konrad Hochedlinger[1,2,3,*]
[1]Howard Hughes Medical Institute at Massachusetts General Hospital Cancer Center and Center for Regenerative Medicine, 185 Cambridge Street, Boston, MA 02114, USA
[2]Department of Stem Cell and Regenerative Biology, Harvard University and Harvard Medical School, 7 Divinity Avenue, Cambridge, MA 02138, USA
[3]Harvard Stem Cell Institute, 1350 Massachusetts Avenue, Cambridge, MA 02138, USA
*Correspondence: khochedlinger@helix.mgh.harvard.edu
http://dx.doi.org/10.1016/j.stem.2012.12.007

Sox family transcription factors are well-established regulators of cell fate decisions during development. Accumulating evidence documents that they play additional roles in adult tissue homeostasis and regeneration. Remarkably, forced expression of Sox factors, in combination with other synergistic factors, reprograms differentiated cells into somatic or pluripotent stem cells. Dysregulation of Sox factors has been further implicated in diseases including cancer. Here, we review molecular and functional evidence linking Sox proteins with stem cell biology, cellular reprogramming, and disease with an emphasis on Sox2.

Introduction

Stem cells are characterized by the capacity to continuously self-renew and the potential to differentiate into one or more mature cellular lineages (Simons and Clevers, 2011). They serve to form tissues and organs during mammalian development, and they maintain ongoing cellular turnover and provide regenerative capacity in certain adult tissues. One can distinguish between pluripotent embryonic stem cells (ESCs), which give rise to all embryonic lineages, and somatic stem cells, which give rise to one or more specialized lineages within the tissues they reside in. A stem cell's decision for self-renewal or differentiation is intrinsically controlled by the interplay of cell type-specific transcription factors and chromatin regulators. Although several such molecules have been implicated in stem cell biology over the last few years, the mechanistic modes of action of these molecules remain incompletely understood.

Research on the Sox gene family began with the seminal discovery of the mammalian testis-determining factor, *Sry* (Gubbay et al., 1990; Sinclair et al., 1990). Sry carries a characteristic high-mobility-group (HMG) domain that binds DNA in a sequence-specific manner. In general, proteins containing an HMG domain with 50% or higher amino acid similarity to the HMG domain of Sry are referred to as Sox proteins (Sry-related HMG box). So far, 20 different Sox genes have been discovered in mice and humans (Schepers et al., 2002). In addition, two Sox-like genes have been identified in the unicellular choanoflagellate *Monosiga brevicollis*, suggesting that the origin of Sox proteins predates multicellularity or possibly marks the transition of unicellular to multicellular organisms (Guth and Wegner, 2008; King et al., 2008).

Sox proteins that share an HMG domain with more than 80% sequence identity are divided into different groups termed A to H (Table 1). Individual members within a group share biochemical properties and thus have overlapping functions (Wegner, 2010). In contrast, Sox factors from different groups have acquired distinct biological functions despite recognizing the same DNA consensus motif. Target gene selectivity by different Sox factors can be achieved through differential affinity for particular flanking sequences next to consensus *Sox* sites, homo- or heterodimerization among Sox proteins, posttranslational modifications of Sox factors, or interaction with other cofactors (Wegner, 2010). This molecular versatility may thus explain why the same Sox factors can play very different molecular and functional roles in distinct biological contexts.

Here, we review the biology of Sox factors that are implicated in stem cell biology in the context of development, tissue homeostasis, reprogramming, and cancer. We place particular emphasis on the well-studied SoxB1 group member Sox2 with the goal of deriving general molecular and cellular principles by which Sox factors control stem and progenitor cell fates.

Sox Factors in Preimplantation Development and Pluripotency

The formation of the trophectoderm (TE) and inner cell mass (ICM) within the blastocyst is the first lineage specification event in the mammalian embryo (Rossant and Tam, 2009). The ICM contains pluripotent founder cells, which give rise to all embryonic lineages, and a population of extraembryonic endoderm (ExEn) cells that contribute to the yolk sac. Similarly, the TE contains a population of multipotent stem cells that form the extraembryonic ectoderm and give rise to the placenta. Sox2 is initially present in both the ICM and the TE but is later confined to the ICM (Avilion et al., 2003). Zygotic deletion of *Sox2* results in early embryonic lethality due to a failure to form the pluripotent epiblast but leaves the TE unperturbed (Avilion et al., 2003). Interestingly, subsequent studies showed that maternal Sox2 protein persists in preimplantation embryos, which might have masked a phenotype in the TE in zygotic *Sox2* mutants (Keramari et al., 2010). Indeed, depletion of both maternal and zygotic transcripts by RNAi causes an early arrest of embryos at the morula stage and a failure to form TE, suggesting that Sox2 is required for the segregation of the TE and ICM (Keramari et al., 2010).

Table 1. Sox Factors Implicated in Stem Cell Biology

Group	Sox Member	Expression			Function	Citations for Functional Role
		Preimplantation Embryo	Fetus	Adult		
SoxA	Sry	Founding member of the Sox family, expression/role in stem cells undefined				
SoxB1	Sox1	N/A	Neural progenitor cells (NPCs)	NPCs	Required for specification and maintenance of undifferentiated stem cells	Bylund et al. (2003); Graham et al. (2003); Pevny et al. (1998); Zhao et al. (2004)
	Sox2	Expression/role in ectoderm, endoderm, and mesoderm derivatives, refer to Figure 1 and text for details				
	Sox3	N/A	NPCs	NPCs	Same as Sox1	Bylund et al. (2003); Bergsland et al. (2011)
		N/A	N/A	Spermatogonia	Genetic deletion leads to loss of undifferentiated spermatogonia	Raverot et al. (2005)
SoxB2	Sox14, Sox21	Expression/role in stem cells largely undefined*				
SoxC	Sox4, Sox11, Sox12	Expression/role in stem cells largely undefined*				
SoxD	Sox5, Sox6, Sox13	Expression/role in stem cells largely undefined*				
SoxE	Sox8	N/A	N/A	Muscle satellite cells	N/A	Schmidt et al. (2003)
	Sox9	N/A	Hair follicle stem cells	Hair follicle stem cells	Deletion leads to loss of specification of early bulge cells needed to form the hair follicle and sebaceous gland	Vidal et al. (2005); Nowak et al. (2008)
		N/A	Distal tip cells (lung)	N/A	N/A	Rawlins (2011)
		N/A	NPCs	NPCs	Required for specification and maintenance of stem cells (LOF and GOF studies)	Scott et al. (2010)
		N/A	Premigratory NCSCs (neural crest stem cells) and migratory cranial NCSCs	N/A		Cheung and Briscoe (2003)
		N/A	Retinal progenitor cells (RPCs)	N/A	Genetic deletion leads to a loss of stem cell differentiation potential to Muller glial lineage	Poché et al. (2008)
		N/A	Pancreatic progenitors	Exocrine pancreatic duct cells	Fetal LT marks all pancreatic lineages, adult LT marks all exocrine lineages. Genetic deletion leads to loss of pancreatic progenitors	Seymour et al. (2007); Furuyama et al. (2011); Kopp et al. (2011)
		N/A	N/A	Liver duct cells	LT labels hepatocytes after injury	Furuyama et al. (2011)
		N/A	N/A	Intestinal stem/ progenitor cells	Embryonic and adult LT labels all intestinal lineages. Genetic deletion depletes stem cells and Paneth cells	Furuyama et al. (2011); Sato et al. (2011)
		N/A	N/A	Mammary stem cells (MaSCs)	Knockdown leads to loss of stem cell maintenance	Guo et al. (2012)
	Sox10	N/A	Migratory NCSCs	N/A	Required for maintenance of stem cells (LOF and GOF studies in chick embryos)	Kim et al. (2003)

Table 1. *Continued*

Group	Sox Member	Expression			Function	Citations for Functional Role
		Preimplantation Embryo	Fetus	Adult		
SoxF	Sox7	Expression/role in stem cells largely undefined*				
	Sox17	Extraembryonic endoderm (XEN) cells	N/A	N/A	XEN cells, required for derivation	Niakan et al. (2010)
		N/A	Hematopoietic stem cells (HSCs)	N/A	HSCs, genetic deletion leads to loss of fetal HSCs	Kim et al. (2007)
	Sox18	Expression/role in stem cells largely undefined*				
SoxG	Sox15	ESCs	N/A	N/A	Genetic deletion has no obvious functional consequence	Maruyama et al. (2005)
		N/A	N/A	Satellite cells	N/A	Meeson et al. (2007)
SoxH	Sox30	Expression/role in stem cells largely undefined*				

Note: only those Sox factors that are linked to stem cells by expression and functional evidence have been highlighted in this table. LT, lineage tracing; LOF, loss of function; GOF, gain of function. N/A, not assessed; (*), some of these Sox factors have been implicated in progenitor cell biology but will not be covered in this review due to space limitations.

Consistent with its role in preimplantation development, *Sox2*-deficient embryos neither support the derivation of ESCs from the ICM nor the derivation of trophoblast stem cells (TSCs) from the TE (Avilion et al., 2003). Furthermore, deletion of *Sox2* in already established ESCs results in their inappropriate differentiation into trophectoderm-like cells, indicating that Sox2 is also critical for the maintenance of ESCs (Masui et al., 2007).

Interestingly, Sox2's effect on self-renewal and differentiation of ESCs is highly dosage dependent (Kopp et al., 2008), suggesting that its expression needs to be in equilibrium with other cofactors to maintain pluripotency. Supporting this concept is the observation that Sox2 acts cooperatively with other dosage-sensitive transcription factors, such as Oct4 and Nanog, to maintain the regulatory networks responsible for self-renewal and to repress differentiation programs in ESCs (Boyer et al., 2005; Chen et al., 2008; Kim et al., 2008; Orkin and Hochedlinger, 2011). Cobinding of these factors at targets associated with self-renewal facilitates recruitment of the coactivator p300 and consequently transcriptional activation (Chen et al., 2008), whereas cobinding at developmental target genes causes gene silencing in concert with the repressive polycomb complex (Boyer et al., 2006). Notably, a large fraction of target genes bound by these factors contain composite *Oct4/Sox2* consensus binding sites (Masui et al., 2007; Tomioka et al., 2002), suggesting that Sox2 closely collaborates with Oct4 in order to efficiently bind to DNA and recruit other factors important for gene activation. In support of the notion that Oct4 and Sox2 jointly activate many targets is the finding that overexpression of *Oct4* can partially compensate for the loss of *Sox2* (Masui et al., 2007).

Upon specification of the ICM, the SoxF group member Sox17 becomes detectable in a rare population of cells destined to form the ExEn lineage (Kanai-Azuma et al., 2002; Niakan et al., 2010). Similar to the requirement for Sox2 in ESC and TSC derivation, Sox17 is essential for the establishment of extraembryonic endoderm cell lines, termed XEN cells (Kunath et al., 2005; Niakan et al., 2010). At the molecular level, Sox17 has been placed downstream of the master regulator for primitive endoderm, Gata6 (Niakan et al., 2010). Accordingly, forced expression of *Sox17* or its related group member *Sox7* in ESCs results in a downregulation of the pluripotency gene expression program and an upregulation of the primitive endoderm-associated program, giving rise to endodermal progenitors (Niakan et al., 2010; Séguin et al., 2008). Mechanistically, Sox17 seems to oppose Sox2's function by repressing pluripotency targets and activating endoderm targets when ectopically expressed in ESCs. Chromatin immunoprecipitation (ChIP) experiments for Sox17 further suggest that this opposition is in part accomplished by displacing Nanog from silenced Sox2/Nanog targets, resulting in their transcriptional activation (Niakan et al., 2010).

Collectively, these results obtained from in vivo or in vitro studies document that different Sox factors play important and often dosage-dependent roles in the establishment of cell lines of the three main cell lineages of the preimplantation embryo, the ICM, TE, and ExEn.

Sox2 in Fetal Development

After gastrulation of the embryo, *Sox2* expression becomes largely restricted to the presumptive neuroectoderm, sensory

placodes, brachial arches, gut endoderm, and primordial germ cells (Avilion et al., 2003; Wood and Episkopou, 1999; Yabuta et al., 2006). Since *Sox2* deficiency causes early postimplantation lethality (Avilion et al., 2003), functional evidence for its role in the fetus has required analyses of hypomorphic and conditional mutants in *Xenopus*, chick, and mouse embryos. These studies have demonstrated the importance of Sox2 in lineage specification, morphogenesis, proliferation, and differentiation in a variety of developing tissues of the fetus. In addition, these data have documented that the function of Sox2 is highly dosage and context dependent. In the following paragraphs, we will briefly summarize Sox2's roles in developing endodermal, ectodermal, and mesodermal cell lineages.

Sox2 in Ectoderm Development

Sox2 is expressed during the earliest stages of ESC differentiation toward the neural lineage in vitro, supporting a role in neural commitment. At the molecular level, Sox2 promotes early neuroectodermal fate by directly suppressing key regulators of the alternative mesendodermal fate such as *brachyury* (Thomson et al., 2011; Wang et al., 2012). Sox2 is involved in a similar cell fate decision in vivo during the differentiation of bipotential axial stem cells into either paraxial mesoderm or neural plate (Takemoto et al., 2011). Paraxial mesoderm gives rise to the vertebral column, dermis, and skeletal muscle, whereas neural tube develops into the CNS. In the absence of competing factors, Sox2 drives axial stem cells toward a neural plate fate. However, in the presence of Tbx6, a regulator of presomitic mesoderm development, *Sox2*'s N1 enhancer becomes directly suppressed and axial stem cells are fated toward paraxial mesoderm. In agreement, *Tbx6* loss or ectopic *Sox2* expression results in the formation of ectopic neural tubes at the expense of paraxial mesoderm (Takemoto et al., 2011). Together, these results emphasize the importance of Sox2 in regulating early neural specification in the embryo and in differentiating ESCs. The antagonism between Sox2 and Tbx6 in axial stem cells further exemplifies a general principle by which Sox factors regulate cell fate decisions during development and will be discussed later on.

Sox2 continues to play major roles in the developing CNS and peripheral nervous system (PNS) by controlling the proliferation and differentiation of fetal progenitor cells (Pevny and Nicolis, 2010; Wegner and Stolt, 2005). Notably, *Sox2* expression overlaps and functions redundantly with that of the other two SoxB1 group factors, *Sox1* and *Sox3* in the CNS (Bylund et al., 2003; Graham et al., 2003; Wood and Episkopou, 1999) (Table 1). In general, overexpression of any of the SoxB1 factors promotes CNS progenitor cell proliferation, whereas depletion of these factors induces cell-cycle exit and onset of differentiation (Bylund et al., 2003; Cavallaro et al., 2008; Ferri et al., 2004; Graham et al., 2003; Kishi et al., 2000; Miyagi et al., 2008). Likewise, Sox2 expression is essential for neural progenitor cell proliferation and differentiation in the retina, in part through its direct activation of the *Notch1* gene (Taranova et al., 2006). Comparison of *Sox2* hypomorphs of various strengths with Sox2 conditional null mice further suggests that Sox2 function in retinal progenitor cells (RPCs) is highly dosage dependent. RPCs lacking *Sox2* expression lose the competence to proliferate and differentiate, while reductions in Sox2 levels cause variable microphthalmia. In addition to neural progenitors of the brain and eye, *Sox2* is transiently expressed in the Schwann cell lineage, which is of neural crest origin and responsible for the myelination of axons of the PNS. Similar to its role in CNS and retinal progenitors, Sox2 prevents terminal differentiation of Schwann cell precursors (Le et al., 2005).

Surprisingly, *Sox2* expression has also been reported to be important for the differentiation of subsets of neurons, indicating that its function is not always confined to the maintenance of progenitors and stem cells. For example, *Sox2* hypomorphic or knockout mice have reduced GABAergic interneurons in the newborn cortex and adult olfactory bulb (Cavallaro et al., 2008). Consistently, *Sox2* mutant NPC cultures generate beta-tubulin-positive neuronal-like cells that are poorly arborized and are negative for markers of mature neurons and GABAergic neurons (Cavallaro et al., 2008; Ferri et al., 2004). In an independent in vitro differentiation paradigm, Sox2 was shown to promote the maturation of migrating neural crest progenitor cells into sensory ganglia (Cimadamore et al., 2011). Collectively, these studies demonstrate that SoxB1 proteins play key roles in the development of the CNS and the PNS by controlling both the proliferation and differentiation of various progenitor cell populations. It will be important to define the mechanisms by which the same transcription factor regulates progenitor cell maintenance and differentiation within the same lineage (see also Mechanisms section/Pioneer factors). *Sox2* is expressed in other developing ectoderm-derived tissues including the inner ear and dental epithelium, which will not be discussed here because of space constraints (see Figure 1 for summary) (Dabdoub et al., 2008; Juuri et al., 2012; Kiernan et al., 2005).

Sox2 in Endoderm Development

Whereas Sox2 counteracts mesoderm specification in vivo and during ESC differentiation, elegant work by Hogan and colleagues showed that it plays multiple additional roles in organ specification of the foregut endoderm (Figure 1). *Sox2* is highly expressed in the anterior part of the foregut, giving rise to esophagus and forestomach. However, it is lowly expressed in the future trachea and posterior stomach, respectively (Que et al., 2007). A severe decrease in Sox2 levels in hypomorphic embryos causes a transformation of esophagus into trachea, resulting in a failure to separate future trachea and esophagus (tracheoesophageal fistula) (Que et al., 2007). Interestingly, Sox2 appears to play an independent role in defining the boundary between the keratinized forestomach/esophagus and the glandular hindstomach/intestine based on the observation that *Sox2* mutant esophagus and forestomach exhibit histological and molecular signs of glandular stomach and intestine. Experiments regulating Sox2 dosage have further demonstrated that Sox2 is required for patterning and morphogenesis of the embryonic tongue into taste bud sensory cells (Okubo et al., 2006), branching and differentiation of primary lung bud into the lung (Gontan et al., 2008; Ishii et al., 1998), and proper differentiation of the tracheal cartilage (Que et al., 2009).

These experiments document an interesting commonality and difference in how Sox2 controls stem and progenitor cells in distinct developing tissues. A commonality among stem and progenitor cells of the retina, foregut-derived tissues, and pluripotent cells is a sensitivity to changes in Sox2 dose. This observation is consistent with the presence of cooperative and/or antagonistic factors whose function depends on finely

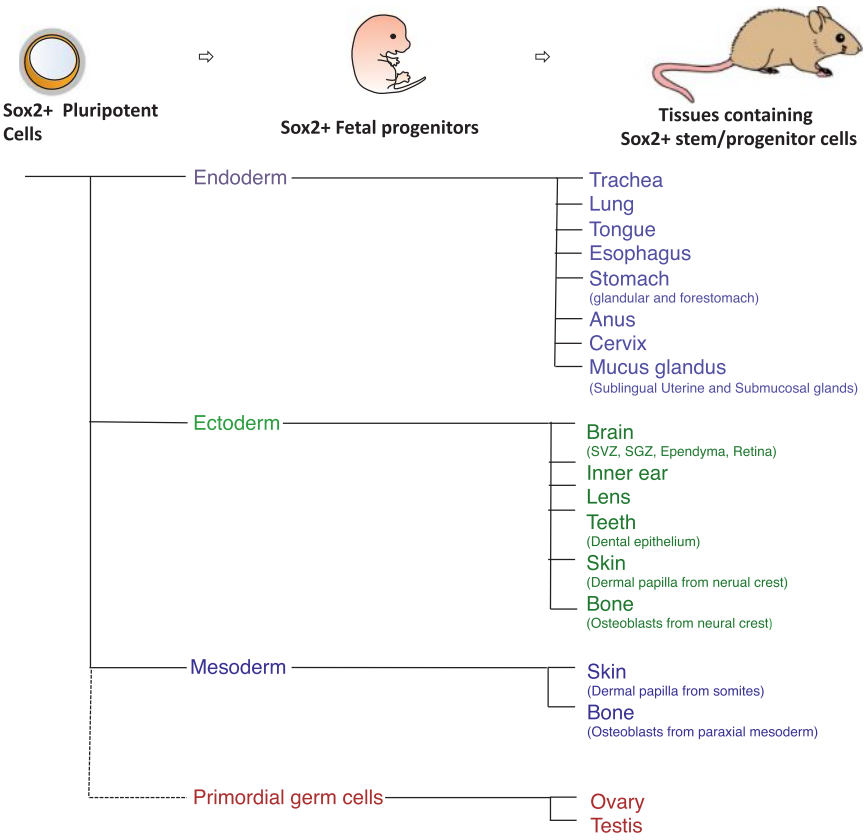

Figure 1. Sox2 Expression in Pluripotent, Fetal, and Adult Progenitor and Stem Cells
Sox2 is expressed throughout development, initially in pluripotent founder cells of the blastocyst and subsequently in ectodermal, endodermal, and mesodermal derivatives as well as in primordial germ cells. Sox2 expression is maintained in fetal and adult tissues derived from Sox2+ fetal progenitor cells and marks stem and progenitor cells and in some cases also differentiated cells.

tuned Sox2 levels and will be discussed below. A notable difference among these tissues is the effect *Sox2* deletion has on cell proliferation. While neural progenitors generally exit the cell cycle upon *Sox2* deletion, trachea, tongue, and esophagus exhibit altered differentiation programs without changes in cell proliferation. Thus, Sox2 seems to control tissue formation in cell proliferation-dependent and independent ways that vary from tissue to tissue. Future studies of Sox2 targets in the respective cell types might give insights into the molecular mechanisms responsible for these different outcomes.

Sox2 in Mesoderm Development

During skin development, *Sox2* is initially expressed in groups of mesenchymal cells called dermal condensates, which precede hair and whisker follicle formation and eventually give rise to the so-called dermal sheath and dermal papilla (DP) (Driskell et al., 2009; Rendl et al., 2005). The DP cyclically provides signals to the surrounding hair follicle to induce hair growth. While all DPs express Sox2 until shortly before birth, only a subset of them continues to be Sox2+ after birth (Driskell et al., 2009). This coincides with the emergence of different types of DP-associated hair follicles during development. In postnatal mice, Sox2+ DPs are associated with so-called guard, auchene, and awl follicles, which form earlier in development, whereas Sox2− DPs are associated with zigzag follicles that form late in development. Of note, Sox2+ dermal cells appear to be the cells of origin of multipotent, self-renewing skin-derived precursors (SKPs) (Fernandes et al., 2004). Both primary *Sox2*+ dermal cells and clonally derived SKPs induce hair morphogenesis upon transplantation into nude mice and differentiate into multiple dermal cell types in vivo and neural cells in vitro (Biernaskie et al., 2009; Driskell et al., 2009). These characteristics identify Sox2+ dermal cells as putative dermal stem cells. DP cells and derivative SKPs were originally thought to originate exclusively from the neural crest (ectoderm). However, recent lineage-tracing analyses with a somite-specific cre (Myf5-cre) driver have refined this interpretation. Trunk-derived DP cells and SKPs originate from somites (mesoderm), while facial-derived DP cells and SKPs originate from the neural crest (ectoderm) (Jinno et al., 2010). Evidence for a functional role for DP-specific Sox2 expression on hair follicle growth has been provided by the Rendl laboratory (Clavel et al., 2012). DP-specific *Sox2* ablation leads to derepression of its target *Sostdc1*, which normally inhibits Bmp signaling. A decrease in Bmp signaling from the DP results in a reduction of hair shaft progenitor cell migration in the adjacent follicle and thus impaired hair growth, which resembles that of Sox2-zigzag hairs. Whether Sox2 also plays a functional role in wound repair and SKP self-renewal is an interesting question that remains to be addressed.

Sox2 has also been implicated in the proliferation of osteoblast progenitors in vitro and in vivo. Deletion of *Sox2* in cultured osteoblast cell lines leads to a senescence-like phenotype, while its overexpression prevents differentiation (Mansukhani et al., 2005). Similarly, ablation of *Sox2* in the osteoblast lineage in vivo using a Collagen (2.3 kb)-driven Cre line results in reduced bone mineral density and bone volume (Basu-Roy et al., 2010), while transgenic overexpression inhibits mature osteoblast function (Holmes et al., 2011). Given that osteoblasts, like DP cells, can originate from both neural crest and paraxial mesoderm, it remains to be formally shown that Sox2 is expressed in osteoblasts derived from both germ layers. Collectively, these experiments extend Sox2 expression and function in stem and progenitor cells from ectoderm and endoderm to that in mesoderm. Another important conclusion from these observations is that Sox2 can influence progenitor cell proliferation either directly by preventing cellular differentiation (e.g., in osteoblasts) or indirectly by suppressing prodifferentiation signals produced from adjacent cells (e.g., in DP cells).

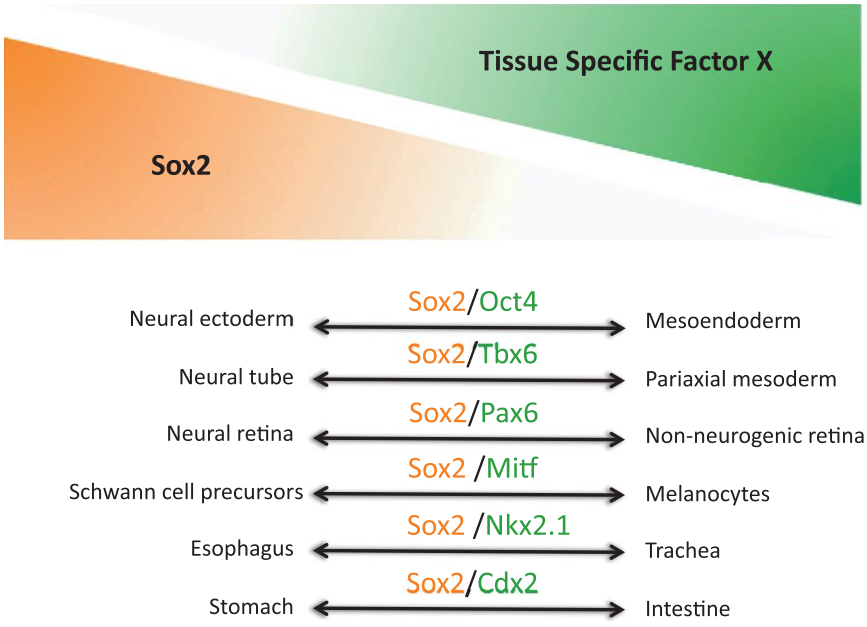

Figure 2. Antagonisms between Sox2 and Other Lineage-Specific Transcription Factors Determine Cell Fate

During organogenesis, Sox2 influences cell fate by inhibiting transcription factors that specify alternative cell lineages. Sox2 is expressed in an inverse gradient with the respective other transcription factor and thus acts in a dosage-dependent manner to establish cellular identities within and boundaries between future tissues.

Sox2 Specifies Cell Fate by Antagonizing Other Transcriptional Regulators

A common theme emerging from the abovementioned observations is that Sox2 often determines cell fate by antagonizing transcription factors of alternative cell lineages (Figure 2). An example already mentioned in this Review is the antagonism between Sox2 and Tbx6 during the specification of bipotential axial stem cells toward either Sox2+ neural tube or Tbx6+ axial mesoderm (Takemoto et al., 2011). Likewise, Sox2 antagonizes the transcription factor Nkx2.1 during foregut development; *Sox2* is expressed most anteriorly in the future esophagus and stomach, whereas *Nkx2.1* is expressed ventrally in the future trachea (Que et al., 2007). Accordingly, embryos deficient for *Nkx2.1* exhibit the reciprocal phenotype to *Sox2* mutants displaying ectopic *Sox2* expression and a transformation of future trachea into esophagus (Que et al., 2007). Furthermore, antagonism between the stomach-specifying Sox2/Barx1/Sfrp pathway and the intestinal fate-promoting Wnt/Cdx2 pathway is responsible for establishing the boundary between the glandular stomach and the intestine (Zorn and Wells, 2009). Lastly, the interaction between Sox2 and Mitf/Egr2 regulates the differentiation of Schwann cell progenitors into either myelinating Schwann cells or melanocytes (Adameyko et al., 2012). Specifically, Sox2 maintains a Schwann cell progenitor state, whereas its cross-regulatory interactions with either Mitf or Egr2 consolidate mature Schwann cell or melanocyte fates, respectively (Adameyko et al., 2012). The suppression of *Mitf* expression by Sox2 may be direct since Sox2 protein was detected at the proximal *Mitf-m* promoter in ESCs and melanoma cell lines (Adameyko et al., 2012). Whether mutual repression between Sox2 and Nkx2.1 or Sox2 and Cdx2 also involves direct binding to the respective regulatory regions remains to be determined. Development of a Sox2 overexpression mouse model showed that Sox2 activates Sox21, which in turn binds to and represses Cdx2 in ESCs and neural progenitors, thus arguing for an indirect mechanism in this particular context (Kuzmichev et al., 2012). Together, these observations underscore a general principle of how Sox2 drives cell fate decisions during development, namely by directly or indirectly inhibiting regulators of alternative cell fates.

It is important to recognize, however, that the antagonisms between Sox2 and other transcription factors are highly cell type and developmental stage specific. In fact, transcription factor pairs that are antagonistic in one cell type or developmental stage may cooperate in other cellular or developmental settings. A case in point is the Sox2/Pax6 pair. Ablation of *Sox2* in multipotent optic cup progenitors biases them toward a nonneurogenic ciliary body epithelium fate (Matsushima et al., 2011). This phenotype is rescued in a *Pax6* heterozygous (haploinsufficient) background (Matsushima et al., 2011), indicating that Sox2 specifies a neurogenic fate, whereas Pax6 instructs a nonneurogenic fate. In contrast to this antagonistic relationship during development of the optic cup, Sox2 and Pax6 cooperate during lens development by forming a complex on lens-specific enhancer elements such as that of the delta crystalline gene (Kamachi et al., 2001). In support of the cooperative role of Sox2 and Pax6 in lens specification, combined expression of both factors is sufficient to differentiate embryonic ectoderm into lens ectoderm.

Sox2 in Tissue Homeostasis and Regeneration

Accumulating data indicate that tissues that require Sox2 during development continue to express this factor in some adult stem and progenitor cells derived from that tissue (Figure 1). Below, we will review the expression patterns and, where available, functional data linking Sox2 with adult stem and progenitor cells.

Using Sox2-GFP knockin mice, Pevny and coworkers first demonstrated that *Sox2* is not only expressed in fetal neural progenitors but also in proliferating cells in the adult CNS, specifically in neurogenic regions, such as the subventricular zone of the lateral ventricle and the subgranular zone of the hippocampus as well as the ependyma of the adult central canal (Ellis et al., 2004). Isolated Sox2+ adult NPCs can be propagated in culture while maintaining their ability to differentiate into neurons, astrocytes, and oligodendrocytes, thus documenting their self-renewal and multipotency in vitro (Ellis et al., 2004). The self-renewal and differentiation capacities of Sox2+ adult NPCs were verified in vivo by Fred Gage's group using lenti- and retroviral-mediated fate mapping approaches (Suh et al., 2007).

Support for a functional role of Sox2 in NPCs came from knockdown experiments in vitro (Cavallaro et al., 2008) and conditional deletion of *Sox2* specifically in the brain (Favaro et al., 2009; Ferri et al., 2004). These experiments revealed that Sox2 depletion in cultured NPCs attenuates their potential to form neurons, whereas its absence in vivo causes a rapid loss of GFAP- and Nestin-expressing precursor cells and a decline in cell proliferation in the dentate gyrus, indicating that Sox2 marks and maintains NPCs and hence neurogenesis in the adult mouse hippocampus. Together, these studies demonstrate that Sox2 regulates both developmental and adult stem cell populations in the brain.

Sox2 marks stem and progenitor cell populations in other adult tissues that depend on *Sox2* expression during development. For example, Sox2+ cells have been detected in progenitors of the adult retina (Taranova et al., 2006), trachea (Que et al., 2009), tongue epithelium (Okubo et al., 2009), and dermal papilla of the hair follicle (Biernaskie et al., 2009; Driskell et al., 2009), as well as in putative progenitors of the pituitary gland (Fauquier et al., 2008). More recently, lineage-tracing experiments from our laboratory and others have demonstrated that immature Sox2+ cells in the adult testes, forestomach, glandular stomach, trachea, anus, cervix, esophagus, lens, and dental epithelium give rise to all mature cell types within these tissues (Arnold et al., 2011; Juuri et al., 2012). Conditional *Sox2* deletion in all tracheal cells has further shown that postnatal expression of *Sox2* is required to sustain tracheal homeostasis by controlling the number of proliferating epithelial cells as well as the proportion of basal, ciliated, and Clara cells. The effect of *Sox2* loss on tracheal cell proliferation thus represents an interesting difference compared with *Sox2* loss in the embryonic trachea, which does not perturb proliferation (Que et al., 2009). Deletion of *Sox2* specifically in bronchiolar Clara cells, which serve as facultative stem cells, also causes reduced cell proliferation and a gradual loss of differentiation markers for Clara, ciliated, and mucous cells (Tompkins et al., 2009). This loss indicates that *Sox2* is required for the self-renewal of Clara cells and their differentiation into ciliated and mucous cells. From a molecular viewpoint, compromised bronchiolar cell proliferation might result from a derepression of the Sox2 target gene Smad3, thus possibly activating the antiproliferative Tgf-β pathway (Tompkins et al., 2009). An important question that remains to be determined is whether *Sox2* expression is required for homeostasis in other Sox2+ adult tissues besides the airways and the brain.

In addition to maintaining tissue homeostasis, Sox2 is involved in tissue repair. For instance, chemically induced damage of the tracheal epithelium in mice is typically repaired within 7–10 days due to the activity of basal stem cells (Que et al., 2009). *Sox2*-deficient trachea, however, fail to undergo efficient tissue repair with severe reductions in the number of basal, ciliated, and Clara cells. Peripheral nerve regeneration is another example for Sox2's role in tissue repair. Upon injury, mature adult Schwann cells re-express *Sox2*, shed their myelin sheaths and dedifferentiate to a progenitor cell-like state (Parrinello et al., 2010). Sox2 seems to play a direct role in this process by organizing Schwann cell clustering, a key event during nerve regeneration, through relocating N-Cadherin molecules. This process then enables Schwann cells to form multicellular cords to guide axon regrowth across the site of injury. It should be interesting to determine whether *Sox2* is reactivated and plays functional roles in other tissues experiencing cellular damage by promoting dedifferentiation into, or expansion of, resident progenitors.

Sox2 and Disease

Sox2 Deficiency in Developmental Disorders

SOX2 mutations have been identified in a number of developmental diseases and cancer. For example, humans carrying a heterozygous mutation for *SOX2* develop anophthalmia-esophageal-genital (AEG) syndrome. These patients have abnormalities in ectodermal and endodermal tissues including microphthalmia (small eyes), trachea-esophageal fistula, hearing loss, and brain abnormalities (Kelberman et al., 2006; Williamson et al., 2006). The heterozygous manifestation of disease in patients is consistent with the dose-dependent functions of Sox2 seen in mice. Surprisingly, however, heterozygous mutant mice are comparatively normal although they exhibit reduced pituitary size and hormone production as well as testicular atrophy and infertility with age, possibly from dose-dependent effects on pituitary and germ cell progenitors (Kelberman et al., 2006).

Sox2 Dysregulation in Cancer

Accumulating evidence suggests that SOX2 acts as an oncogene in some epithelial cancers. The *SOX2* locus is amplified in human squamous cell carcinomas of the lung (23%) and esophagus (15%) as well as in 27% of human small cell lung cancers analyzed (Bass et al., 2009; Rudin et al., 2012). Consistently, overexpression of *Sox2* in the lungs of mice induces rapid hyperproliferation (Tompkins et al., 2011) and, in some cases, adenocarcinomas (Lu et al., 2010), although *SOX2* amplifications have not yet been described in human lung adenocarcinomas. While the molecular function that Sox2 plays in tumorigenesis remains to be determined, recent evidence points toward proproliferative, prosurvial, and/or antidifferentiation roles. For instance, knockdown of SOX2 in human cell lines, derived from squamous cell caricinomas and small cell lung cancer, compromises growth (Bass et al., 2009; Rudin et al., 2012). Moreover, genetic reduction of *Sox2* levels by half in an animal model of pituitary cancer significantly reduces tumor formation (Li et al., 2012a). Lastly, Sox2 was shown to be critical for the proliferation and differentiation of human osteosarcoma cell lines in vitro and in an in vivo transplantation model by antagonizing WNT signaling. *SOX2* expression has also been suggested to contribute to cellular invasion in tumors of neural and neural crest origin such as glioma (Ikushima et al., 2009), melanoma (Laga et al., 2010), and Merkel cell carcinoma (Laga et al., 2010), in which it is overexpressed. Thus, analogous to its multiple roles in development and differentiation, Sox2 appears to function at various levels of carcinogenesis to promote tumor growth.

An important question is whether Sox2 is already expressed in the cell of origin for these tumors or whether it is activated ectopically. While it is plausible that tumors forming within Sox2+ tissues originate from a Sox2+ cell type (e.g., lungs, esophagus, neural cells, and Merkel cells), unequivocal (genetic lineage tracing) evidence for this conclusion is lacking. Interestingly, two reports detected ectopic *Sox2* expression in rare tumor stem cell-like populations isolated from genetically induced mouse models of squamous cell carcinoma of the skin (Beck

et al., 2011; Schober and Fuchs, 2011). Even though skin epidermis (ectoderm) has a similar structure as the Sox2+ squamous epithelia of the gastrointestinal tract (endoderm), *Sox2* is not normally expressed in skin keratinocytes. It remains to be tested whether ectopic Sox2 expression has any functional consequences on these tumors. It is further interesting to note in this context that the ectopic expression of the reprogramming gene *Oct4* in mice results in rapid but reversible tumor formation in several Sox2-expressing squamous epithelia by expanding adult progenitors and preventing their differentiation (Hochedlinger et al., 2005). It is therefore conceivable that Oct4 and Sox2 cooperate in these tissues, like in pluripotent cells, to induce tissue hyperplasia.

Involvement of Other Sox Factors in Stem Cell Biology

Like Sox2, the SoxE group member *Sox9* is expressed in several endoderm-derived and ectoderm-derived tissues. For example, Sox9 marks stem and progenitor cells in the adult intestine, liver, and exocrine pancreas that produce a continuous supply of enterocytes, hepatocytes, and acinar cells, respectively, under both homeostatic and certain injury conditions (Furuyama et al., 2011). In addition to these endodermal tissues, Sox9 functions to maintain stem cells in ectodermal tissue stem cells including the hair follicles of the adult skin (Nowak et al., 2008), multipotent mouse retinal progenitor cells (Poché et al., 2008), NPCs (Scott et al., 2010), neural crest stem cells (Cheung and Briscoe, 2003), and mammary stem cells (Guo et al., 2012). Furthermore, *Sox9* is upregulated in a number of neural tumors and basal cell carcinomas (Kordes and Hagel, 2006; Miller et al., 2006; Nowak et al., 2008), and expression of Sox9 promotes the tumorigenic and metastasis-seeding abilities of human breast cancer cells in a transplant model (Guo et al., 2012), raising the interesting possibility that Sox9 confers stem cell-like properties upon tumor cells.

Other Sox factors have been implicated in stem cell maintenance, which will not be covered in detail in this Review (Table 1). Briefly, expression of Sox10, which like Sox9 is a member of the SoxE group, ensures stem cell survival, maintains multipotency and suppresses neuronal differentiation in neural crest stem cells (Kim et al., 2003). The SoxF group member Sox17 is required for the maintenance of fetal and neonatal hematopoietic stem cells (HSCs) but is dispensable in adult hematopoiesis (Kim et al., 2007). The SoxE group member Sox8 and the SoxG group member Sox15 mark muscle satellite cells, and their individual overexpression in a myoblast cell line prevents MyoD expression and differentiation into myotubes (Meeson et al., 2007; Schmidt et al., 2003). Individual knockout mice for *Sox8* and *Sox15* do not have an overt phenotype, suggesting redundancy. However, *Sox15* mutant mice exhibit defects in muscle regeneration, indicating a requirement for Sox15 after injury (Meeson et al., 2007). Finally, the SoxB1 group member Sox3 marks undifferentiated spermatogonia, and its depletion leads to loss of spermatogenesis and nearly agametic male mice (Raverot et al., 2005).

A few general conclusions can be drawn from these and other studies examining different Sox genes in stem cell biology. First, most Sox factors are expressed in multiple types of stem and progenitor cell types. Second, many Sox factors act redundantly in the maintenance of stem cells (e.g., Sox1, Sox2, Sox3, and Sox9 in NPCs), which may explain why certain Sox gene knockouts do not exhibit obvious phenotypes due to compensation by other Sox factors. Third, different Sox factors may be expressed at subsequent stages of differentiation within a cell lineage (e.g., Sox2/Sox3 and Sox11 during NPC differentiation into neurons or Sox9 and Sox10 during neural crest stem cell differentiation and migration) (Bergsland et al., 2011; Guth and Wegner, 2008). Lastly, Sox factors may be expressed in complementary patterns within a developing or adult tissue (e.g., Sox9 and Sox2 in multipotent distal tip cells and proximal epithelial cells in the developing lung, (Rawlins, 2011) or in bulge stem cells and DP cells of the hair follicle, respectively (Nowak et al., 2008; Driskell et al., 2009)). The broad expression patterns and the partial redundancy of many Sox factors are thought to be the consequence of subfunctionalization and neofunctionalization of Sox genes resulting from an expansion of Sox genes during vertebrate evolution (Guth and Wegner, 2008).

Sox Factors in Cellular Reprogramming

Given that Sox factors play critical roles in establishing and maintaining cell types during development and in the adult, it is conceivable that their ectopic expression in heterologous cell types is sufficient to change cell fates. Indeed, Sox2 is one of the key reprogramming factors for the derivation of induced pluripotent stem cells (iPSCs) from somatic cells. Sox2 is required toward the end of reprogramming (Chen et al., 2011), presumably by activating its own transcription as well as hundreds of pluripotency-associated targets to stabilize the pluripotent state. In fact, a recent study by Jaenisch and colleagues suggested that activation of the endogenous *Sox2* locus during cellular reprogramming initiates a cascade of transcriptional events that takes place exclusively in cells destined to form iPSCs (Buganim et al., 2012). Notably, as a reprogramming factor, Sox2 can be replaced by the most closely related Sox family members, Sox1 and Sox3, but not by more distant members Sox7, Sox15, Sox17, or Sox18 (Nakagawa et al., 2008). The finding that certain Sox factors cannot replace Sox2 despite similar DNA binding characteristics might result from the differential abilities of Sox factors to interact with Oct4 to activate common target genes. In support of this notion single amino acid substitutions within the Oct4 domain that normally interact with Sox2 in ESCs can abrogate its ability to generate iPSCs (Jauch et al., 2011). Conversely, introducing Sox17-compatible amino acid changes into this Oct4 domain generates a variant that no longer recognizes Sox2 and instead endows Sox17 with the potential to induce pluripotency in combination with Oct4, Klf4, and c-Myc (Jauch et al., 2011). This experiment corroborates the notion that the binding partners of Sox2 often confer target gene specificity, resulting in the activation of different gene expression programs in cells that express the same Sox factors.

Surprisingly, Sox2 is dispensable for pluripotency gene activation in somatic cells after cell fusion with ESCs. This nonessential role contrasts with a requirement for Oct4 during cell fusion-mediated reprogramming and might suggest that Oct4 can compensate for the loss of Sox2 in this context, similar to what was seen in self-renewing ESCs (Masui et al., 2007). Alternatively, Sox15, which is also expressed in ESCs (Maruyama et al., 2005), might replace Sox2 exclusively during fusion-induced reprogramming.

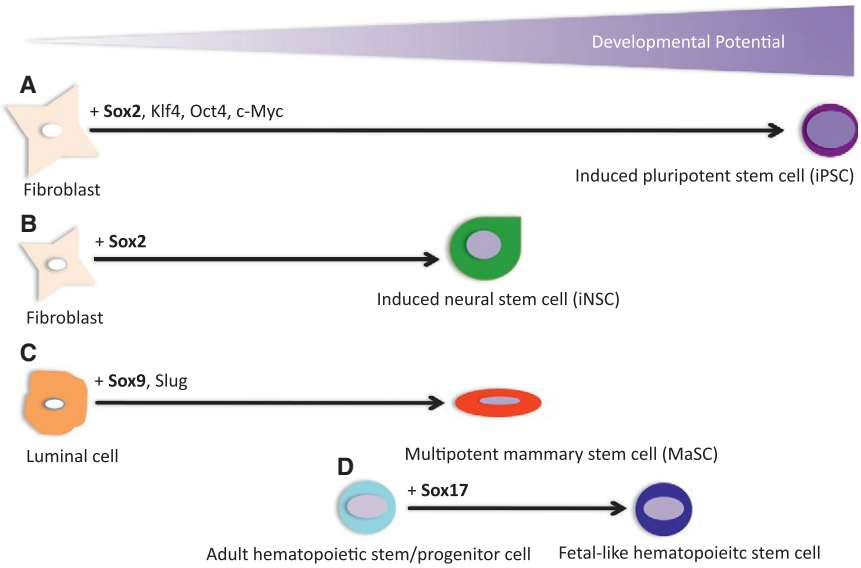

Figure 3. Sox Factors as Inducers of Cellular Reprogramming

Examples of Sox factors whose enforced expression in other cell types induces dedifferentiation.

(A) Ectopic expression of Sox2 in combination with Klf4, Oct4, and c-Myc endows somatic cells with pluripotency, giving rise to induced pluripotent stem cells (iPSCs).

(B) Sox2 expression alone or together with other factors reprograms fibroblasts into induced neural stem cells (iNSCs).

(C) Sox9 expression in combination with Slug expression, converts differentiated luminal cells into mammary stem cells capable of generating an entire mammary ductal tree when transplanted into a mammary fat pad.

(D) Sox17 expression in adult hematopoietic stem and progenitor cells induces a fetal-like hematopoietic stem cell state. These cells have increased self-renewal potential and express HSC markers. However, long-term Sox17 expression in the adult leads to leukemogenesis.

Sox2 expression alone or in combination with different neural transcription factors has been reported to directly reprogram fibroblasts into neural stem cells (Han et al., 2012; Ring et al., 2012; Thier et al., 2012), suggesting that Sox2 can induce different cell fates depending on the presence of cofactors and environmental cues. This notion is in agreement with an earlier finding by Kondo and Raff, who discovered that exposure of rat oligodendrocyte progenitors to PDGF and bFGF induced their reversion into self-renewing multipotent NPC-like cells capable of giving rise to astrocytes, oligodendriocytes, and neurons (Kondo and Raff, 2000, 2004). Interestingly, the authors showed that this growth factor-mediated reversion depends on the reactivation of the *Sox2* locus through a mechanism that involves direct recruitment of the chromatin remodeling factor Brahma and the tumor suppressor Brca1 to its promoter region (Kondo and Raff, 2004).

The ability to induce new cell states from heterologous cell types has recently been demonstrated for other Sox family members including Sox9 and Sox17. Specifically, coexpression of Sox9 and Slug in differentiated luminal cells produces induced multipotent cells which have long-term mammary gland reconstituting potential in transplantation assays (Guo et al., 2012). Similarly, forced expression of the fetal HSC transcription factor Sox17 in adult committed progenitors endows them with fetal HSC characteristics including an enhanced self-renewal potential, long-term multilineage reconstitution ability, and biased erythroid and myeloid differentiation over lymphoid differentiation, although prolonged overexpression causes leukemia (He et al., 2011). Together, these findings underscore the powerful effects Sox factors have in endowing differentiated cells with immature stem cell-like properties (summarized in Figure 3).

Mechanisms by which Sox2 Controls Cell Fate Decisions

Sox2 expression, like that of many other Sox factors, is modulated by extracellular signals and intracellular cofactors. Here, we review examples of how Sox2 expression can be positively or negatively regulated by different extracellular cues in different tissues and discuss intracellular mechanisms by which Sox2 expression is controlled in pluripotent and adult stem cells (Figure 4).

Extracellular Regulators of Sox2 Expression

Sox2 expression is positively and negatively influenced by different extracellular signals in vivo and in vitro. For instance, Fgf signaling from the surrounding ventral mesenchyme negatively regulates *Sox2* expression during embryonic foregut patterning, resulting in a separation of esophagus and trachea (Que et al., 2007). In the developing taste buds, Wnt signaling induces *Sox2* expression in endodermal progenitors, causing their differentiation into taste bud cells at the expense of keratinocytes (Okubo et al., 2006). In calvarial osteoblast progenitors, however, *Sox2* is positively regulated by Fgf signaling. Upregulation of *Sox2*, in turn, inhibits Wnt signaling by means of physical association of Sox2 with beta-catenin (Mansukhani et al., 2005).

In cultured pluripotent ESCs, Sox2 targets are co-occupied by Smad1 and Smad3 proteins, the downstream effectors of Tgf-β signaling that are essential for self-renewal (Chen et al., 2008; Mullen et al., 2011). Notably, one of the genes targeted by Oct4, Sox2, and Smad3 is the Tgf-β inhibitor Lefty1, indicating that tight regulation of this pathway is necessary to maintain pluripotency. Similar to Tgf-β signaling in ESCs, Egf and Shh signaling stimulate *Sox2* expression in NPCs (Favaro et al., 2009). Once activated, Sox2 binds to the *Egfr* and *Shh* genes among many other targets, thus engaging in positive feedback loops that are important for the maintenance of stem cells (Engelen et al., 2011; Hu et al., 2010). In agreement with this molecular link, *Sox2*-deficient NPCs fail to produce sufficient Shh, leading to loss of NPC cultures and dentate gyrus hypoplasia, respectively (Favaro et al., 2009). Remarkably, these phenotypes can be partially restored in vitro and in vivo by supplying recombinant Shh or an Shh agonist (Favaro et al., 2009). A similar connection has been observed between Shh and Sox9 in NPCs (Scott et al., 2010). In contrast to Shh and Egf signaling, which promotes *Sox2* expression, thyroid hormone signaling induces differentiation of neural progenitors into neuroblasts by suppressing *Sox2*

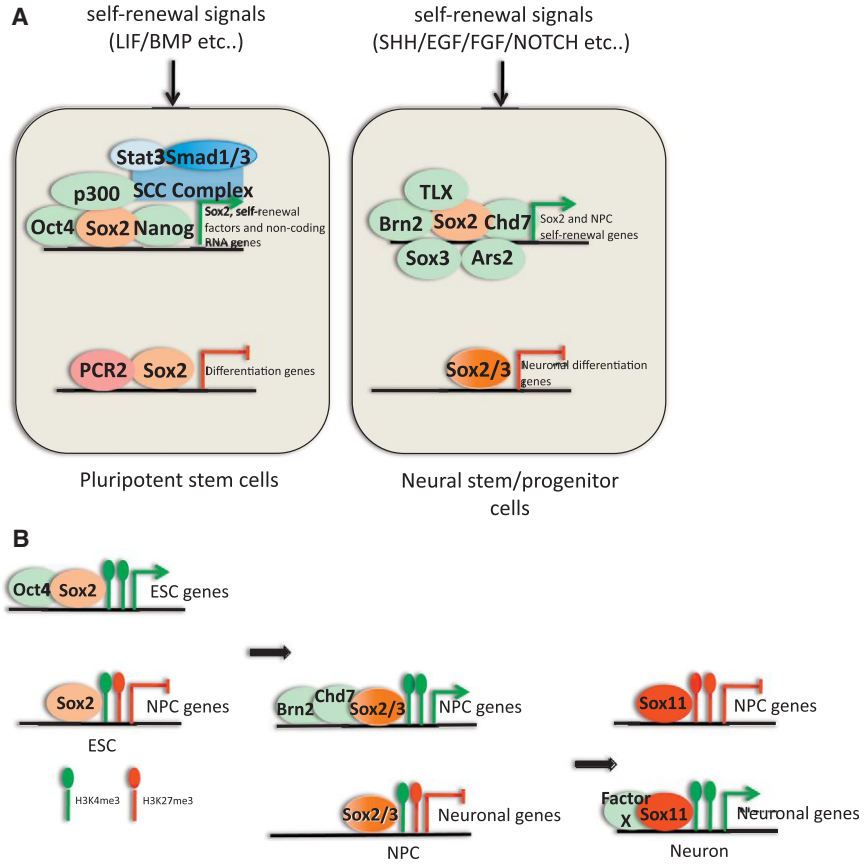

Figure 4. Mechanisms by which Sox2 Controls Self-Renewal and Differentiation in Pluripotent and Multipotent Stem Cells

(A) Sox2 activates self-renewal genes and represses differentiation genes in a cell type-specific manner by (1) interpreting tissue-specific signals and (2) interacting with other cell type-specific cofactors. For example, in ESCs, Sox2 occupies many targets containing Oct4-Sox2 consensus sequences and partners with downstream effectors of ESC-specific signaling pathways including Stat3 (LIF pathway). In NPCs, Sox2 occupies target genes that also contain binding sites for the brain-specific factors Brn2 and Chd7, thus activating different sets of genes. In addition, Sox2 activates its own transcription and regulates components of the signaling pathways that control self-renewal, thereby promoting maintenance of the undifferentiated state.

(B) In addition to activating self-renewal genes and suppressing lineage-specific genes, Sox2 acts as a pioneer factor to prime stem cells for subsequent gene activation. Sox2 occupies silent NPC genes in ESCs, which carry bivalent domains poised for gene activation. Upon differentiation into NPCs, Sox2 and Sox3 cooperate to activate self-renewal genes while keeping neuronal differentiation genes in a silent but bivalent state. When NPCs undergo terminal differentiation, Sox2 and Sox3 disengage from neuronal-specific enhancers and are replaced by Sox11.

expression (López-Juárez et al., 2012). Specifically, thyroid receptor-alpha1 binds to a negative thyroid hormone response element within the *Sox2* enhancer, resulting in *Sox2* repression in a hormone-dependent fashion. Finally, Ephrin signaling causes Sox2 stabilization during Schwann cell regeneration, leading to N-Cadherin remodeling and subsequent Schwann cell clustering (Parrinello et al., 2010). In summary, these and several other examples (Domyan et al., 2011; Takemoto et al., 2006) demonstrate that major signaling pathways can positively or negatively control Sox2 expression levels during embryonic development, stem cell homeostasis, and tissue regeneration in a context-dependent manner. Furthermore, Sox2 itself often modulates these signals by directly activating or repressing key regulators of these pathways.

Intracellular Modulators of Sox2 Expression in Pluripotent Stem Cells

Once Sox2 is activated by extracellular signals, intracellular cofactors ensure that the proper set of target genes is activated in a cell type-specific fashion. One way to achieve this is to collaborate with other cell type-specific transcription factors. As discussed earlier, Sox2 physically associates with and co-occupies targets with other key pluripotency factors including Oct4 and Nanog in ESCs, thus contributing to target gene specificity. Of note, the combination and complexity of these pluripotency transcription factors at individual targets determines whether they will be activated or repressed. That is, targets bound by one or few transcription factors tend to be repressed, whereas targets occupied by multiple factors tend to be expressed in ESCs (Kim et al., 2008; Sridharan et al., 2009). To ensure maintenance of the undifferentiated state of ESCs, Sox2 as well as other pluripotency factors engage in autoregulatory loops to boost their own expression (Boyer et al., 2005).

The observation that ectopic expression of Oct4 and Sox2 alone are insufficient to activate the well-known target gene *Nanog* in a cell-free system (Fong et al., 2011) motivated efforts to identify additional cofactors. Tjian and colleagues employed an elegant biochemical approach to purify the "stem cell coactivation complex" (SCC) that collaborates with Oct4 and Sox2 to transcriptionally activate the *Nanog* promoter. SCC components also occupy hundreds of other Oct4/Sox2 targets in ESCs as determined by ChIP-seq analysis (Fong et al., 2011). The SCC complex contains the trimeric XPC-nucleotide excision repair complex and is thought to act as a molecular link that couples stem cell-specific gene expression programs with genome surveillance and stability in ESCs. Interestingly, the tumor suppressor protein p53 has recently been implicated in a similar role in ESCs. However, unlike the SCC complex, p53 binds to the distal enhancers of ESC-specific genes including *Sox2*, causing their repression upon DNA damage (Li et al., 2012b).

In ESCs, Sox2 additionally requires binding of chromatin modifiers to induce expression of pluripotency-associated targets and repression of differentiation-associated targets. For example, Sox2, Oct4, and Nanog cooperate with WD repeat domain 5 (Wdr5), an effector of activating H3K4 methylation, to maintain robust expression of self-renewal genes in ESCs (Ang et al., 2011). Active Sox2 targets are also cobound by components of the cohesion and mediator complex responsible for

bridging enhancer and promoter elements to ensure efficient gene expression (Kagey et al., 2010). Recent evidence suggests that Sox2 might even interact with ESC-specific long noncoding RNAs (lncRNAs) (Ng et al., 2012) to silence differentiation-associated genes in self-renewing ESCs.

During ESC differentiation, ESC-associated genes need to be rapidly downregulated, which is again achieved by multiple mechanisms. For example, the H3K4/K9 demethylase Lsd1 and HDACs1/2 silence active Oct4/Sox2-occupied enhancers in ESCs (Whyte et al., 2012). Recent evidence further documents an unanticipated role for cell-cycle inhibitors in transcriptional suppression of stem cell genes. The cell-cycle-dependent kinase inhibitor p27, which is rapidly activated as cells differentiate and thus exit the cell cycle, directly binds to and inhibits Sox2's SRR2 enhancer (Li et al., 2012a). In parallel with these transcriptional and epigenetic mechanisms, negative feedback loops kick in during differentiation that shut down the pluripotency program at the posttranscriptional level. This is exemplified by RNA miR-145, which is normally repressed by OCT4 in ESCs, and becomes activated to target OCT4, SOX2, and KLF4 RNAs for degradation when ESCs differentiate (Xu et al., 2009a). Thus, Sox2 interacts at the genic, transcript, and protein levels with other core pluripotency factors, DNA repair complexes, cell-cycle regulators, miRNAs, activating, and repressive chromatin regulators to control specific gene expression programs that balance the decision between self-renewal and differentiation in pluripotent cells.

Intracellular Modulators of Sox2 Expression in Adult Stem Cells

Similar to ESCs, Sox2 induces the expression of self-renewal pathways and inhibits the expression of differentiation genes in NPCs. Because Oct4 and other pluripotency-associated genes are silenced in NPCs, Sox2 partners with different transcription factors to activate alternative targets. In early neural progenitors, Sox2 has been shown to interact with the brain-specific POU factor Brn2 to activate the NPC-associated *Nestin* gene (Tanaka et al., 2004). More recently, the chromatin remodeling ATPase Chd7, which has been associated with CHARGE syndrome, was shown to physically interact and co-occupy targets with Sox2 in NPCs (Engelen et al., 2011). Sox2 and Chd7 coregulate a set of target genes of the Notch and Shh signaling pathways important for stem cell self-renewal. The nuclear receptor tailless (TLX) has been identified as another key target of Sox2 in NPCs. TLX functions as a transcriptional repressor that is important for NPC maintenance and neurogenesis in adult mice. Sox2 physically interacts with TLX and forms complexes on DNA, possibly to suppress differentiation genes (Shimozaki et al., 2012).

Sox2 expression itself is maintained in NPCs by direct transcriptional activation through Ars2, a zinc finger protein typically involved in miRNA biogenesis (Andreu-Agullo et al., 2011). Chromatin immunoprecipiation experiments have shown that Ars2, in a miRNA pathway-independent manner, binds to the promoter region of *Sox2* and activates its expression. Ars2 deletion leads to a loss of NPC self-renewal and multipotency both in vitro and in vivo. Importantly, this defect can be rescued by *Sox2* overexpression (Andreu-Agullo et al., 2011). Similarly, the transcription factor myeloid Elf-1-like factor (MEF) binds to the *Sox2* locus and stimulates its expression in the context of neurospheres and glioma cells (Bazzoli et al., 2012). Forced Sox2 expression also rescues the inability of MEF−/− cells to form neurospheres. In analogy to p27's inhibition of Sox2 expression during ESC differentiation, the cell-cycle-dependent kinase inhibitor p21 was shown to suppress *Sox2* expression during NPC differentiation (Marqués-Torrejón et al., 2013).

Posttranslational modifications, such as acetylation (Baltus et al., 2009; Sikorska et al., 2008), sumoylation (Tsuruzoe et al., 2006), phosphorylation (Jeong et al., 2010), and arginine methylation (Zhao et al., 2011), have also been described to influence the transcriptional activity of Sox2 in ESCs or NPCs. In the case of Sox2, these modifications cause either transcriptional activation (phosphorylation, methylation) or repression (sumoylation, acetylation) by controlling Sox2's stability, nuclear-cytoplasmic localization, or transactivation potential. Collectively, these results demonstrate that Sox2+ adult stem cells utilize some of the same, as well as different, mechanisms as ESCs to control the balance between self-renewal and differentiation. It is worth mentioning that Sox2 has been shown to collaborate with additional transcription factors in the development of other tissues. We refer to an excellent review exploring the various partners of Sox proteins for greater detail (Kondoh and Kamachi, 2010).

Sox Proteins as Pioneer Factors

Pioneer factors are transcription factors that occupy silenced target genes in progenitor cells and keep them in a poised state for activation at subsequent stages of differentiation (Zaret and Carroll, 2011). A classical example is the transcription factor FoxD3, essential for the maintenance of ESC self-renewal (Hanna et al., 2002). FoxD3 occupies the enhancer of the silent liver-specific *Alb1* gene in ESCs, thereby keeping it poised for activation upon differentiation into liver cells, when FoxA1 replaces FoxD3 to activate transcription (Xu et al., 2009b). Recent evidence exploring the genome-wide targets of different Sox factors during neural differentiation from ESCs supports the notion that Sox factors may also function as pioneer factors and thus contribute to differentiated cell fates (Bergsland et al., 2011). In ESCs, Sox2 binds to ESC-specific enhancers, which are active and carry H3K4me3 marks, as well as to neural enhancers, which are silent and carry bivalent H3K4me3/H3K27me3 marks. Upon differentiation into NPCs, Sox2 collaborates with Sox3 to relocate from pluripotent to neural-specific gene enhancers. These enhancers either are active in NPCs and hence carry the H3K4me3 mark or are inactive but poised and hence carry bivalent marks. After neuronal differentiation, both types of enhancers exchange their SoxB1 factors for SoxC factors, including Sox11. At the same time, previously active NPC enhancers acquire the repressive H3K27me3 mark, whereas the poised bivalent enhancers convert to a monvalent H3K4-enriched chromatin signature, resulting in gene activation.

Sox2 might also act as a pioneer factor during hematopoeisis. In ESCs, Sox2 and FoxD3 bind together to the enhancers of the repressed bivalent *lambda5-VpreB1* and *Pax5* genes important in pro/preB cells (Liber et al., 2010). Specifically, Sox2 has been suggested to mediate deposition of a tightly localized peak of H3K4 di and trimethylation at these enhancers whereas Foxd3 suppresses intergenic transcription. Sox2 is subsequently replaced by the SoxC group member Sox4 and FoxD3 by another Forkhead transcription factor in hemangioblasts, which are early progenitors for the hematopoietic and endothelial lineages, leading to robust gene activation during B cell differentiation.

Another interesting question raised by these observations is whether Sox2 along with the transcription factors Oct4, Klf4, and c-Myc may also function as pioneer factors during iPSC generation. An examination of binding patterns of the four factors 48 hr after their induction in fibroblasts showed that Sox2, Oct4, Klf4, and c-Myc mostly bind to enhancers of early reprogramming genes, which are not yet activated (Soufi et al., 2012). While Sox2, Oct4, and Klf4 expression alone allow access of these targets, c-Myc expression alone does not. Thus, Sox2, Oct4, and Klf4 indeed seem to act as pioneer factors for c-Myc early in reprogramming. In addition, c-Myc expression enhances binding of Oct4, Klf4, and Sox2 to their targets, thus facilitating efficient chromatin engagement. Together, these three examples expand the role of Sox2 from a transcriptional activator to a pioneer factor that poises silenced genes for expression during normal development and cellular reprogramming.

Concluding Remarks

The molecular and functional analyses of the Sox family of transcription factors over the past two decades have documented their important roles in various aspects of stem cell biology: Biochemical dissection of protein interaction partners and DNA targets using genome-wide approaches has provided a molecular explanation for the previously observed versatility of individual Sox factors in regulating proliferation and differentiation of progenitor and stem cells in different tissues and at different stages of development. Sox factors respond to different extracellular signals and interact with a host of intracellular cofactors, such as cell type-specific transcription factors and chromatin regulators, to control different sets of genes in distinct cell types. In addition, Sox factors compete with transcription factors of alternative lineages to drive different cell fates during development. At the molecular level, this is often accomplished by directly activating genes that promote their own lineage and repressing genes of alternative lineages. Interestingly, the comparison of genomic binding sites of different Sox proteins along a neural differentiation paradigm demonstrated that Sox factors do not simply serve to activate self-renewal genes and repress differentiation genes but also function as pioneer factors to poise genes for activation by a related Sox factor once differentiation ensues. It should be informative to determine whether this principle also applies to Sox factors in other cellular lineages (e.g., Sox17 in hematopoietic cells or Sox9 in hair follicle cells).

Most insights into the biology of Sox factors have come from developmental studies. The finding that Sox factors are also expressed in numerous adult stem and progenitor cell populations raises interesting questions about the molecular and functional roles they play in tissue homeostasis and regeneration compared with their functions during development. The availability of appropriate mouse models and the ability to maintain rare stem cell populations in culture, combined with genome-wide technologies, should now enable researchers to address this fundamental question at the mechanistic level.

Reprogramming experiments have underscored the power of Sox factors in switching cell fates. However, the underlying mechanisms are still poorly understood. It might be possible to predict from available expression and ChIP-seq data which combinations of Sox factors, together with appropriate partners, are sufficient to generate desired cell states in culture from pluripotent or differentiated cells. Given that certain SOX genes are amplified or overexpressed in human cancer, it is intriguing to speculate that Sox factors also contribute to tumorigenesis by endowing differentiated or progenitor cells with a more primitive stem cell-like state. Indeed, studies manipulating Sox17 in hematopoiesis and Sox9 in mammary stem cells support this notion.

In summary, accumulating evidence implicates many Sox factors in pluripotent and multipotent stem cell biology and tissue regeneration. A better understanding of the mechanisms by which Sox factors induce and maintain stem cell populations should provide important insights into how tissue stem cells are generated and maintained and might lead to strategies to treat degenerative diseases or cancer affecting those tissues.

ACKNOWLEDGMENTS

This Review is dedicated to the memory of Larysa Pevny, who has made seminal contributions to the study of the biology of Sox factors. We apologize to those colleagues whose work we could not cite due to space constraints. We thank Hanno Hock, Michael Rendl, and members of the Hochedlinger laboratory for suggestions and critical reading of the manuscript. K.H. was supported by HHMI, NIH (DP2OD003266, R01HD058013, and R01DK96034), and the Harvard Stem Cell Institute.

REFERENCES

Adameyko, I., Lallemend, F., Furlan, A., Zinin, N., Aranda, S., Kitambi, S.S., Blanchart, A., Favaro, R., Nicolis, S., Lübke, M., et al. (2012). Sox2 and Mitf cross-regulatory interactions consolidate progenitor and melanocyte lineages in the cranial neural crest. Development *139*, 397–410.

Andreu-Agullo, C., Maurin, T., Thompson, C., and Lai, E. (2011). Ars2 maintains neural stem-cell identity through direct transcriptional activation of Sox2. Nature *481*, 195–198.

Ang, Y.-S., Tsai, S.-Y., Lee, D.-F., Monk, J., Su, J., Ratnakumar, K., Ding, J., Ge, Y., Darr, H., Chang, B., et al. (2011). Wdr5 mediates self-renewal and reprogramming via the embryonic stem cell core transcriptional network. Cell *145*, 183–197.

Arnold, K., Sarkar, A., Yram, M.A., Polo, J.M., Bronson, R., Sengupta, S., Seandel, M., Geijsen, N., and Hochedlinger, K. (2011). Sox2(+) adult stem and progenitor cells are important for tissue regeneration and survival of mice. Cell Stem Cell *9*, 317–329.

Avilion, A.A., Nicolis, S.K., Pevny, L.H., Perez, L., Vivian, N., and Lovell-Badge, R. (2003). Multipotent cell lineages in early mouse development depend on SOX2 function. Genes Dev. *17*, 126–140.

Baltus, G.A., Kowalski, M.P., Zhai, H., Tutter, A.V., Quinn, D., Wall, D., and Kadam, S. (2009). Acetylation of sox2 induces its nuclear export in embryonic stem cells. Stem Cells *27*, 2175–2184.

Bass, A.J., Watanabe, H., Mermel, C.H., Yu, S., Perner, S., Verhaak, R.G., Kim, S.Y., Wardwell, L., Tamayo, P., Gat-Viks, I., et al. (2009). SOX2 is an amplified lineage-survival oncogene in lung and esophageal squamous cell carcinomas. Nat. Genet. *41*, 1238–1242.

Basu-Roy, U., Ambrosetti, D., Favaro, R., Nicolis, S.K., Mansukhani, A., and Basilico, C. (2010). The transcription factor Sox2 is required for osteoblast self-renewal. Cell Death Differ. *17*, 1345–1353.

Bazzoli, E., Pulvirenti, T., Oberstadt, M.C., Perna, F., Wee, B., Schultz, N., Huse, J.T., Fomchenko, E.I., Voza, F., Tabar, V., et al. (2012). MEF Promotes Stemness in the Pathogenesis of Gliomas. Cell Stem Cell *11*, 836–844.

Beck, B., Driessens, G., Goossens, S., Youssef, K.K., Kuchnio, A., Caauwe, A., Sotiropoulou, P.A., Loges, S., Lapouge, G., Candi, A., et al. (2011). A vascular niche and a VEGF-Nrp1 loop regulate the initiation and stemness of skin tumours. Nature *478*, 399–403.

Bergsland, M., Ramsköld, D., Zaouter, C., Klum, S., Sandberg, R., and Muhr, J. (2011). Sequentially acting Sox transcription factors in neural lineage development. Genes Dev. *25*, 2453–2464.

Biernaskie, J., Paris, M., Morozova, O., Fagan, B.M., Marra, M., Pevny, L., and Miller, F.D. (2009). SKPs derive from hair follicle precursors and exhibit properties of adult dermal stem cells. Cell Stem Cell *5*, 610–623.

Boyer, L.A., Lee, T.I., Cole, M.F., Johnstone, S.E., Levine, S.S., Zucker, J.P., Guenther, M.G., Kumar, R.M., Murray, H.L., Jenner, R.G., et al. (2005). Core transcriptional regulatory circuitry in human embryonic stem cells. Cell *122*, 947–956.

Boyer, L.A., Plath, K., Zeitlinger, J., Brambrink, T., Medeiros, L.A., Lee, T.I., Levine, S.S., Wernig, M., Tajonar, A., Ray, M.K., et al. (2006). Polycomb complexes repress developmental regulators in murine embryonic stem cells. Nature *441*, 349–353.

Buganim, Y., Faddah, D.A., Cheng, A.W., Itskovich, E., Markoulaki, S., Ganz, K., Klemm, S.L., van Oudenaarden, A., and Jaenisch, R. (2012). Single-cell expression analyses during cellular reprogramming reveal an early stochastic and a late hierarchic phase. Cell *150*, 1209–1222.

Bylund, M., Andersson, E., Novitch, B.G., and Muhr, J. (2003). Vertebrate neurogenesis is counteracted by Sox1-3 activity. Nat. Neurosci. *6*, 1162–1168.

Cavallaro, M., Mariani, J., Lancini, C., Latorre, E., Caccia, R., Gullo, F., Valotta, M., DeBiasi, S., Spinardi, L., Ronchi, A., et al. (2008). Impaired generation of mature neurons by neural stem cells from hypomorphic Sox2 mutants. Development *135*, 541–557.

Chen, X., Xu, H., Yuan, P., Fang, F., Huss, M., Vega, V.B., Wong, E., Orlov, Y.L., Zhang, W., Jiang, J., et al. (2008). Integration of external signaling pathways with the core transcriptional network in embryonic stem cells. Cell *133*, 1106–1117.

Chen, J., Liu, J., Yang, J., Chen, Y., Chen, J., Ni, S., Song, H., Zeng, L., Ding, K., and Pei, D. (2011). BMPs functionally replace Klf4 and support efficient reprogramming of mouse fibroblasts by Oct4 alone. Cell Res. *21*, 205–212.

Cheung, M., and Briscoe, J. (2003). Neural crest development is regulated by the transcription factor Sox9. Development *130*, 5681–5693.

Cimadamore, F., Fishwick, K., Giusto, E., Gnedeva, K., Cattarossi, G., Miller, A., Pluchino, S., Brill, L.M., Bronner-Fraser, M., and Terskikh, A.V. (2011). Human ESC-derived neural crest model reveals a key role for SOX2 in sensory neurogenesis. Cell Stem Cell *8*, 538–551.

Clavel, C., Grisanti, L., Zemla, R., Rezza, A., Barros, R., Sennett, R., Mazloom, A.R., Chung, C.-Y., Cai, X., Cai, C.-L., et al. (2012). Sox2 in the dermal papilla niche controls hair growth by fine-tuning BMP signaling in differentiating hair shaft progenitors. Dev. Cell *23*, 981–994.

Dabdoub, A., Puligilla, C., Jones, J.M., Fritzsch, B., Cheah, K.S., Pevny, L.H., and Kelley, M.W. (2008). Sox2 signaling in prosensory domain specification and subsequent hair cell differentiation in the developing cochlea. Proc. Natl. Acad. Sci. USA *105*, 18396–18401.

Domyan, E.T., Ferretti, E., Throckmorton, K., Mishina, Y., Nicolis, S.K., and Sun, X. (2011). Signaling through BMP receptors promotes respiratory identity in the foregut via repression of Sox2. Development *138*, 971–981.

Driskell, R.R., Giangreco, A., Jensen, K.B., Mulder, K.W., and Watt, F.M. (2009). Sox2-positive dermal papilla cells specify hair follicle type in mammalian epidermis. Development *136*, 2815–2823.

Ellis, P., Fagan, B.M., Magness, S.T., Hutton, S., Taranova, O., Hayashi, S., McMahon, A., Rao, M., and Pevny, L. (2004). SOX2, a persistent marker for multipotential neural stem cells derived from embryonic stem cells, the embryo or the adult. Dev. Neurosci. *26*, 148–165.

Engelen, E., Akinci, U., Bryne, J.C., Hou, J., Gontan, C., Moen, M., Szumska, D., Kockx, C., van Ijcken, W., Dekkers, D.H., et al. (2011). Sox2 cooperates with Chd7 to regulate genes that are mutated in human syndromes. Nat. Genet. *43*, 607–611.

Fauquier, T., Rizzoti, K., Dattani, M., Lovell-Badge, R., and Robinson, I.C. (2008). SOX2-expressing progenitor cells generate all of the major cell types in the adult mouse pituitary gland. Proc. Natl. Acad. Sci. USA *105*, 2907–2912.

Favaro, R., Valotta, M., Ferri, A.L., Latorre, E., Mariani, J., Giachino, C., Lancini, C., Tosetti, V., Ottolenghi, S., Taylor, V., and Nicolis, S.K. (2009). Hippocampal development and neural stem cell maintenance require Sox2-dependent regulation of Shh. Nat. Neurosci. *12*, 1248–1256.

Fernandes, K.J., McKenzie, I.A., Mill, P., Smith, K.M., Akhavan, M., Barnabé-Heider, F., Biernaskie, J., Junek, A., Kobayashi, N.R., Toma, J.G., et al. (2004). A dermal niche for multipotent adult skin-derived precursor cells. Nat. Cell Biol. *6*, 1082–1093.

Ferri, A.L., Cavallaro, M., Braida, D., Di Cristofano, A., Canta, A., Vezzani, A., Ottolenghi, S., Pandolfi, P.P., Sala, M., DeBiasi, S., and Nicolis, S.K. (2004). Sox2 deficiency causes neurodegeneration and impaired neurogenesis in the adult mouse brain. Development *131*, 3805–3819.

Fong, Y.W., Inouye, C., Yamaguchi, T., Cattoglio, C., Grubisic, I., and Tjian, R. (2011). A DNA repair complex functions as an Oct4/Sox2 coactivator in embryonic stem cells. Cell *147*, 120–131.

Furuyama, K., Kawaguchi, Y., Akiyama, H., Horiguchi, M., Kodama, S., Kuhara, T., Hosokawa, S., Elbahrawy, A., Soeda, T., Koizumi, M., et al. (2011). Continuous cell supply from a Sox9-expressing progenitor zone in adult liver, exocrine pancreas and intestine. Nat. Genet. *43*, 34–41.

Gontan, C., de Munck, A., Vermeij, M., Grosveld, F., Tibboel, D., and Rottier, R. (2008). Sox2 is important for two crucial processes in lung development: branching morphogenesis and epithelial cell differentiation. Dev. Biol. *317*, 296–309.

Graham, V., Khudyakov, J., Ellis, P., and Pevny, L. (2003). SOX2 functions to maintain neural progenitor identity. Neuron *39*, 749–765.

Gubbay, J., Collignon, J., Koopman, P., Capel, B., Economou, A., Münsterberg, A., Vivian, N., Goodfellow, P., and Lovell-Badge, R. (1990). A gene mapping to the sex-determining region of the mouse Y chromosome is a member of a novel family of embryonically expressed genes. Nature *346*, 245–250.

Guo, W., Keckesova, Z., Donaher, J.L., Shibue, T., Tischler, V., Reinhardt, F., Itzkovitz, S., Noske, A., Zürrer-Härdi, U., Bell, G., et al. (2012). Slug and Sox9 cooperatively determine the mammary stem cell state. Cell *148*, 1015–1028.

Guth, S.I., and Wegner, M. (2008). Having it both ways: Sox protein function between conservation and innovation. Cell. Mol. Life Sci. *65*, 3000–3018.

Han, D.W., Tapia, N., Hermann, A., Hemmer, K., Höing, S., Araúzo-Bravo, M.J., Zaehres, H., Wu, G., Frank, S., Moritz, S., et al. (2012). Direct reprogramming of fibroblasts into neural stem cells by defined factors. Cell Stem Cell *10*, 465–472.

Hanna, L.A., Foreman, R.K., Tarasenko, I.A., Kessler, D.S., and Labosky, P.A. (2002). Requirement for Foxd3 in maintaining pluripotent cells of the early mouse embryo. Genes Dev. *16*, 2650–2661.

He, S., Kim, I., Lim, M.S., and Morrison, S.J. (2011). Sox17 expression confers self-renewal potential and fetal stem cell characteristics upon adult hematopoietic progenitors. Genes Dev. *25*, 1613–1627.

Hochedlinger, K., Yamada, Y., Beard, C., and Jaenisch, R. (2005). Ectopic expression of Oct-4 blocks progenitor-cell differentiation and causes dysplasia in epithelial tissues. Cell *121*, 465–477.

Holmes, G., Bromage, T.G., and Basilico, C. (2011). The Sox2 high mobility group transcription factor inhibits mature osteoblast function in transgenic mice. Bone *49*, 653–661.

Hu, Q., Zhang, L., Wen, J., Wang, S., Li, M., Feng, R., Yang, X., and Li, L. (2010). The EGF receptor-sox2-EGF receptor feedback loop positively regulates the self-renewal of neural precursor cells. Stem Cells *28*, 279–286.

Ikushima, H., Todo, T., Ino, Y., Takahashi, M., Miyazawa, K., and Miyazono, K. (2009). Autocrine TGF-beta signaling maintains tumorigenicity of glioma-initiating cells through Sry-related HMG-box factors. Cell Stem Cell *5*, 504–514.

Ishii, Y., Rex, M., Scotting, P., and Yasugi, S. (1998). Region-specific expression of chicken Sox2 in the developing gut and lung epithelium: regulation by epithelial-mesenchymal interactions. Dev. Dyn. *213*, 464–475.

Jauch, R., Aksoy, I., Hutchins, A.P., Ng, C.K., Tian, X.F., Chen, J., Palasingam, P., Robson, P., Stanton, L.W., and Kolatkar, P.R. (2011). Conversion of Sox17 into a pluripotency reprogramming factor by reengineering its association with Oct4 on DNA. Stem Cells *29*, 940–951.

Jeong, C.-H., Cho, Y.-Y., Kim, M.-O., Kim, S.-H., Cho, E.-J., Lee, S.-Y., Jeon, Y.-J., Lee, K.Y., Yao, K., Keum, Y.-S., et al. (2010). Phosphorylation of Sox2 cooperates in reprogramming to pluripotent stem cells. Stem Cells *28*, 2141–2150.

Jinno, H., Morozova, O., Jones, K.L., Biernaskie, J.A., Paris, M., Hosokawa, R., Rudnicki, M.A., Chai, Y., Rossi, F., Marra, M.A., and Miller, F.D. (2010).

Convergent genesis of an adult neural crest-like dermal stem cell from distinct developmental origins. Stem Cells *28*, 2027–2040.

Juuri, E., Saito, K., Ahtiainen, L., Seidel, K., Tummers, M., Hochedlinger, K., Klein, O.D., Thesleff, I., and Michon, F. (2012). Sox2+ stem cells contribute to all epithelial lineages of the tooth via Sfrp5+ progenitors. Dev. Cell *23*, 317–328.

Kagey, M.H., Newman, J.J., Bilodeau, S., Zhan, Y., Orlando, D.A., van Berkum, N.L., Ebmeier, C.C., Goossens, J., Rahl, P.B., Levine, S.S., et al. (2010). Mediator and cohesin connect gene expression and chromatin architecture. Nature *467*, 430–435.

Kamachi, Y., Uchikawa, M., Tanouchi, A., Sekido, R., and Kondoh, H. (2001). Pax6 and SOX2 form a co-DNA-binding partner complex that regulates initiation of lens development. Genes Dev. *15*, 1272–1286.

Kanai-Azuma, M., Kanai, Y., Gad, J.M., Tajima, Y., Taya, C., Kurohmaru, M., Sanai, Y., Yonekawa, H., Yazaki, K., Tam, P.P., and Hayashi, Y. (2002). Depletion of definitive gut endoderm in Sox17-null mutant mice. Development *129*, 2367–2379.

Kelberman, D., Rizzoti, K., Avilion, A., Bitner-Glindzicz, M., Cianfarani, S., Collins, J., Chong, W.K., Kirk, J.M., Achermann, J.C., Ross, R., et al. (2006). Mutations within Sox2/SOX2 are associated with abnormalities in the hypothalamo-pituitary-gonadal axis in mice and humans. J. Clin. Invest. *116*, 2442–2455.

Keramari, M., Razavi, J., Ingman, K.A., Patsch, C., Edenhofer, F., Ward, C.M., and Kimber, S.J. (2010). Sox2 is essential for formation of trophectoderm in the preimplantation embryo. PLoS ONE *5*, e13952.

Kiernan, A.E., Pelling, A.L., Leung, K.K., Tang, A.S., Bell, D.M., Tease, C., Lovell-Badge, R., Steel, K.P., and Cheah, K.S. (2005). Sox2 is required for sensory organ development in the mammalian inner ear. Nature *434*, 1031–1035.

Kim, J., Lo, L., Dormand, E., and Anderson, D.J. (2003). SOX10 maintains multipotency and inhibits neuronal differentiation of neural crest stem cells. Neuron *38*, 17–31.

Kim, I., Saunders, T.L., and Morrison, S.J. (2007). Sox17 dependence distinguishes the transcriptional regulation of fetal from adult hematopoietic stem cells. Cell *130*, 470–483.

Kim, J., Chu, J., Shen, X., Wang, J., and Orkin, S.H. (2008). An extended transcriptional network for pluripotency of embryonic stem cells. Cell *132*, 1049–1061.

King, N., Westbrook, M.J., Young, S.L., Kuo, A., Abedin, M., Chapman, J., Fairclough, S., Hellsten, U., Isogai, Y., Letunic, I., et al. (2008). The genome of the choanoflagellate Monosiga brevicollis and the origin of metazoans. Nature *451*, 783–788.

Kishi, M., Mizuseki, K., Sasai, N., Yamazaki, H., Shiota, K., Nakanishi, S., and Sasai, Y. (2000). Requirement of Sox2-mediated signaling for differentiation of early Xenopus neuroectoderm. Development *127*, 791–800.

Kondo, T., and Raff, M. (2000). Oligodendrocyte precursor cells reprogrammed to become multipotential CNS stem cells. Science *289*, 1754–1757.

Kondo, T., and Raff, M. (2004). Chromatin remodeling and histone modification in the conversion of oligodendrocyte precursors to neural stem cells. Genes Dev. *18*, 2963–2972.

Kondoh, H., and Kamachi, Y. (2010). SOX-partner code for cell specification: Regulatory target selection and underlying molecular mechanisms. Int. J. Biochem. Cell Biol. *42*, 391–399.

Kopp, J.L., Ormsbee, B.D., Desler, M., and Rizzino, A. (2008). Small increases in the level of Sox2 trigger the differentiation of mouse embryonic stem cells. Stem Cells *26*, 903–911.

Kopp, J.L., Dubois, C.L., Schaffer, A.E., Hao, E., Shih, H.P., Seymour, P.A., Ma, J., and Sander, M. (2011). Sox9+ ductal cells are multipotent progenitors throughout development but do not produce new endocrine cells in the normal or injured adult pancreas. Development *138*, 653–665.

Kordes, U., and Hagel, C. (2006). Expression of SOX9 and SOX10 in central neuroepithelial tumor. J. Neurooncol. *80*, 151–155.

Kunath, T., Arnaud, D., Uy, G.D., Okamoto, I., Chureau, C., Yamanaka, Y., Heard, E., Gardner, R.L., Avner, P., and Rossant, J. (2005). Imprinted X-inactivation in extra-embryonic endoderm cell lines from mouse blastocysts. Development *132*, 1649–1661.

Kuzmichev, A., Kim, S.-K., D'Alessio, A., Chenoweth, J., Wittko, I., Campanati, L., and McKay, R. (2012). Sox2 acts through Sox21 to regulate transcription in pluripotent and differentiated cells. Curr. Biol. *22*, 1705–1710.

Laga, A.C., Lai, C.-Y., Zhan, Q., Huang, S.J., Velazquez, E.F., Yang, Q., Hsu, M.-Y., and Murphy, G.F. (2010). Expression of the embryonic stem cell transcription factor SOX2 in human skin: relevance to melanocyte and merkel cell biology. Am. J. Pathol. *176*, 903–913.

Le, N., Nagarajan, R., Wang, J.Y., Araki, T., Schmidt, R.E., and Milbrandt, J. (2005). Analysis of congenital hypomyelinating Egr2Lo/Lo nerves identifies Sox2 as an inhibitor of Schwann cell differentiation and myelination. Proc. Natl. Acad. Sci. USA *102*, 2596–2601.

Li, H., Collado, M., Villasante, A., Matheu, A., Lynch, C.J., Cañamero, M., Rizzoti, K., Carneiro, C., Martínez, G., Vidal, A., et al. (2012a). p27(Kip1) directly represses Sox2 during embryonic stem cell differentiation. Cell Stem Cell *11*, 845–852.

Li, M., He, Y., Dubois, W., Wu, X., Shi, J., and Huang, J. (2012b). Distinct regulatory mechanisms and functions for p53-activated and p53-repressed DNA damage response genes in embryonic stem cells. Mol. Cell *46*, 30–42.

Liber, D., Domaschenz, R., Holmqvist, P.-H., Mazzarella, L., Georgiou, A., Leleu, M., Fisher, A.G., Labosky, P.A., and Dillon, N. (2010). Epigenetic priming of a pre-B cell-specific enhancer through binding of Sox2 and Foxd3 at the ESC stage. Cell Stem Cell *7*, 114–126.

López-Juárez, A., Remaud, S., Hassani, Z., Jolivet, P., Pierre Simons, J., Sontag, T., Yoshikawa, K., Price, J., Morvan-Dubois, G., and Demeneix, B.A. (2012). Thyroid hormone signaling acts as a neurogenic switch by repressing Sox2 in the adult neural stem cell niche. Cell Stem Cell *10*, 531–543.

Lu, Y., Futtner, C., Rock, J.R., Xu, X., Whitworth, W., Hogan, B.L., and Onaitis, M.W. (2010). Evidence that SOX2 overexpression is oncogenic in the lung. PLoS ONE *5*, e11022.

Mansukhani, A., Ambrosetti, D., Holmes, G., Cornivelli, L., and Basilico, C. (2005). Sox2 induction by FGF and FGFR2 activating mutations inhibits Wnt signaling and osteoblast differentiation. J. Cell Biol. *168*, 1065–1076.

Marqués-Torrejón, M.A., Porlan, E., Banito, A., Gómez-Ibarlucea, E., Lopez-Contreras, A.J., Fernández-Capetillo, O., Vidal, A., Gil, J., Torres, J., and Fariñas, I. (2013). Cyclin-dependent kinase inhibitor p21 controls adult neural stem cell expansion by regulating Sox2 gene expression. Cell Stem Cell *12* this issue, 88–100.

Maruyama, M., Ichisaka, T., Nakagawa, M., and Yamanaka, S. (2005). Differential roles for Sox15 and Sox2 in transcriptional control in mouse embryonic stem cells. J. Biol. Chem. *280*, 24371–24379.

Masui, S., Nakatake, Y., Toyooka, Y., Shimosato, D., Yagi, R., Takahashi, K., Okochi, H., Okuda, A., Matoba, R., Sharov, A.A., et al. (2007). Pluripotency governed by Sox2 via regulation of Oct3/4 expression in mouse embryonic stem cells. Nat. Cell Biol. *9*, 625–635.

Matsushima, D., Heavner, W., and Pevny, L.H. (2011). Combinatorial regulation of optic cup progenitor cell fate by SOX2 and PAX6. Development *138*, 443–454.

Meeson, A.P., Shi, X., Alexander, M.S., Williams, R.S., Allen, R.E., Jiang, N., Adham, I.M., Goetsch, S.C., Hammer, R.E., and Garry, D.J. (2007). Sox15 and Fhl3 transcriptionally coactivate Foxk1 and regulate myogenic progenitor cells. EMBO J. *26*, 1902–1912.

Miller, S.J., Rangwala, F., Williams, J., Ackerman, P., Kong, S., Jegga, A.G., Kaiser, S., Aronow, B.J., Frahm, S., Kluwe, L., et al. (2006). Large-scale molecular comparison of human schwann cells to malignant peripheral nerve sheath tumor cell lines and tissues. Cancer Res. *66*, 2584–2591.

Miyagi, S., Masui, S., Niwa, H., Saito, T., Shimazaki, T., Okano, H., Nishimoto, M., Muramatsu, M., Iwama, A., and Okuda, A. (2008). Consequence of the loss of Sox2 in the developing brain of the mouse. FEBS Lett. *582*, 2811–2815.

Mullen, A.C., Orlando, D.A., Newman, J.J., Lovén, J., Kumar, R.M., Bilodeau, S., Reddy, J., Guenther, M.G., DeKoter, R.P., and Young, R.A. (2011). Master transcription factors determine cell-type-specific responses to TGF-β signaling. Cell *147*, 565–576.

Nakagawa, M., Koyanagi, M., Tanabe, K., Takahashi, K., Ichisaka, T., Aoi, T., Okita, K., Mochiduki, Y., Takizawa, N., and Yamanaka, S. (2008). Generation of induced pluripotent stem cells without Myc from mouse and human fibroblasts. Nat. Biotechnol. *26*, 101–106.

Ng, S.-Y., Johnson, R., and Stanton, L.W. (2012). Human long non-coding RNAs promote pluripotency and neuronal differentiation by association with chromatin modifiers and transcription factors. EMBO J. *31*, 522–533.

Niakan, K.K., Ji, H., Maehr, R., Vokes, S.A., Rodolfa, K.T., Sherwood, R.I., Yamaki, M., Dimos, J.T., Chen, A.E., Melton, D.A., et al. (2010). Sox17 promotes differentiation in mouse embryonic stem cells by directly regulating extraembryonic gene expression and indirectly antagonizing self-renewal. Genes Dev. *24*, 312–326.

Nowak, J.A., Polak, L., Pasolli, H.A., and Fuchs, E. (2008). Hair follicle stem cells are specified and function in early skin morphogenesis. Cell Stem Cell *3*, 33–43.

Okubo, T., Pevny, L.H., and Hogan, B.L. (2006). Sox2 is required for development of taste bud sensory cells. Genes Dev. *20*, 2654–2659.

Okubo, T., Clark, C., and Hogan, B.L. (2009). Cell lineage mapping of taste bud cells and keratinocytes in the mouse tongue and soft palate. Stem Cells *27*, 442–450.

Orkin, S.H., and Hochedlinger, K. (2011). Chromatin connections to pluripotency and cellular reprogramming. Cell *145*, 835–850.

Parrinello, S., Napoli, I., Ribeiro, S., Digby, P.W., Fedorova, M., Parkinson, D.B., Doddrell, R.D., Nakayama, M., Adams, R.H., and Lloyd, A.C. (2010). EphB signaling directs peripheral nerve regeneration through Sox2-dependent Schwann cell sorting. Cell *143*, 145–155.

Pevny, L.H., and Nicolis, S.K. (2010). Sox2 roles in neural stem cells. Int. J. Biochem. Cell Biol. *42*, 421–424.

Pevny, L.H., Sockanathan, S., Placzek, M., and Lovell-Badge, R. (1998). A role for SOX1 in neural determination. Development *125*, 1967–1978.

Poché, R.A., Furuta, Y., Chaboissier, M.-C., Schedl, A., and Behringer, R.R. (2008). Sox9 is expressed in mouse multipotent retinal progenitor cells and functions in Müller glial cell development. J. Comp. Neurol. *510*, 237–250.

Que, J., Okubo, T., Goldenring, J.R., Nam, K.-T., Kurotani, R., Morrisey, E.E., Taranova, O., Pevny, L.H., and Hogan, B.L. (2007). Multiple dose-dependent roles for Sox2 in the patterning and differentiation of anterior foregut endoderm. Development *134*, 2521–2531.

Que, J., Luo, X., Schwartz, R.J., and Hogan, B.L. (2009). Multiple roles for Sox2 in the developing and adult mouse trachea. Development *136*, 1899–1907.

Raverot, G., Weiss, J., Park, S.Y., Hurley, L., and Jameson, J.L. (2005). Sox3 expression in undifferentiated spermatogonia is required for the progression of spermatogenesis. Dev. Biol. *283*, 215–225.

Rawlins, E. (2011). The building blocks of mammalian lung development. Dev. Dyn. *240*, 463–476.

Rendl, M., Lewis, L., and Fuchs, E. (2005). Molecular dissection of mesenchymal-epithelial interactions in the hair follicle. PLoS Biol. *3*, e331.

Ring, K.L., Tong, L.M., Balestra, M.E., Javier, R., Andrews-Zwilling, Y., Li, G., Walker, D., Zhang, W.R., Kreitzer, A.C., and Huang, Y. (2012). Direct reprogramming of mouse and human fibroblasts into multipotent neural stem cells with a single factor. Cell Stem Cell *11*, 100–109.

Rossant, J., and Tam, P.P. (2009). Blastocyst lineage formation, early embryonic asymmetries and axis patterning in the mouse. Development *136*, 701–713.

Rudin, C.M., Durinck, S., Stawiski, E.W., Poirier, J.T., Modrusan, Z., Shames, D.S., Bergbower, E.A., Guan, Y., Shin, J., Guillory, J., et al. (2012). Comprehensive genomic analysis identifies SOX2 as a frequently amplified gene in small-cell lung cancer. Nat. Genet. *44*, 1111–1116.

Sato, T., van Es, J.H., Snippert, H.J., Stange, D.E., Vries, R.G., van den Born, M., Barker, N., Shroyer, N.F., van de Wetering, M., and Clevers, H. (2011). Paneth cells constitute the niche for Lgr5 stem cells in intestinal crypts. Nature *469*, 415–423.

Schepers, G.E., Teasdale, R.D., and Koopman, P. (2002). Twenty pairs of sox: extent, homology, and nomenclature of the mouse and human sox transcription factor gene families. Dev. Cell *3*, 167–170.

Schmidt, K., Glaser, G., Wernig, A., Wegner, M., and Rosorius, O. (2003). Sox8 is a specific marker for muscle satellite cells and inhibits myogenesis. J. Biol. Chem. *278*, 29769–29775.

Schober, M., and Fuchs, E. (2011). Tumor-initiating stem cells of squamous cell carcinomas and their control by TGF-β and integrin/focal adhesion kinase (FAK) signaling. Proc. Natl. Acad. Sci. USA *108*, 10544–10549.

Scott, C.E., Wynn, S.L., Sesay, A., Cruz, C., Cheung, M., Gomez Gaviro, M.-V., Booth, S., Gao, B., Cheah, K.S., Lovell-Badge, R., and Briscoe, J. (2010). SOX9 induces and maintains neural stem cells. Nat. Neurosci. *13*, 1181–1189.

Séguin, C.A., Draper, J.S., Nagy, A., and Rossant, J. (2008). Establishment of endoderm progenitors by SOX transcription factor expression in human embryonic stem cells. Cell Stem Cell *3*, 182–195.

Seymour, P.A., Freude, K.K., Tran, M.N., Mayes, E.E., Jensen, J., Kist, R., Scherer, G., and Sander, M. (2007). SOX9 is required for maintenance of the pancreatic progenitor cell pool. Proc. Natl. Acad. Sci. USA *104*, 1865–1870.

Shimozaki, K., Zhang, C.-L., Suh, H., Denli, A., Evans, R., and Gage, F. (2012). SRY-box-containing gene 2 regulation of nuclear receptor tailless (Tlx) transcription in adult neural stemcells. J. Biol. Chem. *287*, 5969–5978.

Sikorska, M., Sandhu, J.K., Deb-Rinker, P., Jezierski, A., Leblanc, J., Charlebois, C., Ribecco-Lutkiewicz, M., Bani-Yaghoub, M., and Walker, P.R. (2008). Epigenetic modifications of SOX2 enhancers, SRR1 and SRR2, correlate with in vitro neural differentiation. J. Neurosci. Res. *86*, 1680–1693.

Simons, B.D., and Clevers, H. (2011). Strategies for homeostatic stem cell self-renewal in adult tissues. Cell *145*, 851–862.

Sinclair, A.H., Berta, P., Palmer, M.S., Hawkins, J.R., Griffiths, B.L., Smith, M.J., Foster, J.W., Frischauf, A.M., Lovell-Badge, R., and Goodfellow, P.N. (1990). A gene from the human sex-determining region encodes a protein with homology to a conserved DNA-binding motif. Nature *346*, 240–244.

Soufi, A., Donahue, G., and Zaret, K.S. (2012). Facilitators and impediments of the pluripotency reprogramming factors' initial engagement with the genome. Cell *151*, 994–1004.

Sridharan, R., Tchieu, J., Mason, M.J., Yachechko, R., Kuoy, E., Horvath, S., Zhou, Q., and Plath, K. (2009). Role of the murine reprogramming factors in the induction of pluripotency. Cell *136*, 364–377.

Suh, H., Consiglio, A., Ray, J., Sawai, T., D'Amour, K.A., and Gage, F.H. (2007). In vivo fate analysis reveals the multipotent and self-renewal capacities of Sox2+ neural stem cells in the adult hippocampus. Cell Stem Cell *1*, 515–528.

Takemoto, T., Uchikawa, M., Kamachi, Y., and Kondoh, H. (2006). Convergence of Wnt and FGF signals in the genesis of posterior neural plate through activation of the Sox2 enhancer N-1. Development *133*, 297–306.

Takemoto, T., Uchikawa, M., Yoshida, M., Bell, D.M., Lovell-Badge, R., Papaioannou, V.E., and Kondoh, H. (2011). Tbx6-dependent Sox2 regulation determines neural or mesodermal fate in axial stem cells. Nature *470*, 394–398.

Tanaka, S., Kamachi, Y., Tanouchi, A., Hamada, H., Jing, N., and Kondoh, H. (2004). Interplay of SOX and POU factors in regulation of the Nestin gene in neural primordial cells. Mol. Cell. Biol. *24*, 8834–8846.

Taranova, O.V., Magness, S.T., Fagan, B.M., Wu, Y., Surzenko, N., Hutton, S.R., and Pevny, L.H. (2006). SOX2 is a dose-dependent regulator of retinal neural progenitor competence. Genes Dev. *20*, 1187–1202.

Thier, M., Wörsdörfer, P., Lakes, Y.B., Gorris, R., Herms, S., Opitz, T., Seiferling, D., Quandel, T., Hoffmann, P., Nöthen, M.M., et al. (2012). Direct conversion of fibroblasts into stably expandable neural stem cells. Cell Stem Cell *10*, 473–479.

Thomson, M., Liu, S.J., Zou, L.-N., Smith, Z., Meissner, A., and Ramanathan, S. (2011). Pluripotency factors in embryonic stem cells regulate differentiation into germ layers. Cell *145*, 875–889.

Tomioka, M., Nishimoto, M., Miyagi, S., Katayanagi, T., Fukui, N., Niwa, H., Muramatsu, M., and Okuda, A. (2002). Identification of Sox-2 regulatory region which is under the control of Oct-3/4-Sox-2 complex. Nucleic Acids Res. *30*, 3202–3213.

Tompkins, D.H., Besnard, V., Lange, A.W., Wert, S.E., Keiser, A.R., Smith, A.N., Lang, R., and Whitsett, J.A. (2009). Sox2 is required for maintenance and differentiation of bronchiolar Clara, ciliated, and goblet cells. PLoS ONE *4*, e8248.

Tompkins, D.H., Besnard, V., Lange, A.W., Keiser, A.R., Wert, S.E., Bruno, M.D., and Whitsett, J.A. (2011). Sox2 activates cell proliferation and differentiation in the respiratory epithelium. Am. J. Respir. Cell Mol. Biol. *45*, 101–110.

Tsuruzoe, S., Ishihara, K., Uchimura, Y., Watanabe, S., Sekita, Y., Aoto, T., Saitoh, H., Yuasa, Y., Niwa, H., Kawasuji, M., et al. (2006). Inhibition of DNA binding of Sox2 by the SUMO conjugation. Biochem. Biophys. Res. Commun. *351*, 920–926.

Vidal, V.P., Chaboissier, M.C., Lützkendorf, S., Cotsarelis, G., Mill, P., Hui, C.C., Ortonne, N., Ortonne, J.P., and Schedl, A. (2005). Sox9 is essential for outer root sheath differentiation and the formation of the hair stem cell compartment. Current Biol. *15*, 1340–1351.

Wang, Z., Oron, E., Nelson, B., Razis, S., and Ivanova, N. (2012). Distinct lineage specification roles for NANOG, OCT4, and SOX2 in human embryonic stem cells. Cell Stem Cell *10*, 440–454.

Wegner, M. (2010). All purpose Sox: The many roles of Sox proteins in gene expression. Int. J. Biochem. Cell Biol. *42*, 381–390.

Wegner, M., and Stolt, C.C. (2005). From stem cells to neurons and glia: a Soxist's view of neural development. Trends Neurosci. *28*, 583–588.

Whyte, W.A., Bilodeau, S., Orlando, D.A., Hoke, H.A., Frampton, G.M., Foster, C.T., Cowley, S.M., and Young, R.A. (2012). Enhancer decommissioning by LSD1 during embryonic stem cell differentiation. Nature *482*, 221–225.

Williamson, K.A., Hever, A.M., Rainger, J., Rogers, R.C., Magee, A., Fiedler, Z., Keng, W.T., Sharkey, F.H., McGill, N., Hill, C.J., et al. (2006). Mutations in SOX2 cause anophthalmia-esophageal-genital (AEG) syndrome. Hum. Mol. Genet. *15*, 1413–1422.

Wood, H.B., and Episkopou, V. (1999). Comparative expression of the mouse Sox1, Sox2 and Sox3 genes from pre-gastrulation to early somite stages. Mech. Dev. *86*, 197–201.

Xu, N., Papagiannakopoulos, T., Pan, G., Thomson, J.A., and Kosik, K.S. (2009a). MicroRNA-145 regulates OCT4, SOX2, and KLF4 and represses pluripotency in human embryonic stem cells. Cell *137*, 647–658.

Xu, J., Watts, J.A., Pope, S.D., Gadue, P., Kamps, M., Plath, K., Zaret, K.S., and Smale, S.T. (2009b). Transcriptional competence and the active marking of tissue-specific enhancers by defined transcription factors in embryonic and induced pluripotent stem cells. Genes Dev. *23*, 2824–2838.

Yabuta, Y., Kurimoto, K., Ohinata, Y., Seki, Y., and Saitou, M. (2006). Gene expression dynamics during germline specification in mice identified by quantitative single-cell gene expression profiling. Biol. Reprod. *75*, 705–716.

Zaret, K.S., and Carroll, J.S. (2011). Pioneer transcription factors: establishing competence for gene expression. Genes Dev. *25*, 2227–2241.

Zhao, S., Nichols, J., Smith, A.G., and Li, M. (2004). SoxB transcription factors specify neuroectodermal lineage choice in ES cells. Mol. Cell Neurosci. *27*, 332–342.

Zhao, H.Y., Zhang, Y.J., Dai, H., Zhang, Y., and Shen, Y.F. (2011). CARM1 mediates modulation of Sox2. PLoS ONE *6*, e27026.

Zorn, A.M., and Wells, J.M. (2009). Vertebrate endoderm development and organ formation. Annu. Rev. Cell Dev. Biol. *25*, 221–251.

WELCOME HOME
TO THE NEW CELL.COM

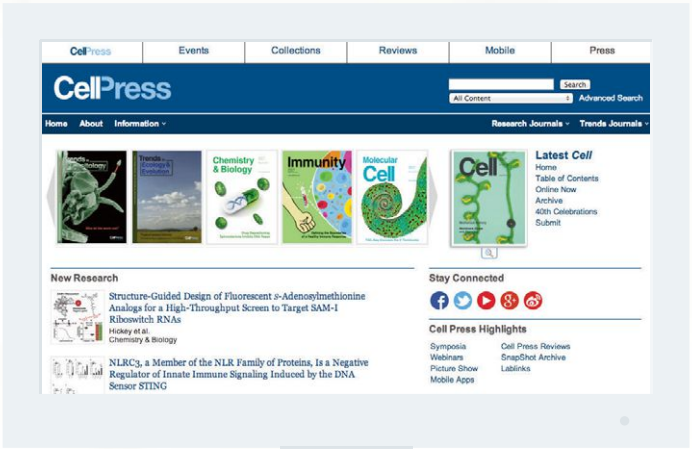

It's not just a website, it's a destination designed to meet your needs.

Cell.com is your resource for the most pioneering science in your field. Read highlights on the latest groundbreaking research, find insightful and provocative reviews, and discover the next Cell Press conference where you can connect with colleagues and collaborators around the world.

Interacting with the high-quality science that comes from Cell Press journals, conference, and learning resources is now even more immersive and intuitive.

See for yourself at **www.cell.com**

CellPress

Cell Stem Cell
Review

Mechanisms that Regulate Stem Cell Aging and Life Span

Robert A.J. Signer[1] and Sean J. Morrison[1,2,*]
[1]Children's Research Institute, Department of Pediatrics, University of Texas Southwestern Medical Center, Dallas, TX 75390, USA
[2]Howard Hughes Medical Institute
*Correspondence: sean.morrison@utsouthwestern.edu
http://dx.doi.org/10.1016/j.stem.2013.01.001

Mammalian aging is associated with reduced tissue regeneration, increased degenerative disease, and cancer. Because stem cells regenerate many adult tissues and contribute to the development of cancer by accumulating mutations, age-related changes in stem cells likely contribute to age-related morbidity. Consistent with this, stem cell function declines with age in numerous tissues as a result of gate-keeping tumor suppressor expression, DNA damage, changes in cellular physiology, and environmental changes in tissues. It remains unknown whether declines in stem cell function during aging influence organismal longevity. However, mechanisms that influence longevity also modulate age-related morbidity, partly through effects on stem cells.

Introduction

Damage accumulates in biological macromolecules during aging, impairing cellular processes, tissue homeostasis, and organ function. This contributes to the onset of age-related diseases, including cognitive (Yankner et al., 2008), neoplastic (Hoeijmakers, 2009), immunologic (Dorshkind et al., 2009), and metabolic (Wallace, 2005) disorders. Age-related morbidity is determined partly by changes in nondividing differentiated cells, such as neurons (Lu et al., 2004), and partly by changes in mitotic cells, including stem cells, restricted progenitors, and differentiated cells (Sharpless and DePinho, 2007).

Stem cells persist throughout life in numerous mammalian tissues, replacing cells lost to homeostatic turnover, injury, and disease. However, stem cell function declines with age in a number of tissues, including the blood (Morrison et al., 1996b; de Haan et al., 1997; Chen et al., 2000), forebrain (Kuhn et al., 1996; Maslov et al., 2004; Molofsky et al., 2006), skeletal muscle (Conboy et al., 2003, 2005), and skin (Nishimura et al., 2005) (Table 1). These declines in stem cell function may contribute to degeneration and dysfunction in aging regenerative tissues (Sharpless and DePinho, 2007). Thus, age-related changes in the function of stem cells and other progenitors may contribute to some diseases of aging, particularly in regenerative tissues, even while other diseases of aging may not be influenced by stem cell aging at all.

It is unknown whether stem cell aging influences mammalian life span. However, in *Drosophila* genetic changes that improve homeostasis in the intestinal epithelium by blocking stem cell overproliferation and differentiation defects during aging do extend life span (Biteau et al., 2010). This raises the possibility that some age-related changes in mammalian stem cells promote homeostasis in aging tissues despite declines in stem cell function.

It is important to emphasize that stem cells are not the only mitotic cells that persist throughout life and whose aging might influence age-related diseases. Like stem cells, some restricted progenitors and differentiated cells are also perpetuated throughout life by intermittent self-renewing divisions. Such cells include pancreatic β cells and memory B and T cells. During aging, declines in the number or function of pancreatic β cells (Teta et al., 2005) and memory T cells (Liu et al., 2011) contribute to the development of type 2 diabetes (Butler et al., 2003) and reduced immune function (Dorshkind et al., 2009). There is at least some overlap in self-renewal mechanisms between these differentiated cells and stem cells (Luckey et al., 2006). This suggests that some of the mechanisms that regulate stem cell aging may also regulate the aging of mitotic differentiated cells, and both classes of progenitors may contribute to age-related morbidity.

Stem cells must change their properties throughout life to match the changing growth and regeneration demands of tissues. Stem cells divide rapidly during fetal development to support rapid growth. By young adulthood, growth has slowed or ceased in mammalian tissues and most stem cells are quiescent most of the time, intermittently dividing to maintain tissue homeostasis. In old adults, stem cells increase gate-keeping tumor suppressor expression. This may reduce the incidence of cancer in aging tissues, but also reduces regenerative capacity (Janzen et al., 2006; Krishnamurthy et al., 2006; Molofsky et al., 2006). These changes in stem cells likely reflect regulation by heterochronic genes—genes whose expression changes over time in a way that causes temporal changes in stem cell function (Nishino et al., 2008; Toledano et al., 2012). Heterochronic genes were originally identified as regulating the timing of developmental transitions in *C. elegans* (Ambros and Horvitz, 1984). This raises the question of whether the increase in tumor suppressor expression and the temporal changes in stem cell function in aging mammalian tissues are partly developmentally programmed.

Mitochondrial activity, tissue growth, and metabolic rates during development can also influence life span and the rates of cellular aging at later stages of life (Dillin et al., 2002). Thus, the aging of stem cells cannot be considered in isolation but rather in the context of temporal changes in stem cell and tissue properties that occur throughout life.

Like all cells, stem cell aging is determined partly by the accumulation of damage over time. Declines in stem cell function

Table 1. Summary of Age-Related Changes in Various Mammalian Stem Cell Populations

Stem Cell Population	Frequency	Proliferation	Differentiation	Other Defects
Hematopoietic	↑ long-lived mouse strains, ↓ short-lived mouse strains	↑ cycling, ↓ self-renewal	↓ lymphoid, ↑ myeloid	↓ homing, ↓ mobilization, ↓ engraftment,
Neural	↓ lateral ventricle SVZ, ↓ dentate gyrus subgranular layer	↓ cycling, ↓ self-renewal (SVZ)	↓ neurogenesis, ↑ gliogenesis	
Muscle	↓ satellite cells associated with muscle fibers	↓ proliferation	↓ myogenic, ↑ fibrogenic, ↑ adipogenic	
Melanonocyte stem cells in hair bulge	↓ melanocyte stem cells		↑ terminal differentiation of melanocytes	

during aging can be precipitated by telomere shortening, DNA damage, and mitochondrial damage (Choudhury et al., 2007; Rossi et al., 2007; Sahin and Depinho, 2010) (Figure 1). Stem cell aging can be slowed by dietary restriction (Lee et al., 2000; Chen et al., 2003; Mair et al., 2010; Cerletti et al., 2012) and by exposure to humoral factors from a young parabiont (sharing circulation with an old mouse) (Conboy et al., 2005; Villeda et al., 2011). In this review we discuss all of these mechanisms that influence stem cell aging in the context of mechanisms that are known to influence general cellular aging and life span.

Gate-Keeping Tumor Suppressors

Gate-keeping tumor suppressors (such as $p16^{Ink4a}$, $p19^{Arf}$, and p53—see Figure 2) negatively regulate cellular proliferation and survival (Kinzler and Vogelstein, 1997). These gene products were first discovered by virtue of their role in cancer, but probably evolved to regulate homeostasis in normal tissues by regulating the proliferation and survival of normal cells. Their role in cancer reflects the ability of cancer cells to evade normal homeostatic controls by deleting these genes. Gate-keeping tumor suppressors tend to negatively regulate stem cell function (He et al., 2009) and regulate stem cell aging because their expression and/or function increase with age (Krishnamurthy et al., 2004, 2006; Janzen et al., 2006; Molofsky et al., 2006).

A regulatory pathway of heterochronic genes increases gate-keeping tumor suppressor expression in aging stem cells (Figure 2A). *let-7* microRNA expression increases with age, probably in many types of stem cells, eliminating the expression of the high mobility group transcriptional regulator, Hmga2, in stem cells from old mice (Nishino et al., 2008). Hmga2 is a proto-oncogene and *let-7* target. The loss of Hmga2 expression from neural stem cells reduces their frequency and self-renewal potential by increasing the expression of $p16^{Ink4a}$ and $p19^{Arf}$ (Nishino et al., 2008). $p16^{Ink4a}$ is a cyclin-dependent kinase inhibitor (Figure 2B) whose expression increases in aging mouse and human tissues (Krishnamurthy et al., 2004), reducing stem cell frequency and self-renewal potential in multiple tissues (Janzen et al., 2006; Krishnamurthy et al., 2006; Molofsky et al., 2006). Elevated $p16^{Ink4a}$ expression also depletes certain differentiated progenitors during aging, including pancreatic β cells (Krishnamurthy et al., 2006) and memory T cells (Liu et al., 2011).

$p19^{Arf}$ ($p14^{Arf}$ in humans) also increases with age in mouse tissues (Zindy et al., 1997; Krishnamurthy et al., 2004). $p19^{Arf}$ promotes p53 protein stability by inhibiting Mdm2-mediated degradation (Figure 2B). It has not yet been tested whether $p19^{Arf}$ negatively regulates stem cell function in aging tissues.

Beyond the mechanisms described above, there are likely to be a number of other mechanisms that regulate changes in $p16^{Ink4a}$ and $p19^{Arf}$ expression during aging, including yet undiscovered mechanisms. A decline in the expression of the polycomb complex component, Ezh2, contributes to increased $p16^{Ink4a}$ and $p19^{Arf}$ expression in aging pancreatic β cells (Chen et al., 2009b). Whether a change in polycomb complex activity contributes generally to changes in $p16^{Ink4a}$ and $p19^{Arf}$ expression in aging stem cells remains untested.

The increase in gate-keeping tumor suppressor expression in aging tissues, and the onset of senescence in some aging cells, may oppose the increased incidence of cancer during aging (Campisi, 2005; Signer et al., 2008). Indeed, $p16^{Ink4a}$ and/or $p19^{Arf}$ deficiency increase the incidence of cancer in adult mice (Serrano et al., 1996; Kamijo et al., 1997), and humans with germline loss-of-function mutations in $p16^{Ink4a}/p14^{Arf}$ have more adult-onset cancers (Ruas and Peters, 1998). However, it remains unclear whether the physiological increase in $p16^{Ink4a}$ and $p19^{Arf}$ expression in aging cells suppresses cancer or whether an even higher level of $p16^{Ink4a}$ and $p19^{Arf}$ expression, induced by oncogenic stimuli, is responsible for cancer suppression. Transgenic mice with an extra copy of the $p16^{Ink4a}/p19^{Arf}/p15^{Ink4b}$ and *p53* loci have a lower cancer incidence, though this may reflect the inability of cancer cells to delete the extra copy of the locus rather than the modestly increased expression of these tumor suppressors under physiological conditions (García-Cao et al., 2002; Matheu et al., 2004, 2007).

While p53 expression promotes the maintenance of genomic integrity (Schoppy et al., 2010), the net effect of p53 in a wild-type background is to negatively regulate stem cell function, at least in hematopoietic stem cells (HSCs) from young adult mice (TeKippe et al., 2003), presumably by opposing cell cycle entry, blocking symmetric division, or inducing cell death (Cicalese et al., 2009; Liu et al., 2009b) (Figure 2 and Figure 3). Elevated p53 expression or constitutive p53 activation can deplete stem cells (Lee et al., 2010), cause premature aging, and shorten life span despite reducing cancer incidence (Tyner et al., 2002; Dumble et al., 2007; Gannon et al., 2011) (Figure 3). These effects in mice also appear to reflect similar functions in humans because a polymorphism in *p53* that reduces p53 function increases cancer incidence and life span in humans (van Heemst et al., 2005). This suggests that increased p53 activity protects against cancer but can promote aging and shorten life span, at least when a certain threshold of activity is reached.

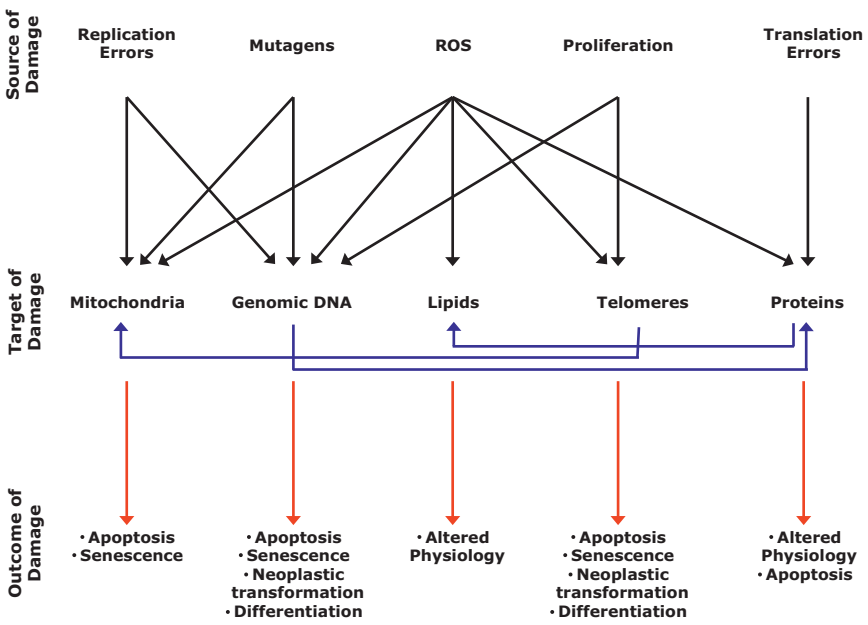

Figure 1. Multiple Sources of Damage to Biological Macromolecules Reduce Stem Cell Function during Aging

Sources of damage (top row) including ROS, exogenous mutagens, proliferation, infidelity of DNA replication, and errors in protein translation can damage macromolecules or organelles within a cell (middle row). Damage accumulates in DNA, proteins, mitochondria, and lipids during aging and contributes to declines in stem cell function, tissue regeneration, and life span. The cellular consequences of this damage (bottom row) include cell death, cellular senescence, differentiation, altered cellular physiology, and cancer. All of these mechanisms are interrelated; damage to one component, such as telomeres, can influence the function of other components, such as mitochondria (Sahin and Depinho, 2010).

The functions of the $p16^{Ink4a}$, $p19^{Arf}$, and p53 tumor suppressors depend on expression level and context (Figure 3), promoting the maintenance of mitotically active cells in some contexts while promoting cell death or senescence in other contexts. For example, p53 promotes the maintenance of genomic integrity (Schoppy et al., 2010) and promotes tissue regeneration in *Atr* mutant mice by promoting DNA repair and/or by promoting the death of cells with DNA damage (Ruzankina et al., 2009); however, in response to oncogenic stimuli or telomere attrition, p53 depletes stem cells (Begus-Nahrmann et al., 2009; Lee et al., 2010). Increased p53 function in HSCs reduces proliferative potential but slows the expression of some molecular markers of aging (Chambers et al., 2007). Moreover, transgenic mice that constitutively express moderately increased levels of $p15^{Ink4b}$, $p16^{Ink4a}$, $p19^{Arf}$, and/or p53 exhibit no signs of accelerated aging and may even show increased median life span that cannot be explained by reduced cancer incidence (García-Cao et al., 2002; Matheu et al., 2004, 2007). Not all normal cell proliferation in aging tissues is advantageous, as illustrated by atherosclerosis. Therefore, cancer suppression may not be the only function of gate-keeping tumor suppressors in aging stem/progenitor cells, as these tumor suppressors might also help sustain tissue homeostasis by suppressing pathological or dysplastic proliferation, or aberrant differentiation, in aging tissues.

$p16^{Ink4a}$ and $p14^{Arf}$ may also regulate human aging. A series of genome-wide association studies have found significant associations between polymorphisms in or near the *p16*^{Ink4a}/*p14*^{Arf} locus in humans and the risk of age-related diseases, including type 2 diabetes and heart disease (Jeck et al., 2012). However, it is not clear whether the polymorphisms increase or decrease $p16^{Ink4a}$/$p14^{Arf}$ function. Overall, gate-keeping tumor suppressors have pleiotropic functions that promote stem cell function in some ways and negatively regulate stem cell function in other ways, with complex and context-dependent consequences for aging.

Care-Taking Tumor Suppressors and Genomic Integrity

Care-taking tumor suppressors, including DNA repair pathway components, promote stem cell function and tissue regeneration by maintaining genomic integrity (Kinzler and Vogelstein, 1997). Various forms of DNA damage accumulate throughout life as a result of DNA replication errors, exposure to endogenous mutagens such as reactive oxygen species (ROS), and exposure to exogenous mutagens such as UV light. To attenuate the accumulation of mutations, a DNA damage response network can sense DNA damage and activate a variety of repair mechanisms, including nucleotide excision repair, mismatch repair, nonhomologous end joining, and homologous recombination (Ciccia and Elledge, 2010). Activation of the DNA damage response network can transiently halt the cell cycle and repair damaged DNA through p53-dependent mechanisms. If the damage is too extensive to be repaired, the network can trigger the onset of senescence or cell death to eliminate the cells. Abundant cell death and senescence, however, can lead to tissue degeneration. Alternatively, unrepaired DNA damage can lead to the development of cancer, the incidence of which rises dramatically with age.

DNA repair pathway components thus delay cellular aging by maintaining genomic integrity. A number of single gene mutations that impair DNA repair cause segmental progeria syndromes. Segmental progeria syndromes are rare human diseases defined by reduced life span and premature aging phenotypes, including cataracts, osteoporosis, skin atrophy, hair graying, heart disease, cancer, cerebellum degeneration, and immunodeficiency. Segmental progeria syndromes caused by defects in DNA repair include Werner syndrome, a recessive trait caused by loss of function in the RecQ DNA helicase WRN, and Ataxia Telangiectasia, a recessive trait caused by loss of function in the DNA damage signaling protein ATM (Martin, 2005). Mice engineered to carry mutations in the genes associated with human progeroid syndromes similarly display phenotypes consistent with accelerated aging (Wong et al., 2003; Chang et al., 2004). The observation that progeria syndromes are frequently caused by defects in DNA repair suggests that DNA damage may be a fundamental underlying cause of aging.

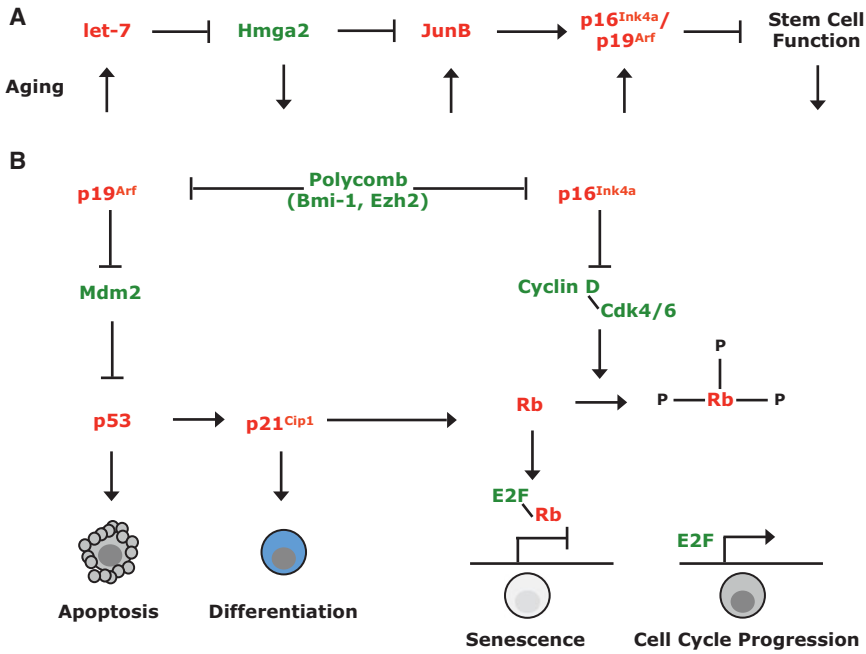

Figure 2. Heterochronic Genes Regulate Increases in the Expression of Gate-Keeping Tumor Suppressors and Declines in Aging Stem Cell Function

Stem cell self-renewal and stem cell aging are regulated by networks of proto-oncogenes (green) and tumor suppressors (red).

(A) *let-7* microRNA is an evolutionarily conserved heterochronic gene that regulates the timing of developmental events from *C. elegans* to mammals (Pasquinelli et al., 2000). *let-7b* expression increases with age in mammals, reducing the expression of the Hmga2 chromatin-associated factor, and increasing the expression of the JunB, $p16^{Ink4a}$, and $p19^{Arf}$ tumor suppressors (Nishino et al., 2008). The increase in $p16^{Ink4a}$ expression during aging reduces stem cell function in multiple tissues (Janzen et al., 2006; Krishnamurthy et al., 2006; Molofsky et al., 2006). *let-7* microRNA also increases with age in *Drosophila*, acting in the niche to non-cell-autonomously reduce spermatogonial stem cell function by impairing the secretion of Unpaired (Toledano et al., 2012).

(B) $p16^{Ink4a}$ and $p19^{Arf}$ expression are also repressed in mammalian stem cells by polycomb proteins, including Bmi-1 and Ezh2 (Jacobs et al., 1999; Lessard and Sauvageau, 2003; Molofsky et al., 2003; Park et al., 2003; Chen et al., 2009b). In the absence of Bmi-1, $p16^{Ink4a}$ and $p19^{Arf}$ expression are induced in postnatal stem cells from multiple tissues, inducing cell death, cellular senescence, or premature differentiation. These pathways illustrate how networks of proto-oncogenes and tumor suppressors regulate stem cell maintenance and homeostasis in adult tissues. The way in which proto-oncogenic and tumor suppressor signals are balanced within these networks changes with age in stem cells.

Mice with loss-of-function mutations in DNA repair pathway components exhibit stem cell defects in multiple tissues. Loss of the DNA damage sensor ATM depletes HSCs (Ito et al., 2004), exacerbates the loss of melanocyte stem cells in response to low dose radiation (Inomata et al., 2009), and promotes the loss of undifferentiated spermatogonia (Takubo et al., 2008). Loss of a related DNA damage sensor, ATR, depletes HSCs and hair follicle stem cells (Ruzankina et al., 2007). Mice deficient in nucleotide excision repair (Xpd^{TTD}), mismatch repair ($Msh2^{-/-}$), nonhomologous end joining (*Lig4*(Y288C) and $Ku80^{-/-}$), or homologous recombination ($Brca2^{-/-}$) all exhibit reduced HSC function (Reese et al., 2003; Navarro et al., 2006; Nijnik et al., 2007; Rossi et al., 2007). The mechanism by which deficiency for DNA repair genes depletes stem cells involves accumulation of DNA damage, induction of p53 and $p21^{cip1}$ (Merritt et al., 1994; Choudhury et al., 2007; Takubo et al., 2008; Begus-Nahrmann et al., 2009), elevated ROS levels (Ito et al., 2004), and premature differentiation (Inomata et al., 2009; Wang et al., 2012).

DNA damage accumulates with age in HSCs and epidermal stem cells from mice (Rossi et al., 2007; Sotiropoulou et al., 2010). It remains to be determined whether the amount of DNA damage that accumulates with age in normal stem cells actually contributes to declines in stem cell function under physiological conditions. However, DNA damage in stem cells may nonetheless have profound consequences. Most somatic cells are postmitotic and are therefore unlikely to be transformed into cancer cells by mutations or to pass their mutations onto progeny. Most dividing cells are short-lived and therefore produce a limited number of progeny or do not persist long enough to accumulate mutations over time. In contrast, stem cells remain mitotically active throughout life, generating large numbers of progeny in some tissues. Given that transformation of normal cells into cancer cells requires a series of mutations that accumulate over a period of years, the ability of stem cells to accumulate mutations and then expand the pool of mutated cells may be critical for the evolution of cancer in regenerative tissues (Rossi et al., 2008). Nonetheless, this does not mean that most cancers arise from stem cells. Even if most carcinogenic mutations accumulate in stem cells, the final mutation that causes frank transformation may occur in the numerically expanded restricted progenitors or differentiated cells that arise from stem cells.

Telomeres

Telomeres are specialized nucleoprotein caps that contain thousands of base pairs of repetitive DNA sequences that protect the ends of chromosomes from end-to-end fusions that induce DNA damage responses (Palm and de Lange, 2008; Sahin and Depinho, 2010). Because of the way DNA is replicated, telomeres shorten with each round of cell division such that the replicative potential of cells is limited by the length of their telomeres, unless the cells express telomerase, which can lengthen telomeres and increase replicative capacity. Telomeres shorten with age in many human cells, including HSCs (Vaziri et al., 1994, and references therein). When telomeres reach a critically short length, cells can exhibit genomic instability and undergo cell cycle arrest, senescence, or apoptosis (Chin et al., 1999; Choudhury et al., 2007; Begus-Nahrmann et al., 2009; Sperka et al., 2012). In addition to protecting against genomic instability, p53 activation following telomere dysfunction also impairs mitochondrial biogenesis, mitochondrial activity, and metabolic function (Sahin et al., 2011). It has been proposed that cellular aging

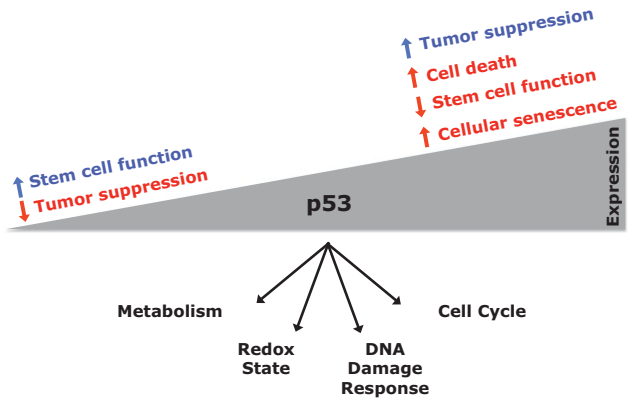

Figure 3. The Multifaceted and Context-Dependent Effects of p53 in Stem Cells

The consequences of tumor suppressor expression in stem cells can be context dependent. p53 can have both positive (blue) and negative (red) effects on stem cell function, depending on context and expression level. When expressed at low levels, p53 can promote stem cell maintenance by promoting the maintenance of genomic integrity and by regulating metabolism. When expressed at high levels, p53 can promote stem cell depletion through cell death or cellular senescence. The aggregate effect of these functions influences longevity, cancer incidence, and tissue regeneration during aging (Tyner et al., 2002; TeKippe et al., 2003; van Heemst et al., 2005; Dumble et al., 2007; Schoppy et al., 2010; Gannon et al., 2011).

is determined partly by telomere erosion, and partly by the DNA damage and loss of replicative potential that ensue (Harley et al., 1992).

Most human cells do not express telomerase, though telomerase is commonly expressed in cancer cells and other immortalized cells (Kim et al., 1994). Loss of telomerase function in mice reduces the regenerative capacity of proliferative organs (Lee et al., 1998), accelerates the development of aging phenotypes (like hair graying), reduces life span, and increases cancer incidence (particularly in the absence of p53) (Blasco et al., 1997; Rudolph et al., 1999; Artandi et al., 2000). Telomerase-deficient mice exhibit defects in stem cell function in the forebrain, epidermis, intestinal epithelium, and hematopoietic system through cell-autonomous (Lee et al., 1998; Allsopp et al., 2003; Choudhury et al., 2007; Ferrón et al., 2009; Jaskelioff et al., 2011) and non-cell-autonomous effects on stem cells (Ju et al., 2007). HSCs express telomerase (Morrison et al., 1996a), slowing, but not eliminating, the decline in telomere length with age (Vaziri et al., 1994). An important caveat is that profound defects are not apparent in germline telomerase-deficient mice for three generations after they are generated because inbred mice have relatively long telomeres (Kipling and Cooke, 1990). This suggests that telomerase is not required during a single generation in inbred mice under normal circumstances. In contrast, telomere length in young zebra finches is predictive of life span (Heidinger et al., 2012), suggesting that telomere length may limit life span in some species. This raises the question of whether telomere length limits proliferative potential during a normal human life span or whether telomere length only becomes limiting in the context of conditions that promote chronic tissue regeneration.

Defects in human telomerase function cause diseases with features of premature aging, including impaired regeneration of proliferative tissues (Lansdorp, 2009). Dyskeratosis congenita is a rare form of ectodermal dysplasia caused by very short telomeres that result from loss-of-function mutations in telomerase components or telomere binding proteins (reviewed by Walne and Dokal, 2009). Indeed, loss-of-function mutations in only a single copy of telomerase lead to accelerated telomere shortening and reduced tissue regeneration (Hao et al., 2005). Accelerated shortening of telomeres has also been observed in other conditions with premature aging phenotypes, including trisomy 21 (Vaziri et al., 1993). Telomere preservation is thus a key aspect of genomic integrity in which defects impair regeneration and accelerate aging.

Oxygen, Energy Metabolism, and ROS

Aging is proposed to result from cellular damage caused by free radicals, principally ROS generated as a consequence of oxidative phosphorylation in the mitochondrial electron transport chain (Wallace, 2005). ROS, such as superoxide and hydroxyl radical, are highly reactive and can damage mitochondrial and nuclear DNA, as well as proteins and lipids, by chemically modifying them. Oxidized macromolecules, such as 8-hydroxy-2-deoxyguanosine, accumulate with age in rats (Fraga et al., 1990). Increased expression of enzymes such as superoxide dismutases or catalase, which convert ROS into less reactive or nonreactive species, reduce the accumulation of oxidized macromolecules, increase maximum life span, and decrease the incidence of certain diseases of aging, including cancer (Wallace, 2005).

Stem cells appear to be particularly sensitive to elevated ROS levels. Under normal conditions, ROS can function as signaling molecules that regulate the differentiation of stem/progenitor cells, such as in *Drosophila* hematopoietic cells (Owusu-Ansah and Banerjee, 2009). However, ROS levels increase in HSCs with age, and prolonged treatment with the antioxidant N-acetyl-L-cysteine increases the replicative potential of HSCs upon serial transplantation in irradiated mice (Ito et al., 2006). Overexpression of superoxide dismutase in either stem cells or their supporting cells in the niche can prolong stem cell function during aging, as shown by work performed in the *Drosophila* ovary (Pan et al., 2007b).

Although the consequences of elevated ROS for stem cell function have been widely studied, we have only glimpses of how ROS levels are regulated in stem cells. FoxO transcription factors regulate metabolism and oxidative stress, partly by promoting the expression of antioxidant enzymes (Salih and Brunet, 2008). Conditional deletion of *FoxO1*, *FoxO3*, and *FoxO4* in mice increases ROS levels and depletes HSCs and neural stem cells (Tothova et al., 2007; Paik et al., 2009). Treatment with N-acetyl-L-cysteine partially rescues the stem cell defects in these mice. FoxO3 appears to be particularly important, because deficiency for *FoxO3* alone leads to oxidative stress and depletion of HSCs and neural stem cells (Miyamoto et al., 2007; Yalcin et al., 2008; Renault et al., 2009). Multiple other mechanisms promote stem cell maintenance at least partly by regulating oxidative stress, including the transcription factor Prdm16 (Chuikov et al., 2010), the polycomb family chromatin regulator, Bmi-1 (Liu et al., 2009a), and the DNA damage signaling molecule ATM (Ito et al., 2004; Maryanovich et al., 2012). There are likely to be many additional transcriptional

and metabolic mechanisms that influence the generation and response to ROS.

Consistent with the sensitivity of stem cells to ROS, responses to oxygen levels and mitochondrial function are highly regulated in stem cells. The Hypoxia inducible factor 1α (*Hif1α*) transcription factor regulates stem cell function and aging. Under normoxic conditions, the E3 ubiquitin ligase von Hippel Lindau (VHL) targets Hif1α for degradation (Majmundar et al., 2010). However, Hif1α is stabilized in low oxygen conditions, activating the transcription of heat shock proteins, glucose transporters, and glycolytic enzymes that allow a cell to survive in a low oxygen environment. Some hematopoietic and neural stem cells are thought to reside in hypoxic microenvironments (Parmar et al., 2007), and Hif1α is stabilized within these cells to promote their maintenance. Deficiency for *Hif1α* depletes neurogenic progenitors in the dentate gyrus and HSCs during aging (Mazumdar et al., 2010; Takubo et al., 2010). However, increased stabilization of Hif1α by reduced VHL function also impairs HSC function, suggesting that Hif1α levels must be tightly controlled for stem cell maintenance (Takubo et al., 2010).

Mitochondrial function is regulated in concert with ROS levels. For example, the PGC-1 transcriptional coactivator is a potent activator of mitochondrial biogenesis and oxidative phosphorylation (Puigserver et al., 1998). To avoid inducing oxidative stress, PGC-1 also promotes the expression of ROS-detoxifying enzymes, including GPx1 and SOD2 (St-Pierre et al., 2006). Overexpression of PGC-1 in *Drosophila* intestinal stem cells is sufficient to increase life span in flies, delaying age-related changes in the intestine and improving tissue homeostasis during aging (Rera et al., 2011). The authors of this study speculated that PGC-1 function within stem cells may be an important determinant of aging and longevity. This idea has not yet been tested in mammals.

Defects in mitochondrial function, such as those caused by an error-prone mitochondrial DNA polymerase, can also accelerate aging phenotypes and reduce life span (Trifunovic et al., 2004). The progeroid phenotypes in these mice include defects in the function of hematopoietic and neural progenitors that can be partially rescued by N-acetyl-L-cysteine treatment (Norddahl et al., 2011; Ahlqvist et al., 2012). But while these studies demonstrate that mitochondrial defects can lead to phenotypes that are reminiscent of premature aging, they do not necessarily demonstrate that mutations to mitochondrial DNA are a mechanism underlying physiological aging because the rate of mitochondrial DNA mutations in aging wild-type mice is 500-fold lower than in the mitochondrial mutator mice (Vermulst et al., 2007).

Non-Cell-Autonomous Regulation of Cellular Aging

Extrinsic factors in the stem cell microenvironment regulate stem cell aging. Stem cells typically reside in specialized microenvironments that promote stem cell maintenance and regulate stem cell function (Morrison and Spradling, 2008). Aging of the niche cells can cause changes in stem cell function. In *Drosophila*, the number of germline stem cells, their mitotic activity, and the number of progeny all decline with age due to both cell autonomous and non-cell-autonomous changes (Wallenfang et al., 2006; Pan et al., 2007b). In the male testis, these changes are partially caused by changes within the niche, as hub cells from older animals express reduced levels of DE-cadherin and Unpaired, both of which are necessary for germline stem cell maintenance (Boyle et al., 2007). Reduced Unpaired expression is caused partly by an increase in mRNA degradation from *let-7*-targeting of IGF-II messenger RNA binding protein (IMP) expression in aging hub cells (Toledano et al., 2012). Overexpression of Unpaired in the hub cells of older males rescues the age-related decline in germline stem cell frequency (Boyle et al., 2007). Similarly, in the *Drosophila* ovary, E-cadherin and BMP expression within the niche decline with age, and genetically increasing expression can enhance the function of old stem cells (Pan et al., 2007b).

Work on muscle stem cells (a subpopulation of satellite cells) suggests that similar age-related changes in the microenvironment within mammalian tissues, as well as in circulation, reduce somatic stem cell function. Aging is associated with a reduced capacity for muscle regeneration after injury, partly as a result of reduced expression of Notch ligand by satellite muscle cells, which reduces satellite cell proliferation after injury (Conboy et al., 2003). Aging muscles also produce elevated levels of TGF-β, which impedes regeneration and satellite cell proliferation (Carlson et al., 2008). However, exposure of old mice to young systemic factors by making old and young mice parabiotic can rejuvenate stem cell function (Conboy et al., 2005). Exposure of satellite cells from old mice to serum from young mice increases Notch ligand expression and proliferation (Conboy et al., 2005). This demonstrates that age-related changes in stem cells are partially reversible and influenced by circulating factors that change with age.

A combination of cell-autonomous and non-cell-autonomous mechanisms regulate the aging of stem cells in other tissues as well. Within the nervous system astrocytes and neural stem cells in the dentate gyrus promote the self-renewal of stem cells and the expansion of neuroblasts by secreting Wnts (Song et al., 2002; Lie et al., 2005). Expression of the Wnt antagonist Dkk1 increases in the aging dentate gyrus, and conditional deletion of *Dkk1* from neural stem and progenitor cells increases neural stem cell self-renewal, neurogenesis, and spatial learning and memory in old mice (Seib et al., 2013).

Circulating blood-borne factors also regulate changes in stem cell function in the aging central nervous system where stem cell frequency, overall mitotic activity, and rates of neurogenesis decline profoundly with age in the mouse forebrain (Kuhn et al., 1996; Maslov et al., 2004; Molofsky et al., 2006). In heterochronic parabionts, rates of neurogenesis and other measures of neural function decline in the young parabiont and increase in the old parabiont (Villeda et al., 2011). These effects appear to be partially explained by an age-related increase in the level of CCL11 chemokine in the plasma, which is sufficient to reduce neurogenesis, learning, and memory when administered to young mice. Heterochronic parabiosis also enhances the rate of remyelination after experimentally induced demyelination in old mice, a process that normally declines with age (Ruckh et al., 2012). The enhanced remyelination is associated with the recruitment of blood monocytes from the young parabiont, suggesting that the young circulating agents that enhance the regeneration of aging tissues can be cellular as well as soluble factors.

The circulating hormones insulin and insulin-like growth factor 1 (Igf1) also regulate aging and stem cells. The insulin/Igf1

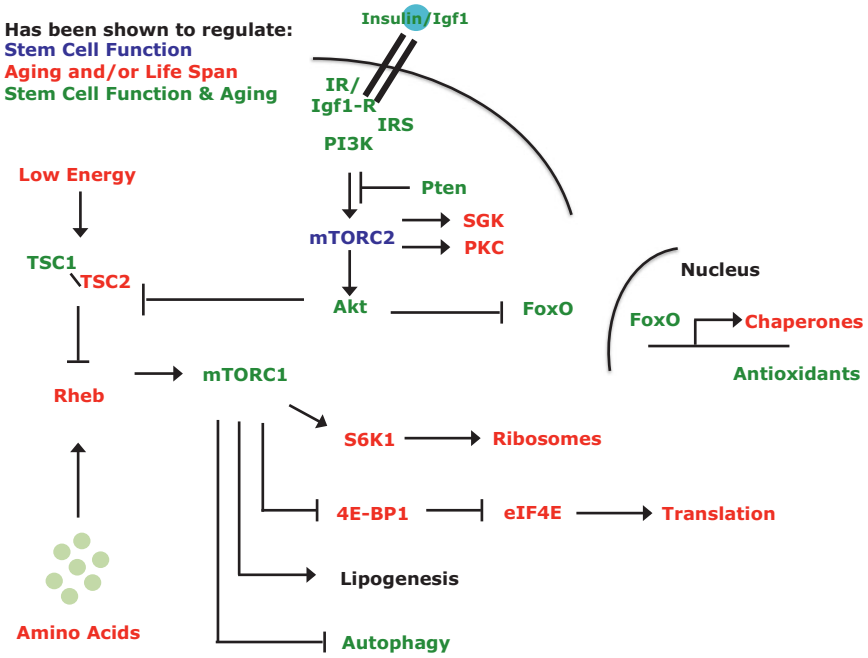

Figure 4. Many Components of the Insulin/PI3K Signaling Pathway Regulate Stem Cell Function and Aging

A variety of tyrosine kinase receptors, including the insulin receptor, activate the PI3K pathway, which leads to the activation of both mTORC1 and mTOCR2 (Laplante and Sabatini, 2012). mTORC2 can phosphorylate and activate Akt, SGK, and protein kinase C (PKC). Activated Akt can phosphorylate FoxO transcription factors, restricting their localization to the cytosol. FoxOs that translocate to the nucleus can transcriptionally activate the expression of a variety of genes, including protein folding chaperones, antioxidant enzymes, and metabolic regulators (Salih and Brunet, 2008). Activated Akt can also activate mTORC1 by phosphorylating TSC2, which relieves the inhibitory effects of the TSC1/TSC2 complex on Rheb. mTORC1 activates mechanisms that promote protein translation and lipid and nucleic acid synthesis and inhibit autophagy. The components of these pathways that have not yet been studied in stem cells are likely to regulate stem cell function and perhaps even stem cell aging.

signaling pathway coordinates growth and development in response to nutrient availability by activating the phosphatidylinositol-3-kinase (PI3K) signaling pathway and inactivating FoxO transcription factors. In *C. elegans*, mutations in *daf-2* (an *IGFR* ortholog) or other downstream signaling components extend life span in a manner that depends upon *daf-16* (a *FoxO* ortholog) (Kenyon et al., 1993; Lin et al., 1997; Ogg et al., 1997). In *Drosophila*, reducing insulin signaling by ablating insulin receptors, insulin receptor substrates, insulin producing cells, or overexpression of *dFOXO* all extend life span (Clancy et al., 2001; Tatar et al., 2001; Broughton et al., 2005; Giannakou et al., 2007). Homozygosity for a polymorphism in *FOXO3A* is associated with longevity in humans (Willcox et al., 2008). Mice with reduced insulin or Igf1 signaling, systemically or only in certain tissues, all exhibit slowed aging and increased life span (Tatar et al., 2001). The ability of the insulin signaling pathway to regulate aging and life span is thus evolutionarily conserved (Tatar et al., 2003).

Insulin signaling is known to regulate stem cells, though stem cell aging in long-lived mutants has not yet been closely examined. In *Drosophila,* reduced insulin signaling leads to declines in germline stem cell proliferation and fecundity (LaFever and Drummond-Barbosa, 2005), though data on mammalian stem cells are surprisingly limited. It will be interesting to determine whether long-lived insulin pathway mutants have increased stem cell function and regenerative capacity in aging tissues.

The accumulation of senescent cells in aging tissues can also non-cell-autonomously affect the function of other cells. Senescence is a cellular state associated with an irreversible loss in the ability to divide. Senescent cells undergo a series of changes, including the secretion of inflammatory factors, growth regulators, proteases, and other signaling molecules (Coppé et al., 2010). These secreted factors affect other cells in the local environment, promoting senescence and inflammation and promoting or inhibiting tumor growth. Life-long clearance of senescent cells from adult mouse tissues resulting from genetic ablation of $p16^{Ink4a}$-expressing cells delays the onset of pathologies in multiple aging tissues (Baker et al., 2011). Clearance of senescent cells only late in life did not improve age-related pathologies but did attenuate their progression. This raises the question of the extent to which $p16^{Ink4a}$ non-cell-autonomously or cell-autonomously influences stem cell function in aging tissues.

Dietary Restriction and TOR Signaling

Dietary restriction, defined as reducing food intake below ad libitum (free feeding) levels without causing malnutrition, extends life span in certain contexts while also delaying the onset of age-related pathologies (Mair and Dillin, 2008). Dietary restriction can also increase stem cell function or slow the decline in stem cell function during aging in multiple tissues (Lee et al., 2000; Mair et al., 2010). Short-term dietary restriction increases the frequency and function of satellite cells in skeletal muscle of both young and old mice, partly by increasing mitochondrial content and promoting oxidative metabolism (Cerletti et al., 2012). In at least one short-lived mouse strain, dietary restriction attenuates age-related declines in HSC frequency and reconstituting activity (Chen et al., 2003). However, these effects of dietary restriction may not be universal. Life span extension was not observed in certain mouse strains (Harrison and Archer, 1987) and was observed in monkeys in one study (Colman et al., 2009) but not in another (Mattison et al., 2012).

The effects of dietary restriction on aging and life span are thought to occur partly through modulation of target of rapamycin (TOR) signaling (Figure 4). TOR is a conserved serine/threonine kinase that promotes protein synthesis and cellular growth and is activated by signals that sense nutrient, growth factor, amino acid, and energy availability (Laplante and Sabatini,

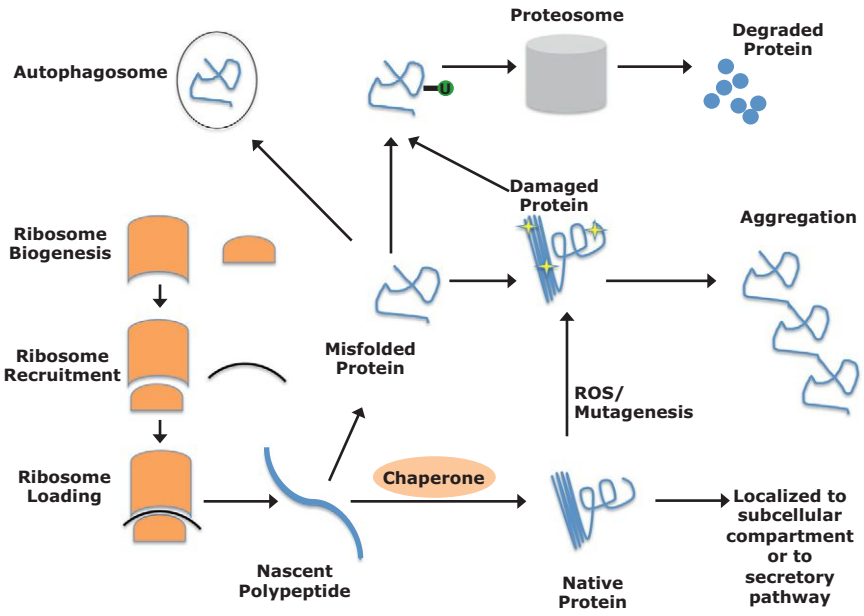

Figure 5. Proteostasis Is Required for Cellular Homeostasis during Aging

Proteostasis is regulated by protein translation rates, which are controlled by ribosome biogenesis, recruitment, and loading. Chaperones promote folding of nascent polypeptides or refolding of misfolded proteins to prevent protein aggregation. Misfolded or damaged proteins can be ubiquitylated and targeted for proteosomal degradation or engulfed and degraded by autophagosomes. Interventions that promote proteostasis can slow aging, reduce the incidence of age-related diseases, and increase life span (Cohen et al., 2009; Durieux et al., 2011; Taylor and Dillin, 2011). These mechanisms are likely to influence tissue regeneration and stem cell function during aging, but this remains largely unstudied.

2012). TOR is the kinase within at least two multiprotein complexes, TORC1 and TORC2, which contain the Raptor and Rictor binding partners, respectively (Laplante and Sabatini, 2012). Activated TORC1 promotes protein synthesis by phosphorylating ribosomal protein S6 kinase 1 (S6K1), which activates ribosome biogenesis partly by phosphorylating the ribosomal protein S6, and 4E-BP1, which frees eIF4E to bind 5′-capped mRNAs, recruiting them to the ribosomal initiation complex (Laplante and Sabatini, 2012) (Figure 4). In contrast, TORC2 promotes cell growth, proliferation, survival, and aspects of cellular metabolism by phosphorylating AKT (Sarbassov et al., 2005), SGK (García-Martínez and Alessi, 2008), and protein kinase C (Guertin et al., 2006) (Figure 4). TOR therefore has distinct functions in different signaling complexes.

Reduced TOR signaling, and TORC1 signaling in particular, can slow organismal aging and extend life span (Figure 4). In *C. elegans*, heterozygosity for the Raptor ortholog *daf-15* significantly increases maximum life span (Jia et al., 2004). Reducing the expression of various downstream targets of TORC1, such as *rsks-1* (an *S6K1* ortholog), *ifg-1* (*eIF4G* ortholog), and other translation initiation complex factors, also extend *C. elegans* life span (Hansen et al., 2007; Pan et al., 2007a). In mammals, reduced mammalian TOR (mTOR) signaling also extends life span, such as is observed upon feeding mice the mTORC1 inhibitor rapamycin (Harrison et al., 2009). The beneficial effects of rapamycin on longevity were evident even when treatment was initiated at 270 days of age, suggesting that interventions late in life can influence health and longevity. Mice that are deficient for *S6K1* also have increased life span and improved motor function, T cell abundance, bone volume, and insulin sensitivity in old age (Selman et al., 2009). TORC1 signaling is thus a key regulator of aging.

TOR also regulates stem cell function (Figure 4). Dietary restriction reduces mTOR signaling in Paneth cells (a component of the intestinal stem cell niche), which non-cell-autonomously increases the proliferation of intestinal stem cells (Yilmaz et al., 2012). Hyperactivation of mTORC1 and/or mTORC2 by deletion of *Pten* or *TSC1* aberrantly increases the proliferation of neural stem/progenitor cells (Groszer et al., 2001) and HSCs (Yilmaz et al., 2006; Zhang et al., 2006; Gan et al., 2008). However, hyperactivation of mTOR in vivo leads to the depletion of some adult neural stem cells (Bonaguidi et al., 2011) as well as HSCs through mTORC1 and mTORC2-dependent mechanisms (Lee et al., 2010; Kalaitzidis et al., 2012; Magee et al., 2012).

The studies described above would predict that reduced mTOR signaling should also attenuate the decline in stem cell function during aging. However, there remain little data on this point. One study reported that mTORC1 signaling is increased in HSCs isolated from old mice, and that age-related declines in HSC reconstituting activity and lymphoid differentiation could be rescued by rapamycin treatment (Chen et al., 2009a). However, rapamycin treatment also increases HSC frequency in young mice, raising questions about the extent to which these effects reflected a rescue of aging phenotypes. Additional studies examining the consequences of reduced mTOR signaling in young and old stem cells are needed to address its role in stem cell aging.

Proteostasis

A major challenge for aging cells is homeostasis of the proteome (proteostasis) (Taylor and Dillin, 2011). Misfolded or damaged proteins can disrupt membranes, form toxic aggregates, and cause cell death (Bucciantini et al., 2002). Several age-related diseases are associated with protein misfolding, including Alzheimer's disease, Parkinson's disease, and Huntington's disease (Ross and Poirier, 2004). Emerging evidence suggests that proteotoxic stress may be an underlying mechanism in metabolic disorders such as diabetes and a determinant of life span (Balch et al., 2008; Durieux et al., 2011; Vilchez et al., 2012b).

A complex network of cellular machinery regulates proteostasis by monitoring proteins throughout their life cycle (Figure 5). The rate at which proteins are produced is tightly controlled by stringent regulation of translation through control of ribosome biogenesis, ribosome recruitment, and ribosome loading

(Gebauer and Hentze, 2004). Protein folding and localization are regulated by molecular chaperones, which trap nascent proteins in tight binding pockets to assist folding, to prevent unwanted aggregation, and to protect them from thermal or oxidative stress (Hartl et al., 2011). Unneeded, misfolded, damaged, and aggregated proteins can be eliminated by the ubiquitin proteasome system (Finley, 2009) or through autophagy (Rubinsztein et al., 2011). Each of these proteostasis mechanisms are capable of eliminating damaged proteins or triggering a more global response, such as cell cycle arrest or apoptosis in the context of severe proteotoxic stress (Ron and Walter, 2007; Boulon et al., 2010).

The accumulation of damaged proteins during aging suggests that the capacity to regulate proteostasis declines with age. Protein damage can occur by misfolding, aggregation, glycation, carbonylation, or oxidation, or from translation errors, genetic mutations (Chiti et al., 2003), and reactive metabolites (Berlett and Stadtman, 1997). Mutations and damage from reactive metabolites accumulate with age. In addition, some proteostasis mechanisms are known to decline during aging, including the endoplasmic reticulum stress response (Ben-Zvi et al., 2009) and autophagy (Rubinsztein et al., 2011). Furthermore, interventions that promote proteostasis can slow aging, reduce the incidence of age-related diseases, and increase life span (Cohen et al., 2009; Durieux et al., 2011; Taylor and Dillin, 2011). Decreasing translation by reducing ribosomal protein levels in yeast increases replicative life span (Chiocchetti et al., 2007), and reduced expression of a variety of translation initiation factors increases life span in *C. elegans* (Pan et al., 2007a) and mammals (Selman et al., 2009).

Many mechanisms that regulate aging and proteostasis also regulate stem cells (Buckley et al., 2012; Vilchez et al., 2012a). Autophagy is likely to be important for HSC maintenance, because deletion of either *Atg7* (Mortensen et al., 2011) or Fip200 (Liu et al., 2010), both of which are necessary for autophagy, increases ROS levels and depletes HSCs. FoxO, which promotes longevity and stem cell function, transcriptionally activates the expression of multiple protein-folding chaperones (Murphy et al., 2003; Oh et al., 2006; Demontis and Perrimon, 2010), some of which regulate aging (Tatar et al., 1997; Walker and Lithgow, 2003; Morley and Morimoto, 2004); however, it is unclear to what extent the chaperones regulate stem cell function or stem cell aging. FOXO4 promotes proteasome activity in human embryonic stem cells, promoting proteostasis and maintenance of pluripotency (Vilchez et al., 2012a). In addition, mTOR is a potent activator of protein translation and inhibitor of autophagy (Laplante and Sabatini, 2012), but it is not clear to what extent these proteostasis pathways mediate the effects of mTOR on stem cell function or aging. It will be important to characterize the mechanisms that regulate proteostasis in stem cells to determine whether they differ from other cells and whether they influence changes in stem cell function during aging.

Conclusions

Many aspects of cellular physiology are regulated differently in stem cells as compared to other kinds of cells (He et al., 2009). Some regulators of stem cell self-renewal are broadly required by many types of dividing cells while other key self-renewal regulators do not regulate the proliferation of restricted progenitors in the same tissues. This suggests that some mechanisms that regulate stem cell aging may broadly regulate the aging of many cells, while other mechanisms will preferentially regulate stem cell aging. So far, the data suggest that the mechanisms that promote the onset of aging phenotypes in other cells (DNA damage, ROS, proteotoxicity, circulating factors from old mice, and telomere erosion) also reduce stem cell function in a manner that is consistent with premature aging, at least in certain tissues (Figure 1). Nonetheless, the details of how these mechanisms influence stem cells may differ from how they influence restricted progenitors and postmitotic cells. For example, gate-keeping tumor suppressors may regulate different cells in different ways, potentially slowing the onset of aging phenotypes in some cells while accelerating aging phenotypes in others. It is not surprising that such mechanisms would influence dividing and nondividing cells in different ways; however, there are also likely to be less obvious differences in how these mechanisms influence stem cells versus restricted progenitors.

There are also likely to be important undiscovered mechanisms, including those that preferentially regulate stem cell aging. For example, there is a centrosome orientation checkpoint in *Drosophila* that prevents spermatogonial stem cells from dividing unless the centrosomes align in a way that facilitates asymmetric division (Cheng et al., 2008). The frequency of stem cells with misaligned centrosomes increases with age, reducing stem cell activity and spermatogenesis. While this is a major cause of the physiological decline in spermatogenesis that occurs with age in flies it remains uncertain whether a similar checkpoint contributes to mammalian stem cell aging. This work illustrates the existence of previously unsuspected mechanisms that regulate declines in stem cell function with age, and that do not fit neatly into the themes emphasized by common theories of aging. Much work remains to be done to understand the mechanisms that regulate stem cell aging. Elucidating these mechanisms will be critical to understanding how regenerative capacity is preserved in certain tissues throughout adult life, and why that capacity declines with age.

ACKNOWLEDGMENTS

This work was supported by the Howard Hughes Medical Institute, the Cancer Prevention and Research Institute of Texas, and the National Institute on Aging (R37 AG024945). R.A.J.S. is supported by fellowships from the Leukemia & Lymphoma Society (5541-11) and the Canadian Institutes of Health Research (MFE-106993). We apologize to authors whose papers we could not cite due to space limitations.

REFERENCES

Ahlqvist, K.J., Hämäläinen, R.H., Yatsuga, S., Uutela, M., Terzioglu, M., Götz, A., Forsström, S., Salven, P., Angers-Loustau, A., Kopra, O.H., et al. (2012). Somatic progenitor cell vulnerability to mitochondrial DNA mutagenesis underlies progeroid phenotypes in Polg mutator mice. Cell Metab. *15*, 100–109.

Allsopp, R.C., Morin, G.B., DePinho, R., Harley, C.B., and Weissman, I.L. (2003). Telomerase is required to slow telomere shortening and extend replicative lifespan of HSCs during serial transplantation. Blood *102*, 517–520.

Ambros, V., and Horvitz, H.R. (1984). Heterochronic mutants of the nematode Caenorhabditis elegans. Science *226*, 409–416.

Artandi, S.E., Chang, S., Lee, S.L., Alson, S., Gottlieb, G.J., Chin, L., and DePinho, R.A. (2000). Telomere dysfunction promotes non-reciprocal translocations and epithelial cancers in mice. Nature *406*, 641–645.

Baker, D.J., Wijshake, T., Tchkonia, T., LeBrasseur, N.K., Childs, B.G., van de Sluis, B., Kirkland, J.L., and van Deursen, J.M. (2011). Clearance of p16Ink4a-positive senescent cells delays ageing-associated disorders. Nature *479*, 232–236.

Balch, W.E., Morimoto, R.I., Dillin, A., and Kelly, J.W. (2008). Adapting proteostasis for disease intervention. Science *319*, 916–919.

Begus-Nahrmann, Y., Lechel, A., Obenauf, A.C., Nalapareddy, K., Peit, E., Hoffmann, E., Schlaudraff, F., Liss, B., Schirmacher, P., Kestler, H., et al. (2009). p53 deletion impairs clearance of chromosomal-instable stem cells in aging telomere-dysfunctional mice. Nat. Genet. *41*, 1138–1143.

Ben-Zvi, A., Miller, E.A., and Morimoto, R.I. (2009). Collapse of proteostasis represents an early molecular event in Caenorhabditis elegans aging. Proc. Natl. Acad. Sci. USA *106*, 14914–14919.

Berlett, B.S., and Stadtman, E.R. (1997). Protein oxidation in aging, disease, and oxidative stress. J. Biol. Chem. *272*, 20313–20316.

Biteau, B., Karpac, J., Supoyo, S., Degennaro, M., Lehmann, R., and Jasper, H. (2010). Lifespan extension by preserving proliferative homeostasis in Drosophila. PLoS Genet. *6*, e1001159.

Blasco, M.A., Lee, H.W., Hande, M.P., Samper, E., Lansdorp, P.M., DePinho, R.A., and Greider, C.W. (1997). Telomere shortening and tumor formation by mouse cells lacking telomerase RNA. Cell *91*, 25–34.

Bonaguidi, M.A., Wheeler, M.A., Shapiro, J.S., Stadel, R.P., Sun, G.J., Ming, G.L., and Song, H. (2011). In vivo clonal analysis reveals self-renewing and multipotent adult neural stem cell characteristics. Cell *145*, 1142–1155.

Boulon, S., Westman, B.J., Hutten, S., Boisvert, F.M., and Lamond, A.I. (2010). The nucleolus under stress. Mol. Cell *40*, 216–227.

Boyle, M., Wong, C., Rocha, M., and Jones, D.L. (2007). Decline in self-renewal factors contributes to aging of the stem cell niche. Cell Stem Cell *1*, 470–478.

Broughton, S.J., Piper, M.D., Ikeya, T., Bass, T.M., Jacobson, J., Driege, Y., Martinez, P., Hafen, E., Withers, D.J., Leevers, S.J., and Partridge, L. (2005). Longer lifespan, altered metabolism, and stress resistance in Drosophila from ablation of cells making insulin-like ligands. Proc. Natl. Acad. Sci. USA *102*, 3105–3110.

Bucciantini, M., Giannoni, E., Chiti, F., Baroni, F., Formigli, L., Zurdo, J., Taddei, N., Ramponi, G., Dobson, C.M., and Stefani, M. (2002). Inherent toxicity of aggregates implies a common mechanism for protein misfolding diseases. Nature *416*, 507–511.

Buckley, S.M., Aranda-Orgilles, B., Strikoudis, A., Apostolou, E., Loizou, E., Moran-Crusio, K., Farnsworth, C.L., Koller, A.A., Dasgupta, R., Silva, J.C., et al. (2012). Regulation of pluripotency and cellular reprogramming by the ubiquitin-proteasome system. Cell Stem Cell *11*, 783–798.

Butler, A.E., Janson, J., Bonner-Weir, S., Ritzel, R., Rizza, R.A., and Butler, P.C. (2003). Beta-cell deficit and increased beta-cell apoptosis in humans with type 2 diabetes. Diabetes *52*, 102–110.

Campisi, J. (2005). Senescent cells, tumor suppression, and organismal aging: good citizens, bad neighbors. Cell *120*, 513–522.

Carlson, M.E., Hsu, M., and Conboy, I.M. (2008). Imbalance between pSmad3 and Notch induces CDK inhibitors in old muscle stem cells. Nature *454*, 528–532.

Cerletti, M., Jang, Y.C., Finley, L.W., Haigis, M.C., and Wagers, A.J. (2012). Short-term calorie restriction enhances skeletal muscle stem cell function. Cell Stem Cell *10*, 515–519.

Chambers, S.M., Shaw, C.A., Gatza, C., Fisk, C.J., Donehower, L.A., and Goodell, M.A. (2007). Aging hematopoietic stem cells decline in function and exhibit epigenetic dysregulation. PLoS Biol. *5*, e201.

Chang, S., Multani, A.S., Cabrera, N.G., Naylor, M.L., Laud, P., Lombard, D., Pathak, S., Guarente, L., and DePinho, R.A. (2004). Essential role of limiting telomeres in the pathogenesis of Werner syndrome. Nat. Genet. *36*, 877–882.

Chen, J., Astle, C.M., and Harrison, D.E. (2000). Genetic regulation of primitive hematopoietic stem cell senescence. Exp. Hematol. *28*, 442–450.

Chen, J., Astle, C.M., and Harrison, D.E. (2003). Hematopoietic senescence is postponed and hematopoietic stem cell function is enhanced by dietary restriction. Exp. Hematol. *31*, 1097–1103.

Chen, C., Liu, Y., Liu, Y., and Zheng, P. (2009a). mTOR regulation and therapeutic rejuvenation of aging hematopoietic stem cells. Sci. Signal. *2*, ra75.

Chen, H., Gu, X., Su, I.H., Bottino, R., Contreras, J.L., Tarakhovsky, A., and Kim, S.K. (2009b). Polycomb protein Ezh2 regulates pancreatic beta-cell Ink4a/Arf expression and regeneration in diabetes mellitus. Genes Dev. *23*, 975–985.

Cheng, J., Türkel, N., Hemati, N., Fuller, M.T., Hunt, A.J., and Yamashita, Y.M. (2008). Centrosome misorientation reduces stem cell division during ageing. Nature *456*, 599–604.

Chin, L., Artandi, S.E., Shen, Q., Tam, A., Lee, S.L., Gottlieb, G.J., Greider, C.W., and DePinho, R.A. (1999). p53 deficiency rescues the adverse effects of telomere loss and cooperates with telomere dysfunction to accelerate carcinogenesis. Cell *97*, 527–538.

Chiocchetti, A., Zhou, J., Zhu, H., Karl, T., Haubenreisser, O., Rinnerthaler, M., Heeren, G., Oender, K., Bauer, J., Hintner, H., et al. (2007). Ribosomal proteins Rpl10 and Rps6 are potent regulators of yeast replicative life span. Exp. Gerontol. *42*, 275–286.

Chiti, F., Stefani, M., Taddei, N., Ramponi, G., and Dobson, C.M. (2003). Rationalization of the effects of mutations on peptide and protein aggregation rates. Nature *424*, 805–808.

Choudhury, A.R., Ju, Z., Djojosubroto, M.W., Schienke, A., Lechel, A., Schaetzlein, S., Jiang, H., Stepczynska, A., Wang, C., Buer, J., et al. (2007). Cdkn1a deletion improves stem cell function and lifespan of mice with dysfunctional telomeres without accelerating cancer formation. Nat. Genet. *39*, 99–105.

Chuikov, S., Levi, B.P., Smith, M.L., and Morrison, S.J. (2010). Prdm16 promotes stem cell maintenance in multiple tissues, partly by regulating oxidative stress. Nat. Cell Biol. *12*, 999–1006.

Cicalese, A., Bonizzi, G., Pasi, C.E., Faretta, M., Ronzoni, S., Giulini, B., Brisken, C., Minucci, S., Di Fiore, P.P., and Pelicci, P.G. (2009). The tumor suppressor p53 regulates polarity of self-renewing divisions in mammary stem cells. Cell *138*, 1083–1095.

Ciccia, A., and Elledge, S.J. (2010). The DNA damage response: making it safe to play with knives. Mol. Cell *40*, 179–204.

Clancy, D.J., Gems, D., Harshman, L.G., Oldham, S., Stocker, H., Hafen, E., Leevers, S.J., and Partridge, L. (2001). Extension of life-span by loss of CHICO, a Drosophila insulin receptor substrate protein. Science *292*, 104–106.

Cohen, E., Paulsson, J.F., Blinder, P., Burstyn-Cohen, T., Du, D., Estepa, G., Adame, A., Pham, H.M., Holzenberger, M., Kelly, J.W., et al. (2009). Reduced IGF-1 signaling delays age-associated proteotoxicity in mice. Cell *139*, 1157–1169.

Colman, R.J., Anderson, R.M., Johnson, S.C., Kastman, E.K., Kosmatka, K.J., Beasley, T.M., Allison, D.B., Cruzen, C., Simmons, H.A., Kemnitz, J.W., and Weindruch, R. (2009). Caloric restriction delays disease onset and mortality in rhesus monkeys. Science *325*, 201–204.

Conboy, I.M., Conboy, M.J., Smythe, G.M., and Rando, T.A. (2003). Notch-mediated restoration of regenerative potential to aged muscle. Science *302*, 1575–1577.

Conboy, I.M., Conboy, M.J., Wagers, A.J., Girma, E.R., Weissman, I.L., and Rando, T.A. (2005). Rejuvenation of aged progenitor cells by exposure to a young systemic environment. Nature *433*, 760–764.

Coppé, J.P., Desprez, P.Y., Krtolica, A., and Campisi, J. (2010). The senescence-associated secretory phenotype: the dark side of tumor suppression. Annu. Rev. Pathol. *5*, 99–118.

de Haan, G., Nijhof, W., and Van Zant, G. (1997). Mouse strain-dependent changes in frequency and proliferation of hematopoietic stem cells during aging: correlation between lifespan and cycling activity. Blood *89*, 1543–1550.

Demontis, F., and Perrimon, N. (2010). FOXO/4E-BP signaling in Drosophila muscles regulates organism-wide proteostasis during aging. Cell *143*, 813–825.

Dillin, A., Hsu, A.L., Arantes-Oliveira, N., Lehrer-Graiwer, J., Hsin, H., Fraser, A.G., Kamath, R.S., Ahringer, J., and Kenyon, C. (2002). Rates of behavior and aging specified by mitochondrial function during development. Science *298*, 2398–2401.

Dorshkind, K., Montecino-Rodriguez, E., and Signer, R.A. (2009). The ageing immune system: is it ever too old to become young again? Nat. Rev. Immunol. *9*, 57–62.

Dumble, M., Moore, L., Chambers, S.M., Geiger, H., Van Zant, G., Goodell, M.A., and Donehower, L.A. (2007). The impact of altered p53 dosage on hematopoietic stem cell dynamics during aging. Blood *109*, 1736–1742.

Durieux, J., Wolff, S., and Dillin, A. (2011). The cell-non-autonomous nature of electron transport chain-mediated longevity. Cell *144*, 79–91.

Ferrón, S.R., Marqués-Torrejón, M.A., Mira, H., Flores, I., Taylor, K., Blasco, M.A., and Fariñas, I. (2009). Telomere shortening in neural stem cells disrupts neuronal differentiation and neuritogenesis. J. Neurosci. *29*, 14394–14407.

Finley, D. (2009). Recognition and processing of ubiquitin-protein conjugates by the proteasome. Annu. Rev. Biochem. *78*, 477–513.

Fraga, C.G., Shigenaga, M.K., Park, J.W., Degan, P., and Ames, B.N. (1990). Oxidative damage to DNA during aging: 8-hydroxy-2′-deoxyguanosine in rat organ DNA and urine. Proc. Natl. Acad. Sci. USA *87*, 4533–4537.

Gan, B., Sahin, E., Jiang, S., Sanchez-Aguilera, A., Scott, K.L., Chin, L., Williams, D.A., Kwiatkowski, D.J., and DePinho, R.A. (2008). mTORC1-dependent and -independent regulation of stem cell renewal, differentiation, and mobilization. Proc. Natl. Acad. Sci. USA *105*, 19384–19389.

Gannon, H.S., Donehower, L.A., Lyle, S., and Jones, S.N. (2011). Mdm2-p53 signaling regulates epidermal stem cell senescence and premature aging phenotypes in mouse skin. Dev. Biol. *353*, 1–9.

García-Cao, I., García-Cao, M., Martín-Caballero, J., Criado, L.M., Klatt, P., Flores, J.M., Weill, J.C., Blasco, M.A., and Serrano, M. (2002). "Super p53" mice exhibit enhanced DNA damage response, are tumor resistant and age normally. EMBO J. *21*, 6225–6235.

García-Martínez, J.M., and Alessi, D.R. (2008). mTOR complex 2 (mTORC2) controls hydrophobic motif phosphorylation and activation of serum- and glucocorticoid-induced protein kinase 1 (SGK1). Biochem. J. *416*, 375–385.

Gebauer, F., and Hentze, M.W. (2004). Molecular mechanisms of translational control. Nat. Rev. Mol. Cell Biol. *5*, 827–835.

Giannakou, M.E., Goss, M., Jacobson, J., Vinti, G., Leevers, S.J., and Partridge, L. (2007). Dynamics of the action of dFOXO on adult mortality in Drosophila. Aging Cell *6*, 429–438.

Groszer, M., Erickson, R., Scripture-Adams, D.D., Lesche, R., Trumpp, A., Zack, J.A., Kornblum, H.I., Liu, X., and Wu, H. (2001). Negative regulation of neural stem/progenitor cell proliferation by the Pten tumor suppressor gene in vivo. Science *294*, 2186–2189.

Guertin, D.A., Stevens, D.M., Thoreen, C.C., Burds, A.A., Kalaany, N.Y., Moffat, J., Brown, M., Fitzgerald, K.J., and Sabatini, D.M. (2006). Ablation in mice of the mTORC components raptor, rictor, or mLST8 reveals that mTORC2 is required for signaling to Akt-FOXO and PKCalpha, but not S6K1. Dev. Cell *11*, 859–871.

Hansen, M., Taubert, S., Crawford, D., Libina, N., Lee, S.J., and Kenyon, C. (2007). Lifespan extension by conditions that inhibit translation in Caenorhabditis elegans. Aging Cell *6*, 95–110.

Hao, L.Y., Armanios, M., Strong, M.A., Karim, B., Feldser, D.M., Huso, D., and Greider, C.W. (2005). Short telomeres, even in the presence of telomerase, limit tissue renewal capacity. Cell *123*, 1121–1131.

Harley, C.B., Vaziri, H., Counter, C.M., and Allsopp, R.C. (1992). The telomere hypothesis of cellular aging. Exp. Gerontol. *27*, 375–382.

Harrison, D.E., and Archer, J.R. (1987). Genetic differences in effects of food restriction on aging in mice. J. Nutr. *117*, 376–382.

Harrison, D.E., Strong, R., Sharp, Z.D., Nelson, J.F., Astle, C.M., Flurkey, K., Nadon, N.L., Wilkinson, J.E., Frenkel, K., Carter, C.S., et al. (2009). Rapamycin fed late in life extends lifespan in genetically heterogeneous mice. Nature *460*, 392–395.

Hartl, F.U., Bracher, A., and Hayer-Hartl, M. (2011). Molecular chaperones in protein folding and proteostasis. Nature *475*, 324–332.

He, S., Nakada, D., and Morrison, S.J. (2009). Mechanisms of stem cell self-renewal. Annu. Rev. Cell Dev. Biol. *25*, 377–406.

Heidinger, B.J., Blount, J.D., Boner, W., Griffiths, K., Metcalfe, N.B., and Monaghan, P. (2012). Telomere length in early life predicts lifespan. Proc. Natl. Acad. Sci. USA *109*, 1743–1748.

Hoeijmakers, J.H. (2009). DNA damage, aging, and cancer. N. Engl. J. Med. *361*, 1475–1485.

Inomata, K., Aoto, T., Binh, N.T., Okamoto, N., Tanimura, S., Wakayama, T., Iseki, S., Hara, E., Masunaga, T., Shimizu, H., and Nishimura, E.K. (2009). Genotoxic stress abrogates renewal of melanocyte stem cells by triggering their differentiation. Cell *137*, 1088–1099.

Ito, K., Hirao, A., Arai, F., Matsuoka, S., Takubo, K., Hamaguchi, I., Nomiyama, K., Hosokawa, K., Sakurada, K., Nakagata, N., et al. (2004). Regulation of oxidative stress by ATM is required for self-renewal of haematopoietic stem cells. Nature *431*, 997–1002.

Ito, K., Hirao, A., Arai, F., Takubo, K., Matsuoka, S., Miyamoto, K., Ohmura, M., Naka, K., Hosokawa, K., Ikeda, Y., and Suda, T. (2006). Reactive oxygen species act through p38 MAPK to limit the lifespan of hematopoietic stem cells. Nat. Med. *12*, 446–451.

Jacobs, J.J.L., Kieboom, K., Marino, S., DePinho, R.A., and van Lohuizen, M. (1999). The oncogene and Polycomb-group gene bmi-1 regulates cell proliferation and senescence through the ink4a locus. Nature *397*, 164–168.

Janzen, V., Forkert, R., Fleming, H.E., Saito, Y., Waring, M.T., Dombkowski, D.M., Cheng, T., DePinho, R.A., Sharpless, N.E., and Scadden, D.T. (2006). Stem-cell ageing modified by the cyclin-dependent kinase inhibitor p16INK4a. Nature *443*, 421–426.

Jaskelioff, M., Muller, F.L., Paik, J.H., Thomas, E., Jiang, S., Adams, A.C., Sahin, E., Kost-Alimova, M., Protopopov, A., Cadiñanos, J., et al. (2011). Telomerase reactivation reverses tissue degeneration in aged telomerase-deficient mice. Nature *469*, 102–106.

Jeck, W.R., Siebold, A.P., and Sharpless, N.E. (2012). Review: a meta-analysis of GWAS and age-associated diseases. Aging Cell *11*, 727–731.

Jia, K., Chen, D., and Riddle, D.L. (2004). The TOR pathway interacts with the insulin signaling pathway to regulate C. elegans larval development, metabolism and life span. Development *131*, 3897–3906.

Ju, Z., Jiang, H., Jaworski, M., Rathinam, C., Gompf, A., Klein, C., Trumpp, A., and Rudolph, K.L. (2007). Telomere dysfunction induces environmental alterations limiting hematopoietic stem cell function and engraftment. Nat. Med. *13*, 742–747.

Kalaitzidis, D., Sykes, S.M., Wang, Z., Punt, N., Tang, Y., Ragu, C., Sinha, A.U., Lane, S.W., Souza, A.L., Clish, C.B., et al. (2012). mTOR complex 1 plays critical roles in hematopoiesis and Pten-loss-evoked leukemogenesis. Cell Stem Cell *11*, 429–439.

Kamijo, T., Zindy, F., Roussel, M.F., Quelle, D.E., Downing, J.R., Ashmun, R.A., Grosveld, G., and Sherr, C.J. (1997). Tumor suppression at the mouse INK4a locus mediated by the alternative reading frame product p19ARF. Cell *91*, 649–659.

Kenyon, C., Chang, J., Gensch, E., Rudner, A., and Tabtiang, R. (1993). A C. elegans mutant that lives twice as long as wild type. Nature *366*, 461–464.

Kim, N.W., Piatzszek, M.A., Prowse, K.R., Harley, C.B., West, M.D., Ho, P.L.C., Coviello, G.M., Wright, W.E., Weinrich, S.L., and Shay, J.W. (1994). Specific association of human telomerase activity with immortal cells and cancer. Science *266*, 2011–2015.

Kinzler, K.W., and Vogelstein, B. (1997). Cancer-susceptibility genes. Gatekeepers and caretakers. Nature *386*, 761–763.

Kipling, D., and Cooke, H.J. (1990). Hypervariable ultra-long telomeres in mice. Nature *347*, 400–402.

Krishnamurthy, J., Torrice, C., Ramsey, M.R., Kovalev, G.I., Al-Regaiey, K., Su, L., and Sharpless, N.E. (2004). Ink4a/Arf expression is a biomarker of aging. J. Clin. Invest. *114*, 1299–1307.

Krishnamurthy, J., Ramsey, M.R., Ligon, K.L., Torrice, C., Koh, A., Bonner-Weir, S., and Sharpless, N.E. (2006). p16INK4a induces an age-dependent decline in islet regenerative potential. Nature *443*, 453–457.

Kuhn, H.G., Dickinson-Anson, H., and Gage, F.H. (1996). Neurogenesis in the dentate gyrus of the adult rat: age-related decrease of neuronal progenitor proliferation. J. Neurosci. *16*, 2027–2033.

LaFever, L., and Drummond-Barbosa, D. (2005). Direct control of germline stem cell division and cyst growth by neural insulin in Drosophila. Science *309*, 1071–1073.

Lansdorp, P.M. (2009). Telomeres and disease. EMBO J. *28*, 2532–2540.

Laplante, M., and Sabatini, D.M. (2012). mTOR signaling in growth control and disease. Cell *149*, 274–293.

Lee, H.W., Blasco, M.A., Gottlieb, G.J., Horner, J.W., 2nd, Greider, C.W., and DePinho, R.A. (1998). Essential role of mouse telomerase in highly proliferative organs. Nature *392*, 569–574.

Lee, J., Duan, W., Long, J.M., Ingram, D.K., and Mattson, M.P. (2000). Dietary restriction increases the number of newly generated neural cells, and induces BDNF expression, in the dentate gyrus of rats. J. Mol. Neurosci. *15*, 99–108.

Lee, J.Y., Nakada, D., Yilmaz, O.H., Tothova, Z., Joseph, N.M., Lim, M.S., Gilliland, D.G., and Morrison, S.J. (2010). mTOR activation induces tumor suppressors that inhibit leukemogenesis and deplete hematopoietic stem cells after Pten deletion. Cell Stem Cell *7*, 593–605.

Lessard, J., and Sauvageau, G. (2003). Bmi-1 determines the proliferative capacity of normal and leukaemic stem cells. Nature *423*, 255–260.

Lie, D.C, Colamarino, S.A., Song, H.J., Desire, L., Mira, H., Consiglio, A., Lein, E.S., Jessberger, S., Lansford, H., Dearie, A.R., and Gage, F.H. (2005). Wnt signalling regulates adult hippocampal neurogenesis. Nature *437*, 1370–1375.

Lin, K., Dorman, J.B., Rodan, A., and Kenyon, C. (1997). daf-16: An HNF-3/forkhead family member that can function to double the life-span of Caenorhabditis elegans. Science *278*, 1319–1322.

Liu, J., Cao, L., Chen, J., Song, S., Lee, I.H., Quijano, C., Liu, H., Keyvanfar, K., Chen, H., Cao, L.Y., et al. (2009a). Bmi1 regulates mitochondrial function and the DNA damage response pathway. Nature *459*, 387–392.

Liu, Y., Elf, S.E., Miyata, Y., Sashida, G., Liu, Y., Huang, G., Di Giandomenico, S., Lee, J.M., Deblasio, A., Menendez, S., et al. (2009b). p53 regulates hematopoietic stem cell quiescence. Cell Stem Cell *4*, 37–48.

Liu, F., Lee, J.Y., Wei, H., Tanabe, O., Engel, J.D., Morrison, S.J., and Guan, J.L. (2010). FIP200 is required for the cell-autonomous maintenance of fetal hematopoietic stem cells. Blood *116*, 4806–4814.

Liu, Y., Johnson, S.M., Fedoriw, Y., Rogers, A.B., Yuan, H., Krishnamurthy, J., and Sharpless, N.E. (2011). Expression of p16(INK4a) prevents cancer and promotes aging in lymphocytes. Blood *117*, 3257–3267.

Lu, T., Pan, Y., Kao, S.Y., Li, C., Kohane, I., Chan, J., and Yankner, B.A. (2004). Gene regulation and DNA damage in the ageing human brain. Nature *429*, 883–891.

Luckey, C.J., Bhattacharya, D., Goldrath, A.W., Weissman, I.L., Benoist, C., and Mathis, D. (2006). Memory T and memory B cells share a transcriptional program of self-renewal with long-term hematopoietic stem cells. Proc. Natl. Acad. Sci. USA *103*, 3304–3309.

Magee, J.A., Ikenoue, T., Nakada, D., Lee, J.Y., Guan, K.L., and Morrison, S.J. (2012). Temporal changes in PTEN and mTORC2 regulation of hematopoietic stem cell self-renewal and leukemia suppression. Cell Stem Cell *11*, 415–428.

Mair, W., and Dillin, A. (2008). Aging and survival: the genetics of life span extension by dietary restriction. Annu. Rev. Biochem. *77*, 727–754.

Mair, W., McLeod, C.J., Wang, L., and Jones, D.L. (2010). Dietary restriction enhances germline stem cell maintenance. Aging Cell *9*, 916–918.

Majmundar, A.J., Wong, W.J., and Simon, M.C. (2010). Hypoxia-inducible factors and the response to hypoxic stress. Mol. Cell *40*, 294–309.

Martin, G.M. (2005). Genetic modulation of senescent phenotypes in Homo sapiens. Cell *120*, 523–532.

Maryanovich, M., Oberkovitz, G., Niv, H., Vorobiyov, L., Zaltsman, Y., Brenner, O., Lapidot, T., Jung, S., and Gross, A. (2012). The ATM-BID pathway regulates quiescence and survival of haematopoietic stem cells. Nat. Cell Biol. *14*, 535–541.

Maslov, A.Y., Barone, T.A., Plunkett, R.J., and Pruitt, S.C. (2004). Neural stem cell detection, characterization, and age-related changes in the subventricular zone of mice. J. Neurosci. *24*, 1726–1733.

Matheu, A., Pantoja, C., Efeyan, A., Criado, L.M., Martín-Caballero, J., Flores, J.M., Klatt, P., and Serrano, M. (2004). Increased gene dosage of Ink4a/Arf results in cancer resistance and normal aging. Genes Dev. *18*, 2736–2746.

Matheu, A., Maraver, A., Klatt, P., Flores, I., Garcia-Cao, I., Borras, C., Flores, J.M., Viña, J., Blasco, M.A., and Serrano, M. (2007). Delayed ageing through damage protection by the Arf/p53 pathway. Nature *448*, 375–379.

Mattison, J.A., Roth, G.S., Beasley, T.M., Tilmont, E.M., Handy, A.M., Herbert, R.L., Longo, D.L., Allison, D.B., Young, J.E., Bryant, M., et al. (2012). Impact of caloric restriction on health and survival in rhesus monkeys from the NIA study. Nature *489*, 318–321.

Mazumdar, J., O'Brien, W.T., Johnson, R.S., LaManna, J.C., Chavez, J.C., Klein, P.S., and Simon, M.C. (2010). O2 regulates stem cells through Wnt/β-catenin signalling. Nat. Cell Biol. *12*, 1007–1013.

Merritt, A.J., Potten, C.S., Kemp, C.J., Hickman, J.A., Balmain, A., Lane, D.P., and Hall, P.A. (1994). The role of p53 in spontaneous and radiation-induced apoptosis in the gastrointestinal tract of normal and p53-deficient mice. Cancer Res. *54*, 614–617.

Miyamoto, K., Araki, K.Y., Naka, K., Arai, F., Takubo, K., Yamazaki, S., Matsuoka, S., Miyamoto, T., Ito, K., Ohmura, M., et al. (2007). Foxo3a is essential for maintenance of the hematopoietic stem cell pool. Cell Stem Cell *1*, 101–112.

Molofsky, A.V., Pardal, R., Iwashita, T., Park, I.K., Clarke, M.F., and Morrison, S.J. (2003). Bmi-1 dependence distinguishes neural stem cell self-renewal from progenitor proliferation. Nature *425*, 962–967.

Molofsky, A.V., Slutsky, S.G., Joseph, N.M., He, S., Pardal, R., Krishnamurthy, J., Sharpless, N.E., and Morrison, S.J. (2006). Increasing p16INK4a expression decreases forebrain progenitors and neurogenesis during ageing. Nature *443*, 448–452.

Morley, J.F., and Morimoto, R.I. (2004). Regulation of longevity in Caenorhabditis elegans by heat shock factor and molecular chaperones. Mol. Biol. Cell *15*, 657–664.

Morrison, S.J., and Spradling, A.C. (2008). Stem cells and niches: mechanisms that promote stem cell maintenance throughout life. Cell *132*, 598–611.

Morrison, S.J., Prowse, K.R., Ho, P., and Weissman, I.L. (1996a). Telomerase activity in hematopoietic cells is associated with self-renewal potential. Immunity *5*, 207–216.

Morrison, S.J., Wandycz, A.M., Akashi, K., Globerson, A., and Weissman, I.L. (1996b). The aging of hematopoietic stem cells. Nat. Med. *2*, 1011–1016.

Mortensen, M., Soilleux, E.J., Djordjevic, G., Tripp, R., Lutteropp, M., Sadighi-Akha, E., Stranks, A.J., Glanville, J., Knight, S., Jacobsen, S.E., et al. (2011). The autophagy protein Atg7 is essential for hematopoietic stem cell maintenance. J. Exp. Med. *208*, 455–467.

Murphy, C.T., McCarroll, S.A., Bargmann, C.I., Fraser, A., Kamath, R.S., Ahringer, J., Li, H., and Kenyon, C. (2003). Genes that act downstream of DAF-16 to influence the lifespan of Caenorhabditis elegans. Nature *424*, 277–283.

Navarro, S., Meza, N.W., Quintana-Bustamante, O., Casado, J.A., Jacome, A., McAllister, K., Puerto, S., Surrallés, J., Segovia, J.C., and Bueren, J.A. (2006). Hematopoietic dysfunction in a mouse model for Fanconi anemia group D1. Mol. Ther. *14*, 525–535.

Nijnik, A., Woodbine, L., Marchetti, C., Dawson, S., Lambe, T., Liu, C., Rodrigues, N.P., Crockford, T.L., Cabuy, E., Vindigni, A., et al. (2007). DNA repair is limiting for haematopoietic stem cells during ageing. Nature *447*, 686–690.

Nishimura, E.K., Granter, S.R., and Fisher, D.E. (2005). Mechanisms of hair graying: incomplete melanocyte stem cell maintenance in the niche. Science *307*, 720–724.

Nishino, J., Kim, I., Chada, K., and Morrison, S.J. (2008). Hmga2 promotes neural stem cell self-renewal in young but not old mice by reducing p16Ink4a and p19Arf Expression. Cell *135*, 227–239.

Norddahl, G.L., Pronk, C.J., Wahlestedt, M., Sten, G., Nygren, J.M., Ugale, A., Sigvardsson, M., and Bryder, D. (2011). Accumulating mitochondrial DNA mutations drive premature hematopoietic aging phenotypes distinct from physiological stem cell aging. Cell Stem Cell *8*, 499–510.

Ogg, S., Paradis, S., Gottlieb, S., Patterson, G.I., Lee, L., Tissenbaum, H.A., and Ruvkun, G. (1997). The Fork head transcription factor DAF-16 transduces insulin-like metabolic and longevity signals in C. elegans. Nature *389*, 994–999.

Oh, S.W., Mukhopadhyay, A., Dixit, B.L., Raha, T., Green, M.R., and Tissenbaum, H.A. (2006). Identification of direct DAF-16 targets controlling longevity, metabolism and diapause by chromatin immunoprecipitation. Nat. Genet. *38*, 251–257.

Owusu-Ansah, E., and Banerjee, U. (2009). Reactive oxygen species prime Drosophila haematopoietic progenitors for differentiation. Nature *461*, 537–541.

Paik, J.H., Ding, Z., Narurkar, R., Ramkissoon, S., Muller, F., Kamoun, W.S., Chae, S.S., Zheng, H., Ying, H., Mahoney, J., et al. (2009). FoxOs cooperatively regulate diverse pathways governing neural stem cell homeostasis. Cell Stem Cell *5*, 540–553.

Palm, W., and de Lange, T. (2008). How shelterin protects mammalian telomeres. Annu. Rev. Genet. *42*, 301–334.

Pan, K.Z., Palter, J.E., Rogers, A.N., Olsen, A., Chen, D., Lithgow, G.J., and Kapahi, P. (2007a). Inhibition of mRNA translation extends lifespan in Caenorhabditis elegans. Aging Cell *6*, 111–119.

Pan, L., Chen, S., Weng, C., Call, G., Zhu, D., Tang, H., Zhang, N., and Xie, T. (2007b). Stem cell aging is controlled both intrinsically and extrinsically in the Drosophila ovary. Cell Stem Cell *1*, 458–469.

Park, I.K., Qian, D., Kiel, M., Becker, M.W., Pihalja, M., Weissman, I.L., Morrison, S.J., and Clarke, M.F. (2003). Bmi-1 is required for maintenance of adult self-renewing haematopoietic stem cells. Nature *423*, 302–305.

Parmar, K., Mauch, P., Vergilio, J.A., Sackstein, R., and Down, J.D. (2007). Distribution of hematopoietic stem cells in the bone marrow according to regional hypoxia. Proc. Natl. Acad. Sci. USA *104*, 5431–5436.

Pasquinelli, A.E., Reinhart, B.J., Slack, F., Martindale, M.Q., Kuroda, M.I., Maller, B., Hayward, D.C., Ball, E.E., Degnan, B., Müller, P., et al. (2000). Conservation of the sequence and temporal expression of let-7 heterochronic regulatory RNA. Nature *408*, 86–89.

Puigserver, P., Wu, Z., Park, C.W., Graves, R., Wright, M., and Spiegelman, B.M. (1998). A cold-inducible coactivator of nuclear receptors linked to adaptive thermogenesis. Cell *92*, 829–839.

Reese, J.S., Liu, L., and Gerson, S.L. (2003). Repopulating defect of mismatch repair-deficient hematopoietic stem cells. Blood *102*, 1626–1633.

Renault, V.M., Rafalski, V.A., Morgan, A.A., Salih, D.A., Brett, J.O., Webb, A.E., Villeda, S.A., Thekkat, P.U., Guillerey, C., Denko, N.C., et al. (2009). FoxO3 regulates neural stem cell homeostasis. Cell Stem Cell *5*, 527–539.

Rera, M., Bahadorani, S., Cho, J., Koehler, C.L., Ulgherait, M., Hur, J.H., Ansari, W.S., Lo, T., Jr., Jones, D.L., and Walker, D.W. (2011). Modulation of longevity and tissue homeostasis by the Drosophila PGC-1 homolog. Cell Metab. *14*, 623–634.

Ron, D., and Walter, P. (2007). Signal integration in the endoplasmic reticulum unfolded protein response. Nat. Rev. Mol. Cell Biol. *8*, 519–529.

Ross, C.A., and Poirier, M.A. (2004). Protein aggregation and neurodegenerative disease. Nat. Med. Suppl. *10*, S10–S17.

Rossi, D.J., Bryder, D., Seita, J., Nussenzweig, A., Hoeijmakers, J., and Weissman, I.L. (2007). Deficiencies in DNA damage repair limit the function of haematopoietic stem cells with age. Nature *447*, 725–729.

Rossi, D.J., Jamieson, C.H., and Weissman, I.L. (2008). Stems cells and the pathways to aging and cancer. Cell *132*, 681–696.

Ruas, M., and Peters, G. (1998). The p16INK4a/CDKN2A tumor suppressor and its relatives. Biochim. Biophys. Acta *1378*, F115–F177.

Rubinsztein, D.C., Mariño, G., and Kroemer, G. (2011). Autophagy and aging. Cell *146*, 682–695.

Ruckh, J.M., Zhao, J.W., Shadrach, J.L., van Wijngaarden, P., Rao, T.N., Wagers, A.J., and Franklin, R.J. (2012). Rejuvenation of regeneration in the aging central nervous system. Cell Stem Cell *10*, 96–103.

Rudolph, K.L., Chang, S., Lee, H.W., Blasco, M., Gottlieb, G.J., Greider, C., and DePinho, R.A. (1999). Longevity, stress response, and cancer in aging telomerase-deficient mice. Cell *96*, 701–712.

Ruzankina, Y., Pinzon-Guzman, C., Asare, A., Ong, T., Pontano, L., Cotsarelis, G., Zediak, V.P., Velez, M., Bhandoola, A., and Brown, E.J. (2007). Deletion of the developmentally essential gene ATR in adult mice leads to age-related phenotypes and stem cell loss. Cell Stem Cell *1*, 113–126.

Ruzankina, Y., Schoppy, D.W., Asare, A., Clark, C.E., Vonderheide, R.H., and Brown, E.J. (2009). Tissue regenerative delays and synthetic lethality in adult mice after combined deletion of Atr and Trp53. Nat. Genet. *41*, 1144–1149.

Sahin, E., and Depinho, R.A. (2010). Linking functional decline of telomeres, mitochondria and stem cells during ageing. Nature *464*, 520–528.

Sahin, E., Colla, S., Liesa, M., Moslehi, J., Müller, F.L., Guo, M., Cooper, M., Kotton, D., Fabian, A.J., Walkey, C., et al. (2011). Telomere dysfunction induces metabolic and mitochondrial compromise. Nature *470*, 359–365.

Salih, D.A., and Brunet, A. (2008). FoxO transcription factors in the maintenance of cellular homeostasis during aging. Curr. Opin. Cell Biol. *20*, 126–136.

Sarbassov, D.D., Guertin, D.A., Ali, S.M., and Sabatini, D.M. (2005). Phosphorylation and regulation of Akt/PKB by the rictor-mTOR complex. Science *307*, 1098–1101.

Schoppy, D.W., Ruzankina, Y., and Brown, E.J. (2010). Removing all obstacles: a critical role for p53 in promoting tissue renewal. Cell Cycle *9*, 1313–1319.

Seib, D., Corsini, N.S., Ellwanger, K., Plaas, C., Mateos, A., Pitzer, C., Niehrs, C., Celikel, T., and Martin-Villalba, A. (2013). Loss of Dickkopf-1 restores neurogenesis in old age and counteracts cognitive decline. Cell Stem Cell *12,* this issue, 204–214.

Selman, C., Tullet, J.M., Wieser, D., Irvine, E., Lingard, S.J., Choudhury, A.I., Claret, M., Al-Qassab, H., Carmignac, D., Ramadani, F., et al. (2009). Ribosomal protein S6 kinase 1 signaling regulates mammalian life span. Science *326*, 140–144.

Serrano, M., Lee, H., Chin, L., Cordon-Cardo, C., Beach, D., and DePinho, R.A. (1996). Role of the INK4a locus in tumor suppression and cell mortality. Cell *85*, 27–37.

Sharpless, N.E., and DePinho, R.A. (2007). How stem cells age and why this makes us grow old. Nat. Rev. Mol. Cell Biol. *8*, 703–713.

Signer, R.A., Montecino-Rodriguez, E., Witte, O.N., and Dorshkind, K. (2008). Aging and cancer resistance in lymphoid progenitors are linked processes conferred by p16Ink4a and Arf. Genes Dev. *22*, 3115–3120.

Song, H., Stevens, C.F., and Gage, F.H. (2002). Astroglia induce neurogenesis from adult neural stem cells. Nature *417*, 39–44.

Sotiropoulou, P.A., Candi, A., Mascré, G., De Clercq, S., Youssef, K.K., Lapouge, G., Dahl, E., Semeraro, C., Denecker, G., Marine, J.C., and Blanpain, C. (2010). Bcl-2 and accelerated DNA repair mediates resistance of hair follicle bulge stem cells to DNA-damage-induced cell death. Nat. Cell Biol. *12*, 572–582.

Sperka, T., Song, Z., Morita, Y., Nalapareddy, K., Guachalla, L.M., Lechel, A., Begus-Nahrmann, Y., Burkhalter, M.D., Mach, M., Schlaudraff, F., et al. (2012). Puma and p21 represent cooperating checkpoints limiting self-renewal and chromosomal instability of somatic stem cells in response to telomere dysfunction. Nat. Cell Biol. *14*, 73–79.

St-Pierre, J., Drori, S., Uldry, M., Silvaggi, J.M., Rhee, J., Jäger, S., Handschin, C., Zheng, K., Lin, J., Yang, W., et al. (2006). Suppression of reactive oxygen species and neurodegeneration by the PGC-1 transcriptional coactivators. Cell *127*, 397–408.

Takubo, K., Ohmura, M., Azuma, M., Nagamatsu, G., Yamada, W., Arai, F., Hirao, A., and Suda, T. (2008). Stem cell defects in ATM-deficient undifferentiated spermatogonia through DNA damage-induced cell-cycle arrest. Cell Stem Cell *2*, 170–182.

Takubo, K., Goda, N., Yamada, W., Iriuchishima, H., Ikeda, E., Kubota, Y., Shima, H., Johnson, R.S., Hirao, A., Suematsu, M., and Suda, T. (2010). Regulation of the HIF-1alpha level is essential for hematopoietic stem cells. Cell Stem Cell *7*, 391–402.

Tatar, M., Khazaeli, A.A., and Curtsinger, J.W. (1997). Chaperoning extended life. Nature *390*, 30.

Tatar, M., Kopelman, A., Epstein, D., Tu, M.P., Yin, C.M., and Garofalo, R.S. (2001). A mutant Drosophila insulin receptor homolog that extends life-span and impairs neuroendocrine function. Science *292*, 107–110.

Tatar, M., Bartke, A., and Antebi, A. (2003). The endocrine regulation of aging by insulin-like signals. Science *299*, 1346–1351.

Taylor, R.C., and Dillin, A. (2011). Aging as an event of proteostasis collapse. Cold Spring Harb. Perspect. Biol. *3*, 3.

TeKippe, M., Harrison, D.E., and Chen, J. (2003). Expansion of hematopoietic stem cell phenotype and activity in Trp53-null mice. Exp. Hematol. *31*, 521–527.

Teta, M., Long, S.Y., Wartschow, L.M., Rankin, M.M., and Kushner, J.A. (2005). Very slow turnover of beta-cells in aged adult mice. Diabetes *54*, 2557–2567.

Toledano, H., D'Alterio, C., Czech, B., Levine, E., and Jones, D.L. (2012). The let-7-Imp axis regulates ageing of the Drosophila testis stem-cell niche. Nature *485*, 605–610.

Tothova, Z., Kollipara, R., Huntly, B.J., Lee, B.H., Castrillon, D.H., Cullen, D.E., McDowell, E.P., Lazo-Kallanian, S., Williams, I.R., Sears, C., et al. (2007). FoxOs are critical mediators of hematopoietic stem cell resistance to physiologic oxidative stress. Cell *128*, 325–339.

Trifunovic, A., Wredenberg, A., Falkenberg, M., Spelbrink, J.N., Rovio, A.T., Bruder, C.E., Bohlooly-Y, M., Gidlöf, S., Oldfors, A., Wibom, R., et al. (2004). Premature ageing in mice expressing defective mitochondrial DNA polymerase. Nature *429*, 417–423.

Tyner, S.D., Venkatachalam, S., Choi, J., Jones, S., Ghebranious, N., Igelmann, H., Lu, X., Soron, G., Cooper, B., Brayton, C., et al. (2002). p53 mutant mice that display early ageing-associated phenotypes. Nature *415*, 45–53.

van Heemst, D., Mooijaart, S.P., Beekman, M., Schreuder, J., de Craen, A.J., Brandt, B.W., Slagboom, P.E., and Westendorp, R.G.; Long Life study group. (2005). Variation in the human TP53 gene affects old age survival and cancer mortality. Exp. Gerontol. *40*, 11–15.

Vaziri, H., Schächter, F., Uchida, I., Wei, L., Zhu, X., Effros, R., Cohen, D., and Harley, C.B. (1993). Loss of telomeric DNA during aging of normal and trisomy 21 human lymphocytes. Am. J. Hum. Genet. *52*, 661–667.

Vaziri, H., Dragowska, W., Allsopp, R.C., Thomas, T.E., Harley, C.B., and Lansdorp, P.M. (1994). Evidence for a mitotic clock in human hematopoietic stem cells: loss of telomeric DNA with age. Proc. Natl. Acad. Sci. USA *91*, 9857–9860.

Vermulst, M., Bielas, J.H., Kujoth, G.C., Ladiges, W.C., Rabinovitch, P.S., Prolla, T.A., and Loeb, L.A. (2007). Mitochondrial point mutations do not limit the natural lifespan of mice. Nat. Genet. *39*, 540–543.

Vilchez, D., Boyer, L., Morantte, I., Lutz, M., Merkwirth, C., Joyce, D., Spencer, B., Page, L., Masliah, E., Berggren, W.T., et al. (2012a). Increased proteasome activity in human embryonic stem cells is regulated by PSMD11. Nature *489*, 304–308.

Vilchez, D., Morantte, I., Liu, Z., Douglas, P.M., Merkwirth, C., Rodrigues, A.P., Manning, G., and Dillin, A. (2012b). RPN-6 determines C. elegans longevity under proteotoxic stress conditions. Nature *489*, 263–268.

Villeda, S.A., Luo, J., Mosher, K.I., Zou, B., Britschgi, M., Bieri, G., Stan, T.M., Fainberg, N., Ding, Z., Eggel, A., et al. (2011). The ageing systemic milieu negatively regulates neurogenesis and cognitive function. Nature *477*, 90–94.

Walker, G.A., and Lithgow, G.J. (2003). Lifespan extension in C. elegans by a molecular chaperone dependent upon insulin-like signals. Aging Cell *2*, 131–139.

Wallace, D.C. (2005). A mitochondrial paradigm of metabolic and degenerative diseases, aging, and cancer: a dawn for evolutionary medicine. Annu. Rev. Genet. *39*, 359–407.

Wallenfang, M.R., Nayak, R., and DiNardo, S. (2006). Dynamics of the male germline stem cell population during aging of Drosophila melanogaster. Aging Cell *5*, 297–304.

Walne, A.J., and Dokal, I. (2009). Advances in the understanding of dyskeratosis congenita. Br. J. Haematol. *145*, 164–172.

Wang, J., Sun, Q., Morita, Y., Jiang, H., Gross, A., Lechel, A., Hildner, K., Guachalla, L.M., Gompf, A., Hartmann, D., et al. (2012). A differentiation checkpoint limits hematopoietic stem cell self-renewal in response to DNA damage. Cell *148*, 1001–1014.

Willcox, B.J., Donlon, T.A., He, Q., Chen, R., Grove, J.S., Yano, K., Masaki, K.H., Willcox, D.C., Rodriguez, B., and Curb, J.D. (2008). FOXO3A genotype is strongly associated with human longevity. Proc. Natl. Acad. Sci. USA *105*, 13987–13992.

Wong, K.K., Maser, R.S., Bachoo, R.M., Menon, J., Carrasco, D.R., Gu, Y., Alt, F.W., and DePinho, R.A. (2003). Telomere dysfunction and Atm deficiency compromises organ homeostasis and accelerates ageing. Nature *421*, 643–648.

Yalcin, S., Zhang, X., Luciano, J.P., Mungamuri, S.K., Marinkovic, D., Vercherat, C., Sarkar, A., Grisotto, M., Taneja, R., and Ghaffari, S. (2008). Foxo3 is essential for the regulation of ataxia telangiectasia mutated and oxidative stress-mediated homeostasis of hematopoietic stem cells. J. Biol. Chem. *283*, 25692–25705.

Yankner, B.A., Lu, T., and Loerch, P. (2008). The aging brain. Annu. Rev. Pathol. *3*, 41–66.

Yilmaz, O.H., Valdez, R., Theisen, B.K., Guo, W., Ferguson, D.O., Wu, H., and Morrison, S.J. (2006). Pten dependence distinguishes haematopoietic stem cells from leukaemia-initiating cells. Nature *441*, 475–482.

Yilmaz, O.H., Katajisto, P., Lamming, D.W., Gültekin, Y., Bauer-Rowe, K.E., Sengupta, S., Birsoy, K., Dursun, A., Yilmaz, V.O., Selig, M., et al. (2012). mTORC1 in the Paneth cell niche couples intestinal stem-cell function to calorie intake. Nature *486*, 490–495.

Zhang, J., Grindley, J.C., Yin, T., Jayasinghe, S., He, X.C., Ross, J.T., Haug, J.S., Rupp, D., Porter-Westpfahl, K.S., Wiedemann, L.M., et al. (2006). PTEN maintains haematopoietic stem cells and acts in lineage choice and leukaemia prevention. Nature *441*, 518–522.

Zindy, F., Quelle, D.E., Roussel, M.F., and Sherr, C.J. (1997). Expression of the p16INK4a tumor suppressor versus other INK4 family members during mouse development and aging. Oncogene *15*, 203–211.

Cell Symposia

Stem Cell Energetics

December 9-11, 2014 — Berkeley, CA, USA

Abstract submission deadline:

August 22 2014

Early bird deadline:

October 3 2014

Stem Cell Energetics will bring together academic researchers, clinicians and drug developers working in the fields of metabolism and stem cells to provide a forum for interdisciplinary discussion and cross-collaboration amongst experts in these rapidly advancing fields.

Symposium themes:

- Metabolic regulation of stem cell self renewal
- Niche influence on stem cell metabolism
- Energetics of stem cell flux
- Mitochondria regulation of stem cell fate
- Metabolites in stem cell epigenetics and reprogramming
- Altered stem cell metabolism in aging and disease

Organizers

Nikla Emambokus, Editor, *Cell Metabolism*
Sheila Chari, Scientific Editor, *Cell Stem Cell*
Emmanuelle Passegue, *University of California, San Francisco, USA*
Michael Teitell, *University of California, Los Angeles, USA*

www.cell-symposia-stem-cell-energetics.com

Cell Stem Cell
Brief Report

Functional Repair of CFTR by CRISPR/Cas9 in Intestinal Stem Cell Organoids of Cystic Fibrosis Patients

Gerald Schwank,[1,2,7] Bon-Kyoung Koo,[1,2,7,8] Valentina Sasselli,[1,2] Johanna F. Dekkers,[3,4] Inha Heo,[1,2] Turan Demircan,[1] Nobuo Sasaki,[1,2] Sander Boymans,[1] Edwin Cuppen,[1,6] Cornelis K. van der Ent,[3] Edward E.S. Nieuwenhuis,[5] Jeffrey M. Beekman,[5,6] and Hans Clevers[1,2,*]
[1]Hubrecht Institute/KNAW
[2]University Medical Center Utrecht
Uppsalalaan 8, Utrecht 3584 CT, The Netherlands
[3]Department of Pediatric Pulmonology
[4]Department of Immunology
[5]Department of Pediatric Gastroenterology
Wilhelmina Children's Hospital, University Medical Center, Lundlaan 6, Utrecht 3584 EA, The Netherlands
[6]Department of Medical Genetics, UMC Utrecht, Universiteitsweg 100, Utrecht 3584 GG, The Netherlands
[7]These authors contributed equally to this work
[8]Present address: Wellcome Trust: Medical Research Council Stem Cell Institute, University of Cambridge, Cambridge CB2 1QR, UK
*Correspondence: h.clevers@hubrecht.eu
http://dx.doi.org/10.1016/j.stem.2013.11.002

SUMMARY

Single murine and human intestinal stem cells can be expanded in culture over long time periods as genetically and phenotypically stable epithelial organoids. Increased cAMP levels induce rapid swelling of such organoids by opening the cystic fibrosis transmembrane conductor receptor (CFTR). This response is lost in organoids derived from cystic fibrosis (CF) patients. Here we use the CRISPR/Cas9 genome editing system to correct the CFTR locus by homologous recombination in cultured intestinal stem cells of CF patients. The corrected allele is expressed and fully functional as measured in clonally expanded organoids. This study provides proof of concept for gene correction by homologous recombination in primary adult stem cells derived from patients with a single-gene hereditary defect.

We have previously described a culture system that allows apparently indefinite in vitro expansion (for >1 year) of single murine Lgr5$^+$ intestinal stem cells into a 3D small intestinal epithelium (Sato et al., 2009). A crucial ingredient is the Wnt agonistic R-spondin1, a ligand of Lgr5 (Carmon et al., 2011; de Lau et al., 2011). Intestinal organoids or "miniguts" comprise nearly intact physiology; self-renewing Lgr5$^+$ stem cells and the niche-supporting Paneth cells are located in a domain that resembles the crypt, and enterocytes as well as goblet and enteroendocrine cells move upward to build a villus-like domain that lines the central lumen. Minor adaptation of this culture condition allowed us to develop similar types of organoid cultures for colon, stomach, liver, and pancreas using mouse and human tissues (Barker et al., 2010; Huch et al., 2013b, 2013c; Jung et al., 2011; Sato et al., 2011). Successful transplantation of clonal organoids derived from single Lgr5$^+$ stem cells into damaged tissue has been demonstrated for mouse colon and liver, making the organoid system a promising tool for adult stem cell/gene therapy (Huch et al., 2013a; Yui et al., 2012). Recently, several groups have demonstrated the use of the CRISPR/Cas9 system for genome engineering in various species (Chang et al., 2013; Cho et al., 2013; Cong et al., 2013; Friedland et al., 2013; Hou et al., 2013; Hwang et al., 2013; Jinek et al., 2013; Li et al., 2013; Mali et al., 2013; Nekrasov et al., 2013; Shen et al., 2013; Wang et al., 2013; Xiao et al., 2013; Yu et al., 2013). The system utilizes the type II prokaryotic CRISPR/Cas9 adaptive immune system and targets the Cas9 nuclease by a 20 nt guide sequence cloned upstream of a 5′-NGG "protospacer adjacent motif" (PAM) (Jinek et al., 2012). The induced site-specific double-strand breaks are repaired either by nonhomologous end-joining (NHEJ) to yield indels (Barnes, 2001) or by homologous recombination (HR) if homologous donor templates are available (van den Bosch et al., 2002), thereby enhancing the efficiency of HR-based gene targeting (Bibikova et al., 2003; Porteus and Carroll, 2005; Thomas and Capecchi, 1987; Urnov et al., 2005). The high efficiency and simple design principle of the CRISPR/Cas9 system prompted us to evaluate its use for gene manipulation of adult stem cells in Lgr5/R-spondin-based organoid cultures.

We first optimized the CRISPR/Cas9 system by targeting the murine *APC* locus in adult intestinal stem cells. The optimized protocol involves culturing intestinal organoids in Wnt-conditioned media, trypsinization to obtain a single cell suspension, and Lipofectamine-mediated transfection with plasmids expressing Cas9 and sgRNAs targeting *APC* (Figures S1A and S1B available online) (Schwank et al., 2013). Of note, only Lgr5$^+$ stem cells—and none of the other epithelial cell types—will grow out in a clonal fashion into secondary organoids in culture (Sato et al., 2009, 2011). As APC is a negative regulator of the Wnt pathway, stem cells in which both *APC* alleles are inactivated will grow out in the absence of the normally essential

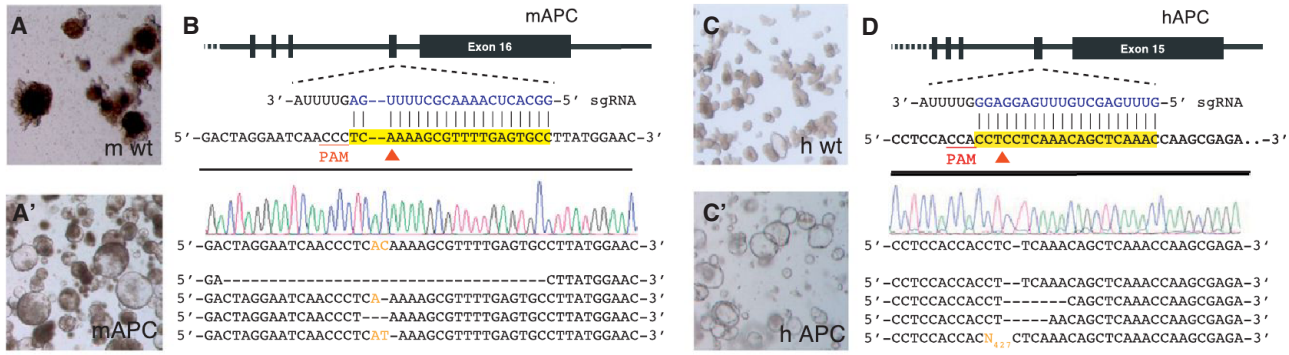

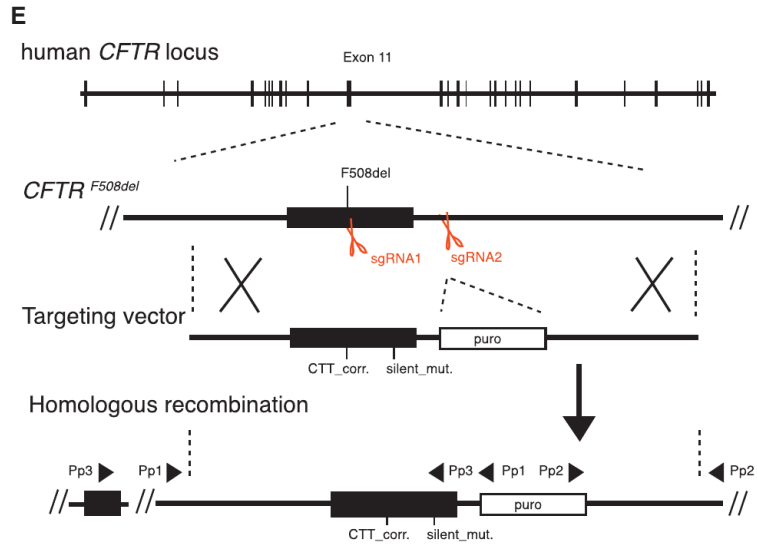

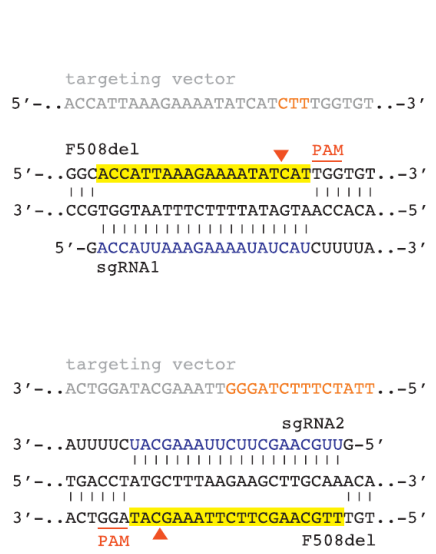

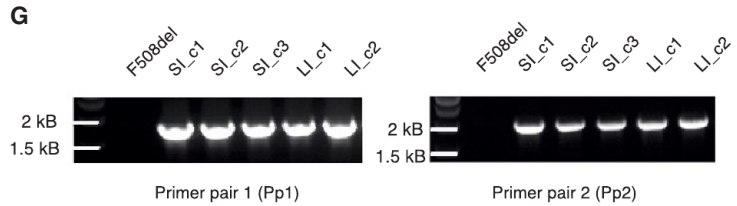

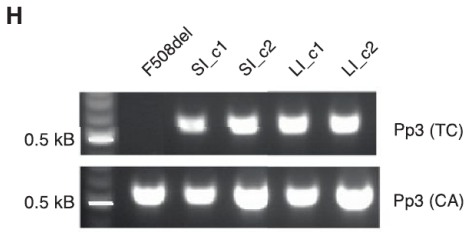

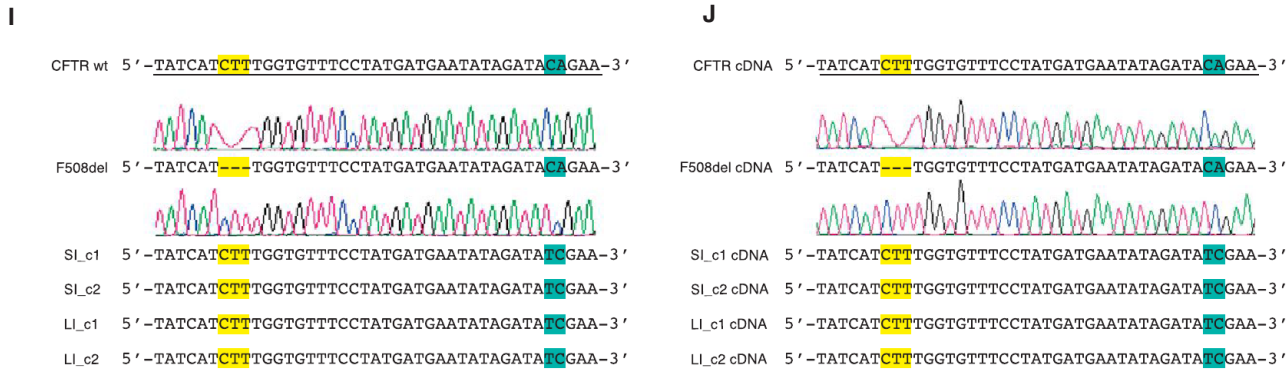

(legend on next page)

Wnt agonist R-spondin1. Two weeks after seeding transfected single cells, multiple organoids grew out from the pool of cells cotransfected with each of five different sgRNAs. In contrast to budding wild-type organoids, selected *APC* mutant organoids showed a cystic morphology (Figures 1A and 1A′), and sequencing of isolated clones confirmed mutations in the targeted *APC* locus (Figure 1B, Figure S1C). No organoids grew in control transfections without the specific sgRNAs. Double-targeting of the two negative Wnt regulators RNF43 and its homolog Znrf3 (Hao et al., 2012; Koo et al., 2012) also resulted in surviving organoids with frameshifts in both targeted loci (Figure S1D), demonstrating the possibility to efficiently generate four-allele knockout organoids in a single transfection. We then tested the CRISPR/Cas9 system on human adult intestinal stem cells by targeting the *APC* locus. As human intestinal stem cells in culture require additional Wnt for self-renewal and expansion (Jung et al., 2011; Sato et al., 2011), transfected stem cells were seeded in medium lacking both Wnt and R-spondin. Organoids only grew out from the pool of cells cotransfected with the specific sgRNA, and selected clones showed a cystic morphology (Figure 1C′). Sequencing confirmed mutations in the targeted region (Figure 1D), demonstrating the potential of the CRISPR/Cas9 system for genome editing of adult human stem cells in primary intestinal organoids.

To investigate the possibility of gene correction in adult stem cells using CRISPR/Cas9, we focused on the cystic fibrosis transmembrane conductor receptor (CFTR) in primary cultured small intestinal (SI) and large intestinal (LI) stem cells. *CFTR* encodes an anion channel essential for fluid and electrolyte homeostasis of epithelia. Mutations in this receptor cause cystic fibrosis (CF) (Kerem et al., 1989; Riordan et al., 1989; Rommens et al., 1989), a disease that leads to the accumulation of viscous mucus in the pulmonary and gastrointestinal tract and to a current median life expectancy of approximately 40 years (Ratjen and Döring, 2003). We established SI and LI organoids from two different pediatric CF patients. Both patients were homozygous for the most common *CFTR* mutation, a deletion of phenylalanine at position 508 (CFTR F508 del) in exon 11, which causes misfolding, endoplasmic reticulum retention, and early degradation of the CFTR protein (Cheng et al., 1990). To first demonstrate the loss of the CFTR function, we performed the previously established forskolin-induced swelling assay. Forskolin activates CFTR by raising the amount of intracellular cyclic AMP, leading to fluid secretion into the lumen and swelling of organoids (Dekkers et al., 2013). Unlike wild-type organoids, the CFTR F508 del patient organoids did not expand their surface area upon forskolin treatment (Figures 2A, 2C, and 2D), confirming loss of function of CFTR as published previously.

We then transfected the patient organoids independently with two different sgRNAs targeting either *CFTR* exon 11 or intron 11, together with a donor plasmid encoding wild-type CFTR sequences (Figure 1E). Downstream of the corrected F508 del mutation, we introduced a silent mutation into the donor sequence enabling allele-specific PCR testing. Within the intronic sequence, we incorporated a puromycin resistance cassette (Figure 1E). The sgRNAs were designed to cut the genomic CFTR sequence, but not the homologous sequence within the targeting vector (Figure 1F). After transfection single cells were plated, and organoids derived from puromycin-resistant individual stem cells were selected and tested for site-specific integration of the donor plasmid by PCR with primers outside of the 5′ and 3′ homology arms and within the puromycin selection cassette (Figure 1E). For both patients, we retrieved several organoid clones with each of the two sgRNAs (Table S1; selected clones are shown in Figure 1G). We confirmed site-specific knockin events and correction of the F508 del allele by sequencing the recombined allele (Figure 1I). Note that sequencing the second allele revealed heterozygous CFTR repair in the majority of clones (Table S1). Transfection with sgRNA2, which induces a double-strand break 203 base pairs (bp) downstream of the F508 del mutation also generated a clone with an anecdotal knockin event where the recombination appeared downstream of the mutation and repair was not achieved (SI_c3 in Figure 1G). To validate expression of the corrected allele, we performed RT-PCR using a forward primer in exon 10 and an allele-specific reverse primer that binds

Figure 1. CRISPR/Cas9-Mediated Genome Editing in Adult Stem Cells

(A–D) Generation of indels in the mouse and human *APC* locus. (A) Wild-type mouse intestinal organoids in complete growth medium, and (A′) *APC* mutant mouse intestinal organoids generated with the CRISP/Cas9 system and selected in medium without R-spondin. Note that organoids change their morphology from budding structures (wild-type) to cystic structures (APC). (B) Schematic of the targeted region of the mouse *APC* locus, and sequences of five mutant alleles from selected clones. Regions of the sgRNA complementary to the protospacer (yellow) are shown in blue. Red arrowheads indicate cleavage sites. (C) Wild-type human intestinal organoids in complete growth medium, and (C′) *APC* mutant human intestinal organoids selected in medium without Wnt and R-spondin. (D) Schematic of the targeted region of the human *APC* locus, and sequences of five mutant alleles from selected clones.

(E–J) Correction of the human *CFTR F508del* allele by induced homologous recombination. (E) Strategy of the genome modification using CRISPR/Cas9 to induce double-strand breaks in the *CFTR* locus, and a template for homology directed repair. Top line, structure of the *CFTR* gene. Black boxes illustrate exons, and thin strokes illustrate introns. Red scissors show cleavage sites of sgRNA1 and sgRNA2, and white box in the targeting vector indicates the puromycin selection cassette. A 2 bp silent mutation is introduced downstream of the CTT F508del correction and allows allele-specific PCR testing. Pp1, Pp2, and Pp3 illustrate PCR primer pairs. (F) Schematic representation of base pairing of the targeting locus with sgRNA1 (upper panel) and sgRNA2 (lower panel). Top lines illustrate the corresponding sequences in the targeting vector. Nonmatching bases are shown in orange and are based on the F508del correction (CTT addition) and insertion of the selection cassette, respectively. (G) PCR analysis showing insertion of the targeting vector by homologous recombination. Positions of Pp1 and Pp2 primers-pairs are illustrated in (E). SI_c1: clone derived from SI organoids of patient 1 corrected by cleavage with sgRNA1. SI_c2: clone derived from SI organoids of patient 1 corrected by cleavage with sgRNA2. SI_c3: same as SI_c2, but integration of the selection cassette did not result in F508 del correction. LI_c1: clone derived from LI organoids of patient 2, corrected by cleavage with sgRNA1. LI_c2: clone derived from LI organoids of patient 2, corrected by cleavage with sgRNA2. (H) RT-PCR analysis of the CFTR cDNA with primers specific for the corrected allele Pp3(TC) and the uncorrected allele Pp3(CA), respectively. Pp3 forward primer is located in exon 10. (I and J) PCR amplification products of the corrected alleles (from G and H) were sequenced. This revealed correction of the F508 del mutation in the genomic locus (I) and cDNA (J). Note that the clones shown here are heterozygous for the corrected allele and retained one copy of the mutant allele (data not shown).

See also Figure S1, Table S1, and Table S2.

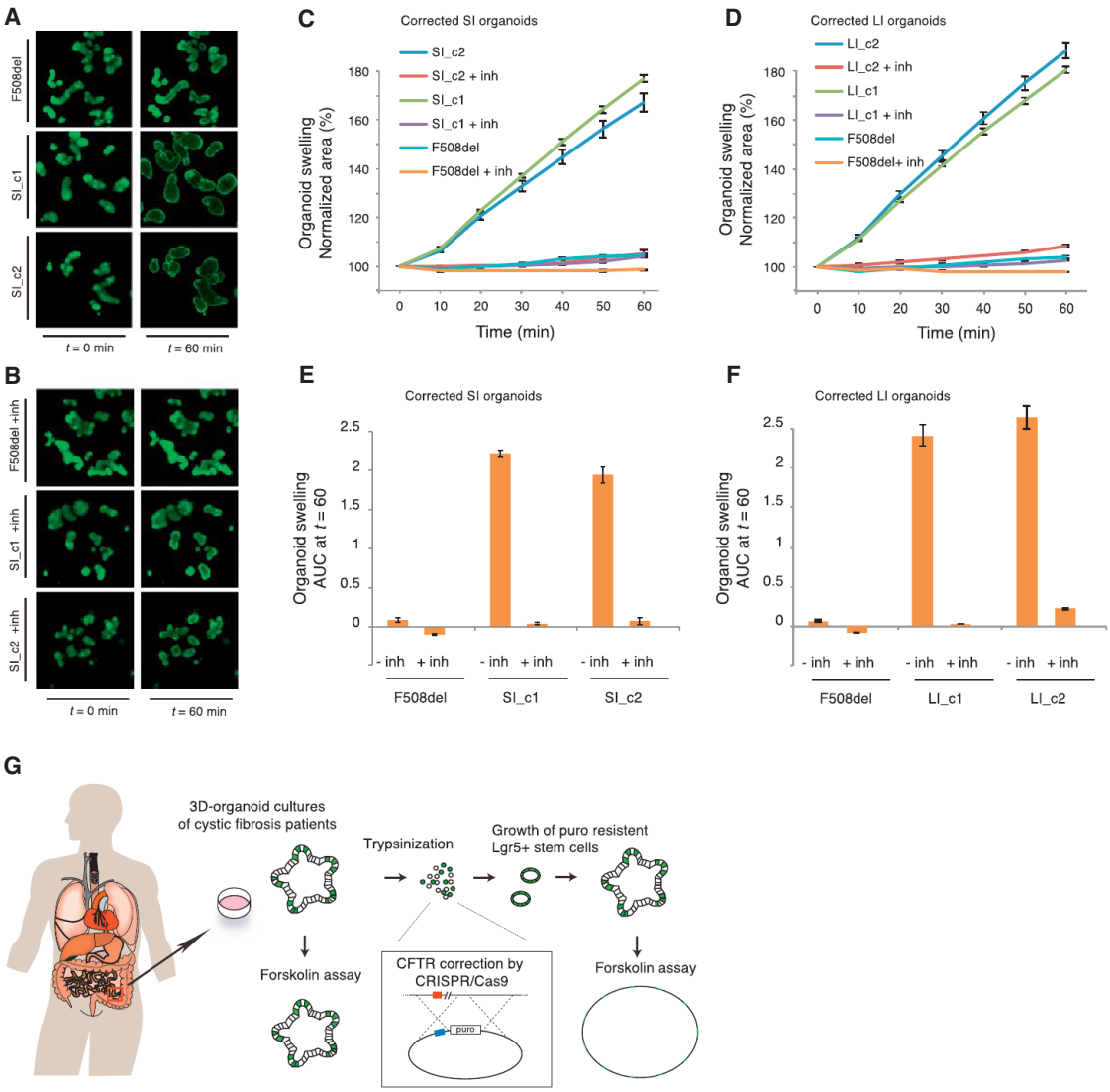

Figure 2. Functional Analysis of the Restored CFTR Function in Corrected Organoids

(A and B) Confocal images of calcein-green-labeled and forskolin-stimulated SI organoids (A) without and (B) in the presence of a chemical CFTR inhibitor. SI_c1, SI_c2: clones derived from SI organoids corrected by cleavage with sgRNA1 and sgRNA2, respectively. F508 del: uncorrected control organoids of the corresponding patient. t = 0 min, t = 60 min indicate time points after forskolin induction.

(C and D) Quantification of organoid swelling of corrected SI organoid clones (C) and LI organoid clones (D). The total organoid surface area is normalized to t_0 min and measured in three independent wells. Error bars indicate the standard error of the mean (SEM). inh, chemical CFTR inhibitor.

(E and F) Forskolin-induced swelling expressed as the absolute area under the curve calculated from (C) and (D), respectively (baseline = 100%, t = 60 min). Error bars indicate SEM.

(G) Schematic illustration of the gene correction protocol. Stem cells are labeled in green. Note that after transfection only stem cells that integrated the selection cassette can grow out and form new organoids.

See also Movie S1.

exclusively to the introduced silent mutations in exon 11. Expression of the repaired allele was absent in uncorrected control organoids and detected in all transgenic clones (Figures 1H and 1J). RT-PCR with a reverse primer specific for the uncorrected allele confirms heterozygousity of the knockin events.

It has been reported that sgRNAs can potentially tolerate mismatches in the 20 bp protospacer target sequence, which can lead to the generation of undesirable "off-target" indels (Hsu et al., 2013; Mali et al., 2013; Pattanayak et al., 2013). To assess off-target effects of the CRISPR/Cas9 system in our adult primary stem cell system, we computationally identified possible off-target sites for each of the two sgRNAs (sequences with one to three mismatches to the protospacer followed by the NGG-PAM motif). We identified 29 potential off-target sites for sgRNA1, of which 25 were sequenced and analyzed in an individual clone. Only one site contained a 4 bp insertion in the protospacer sequence (Table S2). Notably, the mutation was heterozygous and located within an intron, making phenotypic consequences highly unlikely. For sgRNA2, we identified and sequenced 17 off-target sites in one clone, and no mutations

were found (Table S2). Also, when protospacer-homology regions with 4 mismatches (10 sites for sgRNA1 and 8 sites for sgRNA2) were analyzed, we did not find any indels (Table S2), confirming previous studies that suggest off-target effects to be limited to sites with only one to three mismatches (Mali et al., 2013). Our results therefore demonstrated high specificity of the CRISPR/Cas9 system in adult stem cells.

To assess whether the CFTR function in corrected organoids was restored, we performed the forskolin assay with transgenic lines. By live-cell microscopy, we observed rapid expansion of the organoid surface area in the corrected organoids, whereas swelling was absent in untransfected control organoids (Figure 2A, Movie S1). Quantification of swelling by automated image analysis demonstrated a relative increase of the total organoid surface area to 177% (±1.4 SEM) and 167% (±3.8 SEM) for two corrected SI organoid clones (Figures 2C and 2E), and to 187% (±3 SEM) and 180% (±1.5 SEM) for two corrected LI organoid clones (Figures 2D and 2F). These numbers are comparable to forskolin-induced surface area increase of wild-type organoids and exceed CFTR rescue capacities obtained with chemical correctors (Dekkers et al., 2013). Untransfected F508 del organoids increased only marginally in surface area (Figures 2C–2F), which is consistent with very limited residual CFTR function of the F508 del allele (Dekkers et al., 2013). We next tested whether the forskolin-induced swelling of the corrected organoids was sensitive to chemical inhibition of CFTR by CFTRinh-172 (Thiagarajah et al., 2004). Indeed, forskolin-induced swelling was fully abolished in presence of the inhibitor (Figures 2C–2F, Movie S1). Together, these data demonstrated that the corrected F508 del allele was fully functional and was able to rescue the CFTR phenotype in organoids.

In summary, we have isolated and expanded adult intestinal stem cells from two CF patients, corrected the mutant F508 del allele using the CRISPR/Cas9 mediated homologous recombination, and demonstrated functionality of the corrected allele in the organoid system (Figure 2G). Together with previous studies, in which in vitro expanded organoids were successfully transplanted into colons of mice (Yui et al., 2012), this work provides a potential strategy for future gene therapy in patients. Although given its multiorgan involvement CF does not appear to be a prime candidate for clinical application of adult stem cell gene therapy, this approach may present a safe complement to induced-pluripotent-stem-cell-based approaches, and in the future it could be applied to different single-gene hereditary defects. The advantage of combining HR-based gene correction strategies with organoid culture technology rests in the possibility of clonal expansion of single adult patient stem cells and the selection of recombinant clonal organoid cultures harboring the desired, exact genetic change.

SUPPLEMENTAL INFORMATION

Supplemental Information for this article includes Supplemental Experimental Procedures, one figure, two tables, and one movie and can be found with this article online at http://dx.doi.org/10.1016/j.stem.2013.11.002.

ACKNOWLEDGMENTS

We thank K. Tenbrock (Department of Pediatrics, the RWTH Aachen University, Germany) for providing intestinal rest-material and A. Smith (Wellcome Trust Centre for Stem Cell Research, University of Cambridge) for providing Rosa-CreERT2 mice. This work was funded by grants from the European Research Council (EU/232814-StemCeLLMark), the KNAW/3V-fund, the SNF fellowship for advanced researchers PA00P3 139732 (G.S.), the Human Frontiers in Science Program long-term fellowship LT000422/2012 (G.S.), the Wellcome Trust (097922/C/11/Z) (B.-K.K.), the EU Marie Curie Fellowship EU/330571-FP7-IIF (I.H.), the Astellas Foundation (N.S.), and JSPS (N.S.).

Received: October 21, 2013
Revised: October 31, 2013
Accepted: November 1, 2013
Published: December 5, 2013

REFERENCES

Barker, N., Huch, M., Kujala, P., van de Wetering, M., Snippert, H.J., van Es, J.H., Sato, T., Stange, D.E., Begthel, H., van den Born, M., et al. (2010). Lgr5(+ve) stem cells drive self-renewal in the stomach and build long-lived gastric units in vitro. Cell Stem Cell *6*, 25–36.

Barnes, D.E. (2001). Non-homologous end joining as a mechanism of DNA repair. Curr. Biol. *11*, R455–R457.

Bibikova, M., Beumer, K., Trautman, J.K., and Carroll, D. (2003). Enhancing gene targeting with designed zinc finger nucleases. Science *300*, 764.

Carmon, K.S., Gong, X., Lin, Q., Thomas, A., and Liu, Q. (2011). R-spondins function as ligands of the orphan receptors LGR4 and LGR5 to regulate Wnt/beta-catenin signaling. Proc. Natl. Acad. Sci. USA *108*, 11452–11457.

Chang, N., Sun, C., Gao, L., Zhu, D., Xu, X., Zhu, X., Xiong, J.W., and Xi, J.J. (2013). Genome editing with RNA-guided Cas9 nuclease in zebrafish embryos. Cell Res. *23*, 465–472.

Cheng, S.H., Gregory, R.J., Marshall, J., Paul, S., Souza, D.W., White, G.A., O'Riordan, C.R., and Smith, A.E. (1990). Defective intracellular transport and processing of CFTR is the molecular basis of most cystic fibrosis. Cell *63*, 827–834.

Cho, S.W., Kim, S., Kim, J.M., and Kim, J.S. (2013). Targeted genome engineering in human cells with the Cas9 RNA-guided endonuclease. Nat. Biotechnol. *31*, 230–232.

Cong, L., Ran, F.A., Cox, D., Lin, S., Barretto, R., Habib, N., Hsu, P.D., Wu, X., Jiang, W., Marraffini, L.A., and Zhang, F. (2013). Multiplex genome engineering using CRISPR/Cas systems. Science *339*, 819–823.

de Lau, W., Barker, N., Low, T.Y., Koo, B.K., Li, V.S., Teunissen, H., Kujala, P., Haegebarth, A., Peters, P.J., van de Wetering, M., et al. (2011). Lgr5 homologues associate with Wnt receptors and mediate R-spondin signalling. Nature *476*, 293–297.

Dekkers, J.F., Wiegerinck, C.L., de Jonge, H.R., Bronsveld, I., Janssens, H.M., de Winter-de Groot, K.M., Brandsma, A.M., de Jong, N.W., Bijvelds, M.J., Scholte, B.J., et al. (2013). A functional CFTR assay using primary cystic fibrosis intestinal organoids. Nat. Med. *19*, 939–945.

Friedland, A.E., Tzur, Y.B., Esvelt, K.M., Colaiácovo, M.P., Church, G.M., and Calarco, J.A. (2013). Heritable genome editing in C. elegans via a CRISPR-Cas9 system. Nat. Methods *10*, 741–743.

Hao, H.X., Xie, Y., Zhang, Y., Charlat, O., Oster, E., Avello, M., Lei, H., Mickanin, C., Liu, D., Ruffner, H., et al. (2012). ZNRF3 promotes Wnt receptor turnover in an R-spondin-sensitive manner. Nature *485*, 195–200.

Hou, Z., Zhang, Y., Propson, N.E., Howden, S.E., Chu, L.F., Sontheimer, E.J., and Thomson, J.A. (2013). Efficient genome engineering in human pluripotent stem cells using Cas9 from Neisseria meningitidis. Proc. Natl. Acad. Sci. USA *110*, 15644–15649.

Hsu, P.D., Scott, D.A., Weinstein, J.A., Ran, F.A., Konermann, S., Agarwala, V., Li, Y., Fine, E.J., Wu, X., Shalem, O., et al. (2013). DNA targeting specificity of RNA-guided Cas9 nucleases. Nat. Biotechnol. *31*, 827–832.

Huch, M., Boj, S.F., and Clevers, H. (2013a). Lgr5(+) liver stem cells, hepatic organoids and regenerative medicine. Regen. Med. *8*, 385–387.

Huch, M., Bonfanti, P., Boj, S.F., Sato, T., Loomans, C.J., van de Wetering, M., Sojoodi, M., Li, V.S., Schuijers, J., Gracanin, A., et al. (2013b). Unlimited in vitro

expansion of adult bi-potent pancreas progenitors through the Lgr5/R-spondin axis. EMBO J. *32*, 2708–2721.

Huch, M., Dorrell, C., Boj, S.F., van Es, J.H., Li, V.S., van de Wetering, M., Sato, T., Hamer, K., Sasaki, N., Finegold, M.J., et al. (2013c). In vitro expansion of single Lgr5+ liver stem cells induced by Wnt-driven regeneration. Nature *494*, 247–250.

Hwang, W.Y., Fu, Y., Reyon, D., Maeder, M.L., Tsai, S.Q., Sander, J.D., Peterson, R.T., Yeh, J.R., and Joung, J.K. (2013). Efficient genome editing in zebrafish using a CRISPR-Cas system. Nat. Biotechnol. *31*, 227–229.

Jinek, M., Chylinski, K., Fonfara, I., Hauer, M., Doudna, J.A., and Charpentier, E. (2012). A programmable dual-RNA-guided DNA endonuclease in adaptive bacterial immunity. Science *337*, 816–821.

Jinek, M., East, A., Cheng, A., Lin, S., Ma, E., and Doudna, J. (2013). RNA-programmed genome editing in human cells. Elife *2*, e00471.

Jung, P., Sato, T., Merlos-Suárez, A., Barriga, F.M., Iglesias, M., Rossell, D., Auer, H., Gallardo, M., Blasco, M.A., Sancho, E., et al. (2011). Isolation and in vitro expansion of human colonic stem cells. Nat. Med. *17*, 1225–1227.

Kerem, B., Rommens, J.M., Buchanan, J.A., Markiewicz, D., Cox, T.K., Chakravarti, A., Buchwald, M., and Tsui, L.C. (1989). Identification of the cystic fibrosis gene: genetic analysis. Science *245*, 1073–1080.

Koo, B.K., Spit, M., Jordens, I., Low, T.Y., Stange, D.E., van de Wetering, M., van Es, J.H., Mohammed, S., Heck, A.J., Maurice, M.M., and Clevers, H. (2012). Tumour suppressor RNF43 is a stem-cell E3 ligase that induces endocytosis of Wnt receptors. Nature *488*, 665–669.

Li, J.F., Norville, J.E., Aach, J., McCormack, M., Zhang, D., Bush, J., Church, G.M., and Sheen, J. (2013). Multiplex and homologous recombination-mediated genome editing in Arabidopsis and Nicotiana benthamiana using guide RNA and Cas9. Nat. Biotechnol. *31*, 688–691.

Mali, P., Aach, J., Stranges, P.B., Esvelt, K.M., Moosburner, M., Kosuri, S., Yang, L., and Church, G.M. (2013). CAS9 transcriptional activators for target specificity screening and paired nickases for cooperative genome engineering. Nat. Biotechnol. *31*, 833–838.

Nekrasov, V., Staskawicz, B., Weigel, D., Jones, J.D., and Kamoun, S. (2013). Targeted mutagenesis in the model plant Nicotiana benthamiana using Cas9 RNA-guided endonuclease. Nat. Biotechnol. *31*, 691–693.

Pattanayak, V., Lin, S., Guilinger, J.P., Ma, E., Doudna, J.A., and Liu, D.R. (2013). High-throughput profiling of off-target DNA cleavage reveals RNA-programmed Cas9 nuclease specificity. Nat. Biotechnol. *31*, 839–843.

Porteus, M.H., and Carroll, D. (2005). Gene targeting using zinc finger nucleases. Nat. Biotechnol. *23*, 967–973.

Ratjen, F., and Döring, G. (2003). Cystic fibrosis. Lancet *361*, 681–689.

Riordan, J.R., Rommens, J.M., Kerem, B., Alon, N., Rozmahel, R., Grzelczak, Z., Zielenski, J., Lok, S., Plavsic, N., Chou, J.L., et al. (1989). Identification of the cystic fibrosis gene: cloning and characterization of complementary DNA. Science *245*, 1066–1073.

Rommens, J.M., Iannuzzi, M.C., Kerem, B., Drumm, M.L., Melmer, G., Dean, M., Rozmahel, R., Cole, J.L., Kennedy, D., Hidaka, N., et al. (1989). Identification of the cystic fibrosis gene: chromosome walking and jumping. Science *245*, 1059–1065.

Sato, T., Vries, R.G., Snippert, H.J., van de Wetering, M., Barker, N., Stange, D.E., van Es, J.H., Abo, A., Kujala, P., Peters, P.J., and Clevers, H. (2009). Single Lgr5 stem cells build crypt-villus structures in vitro without a mesenchymal niche. Nature *459*, 262–265.

Sato, T., Stange, D.E., Ferrante, M., Vries, R.G., Van Es, J.H., Van den Brink, S., Van Houdt, W.J., Pronk, A., Van Gorp, J., Siersema, P.D., and Clevers, H. (2011). Long-term expansion of epithelial organoids from human colon, adenoma, adenocarcinoma, and Barrett's epithelium. Gastroenterology *141*, 1762–1772.

Schwank, G., Andersson-Rolf, A., Koo, B.K., Sasaki, N., and Clevers, H. (2013). Generation of BAC transgenic epithelial organoids. PLoS ONE *8*, e76871.

Shen, B., Zhang, J., Wu, H., Wang, J., Ma, K., Li, Z., Zhang, X., Zhang, P., and Huang, X. (2013). Generation of gene-modified mice via Cas9/RNA-mediated gene targeting. Cell Res. *23*, 720–723.

Thiagarajah, J.R., Song, Y., Haggie, P.M., and Verkman, A.S. (2004). A small molecule CFTR inhibitor produces cystic fibrosis-like submucosal gland fluid secretions in normal airways. FASEB J. *18*, 875–877.

Thomas, K.R., and Capecchi, M.R. (1987). Site-directed mutagenesis by gene targeting in mouse embryo-derived stem cells. Cell *51*, 503–512.

Urnov, F.D., Miller, J.C., Lee, Y.L., Beausejour, C.M., Rock, J.M., Augustus, S., Jamieson, A.C., Porteus, M.H., Gregory, P.D., and Holmes, M.C. (2005). Highly efficient endogenous human gene correction using designed zinc-finger nucleases. Nature *435*, 646–651.

van den Bosch, M., Lohman, P.H., and Pastink, A. (2002). DNA double-strand break repair by homologous recombination. Biol. Chem. *383*, 873–892.

Wang, H., Yang, H., Shivalila, C.S., Dawlaty, M.M., Cheng, A.W., Zhang, F., and Jaenisch, R. (2013). One-step generation of mice carrying mutations in multiple genes by CRISPR/Cas-mediated genome engineering. Cell *153*, 910–918.

Xiao, A., Wang, Z., Hu, Y., Wu, Y., Luo, Z., Yang, Z., Zu, Y., Li, W., Huang, P., Tong, X., et al. (2013). Chromosomal deletions and inversions mediated by TALENs and CRISPR/Cas in zebrafish. Nucleic Acids Res. *41*, e141.

Yu, Z., Ren, M., Wang, Z., Zhang, B., Rong, Y.S., Jiao, R., and Gao, G. (2013). Highly efficient genome modifications mediated by CRISPR/Cas9 in Drosophila. Genetics *195*, 289–291.

Yui, S., Nakamura, T., Sato, T., Nemoto, Y., Mizutani, T., Zheng, X., Ichinose, S., Nagaishi, T., Okamoto, R., Tsuchiya, K., et al. (2012). Functional engraftment of colon epithelium expanded in vitro from a single adult Lgr5$^+$ stem cell. Nat. Med. *18*, 618–623.

Cell Stem Cell
Article

Replacement of Oct4 by Tet1 during iPSC Induction Reveals an Important Role of DNA Methylation and Hydroxymethylation in Reprogramming

Yawei Gao,[1,2,4] Jiayu Chen,[1,2,4] Ke Li,[2] Tong Wu,[2] Bo Huang,[2] Wenqiang Liu,[2] Xiaochen Kou,[2] Yu Zhang,[2] Hua Huang,[3] Yonghua Jiang,[2] Chao Yao,[2] Xiaolei Liu,[2] Zhiwei Lu,[2] Zijian Xu,[2] Lan Kang,[2] Jun Chen,[2] Hailin Wang,[3] Tao Cai,[2,*] and Shaorong Gao[1,2,*]

[1]Graduate School of Peking Union Medical College, Beijing 100730, China
[2]National Institute of Biological Sciences, Beijing 102206, China
[3]State Key Laboratory of Environmental Chemistry and Ecotoxicology, Research Center for Eco-Environmental Sciences, Chinese Academy of Science, Beijing 100085, China
[4]These authors contributed equally to this work
*Correspondence: caitao@nibs.ac.cn (T.C.), gaoshaorong@nibs.ac.cn (S.G.)
http://dx.doi.org/10.1016/j.stem.2013.02.005

SUMMARY

DNA methylation and demethylation have been proposed to play an important role in somatic cell reprogramming. Here, we demonstrate that the DNA hydroxylase Tet1 facilitates pluripotent stem cell induction by promoting *Oct4* demethylation and reactivation. Moreover, Tet1 (T) can replace Oct4 and initiate somatic cell reprogramming in conjunction with Sox2 (S), Klf4 (K), and c-Myc (M). We established an efficient TSKM secondary reprogramming system and used it to characterize the dynamic profiles of 5-methylcytosine (5mC), 5-hydroxymethylcytosine (5hmC), and gene expression during reprogramming. Our analysis revealed that both 5mC and 5hmC modifications increased at an intermediate stage of the process, correlating with a transition in the transcriptional profile. We also found that 5hmC enrichment is involved in the demethylation and reactivation of genes and regulatory regions that are important for pluripotency. Our data indicate that changes in DNA methylation and hydroxymethylation play important roles in genome-wide epigenetic remodeling during reprogramming.

INTRODUCTION

The direct reprogramming of differentiated somatic cells to induced pluripotent stem cells (iPSCs) can be achieved through the overexpression of a set of defined transcription factors such as Oct4 (O), Sox2 (S), Klf4 (K), and c-Myc (M) (Maherali et al., 2007; Okita et al., 2007; Takahashi et al., 2007; Takahashi and Yamanaka, 2006; Wernig et al., 2007). The full pluripotency of iPSCs has been confirmed by the production of viable all-iPSC mice through tetraploid complementation (Boland et al., 2009; Kang et al., 2009; Zhao et al., 2009).

Global epigenetic reprogramming of DNA and histones is crucial for the reprogramming process overall and involves the removal of the original somatic cell epigenetic landscape and the establishment of a pluripotent stem cell-specific epigenetic landscape in its place. Many regulators of chromatin modification play important roles in reprogramming to iPSCs (Onder et al., 2012; Singhal et al., 2010; Surani et al., 2007; Wang et al., 2011; Yang et al., 2011), and inhibitors of histone deacetylases or DNA methylation have also been useful in improving reprogramming efficiency (Plath and Lowry, 2011). Uncovering the molecular mechanisms involved may lead to improvements in both reprogramming efficiency and iPSC quality, and thus ultimately advance therapeutic application.

The generation of iPSCs can be affected significantly by the initial expression of reprogramming factors, starting cell types, and induction methods. Through the development of a secondary (2°) reprogramming system, iPSC generation was initially described as a multistep process characterized by phenotypic, transcriptional, and chromatin changes (Plath and Lowry, 2011). More recently, genome-wide analysis of specific chromatin modification dynamics (gain of H3K4me2) at early stages of reprogramming indicated that this progress might be constrained by repressive epigenetic modifications, such as H3K9me3 and DNA methylation (Koche et al., 2011; Soufi et al., 2012). H3K9me3 and DNA methylation are considered major barriers to faithful reprogramming (Chen et al., 2013; Meissner et al., 2008).

It has been proposed that DNA methylation functions in the silencing of somatic genes and chromatin remodeling during iPSC generation (Plath and Lowry, 2011), and DNA demethylation appears to play an important role in reactivating pluripotency genes, which are hypermethylated and silenced in somatic cells, particularly in the late stages of the reprogramming process (Mikkelsen et al., 2008). Recently, 5-hydroxymethylcytosine (5hmC), formed by hydroxylation of 5-methylcytosine (5mC) by Tet1–Tet3 proteins, has been detected in a broad range of cell types and is thought to be involved in active and/or passive DNA demethylation (Tahiliani et al., 2009; Wu and Zhang, 2011). Two recent studies have shown that some of the erasure of CpG methylation during primordial germ cell (PGC) specification occurs via 5mC-to-5hmC conversion driven by Tet1 and Tet2 (Hackett et al., 2013; Vincent et al., 2013). In addition, Tet2-mediated 5hmC conversion on *Nanog* and *Esrrb* has

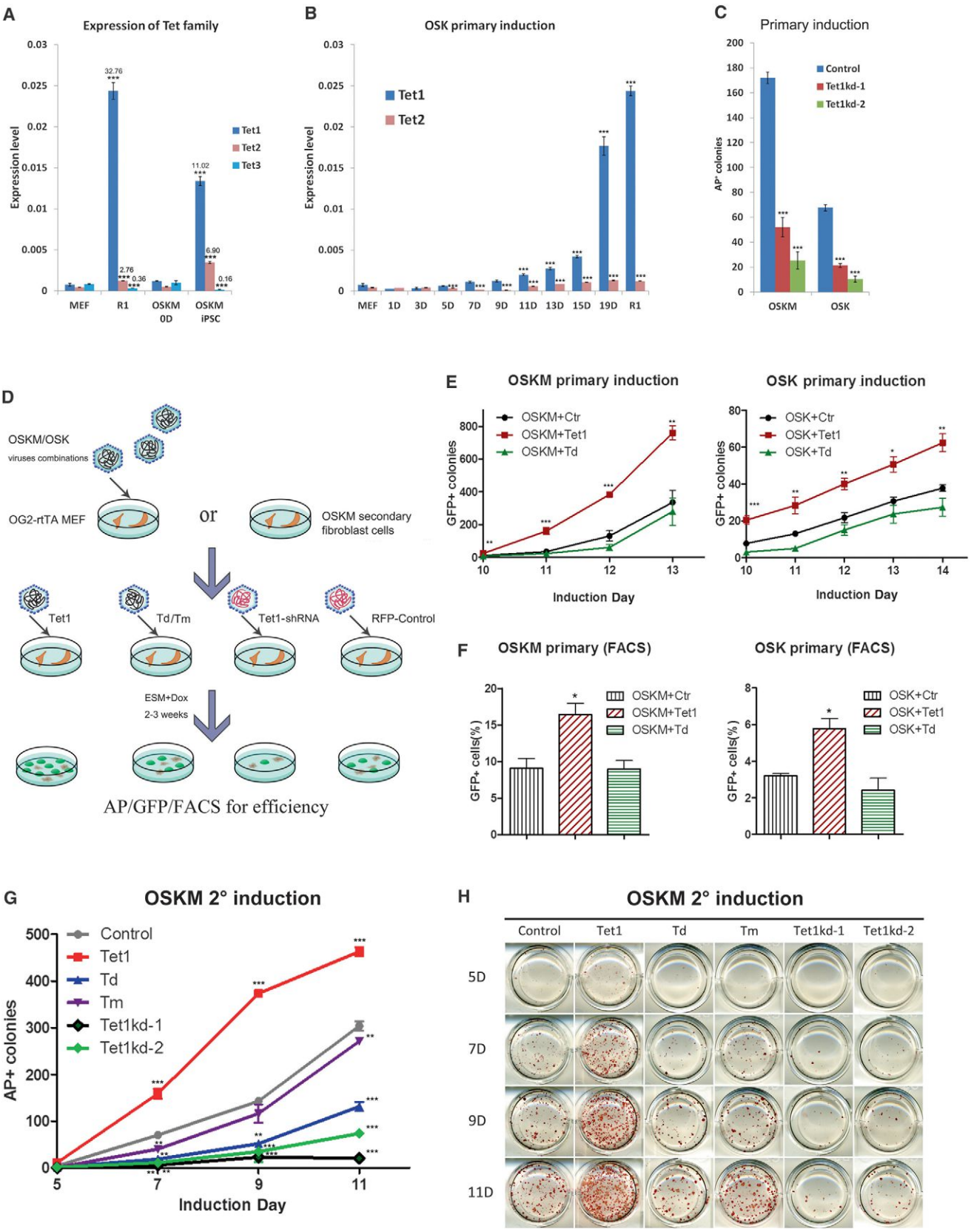

(legend on next page)

been observed in the OSKM reprogramming system (Doege et al., 2012). However, overall understanding of the global dynamics of DNA modification and the molecular mechanisms for DNA demethylation during reprogramming remains poor.

In the present study, we show that Tet1 acts at the *Oct4* loci to promote 5mC-to-5hmC conversion and facilitates the DNA demethylation and transcriptional reactivation during OSKM iPSC induction. Importantly, we found that Tet1 can replace Oct4 in the initiation of reprogramming in combination with SKM. We established an efficient TSKM 2° reprogramming system, which was used to identify an intermediate stage in the reprogramming process and to dissect the molecular events involved. Overall, we characterized a unique DNA methylation and hydroxymethylation state map, and our data further suggest that 5mC-to-5hmC conversion represents a crucial step in the initiation of epigenetic remodeling and transcriptome resetting to achieve a pluripotent state.

RESULTS

Tet1 Can Facilitate Traditional iPSC Induction in a Hydroxylase-Dependent Manner

To investigate the role of DNA methylation and demethylation during reprogramming, we focused on the Tet family proteins, which have been proposed to play important roles in initiating DNA demethylation through 5mC oxidation (Wu and Zhang, 2011). We first examined the expression dynamics of *Tet1–Tet3* during reprogramming and in iPSCs. Consistent with previous reports (Koh et al., 2011; Polo et al., 2012), *Tet1* was more significantly upregulated than *Tet2* in iPSCs, whereas *Tet3* was repressed (Figure 1A). Although *Tet2* was upregulated as early as day 3 in OSKM-induced reprogramming, only *Tet1* showed a progressive upregulation in both OSKM- and OSK-induced reprogramming systems (Figure 1B; Figure S1A available online). We further demonstrated that the formation of iPSC colonies was abolished by short hairpin RNA (shRNA)-mediated *Tet1* knockdown (Tet1kd) in both the OSKM and OSK (4F and 3F) induction systems (Figure 1C).

To further explore the potential function of Tet1 in reprogramming, we performed both gain- and loss-of-function studies (Figure 1D). We used lentiviral-based doxycycline (Dox)-inducible expression vectors to exogenously express genes. The OSKM and OSK primary induction system (fibroblasts with the *Oct4-GFP/Rosa26-M2rtTA* background) was used for first verifying whether Tet1 could increase reprogramming efficiency. We found that the formation of Oct4-GFP$^+$ colonies was promoted markedly by ectopic expression of *Tet1* in both the OSKM and OSK induction systems (Figures 1E and S1B–S1D). The percentage of Oct4-GFP$^+$ cells also increased (Figures 1F and S1E). Importantly, the catalytic domain (CD) of *Tet1* appeared to be essential for its function in this context, because ectopic expression of CD-deleted *Tet1* (Td) did not have a positive effect on reprogramming (Figures 1E, 1F, and S1B–S1E).

For ruling out the possible influence of variation in transgene expression, an OSKM 2° reprogramming system established in our lab was used for further studies (Kang et al., 2009; Kou et al., 2010). We optimized the expression of exogenous *Tet1* (Figures S1F and S1G) and constructed a mutant *Tet1* (Tm) that is full length but lacks DNA hydroxylase activity (Figures S1B and S1C). OSKM 2° fibroblasts were infected with similar amounts of Tet1, Td, Tm, control, or Tet1-shRNA viruses and were then induced by Dox under the same culture conditions (Figure 1D). Total *Tet1* expression levels were confirmed using primers on the CD on induction day 3 (Figure S1H).

The percentage of SSEA1$^+$ cells (as determined using fluorescence-activated cell sorting [FACS] analysis) and the number of AP$^+$ colonies were used for measuring the kinetics and the efficiency of reprogramming, respectively. We found that when Tet1 was repressed by shRNA, the increase in SSEA1$^+$ cells was delayed, and colony formation was abolished (Figures 1G, 1H, S1I, and S1J). In contrast, ectopic expression of wild-type Tet1 accelerated the reprogramming process and increased the efficiency significantly. Although the overexpression of Td and Tm also promoted the expression of SSEA1 (Figures S1I and S1J), the number of AP$^+$ colonies showed no significant differences compared with the control (Figures 1G and 1H). Taken together, these results demonstrate that Tet1 facilitates OSKM-mediated iPSC induction in a hydroxylase-activity-dependent manner.

Tet1 and 5hmC Involve Demethylation of the *Oct4* Enhancer and Promoter during OSKM Reprogramming

The demethylation and reactivation of *Oct4* is a crucial step in reprogramming (Plath and Lowry, 2011). We examined *Oct4* expression levels in SSEA1$^+$ cells sorted on induction day 11 and found that only wild-type Tet1, but not Td or Tm, promoted

Figure 1. Tet1 Can Facilitate Traditional iPSC Induction

(A) *Tet1* is highly expressed in pluripotent stem cells. The expression levels of the *Tet*s were normalized to glyceraldehyde-3-phosphate dehydrogenase (*Gapdh*) and compared via fold changes from differentiated cells to pluripotent cells (MEF versus R1 ESC, and OSKM 0D versus OSKM iPSC).

(B) *Tet1* is progressively upregulated in OSK iPSC induction. qRT-PCR analyses of *Tet1* and *Tet2* expression were normalized to *Gapdh* and compared with MEF, respectively.

(C) Tet1 deficiency reduces the alkaline phosphatase (AP)-positive colonies in iPSC induction. AP staining was performed at day 12 and day 16 in OSKM and OSK induction, respectively.

(D) Strategy for functional studies of Tet1 in reprogramming. Parallel experiments were performed using wild-type *Tet1* (Tet1), truncated *Tet1* (Td), mutated *Tet1* (Tm), shRNA for *Tet1* (Tet1kd-1 and Tet1kd-2) and RFP control (Ctr). rtTA, reverse tetracycline transactivator; ESM, ESC culture media.

(E) Expression of *Tet1*, but not Td, facilitates the formation of Oct4-GFP$^+$ colonies. The Oct4-GFP$^+$ colonies were counted on days 10–13 in OSKM (left) and days 10–14 in OSK (right) after Dox induction.

(F) The percentage of Oct4-GFP$^+$ cells is increased by Tet1. FACS analysis was performed by the end of primary iPSC induction: OSKM (left) at day 13 and OSK (right) at day 14.

(G and H) Kinetics of the AP$^+$ colony formation are facilitated by Tet1 and abolished by Tet1kds from day 5 to day 11 in OSKM 2° induction. The number of AP$^+$ colonies was counted and compared with the control in (G). Representative AP-stained plates during reprogramming are shown in (H).

Data in (A)–(C) are represented as the mean ± SD (n = 3). Data in E–G are represented as the mean ± SEM (n = 3 in E and F; n = 2 in G). *$p < 0.05$; **$p < 0.01$; ***$p < 0.001$ by ANOVA or Student's t test for comparison. See also Figure S1.

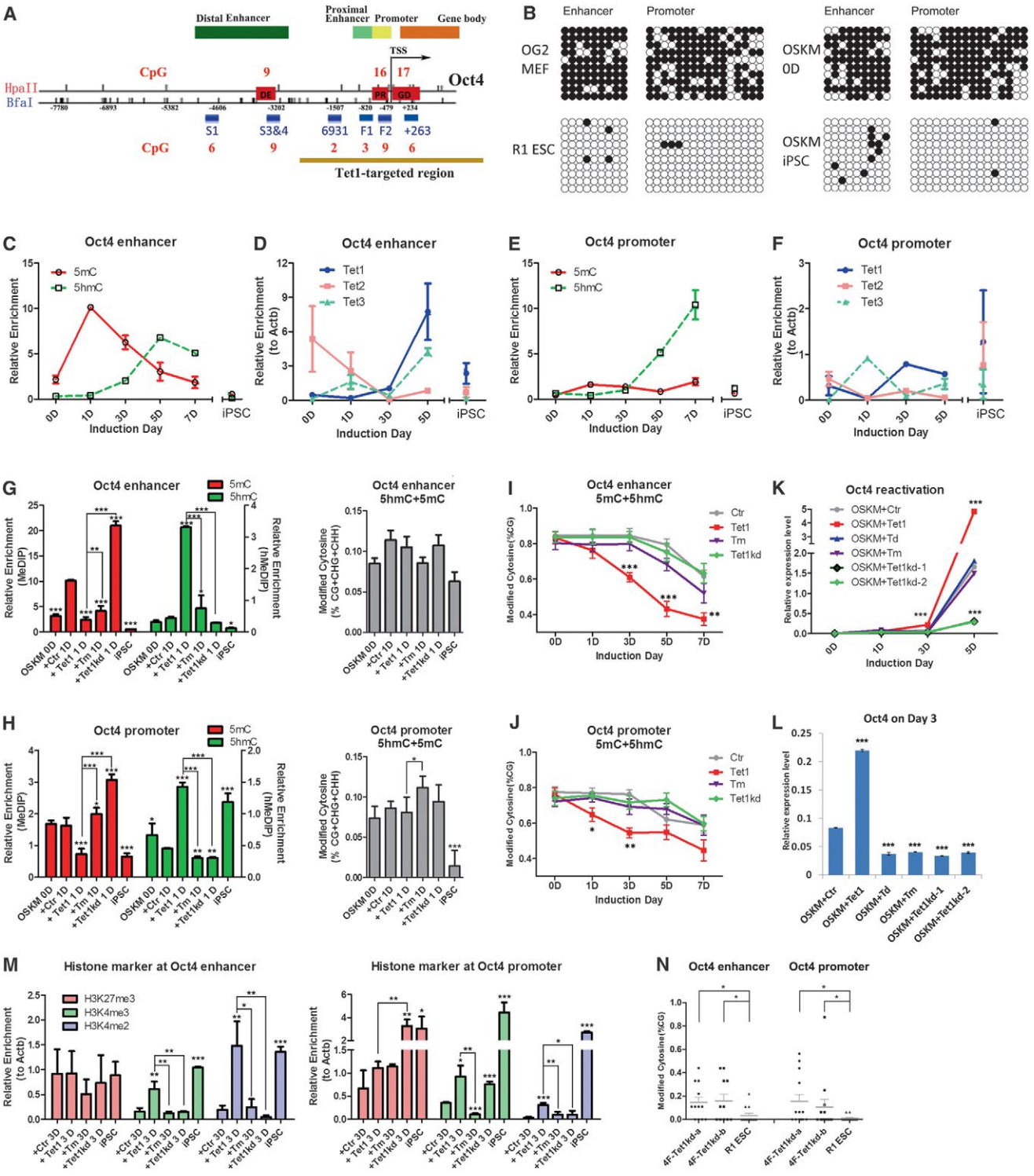

Figure 2. Tet1 Can Reactivate *Oct4* during OSKM Reprogramming

(A) Diagram of the analyzed regions of *Oct4*. The reported T-DMRs and Tet1-targeted regions in ESCs, as well as the number of CpG dinucleotides in *BfaI*-defined regions, are labeled. The enhancer (S3&4, DE) and promoter (F2, PR) were identified as R-DMRs of *Oct4*.

(B) CpG dinucleotides of *Oct4* R-DMRs were demethylated through OSKM induction. Bisulfite sequencing analysis was performed on differentiated cells and pluripotent cells (OG2 MEF versus R1 ESC and OSKM 0D versus OSKM iPSC). The open circles indicate unmethylated CpG dinucleotides, and the closed circles indicate methylated CpG dinucleotides.

(C and E) Time course of relative 5mC/5hmC enrichment at *Oct4* enhancer (C) and promoter (E) during OSKM 2° induction.

(D and F) Time course of Tet1–Tet3 occupancy at *Oct4* enhancer (D) and promoter (F) during OSKM 2° induction.

(legend continued on next page)

Oct4 reactivation (Figure S2A). Expression of *Oct4* is highly regulated by the CpG methylation levels of tissue-dependent, differentially methylated regions (T-DMRs) (Hattori et al., 2004), and Oct4 can be targeted directly by Tet1 in embryonic stem cells (ESCs) (Wu et al., 2011). Therefore, we next examined whether Tet1 and 5hmC are involved in *Oct4* demethylation and reactivation during OSKM reprogramming.

We identified two reprogramming-related, differentially methylated regions (R-DMRs) in the *Oct4* gene (including enhancer and promoter regions) that undergo DNA demethylation during reprogramming (Figures 2A and 2B). We used methylated or hydroxymethylated DNA immunoprecipitation quantitative PCR (MeDIP or hMeDIP qPCR) to track the dynamics of the relative 5mC or 5hmC levels, respectively, at *Oct4* R-DMRs from induction day 1 to day 7 in the OSKM 2° system. We also quantified the total cytosine methylation level (5mC plus 5hmC) through bisulfite sequencing analysis of the same regions.

We found that 5hmC enrichment increased in parallel with a decrease in 5mC at these loci from day 1 to day 5 of the reprogramming process (Figures 2C and 2E). In addition, chromatin immunoprecipitation (ChIP) demonstrated that the occupancy of Tet proteins at these two loci was different (Figures 2D and 2F). The binding of Tet1, but not Tet2 or Tet3, was increased from day 1 to day 5, which coincided perfectly with the 5hmC increase (Figures 2C–2F). These results suggest that Tet1 and 5hmC may function since the early stage of reprogramming and might be directly involved in the DNA demethylation of *Oct4* R-DMRs.

Unexpectedly, we noticed an increase in 5mC levels at *Oct4* R-DMRs at day 1 of OSKM-mediated reprogramming (Figures 2C and 2E). We performed bisulfite analyses (Gruntman et al., 2008) to quantify the methylated cytosine levels during reprogramming and their dynamics on CG, CHG (H = C/A/T), and CHH (H = C/A/T) sites. We found that the major demethylation events in these two regions took place at a relatively late stage on CG sites (from day 5) in reprogramming, whereas de novo non-CpG DNA methylation occurred primarily on CHG and CHH sites, potentially explaining the observed increase in 5mC (Figure S2B). This finding is also consistent with previous data indicating that DNA demethylation at the *Oct4* gene occurs at a late stage in reprogramming (Mikkelsen et al., 2008; Polo et al., 2012).

Tet1 Promotes *Oct4* Demethylation and Reactivation via 5hmC Conversion during OSKM Reprogramming

We next explored the role of Tet1 and 5hmC in *Oct4* reactivation using established gain- and loss-of-function systems (Figure 1D). The molecular changes at the *Oct4* R-DMRs were analyzed and compared to Tet1 overexpression or repression during OSKM 2° reprogramming.

When compared to control OSKM-mediated reprogramming (OSKM+Ctr) at day 1, overexpression of Tet1, but not Tm, led to a significant and consistent increase in 5hmC and a corresponding decrease in 5mC at both loci after 24 hr of Dox induction, whereas the total amount of modified cytosine was comparable (Figures 2G and 2H). By contrast, Tet1kd by shRNA resulted in an increase in 5mC and a decrease in 5hmC at these two loci (Figures 2G and 2H). These results suggest that Tet1 expression converts 5mC to 5hmC at both the *Oct4* enhancer and promoter at the very beginning of reprogramming.

Importantly, overexpression of Tet1 also significantly promoted the CpG demethylation process at both regions (Figures 2I and 2J) and facilitated *Oct4* transcriptional reactivation as early as day 3 (Figures 2K and 2L). Interestingly, we noticed that Tet1 expression limited the increase in total 5mC at early stages (Figures S2C and S2D). However, Tet1 deficiency impeded the increase in 5hmC during the entire process and led to a more significant increase in 5mC on day 1 at both loci (Figures S2C and S2D). These results suggest that the function of Tet1 may not be limited to the CpG sites. ChIP analysis on day 3 also revealed a significant enrichment of activation-associated histone modifications, including H3K4me3 and H3K4me2, but not the repressive mark H3K27me3, at the two loci when Tet1 was overexpressed (Figure 2M).

After day 1, the changes in 5hmC and Tet binding at both loci became more complicated. For example, compared with the control, H3K4me3 and H3K27me3 were enriched at the *Oct4* promoter, but not the enhancer, in OSKM+Tet1kd day 3 cells. ChIP analysis further revealed increased occupancy of Tet1 and Tet3 (but not Tet2) at the *Oct4* promoter, whereas the binding of all Tets at the *Oct4* enhancer was comparable to the OSKM+Ctr cells on day 3 (Figures S2E and S2F). Overall, though, *Oct4* demethylation and reactivation were repressed by Tet1kd on day 3 (Figures 2I, 2J, and 2L).

Although redundant binding of Tets might occur, Tet1 expression during reprogramming appears to be more significant for *Oct4* reactivation. It is interesting that even in the Tet1-deficient primary OSKM reprogramming, some Dox-independent AP^+ iPSC lines were established, but they had a low Oct4-GFP signal (Figure S2G). *Oct4* demethylation and reactivation were incomplete in these Tet1-deficient iPSC lines (4F-Tet1kd iPSC a and b) compared to ESCs and Tet1-deficient ESCs, even though *Sox2* expression (demethylation independent) was reactivated normally, and *Tet2* and *Tet3* were also highly expressed in one of the lines (4F-Tet1kd-b) (Figures 2N and S2H).

(G and H) DNA modification changes at *Oct4* enhancer (G) and promoter (H) at induction day 1 in the OSKM 2° system. Relative 5mC/5hmC enrichment (left) and content of modified cytosine (right) of different conditions are presented.
(I and J) Tet1 can promote CpG demethylation at *Oct4* enhancer (I) and promoter (J) during OSKM 2° induction.
(K and L) Tet1 can promote the reactivation of *Oct4* during OSKM 2° induction. The time course is compared in (K), and the comparison on day 3 is shown in (L).
(M) Occupancy of H3K27me3, H3K4me3, and H3K4me2 at *Oct4* enhancer (left) and promoter (right) in cultures as indicated.
(N) The CpG demethylation at the *Oct4* enhancer and promoter is incomplete in two OSKM-Tet1kd iPSC lines, as compared with R1 ESCs.
Gene expression was assessed by qRT-PCR, normalized by *Actb*, and compared to those observed in R1 ESCs. Content of modified cytosines (5hmC+5mC) was determined by bisulfite sequencing and further analyzed on CGs, CHGs, and CHHs. The relative 5mC and 5hmC levels were determined by MeDIP- and hMeDIP-qPCR, respectively, relative to input (1/40) DNA. Occupancy of Tet1–Tet3 and the histone markers was determined by ChIP-qPCR, relative to input (1/10) and normalized by *Actb*. The cells for each kind of analysis during reprogramming were collected from the same or parallel culture plates every 2 days after Dox induction. Data in (C)–(H) and (K)–(M) are represented as the mean ± SD (n = 3). Data in (I), (J), and (N) are represented as the mean ± SEM (n = 10∼16). *$p < 0.05$; **$p < 0.01$; ***$p < 0.001$ by ANOVA or Student's t test for comparison. See also Figure S2.

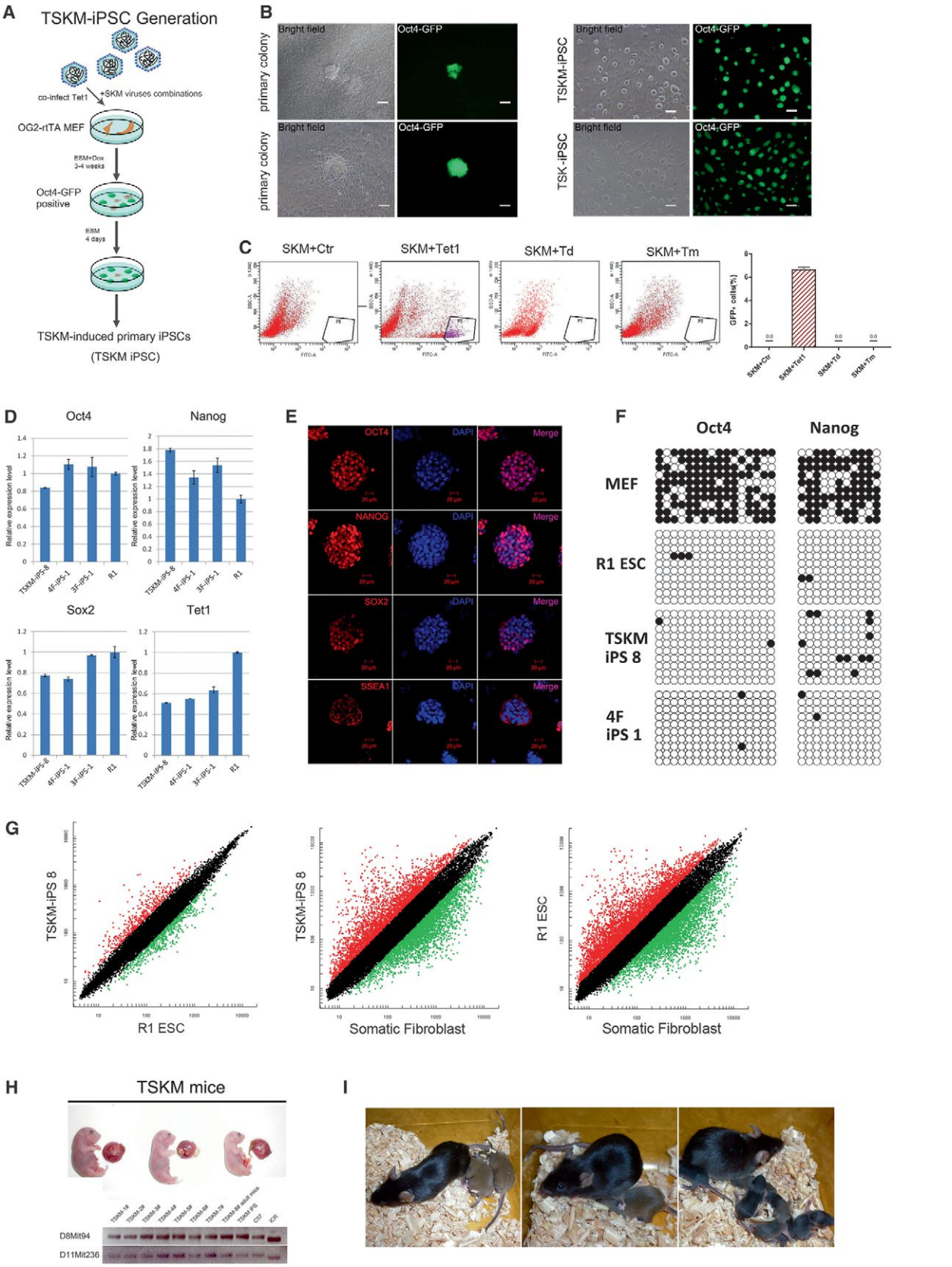

(legend on next page)

Collectively, these results indicate that Tet1 promotes *Oct4* demethylation and reactivation through 5mC-to-5hmC conversion at a very early stage in OSKM-mediated reprogramming.

Tet1 Can Replace Oct4 in the Induction of Reprogramming

After establishing that Tet1 promotes *Oct4* reactivation early in reprogramming, we next investigated whether Tet1 could replace Oct4 during iPSC induction. To this end, we infected mouse embryonic fibroblasts (MEFs) (*Oct4-GFP*/*Rosa26-M2rtTA*) with viruses expressing *Tet1*, *Sox2*, *Klf4*, and c-*Myc* (TSKM) using a traditional infection method (Figures 3A and S3A). Interestingly, we observed Oct4-GFP$^+$ colonies (68 ± 12 per 100,000 MEFs plated) within 3–4 weeks of induction, and FACS analysis revealed that 6.6% of the cells were Oct4-GFP$^+$ by the end of the reprogramming process (Figures 3B and 3C). By contrast, we saw no Oct4-GFP$^+$ colonies or cells from MEFs infected with SKM+Td, SKM+Tm, or SKM+Ctr combinations under the same conditions. We also found that c-Myc was dispensable for reprogramming with this approach (Figure 3B), and that other cell types such as trophoblast stem cells (TSCs) could be reprogrammed successfully using TSKM (Figure S3B).

TSKM-Reprogrammed iPSCs Are Fully Pluripotent

We selected and propagated Oct4-GFP$^+$ colonies without Dox to generate TSKM iPSC lines and characterized their pluripotency further. One representative cell line, TSKM-iPS8 (40 chromosomes, XY; Figure S3C), was analyzed with regard to transcription, epigenetic modification, and developmental potential. The reported fully pluripotent 4F iPSCs and 3F iPSCs (Kang et al., 2009; Kang et al., 2011) and the R1 ESCs were used as controls.

In TSKM-iPS8 cells, the exogenous vectors were silenced (Figure S3D), and pluripotency-marker expression was the same as that seen in fully pluripotent 4F iPSCs and 3F iPSCs and in R1 ESCs (Figures 3D, 3E, and S3E). The global gene-expression profiles of TSKM-iPS8 cells resembled R1 ESCs but were distinct from those of somatic fibroblasts (Figures 3G and S3F). Bisulfite sequencing analysis indicated that successful demethylation occurred at the promoters of *Oct4* and *Nanog* during TSKM reprogramming (Figure 3F).

TSKM-iPS8 cells also showed development potential both in vitro and in vivo. Embryoid bodies (EBs) were formed using TSKM-iPS8 cells, and marker genes for the three germ layers were detected in the plated EBs (Figures S3G and S3H). Teratomas with three germ layers and chimeric mice with germline transmission could be generated by TSKM-iPS8 cells (Figures S3I and S3J).

Strikingly, through tetraploid complementation, we successfully obtained full-term, all-iPSC mice from this TSKM iPSC line, which we referred to as TSKM mice. We produced 20 living TSKM all-iPSC mice through Caesarean-section (C-section) deliveries at embryonic day 19.5 (E19.5) (Figure 3H). We used some of these full-term TSKM mice to derive somatic cells for a 2° induction system. Three of the remaining TSKM mice reached adulthood and were fertile (Figure 3I). Most strikingly, we found that, thus far, all TSKM mice have been free of tumors, unlike the OSKM mice (Figure S3K), and the oldest TSKM mouse is now 2 years old.

These results demonstrate that fully reprogrammed iPSCs can be obtained via TSKM-mediated reprogramming.

A TSKM 2° Reprogramming System Can Initiate Efficient Reprogramming

We established a secondary reprogramming system, referred to as the TSKM 2° system, using fibroblasts derived from full-term, TSKM mice (Figure 4A). After the addition of Dox, ectopic expression of exogenous factors was detected (Figure S4A). We analyzed the reprogramming process in the TSKM 2° system using FACS analysis every 2 days. During TSKM 2° reprogramming, the fibroblasts morphed into smaller, round cells at day 3 when SSEA1$^+$ cells appeared; cell death was observed later, and some cells clustered at approximately day 5. Oct4-GFP$^+$ colonies appeared at day 7, and we analyzed the efficiency at these points (Figures 4B and S4B–S4E). Interestingly, we found that the percentage of double-positive cells (Oct4-GFP$^+$, SSEA1$^+$) within the SSEA1$^+$ population was much higher in the TSKM 2° induction system than with OSKM (Figure S4F). Subsequently, we generated TSKM 2° iPSC lines (TSKM 2-iPSC) (Figure 4C), which also possessed full pluripotency and the ability to generate full-term, all-iPSC mice (TSKM 2-iPSC mice; Figure 4D).

These results indicate that faithful somatic cell reprogramming can be achieved efficiently in the TSKM 2° reprogramming system and that it provides a useful tool to further explore the molecular dynamics of TSKM-mediated reprogramming.

Figure 3. Tet1 Can Replace Oct4 and Generate Fully Pluripotent iPSCs

(A) Strategy for generating TSKM iPSCs.

(B) Morphology of Oct4-GFP$^+$ TSKM and TSK iPSC colonies.

(C) Only wild-type Tet1 can generate Oct4-GFP$^+$ cells in combination with SKM. FACS was performed at induction day 28 after infection with different combinations. Data are represented as the mean ± SEM (n = 3).

(D) qRT-PCR analysis of pluripotency genes expression in TSKM iPSCs and 4F-/3F-iPSCs. Both 4F- and 3F-iPSCs can produce all-iPS mice. The expression levels were normalized to those observed in R1 ESCs and represented as mean ± SD (n = 3).

(E) Immunofluorescent staining of pluripotency markers in TSKM iPSCs. Scale bars represent 20 μm.

(F) The *Oct4* and *Nanog* promoter regions in MEFs undergo demethylation in TSKM iPSCs, similar to that in R1 ESCs and 4F iPSCs as analyzed by bisulfite sequencing. Open and closed circles indicate the unmethylated and methylated CpGs, respectively.

(G) Scatter-plot analysis comparison of the gene-expression profiles in TSKM iPSCs, fibroblasts, and R1 ESCs.

(H) TSKM iPS8 can generate full-term TSKM-iPSC mice through tetraploid complementation. The newborn mice were alive after C-section (upper row) and simple sequence length polymorphism analysis (lower row) of the TSKM-iPSC mice were performed. TSKM iPSCs and C57BL/6J mice were used as positive controls and ICR mice were used as a negative control.

(I) Three adult TSKM-iPSC mice with germline transmission ability. The left mouse is 2 years old, and the other two mice are 6 months old.

See also Figure S3.

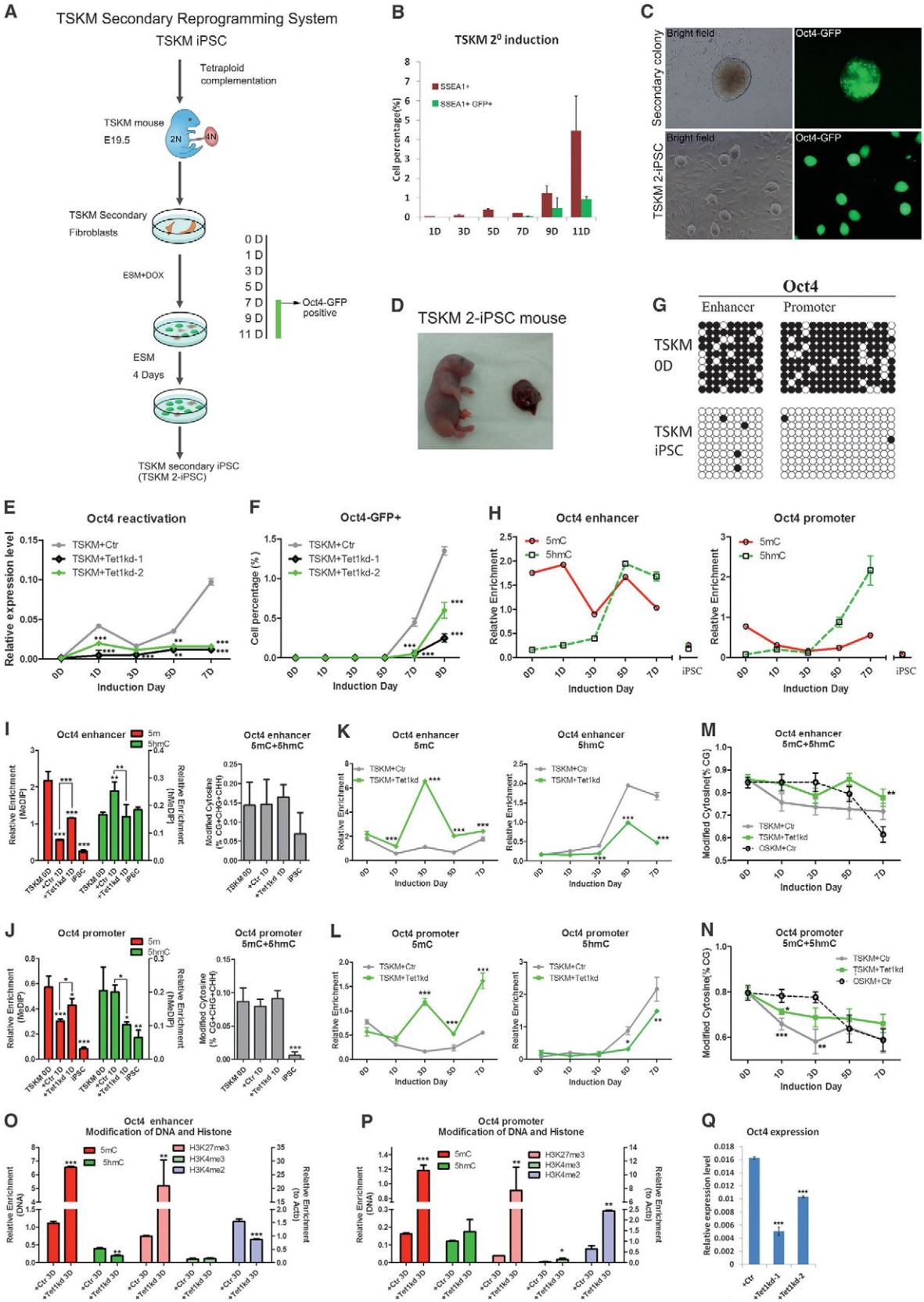

(legend on next page)

Efficient Reactivation of Oct4 Involves Tet1 and 5hmC during TSKM Reprogramming

To examine the role of Tet1 in TSKM-mediated programming, we used gain- and loss-of-function analysis in the TSKM 2° system. As in the OSKM system (Figures 1G, 1H, 2K, S1I, and S1J), Tet1 deficiency (Tet1 shRNA) in the TSKM 2° system delayed the production of SSEA1$^+$ and Oct4-GFP$^+$ cells, and colony formation and *Oct4* reactivation were abolished (Figures 4E, 4F, and S4G–S4I). Although Tm and Td can facilitate the expression of SSEA1, only wild-type Tet1 greatly promoted the generation of Oct4-GFP$^+$ cells, further improved colony formation, and facilitated Oct4 reactivation. The entire reprogramming process was shortened by 2 days with additional Tet1 expression (Figures S4G–S4I).

We also performed a side-by-side analysis of Oct4 reactivation in the TSKM 2° system. As in OSKM-mediated reprogramming (Figure 2B), the *Oct4* R-DMRs underwent demethylation during TSKM-mediated reprogramming (Figure 4G). Compared with OSKM reprogramming (Figures 2C, 2E, and S2B), we observed a consistent increase in 5hmC in the TSKM 2° system, but we no longer saw the sharp increase in 5mC on day 1 (Figure 4H). Bisulfite sequencing analysis further revealed that de novo non-CpG methylation was repressed during TSKM reprogramming (Figure S4J).

Compared with the control in day 1, Tet1kd by shRNA on day 1 (TSKM+Tet1kd 1D) resulted in a consistent increase in 5mC and a decrease in 5hmC at both *Oct4* R-DMRs (Figures 4I and 4J). Tet1 deficiency also diminished the gain of 5hmC and led to increased 5mC on both loci during the whole reprogramming process (Figures 4K and 4L). Furthermore, Tet1 deficiency abolished the demethylation of CpG sites, which were more efficiently demethylated in TSKM+Ctr cells than in OSKM+Ctr (Figures 4M and 4N). Moreover, when additional Tet1 was applied in the TSKM system, the 5hmC levels were significantly increased, and the demethylation of CpG sites was facilitated on both loci (Figures S4K and S4L).

ChIP analysis on cells at induction day 3 revealed that Tet1 deficiency led to significantly higher 5mC levels and H3K27me3 occupancy relative to TSKM+Ctr at the two loci (Figures 4O and 4P). Although Tet1 deficiency also affected 5hmC and active histone marks, these effects were not as obvious as the changes observed on the repressive marks. qRT-PCR analysis revealed that expression of endogenous *Oct4* was repressed by Tet1kd on day 3 relative to controls (Figure 4Q).

These results suggest that *Oct4* reactivation depends on Tet1 and 5hmC conversion in the TSKM 2° system. Thus, it seems that Tet1 can reactivate endogenous *Oct4* during reprogramming without a requirement for exogenous Oct4.

An Intermediate Reprogramming Stage in the TSKM 2° System Is Characterized by an Apparent Transcriptional Transition

We achieved successful reprogramming within one week using the TSKM 2° system, suggesting that changes occur rapidly at both the transcriptional and epigenetic levels (Figure 5A). We realized that for gaining insight into the molecular mechanism of TSKM-mediated reprogramming it would be important to identify a distinct intermediate stage where changes are evident. To this end, we examined the expression level of pluripotency markers in three groups of cells sorted by FACS, which included SSEA1$^+$ cells (S$^+$) and two groups of SSEA1$^-$ cells (R2 and R7), from day 3 to day 7 during TSKM 2° reprogramming. We found that the gene-expression levels among the three groups of cells were comparable at day 3 (TSKM 3D), but obvious diversity appeared from day 5 (TSKM 5D; Figures S5A and S5B). Therefore, the TSKM 3D cells seemed to be a relatively homogeneous state that could be utilized for high-throughput analysis. We performed 5hmC dot blot assays and found a sharp increase in 5hmC on day 3 (Figure S5C). Therefore, we concluded that TSKM 3D cells constitute an identifiable intermediate stage that could be used to explore the molecular mechanism of TSKM-mediated reprogramming.

Figure 4. TSKM 2° System Can Initiate Reprogramming Rapidly and Efficiently

(A) Schematic of the TSKM 2° system. Fibroblasts were derived from the TSKM mice (E19.5) and induced by Dox. The TSKM 2-iPSC line could be established after 7 day induction and was further used to produce TSKM 2-iPSC mice through tetraploid complementation.

(B) Kinetics of TSKM 2° induction by FACS at the indicated time points. SSEA1$^+$ cells emerged at day 3, and SSEA1 and Oct4-GFP double-positive cells emerged at day 7.

(C) Morphology of TSKM 2-iPSC colonies. The original Oct4-GFP$^+$ colonies appeared since induction day 7 (upper panels). After withdrawal of Dox for 4 days, TSKM 2-iPSC lines could be established (lower panels).

(D) A TSKM 2-iPSC mouse. A full-term TSKM 2-iPSC mouse could be produced through tetraploid complementation and was alive when C-section was performed.

(E) Tet1 deficiency represses the reactivation of *Oct4* in TSKM 2° induction.

(F) Tet1 deficiency represses the reprogramming kinetics of TSKM 2° induction. FACS was performed to determine the percentage of Oct4-GFP$^+$ cells.

(G) CpG dinucleotides of *Oct4* R-DMRs undergo demethylation during TSKM 2° induction.

(H) Time course of relative 5mC/5hmC enrichment at *Oct4* enhancer (left) and promoter (right) in TSKM 2° induction.

(I and J) DNA modification changes at *Oct4* enhancer (I) and promoter (J) at induction day 1 in the TSKM 2° system. Relative 5mC/5hmC enrichment (left) and content of modified cytosine (right) of different conditions are presented.

(K and L) Tet1 deficiency results in 5mC increase and 5hmC decrease at *Oct4* R-DMRs in TSKM 2° induction. Time course of relative 5mC/5hmC enrichment at *Oct4* enhancer (K) and promoter (L) is shown.

(M and N) TSKM-mediated reprogramming promotes more efficient CpG demethylation on *Oct4* R-DMRs as compared to OSKM 2° induction. CpG demethylation on *Oct4* enhancer (M) and promoter (N) in TSKM 2° induction is represented by the time course of 5hmC+5mC content on CGs as indicated.

(O and P) Occupancy of histone markers and relative enrichment of 5mC/5hmC at *Oct4* enhancer (O) and promoter (P) at induction day 3 in cultures as indicated in TSKM 2° induction.

(Q) The relative expression level of *Oct4* at day 3 in TSKM 2° induction.

The analyses in the TSKM 2° system were performed in parallel to those in the OSKM 2° system. Data in (B), (E)–(L), and (O)–(Q) are represented as the mean ± SD (n = 3). Data in (M) and (N) are represented as the mean ± SEM (n = 10∼16). *p < 0.05; **p < 0.01; ***p < 0.001 by ANOVA or Student's t test for comparison. See also Figure S4.

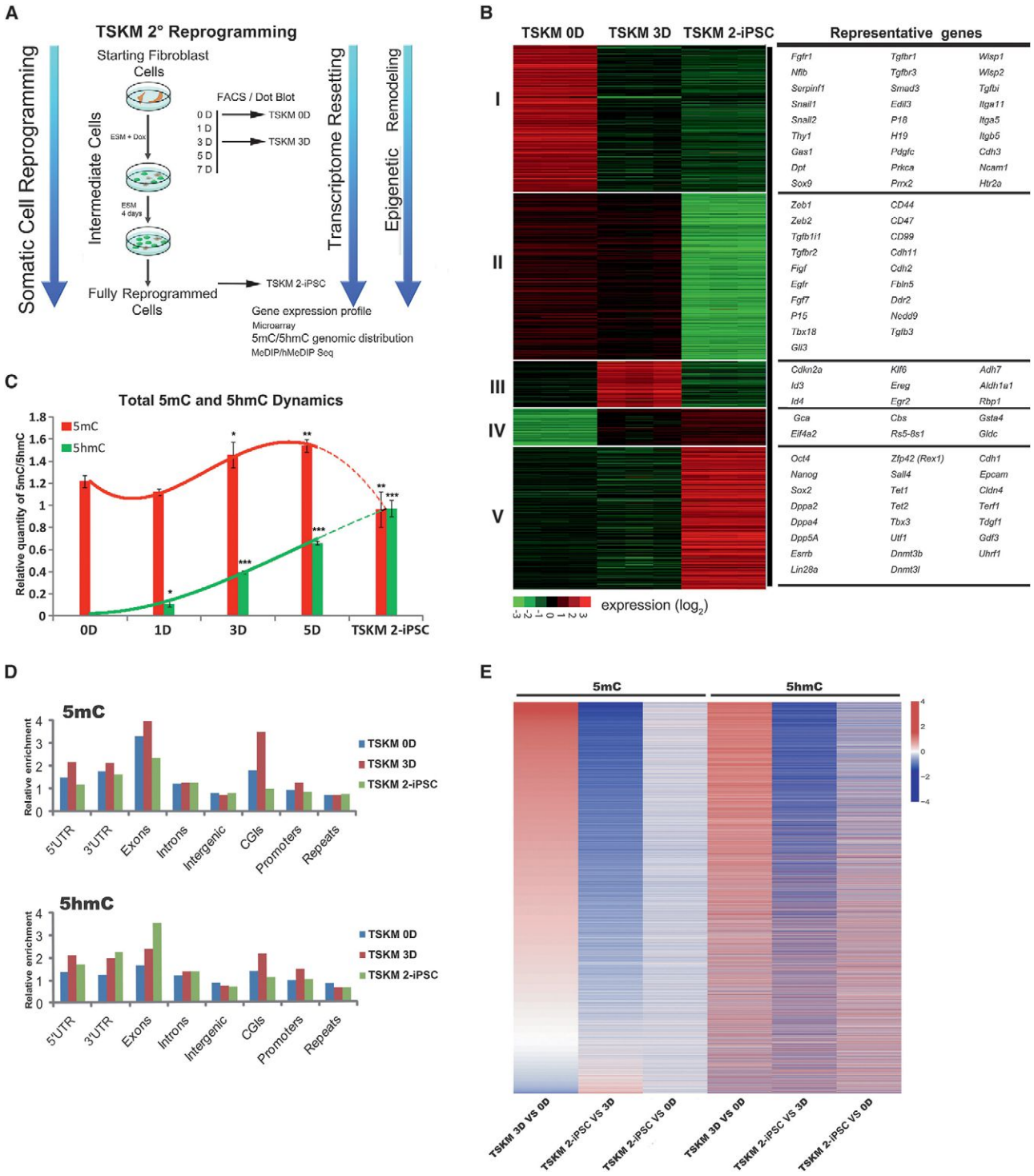

Figure 5. The Transcriptome Transition and DNA Modification Dynamics in the TSKM 2° System

(A) Strategy for molecular analysis of TSKM 2° reprogramming. Microarray, MeDIP-seq, and hMeDIP-seq were used for systemic analysis of molecular events in the TSKM 2° system from fibroblasts to iPSCs.

(B) Clustering of gene-expression profiles based on transcriptional dynamic during TSKM 2° reprogramming. The genes were clustered into five groups (I–V), according to the expression correlation using *k*-means algorithms. Each row is a gene (representative genes are listed in the right panel), and each column represents a sample with repeats. The gene-expression intensity was scaled across samples (red for high expression and green for low expression).

(C) The unique 5mC and 5hmC dynamics during TSKM 2° reprogramming. Quantification of the total 5mC and 5hmC in each cell sample was performed by LC-MS/MS analysis and normalized to that in R1 ESCs. Data are represented as the mean ± SD (n = 3). *p < 0.05; **p < 0.01; ***p < 0.001 by ANOVA for comparison to TSKM 0D.

(legend continued on next page)

We then performed a microarray analysis using the starting fibroblasts (TSKM 0D cells), intermediate stage cells (TSKM 3D cells) and fully reprogrammed iPSCs (TSKM 2-iPSCs; Figure 5A). As expected, we observed an obvious transcriptional transition from a somatic to a pluripotent state during TSKM-mediated reprogramming. The gene-expression profiles of TSKM 3D cells clearly represented an intermediate stage of this transition with widespread changes (Figure S5D). Importantly, similar transcriptional transitions were observed in OSKM-mediated reprogramming when pre-iPSCs were used as the intermediate-stage cells (Mikkelsen et al., 2008) (Figure S5D).

Based on the gene-expression dynamics, we clustered the significantly changed genes into five groups (2,508 genes in total), representing the major transcriptional events in TSKM-mediated reprogramming (Figure 5B). A large set of genes (clusters I, II, and III), including many lineage-specific genes, are repressed in iPSCs. The reported mesenchymal-related genes (Samavarchi-Tehrani et al., 2010), such as *Snail1*, *Snail2*, *Zeb1*, *Zeb2*, and the fibroblast markers *Cdh2* and *Thy1*, were included (clusters I and II). In contrast, some pluripotency-related genes, including the key pluripotency factors *Oct4*, *Nanog*, *Sox2*, *Dppa4*, and *Zfp42*, and some reported epithelial genes, such as *Epcam* and *Cdh1*, were reactivated and highly expressed in TSKM 2-iPSCs (clusters IV and V; Figure 5B).

During epigenetic reprogramming in PGCs, the high expression of *Tet1* and *Tet2* and the repression of DNA-methylation-related genes (*Dnmt3a*, *Dnmt3b*, *Dnmt3l*, and *Uhrf1*) are believed to account for the 5hmC conversion and passive 5mC depletion (Hackett et al., 2013; Vincent et al., 2013). Interestingly, we found that not only *Tet1* and *Tet2* but also DNA-methylation-related genes were upregulated during TSKM reprogramming (Figures 5B and S5E). Therefore, a unique mechanism might be employed to reset an ESC-like DNA modification landscape during iPSC generation, and this process may further contribute to the genome-wide epigenetic reprogramming and transcriptional transition to ensure the attainment of pluripotency.

DNA Modification toward an ESC-like State Is Characterized by an Increase in 5mC and 5hmC at the Intermediate Stage

To examine the dynamic changes of 5mC and 5hmC in the TSKM 2° system, we performed mass spectrometry to quantify the total amount of 5mC and 5hmC modifications during TSKM 2° induction (Figures 5C and S5F). In TSKM 0D cells, the total amount of 5hmC was very low (approximately 3% of that in ESCs), whereas the 5mC content was approximately 20% higher than that in ESCs. Mass-spectrometry analysis further revealed that 5hmC showed a consistent increase during TSKM 2° induction (Figure 5C). In contrast, 5mC increased in TSKM cells at days 3 and 5, and depletion of 5mC appeared to occur much later (Figure 5C). Immunofluorescent staining of cells from TSKM 0D to TSKM 5D also indicated that the increase in 5mC and 5hmC could be detected at the same time in cells on day 3 and in clustered cells on day 5 (Figure S5G).

We then performed MeDIP and hMeDIP sequencing (MeDIP-seq and hMeDIP-seq) using TSKM 0D and TSKM 3D cells and TSKM 2-iPSCs (Figure 5A) and used that to generate a DNA methylation-hydroxymethylation-state map of TSKM-mediated reprogramming. Consistent with the mass-spectrometry analysis, we found that the predicted 5mC hot-spot regions first increased from TSKM 0D to TSKM 3D and decreased in TSKM 2-iPSC (104,011; 165,869; and 61,171, respectively). In addition, the predicted 5hmC hot-spot regions increased from TSKM 0D to TSKM 3D and then to TSKM 2-iPSC (42,301; 116,087; and 174,079, respectively; Table S1). We have summarized the relative enrichment of 5mC and 5hmC modifications at the different genomic regions. We also noticed that the changes in 5mC and 5hmC did not simply occur over the whole genome but instead increased at the CpG islands (CGIs) and gene-related regions (promoters, 5′ UTRs, 3′ UTRs, and exons; Figure 5D).

We further explored the 5mC and 5hmC changes on transcription start site (TSS) regions (2 kb around the TSS) for each individual gene. When the genes were ranked according to the fold changes of 5mC from TSKM 0D to TSKM 3D, a similar pattern of gradual color change between 5mC and 5hmC suggested that most TSS regions showed an increase in both 5mC and 5hmC during the early stage of reprogramming (from TSKM 0D to TSKM 3D) (Figure 5E). We observed a general decrease in 5mC later in the reprogramming process, whereas the 5hmC enrichment pattern underwent further significant changes (Figure 5E). Consistent with the increase of 5hmC on some loci, *Tet1*, *Tet2*, and Tet1-activity regulators (*Idh1* and *Idh2*) were upregulated during the TSKM reprogramming (Figures S7A and S7B).

The highly coordinated dynamics of 5mC and 5hmC indicated a genome-wide 5mC-to-5hmC conversion in TSKM-mediated reprogramming. This type of genome-wide 5hmC conversion from 5mC could potentially account for the de novo gain of 5hmC early in the reprogramming process and the 5mC depletion at later stages.

The Transcriptional Transition May Be Regulated by the Dynamic Change of DNA Modification

As a repressive mark, 5mC is believed to have a significant impact on transcription. We therefore compared the 5mC and 5hmC enrichments on the TSS regions in different gene clusters to investigate the impact of DNA modification dynamics on transcription during reprogramming. We found that most of the genes silenced in iPSCs (clusters I, II, and III) are not associated with significant 5mC increases in TSKM 2-iPSC relative to TSKM 0D (green versus blue lines in Figure S6A). However, we did observe an increase in 5mC and 5hmC at TSKM 3D (red lines in Figure S6A). In addition, the genes in cluster I that are strongly repressed in TSKM 3D cells possess the highest 5mC

(D) The relative enrichment of 5mC (upper panel) and 5hmC (lower panel) in different genomic regions. Promoters are defined as −1 to +0.5 kb regions around the gene TSS.

(E) The comparison of 5hmC and 5mC modifications in TSS regions during TSKM 2° reprogramming. The reads in the gene TSS region were compared among the samples; e.g., TSKM 3D versus 0D is the log ratio of 5mC/5hmC reads in TSKM 3D divided by the reads in TSKM 0D. The genes were ordered by the strength of the log ratio in 5mC-TSKM 3D versus 0D. The color indicates a trend of increased enrichment (red) or decreased enrichment (blue) between the two samples. See also Figures S5 and S7 and Table S1.

enrichment and the lowest 5hmC enrichment at the TSS, whereas the genes in cluster III that have the highest level of 5hmC levels and the lowest 5mC levels expressed highly in TSKM 3D cells (Figure 6A).

Among the genes activated by reprogramming (clusters IV and V), demethylation was observed in TSKM 2-iPSC relative to TSKM 0D (green versus blue lines in Figure S6B). Similarly, the genes in cluster IV, which were apparently upregulated in TSKM 3D, contain relatively low 5mC and high 5hmC enrichment in TSKM 3D cells (Figure 6B).

These results suggest that during TSKM-mediated reprogramming the repressive mark seen at most iPSC-silenced genes might be established through an increase in 5mC during the induction process. Moreover, at an intermediate stage of TSKM reprogramming, the expression status of genes might be regulated by the DNA modification state around the TSS, with 5mC acting to silence gene expression and 5hmC having converse activity.

5hmC Conversion Is Important for DNA Demethylation of Both Pluripotency Genes and ESC-Active Regulatory Regions during Reprogramming

Demethylation of pluripotency genes during reprogramming is considered to be extremely important for iPSC formation. Our data indicated that the genes in clusters IV and V undergo demethylation to reach stable transcriptional activity in iPSCs (Figure S6B). To investigate whether demethylation of key pluripotency genes occurs in a Tet1- and 5hmC-mediated manner similar to that seen for *Oct4*, we looked for demethylation-reactivated genes that are significantly upregulated with apparent demethylation during TSKM-mediated reprogramming and identified several important pluripotency genes, including *Oct4*, *Nanog*, *Gdf3*, *Zfp42* (*Rex1*), and *Dppa4* (Figures S6C and S6D).

We further analyzed the expression dynamics of these genes in TSKM-mediated reprogramming and found that reactivation of these genes was repressed by Tet1 deficiency and facilitated by additional Tet1 expression (Figures 6E and S6E). These dynamics were similar to that seen for *Oct4* (Figures 4E and S4I). We generated 5mC and 5hmC profiles for these genes calculated at the demethylated loci (Figures 6C and 6D) and found that the decrease in 5mC was coupled with 5hmC conversion from 5mC, which peaked in either TSKM 3D or TSKM 2-iPSCs at these loci (Figures 6C and 6D). hMeDIP-qPCR analysis further revealed that the 5hmC enrichment on these genes in TSKM 3D cells could be regulated by the Tet1 expression level (Figure S6F). Therefore, 5hmC conversion from 5mC may be involved in the demethylation and reactivation of these pluripotency factors during TSKM reprogramming as well. Importantly, the reactivation of these genes was also affected by the Tet1 expression level in the OSKM 2° system (Figure S6G), which further suggests that the underlying mechanism for reactivation of these genes may be shared across different factor-induced reprogramming systems.

In addition to regulating the expression of pluripotency genes, epigenetic modification of other regulatory regions may also be important for establishing pluripotency. We selected two defined ESC-active regulatory regions: ESC low-methylated regions (LMRs) and ESC H3K4me3 regions. The LMRs, with an average methylation of 30%, represent CpG-poor, distal regulatory regions, as evidenced by location, DNase I hypersensitivity, and the presence of enhancer marks and enhancer activities (Stadler et al., 2011). The H3K4me3 modification is usually associated with active regulatory regions and can also be used to predict active promoters (Heintzman et al., 2007). Consistent with previous studies (Stadler et al., 2011; Yu et al., 2012), these regions appeared to have relatively low levels of 5mC enrichment and higher 5hmC levels than neighboring regions in ESCs (Figure S6H). The average profile of 5mC and 5hmC showed that ESC-defined LMRs and H3K4me3 regions were highly enriched for 5mC in TSKM 0D cells, whereas the 5hmC level was low (Figure 6F). During TSKM-mediated reprogramming, the 5mC and 5hmC distributions were driven to an ESC-like state via both demethylation and relative 5hmC enrichment at the center of these regions. The accompanying increase in 5mC and 5hmC was observed in these centers from TSKM 0D to TSKM 3D, and localization-related DNA demethylation was observed from TSKM 3D to TSKM 2-iPSCs (Figure 6F). Overall, the data suggest that at these ESC-active regulatory regions, 5hmC converted from 5mC might be important for achieving demethylation and obtaining an ESC-like DNA modification state in iPSCs through TSKM-mediated reprogramming.

DISCUSSION

In this study, we explored the role of Tet1 and the 5hmC modification in iPSC generation. We demonstrated that Tet1 facilitated conventional iPSC induction. In the OSKM induction system, Tet1 promoted *Oct4* demethylation and reactivation through 5hmC conversion at the *Oct4* R-DMRs. Moreover, we discovered that Tet1 could replace Oct4 to initiate somatic cell reprogramming and generate fully pluripotent iPSCs in conjunction with SKM. Based on that, we established a rapid and efficient TSKM 2° reprogramming system. We showed that the demethylation and reactivation of endogenous *Oct4* is Tet1- and 5hmC-dependent in the TSKM reprogramming system. Using mass spectrometry and hMeDIP-seq analysis, we generated a unique state map of 5mC and 5hmC in TSKM-mediated reprogramming, which is characterized by an increase in both 5mC and 5hmC at an intermediate stage. Genome-wide analysis of transcriptome and DNA modifications revealed that both DNA methylation and hydroxymethylation play important roles in transcriptome resetting during reprogramming. Moreover, the conversion of 5mC to 5hmC may be important for DNA demethylation of both pluripotency genes and ESC-active regulatory regions in TSKM-mediated reprogramming.

One major contribution of the present study is that we successfully established a TSKM 2° reprogramming system and used it to identify an intermediate reprogramming stage (TSKM 3D) with relatively homogeneous cells, a clear-cut transcriptional transition, and an apparent 5hmC increase, which we then used to dissect molecular events in reprogramming at transcriptional and epigenetic levels. We generated state maps of transcriptome and DNA methylation and hydroxymethylation; these maps revealed a two-phase dynamic process during TSKM-mediated reprogramming (Figure 7A). Phase I (TSKM 0D to TSKM 3D) mainly involved disruption of the somatic epigenetic landscape. During this phase, an increase in both 5mC and

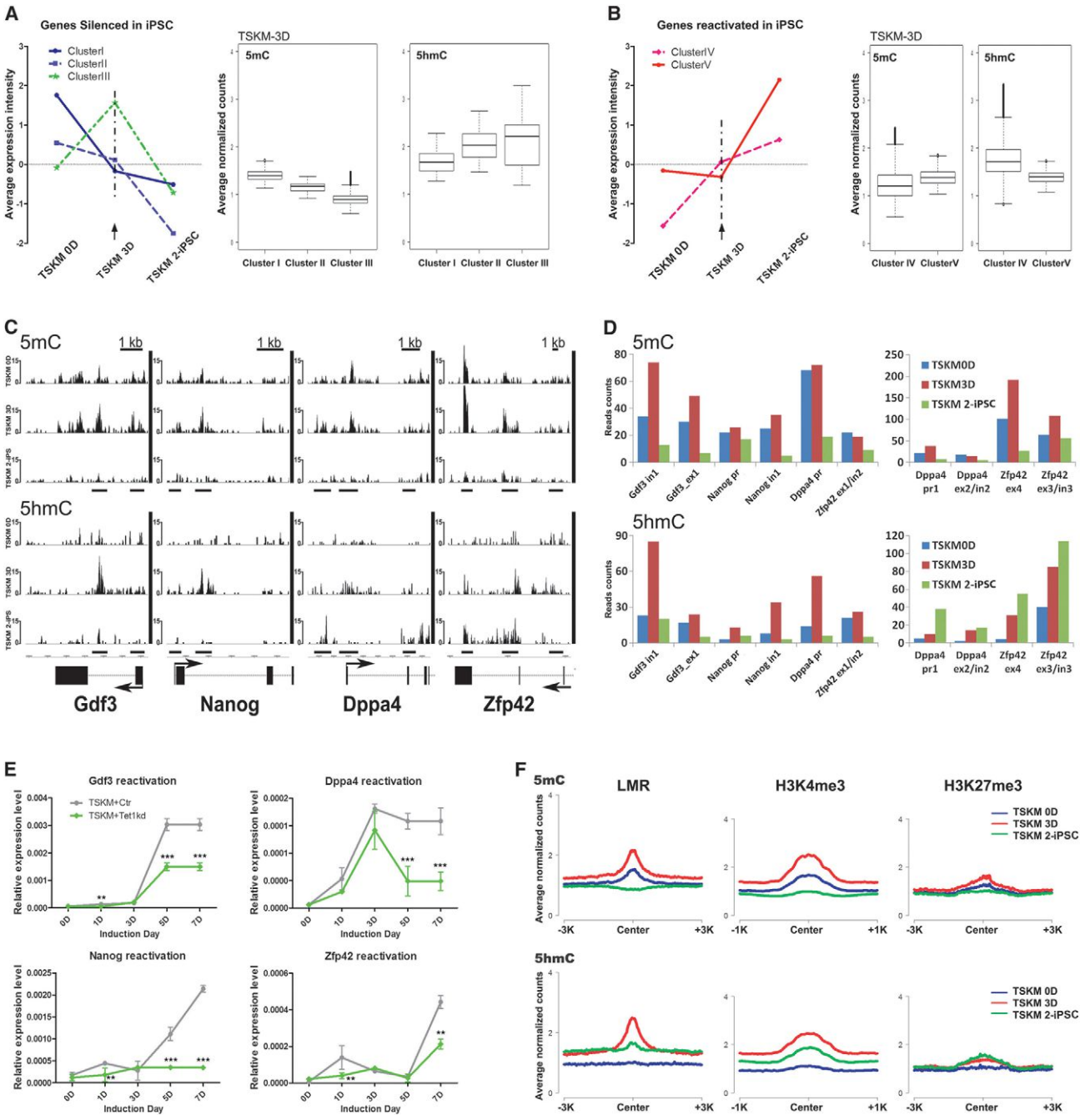

Figure 6. Reactivation of Pluripotency Genes and ESC-Active Regulatory Regions in TSKM 2° Reprogramming

(A and B) Transcriptional dynamics are related to the DNA modification state at the intermediate stage of TSKM 2° reprogramming. The average expression intensity for the genes in each cluster (Figure 5B) was displayed, and the average normalized 5mC and 5hmC reads in the gene TSS region were calculated, respectively. The counts' distributions were plotted (the box drawn by the "boxplot" command in R statistical language indicated the center quartiles of counts) for genes silenced in iPSCs (A) and for the genes reactivated in iPSCs (B).

(C and D) 5hmC peaks at the demethylation loci on indicated pluripotent genes at either intermediate or final stage in TSKM 2° induction. The pluripotency genes were demethylation-reactivated genes, as identified in Figure S6C. The demethylation loci are marked (C). Normalized 5mC (upper panels) and 5hmC (lower panels) counts on these loci are summarized (D).

(E) Tet1 deficiency represses the reactivation of indicated pluripotent genes. Data are represented as the mean ± SD (n = 3). *$p < 0.05$; **$p < 0.01$; ***$p < 0.001$ by Student's t test.

(F) The profiles of 5mC and 5hmC modifications in ESC-LMRs (left panels), ESC-H3K4me3 (middle panels), and ESC-H3K27me3 (right panels, represented as control) in TSKM 2° induction. The histone-modification-enriched regions are from the unpublished data set, which will be submitted soon (G. Chang and S.G., unpublished data). The identification of LMRs was from published data (Stadler et al., 2011).

See also Figure S6.

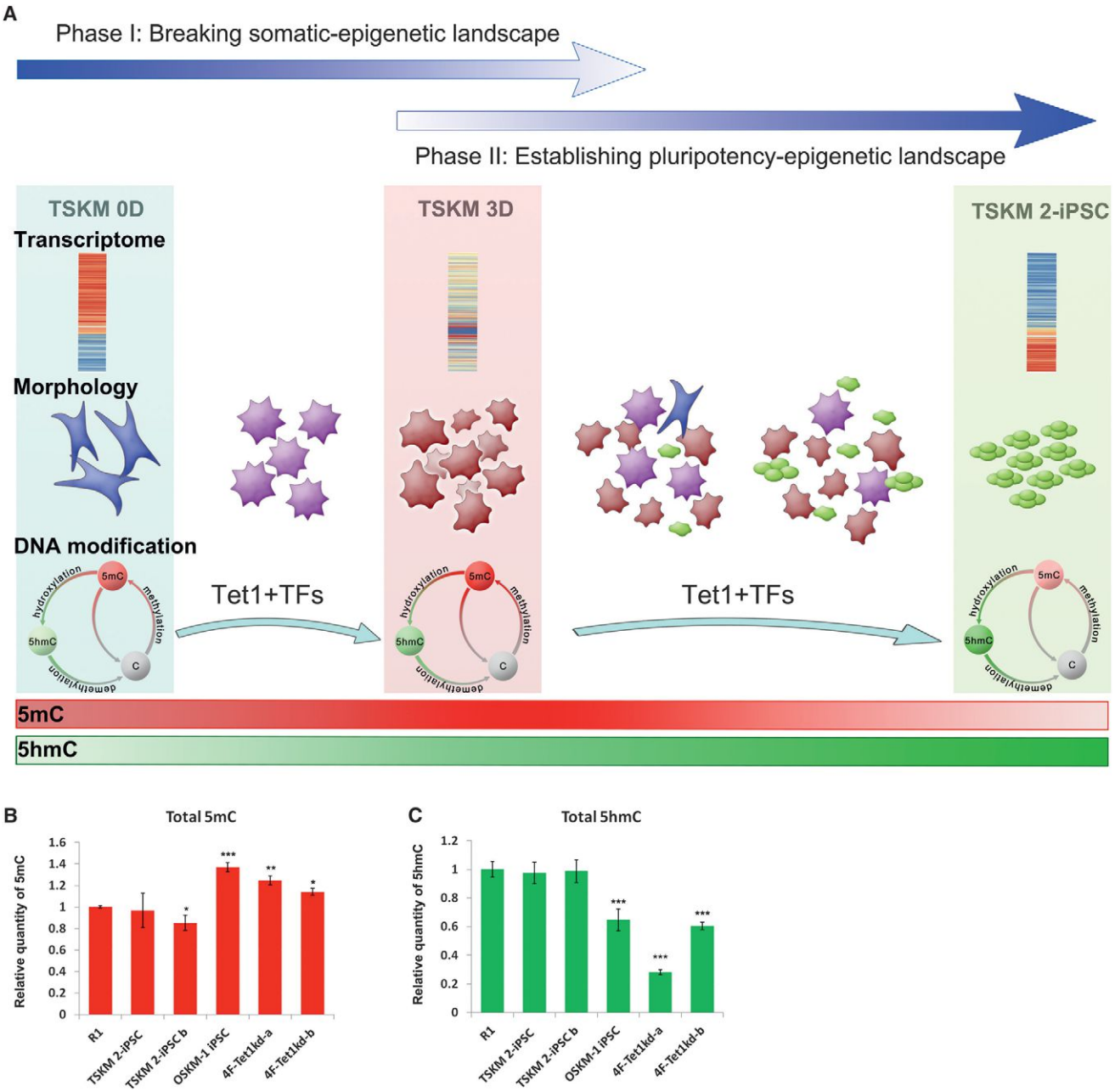

Figure 7. A Schematic Model of TSKM-Mediated Reprogramming and Quantification of 5mC and 5hmC in iPSCs

(A) The transcriptional transition and cell morphological changes are coupled with the DNA modification dynamics in TSKM 2° reprogramming.

(B and C) Quantification of genomic 5mC and 5hmC in indicated iPSCs. LC-MS/MS analysis of 5mC (B) and 5hmC (C) were performed with genomic DNA extracted from R1 ESCs, TSKM iPSCs, OSKM iPSCs, and 4F-Tet1kd-a# and -b# iPSCs. The values were normalized and compared to those in R1 ESCs. Data are shown as the mean ± SD (n = 3). *p < 0.05, **p < 0.01, ***p < 0.001 by ANOVA for comparison to TSKM 0D.

See also Figure S7.

5hmC can be observed, which may be related to Tet-mediated 5hmC conversion. Moreover, the correlation between 5mC, 5hmC, and the transcriptional state at this stage suggests that genome-wide DNA methylation and hydroxymethylation dynamics may contribute to the transcriptional transition in TSKM-mediated reprogramming (Figures 5B, 5E, 6A, and S6A). Phase II (TSKM 3D to TSKM 2-iPSC) is characterized by the re-establishment of an ESC-like epigenetic landscape. In this phase, widespread DNA demethylation, especially at the pluripotency genes and ESC-active regulatory regions, is accompanied by enrichment of 5hmC, which peaks at either the intermediate or at the final stage of reprogramming depending on the particular location (Figures 6C, 6D, 6F, S6B, and S6C). Our analysis therefore complements other recent studies looking

at the different stages that occur during the reprogramming process (Buganim et al., 2012; Golipour et al., 2012; Hansson et al., 2012; Polo et al., 2012) by focusing on the epigenetic reorganization events involved.

As reported previously, DNA demethylation involving 5hmC conversion plays important roles in epigenetic reprogramming in zygotes and PGC specification (Gu et al., 2011; Hackett et al., 2013; Inoue and Zhang, 2011; Iqbal et al., 2011). The dynamic changes of 5mC and 5hmC during somatic cell reprogramming appear distinct from those observed in zygotes and PGCs.

We noticed that expression of the enzymes responsible for de novo and maintenance DNA methylation was upregulated during iPSC induction (Figures 5B and S5E), and these enzymes could in principle hinder 5mC depletion during the later stage of reprogramming (from TSKM 5D to TSKM 2-iPSC). However, the simultaneous upregulation of active demethylase candidates (*Apobec 2*, *Apobec 3*, *Tdg*, *Parp1*, and *Mbd4*) during TSKM reprogramming (Figure S7B) suggests that active demethylation through 5hmC might function during later stages of iPSC induction. Therefore, a unique mechanism might be employed in TSKM iPSC generation to ensure that an ESC-like DNA methylation and hydroxylation state could be re-established rather than genome-wide erasure of both 5mC and 5hmC.

As an important epigenetic mark in iPSCs, 5hmC should be acquired and reset to an ESC-like state. A very recent report also proposed the important role of 5hmC in establishment of pluritotency (Costa et al., 2013). Therefore, the establishment of 5hmC distribution might be conserved in factor-induced somatic cell reprogramming. We demonstrate that the increase of 5hmC also occurred in the OSKM 2° system, albeit with somewhat different timing (Figure S7C).

However, we then noted that TSKM iPSCs contain comparable levels of 5mC and 5hmC to those in normal ESCs, whereas OSKM iPSCs and the 4F-Tet1kd iPSCs have less 5hmC and more 5mC (Figures 7B and 7C). Aberrant DNA methylation is observed widely in multiple cancers (Dawson and Kouzarides, 2012), and the loss of Tet1 and 5hmC may correlate with many types of cancers, and 5hmC loss has been recently identified as an epigenetic hallmark of melanoma (Ko et al., 2010; Kudo et al., 2012; Lian et al., 2012; Yang et al., 2013). The ESC-like levels of 5mC and 5hmC in TSKM iPSCs relative to OSKM iPSCs might partially account for the low tumor incidence observed in TSKM mice (Figure S3K). It will be important to investigate whether the 5hmC content is related to the risk of tumorigenesis of iPSCs, as this is a key issue for future clinical applications.

In summary, our study provides direct evidence that the DNA hydroxylase Tet1 promotes reprogramming to pluripotency and can in fact replace exogenous Oct4 in this process. The TSKM 2° reprogramming system that we have established will be a valuable tool for further investigation of the mechanisms of epigenetic remodeling involved in somatic cell reprogramming and for developing a systematic understanding of the events that occur in this exciting process.

EXPERIMENTAL PROCEDURES

Tet1 Lentiviral Vector Construction and TSKM iPSC Derivation

Full-length mouse *Tet1* (GU079948) was cloned from R1 ESCs and inserted into the FUW-TET-On vector. Inducible TSKM iPSCs were generated as previously described (Brambrink et al., 2008; Stadtfeld et al., 2008). ESC-like colonies appeared 3 to 5 weeks after induction. The colonies were selected and propagated after Dox withdrawal.

ChIP

The cells used for the ChIP assay were collected from the same dish or a parallel dish for FACS, qPCR, hMedIP-qPCR, and bisulfate analysis. ChIP was performed with the MAGnify kit (Invitrogen) and the following antibodies: anti-Tet1 (Xu et al., 2011), anti-Tet2 (Santa Cruz Biotechnology), anti-Tet3 (Santa Cruz Biotechnology), anti-dimethyl K4 of H3 (Millipore), anti-trimethyl K4 of H3 (Abcam), anti-trimethyl K27 of H3 (Millipore), and normal rabbit immunoglobulin G (MAGnify, Invitrogen).

hMeDIP-Seq

Genomic DNA was prepared using the QIAGEN DNeasy Blood & Tissue Kit or QIAGEN AllPrep DNA/RNA Mini Kit (treated with ribonuclease A). hMeDIP- and MeDIP-seq were performed as previously described (Ficz et al., 2011) using anti-5hmC (Active Motif) and anti-5mC (Calbiochem), respectively. Genomic DNA treated with *Bfa*I digestion was further analyzed via qPCR with the designed primers (Table S2). Sonicated genomic DNA (treated with NEBNext Master Mix) was used for hMeDIP-seq.

Liquid Chromatography-Mass Spectrometry

Cells undergoing reprogramming from day 0 to day 5 in the TSKM 2° system, R1 ESCs, and iPSCs from different induction systems were used for the 5mC and 5hmC quantity analysis. Liquid chromatography-tandem mass spectrometry (LC-MS/MS) analysis was performed for analyzing the quantity of 5mC and 5hmC in the genomic DNA of different cell samples, as detailed in the Supplemental Experimental Procedures.

Microarray Analysis

Total RNA was extracted using Trizol reagent (Invitrogen) from starting fibroblasts, intermediate-stage reprogrammed cells, and the fully reprogrammed iPSCs in three separate experiments. Analysis with the Mouse Gene 1.0 ST array (Affymetrix) was performed at CapitalBio in Beijing.

Mice

All of our study procedures were consistent with the National Institute of Biological Sciences guide for the care and use of laboratory animals.

Statistics

The Holm-Sidak test (for ANOVA) or Student's t test was performed using SigmaStat 3.5 software for statistics comparison.

ACCESSION NUMBERS

The microarray data sets and MeDIP and hMeDIP deep-sequencing data sets have been deposited in NCBI's Gene Expression Omnibus (GEO) under accession number GSE39639.

SUPPLEMENTAL INFORMATION

Supplemental Information includes seven figures, two tables, and Supplemental Experimental Procedures and can be found with this article online at http://dx.doi.org/10.1016/j.stem.2013.02.005.

ACKNOWLEDGMENTS

We thank Professor Rudolf Jaenisch from the Whitehead Institute of MIT for generously supplying the lentiviral vectors containing the cDNAs of the original four transcription factors. We thank Dr. Guo-Liang Xu from the Shanghai Institute of Biological Sciences for providing the Tet1 antibody. We thank Dr. Lijun Liu from Lanzhou University for assistance with the karyotype analysis of the TSKM-iPS8 cells. We thank Mr. Ning Yang for assistance with the design of the schematic model. We thank Dr. Bing Zhu and Dr. Dangsheng Li for their comments. We are also grateful to our laboratory colleagues for their assistance with experiments and in the preparation of the manuscript. This work

was supported by the Ministry of Science and Technology (grants 2010CB944900, 2011CB812700, and 2011CB964800).

Received: February 6, 2012
Revised: September 12, 2012
Accepted: February 19, 2013
Published: March 14, 2013

REFERENCES

Boland, M.J., Hazen, J.L., Nazor, K.L., Rodriguez, A.R., Gifford, W., Martin, G., Kupriyanov, S., and Baldwin, K.K. (2009). Adult mice generated from induced pluripotent stem cells. Nature *461*, 91–94.

Brambrink, T., Foreman, R., Welstead, G.G., Lengner, C.J., Wernig, M., Suh, H., and Jaenisch, R. (2008). Sequential expression of pluripotency markers during direct reprogramming of mouse somatic cells. Cell Stem Cell *2*, 151–159.

Buganim, Y., Faddah, D.A., Cheng, A.W., Itskovich, E., Markoulaki, S., Ganz, K., Klemm, S.L., van Oudenaarden, A., and Jaenisch, R. (2012). Single-cell expression analyses during cellular reprogramming reveal an early stochastic and a late hierarchic phase. Cell *150*, 1209–1222.

Chen, J., Liu, H., Liu, J., Qi, J., Wei, B., Yang, J., Liang, H., Chen, Y., Chen, J., Wu, Y., et al. (2013). H3K9 methylation is a barrier during somatic cell reprogramming into iPSCs. Nat. Genet. *45*, 34–42.

Costa, Y., Ding, J., Theunissen, T.W., Faiola, F., Hore, T.A., Shliaha, P.V., Fidalgo, M., Saunders, A., Lawrence, M., Dietmann, S., et al. (2013). NANOG-dependent function of TET1 and TET2 in establishment of pluripotency. Nature. Published online February 10, 2013. http://dx.doi.org/10.1038/nature11925.

Dawson, M.A., and Kouzarides, T. (2012). Cancer epigenetics: from mechanism to therapy. Cell *150*, 12–27.

Doege, C.A., Inoue, K., Yamashita, T., Rhee, D.B., Travis, S., Fujita, R., Guarnieri, P., Bhagat, G., Vanti, W.B., Shih, A., et al. (2012). Early-stage epigenetic modification during somatic cell reprogramming by Parp1 and Tet2. Nature *488*, 652–655.

Ficz, G., Branco, M.R., Seisenberger, S., Santos, F., Krueger, F., Hore, T.A., Marques, C.J., Andrews, S., and Reik, W. (2011). Dynamic regulation of 5-hydroxymethylcytosine in mouse ES cells and during differentiation. Nature *473*, 398–402.

Golipour, A., David, L., Liu, Y., Jayakumaran, G., Hirsch, C.L., Trcka, D., and Wrana, J.L. (2012). A late transition in somatic cell reprogramming requires regulators distinct from the pluripotency network. Cell Stem Cell *11*, 769–782.

Gruntman, E., Qi, Y., Slotkin, R.K., Roeder, T., Martienssen, R.A., and Sachidanandam, R. (2008). Kismeth: analyzer of plant methylation states through bisulfite sequencing. BMC Bioinformatics *9*, 371.

Gu, T.P., Guo, F., Yang, H., Wu, H.P., Xu, G.F., Liu, W., Xie, Z.G., Shi, L., He, X., Jin, S.G., et al. (2011). The role of Tet3 DNA dioxygenase in epigenetic reprogramming by oocytes. Nature *477*, 606–610.

Hackett, J.A., Sengupta, R., Zylicz, J.J., Murakami, K., Lee, C., Down, T.A., and Surani, M.A. (2013). Germline DNA demethylation dynamics and imprint erasure through 5-hydroxymethylcytosine. Science *339*, 448–452.

Hansson, J., Rafiee, M.R., Reiland, S., Polo, J.M., Gehring, J., Okawa, S., Huber, W., Hochedlinger, K., and Krijgsveld, J. (2012). Highly coordinated proteome dynamics during reprogramming of somatic cells to pluripotency. Cell Rep *2*, 1579–1592.

Hattori, N., Nishino, K., Ko, Y.G., Hattori, N., Ohgane, J., Tanaka, S., and Shiota, K. (2004). Epigenetic control of mouse Oct-4 gene expression in embryonic stem cells and trophoblast stem cells. J. Biol. Chem. *279*, 17063–17069.

Heintzman, N.D., Stuart, R.K., Hon, G., Fu, Y., Ching, C.W., Hawkins, R.D., Barrera, L.O., Van Calcar, S., Qu, C., Ching, K.A., et al. (2007). Distinct and predictive chromatin signatures of transcriptional promoters and enhancers in the human genome. Nat. Genet. *39*, 311–318.

Inoue, A., and Zhang, Y. (2011). Replication-dependent loss of 5-hydroxymethylcytosine in mouse preimplantation embryos. Science *334*, 194.

Iqbal, K., Jin, S.G., Pfeifer, G.P., and Szabó, P.E. (2011). Reprogramming of the paternal genome upon fertilization involves genome-wide oxidation of 5-methylcytosine. Proc. Natl. Acad. Sci. USA *108*, 3642–3647.

Kang, L., Wang, J., Zhang, Y., Kou, Z., and Gao, S. (2009). iPS cells can support full-term development of tetraploid blastocyst-complemented embryos. Cell Stem Cell *5*, 135–138.

Kang, L., Wu, T., Tao, Y., Yuan, Y., He, J., Zhang, Y., Luo, T., Kou, Z., and Gao, S. (2011). Viable mice produced from three-factor induced pluripotent stem (iPS) cells through tetraploid complementation. Cell Res. *21*, 546–549.

Ko, M., Huang, Y., Jankowska, A.M., Pape, U.J., Tahiliani, M., Bandukwala, H.S., An, J., Lamperti, E.D., Koh, K.P., Ganetzky, R., et al. (2010). Impaired hydroxylation of 5-methylcytosine in myeloid cancers with mutant TET2. Nature *468*, 839–843.

Koche, R.P., Smith, Z.D., Adli, M., Gu, H., Ku, M., Gnirke, A., Bernstein, B.E., and Meissner, A. (2011). Reprogramming factor expression initiates widespread targeted chromatin remodeling. Cell Stem Cell *8*, 96–105.

Koh, K.P., Yabuuchi, A., Rao, S., Huang, Y., Cunniff, K., Nardone, J., Laiho, A., Tahiliani, M., Sommer, C.A., Mostoslavsky, G., et al. (2011). Tet1 and Tet2 regulate 5-hydroxymethylcytosine production and cell lineage specification in mouse embryonic stem cells. Cell Stem Cell *8*, 200–213.

Kou, Z., Kang, L., Yuan, Y., Tao, Y., Zhang, Y., Wu, T., He, J., Wang, J., Liu, Z., and Gao, S. (2010). Mice cloned from induced pluripotent stem cells (iPSCs). Biol. Reprod. *83*, 238–243.

Kudo, Y., Tateishi, K., Yamamoto, K., Yamamoto, S., Asaoka, Y., Ijichi, H., Nagae, G., Yoshida, H., Aburatani, H., and Koike, K. (2012). Loss of 5-hydroxymethylcytosine is accompanied with malignant cellular transformation. Cancer Sci. *103*, 670–676.

Lian, C.G., Xu, Y., Ceol, C., Wu, F., Larson, A., Dresser, K., Xu, W., Tan, L., Hu, Y., Zhan, Q., et al. (2012). Loss of 5-hydroxymethylcytosine is an epigenetic hallmark of melanoma. Cell *150*, 1135–1146.

Maherali, N., Sridharan, R., Xie, W., Utikal, J., Eminli, S., Arnold, K., Stadtfeld, M., Yachechko, R., Tchieu, J., Jaenisch, R., et al. (2007). Directly reprogrammed fibroblasts show global epigenetic remodeling and widespread tissue contribution. Cell Stem Cell *1*, 55–70.

Meissner, A., Mikkelsen, T.S., Gu, H., Wernig, M., Hanna, J., Sivachenko, A., Zhang, X., Bernstein, B.E., Nusbaum, C., Jaffe, D.B., et al. (2008). Genome-scale DNA methylation maps of pluripotent and differentiated cells. Nature *454*, 766–770.

Mikkelsen, T.S., Hanna, J., Zhang, X., Ku, M., Wernig, M., Schorderet, P., Bernstein, B.E., Jaenisch, R., Lander, E.S., and Meissner, A. (2008). Dissecting direct reprogramming through integrative genomic analysis. Nature *454*, 49–55.

Okita, K., Ichisaka, T., and Yamanaka, S. (2007). Generation of germline-competent induced pluripotent stem cells. Nature *448*, 313–317.

Onder, T.T., Kara, N., Cherry, A., Sinha, A.U., Zhu, N., Bernt, K.M., Cahan, P., Marcarci, B.O., Unternaehrer, J., Gupta, P.B., et al. (2012). Chromatin-modifying enzymes as modulators of reprogramming. Nature *483*, 598–602.

Plath, K., and Lowry, W.E. (2011). Progress in understanding reprogramming to the induced pluripotent state. Nat. Rev. Genet. *12*, 253–265.

Polo, J.M., Anderssen, E., Walsh, R.M., Schwarz, B.A., Nefzger, C.M., Lim, S.M., Borkent, M., Apostolou, E., Alaei, S., Cloutier, J., et al. (2012). A molecular roadmap of reprogramming somatic cells into iPS cells. Cell *151*, 1617–1632.

Samavarchi-Tehrani, P., Golipour, A., David, L., Sung, H.K., Beyer, T.A., Datti, A., Woltjen, K., Nagy, A., and Wrana, J.L. (2010). Functional genomics reveals a BMP-driven mesenchymal-to-epithelial transition in the initiation of somatic cell reprogramming. Cell Stem Cell *7*, 64–77.

Singhal, N., Graumann, J., Wu, G., Araúzo-Bravo, M.J., Han, D.W., Greber, B., Gentile, L., Mann, M., and Schöler, H.R. (2010). Chromatin-Remodeling Components of the BAF Complex Facilitate Reprogramming. Cell *141*, 943–955.

Soufi, A., Donahue, G., and Zaret, K.S. (2012). Facilitators and impediments of the pluripotency reprogramming factors' initial engagement with the genome. Cell *151*, 994–1004.

Stadler, M.B., Murr, R., Burger, L., Ivanek, R., Lienert, F., Schöler, A., van Nimwegen, E., Wirbelauer, C., Oakeley, E.J., Gaidatzis, D., et al. (2011). DNA-binding factors shape the mouse methylome at distal regulatory regions. Nature *480*, 490–495.

Stadtfeld, M., Maherali, N., Breault, D.T., and Hochedlinger, K. (2008). Defining molecular cornerstones during fibroblast to iPS cell reprogramming in mouse. Cell Stem Cell *2*, 230–240.

Surani, M.A., Hayashi, K., and Hajkova, P. (2007). Genetic and epigenetic regulators of pluripotency. Cell *128*, 747–762.

Tahiliani, M., Koh, K.P., Shen, Y., Pastor, W.A., Bandukwala, H., Brudno, Y., Agarwal, S., Iyer, L.M., Liu, D.R., Aravind, L., and Rao, A. (2009). Conversion of 5-methylcytosine to 5-hydroxymethylcytosine in mammalian DNA by MLL partner TET1. Science *324*, 930–935.

Takahashi, K., and Yamanaka, S. (2006). Induction of pluripotent stem cells from mouse embryonic and adult fibroblast cultures by defined factors. Cell *126*, 663–676.

Takahashi, K., Tanabe, K., Ohnuki, M., Narita, M., Ichisaka, T., Tomoda, K., and Yamanaka, S. (2007). Induction of pluripotent stem cells from adult human fibroblasts by defined factors. Cell *131*, 861–872.

Vincent, J.J., Huang, Y., Chen, P.Y., Feng, S., Calvopiña, J.H., Nee, K., Lee, S.A., Le, T., Yoon, A.J., Faull, K., et al. (2013). Stage-Specific Roles for Tet1 and Tet2 in DNA Demethylation in Primordial Germ Cells. Cell Stem Cell. Published online February 13, 2013. http://dx.doi.org/10.1016/j.stem.2013.01.016.

Wang, T., Chen, K., Zeng, X., Yang, J., Wu, Y., Shi, X., Qin, B., Zeng, L., Esteban, M.A., Pan, G., and Pei, D. (2011). The histone demethylases Jhdm1a/1b enhance somatic cell reprogramming in a vitamin-C-dependent manner. Cell Stem Cell *9*, 575–587.

Wernig, M., Meissner, A., Foreman, R., Brambrink, T., Ku, M., Hochedlinger, K., Bernstein, B.E., and Jaenisch, R. (2007). In vitro reprogramming of fibroblasts into a pluripotent ES-cell-like state. Nature *448*, 318–324.

Wu, H., and Zhang, Y. (2011). Mechanisms and functions of Tet protein-mediated 5-methylcytosine oxidation. Genes Dev. *25*, 2436–2452.

Wu, H., D'Alessio, A.C., Ito, S., Xia, K., Wang, Z., Cui, K., Zhao, K., Sun, Y.E., and Zhang, Y. (2011). Dual functions of Tet1 in transcriptional regulation in mouse embryonic stem cells. Nature *473*, 389–393.

Xu, Y., Wu, F., Tan, L., Kong, L., Xiong, L., Deng, J., Barbera, A.J., Zheng, L., Zhang, H., Huang, S., et al. (2011). Genome-wide regulation of 5hmC, 5mC, and gene expression by Tet1 hydroxylase in mouse embryonic stem cells. Mol. Cell *42*, 451–464.

Yang, H., Liu, Y., Bai, F., Zhang, J.Y., Ma, S.H., Liu, J., Xu, Z.D., Zhu, H.G., Ling, Z.Q., Ye, D., et al. (2013). Tumor development is associated with decrease of TET gene expression and 5-methylcytosine hydroxylation. Oncogene *32*, 663–669.

Yang, P., Wang, Y., Chen, J., Li, H., Kang, L., Zhang, Y., Chen, S., Zhu, B., and Gao, S. (2011). RCOR2 is a subunit of the LSD1 complex that regulates ESC property and substitutes for SOX2 in reprogramming somatic cells to pluripotency. Stem Cells *29*, 791–801.

Yu, M., Hon, G.C., Szulwach, K.E., Song, C.X., Zhang, L., Kim, A., Li, X., Dai, Q., Shen, Y., Park, B., et al. (2012). Base-resolution analysis of 5-hydroxymethylcytosine in the mammalian genome. Cell *149*, 1368–1380.

Zhao, X.Y., Li, W., Lv, Z., Liu, L., Tong, M., Hai, T., Hao, J., Guo, C.L., Ma, Q.W., Wang, L., et al. (2009). iPS cells produce viable mice through tetraploid complementation. Nature *461*, 86–90.

Cell Symposia

Hallmarks of Cancer: Asia

November 9-11, 2014 — Beijing, China

In partnership with

2014 相约在北京，交流癌症机理及临床研究的世界最新动向

Hallmarks of Cancer: Asia will convene global leaders in cancer research to promote rapid translation of new findings, idea exchanges, and future collaborations among oncologists, drug development industries and scientists.

Symposium themes:

- Understanding cancer hallmarks - new frontiers
- Cancer hallmarks as therapeutic targets
- Tumor immunology and immunotherapy
- Clinical progress and obstacles
- Managing cancer in the “omics” era

Abstract submission deadline:

July 11 2014

Early bird deadline:

Sept 12 2014

Co-organizers:

Xuetao Cao, *President of the Chinese Academy of Medical Sciences, Beijing, China*

Xiaohong Helena Yang, Senior Editor, *Cancer Cell*

Angela Messmer-Blust, Scientific Editor, *Conferences*

www.cell-symposia-hallmarksofcancer-2014.com

Cell Stem Cell
Article

Genome-wide Chromatin Interactions of the *Nanog* Locus in Pluripotency, Differentiation, and Reprogramming

Effie Apostolou,[1,2,3,11] Francesco Ferrari,[4,11] Ryan M. Walsh,[1,2,3] Ori Bar-Nur,[1,2,3] Matthias Stadtfeld,[1,2,3,9] Sihem Cheloufi,[1,2,3] Hannah T. Stuart,[1,2,3] Jose M. Polo,[1,2,3,10] Toshiro K. Ohsumi,[5] Mark L. Borowsky,[5] Peter V. Kharchenko,[4,6] Peter J. Park,[4,7,8,*] and Konrad Hochedlinger[1,2,3,*]

[1]Massachusetts General Hospital Cancer Center and Center for Regenerative Medicine, 185 Cambridge Street, Boston, MA 02114, USA
[2]Harvard Stem Cell Institute, 1350 Massachusetts Avenue, Cambridge, MA 02138, USA
[3]Howard Hughes Medical Institute and Department of Stem Cell and Regenerative Biology, Harvard University and Harvard Medical School, 7 Divinity Avenue, Cambridge, MA 02138, USA
[4]Center for Biomedical Informatics, Harvard Medical School, 10 Shattuck Street, Boston, MA 02115, USA
[5]Department of Molecular Biology, Massachusetts General Hospital and Harvard Medical School, 185 Cambridge Street, Boston, MA 02114, USA
[6]Division of Hematology/Oncology
[7]Informatics Program
Children's Hospital, Boston, MA 02115, USA
[8]Division of Genetics, Brigham and Women's Hospital, Boston, MA 02115, USA
[9]Present address: The Helen L. and Martin S. Kimmel Center for Biology and Medicine, The Skirball Institute of Biomolecular Medicine, New York University, New York, NY 10016, USA
[10]Present address: Australian Regenerative Medicine Institute and Department of Anatomy and Developmental Biology, Monash University, Wellington Rd, Clayton, Vic 3800, Australia
[11]These authors contributed equally to this work
*Correspondence: peter_park@harvard.edu (P.J.P.), khochedlinger@helix.mgh.harvard.edu (K.H.)
http://dx.doi.org/10.1016/j.stem.2013.04.013

SUMMARY

The chromatin state of pluripotency genes has been studied extensively in embryonic stem cells (ESCs) and differentiated cells, but their potential interactions with other parts of the genome remain largely unexplored. Here, we identified a genome-wide, pluripotency-specific interaction network around the *Nanog* promoter by adapting circular chromosome conformation capture sequencing. This network was rearranged during differentiation and restored in induced pluripotent stem cells. A large fraction of *Nanog*-interacting loci were bound by Mediator or cohesin in pluripotent cells. Depletion of these proteins from ESCs resulted in a disruption of contacts and the acquisition of a differentiation-specific interaction pattern prior to obvious transcriptional and phenotypic changes. Similarly, the establishment of *Nanog* interactions during reprogramming often preceded transcriptional upregulation of associated genes, suggesting a causative link. Our results document a complex, pluripotency-specific chromatin "interactome" for *Nanog* and suggest a functional role for long-range genomic interactions in the maintenance and induction of pluripotency.

INTRODUCTION

Three-dimensional (3D) chromatin architecture is important for many biological processes including transcriptional regulation. For example, looping between promoter and enhancer or insulator elements controls the transcriptional activation or repression of genes, respectively (Engel and Tanimoto, 2000; Ling et al., 2006; Zhao et al., 2006). Although long-range chromatin interactions have been observed mostly in *cis* along the same chromosome (Schoenfelder et al., 2010), they can also occur in *trans* between different chromosomes. Interactions in *trans* are associated with coregulation of imprinted genes (Zhao et al., 2006) or genes associated with erythropoiesis (Schoenfelder et al., 2010), with stochastic selection for monoallelic activation of the *IFN-β* locus (Apostolou and Thanos, 2008) and olfactory genes (Clowney et al., 2012; Lomvardas et al., 2006), and with activation-induced cytidine deaminase-mediated translocations (Klein et al., 2011; Rocha et al., 2012). Although the organization of chromosomes into defined territories was reported three decades ago (Schardin et al., 1985), the molecular principles of global chromatin architecture have only recently been explored with high-throughput technologies such as the Hi-C method (Dixon et al., 2012; Duan et al., 2010; Lieberman-Aiden et al., 2009; Sexton et al., 2012; Zhang et al., 2012).

Chromatin organization also plays a role in the control of pluripotency and cellular differentiation. For instance, pluripotency-associated genes such as *Sox2*, *Nanog*, and *Klf4* relocate from the nuclear center to the nuclear periphery upon differentiation of mouse embryonic stem cells (ESCs) (Peric-Hupkes et al., 2010). Moreover, the loss of promoter-enhancer interactions at key pluripotency genes, including *Nanog* and *Oct4*, during ESC differentiation has been associated with silencing of these genes (Kagey et al., 2010; Levasseur et al., 2008). Proteins involved in chromatin looping, including CTCF, cohesin, and Mediator, co-occupy many genomic targets of pluripotency factors (Kagey et al., 2010; Nitzsche et al., 2011) or directly interact with them

(Donohoe et al., 2009; Tutter et al., 2009). These molecules might therefore cooperate to arrange a higher-order chromatin structure that maintains pluripotency. Indeed, depletion of Mediator and cohesin subunits from ESCs results in unscheduled differentiation (Kagey et al., 2010). A more recent study using the Hi-C technology in mouse and human ESCs and differentiated cells identified a network of local chromatin-interaction domains, so-called topological domains, with conserved boundaries among different species and cell types (Dixon et al., 2012). Although that report documented important general principles of chromatin organization in pluripotent and differentiated cells, a high-resolution map of genome-wide interactions of pluripotency genes in ESCs is lacking. It also remains unclear which molecules might be involved in establishing such putative connections, and whether and how these patterns change upon differentiation.

Forced expression of the transcription factors Oct4, Sox2, Klf4, and c-Myc is sufficient for endowing somatic cells with pluripotency, giving rise to induced pluripotent stem cells (iPSCs) (Takahashi and Yamanaka, 2006). In-depth molecular analysis of reprogramming intermediates has been achieved only recently with improved technologies for studying rare and defined cell populations (Buganim et al., 2012; Golipour et al., 2012; Polo et al., 2012; Soufi et al., 2012). In addition, molecular characterization of stable partially reprogrammed iPSC (piPSC) lines sheds light on the earliest events in cellular reprogramming (Mikkelsen et al., 2008; Sridharan et al., 2009). Although these studies reported the reestablishment of an ESC-like transcriptional and epigenetic state, it remains unclear whether, when, and how the 3D chromatin structure is reset during cellular reprogramming into iPSCs.

In this study, we have investigated the genome-wide interaction network of the *Nanog* gene, which is indispensable for development as well as for the derivation of ESCs (Mitsui et al., 2003; Chambers et al., 2003) and iPSCs (Silva et al., 2009). We developed a modified version of circular chromosome conformation capture sequencing (m4C-seq) to determine the genome-wide interaction partners of the *Nanog* locus in ESCs, iPSCs, and mouse embryonic fibroblasts (MEFs) at high resolution. Our study provides the first detailed chromatin-interaction map of a key pluripotency locus on a genomic scale and offers mechanistic insights into the regulation of chromatin architecture during the acquisition and maintenance of pluripotency.

RESULTS

The *Nanog* Locus Engages in Distinct Genome-wide Interactions in Pluripotent and Differentiated Cells

We developed a modified version of 4C-seq for unbiased genome-wide capture of *Nanog*'s interactions in pluripotent and differentiated cells (Figure 1A; see Experimental Procedures). In brief, 4C technology is based on the proximity-ligation principle, in which unknown chromatin loci that interact with a known "bait" locus (e.g., *Nanog*) are ligated into chimeric DNA molecules and then identified by deep sequencing (Dekker et al., 2002). m4C-seq involves ligation of universal adapters to the linearized hybrid molecules, followed by ligation-mediated PCR with an adaptor-specific oligonucleotide and a biotinylated primer recognizing the *Nanog* locus. This allows specific enrichment and purification of the *Nanog*-interacting regions using streptavidin beads and avoids the less-efficient recircularization and inverse-PCR steps of published 4C methods.

To increase confidence in observed interactions, we used biological replicates, applied multiple filtering and normalization steps, and adjusted for random ligation events and possible technical biases based on a control sample (noncrosslinked genomic DNA; see Experimental Procedures). Technical replicates generated by independent ligation, amplification, and sequencing showed a high level of concordance (Spearman's rank correlation coefficient $\approx$ 0.9) (Figure S1A available online). We then analyzed three independent biological replicates for ESC lines (R1, V6.5, and KH2-ESC1), MEFs, and fibroblast-derived iPSC clones previously shown to give rise to entirely iPSC-derived mice, thus satisfying the most stringent criteria of pluripotency (Stadtfeld et al., 2010a). The biological replicates of pluripotent cells showed higher variability than the technical replicates, as expected, but nevertheless exhibited high correlation (Spearman's coefficient $\approx$ 0.7) (Figures S1A–S1D). However, MEF replicates showed notably lower correlation (Spearman's coefficient $\approx$ 0.3), suggesting that *Nanog* may have less-stable interactions in MEFs, perhaps because the gene is not active.

Unsupervised clustering (Figure 1B) highlighted similarities between ESCs and iPSCs, which clustered separately from MEFs. Consistent with this observation, we found extensive overlap ($\sim$70%) among the conserved *Nanog* interactions in ESCs and iPSCs (Table S1), but much less overlap between these pluripotent samples and MEFs (<10% of pluripotent interactions) (Figure 1C). The higher variability in MEF samples resulted in a smaller set of conserved interactions among replicates (Figures 1C and S1C; Table S1). These results show distinct *Nanog* interactomes in differentiated and pluripotent cells.

Given that *Nanog* is located in a gene-rich genomic region containing other pluripotency loci, we first examined a 200 kb window around its promoter. We detected several interaction partners, including the *Nanog* enhancer, *Aicda*, *Apobec1*, and *Scl2a3* genes (Figure S1E). We obtained reads for 11 out of 12 loci that have previously been tested in ESCs by chromosome conformation capture (3C) (Levasseur et al., 2008). We also identified broad interaction domains in distal regions on chromosome 6, visualized in the form of a "domainogram" (Figure S2A) (Bantignies et al., 2011). Randomly selected interactions within the broad domains were verified by 3D DNA fluorescence in situ hybridization (FISH) (Figures 1D, 1E, and S2B) and by 3C analysis among single HindIII fragments using independent cell preparations (Figure S2D). FISH results were independently confirmed for a subset of nuclei ($\sim$250 nuclei for three probes in total) at a higher resolution, which allowed for more accurate measurement of colocalized signals (<250 nm, Figure S2C).

Broad interaction domains with differential strengths in ESCs and MEFs are shown in Figure 1F. MEF-derived iPSCs and ESCs showed similar differential domainogram patterns when compared to MEFs, suggesting that reprogramming restored the ESC-specific 3D structure along chromosome 6. Furthermore, *cis* interaction patterns observed in published Hi-C data for ESCs (Dixon et al., 2012) exhibited a higher correlation to those we detected in ESCs and iPSCs than to those in MEFs (Figure S2E). Together, these data document that *Nanog* forms a pluripotency-specific interactome with multiple genomic regions along its entire chromosome in both ESCs and iPSCs.

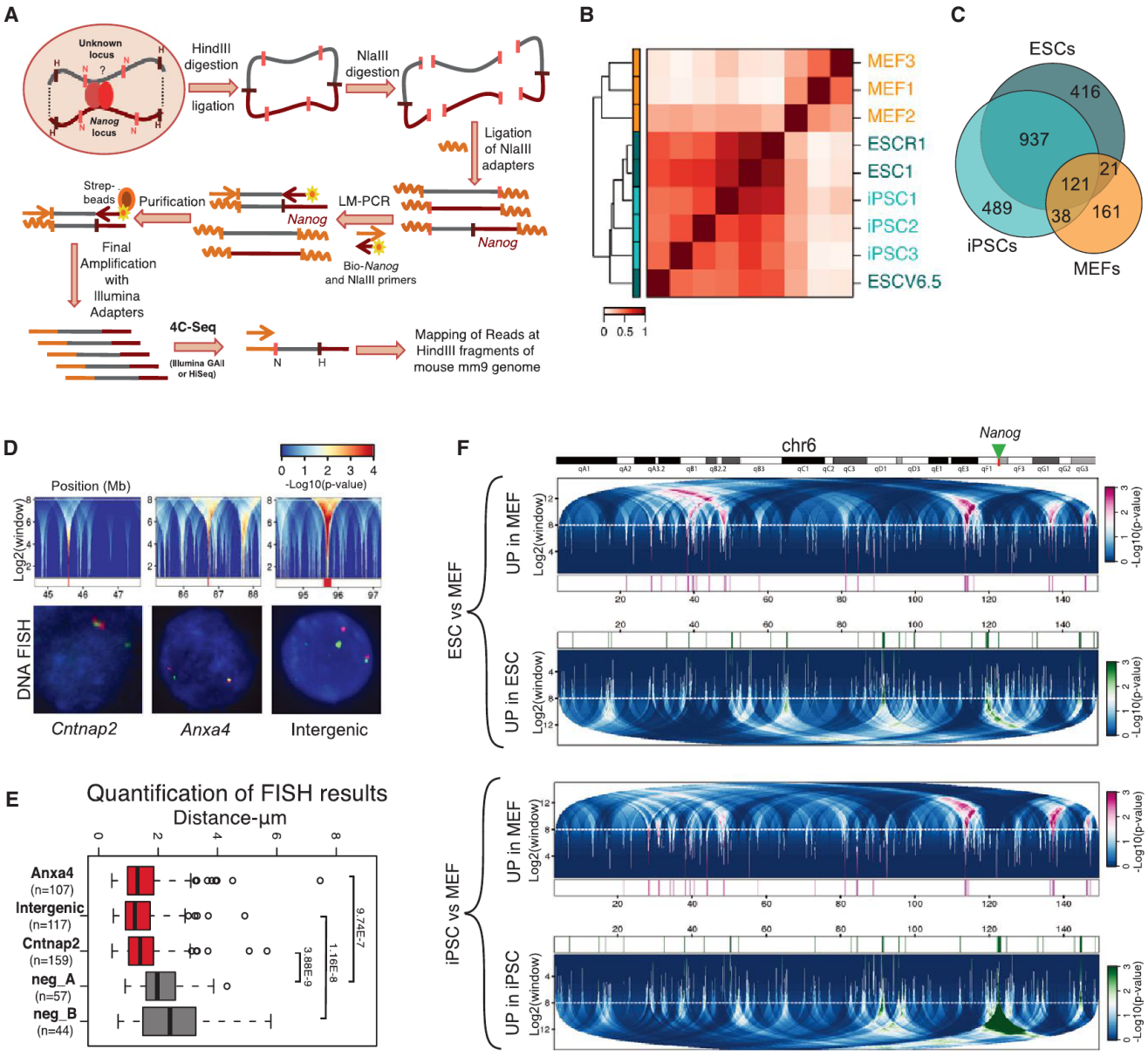

Figure 1. Genome-wide Interactions of the *Nanog* Locus in Differentiated and Pluripotent Cells

(A) Schematic representation of m4C-seq. LM-PCR, ligation-mediated PCR; Strep-beads, streptavidin-conjugated beads; H, HindIII site; N, NlaIII site.

(B) Unsupervised clustering and correlation matrix of pluripotent and differentiated cells (three ESCs, three iPSCs, and three MEFs). Normalized (observed over expected) m4C-seq signals at individual HindIII fragments are clustered, with Spearman's correlation (color gradient) and average linkage shown. Fragments detected in at least three out of nine samples are used.

(C) Venn diagram showing the degree of overlap among the *Nanog*-interacting HindIII fragments common within each group: ESCs, iPSCs, and MEFs.

(D) The upper panels show details of domainogram analysis for broad intrachromosomal interaction domains (*Cntnap2*, *Anxa4*, and an intergenic region) in individual samples. Regions around broad interaction domains are shown for a representative ESC sample (ESC1 cell line). The centers of interacting domains are marked in red at the bottom (p value < 0.0001). The dashed horizontal white line indicates the maximum-window-size cutoff. The bottom panels show representative 3D DNA FISH in ESCs confirming the interaction of *Nanog* (green fluorescein isothiocyanate [FITC] signals) with each of those domains (magenta Alexa 568 signals).

(E) Boxplot for distances between the *Nanog* locus and the tested domains (n = number of measured nuclei). Intrachromosomal regions between the positive hits and the bait position were used as negative controls (neg_A and neg_B). p values for the Wilcoxon signed-rank test are reported (see also Figure S2C). Whiskers extend to the most extreme values within 1.5 times the interquartile range from the upper or lower quartile.

(F) Differential interactions over large domains (domainogram) for ESCs versus MEFs (upper panel) and iPSCs versus MEFs (bottom panel) on chromosome 6. The green arrow indicates the *Nanog* position. Top: interacting domains upregulated in MEFs (magenta); bottom: interacting domains upregulated in ESCs or iPSCs, respectively (green). In the central part, magenta and green marks indicate the regions significantly upregulated (p value < 0.001) in MEFs and ESCs or iPSCs, respectively. The dashed horizontal white line indicates the maximum-window-size cutoff. All replicates for each cell type are taken into account for computing the score for differential interactions.

See also Figures S1 and S2 and Tables S1 and S6.

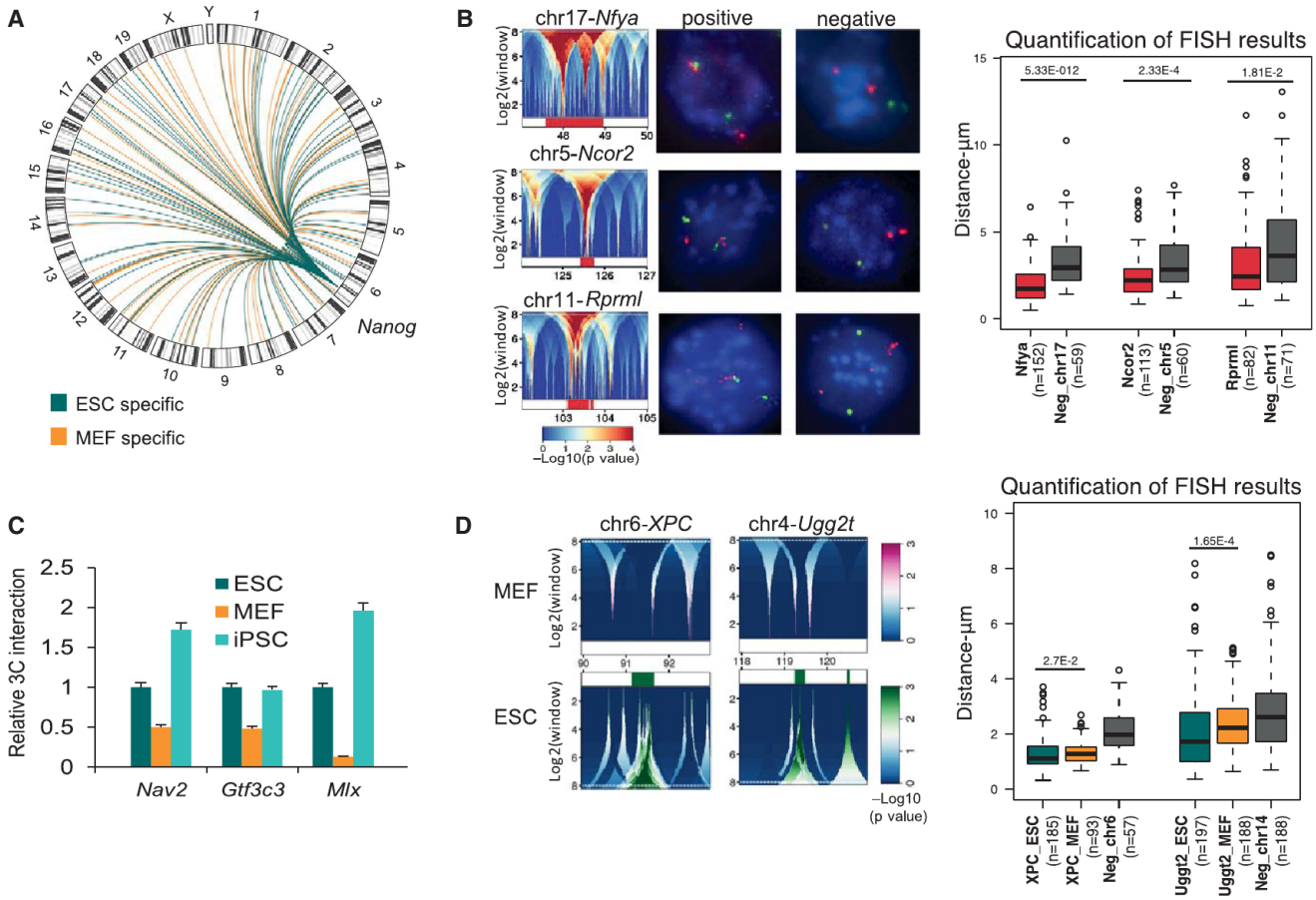

Figure 2. Detection and Validation of Interchromosomal Associations of the *Nanog* Locus in Pluripotent and Differentiated Cells

(A) Circos plot for differential interchromosomal interactions in ESCs (green) compared to MEFs (orange) as detected from broad domain analysis using domainograms (Figure 1F) in each chromosome.

(B) Three interchromosomal *Nanog*-interacting domains confirmed by 3D DNA FISH in ESCs. The domainograms refer to the ESC1 line and are representative of other ESCs. Representative 3D DNA FISH images show the *Nanog* alleles (green FITC signals) interacting with each of those domains (left) or their corresponding negative controls (right) (magenta Alexa 568 signals). The boxplots report 3D DNA FISH results (n = number of nuclei; p = Wilcoxon test p value) (whiskers are as in Figure 1E). Negative controls were selected in regions within 2 Mb of the targets.

(C) 3C PCR confirmation of selected differential interchromosomal interactions of the *Nanog* locus in ESCs and iPSCs versus MEFs. For each primer pair, the PCR signal was calculated relative to the corresponding signal in ESCs ("Relative 3C Interaction") after normalization with the PCR signal of primers designed at the bait locus (see Table S6). Error bars indicate SD (n = 3 technical replicates). All 3C PCR products were isolated and analyzed by Sanger sequencing.

(D) Domainogram details for differential interactions around *XPC* and *Ugg2t*, which were found to interact with *Nanog* preferentially in ESCs. Top (magenta) and bottom panels (green) refer to interaction enrichment in MEFs and pluripotent cells, respectively. 3D DNA FISH results for the two regions are shown in the boxplot, similarly to (B) (whiskers are as in Figure 1E).

See also Figure S2 and Tables S2 and S6.

Nanog Participates in Pluripotency-Specific Interchromosomal Associations

Many of the detected contacts were found to be *trans* interactions of *Nanog* with other chromosomes (Figure 2A and Table S1). Although previous studies using conventional 4C-seq protocols did not detect such a high number of *trans* associations (Simonis et al., 2006, 2009), our results are consistent with a similar 4C adaption termed "enhanced 4C" (e4C) (Schoenfelder et al., 2010). We believe that m4C-seq and e4C approaches using universal adapters and streptavidin-based purification and enrichment of the bait locus enable greater sensitivity. The high number of observed interchromosomal interactions is further supported by the tendency of the *Nanog* locus to localize on the edge or outside of its chromosome territory (Figure S2F). Moreover, reanalysis of recently published Hi-C data from mouse ESCs (Dixon et al., 2012) showed that over 60% of *Nanog*'s *trans* interactions overlapped significantly with our m4C-seq interactions in ESCs and iPSCs, but not with those in MEFs (Figure S2G). Selected interacting regions in ESCs, localized on three different chromosomes, were tested by 3D DNA FISH in ESCs, and they showed closer proximity to the *Nanog* locus compared with noninteracting regions on the respective chromosomes (Figure 2B).

The distribution of broad differential intra- and interchromosomal interaction domains in pluripotent (ESCs) versus differentiated (MEFs) cells is visualized in Figure 2A. In addition,

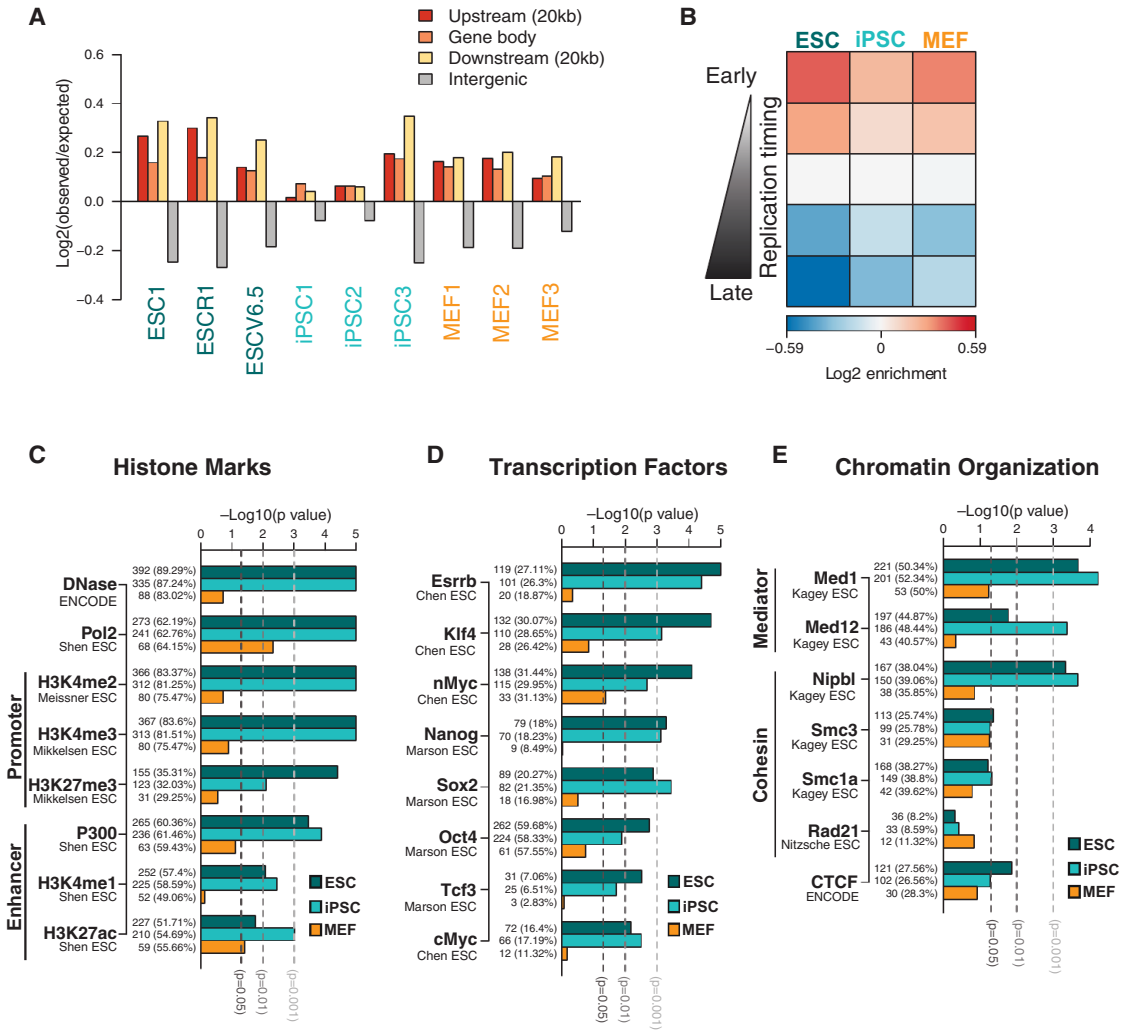

Figure 3. *Nanog*-Interacting Regions Are Enriched for Open Chromatin Features and Pluripotency-Factor Binding in Pluripotent Cells

(A) Distribution of the *Nanog*-interacting loci detected at single-fragment level in each sample. Log ratios of observed over expected fragments in different genomic regions show a consistent overrepresentation of interactions in genes and surrounding regions (20 kb upstream or downstream).

(B) Association of the *Nanog*-interacting regions with replication timing (RT). Genomic segments were divided into five groups (from early to late) based on their RT data in each cell type (Hiratani et al., 2010). The median association of interacting fragments (observed over expected log ratio) across biological replicates is plotted as a heatmap.

(C) Association of conserved *Nanog* interactions within each cell type (ESCs, iPSCs, or MEFs) with active or repressive chromatin features. Conserved *Nanog* interactions were identified by gene-level analysis; ChIP peaks in ESCs were linked to genes when overlapping with a −5 kb-to-+1 kb window at transcriptional start sites. The barplots show the significance of association between *Nanog*-interacting genes and genes enriched for a given mark, tested independently for each cell type. The number and the percentage of interacting genes with a given chromatin mark are reported for each bar.

(D and E) Similar analyses of association to genes bound by pluripotency transcription factors in ESCs (D) and genes bound by components of cohesin and Mediator complexes and CTCF in ESCs (E) are shown.

See also Figure S3 and Table S3.

differential interactions selected at the single-fragment level are reported in Table S2 and shown in Figure S1B. We confirmed several of the differential interactions between MEFs and ESCs, either by 3C (Figure 2C) or 3D DNA FISH analysis (Figure 2D) using independent cell preparations. Collectively, these results show that *Nanog* forms a complex genomic interaction network with multiple chromosomes that differs between pluripotent and differentiated cells and is restored in iPSCs.

Nanog-Interacting Loci Are Enriched for Open Chromatin Features as well as Binding Sites for Pluripotency Factors, Cohesin, and Mediator

To determine whether *Nanog*-interacting loci share common genomic features, we compared our results with published data (Table S3). We first noticed consistent enrichment for gene bodies and surrounding regulatory regions among interactions in ESCs, iPSCs, and MEFs (Figure 3A), as well as for early-replicating domains, which typically exhibit an open

chromatin structure (Figure 3B). The latter correlation is consistent with the fact that *Nanog* replicates early in both cell types despite its transcriptional silencing in MEFs (Hiratani et al., 2008, 2010).

We next examined chromatin features of pluripotent cells including histone marks (Table S3) and DNase I hypersensitivity among *Nanog*-interacting genes using data from the Encyclopedia of DNA Elements project (ENCODE Project Consortium, 2011). *Nanog*-interacting genes in pluripotent cells were enriched for the activating histone marks H3K4me3 and H3K4me2 and enhancer marks (H3K27ac, H3K4me1, and p300), as well as for DNase I-hypersensitive sites characterizing open chromatin areas (Figures 3C and S3A). A weak correlation was also detected for the repressive H3K27me3 mark and for bivalent promoters (p value < 0.05 in ESCs and iPSCs). However, we were unable to detect significant and consistent enrichment for binding sites of the Polycomb complex, which deposits H3K27me3 (Figures 3C and S3A). Thus, *Nanog* interacts mostly with active genes and regulatory elements in pluripotent cells.

To gain mechanistic insights into how the identified interactions are established, we searched for enrichment of pluripotency transcription factor binding sites among the *Nanog*-interacting loci using published chromatin immunoprecipitation sequencing (ChIP-seq) data sets (Table S3). Indeed, target sites for Esrrb, Klf4, c-Myc, and Sox2 were among the most consistently and significantly enriched sequences, whereas enrichment of Nanog and Oct4 targets varied across data sets (Figures 3D and S3B). We also found a pluripotency-specific association with binding of additional factors of the pluripotency network (Chen et al., 2008), including Tcf3, Tcfcp2l1, Nr5a2, and Zfx (Figures 3D and S3B). Together, these data show that genes interacting with *Nanog* in ESCs and iPSCs are strongly enriched for binding of essential pluripotency factors. It remains to be tested whether this result reflects that coregulated genes are spatially connected or that some of these factors are actively involved in chromatin looping.

We also examined occupancy of cohesin, Mediator, and CTCF molecules, proteins reported to mediate long-range interactions, among the ESC-specific contacts (Table S3). We found a significant association of *Nanog* interactions in pluripotent cells with binding of the Mediator (Med1 and Med12) and cohesin (Smc1a, Nipbl, and Smc3) complexes and a less-consistent correlation with CTCF binding depending on the data set (Figures 3E and S3C). Collectively, these results suggest that key pluripotency transcription factors might collaborate with molecules known to mediate promoter-enhancer looping and general chromatin organization to establish the observed pluripotency-specific *Nanog* interactome.

Nanog Interactions Are Dependent on Mediator and Cohesin Subunits in ESCs

We next asked how many of those regions were indeed bound by the Mediator and cohesin complexes in ESCs. To this end, we performed "4C-ChIP-seq" (Figure 4A), wherein ChIP for the Med1 and Smc1 proteins was carried out before sequencing of the *Nanog*-centered m4C libraries (Figure S4A and Experimental Procedures). Loci bound by Med1, Smc1, or both accounted for about 40% of all ESC-specific interactions (Figure 4B; Table S4). These data reinforce the results of our association analysis with published data and show that a large portion of the ESC-specific *Nanog* interactions involve the Mediator and cohesin complexes.

To test whether *Nanog* interactions require the Mediator or the cohesin complex, we performed m4C-seq in ESCs transduced with lentiviral vectors expressing short hairpin RNAs (shRNAs) against *Smc1a* or *Med1* (Figures 4A and S4B; Table S6). Chromatin was isolated 5 days after viral transduction, when protein levels were substantially reduced (Figure S4B) but before the onset of differentiation, as assessed by their undifferentiated morphology (Figure S4C) and the ESC-like messenger RNA (mRNA) and protein levels of several pluripotency factors (Figures 4C, S4D, and S4E). Importantly, *Nanog*'s promoter-enhancer interaction was already disrupted at day 5 of *Med1* or *Smc1a* knockdown (KD) (Figure 4D), although *Nanog* transcription was still detectable by RT-PCR (Figure 4C) and by the presence of Pol II phospho-Ser2 on the *Nanog* promoter (Figure S4F). Med1- and Smc1a-mediated *Nanog* interactions were severely reduced or completely abrogated in the day 5 KD 4C-seq samples (Figure 4E). Loss of chromatin contacts was confirmed by DNA FISH for one of the interacting candidate loci (Figure 4F). RNA sequencing (RNA-seq) analysis of *Med1* and *Smc1a* KD ESCs confirmed downregulation of pluripotency-related genes and upregulation of differentiation-related genes by day 8, whereas these changes were less evident on day 5 (Figure S4G). The altered transcriptional profiles of our KD cells at day 8 resembled those of previously published ESCs infected with shRNAs against *Med12* (another Mediator subunit) or *Smc1a* (Kagey et al., 2010) (Figure S4H). The faster kinetics of differentiation upon *Med12* and *Smc1a* KD reported in that study probably resulted from a more efficient depletion with a different vector system. Remarkably, the m4C-seq profiles of KD ESCs indicated that the majority of the ESC-specific interactions were lost (Figures 4H and S4I), whereas many of the MEF-specific interactions were established, presumably in a Med1- or Smc1a-independent manner (Figures 4G and 4H). Thus, Smc1a and Med1 depletion led to rearrangement of chromatin from a pluripotent- to a differentiation-specific state, even though cells still showed phenotypic and transcriptional features of the pluripotent state.

The *Nanog* Interactome Undergoes Dramatic Changes during Somatic Cell Reprogramming

Given that iPSCs have reset the *Nanog* interactome from a somatic to a pluripotent state, we assessed when chromatin rearrangements occur during reprogramming and how these relate to gene-expression changes. Specifically, we compared the kinetics of chromatin looping with gene expression using piPSC lines and sorted SSEA1$^+$ intermediates at different stages of reprogramming (Figure 5A). Importantly, both piPSCs and SSEA1$^+$ intermediates have exited the somatic state and are poised to form iPSCs under different conditions, consistent with previous observations (Figures S5A and S5B) (Sridharan et al., 2009; Stadtfeld et al., 2008). In further agreement with those previous reports, we found that *Nanog* is not yet expressed in piPSCs, whereas it is gradually upregulated during mid-to-late stages of reprogramming (Figure 5B). Surprisingly, 3C analysis revealed that looping between the *Nanog* enhancer

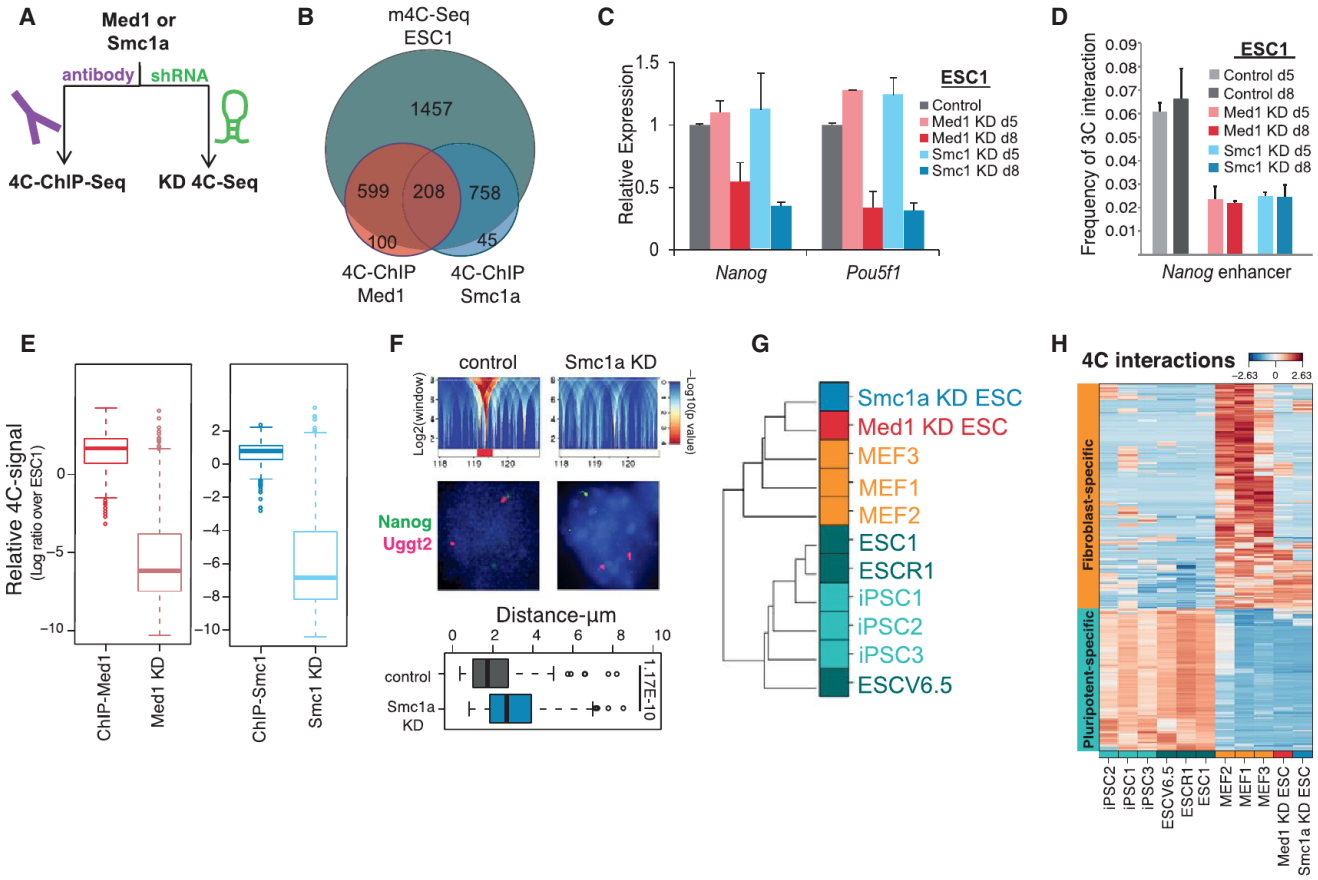

Figure 4. Mediator and Cohesin Coordinate *Nanog*'s Genomic Interactions in Pluripotent Cells

(A) Two-pronged strategy for testing the role of candidate proteins in the *Nanog* interactome in ESCs.

(B) Venn diagram depicting the overlap of *Nanog*-interacting HindIII fragments detected by m4C-ChIP-seq for either Med1 or Smc1a compared to m4C-seq in ESC line ESC1.

(C) RT-PCR analysis for pluripotency genes *Nanog* and *Pou5f1* in ESCs treated with shRNAs against *Med1* or *Smc1* for 5 (d5) or 8 days (d8). Error bars indicate SD (n = 3 technical replicates). m4C-seq analysis was performed on day 5, before downregulation of *Nanog* or *Pou5f1* and apparent differentiation of cells.

(D) 3C PCR quantifying the interaction frequency between the *Nanog* promoter and enhancer in control ESCs and in ESCs harvested 5 (d5) or 8 days (d8) after knocking down Med1 or Smc1a. For each primer pair, the PCR signal was normalized to the PCR signal of primers designed at the bait locus (see Table S6). Error bars indicate SD (n = 3 technical replicates).

(E) Boxplot reporting the relative change in 4C-seq normalized signal of the 4C-ChIP selected fragments compared to ESC1 (log2 ratio) (whiskers are as in Figure 1E).

(F) Top: domainogram details showing the interaction of *Nanog* with the *Uggt2* locus in control ESC1 and its disruption in Smc1a KD ESC1. Middle: representative DNA FISH photos for *Nanog* (FITC signal) and *Uggt2* (magenta signal) in control or *Smc1a* KD ESCs. Bottom: boxplot for distances between the *Nanog* and *Ugg2t* as measured by DNA FISH (whiskers are as in Figure 1E). The difference is significant (Wilcoxon test).

(G) Unsupervised clustering of samples is performed as in Figure 1B with the addition of the ESC samples for *Med1* or *Smc1a* KD.

(H) Heatmap showing the relative change in m4C-seq signal for the set of 4C fragments selected as differential interactions between ESCs and MEFs, clearly showing that the pluripotency-specific interactions have been lost in the *Med1* or *Smc1a* KD sample. The rows refer to individual HindIII fragments, and the columns are different 4C-seq samples. The color refers to standardized values across samples (*Z* score) for log-transformed normalized 4C read counts.

See also Figure S4 and Tables S4 and S6.

and promoter was established in both piPSC and in SSEA1$^+$ intermediates before detectable transcriptional activation of *Nanog* (Figure 5C). We extended this analysis by performing 3C analysis in piPSCs for *Oct4*, *Phc1* and *Lefty1,* which form promoter-enhancer loops in ESCs (Figure S5C) (Kagey et al., 2010). Whereas *Phc1* already exhibited looping and expression in piPSCs, *Oct4* had neither initiated looping nor activated expression. In contrast, *Lefty1* had initiated looping, but not yet expression, akin to the *Nanog* locus. These results support the conclusion that the looping at the examined pluripotency-associated genes precedes, but is not sufficient for, transcriptional activation in the context of cellular reprogramming.

On a genome-wide scale, m4C-seq analysis of piPSCs and SSEA1$^+$ intermediates showed that both cell populations had lost a large fraction of the MEF-specific interactions and had gained a small number of ESC-specific interactions (Figures 5D, S5D, and S5E). Unexpectedly, we also observed a number of reprogramming-specific interactions detectable neither in MEFs nor in iPSCs (Table S5). Transient interactions were variable among SSEA1$^+$ samples from independent reprogramming

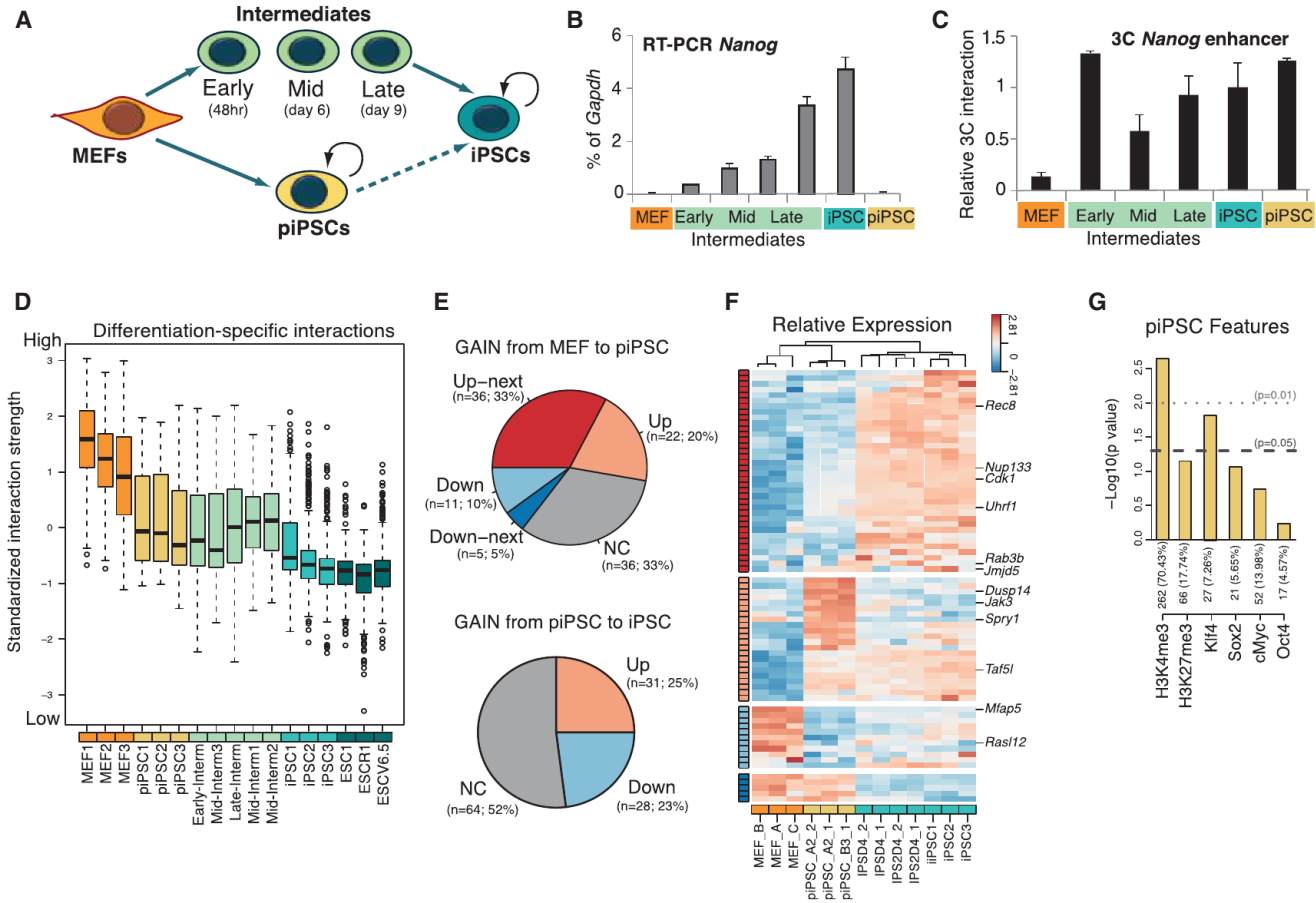

Figure 5. Dynamic Change of *Nanog* Interactome during Cellular Reprogramming into iPSCs

(A) Isolation and study of reprogramming intermediates and piPSCs.

(B) RT-PCR analysis for *Nanog* mRNA in indicated cell populations. The *Nanog* expression is normalized over *Gapdh* (% of *Gapdh*). The error bars indicate SD (n = 3 technical replicates). Late intermediates include SSEA1$^+$ cells from day 9 and day 12.

(C) 3C analysis of relative interaction frequency between the *Nanog* promoter and enhancer during reprogramming and in the piPSCs. The PCR signal is relative to ESCs ("Relative 3C Interaction") after normalization with bait-locus primers (see Table S6). Error bars represent SD (n = 3 technical replicates).

(D) Boxplot for the standardized interaction strength for differentiation-specific fragments (whiskers are as in Figure 1E). The fragments were selected as differential fragments upregulated in MEFs versus ESCs. Five groups of samples are shown: ESCs, iPSCs, SSEA1$^+$ intermediates, piPSCs, and MEFs. SSEA1 intermediates and piPSCs show an intermediate interaction strength between stronger MEFs and weaker ESCs and iPSCs. For each fragment, the log-transformed normalized 4C read counts are standardized by subtracting the mean value across all samples, then dividing over SD (*Z* score) (see also Figure S5D).

(E) Pie charts showing the number of genes, which have established (gain) interactions with *Nanog* during the transition from MEFs to piPSCs (upper panel) or from piPSCs to iPSCs (lower panel). Genes are grouped based on the change of expression detected by microarray data (false discovery rate = 0.05; fold change = 1.3) (Sridharan and Hochedlinger data sets, Table S3 and Figure S5G). Up/Down, up-/downregulated genes in the transition from MEFs to piPSCs (upper panel) or from piSPCs to iPSCs (lower panel); Up-/Down-next (for the upper panel only), represents up-/downregulated genes in the next stage, i.e., the transition from piPSCs to iPSCs (see also F); NC, genes without a statistically significant change in expression. The number of genes and percentage over the total are indicated. We found significant enrichment in the "Up-next" group (one-tailed Fisher's exact test, p = 0.001). Gene-level interactions detected in all piPSC replicates and in none of the MEFs were used.

(F) Heatmap showing expression of *Nanog*-interacting genes gained in the MEF-to-piPSC transition, as in (E). Rows are genes, and columns are microarray samples (Table S3). Expression-pattern groups were defined as in (E) and marked accordingly with the side color bar. Some genes showed significant upregulation in both the MEF-to-piPSC and the piPSC-to-iPSC transitions. In this case, they were assigned to the "Up-next" group as well. The statistically significant enrichment in the "Up-next" pattern is confirmed even if these genes are assigned to the "Up" group. The heatmap shows standardized gene-expression levels across samples (*Z* score).

(G) Association of conserved *Nanog*-interacting genes in piPSCs with H3K4me3, H3K27me3, and pluripotency transcription factors binding in the same cell type. The number and percentage of interacting genes with ChIP enrichment is reported for each bar. The analysis criteria is similar to that in Figure 3.

See also Figure S5 and Table S5.

experiments, probably reflecting their heterogeneity (see single-cell RT-PCR of Figure S5F and Polo et al., 2012). We therefore focused on piPSCs, which are of clonal origin and hence more homogeneous. Notably, these transient interactions in piPSCs (Table S5) were preferentially associated with pluripotency- rather than differentiation-related genes (p value = 0.014). Thus, forced expression of reprogramming factors readily extinguished fibroblast-specific interactions and induced a large

number of transient chromatin interactions enriched for pluripotency-associated genes.

We next correlated the reorganization of *Nanog*'s interactome during reprogramming with transcriptional changes of associated genes. Notably, more than 50% of genes that established interactions with *Nanog* during the transition of MEFs into piPSCs became transcriptionally upregulated in piPSCs ("Up") or at the subsequent (iPSC) stage ("Up-next") (Figures 5E, 5F, and S5G). These results extend, to a genome-wide level, our previous observations that the gain of *Nanog*-centered chromatin contacts during early reprogramming coincides with or precedes transcriptional changes of genes. Unexpectedly, the interactions gained during the piPSC-to-iPSC transition showed a weaker correlation with transcriptional changes, suggesting a lesser impact of *Nanog* interactions on gene expression during the late stages of reprogramming. We conclude that *Nanog*'s chromatin associations during early stages of reprogramming mostly involve genes that are either immediately upregulated or poised for activation in iPSCs.

To investigate which molecules might mediate *Nanog*'s interactions during reprogramming, we compared m4C-seq results on piPSCs with published ChIP-chip data of reprogramming factors and histone modifications in the same cell type (Sridharan et al., 2009). This analysis revealed a positive correlation with the active histone mark H3K4me3 and a significant association of *Nanog*'s interacting loci with Klf4 binding, further supporting its possible role in regulating long-range chromatin interactions (Figures 3D and 5G). Thus, forced expression of Oct4, Sox2, Klf4, and c-Myc induces reorganization of chromatin architecture and facilitates interactions of the *Nanog* locus with other Klf4 target genes, as well as with open chromatin domains.

Reprogramming Factors and Mediator Cooperate during the Establishment of *Nanog*-Centered Interactions

To investigate whether Mediator and cohesin are involved in the acquisition of pluripotency, we assayed the potential to generate iPSCs from reprogrammable MEFs when subunits of Mediator (Med1 and Med12) and/or cohesin (Smc1a, Smc3, and Rad21) were depleted (Figure S6A). Indeed, KD of Mediator and/or cohesin components significantly decreased reprogramming efficiencies (Figure 6A).

Upon KD of Mediator and cohesin components, fewer iPSC colonies could result from either deficient reprogramming or immediate differentiation of newly formed iPSCs. To distinguish between these possibilities, we analyzed early (SSEA1) and late (EpCam) markers of pluripotency at intermediate stages of reprogramming (Polo et al., 2012). We focused on *Med1* KD cells because Med1 is expressed most differentially between somatic and pluripotent cells (Figure S6B) (Kagey et al., 2010; Polo et al., 2012). Figure 6B shows that *Med1* KD MEFs gave rise to fewer $SSEA1^+$ and $EpCam^+$ reprogramming intermediates at day 9 of reprogramming-factor overexpression. 3C analysis at this time point showed that *Nanog* promoter-enhancer looping was not efficiently established in the absence of Med1, concordant with decreased transcription (Figure 6C). Together, these data suggest that Med1 is important for acquiring pluripotency-specific chromatin loops and gene expression in addition to its established role in the maintenance of pluripotency.

We hypothesized that Med1 might cooperate with reprogramming factors to reorganize 3D chromatin architecture and to control gene expression during iPSC formation. Coimmunoprecipitation experiments in piPSCs showed association of Med1 with the reprogramming factors Oct4, Sox2, and Klf4 (Figure 6D), as well as with Med12 and Smc1 (Figure S6C), which have previously been reported to interact with Med1 in ESCs (Borggrefe and Yue, 2011; Kagey et al., 2010). Importantly, these protein-protein interactions were detected as early as 48 hr after expression of the reprogramming factors, suggesting an early function. Med1's interactions with Oct4 and Sox2 were also confirmed in ESCs (Figure S6C). These results indicate that Mediator components and pluripotency factors form a multiprotein complex throughout cellular reprogramming and in pluripotent cells.

Lastly, we asked how reprogramming factors might collaborate with Mediator and/or cohesin to form chromatin loops during reprogramming. We investigated the binding of these proteins to three genomic regions (*Aicda*, *Nanog* enhancer, and *Slc2a3*) found to interact with the *Nanog* promoter in pluripotent cells based on m4C-seq data (Figure 6E). This analysis showed that Klf4, Oct4, Sox2, Med1, and Smc1 were bound to all three loci in pluripotent cells (Figure S6D). Similarly, the loci that had already established chromatin loops with the *Nanog* promoter (*Nanog* enhancer and *Slc2a3*) in piPSC lines were occupied by all tested factors (Figure 6F). In contrast, *Aicda*, which interacted with the *Nanog* promoter in established iPSCs only, but not yet in piPSCs, was bound solely by Klf4 in piPSCs. This result suggests that a minimum set of pluripotency proteins may be required by cohesin and Mediator to bridge distal chromatin elements.

DISCUSSION

Herein, we provide genetic, biochemical, and bioinformatic evidence that *Nanog* engages in a pluripotency-specific genome-wide chromatin network that resolves into a somatic-specific pattern upon differentiation and resets in iPSCs (Figure 7). This is the first genome-wide interaction map of a key mouse pluripotency gene at high resolution. Our results extend previous genome-scale transcription factor occupancy and protein interaction studies for pluripotency factors (Chen et al., 2008; Kim et al., 2008) and reveal an unexpectedly complex genomic interactome in pluripotent cells.

We document *Nanog* promoter interactions with individual loci as well as broader domains on the same and on different chromosomes. These interactions were stable and conserved among different pluripotent cell lines, whereas they were less consistent in MEFs (Figure 7). This finding indicates that pluripotency loci might engage in less stable and/or more random interactions in cell types wherein the bait locus is inactive. Alternatively, it may reflect the heterogeneity of fibroblast populations, which were used as a proxy for differentiated cells. Of note, almost half of the conserved interactions found in MEF samples were also detected in pluripotent cells, indicating a cell-type independent network of presumably structural interactions.

A positive correlation between *Nanog*-centered interactions and active chromatin marks specifically in pluripotent cells is in accordance with previous studies showing that active genes

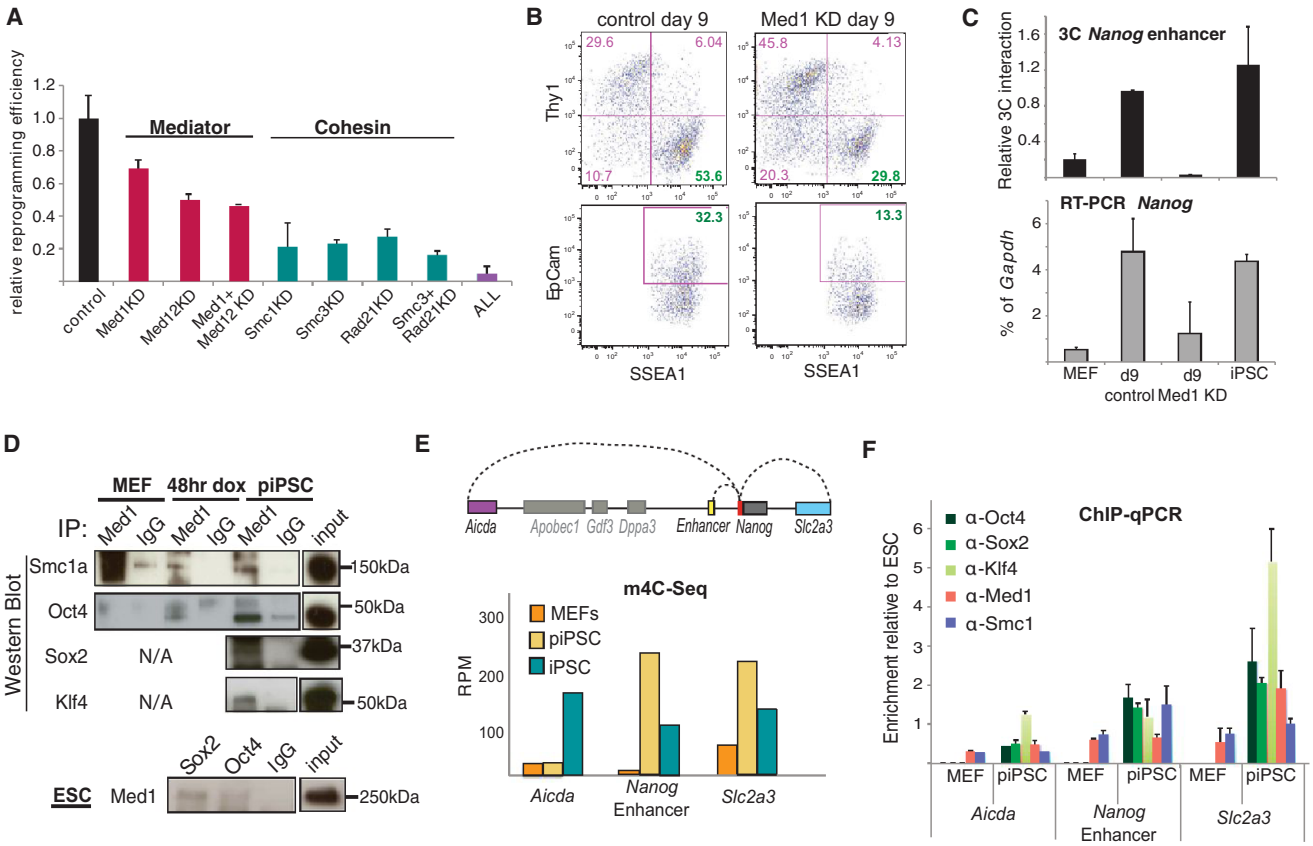

Figure 6. Role of Mediator and Cohesin in the Reprogramming of MEFs to iPSCs

(A) Graph comparing the reprogramming efficiency of tetO-OKSM MEFs after infection with empty vector (control) or shRNA vectors (KD) against individual subunits of Mediator (Med1 and Med12) or cohesin (Smc1a, Smc3, and Rad21) complexes or combinations thereof. The efficiency was calculated as the ratio of alkaline-phosphatase-positive colonies per starting number of cells. Reprogramming efficiency of control MEFs was set at 1. Error bars indicate SD (n = 3 biological replicates).

(B) Fluorescence-activated cell sorting plots of SSEA1-positive or EpCam-positive cells on day 9 of reprogramming, starting with either wild-type (left) or Med1-knocked down (KD, right) reprogrammable MEFs. SSEA1 and EpCam were chosen as early or late surface markers of pluripotency, respectively.

(C) RT-PCR (bottom) for *Nanog* expression and 3C assay (top) for *Nanog* enhancer-promoter interaction in MEFs, iPSCs, and reprogramming intermediates of control or Med1 KD MEFs on day 9. The 3C PCR signal was calculated relative to ESCs ("Relative 3C Interaction") after normalization with bait-locus primers (Table S6). Error bars represent SD (n = 2 technical replicates). The RT-PCR *Nanog* signal was normalized to *Gapdh* levels, and the error bars indicate SD (n = 4 replicates).

(D) Med1 protein immunoprecipitation (upper panels) in reprogrammable MEFs before (MEF) and after (MEF 48 hr) doxycycline induction and in piPSCs. In the bottom panel, the interaction of Med1 with Oct4, Sox2, and Nanog was also confirmed in ESCs, this time using antibodies for the reprogramming factors for the pull-down.

(E) Schematic representation of the genomic regions found to interact in *cis* with the *Nanog* promoter (red) in a pluripotent-specific way (top). Barplot of the m4C-seq signal for each of the indicated regions in MEFs, piPSCs, and ESCs. The signal is expressed in reads per million (RPM) and represents the average value of three biological replicates.

(F) ChIP experiments of the reprogramming factors Oct4, Sox2, and Klf4, as well as Med1 and Smc1a, on the indicated genomic regions in MEFs and piPSCs. All of the ChIP-qPCR signals are first normalized to the input, and then expressed relative to the corresponding signal in ESCs (see also Figure S6). Error bars indicate SD.

See also Figure S6 and Table S6.

tend to colocalize in the genome (Gao et al., 2013; Kalhor et al., 2012; Simonis et al., 2006). Notably, binding sites for the key pluripotency factors Oct4, Sox2, Nanog, Esrrb, c-Myc, and Klf4 were also enriched among the *Nanog*-interacting genes in pluripotent cells (Figure 7), suggesting that these proteins might be involved in bringing coregulated pluripotency-associated genes into physical proximity for subsequent transcriptional activation during the induction and maintenance of pluripotency. Indeed, previous studies documented roles for Oct4 in the maintenance of *cis* DNA loops around *Nanog* (Levasseur et al., 2008), for c-Myc in the spatial organization of ribosomal RNA genes in other cell types (Shiue et al., 2009), and for Klf1 in long-range interactions of erythroid genes during blood cell development (Schoenfelder et al., 2010). It is worth mentioning here that forced expression of either of c-Myc, Nanog, Esrrb, or Klf4 proteins relieves ESCs from leukemia-inhibitory-factor-dependent growth (Festuccia et al., 2012; Jiang et al., 2008; Marks et al., 2012; Smith and Dalton, 2010; Smith et al., 2010), suggesting

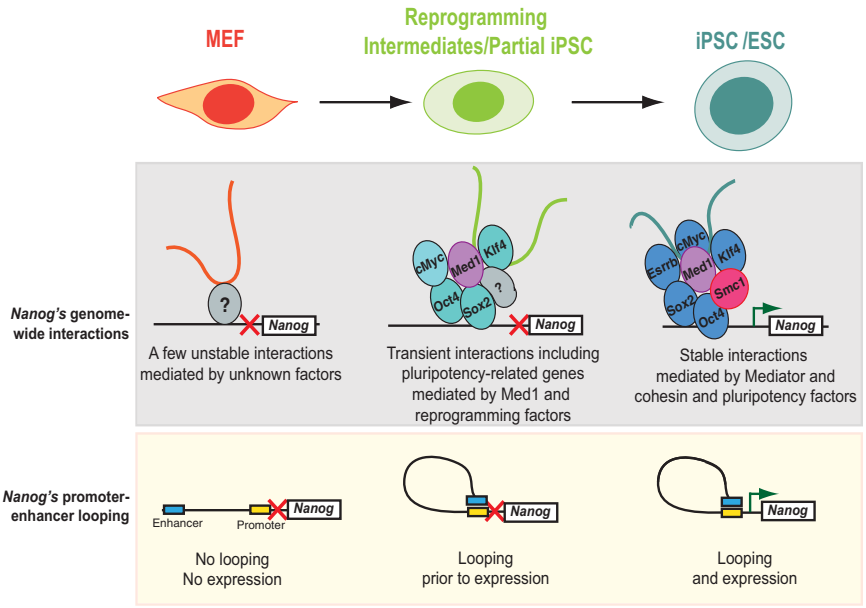

Figure 7. Model Depicting the Dynamics of *Nanog* Interactions during Differentiation and Cellular Reprogramming

The *Nanog* locus engages in genome-wide chromatin interactions in MEFs ("MEF-specific interactome") that are highly variable, possibly because the *Nanog* gene is inactive in differentiated cells. During reprogramming, the complexity of interactions increases, presumably by the cooperative action of the overexpressed reprogramming factors and "bridging" factors, including Mediator components (Med1). The majority of interactions gained in piPSCs lead to upregulation of associated genes immediately or in iPSCs. Once cells reach the pluripotent state, different and more-stable interactions are established. These pluripotency-specific interactions are mainly maintained by cohesin and Mediator complexes, as well as the key pluripotency factors. Upon normal differentiation or depletion of either Med1 or Smc1a, the *Nanog* interactome is rearranged into the less-organized differentiated state.

that the observed interaction network and its constituents may also be functionally connected.

We provide evidence that members of the Mediator and/or cohesin families are responsible for about 40% of the observed interactions in ESCs. Their depletion from ESCs resulted in a rearrangement of chromatin from a pluripotent to a differentiated state before the transcriptional and phenotypic onset of differentiation. Similarly, their reduction during cellular reprogramming impaired iPSC colony formation, suggesting an additional role in establishing pluripotency. Our observation that Med1 associated physically with the overexpressed Oct4, Sox2, and Klf4 factors during reprogramming and with the corresponding endogenous proteins in established ESCs supports this interpretation and extends previous results regarding the direct interactions of cohesin and Mediator subunits with Oct4 and Nanog in ESCs (Costa et al., 2013; Nitzsche et al., 2011; Tutter et al., 2009; van den Berg et al., 2010). Our results therefore suggest that Mediator and cohesin components, in collaboration with pluripotency transcription factors, play a critical role in establishing and maintaining a broader 3D chromatin network centered around *Nanog* and possibly other pluripotency loci (Figure 7). We cannot exclude the possibility that Mediator and cohesin influence iPSC formation and ESC maintenance by additional mechanisms such as cell cycle, cell signaling (Rocha et al., 2010), mesenchymal-to-epithelial transition (Huang et al., 2012), and/or transcriptional regulation (Malik and Roeder, 2010; Wood et al., 2010).

Lastly, we document that the reprogramming of somatic cells into iPSCs resets *Nanog*'s chromatin interactome. We show that fibroblasts rapidly lose MEF-specific interactions upon overexpression of Oct4, Sox2, Klf4, and c-Myc and gradually establish pluripotency-specific interactions. This is in accordance with the transcriptional shutdown of the somatic program prior to the activation of the pluripotency program as described recently (Polo et al., 2012; Soufi et al., 2012; Stadtfeld et al., 2008). Unexpectedly, we detected a number of transient, reprogramming-specific contacts, which involved many pluripotency-related genes (Figure 7). These genes might be physically brought together with *Nanog* by forced reprogramming-factor expression for coordinated gene activation. The observed protein-protein interactions of Oct4, Sox2, and Klf4 with Med1 in piPSCs support a model whereby reprogramming factors and associated bridging factors act synergistically to orchestrate chromatin rearrangements during reprogramming (Figure 7). However, we cannot rule out the possibility that these interactions might be the consequence of global chromatin changes or aberrant binding of the overexpressed transcription factors during reprogramming (Soufi et al., 2012).

Collectively, our data provide a comprehensive analysis of the genomic interactions of a key pluripotency gene and their relationship with transcription, epigenetic marks, and pluripotency-factor binding. Our findings further suggest an important and possibly causative role for chromatin structure in controlling transcriptional patterns and eventually determining cell identity in the context of pluripotency, differentiation, and cellular reprogramming. Identifying the interactomes for other pluripotency loci should allow researchers to construct an integrative view of 3D chromatin architecture in pluripotent cells in the future.

EXPERIMENTAL PROCEDURES

Cell Culture and Reprogramming

ESCs, MEF-derived iPSCs (Stadtfeld et al., 2010a), and piPSCs (Maherali et al., 2007) were cultured as described before. MEFs were isolated from "reprogrammable" mice (Stadtfeld et al., 2010b) and reprogrammed in presence of 1 μg/ml doxycycline and 50 μg/ml ascorbic acid.

shRNA Virus Production and Infection

The shRNA lentiviruses for Med1 and Smc1a were designed according to a previous study (Kagey et al., 2010) and cloned into a different vector (Addgene-pSicoR-GFP). The virus production, transduction, and reprogramming of infected MEFs are described in Supplemental Experimental Procedures. All the shRNA sequences used for this study are shown in Table S6.

RNA-Seq Library Preparation

The RNA-seq library construction is described in the Supplemental Experimental Procedures.

Protein Coimmunoprecipation

The antibodies used for this study were as follows: Med1 (Bethyl Laboratories), Smc1 (Bethyl Laboratories), Oct4 (Santa Cruz Biotechnology for western blotting and R&D Systems for immunoprecipitation), Sox2 (R&D), Klf4 (R&D), Nanog (Bethyl Laboratories), actin-HPRT (Abcam), Med12 (Bethyl Laboratories), Smc3 (Abcam), and Rad21 (Santa Cruz). The exact process is described in the Supplemental Experimental Procedures.

ChIP

ChIP was performed as described previously (Stadtfeld et al., 2012). The antibodies used were as follows: Oct4 (R&D), Sox2 (R&D), Klf4 (R&D), Med1 (Bethyl Laboratories), Smc1 (Bethyl Laboratories), immunoglobulin G (Abcam), and Pol II phospho-Ser2 (Abcam). The primers used for the quantitative PCR (qPCR) analysis are listed in Table S6.

3D DNA FISH and Image Analysis

3D DNA FISH analysis was performed as described previously (Xu et al., 2006). The protocol and the bacterial artificial clones used for this study are listed in the Supplemental Experimental Procedures.

m4C-Seq, m4C-ChIP-Seq, and 3C Analyses

4C and 3C were performed as has been previously described (Schoenfelder et al., 2010) with some modifications, described in detail in the Supplemental Experimental Procedures. For m4C-ChIP-seq, an immunoprecipitation step with Med1 and Smc1 antibodies (Bethyl Laboratories) was included. The primers used for these assays are listed in Table S6.

Bioinformatics Analyses of m4C-Seq and Associations with Public Data Sets

See Supplemental Experimental Procedures.

ACCESSION NUMBERS

The Sequence Read Archive accession number for sequencing data reported in this paper is SRA051554.

SUPPLEMENTAL INFORMATION

Supplemental Information includes Supplemental Experimental Procedures, six figures, and six tables and can be found with this article online at http://dx.doi.org/10.1016/j.stem.2013.04.013.

ACKNOWLEDGMENTS

We acknowledge Peter Fraser, Frank Grosveld, Jane Skok, and Job Dekker for comments and suggestions. We thank Mariann Miscinai and Triantiafyllos Paparountas for discussing bioinformatics analysis, Eda Yildirim and Berni Peyer for advice about FISH experiments, and all members of the Hochedlinger and Park groups for suggestions. E.A. was supported by postdoctoral fellowships from JCCF and HHMI. P.J.P. was supported by a Sloan Research Fellowship and NIH (RC2HL102815), P.V.K was supported by NIH (K25AG037596), and K.H. was supported by NIH (DP2OD003266 and R01HD058013).

Received: April 11, 2012
Revised: March 27, 2013
Accepted: April 16, 2013
Published: May 9, 2013

REFERENCES

Apostolou, E., and Thanos, D. (2008). Virus Infection Induces NF-kappaB-dependent interchromosomal associations mediating monoallelic IFN-beta gene expression. Cell *134*, 85–96.

Bantignies, F., Roure, V., Comet, I., Leblanc, B., Schuettengruber, B., Bonnet, J., Tixier, V., Mas, A., and Cavalli, G. (2011). Polycomb-dependent regulatory contacts between distant Hox loci in Drosophila. Cell *144*, 214–226.

Borggrefe, T., and Yue, X. (2011). Interactions between subunits of the Mediator complex with gene-specific transcription factors. Semin. Cell Dev. Biol. *22*, 759–768.

Buganim, Y., Faddah, D.A., Cheng, A.W., Itskovich, E., Markoulaki, S., Ganz, K., Klemm, S.L., van Oudenaarden, A., and Jaenisch, R. (2012). Single-cell expression analyses during cellular reprogramming reveal an early stochastic and a late hierarchic phase. Cell *150*, 1209–1222.

Chambers, I., Colby, D., Robertson, M., Nichols, J., Lee, S., Tweedie, S., and Smith, A. (2003). Functional expression cloning of Nanog, a pluripotency sustaining factor in embryonic stem cells. Cell *113*, 643–655.

Chen, X., Xu, H., Yuan, P., Fang, F., Huss, M., Vega, V.B., Wong, E., Orlov, Y.L., Zhang, W., Jiang, J., et al. (2008). Integration of external signaling pathways with the core transcriptional network in embryonic stem cells. Cell *133*, 1106–1117.

Clowney, E.J., LeGros, M.A., Mosley, C.P., Clowney, F.G., Markenskoff-Papadimitriou, E.C., Myllys, M., Barnea, G., Larabell, C.A., and Lomvardas, S. (2012). Nuclear aggregation of olfactory receptor genes governs their monogenic expression. Cell *151*, 724–737.

Costa, Y., Ding, J., Theunissen, T.W., Faiola, F., Hore, T.A., Shliaha, P.V., Fidalgo, M., Saunders, A., Lawrence, M., Dietmann, S., et al. (2013). NANOG-dependent function of TET1 and TET2 in establishment of pluripotency. Nature *495*, 370–374.

Dekker, J., Rippe, K., Dekker, M., and Kleckner, N. (2002). Capturing chromosome conformation. Science *295*, 1306–1311.

Dixon, J.R., Selvaraj, S., Yue, F., Kim, A., Li, Y., Shen, Y., Hu, M., Liu, J.S., and Ren, B. (2012). Topological domains in mammalian genomes identified by analysis of chromatin interactions. Nature *485*, 376–380.

Donohoe, M.E., Silva, S.S., Pinter, S.F., Xu, N., and Lee, J.T. (2009). The pluripotency factor Oct4 interacts with Ctcf and also controls X-chromosome pairing and counting. Nature *460*, 128–132.

Duan, Z., Andronescu, M., Schutz, K., McIlwain, S., Kim, Y.J., Lee, C., Shendure, J., Fields, S., Blau, C.A., and Noble, W.S. (2010). A three-dimensional model of the yeast genome. Nature *465*, 363–367.

ENCODE Project Consortium. (2011). A user's guide to the encyclopedia of DNA elements (ENCODE). PLoS Biol. *9*, e1001046.

Engel, J.D., and Tanimoto, K. (2000). Looping, linking, and chromatin activity: new insights into beta-globin locus regulation. Cell *100*, 499–502.

Festuccia, N., Osorno, R., Halbritter, F., Karwacki-Neisius, V., Navarro, P., Colby, D., Wong, F., Yates, A., Tomlinson, S.R., and Chambers, I. (2012). Esrrb is a direct Nanog target gene that can substitute for Nanog function in pluripotent cells. Cell Stem Cell *11*, 477–490.

Gao, F., Wei, Z., An, W., Wang, K., and Lu, W. (2013). The interactomes of POU5F1 and SOX2 enhancers in human embryonic stem cells. Sci. Rep. *3*, 1588.

Golipour, A., David, L., Liu, Y., Jayakumaran, G., Hirsch, C.L., Trcka, D., and Wrana, J.L. (2012). A late transition in somatic cell reprogramming requires regulators distinct from the pluripotency network. Cell Stem Cell *11*, 769–782.

Hiratani, I., Ryba, T., Itoh, M., Yokochi, T., Schwaiger, M., Chang, C.-W., Lyou, Y., Townes, T.M., Schübeler, D., and Gilbert, D.M. (2008). Global reorganization of replication domains during embryonic stem cell differentiation. PLoS Biol. *6*, e245.

Hiratani, I., Ryba, T., Itoh, M., Rathjen, J., Kulik, M., Papp, B., Fussner, E., Bazett-Jones, D.P., Plath, K., Dalton, S., et al. (2010). Genome-wide dynamics of replication timing revealed by in vitro models of mouse embryogenesis. Genome Res. *20*, 155–169.

Huang, S., Hölzel, M., Knijnenburg, T., Schlicker, A., Roepman, P., McDermott, U., Garnett, M., Grernrum, W., Sun, C., Prahallad, A., et al. (2012). MED12 controls the response to multiple cancer drugs through regulation of TGF-β receptor signaling. Cell *151*, 937–950.

Jiang, J., Chan, Y.S., Loh, Y.H., Cai, J., Tong, G.Q., Lim, C.A., Robson, P., Zhong, S., and Ng, H.H. (2008). A core Klf circuitry regulates self-renewal of embryonic stem cells. Nat. Cell Biol. *10*, 353–360.

Kagey, M.H., Newman, J.J., Bilodeau, S., Zhan, Y., Orlando, D.A., van Berkum, N.L., Ebmeier, C.C., Goossens, J., Rahl, P.B., Levine, S.S., et al. (2010). Mediator and cohesin connect gene expression and chromatin architecture. Nature *467*, 430–435.

Kalhor, R., Tjong, H., Jayathilaka, N., Alber, F., and Chen, L. (2012). Genome architectures revealed by tethered chromosome conformation capture and population-based modeling. Nat. Biotechnol. *30*, 90–98.

Kim, J., Chu, J., Shen, X., Wang, J., and Orkin, S.H. (2008). An extended transcriptional network for pluripotency of embryonic stem cells. Cell *132*, 1049–1061.

Klein, I.A., Resch, W., Jankovic, M., Oliveira, T., Yamane, A., Nakahashi, H., Di Virgilio, M., Bothmer, A., Nussenzweig, A., Robbiani, D.F., et al. (2011). Translocation-capture sequencing reveals the extent and nature of chromosomal rearrangements in B lymphocytes. Cell *147*, 95–106.

Levasseur, D.N., Wang, J., Dorschner, M.O., Stamatoyannopoulos, J.A., and Orkin, S.H. (2008). Oct4 dependence of chromatin structure within the extended Nanog locus in ES cells. Genes Dev. *22*, 575–580.

Lieberman-Aiden, E., van Berkum, N.L., Williams, L., Imakaev, M., Ragoczy, T., Telling, A., Amit, I., Lajoie, B.R., Sabo, P.J., Dorschner, M.O., et al. (2009). Comprehensive mapping of long-range interactions reveals folding principles of the human genome. Science *326*, 289–293.

Ling, J.Q., Li, T., Hu, J.F., Vu, T.H., Chen, H.L., Qiu, X.W., Cherry, A.M., and Hoffman, A.R. (2006). CTCF mediates interchromosomal colocalization between Igf2/H19 and Wsb1/Nf1. Science *312*, 269–272.

Lomvardas, S., Barnea, G., Pisapia, D.J., Mendelsohn, M., Kirkland, J., and Axel, R. (2006). Interchromosomal interactions and olfactory receptor choice. Cell *126*, 403–413.

Maherali, N., Sridharan, R., Xie, W., Utikal, J., Eminli, S., Arnold, K., Stadtfeld, M., Yachechko, R., Tchieu, J., Jaenisch, R., et al. (2007). Directly reprogrammed fibroblasts show global epigenetic remodeling and widespread tissue contribution. Cell Stem Cell *1*, 55–70.

Malik, S., and Roeder, R.G. (2010). The metazoan Mediator co-activator complex as an integrative hub for transcriptional regulation. Nat. Rev. Genet. *11*, 761–772.

Marks, H., Kalkan, T., Menafra, R., Denissov, S., Jones, K., Hofemeister, H., Nichols, J., Kranz, A., Stewart, A.F., Smith, A., and Stunnenberg, H.G. (2012). The transcriptional and epigenomic foundations of ground state pluripotency. Cell *149*, 590–604.

Mikkelsen, T.S., Hanna, J., Zhang, X., Ku, M., Wernig, M., Schorderet, P., Bernstein, B.E., Jaenisch, R., Lander, E.S., and Meissner, A. (2008). Dissecting direct reprogramming through integrative genomic analysis. Nature *454*, 49–55.

Mitsui, K., Tokuzawa, Y., Itoh, H., Segawa, K., Murakami, M., Takahashi, K., Maruyama, M., Maeda, M., and Yamanaka, S. (2003). The homeoprotein Nanog is required for maintenance of pluripotency in mouse epiblast and ES cells. Cell *113*, 631–642.

Nitzsche, A., Paszkowski-Rogacz, M., Matarese, F., Janssen-Megens, E.M., Hubner, N.C., Schulz, H., de Vries, I., Ding, L., Huebner, N., Mann, M., et al. (2011). RAD21 cooperates with pluripotency transcription factors in the maintenance of embryonic stem cell identity. PLoS ONE *6*, e19470.

Peric-Hupkes, D., Meuleman, W., Pagie, L., Bruggeman, S.W., Solovei, I., Brugman, W., Gräf, S., Flicek, P., Kerkhoven, R.M., van Lohuizen, M., et al. (2010). Molecular maps of the reorganization of genome-nuclear lamina interactions during differentiation. Mol. Cell *38*, 603–613.

Polo, J.M., Anderssen, E., Walsh, R.M., Schwarz, B.A., Nefzger, C.M., Lim, S.M., Borkent, M., Apostolou, E., Alaei, S., Cloutier, J., et al. (2012). A molecular roadmap of reprogramming somatic cells into iPS cells. Cell *151*, 1617–1632.

Rocha, P.P., Scholze, M., Bleiss, W., and Schrewe, H. (2010). Med12 is essential for early mouse development and for canonical Wnt and Wnt/PCP signaling. Development *137*, 2723–2731.

Rocha, P.P., Micsinai, M., Kim, J.R., Hewitt, S.L., Souza, P.P., Trimarchi, T., Strino, F., Parisi, F., Kluger, Y., and Skok, J.A. (2012). Close proximity to Igh is a contributing factor to AID-mediated translocations. Mol. Cell *47*, 873–885.

Schardin, M., Cremer, T., Hager, H.D., and Lang, M. (1985). Specific staining of human chromosomes in Chinese hamster x man hybrid cell lines demonstrates interphase chromosome territories. Hum. Genet. *71*, 281–287.

Schoenfelder, S., Sexton, T., Chakalova, L., Cope, N.F., Horton, A., Andrews, S., Kurukuti, S., Mitchell, J.A., Umlauf, D., Dimitrova, D.S., et al. (2010). Preferential associations between co-regulated genes reveal a transcriptional interactome in erythroid cells. Nat. Genet. *42*, 53–61.

Sexton, T., Yaffe, E., Kenigsberg, E., Bantignies, F., Leblanc, B., Hoichman, M., Parrinello, H., Tanay, A., and Cavalli, G. (2012). Three-dimensional folding and functional organization principles of the Drosophila genome. Cell *148*, 458–472.

Shiue, C.N., Berkson, R.G., and Wright, A.P. (2009). c-Myc induces changes in higher order rDNA structure on stimulation of quiescent cells. Oncogene *28*, 1833–1842.

Silva, J., Nichols, J., Theunissen, T.W., Guo, G., van Oosten, A.L., Barrandon, O., Wray, J., Yamanaka, S., Chambers, I., and Smith, A. (2009). Nanog is the gateway to the pluripotent ground state. Cell *138*, 722–737.

Simonis, M., Klous, P., Splinter, E., Moshkin, Y., Willemsen, R., de Wit, E., van Steensel, B., and de Laat, W. (2006). Nuclear organization of active and inactive chromatin domains uncovered by chromosome conformation capture-on-chip (4C). Nat. Genet. *38*, 1348–1354.

Simonis, M., Klous, P., Homminga, I., Galjaard, R.-J., Rijkers, E.-J., Grosveld, F., Meijerink, J.P., and de Laat, W. (2009). High-resolution identification of balanced and complex chromosomal rearrangements by 4C technology. Nat. Methods *6*, 837–842.

Smith, K., and Dalton, S. (2010). Myc transcription factors: key regulators behind establishment and maintenance of pluripotency. Regen. Med. *5*, 947–959.

Smith, K.N., Singh, A.M., and Dalton, S. (2010). Myc represses primitive endoderm differentiation in pluripotent stem cells. Cell Stem Cell *7*, 343–354.

Soufi, A., Donahue, G., and Zaret, K.S. (2012). Facilitators and impediments of the pluripotency reprogramming factors' initial engagement with the genome. Cell *151*, 994–1004.

Sridharan, R., Tchieu, J., Mason, M.J., Yachechko, R., Kuoy, E., Horvath, S., Zhou, Q., and Plath, K. (2009). Role of the murine reprogramming factors in the induction of pluripotency. Cell *136*, 364–377.

Stadtfeld, M., Maherali, N., Breault, D.T., and Hochedlinger, K. (2008). Defining molecular cornerstones during fibroblast to iPS cell reprogramming in mouse. Cell Stem Cell *2*, 230–240.

Stadtfeld, M., Apostolou, E., Akutsu, H., Fukuda, A., Follett, P., Natesan, S., Kono, T., Shioda, T., and Hochedlinger, K. (2010a). Aberrant silencing of imprinted genes on chromosome 12qF1 in mouse induced pluripotent stem cells. Nature *465*, 175–181.

Stadtfeld, M., Maherali, N., Borkent, M., and Hochedlinger, K. (2010b). A reprogrammable mouse strain from gene-targeted embryonic stem cells. Nat. Methods *7*, 53–55.

Stadtfeld, M., Apostolou, E., Ferrari, F., Choi, J., Walsh, R.M., Chen, T., Ooi, S.S., Kim, S.Y., Bestor, T.H., Shioda, T., et al. (2012). Ascorbic acid prevents loss of Dlk1-Dio3 imprinting and facilitates generation of all-iPS cell mice from terminally differentiated B cells. Nat. Genet. *44*, 398–405, S1–S2.

Takahashi, K., and Yamanaka, S. (2006). Induction of pluripotent stem cells from mouse embryonic and adult fibroblast cultures by defined factors. Cell *126*, 663–676.

Tutter, A.V., Kowalski, M.P., Baltus, G.A., Iourgenko, V., Labow, M., Li, E., and Kadam, S. (2009). Role for Med12 in regulation of Nanog and Nanog target genes. J. Biol. Chem. *284*, 3709–3718.

van den Berg, D.L., Snoek, T., Mullin, N.P., Yates, A., Bezstarosti, K., Demmers, J., Chambers, I., and Poot, R.A. (2010). An Oct4-centered protein interaction network in embryonic stem cells. Cell Stem Cell *6*, 369–381.

Wood, A.J., Severson, A.F., and Meyer, B.J. (2010). Condensin and cohesin complexity: the expanding repertoire of functions. Nat. Rev. Genet. *11*, 391–404.

Xu, N., Tsai, C.-L., and Lee, J.T. (2006). Transient homologous chromosome pairing marks the onset of X inactivation. Science *311*, 1149–1152.

Zhang, Y., McCord, R.P., Ho, Y.J., Lajoie, B.R., Hildebrand, D.G., Simon, A.C., Becker, M.S., Alt, F.W., and Dekker, J. (2012). Spatial organization of the mouse genome and its role in recurrent chromosomal translocations. Cell *148*, 908–921.

Zhao, Z., Tavoosidana, G., Sjölinder, M., Göndör, A., Mariano, P., Wang, S., Kanduri, C., Lezcano, M., Sandhu, K.S., Singh, U., et al. (2006). Circular chromosome conformation capture (4C) uncovers extensive networks of epigenetically regulated intra- and interchromosomal interactions. Nat. Genet. *38*, 1341–1347.

Cell Stem Cell
Article

Regulation of Glycolysis by Pdk Functions as a Metabolic Checkpoint for Cell Cycle Quiescence in Hematopoietic Stem Cells

Keiyo Takubo,[1,*] Go Nagamatsu,[1] Chiharu I. Kobayashi,[1] Ayako Nakamura-Ishizu,[1] Hiroshi Kobayashi,[1] Eiji Ikeda,[3] Nobuhito Goda,[4,5] Yasmeen Rahimi,[9] Randall S. Johnson,[6] Tomoyoshi Soga,[5,7] Atsushi Hirao,[5,8] Makoto Suematsu,[2] and Toshio Suda[1,*]

[1]Department of Cell Differentiation, The Sakaguchi Laboratory of Developmental Biology, Keio University School of Medicine, 35 Shinano-machi, Shinjuku-ku, Tokyo 160-8582, Japan
[2]Department of Biochemistry, Keio University School of Medicine and Japan Science Technology Agency (JST), Exploratory Research for Advanced Technology (ERATO), Suematsu Gas Biology Project, 35 Shinano-machi, Shinjuku-ku, Tokyo 160-8582, Japan
[3]Department of Pathology, Yamaguchi University Graduate School of Medicine, 1-1-1 Minami-Kogushi, Ube, Yamaguchi 755-8505, Japan
[4]Department of Life Science and Medical Bio-Science, School of Advanced Science and Engineering, Waseda University, 2-2 Wakamatsu-cho, Shinjuku-ku, Tokyo 162-8480, Japan
[5]Core Research for Evolutional Science and Technology, Japan Science and Technology Agency, Chiyoda-ku, Tokyo 102-0075, Japan
[6]Department of Physiology, Development & Neuroscience, University of Cambridge, Downing Street, Cambridge CB2 3EG, UK
[7]Institute for Advanced Biosciences, Keio University, 246-2, Mizukami, Kakuganji, Tsuruoka City, Yamagata 997-0052, Japan
[8]Division of Molecular Genetics, Cancer Research Institute, Kanazawa University, Kakuma-machi, Kanazawa 920-1192, Japan
[9]Department of Biochemistry and Molecular Biology, Indiana University School of Medicine, Richard L. Roudebush VA Medical Center, 1481 W. 10th Street, Indianapolis, IN 46202-2803, USA
*Correspondence: keiyot@gmail.com (K.T.), sudato@z3.keio.jp (T.S.)
http://dx.doi.org/10.1016/j.stem.2012.10.011

SUMMARY

Defining the metabolic programs that underlie stem cell maintenance will be essential for developing strategies to manipulate stem cell capacity. Mammalian hematopoietic stem cells (HSCs) maintain cell cycle quiescence in a hypoxic microenvironment. It has been proposed that HSCs exhibit a distinct metabolic phenotype under these conditions. Here we directly investigated this idea using metabolomic analysis and found that HSCs generate adenosine-5′-triphosphate by anaerobic glycolysis through a pyruvate dehydrogenase kinase (Pdk)-dependent mechanism. Elevated Pdk expression leads to active suppression of the influx of glycolytic metabolites into mitochondria. Pdk overexpression in glycolysis-defective HSCs restored glycolysis, cell cycle quiescence, and stem cell capacity, while loss of both Pdk2 and Pdk4 attenuated HSC quiescence, glycolysis, and transplantation capacity. Moreover, treatment of HSCs with a Pdk mimetic promoted their survival and transplantation capacity. Thus, glycolytic metabolic status governed by Pdk acts as a cell cycle checkpoint that modulates HSC quiescence and function.

INTRODUCTION

Stem cells are tissue-sustaining cells that generate differentiated progeny and are resistant to external stresses (Zon, 2008; Seita and Weissman, 2010). Although stem cells probably exhibit metabolic characteristics allowing them to meet diverse energy demands, it is not known whether their metabolic phenotype differs from that of transiently amplifying progenitors and terminally differentiated cells and, if so, how metabolic phenotypes directly define stem cell identity (Suda et al., 2011). Cells generate adenosine-5′-triphosphate (ATP), the major currency for energy-consuming reactions, through central carbon metabolism, including glycolysis and mitochondrial oxidative phosphorylation (OXPHOS). The mammalian HSC system is maintained by self-renewal of quiescent long-term (LT)-HSCs and subsequent generation of short-term (ST)-HSCs, multipotent progenitors (MPPs), and various lineage-restricted progenies (Zon, 2008; Seita and Weissman, 2010). Adult LT-HSCs are maintained in a hypoxic state in the bone marrow (BM) niche (Parmar et al., 2007; Takubo et al., 2010). LT-HSCs maintain cell cycle quiescence through precise regulation of levels of hypoxia-inducible factor-1α (HIF-1α), a transcription factor responsive to cellular and systemic hypoxia (Takubo et al., 2010).

LT-HSCs, which exhibit fewer mitochondria than progenitors (Kim et al., 1998; Simsek et al., 2010; Norddahl et al., 2011), are hypothesized to utilize anaerobic metabolism in the hypoxic endosteal zone. Although the ratio of ATP generation to glucose consumption under anaerobic glycolysis is inefficient compared with that supported by OXPHOS, the rate of ATP production under hypoxia potentially increases 100-fold compared to that supported by mitochondrial energy production under normoxia (Voet and Voet, 2010). HSCs are particularly sensitive to oxidative stress and show low endogenous ROS levels. Aberrant ROS generation could abrogate various stem cell properties including cell cycle quiescence, self-renewal, survival, and multilineage differentiation capacity in HSCs (Miyamoto et al., 2007; Kobayashi and Suda, 2012). Because various mutant mice defective in LT-HSC maintenance display a wide range of bioenergetic defects in vivo, achieving a stable metabolic state in

LT-HSCs is probably important for their maintenance (Liu et al., 2009; Nakada et al., 2010; Gurumurthy et al., 2010; Gan et al., 2010; Sahin et al., 2011). Recently, Simsek et al. reported that LT-HSCs show higher glycolytic capacity than do cells in whole BM, which consists primarily of lineage marker$^+$-differentiated cells (Lin$^+$ cells) (Simsek et al., 2010). This activity is regulated by Cripto-GRP78 signaling activated by HIF-1α (Miharada et al., 2011). However, it remains unclear whether these metabolic characteristics are common in primitive hematopoietic cells such as LT-HSCs and progenitors and required for their maintenance.

In this study, we addressed the proposed "metabolic stemness" of HSCs, namely glycolytic activation, using metabolomics and genetics. During glycolysis, glucose is converted to pyruvate and then anaerobically to lactate or aerobically to acetyl-CoA for use in mitochondrial metabolism. The conversion of pyruvate to acetyl-CoA is catalyzed by pyruvate dehydrogenase (PDH), whose activity is suppressed by phosphorylation by PDH kinases (Pdks) (Harris et al., 2002). We observed that LT-HSCs show HIF-1α-mediated Pdk activation, resulting in maintenance of glycolytic flow and suppression of the influx of glycolytic metabolites into mitochondria. Also, a glycolytic metabolic state was shown to promote LT-HSC cell cycle quiescence, an activity that could potentially be exploited to regulate the cell cycle in those cells in vitro and in vivo. In mice, loss of Pdk2 and Pdk4 resulted in defective maintenance of cell cycle quiescence and transplantation capacity and altered glycolytic metabolic properties in LT-HSCs. Treatment of LT-HSCs with a competitive inhibitor of PDH promoted maintenance of transplantation capacity in vitro. These observations suggest that Pdk-mediated antagonism of mitochondrial metabolism comprises a checkpoint required to establish a metabolic state favoring cell cycle quiescence of LT-HSCs.

RESULTS

Metabolomic Profiling of Central Carbon Metabolism in LT-HSCs and Their Progeny

To define specific metabolic characteristics of hypoxic LT-HSCs, we performed metabolome analyses with capillary electrophoresis time-of-flight mass spectrometry (CE-TOFMS) (Soga et al., 2003, 2006; Shintani et al., 2009) using at least 1 × 10^6 murine BM LT-HSCs (CD34$^-$Flt3$^-$ Lineage marker$^-$ Sca-1$^+$ c-Kit$^+$; CD34$^-$Flt3$^-$ LSK cells) and their progeny, including ST-HSCs (CD34$^+$Flt3$^-$ LSK cells), MPPs (CD34$^+$Flt3$^+$ LSK cells), myeloid progenitors (MPs; Lin$^-$ c-Kit$^+$ Sca-1$^-$ cells), and differentiated hematopoietic cells (Gr-1/Mac-1+ myeloid cells, CD4/CD8+ T cells, and B220+ B cells) to assess levels of intracellular metabolites functioning in central carbon metabolism. We replicated the analysis and show one representative result in Figure 1A and Figure S1A available online (Figure 1A is an extract of Figure S1A). Notably, fructose 1,6-bisphosphate (F1,6BP), a product of the rate-limiting step of glycolysis catalyzed by phosphofructokinase-1 (Pfk-1), was observed only in LT-HSCs and ST-HSCs (Figures 1A and S1A). Because F1,6BP is a strong allosteric activator of pyruvate kinase (PK) (Voet and Voet, 2010), LT-HSCs probably support glycolytic metabolism required to produce PK-dependent ATP. Because low levels of the Pfk-1 substrate fructose-6-phosphate were also observed in LT-HSCs, the rate-limiting Pfk-1 reaction is probably activated in LT-HSCs (Figures 1A and S1A). In addition, pyruvate, a by-product of PK-dependent ATP generation, accumulated to high levels in LT-HSCs (Figures 1A and S1A), while levels of phosphoenolpyruvate, a PK substrate, remained low (Figures 1A and S1A). Mitochondrial OXPHOS is fueled by the tricarboxylic acid (TCA) cycle. Among TCA cycle-related metabolites, 2-oxoglutarate (2-OG) and both acetyl-CoA and succinyl-CoA were not detected in any hematopoietic fraction (Figure S1A). In support of metabolomics profiling data shown in Figures 1A and S1A, we found that various glycolytic enzymes were more highly expressed in LT-HSCs than in progenitors or terminally differentiated cells (Figure S1B), suggesting that LT-HSCs utilize glycolysis for energy generation (Voet and Voet, 2010).

Interestingly, LT-HSC ATP levels were lowest among various primitive hematopoietic cell fractions in the BM (Figure 1B). The Side Population (SP) phenotype of LT-HSCs is marked by expression of the ATP-dependent transporter Bcrp1 (Goodell et al., 1996, 1997; Zhou et al., 2001) and maintained by intracellular ATP production. The SP phenotype of normal LT-HSCs was sensitive to treatment with the glycolytic inhibitor 2-deoxy-D-glucose (2-DG) (Figure 1C). Treatment of BM mononuclear cells (MNCs) with the respiration inhibitor sodium azide (NaN_3), even at concentrations (20 mM) sufficient to inhibit OXPHOS, moderately reduced SP phenotypes in LT-HSCs (Figure 1C). Glucose uptake by cells from primitive fractions including LT- or ST-HSCs or MPPs was higher than that seen in myeloid progenitor or lineage marker+ fractions (Figure 1D). The activity of pyruvate kinase, which catalyzes an ATP-generating step in glycolysis, was highest in LT-HSCs among various BM fractions (Figure 1E). Overall, these observations suggest that only LT-HSCs, rather than transiently amplifying progenitors or terminally differentiated cells, can survive independent of mitochondrial energy generation, possibly through suppression of the PDH-E1α subunit by Pdk-dependent phosphorylation (depicted schematically in Figure 2A). Expression of all murine Pdk family members (Pdk1–Pdk4) (Harris et al., 2002) was high in LT-HSCs (Figure 2B), and PDH-E1α was more highly phosphorylated in LT-HSCs than in their differentiated progeny (Figures 2C and 2D). The oxygen consumption rate (OCR) was lowest in LT-HSCs, dynamically upregulated after their differentiation into ST-HSCs, and slightly decreased in MPPs or MPs (Figure 2E). The higher OCR seen in fractions other than LT-HSCs was probably maintained by mitochondrial oxygen consumption, as treatment with oligomycin, which inhibits mitochondrial ATP synthase, clearly suppressed the OCR in these cells (Figure 2E). These findings are in accord with the idea that LT-HSCs survive in a hypoxic environment and are less dependent on mitochondrial oxygen-consuming metabolism than more differentiated cells (Figure 2E).

Loss of HIF-1α Alters Energy Metabolism in LT-HSCs

To determine whether a HIF-1α-dependent crucial checkpoint maintains anaerobic metabolic stemness in LT-HSCs, we examined parameters relevant to metabolism in *HIF-1*$\alpha^{\Delta/\Delta}$ LT-HSCs. We found that HIF-1α deficiency was accompanied by decreased expression of various glycolytic enzymes in LT-HSCs (Figure S2). Glucose uptake was identical at various differentiation stages in *HIF-1*$\alpha^{\Delta/\Delta}$ BM (Figure 3A), although an essential glucose transporter, Glut1, was significantly downregulated in

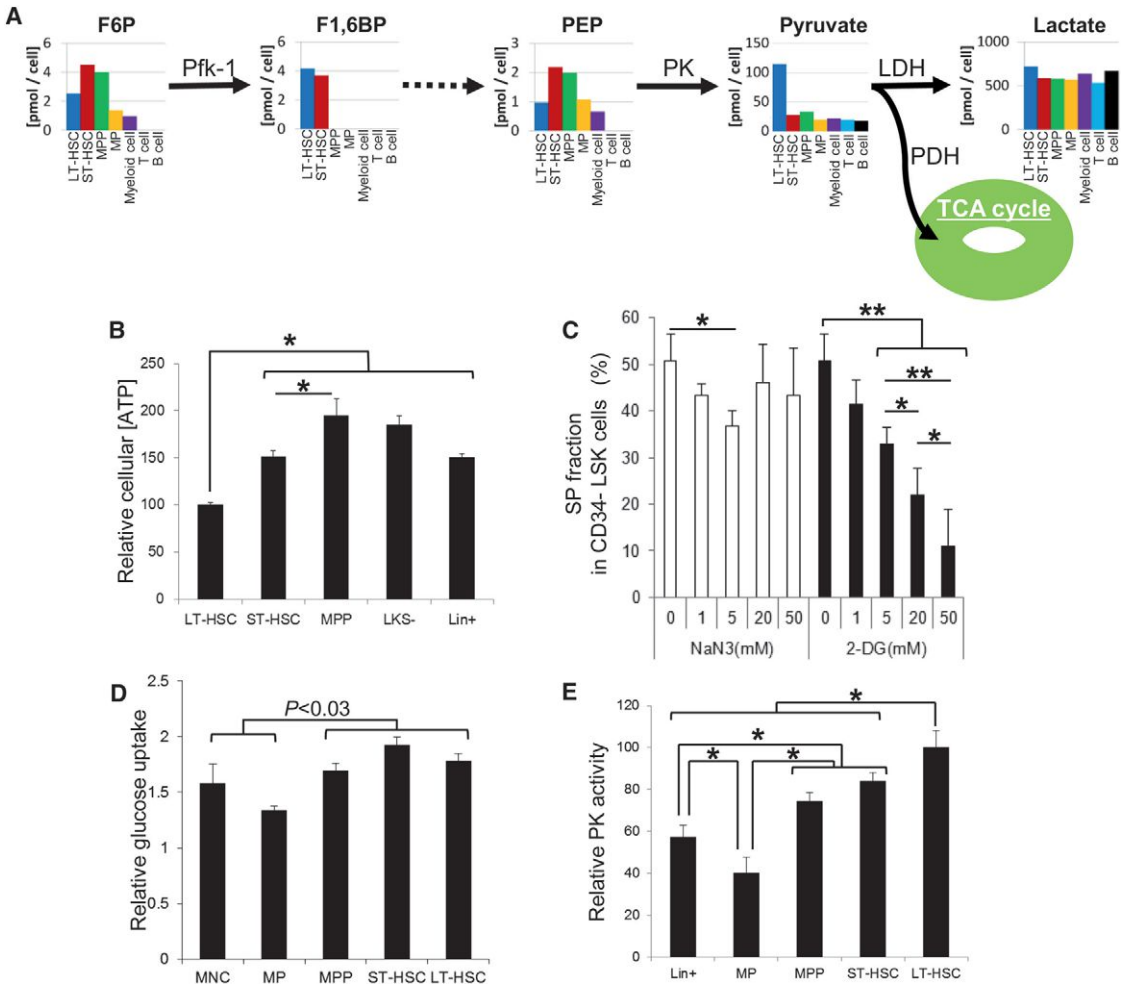

Figure 1. Metabolic Profiling of Glycolytic Metabolism in HSCs and Their Progeny

(A) Quantification of metabolites in glycolytic metabolism based on CE-TOFMS analysis. Bar graphs for independent metabolites plotted in the glycolytic metabolism map are (from left to right): long-term (LT)-hematopoietic stem cells (HSCs) ($CD34^-Flt3^-$ LSK cells; blue bars), short-term (ST)-HSCs ($CD34^+Flt3^-$ LSK cells; red bars), multipotent progenitors (MPPs) ($CD34^+Flt3^+$ LSK cells; green bars), myeloid progenitors (MPs; Lin^- c-Kit^+ $Sca\text{-}1^-$ cells; yellow bars), Gr-1/Mac-1^+ myeloid cells (purple bars), CD4/$CD8^+$ T cells (sky blue bars), and $B220^+$ B lymphocytes (black bars). Data are representative of two independent experiments.

(B) Relative intracellular ATP concentrations in LT-HSC, ST-HSC, MPP, LKS^-, and Lin^+ cells (mean ± SD, n = 6, *p < 0.001).

(C) Effects of NaN_3 (open bars) or 2-DG (closed bars) treatment on the Side Population phenotype of the $CD34^-$ LSK fraction at indicated concentrations (mean ± SD, n = 4, *p < 0.05, **p < 0.0002).

(D) Relative glucose uptake by LT-HSC, ST-HSC, MPP, MP, and Lin^+ cells (mean ± SD, n = 5).

(E) Relative PK activity in LT-HSC, ST-HSC, MPP, MP, and Lin^+ cells (mean ± SD, n = 6, *p < 0.001).

See also Figure S1.

HIF-1α$^{\Delta/\Delta}$ LT-HSCs (Figure S2). Glycolytic LDH activity in normal LT-HSCs was higher than that seen in $CD34^+$ LSK progenitors (the sum of ST-HSCs plus MPPs) and was decreased in *HIF-1α*$^{\Delta/\Delta}$ LT-HSCs (Figure 3B). We found that LT-HSCs release lactate into the culture medium only under hypoxia and those levels decrease in the case of HIF-1α deficiency (Figure 3C). Because intracellular levels of lactate, a product of the LDH reaction, in LT-HSCs and their differentiated progeny were unchanged (Figures 1A and S1A), we conclude that LT-HSCs probably rapidly release lactate generated by glycolysis into the extracellular space. Intracellular pyruvate levels, which are high in LT-HSCs (Figures 1A and S1A), were decreased by HIF-1α deficiency (Figure 3D). These data suggest that, in the hypoxic niche, LT-HSCs suppress flux of glycolytic metabolites into mitochondria for the TCA cycle and *HIF-1α*$^{\Delta/\Delta}$ LT-HSCs show defective conversion of pyruvate to lactate, an activity maintained through the suppression of PDH by Pdk. In support of this, phosphorylation of the α subunit of PDH-E1 is attenuated in *HIF-1α*$^{\Delta/\Delta}$ LT-HSCs (Figure 3E). Overall ATP production was considerably decreased in *HIF-1α*$^{\Delta/\Delta}$ LT-HSCs compared to *HIF-1α*$^{\Delta/\Delta}$ $CD34^+$ LSK progenitors (Figure 3F), suggesting that ATP production in the former is dependent on HIF-1α-dependent glycolysis and that mitochondrial metabolism is suppressed by Pdk. Overall mitochondrial mass in wild-type LT-HSCs was

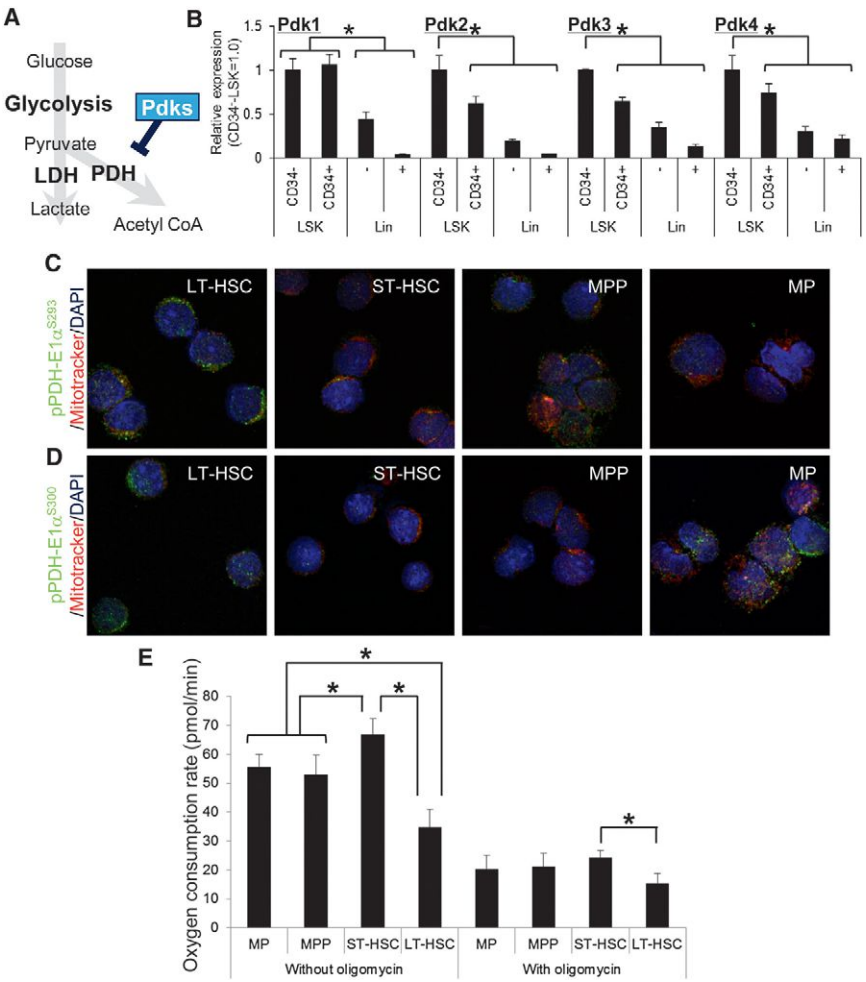

Figure 2. Pdk-Mediated Metabolic Properties of LT-HSCs

(A) Schematic representation of the effect of Pdks on energy metabolism.

(B) qPCR analysis of Pdk family members in $CD34^-$ LSK, $CD34^+$ LSK, Lin^-, or Lin^+ fractions from 12-week-old mice (mean ± SD, n = 4). Each value was normalized to β-actin expression and is expressed as fold induction compared to levels detected in $CD34^-$ LSK samples (*$p < 0.01$).

(C and D) Immunocytochemical staining for phosphorylated S293 (C) or S300 (D) residues of PDH-E1α (green), Mitotracker DeepRed (red), and DAPI (blue) in wild-type LT-HSC ($CD34^-$ $Flt3^-$ LSK), ST-HSC ($CD34^+$ $Flt3^-$ LSK), MPP ($CD34^+$ $Flt3^+$ LSK), or MP (Lineage marker$^-$ c-Kit^+ $Sca\text{-}1^-$) cells.

(E) Oxygen consumption rate in LT-HSC, ST-HSC, MPP, and MP cells treated with or without oligomycin (mean ± SD, n = 6) (*$p < 0.001$).

See also Figure S2.

HIF-1α Maintains Pdk Expression, Glycolysis, and Transplantation Capacity in LT-HSCs

The decreased glycolysis and activated mitochondrial energy metabolism seen in *HIF-1α*$^{\Delta/\Delta}$ LT-HSCs (Figure 3) suggest that HIF-1α-dependent remodeling of metabolic pathways by Pdk-mediated antagonism of PDH activity occurs in LT-HSCs. Notably, among Pdk family members, *Pdk2* and *Pdk4* mRNA levels were positively correlated with HIF-1α expression in LT-HSCs (Figure 4A). Their mRNA levels decreased in the case of HIF-1α deficiency and increased in the presence of VHL deficiency (Figure 4A). Increased Pdk mRNA levels were suppressed by deletion of both HIF-1α and VHL (Figure 4A). Exposure of LT-HSCs to hypoxia increased expression of Pdk4 but not Pdk2 (Figure S4A), suggesting oxygen-dependent and -independent roles for HIF-1α for the expression of these two genes. To verify that Pdks function as HIF-1α effectors in HSC maintenance, we transduced LT-HSCs or LSK cells with retrovirus expressing Pdk2 or Pdk4 (Figures 4B and S4B). Pdk misexpression (at mRNA levels 100- to 1,000-fold greater than normal) by retrovirus-restored phosphorylation of the PDH-E1α subunit in *HIF-1α*$^{\Delta/\Delta}$ LT-HSCs (Figure 4C) and glycolytic activity in *HIF-1α*$^{\Delta/\Delta}$ LSK cells, as measured by LDH activity (Figure 4D), and antagonized increased mitochondrial ROS generation seen under HIF-1α deficiency (Takubo et al., 2010) (Figure S4D). The number of $Ki67^+$ cycling cells also decreased in Pdk-transduced *HIF-1α*$^{\Delta/\Delta}$ LSK cells (Figure 4E). For in vitro analysis of HSCs, we utilized the SLAM marker to detect HSCs in the LSK population because some LT-HSCs tend to express CD34 in vitro (Noda et al., 2008). *HIF-1α*$^{\Delta/\Delta}$ cells cultured in hypoxic conditions could not sustain an LT-HSC fraction, a deficiency rescued by the introduction of Pdk2 or Pdk4 into *HIF-1α*$^{\Delta/\Delta}$ LSK cells (Figures 4F and 4G).

smaller than that seen in wild-type $CD34^+$ LSK progenitors (Figure 3G). In *HIF-1α*$^{\Delta/\Delta}$ LT-HSCs, mitochondrial volume and expression of the mitochondrial respiratory component COX4-1 (Fukuda et al., 2007) were higher than that seen in wild-type LT-HSCs (Figures 3G and 3H). These data suggest that *HIF-1α*$^{\Delta/\Delta}$ LT-HSCs exhibit decreased dependence on anaerobic glycolysis and activate mitochondrial aerobic metabolism due to loss of a metabolic checkpoint regulated by PDH-E1α subunit phosphorylation status.

To directly analyze metabolic changes in *HIF-1α*$^{\Delta/\Delta}$ HSCs, we analyzed the SP phenotype. Overall, the *HIF-1α*$^{\Delta/\Delta}$ LSK fraction showed significant loss of the SP phenotype after treatment with 20 mM NaN_3 (Figure S3A), suggesting that, in the case of HIF-1α deficiency, compensatory mitochondrial aerobic metabolism supports ATP production in the primitive hematopoietic fraction. By contrast, LSK cells deficient in VHL, an E3 ubiquitin ligase targeting HIF-1α (Semenza, 2010), showed significantly reduced mitochondrial volume compared to wild-type LSK cells (Figure S3B). Because normal quiescent HSCs have relatively little cytoplasm and contain few inactive mitochondria (Kim et al., 1998) (Figure 3G), the decreased mitochondrial mass seen in *VHL*$^{\Delta/\Delta}$ LSK cells suggests that active regulatory mechanisms function in HIF-1α dose-dependent energy production in primitive hematopoietic cells.

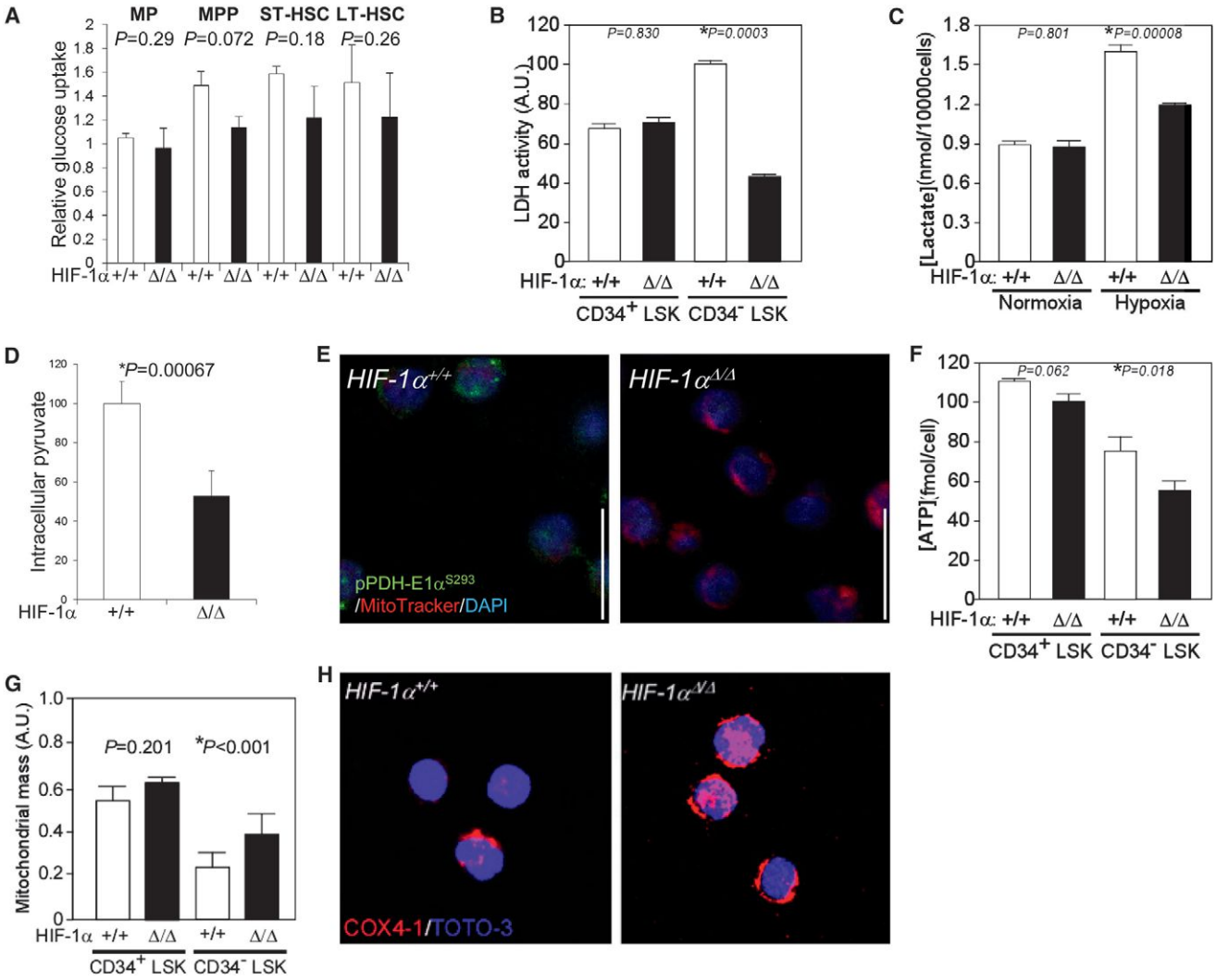

Figure 3. Loss of HIF-1α Alters HSC Energy Metabolism

(A) Relative glucose uptake by LT-HSC, ST-HSC, MPP, and MP cells from *HIF-1α*$^{+/+}$ or *HIF-1α*$^{\Delta/\Delta}$ mice (mean ± SD, n = 4).

(B) LDH activity in CD34$^+$ or CD34$^-$ LSK cells from *HIF-1α*$^{+/+}$ or *HIF-1α*$^{\Delta/\Delta}$ mice (mean ± SD, n = 4). Arbitrary units (a.u.) were calculated as the value relative to LDH activity in the *HIF-1α*$^{+/+}$ CD34$^-$ LSK fraction (set to 100; *p < 0.01).

(C) Lactate production in CD34$^-$ LSK cells under normoxic (20% O_2) or hypoxic (1% O_2) conditions per ten thousand cells (mean ± SD, n = 4; *p < 0.01).

(D) Relative intracellular pyruvate concentrations in LT-HSCs from *HIF-1α*$^{+/+}$ or *HIF-1α*$^{\Delta/\Delta}$ mice (mean ± SD, n = 4; *p < 0.01).

(E) Immunocytochemical staining for phosphorylated S293 residues of PDH-E1α (green), mitochondrial dye Mitotracker DeepRed (red), and DAPI (blue) in *HIF-1α*$^{+/+}$ or *HIF-1α*$^{\Delta/\Delta}$ LT-HSCs.

(F) Intracellular ATP concentration in CD34$^+$ or CD34$^-$ LSK cells from *HIF-1α*$^{+/+}$ or *HIF-1α*$^{\Delta/\Delta}$ mice (mean ± SD, n = 3; *p < 0.05).

(G) Relative mitochondrial mass (mitochondrial fluorescence/nuclear fluorescence) in individual *HIF-1α*$^{\Delta/\Delta}$ CD34$^+$ or CD34$^-$ LSK cells (n = 50). Data are presented as the mean ± SD (*p < 0.001).

(H) Immunocytochemical staining of CD34$^-$ LSK cells for COX4-1 (red) and TOTO-3 (blue).

See also Figure S3.

To test reconstitution capacity, we transplanted 3,000 GFP$^+$-*HIF-1α*$^{\Delta/\Delta}$ LSK cells into lethally irradiated Ly5.1 (CD45.1$^+$) congenic mice together with competitor BM (CD45.1$^+$). Transduced LSK cells in every group contained a similar number of LT-HSCs, as assessed by flow cytometry (data not shown). Twelve weeks after BM transplantation (BMT), *HIF-1α*$^{\Delta/\Delta}$ LSK cells transduced with GFP virus showed significantly decreased repopulation capacity, probably due to upregulation of p16^{Ink4a}/p19^{Arf} in *HIF-1α*$^{\Delta/\Delta}$ LT-HSCs during transduction stress, as previously reported (Takubo et al., 2010). In contrast, *HIF-1α*$^{\Delta/\Delta}$ LSK cells transduced with either Pdk2 or Pdk4 virus showed substantial chimerism and multilineage reconstitution capacity in peripheral blood (PB) compared to control *HIF-1α*$^{\Delta/\Delta}$ cells (Figure 4H and Figure S4E). These experiments suggest that HIF-1α maintains substantial chimerism and multilineage reconstitution capacity through upregulation of Pdk2 and Pdk4 despite expression of other HIF-α family members (Figure S4C).

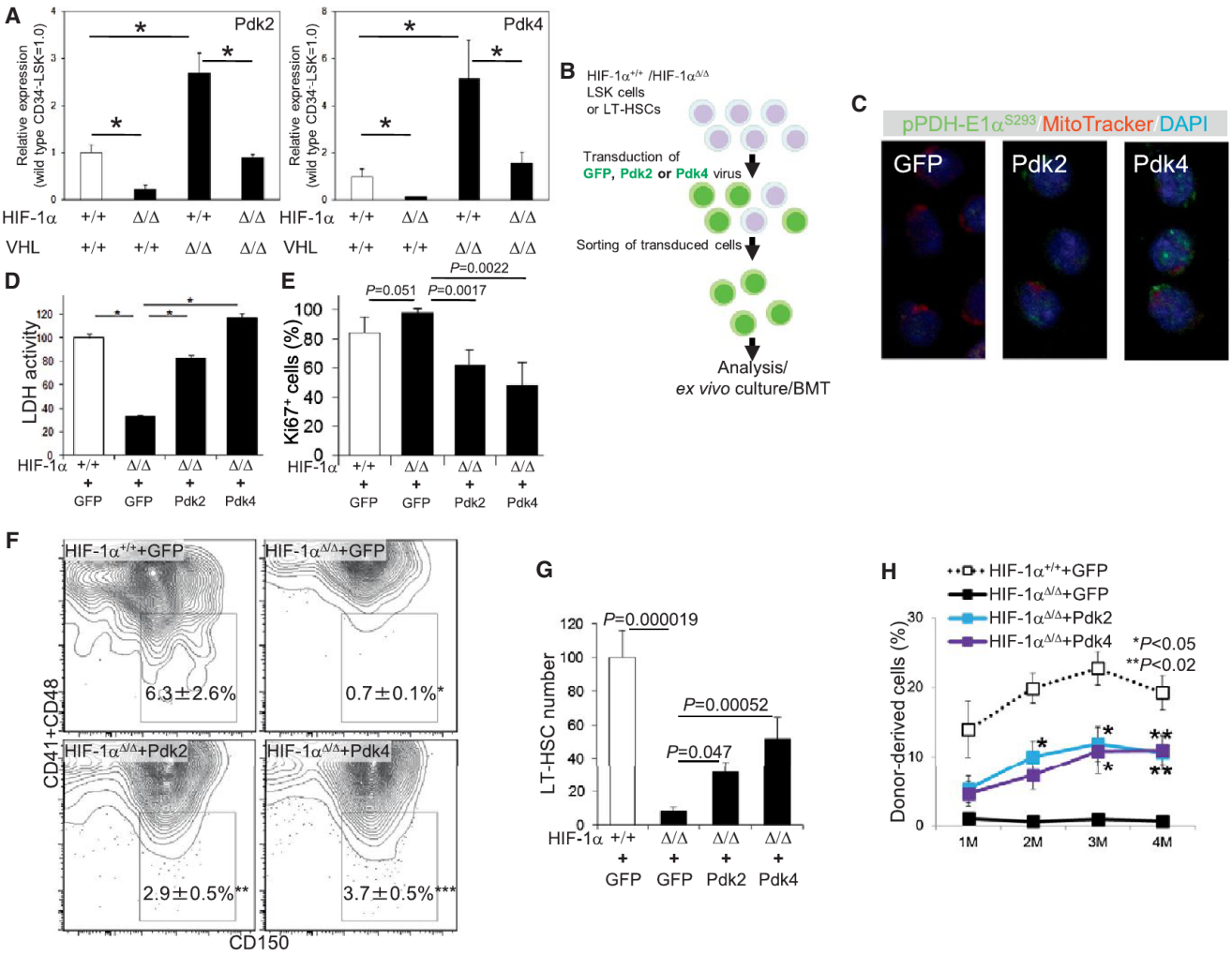

Figure 4. HIF-1α Maintains Pdk Expression, Glycolysis, and Transplantation Capacity in HSCs

(A) qPCR analysis of Pdk2 and Pdk4 expression in the LT-HSC fraction of 12-week-old *HIF-1α*$^{+/+}$, *HIF-1α*$^{Δ/Δ}$, *VHL*$^{Δ/Δ}$ BM, or *HIF-1α*$^{Δ/Δ}$:*VHL*$^{Δ/Δ}$ BM mice (n = 4). Values are normalized to β-actin expression and expressed as fold induction compared to levels detected in *HIF-1α*$^{+/+}$ samples (mean ± SD, n = 4, *p < 0.01).

(B) Design of retroviral rescue of Pdk expression in *HIF-1α*$^{Δ/Δ}$ LSK cells.

(C) Immunocytochemical staining for phosphorylated S293 residues of PDH-E1α (green), Mitotracker DeepRed (red), and DAPI (blue) in *HIF-1α*$^{Δ/Δ}$ LT-HSCs transduced with GFP, Pdk2, or Pdk4 retroviruses.

(D) Intracellular LDH activity in GFP virus-transduced *HIF-1α*$^{+/+}$ LSK cells or in *HIF-1α*$^{Δ/Δ}$ LSK cells transduced with GFP, Pdk2, or Pdk4 retroviruses (mean ± SD, n = 5, *p < 0.000001).

(E) Immunocytochemical assessment of Ki67^{+} in LSK cells transduced with Pdks for 48 hr on a *HIF-1α*$^{+/+}$ or *HIF-1α*$^{Δ/Δ}$ background (mean ± SD, n = 5).

(F) CD150^{+}CD41^{-}CD48^{-} LSK cells after transduction with GFP, Pdk2, or Pdk4 retroviruses and then 7 days of culture under hypoxia (mean ± SD, n = 3, *p < 0.05).

(G) Quantification of total cell number of CD150^{+}CD41^{-}CD48^{-} LSK cells analyzed in (F).

(H) PB chimerism of *HIF-1α*$^{Δ/Δ}$ donor cells transduced with Pdk viruses at 1, 2, 3 and 4 months (M) after BMT (mean ± SEM, n = 5, *p < 0.05, **p < 0.02; compared to *HIF-1α*$^{Δ/Δ}$+GFP virus).

See also Figure S4.

Pdk2 and Pdk4 Are Essential for LT-HSC Transplantation Capacity

To assess whether Pdk functions in LT-HSC maintenance downstream of HIF-1α, we examined hematopoiesis of Pdk2/Pdk4 double knockout mice (Dunford et al., 2011; Jeoung et al., 2006). Peripheral blood counts indicated that these *Pdk2*$^{-/-}$*: Pdk4*$^{-/-}$ mice were mildly but significantly anemic compared to control mice (Figure 5A). Various populations of differentiated and undifferentiated cells in the BM, spleen, and thymus were unchanged in number in *Pdk2*$^{-/-}$*: Pdk4*$^{-/-}$ mice (Figures S5A–S5E). Progenitor capacity of *Pdk2*$^{-/-}$*: Pdk4*$^{-/-}$ LSK cells, as assessed by the colony-forming capacity in semi-solid methylcellulose plus cytokines, was identical to that of control cells (Figure 5B), suggesting that steady-state hematopoiesis and progenitor capacity is maintained in *Pdk2*$^{-/-}$*: Pdk4*$^{-/-}$ mice. To investigate self-renewal and multilineage differentiation capacity of *Pdk2*$^{-/-}$*: Pdk4*$^{-/-}$ LT-HSCs, we performed BM transplantation of these cells with congenic

A

	Control	*Pdk2*$^{-/-}$:*Pdk4*$^{-/-}$	P value
WBC(/ul)	11429±3259	10000±4320	0.498
RBC(x10^4/ul)	1019±34	1007±41	0.583
Hb(g/dl)	15.9±0.4	15.0±0.0	<0.001
HCT(%)	51.3±1.3	49.6±1.0	0.014
MCV(fl)	50.4±1.4	49.3±1.7	0.206
MCH(pg)	15.6±0.4	14.9±0.6	0.043
Plt(x10^4/ul)	88.4±27.4	82.0±36.4	0.716

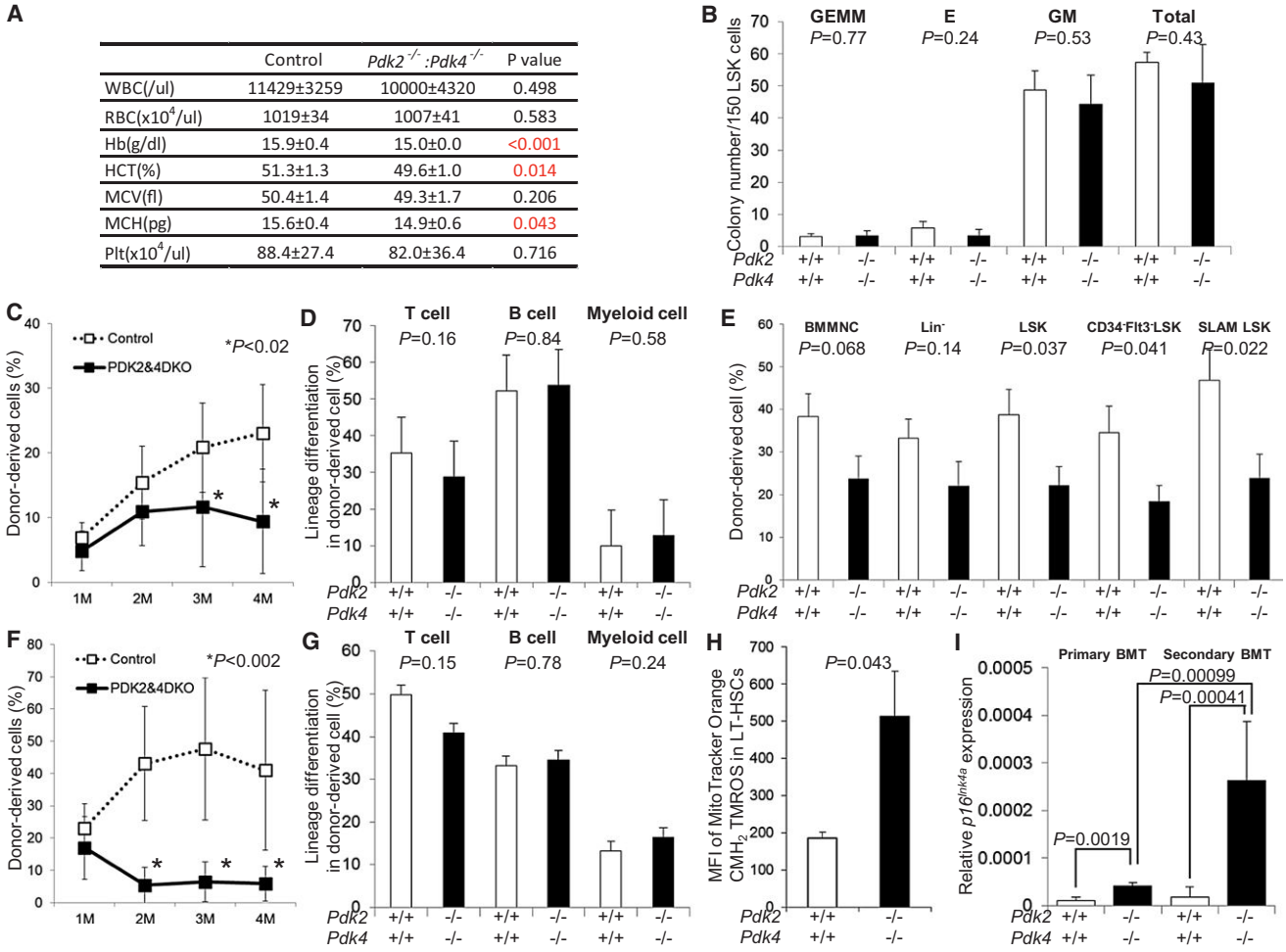

Figure 5. Defective Maintenance of *Pdk2*$^{-/-}$: *Pdk4*$^{-/-}$ HSCs after Transplantation

(A) PB counts in control and *Pdk2*$^{-/-}$: *Pdk4*$^{-/-}$ mice (mean ± SD, n = 7).

(B) Colony-forming capacity of control (open bars) and *Pdk2*$^{-/-}$: *Pdk4*$^{-/-}$ LSK cells (closed bars) (mean ± SD, n = 3). CFU-GEMM, CFU-E, CFU-GM, and total colony numbers are indicated.

(C) PB chimerism in primary BMT recipients of control (open boxes) or *Pdk2*$^{-/-}$: *Pdk4*$^{-/-}$ LT-HSC (closed boxes) cells at 1, 2, 3 and 4 months (M) after BMT (mean ± SD, n = 10).

(D) Differentiation status (CD4/CD8+ T cells, B220+ B cells, or Mac-1/Gr-1+ myeloid cells) of donor-derived (Ly5.2+) PB cells in primary BMT recipients of control (open bars) or *Pdk2*$^{-/-}$: *Pdk4*$^{-/-}$ (closed bars) LT-HSCs (mean ± SD, n = 10).

(E) Donor-derived (Ly5.2+) BM MNC, Lin$^-$, LSK, CD34$^-$Flt3$^-$ LSK, or SLAM-LSK chimerism in primary BMT recipients of control (open bars) or *Pdk2*$^{-/-}$: *Pdk4*$^{-/-}$ (closed bars) LT-HSCs 4 months after primary BMT (mean ± SEM, n = 10).

(F) PB chimerism in secondary recipients of BM derived from primary recipients of control (open boxes) or *Pdk2*$^{-/-}$: *Pdk4*$^{-/-}$ (closed boxes) MNCs, at indicated times after BMT (mean ± SD, n = 10).

(G) Differentiation status (CD4/CD8+ T cells, B220+ B cells, or Mac-1/Gr-1+ myeloid cells) of donor-derived (Ly5.2+) PB cells in secondary BMT recipients of control (open bars) or *Pdk2*$^{-/-}$: *Pdk4*$^{-/-}$ (closed bars) cells (mean ± SD, n = 10).

(H) Redox-sensitive MitoTracker fluorescence in control (open bars) or *Pdk2*$^{-/-}$: *Pdk4*$^{-/-}$ (closed bars) BM LT-HSCs (n = 3, mean ± SD).

(I) Quantitative PCR analysis of p16^{Ink4a} expression in control (open bars) or *Pdk2*$^{-/-}$: *Pdk4*$^{-/-}$ (closed bars) donor-derived LT-HSCs 4 months after primary BMT (n = 4). Values are normalized to β-actin expression and expressed as fold induction compared to levels detected in *HIF-1α*$^{+/+}$ Ly5.2$^+$ LSK samples (mean ± SD). See also Figure S5.

competitors into lethally irradiated recipient mice. In contrast to the capacity of differentiated counterparts, LT-HSCs were defective in repopulation of primary recipient peripheral blood at 3–4 months after transplantation (Figure 5C). Four months after BMT, *Pdk2*$^{-/-}$: *Pdk4*$^{-/-}$ donor-derived cells retained differentiation capacity of T, B, and myeloid cells comparable with control donor-derived cells (Figure 5D). At that time, recipients of *Pdk2*$^{-/-}$: *Pdk4*$^{-/-}$ donor cells exhibited less chimerism than did recipients of control donor cells in the LSK-gated, CD34$^-$Flt3$^-$ LSK-gated, or SLAM-LSK-gated fraction of BM (Figure 5E), indicating that HSC levels decreased. We then isolated and transplanted 1 × 10^6 primary donor-derived MNCs into secondary recipients. We observed a clear defect in long-term reconstitution ability of *Pdk2*$^{-/-}$: *Pdk4*$^{-/-}$

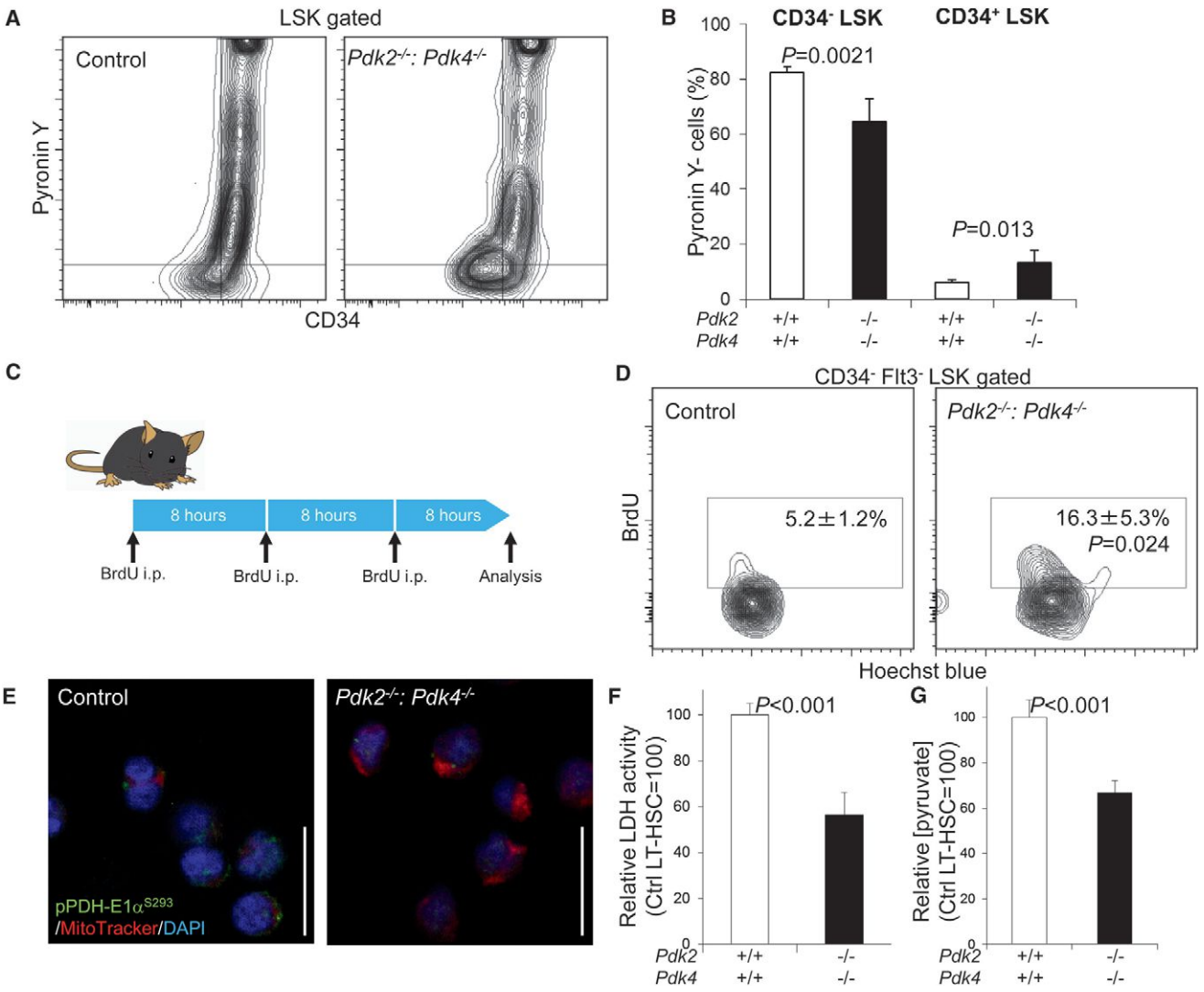

Figure 6. Loss of Cell Cycle Quiescence and Glycolytic Capacity in *Pdk2*$^{-/-}$: *Pdk4*$^{-/-}$ HSCs

(A) Representative flow cytometric plot of Pyronin Y analysis in the LSK-gated fraction of control or *Pdk2*$^{-/-}$: *Pdk4*$^{-/-}$ BM MNCs.

(B) Summary of flow cytometric Pyronin Y analysis of CD34^{-} LSK or CD34^{+} LSK fractions in control or *Pdk2*$^{-/-}$: *Pdk4*$^{-/-}$ BM MNCs (mean ± SD, n = 6).

(C) Design of short-term BrdU labeling assay in control or *Pdk2*$^{-/-}$: *Pdk4*$^{-/-}$ mice.

(D) Representative flow cytometric plot showing BrdU labeling of the LT-HSC-gated fraction from control or *Pdk2*$^{-/-}$: *Pdk4*$^{-/-}$ BM MNCs. Numbers indicate the frequency of the BrdU+ fraction in LT-HSCs (mean ± SD, n = 3).

(E) Immunocytochemical staining for the phosphorylated S293 residue of PDH-E1α (green), Mitotracker DeepRed (red), and DAPI (blue) in control or *Pdk2*$^{-/-}$: *Pdk4*$^{-/-}$ LT-HSCs.

(F) LDH activity in LT-HSCs from control or *Pdk2*$^{-/-}$: *Pdk4*$^{-/-}$ mice (mean ± SD, n = 4). Shown are arbitrary values calculated as the value relative to LDH activity in the control LT-HSC fraction (set to 100).

(G) Intracellular pyruvate concentration in LT-HSCs from control or *Pdk2*$^{-/-}$: *Pdk4*$^{-/-}$ mice (mean ± SD, n = 3). Shown are arbitrary values calculated as the value relative to intracellular pyruvate levels in the control LT-HSC fraction (set to 100).

See also Figure S6.

HSCs in the PB and BM of secondary recipients (Figures 5F and S5F) without any differentiation defect 4 months after secondary transplantation (Figure 5G). We isolated and transplanted 1 × 10^6 secondary donor-derived MNCs into tertiary recipients. We observed no long-term reconstitution ability of *Pdk2*$^{-/-}$: *Pdk4*$^{-/-}$ HSCs in the PB of tertiary recipients (Figure S5G). ROS reportedly induces p16^{Ink4a} expression (Takahashi et al., 2006), and p16^{Ink4a} enhances HSC aging (Janzen et al., 2006). We observed increased mitochondrial ROS production in *Pdk2*$^{-/-}$: *Pdk4*$^{-/-}$ LT-HSCs (Figure 5H). Thus, ROS-mediated senescence of *Pdk2*$^{-/-}$: *Pdk4*$^{-/-}$ LT-HSCs could account for loss of stem cell properties through p16^{Ink4a} upregulation. In support of this idea, we detected significantly elevated levels of p16^{Ink4a} transcripts in *Pdk2*$^{-/-}$: *Pdk4*$^{-/-}$ LT-HSCs from primary and secondary BMT recipients (Figure 5I).

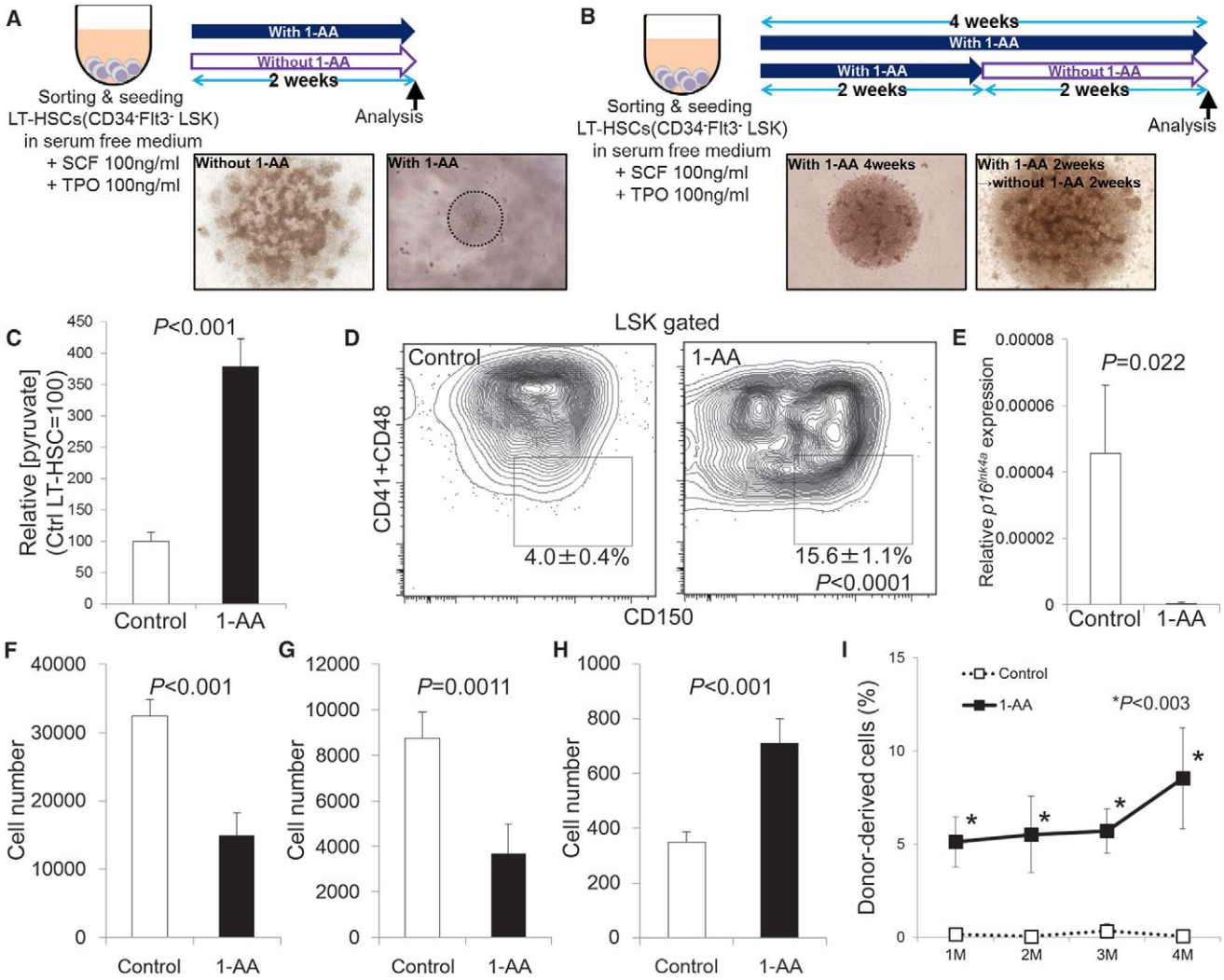

Figure 7. Modulation of HSC Cell Cycle Quiescence by a PDH Inhibitor

(A) Design of LT-HSC cultures treated with or without 1-AA for 2 weeks. Light microscopic data show colony morphology.

(B) Effect of 1-AA withdrawal on LT-HSCs after 2 weeks of treatment. Light microscopic colony morphology after 4 weeks of culture.

(C) Intracellular pyruvate concentrations in LT-HSCs treated with or without 1-AA for 4 days (mean ± SD, n = 3). Shown are arbitrary values calculated as the value relative to intracellular pyruvate in the control LT-HSC fraction (set to 100).

(D) Flow cytometric analysis of LT-HSCs treated with or without 1-AA in vitro for 4 weeks. Numbers indicate the LT-HSC fraction in LSK cells (mean ± SD, n = 4).

(E) Quantitative PCR analysis of *p16*^{Ink4a} expression in control (open bars) or 1-AA-treated (closed bars) LT-HSCs 2 weeks after culture with or without 1-AA (n = 4). Values are normalized to β-actin expression and expressed as fold induction compared to levels detected in control samples (mean ± SD).

(F–H) Quantification of total cells (F), LSK cells (G), or LT-HSCs (H) from LT-HSC-derived colonies in the absence (control) or presence of 1-AA for 4 weeks in vitro (mean ± SD, n = 4).

(I) Donor-derived (Ly5.1$^+$) PB chimerism in BMT recipients of control LT-HSCs or LT-HSCs treated with 1-AA for 4 weeks, at indicated times after BMT (mean ± SD, n = 4–5).

See also Figure S7.

Pdks Are Essential for LT-HSC Cell Cycle Quiescence and Metabolism

The pivotal role played by Pdk2 and Pdk4 in LT-HSC senescence during transplantation suggests that Pdk-mediated antagonism of mitochondrial metabolism prevents LT-HSC senescence by maintaining cell cycle quiescence. To test this hypothesis, we examined cell cycle kinetics of the *Pdk2*$^{-/-}$*: Pdk4*$^{-/-}$ LT-HSCs by multicolor flow cytometry. Although the number of LT-HSCs, ST-HSCs, and MPPs was unchanged in *Pdk2*$^{-/-}$*: Pdk4*$^{-/-}$ mice (Figures S5D and S5E), we detected specific activation of the cell cycle, characterized by a reduction in the Pyronin Y$^-$ G0 fraction and an increase in the Pyronin Y$^+$ G1 fraction, in *Pdk2*$^{-/-}$*: Pdk4*$^{-/-}$ CD34$^-$ LSK cells (Figures 6A and 6B). Recipient mice whose BM was replaced by *Pdk2*$^{-/-}$*: Pdk4*$^{-/-}$ MNCs (*Pdk2*$^{-/-}$*: Pdk4*$^{-/-}$ BM mice) also showed similar loss of the G0 fraction in *Pdk2*$^{-/-}$*: Pdk4*$^{-/-}$ CD34$^-$ LSK cells (Figures S6A and S6B). Interestingly, CD34$^+$ LSK cells showed an increase in the Pyronin Y$^-$ G0 fraction in *Pdk2*$^{-/-}$*: Pdk4*$^{-/-}$ mice (both

hematopoietic cells and hematopoietic microenvironment are *Pdk2*$^{-/-}$*: Pdk4*$^{-/-}$), but not in *Pdk2*$^{-/-}$*: Pdk4*$^{-/-}$ BM mice (*Pdk2*$^{-/-}$*: Pdk4*$^{-/-}$ hematopoietic cells and *Pdk2*$^{+/+}$*: Pdk4*$^{+/+}$ hematopoietic microenvironment) (Figures 6A, 6B, S6A, and S6B). These observations suggest that *Pdk2*$^{-/-}$*: Pdk4*$^{-/-}$ nonhematopoietic cells limit blood cell production by slowing the G0/G1 progression of *Pdk2*$^{-/-}$*: Pdk4*$^{-/-}$ progenitors. Also, short-term BrdU labeling indicated high levels of cycling cells in the *Pdk2*$^{-/-}$*: Pdk4*$^{-/-}$ LT-HSC population (Figures 6C and 6D). In addition to the cell cycle defect, we detected metabolic defects in *Pdk2*$^{-/-}$*: Pdk4*$^{-/-}$ mice. In *Pdk2*$^{-/-}$*: Pdk4*$^{-/-}$ LT-HSCs, PDH-E1α subunit phosphorylation status was decreased (Figures 6E, S6C, and S6D) and intracellular LDH activity and pyruvate content were significantly attenuated (Figures 6F and 6G). These findings indicate that Pdks are necessary to maintain cell cycle quiescence and LT-HSC metabolic properties.

A Pdk Mimetic Modulates Cell Cycle Quiescence in LT-HSCs

To determine whether metabolic reprogramming could be achieved in HSCs, we artificially suppressed PDH activity using the PDH inhibitor, 1-aminoethylphosphinic acid (1-AA). This molecule is converted by aminotransferase to the pyruvate analog acetylphosphinic acid, which competes with pyruvate to suppress PDH enzymatic activity (Laber and Amrhein, 1987; Nemeria et al., 2006). In vitro treatment of isolated LT-HSCs, ST-HSCs, or MPPs with or without 1-AA for 2 weeks maintained LT-HSCs and ST-HSCs (Figures 7A, S7A, and S7B). No viable cells were detected in MPPs in the presence of 1-AA after 2 weeks of culture (Figure S7B). Colony growth of LT- or ST-HSCs in the culture medium was suppressed by 1-AA in vitro (Figure S7B). LT-HSCs cultured with 1-AA for 2 weeks could proliferate again after removal of 1-AA (Figure 7B). Treatment of LT-HSCs with 1-AA in vitro showed higher pyruvate levels than nontreated LT-HSCs (Figure 7C). In vitro treatment of isolated LT-HSCs, ST-HSCs, or MPPs with or without 1-AA for 4 weeks only maintained LT-HSCs (Figure S7C). No viable cells were detected in ST-HSCs and MPPs in the presence of 1-AA after 4 weeks of culture (Figures S7A and S7C). Colony growth of LT-HSCs in the culture medium was suppressed by 1-AA in vitro (Figure S7C). Flow cytometric analysis of LT-HSC-derived colony after 4 weeks of culture revealed preferential maintenance of LT-HSC frequency within LSK cells in the presence of 1-AA compared to control cells (Figure 7D). LT-HSCs treated with 1-AA for 2 weeks lacked expression of $p16^{Ink4a}$ mRNA in LT-HSCs (Figure 7E). Both the total number of cells and that of LSK cells were suppressed by 1-AA treatment after 4 weeks of culture (Figures 7F and 7G). In contrast, 1-AA treatment maintained the LT-HSC fraction in vitro (Figure 7H). Transplanted LT-HSC-derived colonies after 4 weeks of culture retained reconstitution capacity of PB and BM during transplantation (Figures 7I and S7D). These data collectively suggest that metabolic reprogramming by Pdk induction could be a potent tool to modulate the cell cycle of LT-HSCs.

DISCUSSION

The present study provides direct evidence for metabolic specificity of LT-HSCs compared to progenitors or terminally differentiated cells. Our observations indicate that LT-HSCs specifically activate glycolysis and suppress influx of glycolytic metabolites into mitochondria via Pdk activity. We also demonstrate the importance of glycolytic ATP production promoted by the HIF-1α/Pdk regulatory system for HSC stem cell capacity by maintaining cell cycle quiescence. In lower eukaryotes, quiescence is defined not only in terms of the cell cycle but as a metabolically specific state characterized by suppressed catabolism and resulting in a nondividing phase (Allen et al., 2006; Klosinska et al., 2011; Laporte et al., 2011). Establishment of cell cycle quiescence via altered metabolic activity is an effective strategy to survive extreme conditions of starvation or hypoxia.

Our initial metabolomics analysis of purified HSCs, progenitors, and terminally differentiated cells using CE-TOFMS indicated that quiescent LT-HSCs exhibit specific carbon metabolism phenotypes favoring glycolysis (Figures 1A and S1A). Low ATP levels generated in LSK fraction subpopulations, which are maintained by glycolysis, gradually increase during differentiation from LT-HSCs to MPPs through ST-HSCs (Figure 1B). Likewise, various glycolytic regulators are highly expressed in LT-HSCs in a HIF-1α-dependent manner. Among these regulators, levels of Pdk2 and Pdk4 are regulated by HIF-1α levels. Pdk actively suppresses mitochondrial metabolism and maintains ATP generation during hypoxia through PDH-E1α phosphorylation (Harris et al., 2002). Pdk1 is reportedly a direct HIF-1α target in murine embryonic fibroblasts and human solid tumor cell lines (Kim et al., 2006; Papandreou et al., 2006). Our data suggest that Pdk2 and Pdk4 are downstream effectors of HIF-1α in maintaining LT-HSC cell cycle quiescence. Rescue of *HIF-1*$\alpha^{\Delta/\Delta}$ HSCs by Pdk overexpression as well as loss-of-function experiments in HSCs from *Pdk2*$^{-/-}$*: Pdk4*$^{-/-}$ mice indicate an important role for Pdks on LT-HSC cell cycle quiescence in a HIF-1α-dependent manner. Therefore, Pdk probably functions in two ways, via activation of glycolysis and suppression of influx of glycolytic metabolites into mitochondria, to maintain LT-HSCs in a hypoxic, hypoperfused, and low-nutrient niche in the BM. Metabolic activities demonstrated here may also protect HSCs from ROS generation either through mitochondria or through accelerated consumption of NADH by LDH activity, which would ameliorate oxidative stress (Suematsu et al., 1992). In addition, products of the TCA cycle, including citrate, could return to the cytosol to drive lipid metabolism required for cell growth and proliferation (Lum et al., 2007). Thus, Pdk could suppress mitochondrial ROS generation and decrease the lipid supply to modulate cellular proliferation. The characteristic metabolite pool in LT-HSCs may also activate a signaling pathway favoring quiescence. Because the Pdk mimetic 1-AA induced increased levels of pyruvate and enhanced LT-HSC maintenance via cell cycle quiescence in vitro, suppression of glycolytic metabolic influx into mitochondria and activation of glycolysis via the HIF-1α/Pdk system could be the primary event in generating HSC quiescence. Activation of a Pdk/PDH checkpoint results in a decoupling of glycolysis and the mitochondrial TCA cycle and might confer a metabolic robustness through two independent energy factories—glycolysis and TCA cycle—in LT-HSCs. Although 1-AA induced ST-HSC cell cycle suppression and maintained cells for 2 weeks, they died in vitro after 4 weeks in culture. Therefore, cell cycle suppression via the PDH may function not only in LT-HSCs but also in differentiated ST-HSCs, although additional

metabolic programs may also maintain ST-HSCs. In addition, 1-AA treatment not only supported the cell number of LT-HSCs but also had a qualitative effect on transplantation capacity of LT-HSCs, as shown in Figures 7I and S7D. Overall, suppression of mitochondrial metabolite flux by Pdks is an efficient strategy for stem cell maintenance. This observation is in contrast to the activity of cancer cells, which utilize aerobic glycolysis and suppress mitochondrial metabolism to promote proliferation rather than quiescence (DeBerardinis et al., 2008; Jones and Thompson, 2009). Thus, the existence of differing molecular mechanisms underlying identical metabolic phenotypes may suggest strategies for novel tumor-specific therapy.

Although we could rule out the importance of other Pdks, including Pdk1 and Pdk3, on *HIF-1α*$^{\Delta/\Delta}$ HSCs, it is noteworthy that *HIF-1α*$^{\Delta/\Delta}$ LT-HSCs, which show decreased Pdk2/4 expression, exhibit decreased phosphorylation of PDH-E1α and increased mitochondrial size. These size changes may be due to HIF-1α-regulated increases in mitochondrial biogenesis (Zhang et al., 2007) or reduced mitochondrial autophagy (Zhang et al., 2008). However, reduced ATP content resulting from attenuated glycolysis, a hallmark of senescent cells (Zwerschke et al., 2003), seen in *HIF-1α*$^{\Delta/\Delta}$ LT-HSCs could not be rescued by mitochondrial ATP generation (Figure 3F), suggesting an essential role for anaerobic glycolysis in energy production by hypoxic HSCs. Because *VHL*$^{\Delta/\Delta}$ LSK cells show decreased mitochondrial content, mitochondrial mass is probably also regulated by the VHL/HIF-1α regulatory system in HSCs and progenitors. Various studies of HSCs defective in ATP generation indicate that LT-HSCs exhibit mitochondrial defects (Liu et al., 2009; Nakada et al., 2010; Gurumurthy et al., 2010; Gan et al., 2010; Sahin et al., 2011). Therefore, although influx of glycolytic metabolites into mitochondria is suppressed by Pdks, mitochondrial metabolic integrity is apparently important for LT-HSC maintenance. The elucidation of these integrative metabolic programs in LT-HSCs extends the concept of the stem cell niche and suggests a strategy for maintaining and expanding HSC resources by modulating their quiescence via Pdk/PDH modulators or enhancement of HIF-1α signaling.

EXPERIMENTAL PROCEDURES

CE-TOFMS Analysis

For CE-TOFMS analysis, BM cells including CD34$^-$Flt3$^-$ LSK (LT-HSCs), CD34$^+$Flt3$^-$ LSK (ST-HSCs), CD34$^+$Flt3$^+$ LSK (MPPs), Lin$^-$ c-Kit$^+$ Sca-1$^-$ (MPs), Gr-1/Mac-1+ (myeloid cells), CD4/CD8+ (T cells), and B220+ (B cells) (1–2 × 10^6 cells) sorted from 120 C57BL/6 mice (12 weeks old) were lysed to extract metabolites. Metabolomic profiling and data analysis were performed twice essentially as described (Soga et al., 2003, 2006).

Mice

Mx1-cre:HIF-1α $^{flox/flox}$, *Mx1-cre:VHL*$^{flox/flox}$ or *Pdk2*$^{-/-}$*: Pdk4*$^{-/-}$ mice (Takubo et al., 2010; Dunford et al., 2011; Jeoung et al., 2006) were genotyped using PCR-based assays of tail DNA samples. To prepare *HIF-1α*$^{\Delta/\Delta}$ mice, we induced Mx1-cre expression by intraperitoneal injection of 400 μg of pIpC (Amersham or Sigma) into 4- to 8-week-old mice on 3 alternate days. Age-matched pIpC-injected *Mx1-cre:HIF-1α*$^{+/+}$ mice or *Cre(-):HIF-1α* $^{flox/flox}$ mice served as controls (*HIF-1α*$^{+/+}$ mice). C57BL/6-Ly5.1 congenic or C57BL/6-Ly5.1/Ly5.2 F1 mice were used for competitive repopulation assays. To prepare mice with *VHL*$^{\Delta/\Delta}$, *HIF-1α*$^{\Delta/\Delta}$*:VHL*$^{\Delta/\Delta}$ or *Pdk2*$^{-/-}$*: Pdk4*$^{-/-}$ BM (*VHL*$^{\Delta/\Delta}$, *HIF-1α*$^{\Delta/\Delta}$*:VHL*$^{\Delta/\Delta}$ or *Pdk2*$^{-/-}$*: Pdk4*$^{-/-}$ BM mice), we transplanted 6 × 10^6–1 × 10^7 BM MNCs or CD45$^+$ BM MNCs from *Mx1-cre:VHL*$^{flox/flox}$ or *Mx1-cre:HIF-1α* $^{flox/flox}$*: VHL*$^{flox/flox}$ mice into lethally irradiated C57BL/6-Ly5.1 mice. Six weeks after BMT, we checked for peripheral blood chimerism and utilized recipients with more than 90% donor-derived cells. Cre expression in replaced BM was induced by intraperitoneal injection of 250 μg of pIpC (Amersham or Sigma) on 3 alternate days. *Mx1-cre:HIF-1α*$^{+/+}$*:VHL*$^{+/+}$ or *Pdk2*$^{+/+}$*: Pdk4*$^{+/+}$ BM mice served as controls.

Antibodies

The following monoclonal antibodies (mAbs) were used in this study: rat mAbs against c-Kit (2B8), Sca-1 (E13-161.7), CD4 (L3T4), CD8 (53-6.72), B220 (RA3-6B2), TER-119, Gr-1 (RB6-8C5), CD34 (RAM34), Mac-1 (M1/70), CD3 (500A2), Flt-3 (A2F10.1), CD41 (MWReg30), CD48 (HM48-1), CD150 (TC15-12F12.2), CD45.2 (104), and CD45.1 (A20). All rat mAbs were purchased from BD, eBiosciences, or Biolegend. A mixture of mAbs against CD4, CD8, B220, TER-119, Mac-1, and Gr-1 was used as a lineage marker (Lineage). We also utilized anti-Ki67 (SP-6, Labvision), anti-PDH-E1α (pSer293) (Merck), anti-PDH-E1α (pSer300) (Merck), and anti-COX4-1 (MitoSciences) antibodies for immunocytochemical experiments.

Flow Cytometry

Analysis of various HSC fractions, detection of Side Population by Hoechst 33342, and Pyronin Y analysis were performed essentially as described (Arai et al., 2004). For flow cytometry analysis of metabolic properties of quiescent stem cells, we pretreated BM MNCs in vitro with 2-DG and/or NaN_3 10 min before staining with Hoechst 33342. For flow cytometric analysis of glucose uptake, BM cells were isolated and preincubated for 30 min at 37°C with 2-[N-(7-Nitrobenz-2-Oxa-1,3-Diazol-4-yl)Amino]-2-Deoxy-D-Glucose or 2-[N-(7-Nitrobenz-2-Oxa-1,3-Diazol-4-yl)Amino]-2-Deoxy-L-Glucose (negative control) (Peptide Institute) before staining with surface markers. For intracellular flow cytometry analysis of phosphorylated PDH-E1α^{S293}, cells were fixed and permeabilized as previously described (Takubo et al., 2010) and stained with anti-phosphorylated pPDH-E1α^{S293} antibody and a fluorophore-labeled secondary antibody.

Immunocytochemistry

Immunocytochemistry of isolated cells was performed as described (Takubo et al., 2008). In brief, cells were attached to glass slides and fixed with 4% PFA. Slides were then blocked with a protein blocker (DAKO) to avoid nonspecific staining. Specimens were reacted with primary antibodies followed by fluorophore-labeled secondary antibodies and nuclear staining.

Cell Cycle Analysis

For immunocytochemical analysis, Ki67$^+$ cells were detected with an anti-Ki67 antibody (SP-6) followed by incubation with a fluorophore-labeled anti-rabbit Ig antibody (MolecularProbes). The cutoff range for fluorescence was determined by a negative control sample stained with an isotype control Ig followed by secondary Ab treatment. The proportion of Ki67-positive cells in each fraction was determined by counting. At least 500 cells per sample were examined for each specimen. For FACS analysis of the cell cycle, cells were first stained with antibodies for surface markers and then fixed and permeabilized to detect the intracellular BrdU with BrdU Flow Kit (Beckman Coulter).

Analysis of Mitochondrial Mass and ROS Production

For confocal microscopy of mitochondria, sorted cells were stained with anti-COX4-1 antibody or incubated for 30 min at 37°C with 100 nM mitotracker Deep Red (MolecularProbes), which binds to mitochondrial membranes independent of membrane potential. Stained cells were attached to glass slides and counterstained with TOTO-3 or DAPI (MolecularProbes) for 30 min. Samples were then three-dimensionally analyzed by laser confocal microscopy for the relative mitochondrial volume of individual cells under identical acquisition settings in the linear range of the acquired fluorescence. We randomly chose cells in multiple fields (more than five fields per sample). Mitochondrial fluorescence was normalized to nuclear DNA fluorescence. To detect mitochondrial ROS production, we stained sorted cells with 100 nM Mitotracker Orange CMH_2TMROS (MolecularProbes) for 30 min at 37°C and analyzed them by FACS.

Quantitative RT-PCR

Quantitative PCR was performed as described previously (Takubo et al., 2008). The cDNA equivalent of 500 cells per reaction was used as a template

for one PCR reaction. PCR primers for each gene were purchased from TaKaRa Bio.

Virus Transduction

For retrovirus transduction, murine Pdk2 and Pdk4 cDNAs were subcloned upstream of IRES-EGFP in pMY-IRES-EGFP (Nosaka et al., 1999). To produce recombinant retrovirus, we transfected plasmid DNA into Plat-E cells by FuGENE (Roche). Supernatants of transfected cells were used to transduce LSK cells or LT-HSCs precultured with SCF and thrombopoietin (TPO) for 16 hr. At 48 hr posttransduction, GFP^+ cells were sorted by FACS and analyzed, transplanted, or cultured for assays.

Serum-free HSC Culture

Sorted cells were cultured on U-bottomed fibronectin-coated plates. Cultures were maintained in SF-O3 medium (Sanko Junyaku) containing 1.0% BSA, 100 ng/ml SCF, 100 ng/ml TPO with or without 1-AA. After 14 or 28 days of cultivation, cells were collected, stained with fluorophore-labeled mAb, and analyzed by FACS or used for immunocytochemical and metabolic analysis.

Bone Marrow Transplant

For Pdk rescue experiments, transduced GFP^+ LSK cells from *HIF-1*$\alpha^{+/+}$ or *HIF-1*$\alpha^{\Delta/\Delta}$ mice (Ly5.2), together with 4×10^5 BM MNCs from C57BL/6-Ly5.1 mice, were transplanted into lethally irradiated C57BL/6-Ly5.1 congenic mice. For *Pdk2*$^{-/-}$*: Pdk4*$^{-/-}$ mice, 500 $CD34^-Flt3^-$ LSK cells from *Pdk2*$^{+/+}$*: Pdk4*$^{+/+}$ or *Pdk2*$^{-/-}$*: Pdk4*$^{-/-}$ mice (Ly5.2), together with 4×10^5 BM MNCs from C57BL/6-Ly5.1 mice, were transplanted into lethally irradiated C57BL/6-Ly5.1 congenic mice. For 1-AA treatment, 830 $CD34^-Flt3^-$ LSK cells from C57BL/6-Ly5.1 mice were cultured in SF-O3 medium containing 1.0% BSA, 100 ng/ml SCF, 100 ng/ml TPO with or without 1-AA and the colony derived from 830 $CD34^-Flt3^-$ LSK cells at day 28 was harvested and transplanted into lethally irradiated C57BL/6 mice (Ly5.2) with 4×10^5 BM MNCs from C57BL/6 mice. One, two, three, and four months after BMT, peripheral blood was collected and examined to determine the percentage of donor-derived cells and the differentiation status of donor-derived cells by FACS. Four months after BMT, BM MNCs were collected and examined to determine the percentage of donor-derived cells by FACS.

Determination of Intracellular ATP, LDH Activity, Pyruvate Content, and PK Activity

Sorted cells ($1–5 \times 10^4$) were lysed, and intracellular ATP, LDH activity, pyruvate content, or PK activity was measured using the Luciferase ATP Determination Kit (Sigma), the LDH Cytotoxicity Detection Kit (TaKaRa), the Pyruvate Assay Kit (BioVision), or the Pyruvate Kinase Activity Assay Kit (BioVision), respectively, following the manufacturers' instructions.

OCR Determination

Sorted cells (5×10^4) were attached to the bottom of a XF96 Tissue Culture Plate (Seahorse Bioscience) coated with BD Cell-Tak Cell Adhesive. Then, cells were incubated in the presence of SCF and TPO with or without oligomycin and OCR was measured by XF96 Extracellular Flux Analyzer (Seahorse Bioscience).

Analysis of HSC Lactate Production

Sorted cells ($1–5 \times 10^4$) were cultured under normoxic or hypoxic conditions for 26 hr. Culture supernatants were then analyzed using the Lactate Assay Kit (BioVision) following the manufacturer's instructions.

Statistical Analysis

Data are presented as means ± SD unless stated otherwise. Statistical significance was determined by Tukey's multiple comparison test. To compare two-group experiments, we used the two-tailed Student's t test.

SUPPLEMENTAL INFORMATION

Supplemental Information for this article includes seven figures and can be found with this article online at http://dx.doi.org/10.1016/j.stem.2012.10.011.

ACKNOWLEDGMENTS

We thank T. Kitamura for providing the Plat-E packaging cell line and pMY-IRES-EGFP vector, K. Rajewsky for providing *Mx1-Cre* mice, Primetech for OCR analysis by XF96, V. Haase for providing *VHL*$^{flox/flox}$ mice, R.A. Harris for providing *Pdk2*$^{-/-}$*:Pdk4*$^{-/-}$ mice, and T. Muraki, K. Igarashi, K. Saito, and T. Hirose for technical support and laboratory management. K.T. is supported by the Global COE Programs for Human Metabolomic Systems Biology (for M.S.) and for Stem Cell Medicine and in part by a MEXT Grant-in-Aid for Young Scientists (A). A.H. and M.S. were supported in part by a MEXT Grant-in-Aid for Creative Scientific Research (17GS0419). FACS analysis was supported by M.S., the Leader of the JST, ERATO, and Suematsu Gas Biology Project. T.S. and K.T. were supported in part by a MEXT Grant-in-Aid for Scientific Research (A), a MEXT Grant-in-Aid for Scientific Research on Innovative Areas, and the Project for Realization of Regenerative Medicine from MEXT.

Received: July 13, 2011
Revised: July 2, 2012
Accepted: October 12, 2012
Published: January 2, 2013

REFERENCES

Allen, C., Büttner, S., Aragon, A.D., Thomas, J.A., Meirelles, O., Jaetao, J.E., Benn, D., Ruby, S.W., Veenhuis, M., Madeo, F., and Werner-Washburne, M. (2006). Isolation of quiescent and nonquiescent cells from yeast stationary-phase cultures. J. Cell Biol. *174*, 89–100.

Arai, F., Hirao, A., Ohmura, M., Sato, H., Matsuoka, S., Takubo, K., Ito, K., Koh, G.Y., and Suda, T. (2004). Tie2/angiopoietin-1 signaling regulates hematopoietic stem cell quiescence in the bone marrow niche. Cell *118*, 149–161.

DeBerardinis, R.J., Lum, J.J., Hatzivassiliou, G., and Thompson, C.B. (2008). The biology of cancer: metabolic reprogramming fuels cell growth and proliferation. Cell Metab. *7*, 11–20.

Dunford, E.C., Herbst, E.A., Jeoung, N.H., Gittings, W., Inglis, J.G., Vandenboom, R., LeBlanc, P.J., Harris, R.A., and Peters, S.J. (2011). PDH activation during in vitro muscle contractions in PDH kinase 2 knockout mice: effect of PDH kinase 1 compensation. Am. J. Physiol. Regul. Integr. Comp. Physiol. *300*, R1487–R1493.

Fukuda, R., Zhang, H., Kim, J.W., Shimoda, L., Dang, C.V., and Semenza, G.L. (2007). HIF-1 regulates cytochrome oxidase subunits to optimize efficiency of respiration in hypoxic cells. Cell *129*, 111–122.

Gan, B., Hu, J., Jiang, S., Liu, Y., Sahin, E., Zhuang, L., Fletcher-Sananikone, E., Colla, S., Wang, Y.A., Chin, L., and Depinho, R.A. (2010). Lkb1 regulates quiescence and metabolic homeostasis of haematopoietic stem cells. Nature *468*, 701–704.

Goodell, M.A., Brose, K., Paradis, G., Conner, A.S., and Mulligan, R.C. (1996). Isolation and functional properties of murine hematopoietic stem cells that are replicating in vivo. J. Exp. Med. *183*, 1797–1806.

Goodell, M.A., Rosenzweig, M., Kim, H., Marks, D.F., DeMaria, M., Paradis, G., Grupp, S.A., Sieff, C.A., Mulligan, R.C., and Johnson, R.P. (1997). Dye efflux studies suggest that hematopoietic stem cells expressing low or undetectable levels of CD34 antigen exist in multiple species. Nat. Med. *3*, 1337–1345.

Gurumurthy, S., Xie, S.Z., Alagesan, B., Kim, J., Yusuf, R.Z., Saez, B., Tzatsos, A., Ozsolak, F., Milos, P., Ferrari, F., et al. (2010). The Lkb1 metabolic sensor maintains haematopoietic stem cell survival. Nature *468*, 659–663.

Harris, R.A., Bowker-Kinley, M.M., Huang, B., and Wu, P. (2002). Regulation of the activity of the pyruvate dehydrogenase complex. Adv. Enzyme Regul. *42*, 249–259.

Janzen, V., Forkert, R., Fleming, H.E., Saito, Y., Waring, M.T., Dombkowski, D.M., Cheng, T., DePinho, R.A., Sharpless, N.E., and Scadden, D.T. (2006). Stem-cell ageing modified by the cyclin-dependent kinase inhibitor p16INK4a. Nature *443*, 421–426.

Jeoung, N.H., Wu, P., Joshi, M.A., Jaskiewicz, J., Bock, C.B., Depaoli-Roach, A.A., and Harris, R.A. (2006). Role of pyruvate dehydrogenase kinase

isoenzyme 4 (PDHK4) in glucose homoeostasis during starvation. Biochem J *397*, 417–425.

Jones, R.G., and Thompson, C.B. (2009). Tumor suppressors and cell metabolism: a recipe for cancer growth. Genes Dev. *23*, 537–548.

Kim, M., Cooper, D.D., Hayes, S.F., and Spangrude, G.J. (1998). Rhodamine-123 staining in hematopoietic stem cells of young mice indicates mitochondrial activation rather than dye efflux. Blood *91*, 4106–4117.

Kim, J.W., Tchernyshyov, I., Semenza, G.L., and Dang, C.V. (2006). HIF-1-mediated expression of pyruvate dehydrogenase kinase: a metabolic switch required for cellular adaptation to hypoxia. Cell Metab. *3*, 177–185.

Klosinska, M.M., Crutchfield, C.A., Bradley, P.H., Rabinowitz, J.D., and Broach, J.R. (2011). Yeast cells can access distinct quiescent states. Genes Dev. *25*, 336–349.

Kobayashi, C.I., and Suda, T. (2012). Regulation of reactive oxygen species in stem cells and cancer stem cells. J. Cell. Physiol. *227*, 421–430.

Laber, B., and Amrhein, N. (1987). Metabolism of 1-aminoethylphosphinate generates acetylphosphinate, a potent inhibitor of pyruvate dehydrogenase. Biochem. J. *248*, 351–358.

Laporte, D., Lebaudy, A., Sahin, A., Pinson, B., Ceschin, J., Daignan-Fornier, B., and Sagot, I. (2011). Metabolic status rather than cell cycle signals control quiescence entry and exit. J. Cell Biol. *192*, 949–957.

Liu, J., Cao, L., Chen, J., Song, S., Lee, I.H., Quijano, C., Liu, H., Keyvanfar, K., Chen, H., Cao, L.Y., et al. (2009). Bmi1 regulates mitochondrial function and the DNA damage response pathway. Nature *459*, 387–392.

Lum, J.J., Bui, T., Gruber, M., Gordan, J.D., DeBerardinis, R.J., Covello, K.L., Simon, M.C., and Thompson, C.B. (2007). The transcription factor HIF-1alpha plays a critical role in the growth factor-dependent regulation of both aerobic and anaerobic glycolysis. Genes Dev. *21*, 1037–1049.

Miharada, K., Karlsson, G., Rehn, M., Rörby, E., Siva, K., Cammenga, J., and Karlsson, S. (2011). Cripto regulates hematopoietic stem cells as a hypoxic-niche-related factor through cell surface receptor GRP78. Cell Stem Cell *9*, 330–344.

Miyamoto, K., Araki, K.Y., Naka, K., Arai, F., Takubo, K., Yamazaki, S., Matsuoka, S., Miyamoto, T., Ito, K., Ohmura, M., et al. (2007). Foxo3a is essential for maintenance of the hematopoietic stem cell pool. Cell Stem Cell *1*, 101–112.

Nakada, D., Saunders, T.L., and Morrison, S.J. (2010). Lkb1 regulates cell cycle and energy metabolism in haematopoietic stem cells. Nature *468*, 653–658.

Nemeria, N.S., Korotchkina, L.G., Chakraborty, S., Patel, M.S., and Jordan, F. (2006). Acetylphosphinate is the most potent mechanism-based substrate-like inhibitor of both the human and Escherichia coli pyruvate dehydrogenase components of the pyruvate dehydrogenase complex. Bioorg. Chem. *34*, 362–379.

Noda, S., Horiguchi, K., Ichikawa, H., and Miyoshi, H. (2008). Repopulating activity of ex vivo-expanded murine hematopoietic stem cells resides in the CD48-c-Kit+Sca-1+lineage marker- cell population. Stem Cells *26*, 646–655.

Norddahl, G.L., Pronk, C.J., Wahlestedt, M., Sten, G., Nygren, J.M., Ugale, A., Sigvardsson, M., and Bryder, D. (2011). Accumulating mitochondrial DNA mutations drive premature hematopoietic aging phenotypes distinct from physiological stem cell aging. Cell Stem Cell *8*, 499–510.

Nosaka, T., Kawashima, T., Misawa, K., Ikuta, K., Mui, A.L., and Kitamura, T. (1999). STAT5 as a molecular regulator of proliferation, differentiation and apoptosis in hematopoietic cells. EMBO J. *18*, 4754–4765.

Papandreou, I., Cairns, R.A., Fontana, L., Lim, A.L., and Denko, N.C. (2006). HIF-1 mediates adaptation to hypoxia by actively downregulating mitochondrial oxygen consumption. Cell Metab. *3*, 187–197.

Parmar, K., Mauch, P., Vergilio, J.A., Sackstein, R., and Down, J.D. (2007). Distribution of hematopoietic stem cells in the bone marrow according to regional hypoxia. Proc. Natl. Acad. Sci. USA *104*, 5431–5436.

Sahin, E., Colla, S., Liesa, M., Moslehi, J., Müller, F.L., Guo, M., Cooper, M., Kotton, D., Fabian, A.J., Walkey, C., et al. (2011). Telomere dysfunction induces metabolic and mitochondrial compromise. Nature *470*, 359–365.

Seita, J., and Weissman, I.L. (2010). Hematopoietic stem cell: self-renewal versus differentiation. Wiley Interdiscip Rev Syst Biol Med *2*, 640–653.

Semenza, G.L. (2010). Oxygen homeostasis. Wiley Interdiscip Rev Syst Biol Med *2*, 336–361.

Shintani, T., Iwabuchi, T., Soga, T., Kato, Y., Yamamoto, T., Takano, N., Hishiki, T., Ueno, Y., Ikeda, S., Sakuragawa, T., et al. (2009). Cystathionine beta-synthase as a carbon monoxide-sensitive regulator of bile excretion. Hepatology *49*, 141–150.

Simsek, T., Kocabas, F., Zheng, J., Deberardinis, R.J., Mahmoud, A.I., Olson, E.N., Schneider, J.W., Zhang, C.C., and Sadek, H.A. (2010). The distinct metabolic profile of hematopoietic stem cells reflects their location in a hypoxic niche. Cell Stem Cell *7*, 380–390.

Soga, T., Ohashi, Y., Ueno, Y., Naraoka, H., Tomita, M., and Nishioka, T. (2003). Quantitative metabolome analysis using capillary electrophoresis mass spectrometry. J. Proteome Res. *2*, 488–494.

Soga, T., Baran, R., Suematsu, M., Ueno, Y., Ikeda, S., Sakurakawa, T., Kakazu, Y., Ishikawa, T., Robert, M., Nishioka, T., and Tomita, M. (2006). Differential metabolomics reveals ophthalmic acid as an oxidative stress biomarker indicating hepatic glutathione consumption. J. Biol. Chem. *281*, 16768–16776.

Suda, T., Takubo, K., and Semenza, G.L. (2011). Metabolic regulation of hematopoietic stem cells in the hypoxic niche. Cell Stem Cell *9*, 298–310.

Suematsu, M., Suzuki, H., Ishii, H., Kato, S., Yanagisawa, T., Asako, H., Suzuki, M., and Tsuchiya, M. (1992). Early midzonal oxidative stress preceding cell death in hypoperfused rat liver. Gastroenterology *103*, 994–1001.

Takahashi, A., Ohtani, N., Yamakoshi, K., Iida, S., Tahara, H., Nakayama, K., Nakayama, K.I., Ide, T., Saya, H., and Hara, E. (2006). Mitogenic signalling and the p16INK4a-Rb pathway cooperate to enforce irreversible cellular senescence. Nat. Cell Biol. *8*, 1291–1297.

Takubo, K., Ohmura, M., Azuma, M., Nagamatsu, G., Yamada, W., Arai, F., Hirao, A., and Suda, T. (2008). Stem cell defects in ATM-deficient undifferentiated spermatogonia through DNA damage-induced cell-cycle arrest. Cell Stem Cell *2*, 170–182.

Takubo, K., Goda, N., Yamada, W., Iriuchishima, H., Ikeda, E., Kubota, Y., Shima, H., Johnson, R.S., Hirao, A., Suematsu, M., and Suda, T. (2010). Regulation of the HIF-1alpha level is essential for hematopoietic stem cells. Cell Stem Cell *7*, 391–402.

Voet, D., and Voet, J.G. (2010). Biochemistry (Hoboken, NJ: Wiley).

Zhang, H., Gao, P., Fukuda, R., Kumar, G., Krishnamachary, B., Zeller, K.I., Dang, C.V., and Semenza, G.L. (2007). HIF-1 inhibits mitochondrial biogenesis and cellular respiration in VHL-deficient renal cell carcinoma by repression of C-MYC activity. Cancer Cell *11*, 407–420.

Zhang, H., Bosch-Marce, M., Shimoda, L.A., Tan, Y.S., Baek, J.H., Wesley, J.B., Gonzalez, F.J., and Semenza, G.L. (2008). Mitochondrial autophagy is an HIF-1-dependent adaptive metabolic response to hypoxia. J. Biol. Chem. *283*, 10892–10903.

Zhou, S., Schuetz, J.D., Bunting, K.D., Colapietro, A.M., Sampath, J., Morris, J.J., Lagutina, I., Grosveld, G.C., Osawa, M., Nakauchi, H., and Sorrentino, B.P. (2001). The ABC transporter Bcrp1/ABCG2 is expressed in a wide variety of stem cells and is a molecular determinant of the side-population phenotype. Nat. Med. *7*, 1028–1034.

Zon, L.I. (2008). Intrinsic and extrinsic control of haematopoietic stem-cell self-renewal. Nature *453*, 306–313.

Zwerschke, W., Mazurek, S., Stöckl, P., Hütter, E., Eigenbrodt, E., and Jansen-Dürr, P. (2003). Metabolic analysis of senescent human fibroblasts reveals a role for AMP in cellular senescence. Biochem. J. *376*, 403–411.

Cell Stem Cell
Article

Forebrain Engraftment by Human Glial Progenitor Cells Enhances Synaptic Plasticity and Learning in Adult Mice

Xiaoning Han,[1,2] Michael Chen,[1,2] Fushun Wang,[1,2] Martha Windrem,[1,3] Su Wang,[1,3] Steven Shanz,[1,3] Qiwu Xu,[1,2] Nancy Ann Oberheim,[1,2] Lane Bekar,[1,2] Sarah Betstadt,[4] Alcino J. Silva,[5] Takahiro Takano,[1,2] Steven A. Goldman,[1,2,3,*] and Maiken Nedergaard[1,2,3,*]

[1]Center for Translational Neuromedicine
[2]Department of Neurosurgery
[3]Department of Neurology
[4]Department of Obstetrics and Gynecology
University of Rochester Medical Center, Rochester, NY 14642, USA
[5]Departments of Neurobiology, Psychiatry and Psychology, Integrative Center for Learning and Memory, University of California, Los Angeles, David Geffen School of Medicine, Los Angeles, CA 90095, USA
*Correspondence: steven_goldman@urmc.rochester.edu (S.A.G.), nedergaard@urmc.rochester.edu (M.N.)
http://dx.doi.org/10.1016/j.stem.2012.12.015

SUMMARY

Human astrocytes are larger and more complex than those of infraprimate mammals, suggesting that their role in neural processing has expanded with evolution. To assess the cell-autonomous and species-selective properties of human glia, we engrafted human glial progenitor cells (GPCs) into neonatal immunodeficient mice. Upon maturation, the recipient brains exhibited large numbers and high proportions of both human glial progenitors and astrocytes. The engrafted human glia were gap-junction-coupled to host astroglia, yet retained the size and pleomorphism of hominid astroglia, and propagated Ca^{2+} signals 3-fold faster than their hosts. Long-term potentiation (LTP) was sharply enhanced in the human glial chimeric mice, as was their learning, as assessed by Barnes maze navigation, object-location memory, and both contextual and tone fear conditioning. Mice allografted with murine GPCs showed no enhancement of either LTP or learning. These findings indicate that human glia differentially enhance both activity-dependent plasticity and learning in mice.

INTRODUCTION

The unique processing capabilities of the human brain reflect a number of evolutionary adaptations by its cellular constituents (Fields, 2004). One especially distinct feature of the adult human brain's cellular composition is the size and complexity of its astrocytic cohort. Human astrocytes are both morphologically and functionally distinct from those of infraprimate mammals, in that human astroglia are larger and exhibit far greater architectural complexity and cellular pleomorphism, as well as more rapid syncytial calcium signaling, than their murine counterparts (Colombo, 1996; Oberheim et al., 2009). These phylogenetic differences are of particular interest, since astrocytes can both coordinate and modulate neural signal transmission (Rusakov et al., 2011; Verkhratsky et al., 1998). These observations promise to fundamentally transform our view of astrocytes, since current concepts of the role of astrocytes in neural network performance are based almost entirely on studies of astrocytic physiology in the rodent brain (Oberheim et al., 2006).

In this study, we have used a human glial chimeric mouse brain to ask whether the structural complexity and unique functional properties of human astrocytes influence activity-dependent plasticity in an otherwise stable neural network. In particular, we have tested the hypothesis that human astrocytes might enhance synaptic plasticity and learning relative to their murine counterparts.

RESULTS

Human Glial Progenitors Exhibit Cell-Autonomous Astrocytic Differentiation in Mouse Brain

To study human astrocytes in the live adult brain, we generated chimeric mice in which human glial progenitor cells (GPCs)—isolated by being sorted on the basis of an $A2B5^+$/PSA-$NCAM^-$ phenotype, and then being expanded via a protocol that promoted differentiation into hGFAP- and A2B5-expressing astrocytes (Figure S1A available online)—were xenografted into neonatal immune-deficient mice; these matured to become adults chimeric for both mouse and human astroglia (Windrem et al., 2004, 2008) (Figure 1A). The human GPCs were labeled ex vivo, prior to implantation, with VSVg-pseudotyped lentiviral-CMV-EGFP; in antecedent pilot experiments, we had determined that this vector sustained the expression of EGFP by astroglia for at least 1 year in vivo (Figure 1A). The neonatally implanted mice were sacrificed at time points ranging from 0.5 to 20 months of age, and their brains were assessed both histologically and electrophysiologically. Human donor cells were first identified based on their expression of human nuclear antigen (hNuclei). The $hNuclei^+$ cells were found to distribute relatively evenly throughout the forebrain, infiltrating both hippocampus

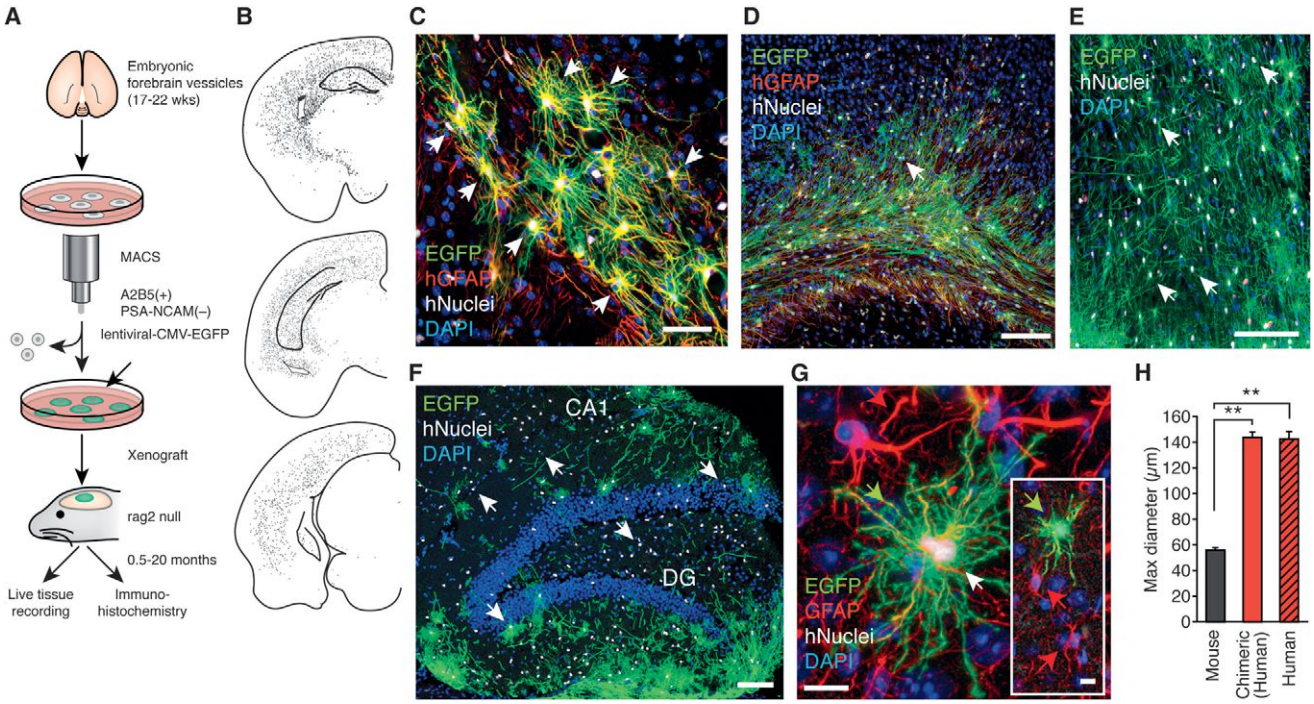

Figure 1. Human Astrocytes Replace Host Glia in Mice Engrafted with Human Glial Progenitors

(A) Schematic outlining the procedure for magnetic cell sort-based isolation (MACS) of human glial progenitors, tagging with EGFP, and xenografting at P1. The chimeric mice brains were analyzed in 0.5- to 20-month-old chimeric mice.

(B) Representative dot map showing the distribution of human nuclear antigen $(hNuclei)^+$ cells in three coronal sections from a 10-month-old human chimeric mouse.

(C) The complex fine structure of human astrocytes in chimeric brain replicates the classical star-shaped appearance of human astrocytes labeled with hGFAP in situ. Most cells in the field are $EGFP^+/hNuclei^+/hGFAP^+$ (hGFAP, red). Arrows in (C) through (F) show representative examples of human cells (hNuclei, white).

(D) At 5 months, $EGFP^+$ cells typically infiltrated corpus callosum and cortical layers V and VI. All $EGFP^+$ cells labeled with an antibody directed against human nuclear antigen (hNuclei) and most of the human cells were also labeled with an antibody directed against human GFAP (hGFAP, red).

(E) At 11 months, many areas of cortex were infiltrated by evenly distributed $EGFP^+/hNuclei^+$ cells.

(F) The hippocampus was also populated with $EGFP^+/hNuclei^+$ cells in a 14-month-old animal, with the highest density in the dentate.

(G) Human $EGFP^+/hNuclei^+/GFAP^+$ cells (green arrows) were significantly larger than host murine astrocytes (red arrow). The anti-GFAP antibody cross-reacted with both human and mouse GFAP (red). Inset shows same field in lower magnification.

(H) Histogram comparing the diameter of mouse cortical astrocytes to human cortical astrocytes in situ (freshly resected surgical samples) and xenografted human astrocytes in cortex of chimeric mouse brain. The maximal diameter of mouse and human astrocytes (in situ and in chimeric mice) was determined in sections stained with an anti-GFAP antibody that labels both human and mouse GFAP. ($n = 50–65$; $^{**}p < 0.01$, Bonferroni t test.)

EGFP, green; hNuclei, white and white arrow; DAPI, blue (B–F). Scale bars: 50 μm (C); 100 μm (D–F); and 10 μm (G). Data graphed as means ± SEM. See also Figure S1.

and cortex (Figure 1B). Human astrocytes were specifically identified by their intricate $EGFP^+$ fluorescent processes and, in fixed tissue, by their coexpression of human glial fibrillary acidic protein (hGFAP) and hNuclei (Figure 1C). By 4–5 months of age, mice engrafted with human GPCs exhibited substantial addition of human astrocytes to both the hippocampus and deep neocortical layers; by 12–20 months, human astrocytes further populated large regions of the amygdala, thalamus, neostriatum, and cortex (Figures 1D–1F). The human astrocytes appeared to develop and mature in a cell-autonomous fashion, maintaining their larger size and more complex structure relative to murine astrocytes (Figures 1G and 1H).

Human astrocytes, defined as $EGFP^+/hGFAP^+/hNuclei^+$, regularly extended processes that terminated in end-feet contiguously arrayed along blood vessel walls (Figures 2A and 2B). Their long processes were often tortuous and resembled the processes of interlaminar astroglia, a phenotype previously described only in adult human and ape brain (Oberheim et al., 2006) (Figure 2C); these cells are characterized by long, unbranched processes that traverse multiple cortical laminae (Colombo, 2001). Many of the engrafted human astrocytes in chimeric mice extended processes that spanned >0.5 mm (Figure 2D). A large number of mitochondria were present in the long processes (Figure 2E). Other engrafted human cells exhibited the long, varicosity-studded processes of varicose projection astrocytes, a second class of hominid astrocytes (Oberheim et al., 2009).

Of note, $rag2^{-/-}$ immunodeficient mice on a C3h background were generally used as recipients for these experiments, although $rag1^{-/-}$ immunodeficient mice (on a C57/Bl6 background) were used for vision-dependent behavioral tests, since the C3h background of the rag2 mice is a visually impaired strain; we observed no difference in xenograft acceptance, cell dispersal, or differentiation patterns between these two hosts.

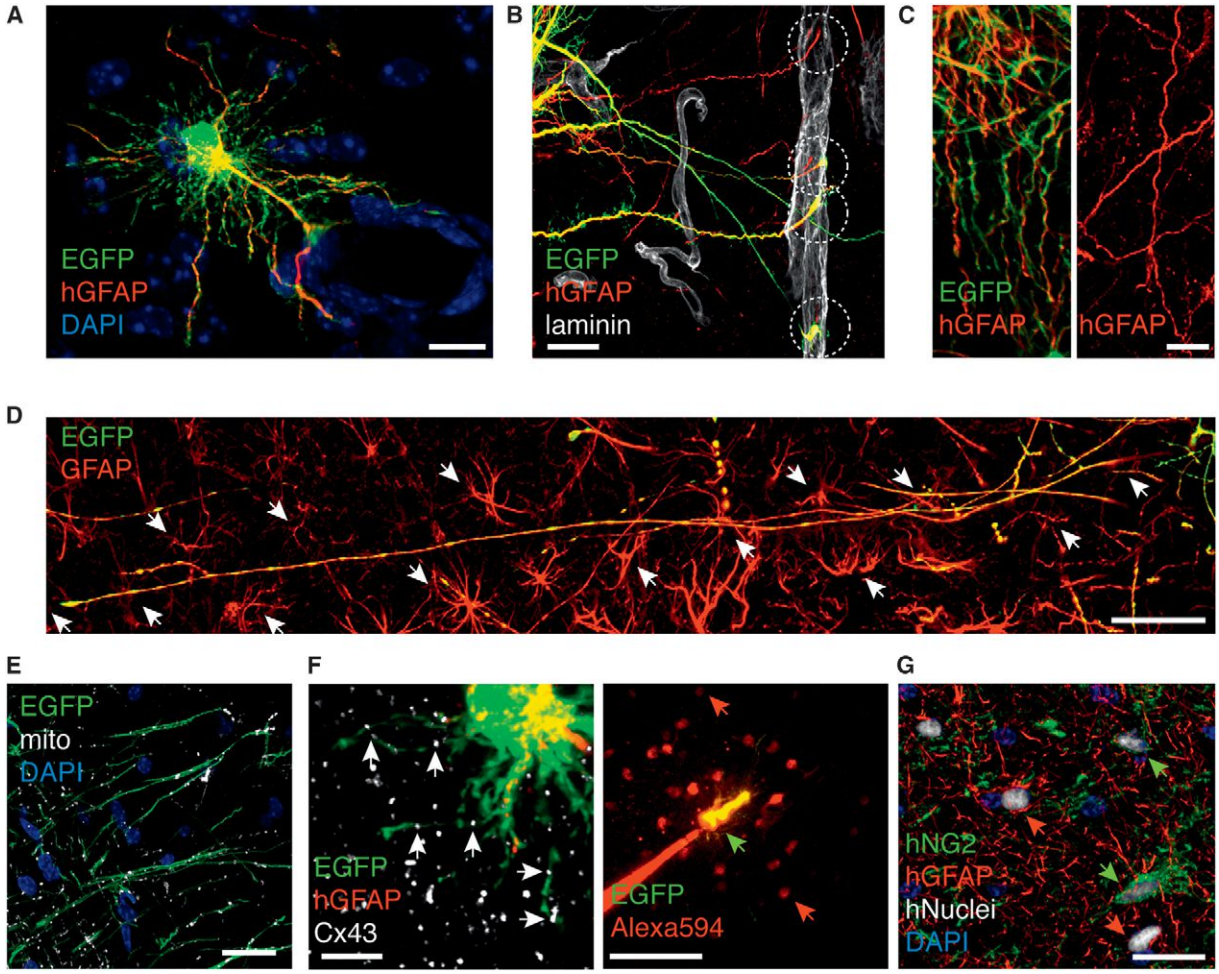

Figure 2. Human Astrocytes Retain Hominid-Specific Morphologies in Chimeric Mice

Human protoplasmic astrocytes matured in a cell-autonomous fashion in the chimeric mouse brain environment and retained the long GFAP$^+$, mitochondrial-enriched processes of native human astroglia.

(A) An EGFP$^+$/hGFAP$^+$ astrocyte makes contact with the vasculature in a 1-month-old chimeric mouse.

(B) Long, unbranched EGFP$^+$ and hGFAP$^+$ astrocytic processes terminated (dashed circle) on the vasculature (laminin; white) 16 days after implantation.

(C) The tortuous shape of EGFP$^+$/hGFAP$^+$ processes in chimeric brains replicate the appearance of GFAP$^+$ processes of interlaminar astroglia in intact human tissue.

(D) An example of an EGFP$^+$/GFAP$^+$ process that spans >600 μm and penetrates the domains of at least 14 host murine astrocytes (white arrow) (GFAP, red).

(E) Long EGFP$^+$ processes contain a large number of mitochondria (white) in an 11-month-old chimeric mouse.

(F) An EGFP$^+$/hGFAP$^+$ human astrocyte expresses Cx43 (white) gap junction plaques (left panel). An EGFP$^+$ cell (green arrow) loaded with a small gap junction permeable tracer, Alexa 594 (MW 760) in a cortical slice (P15), is also shown. Alexa 594 (red) diffused into multiple neighboring EGFP$^-$ cells (red arrows).

(G) Coexistence of hGFAP$^+$ (red)/hNuclei+ (white) cells (red arrows) and hNG2$^+$ (green)/hNuclei$^+$ cells (green arrows) in the dentate of a 12-month-old chimeric mouse.

EGFP, green (A–F); hGFAP, red (A–C). Scale bars: 10 μm (A and C); 20 μm (B, E, and G); 50 μm (D and F, right panel); and 5 μm (F, left panel). See also Figure S2.

In that regard, we found no evidence of microglial activation in the xenografted mice, whether in rag1 null or rag2 null hosts, reflecting both their neonatal engraftment and immunodeficient backgrounds (Figures S1B–S1F).

Human Astrocytes Coupled Structurally and Functionally with Mouse Astrocytes

Their cell-autonomous maturation and morphologies notwithstanding, the engrafted human cells rapidly integrated with murine host cells. The gap junction tracer Alexa 594 (MW 760), once injected into EGFP$^+$ human cells, spread rapidly into multiple neighboring EGFP$^-$ host cells, suggesting the competence of interspecies gap junctions linking human and mouse astroglia, likely derived from the apposition of human and mouse Cx43 hemichannels (Figure 2F). A large number of hNuclei$^+$ cells failed to express GFAP but did express a human-specific isoform of the chondroitin sulfate proteoglycan NG2 (Figure 2G), a prototypic marker of parenchymal glial progenitor cells (Mangin and Gallo, 2011; Robel et al., 2011). Of note, hGFAP$^+$ and hNG2$^+$ human cells often coexisted in close proximity, although their relative ratios exhibited considerable variation across regions as well as between individual

mice (Figure 2G). Transferrin immunostaining failed to detect any human oligodendroglia, consistent with our prior assessment of glial progenitor cell fate upon transplantation to normally myelinated brain (Windrem et al., 2009) (Figures S2A and S2B): whereas a large proportion of engrafted human GPCs differentiate into oligodendrocytes in hypomyelinated shiverer mice, essentially no human oligodendrocytes were found in similarly engrafted wild-type mice (Windrem et al., 2009).

Human GPCs and Astrocytes Exhibited Distinct Physiological Phenotypes in Mouse Brain

To evaluate the electrophysiological properties of human astrocytes engrafted in mice, acute hippocampal slices were prepared from chimeric mice ranging from 4 to 10 months of age (6.5 ± 0.4 months old, mean ± SD). Donor astrocytes could be readily identified by their EGFP fluorescence and by their large, symmetric, highly branched astrocytic morphologies. The tagged donor cells were filled with Alexa 594 or the Ca^{2+} indicator rhod2 during whole-cell recordings, and their phenotype was verified by immunolabeling for GFAP (Figure 3A). $EGFP^+$ human astrocytes exhibited a higher input resistance than that of host murine astrocytes (51.6 ± 2.5 MΩ, n = 37, versus 29.2 ± 3.2 MΩ, n = 17, respectively, means ± SEM; $p < 0.05$, Steel-Dwass test). In contrast, the resting membrane potential of human astrocytes (−69.2 ± 1.5 mV, n = 37) was not significantly different from that of untagged host astrocytes (−73.9 ± 1.7 mV, n = 17, $p > 0.05$) (Figures 3B–3D). Whereas all large and symmetric $EGFP^+$ donor cells exhibited passive membrane currents and linear current to voltage (I/V) curves, another population of smaller $EGFP^+$ human cells with compact, asymmetrically branched morphologies manifested a much higher input resistance (147.8 ± 11.7 MΩ, n = 14). These donor cells manifested voltage-gated currents and depolarization-triggered outward currents with delayed activation (Figure 3B) and expressed a human epitope of chondroitin sulfate proteoglycan NG2, identifying them as persistent glial progenitors (Figure 2G) (Kang et al., 2010; Robel et al., 2011). Together, these histological and electrophysiological analyses supported the notion that a large proportion of engrafted human cells differentiated into protoplasmic astrocytes, forming a functional syncytium with their murine host, and that these were accompanied by large numbers of coengrafted $NG2^+$ human glial progenitors.

Human Astrocytes Propagate Calcium Waves More Quickly than Do Murine Astroglia

Astrocytes are electrically nonexcitable and are incapable of electrochemical communication. Instead, the principle mechanism of astrocytic signaling involves transient elevations of cytosolic Ca^{2+} (Cotrina and Nedergaard, 2005). In light of the larger and more complex architecture of human astrocytes, we next asked whether propagation of intracellular Ca^{2+} signals in human astrocytes differs from that of rodents. To compare intracellular Ca^{2+} wave propagation between human and mouse astrocytes, we initiated localized Ca^{2+} increases by photolysis of caged Ca^{2+} (Parpura and Verkhratsky, 2012; Rusakov et al., 2011). Photolysis of caged Ca^2 loaded specifically into astrocytes was used to avoid potentially confounding alterations in local synaptic activity. Intracellular Ca^{2+} waves were evoked when we directed a UV beam at long processes of astrocytes filled with rhod2 and NP-EGTA by a patch pipette. The subsequent spread of Ca^{2+} signals was visualized using two-photon excitation (Figure 3E). Line scanning with high temporal resolution (2–4 ms) showed that intracellular Ca^{2+} wave propagation was significantly faster in human astrocytes than in murine cells; intracellular Ca^{2+} increases propagated with a velocity of 15.8 ± 0.7 μm/s among human glia compared to 5.7 ± 0.4 μm/s in resident murine astrocytes (n = 22–34, 6.5 ± 0.4 versus 7.0 ± 0.5 months old, mean ± SEM, $p < 0.05$, Steel-Dwass test) (Figures 3F–3H). To determine whether the faster intracellular Ca^{2+} waves in human astrocytes were an artifact of xenograft, we also assessed intracellular Ca^{2+} wave spread in slices of fresh human brain tissue obtained at surgical resection for distant lesions (mean age of patients: 30.6 ± 8.8 years, n = 3). Human astrocytes in these surgical resections similarly propagated intracellular Ca^{2+} waves much more rapidly than did murine astrocytes (n = 10) (Figure 3H). Together, these experiments demonstrated that intracellular Ca^{2+} signals propagate at least 3-fold faster within human astrocytes than in their rodent counterparts, and do so in human glial chimeric mice just as in human brain tissue. Of note, we were unable to evaluate intercellular Ca^{2+} wave propagation, as only slices prepared from young mice pups load well with esterified (AM) Ca^{2+} indicators (Dawitz et al., 2011).

Human Astrocytes Accentuate Excitatory Synaptic Transmission in the Murine Hippocampus

A principal function of astrocytes is to monitor local synaptic activity by their expression of metabotropic neurotransmitter receptors for both glutamate and GABA (Parpura and Verkhratsky, 2012; Rusakov et al., 2011). These receptors activate intracellular signaling pathways, mediated primarily by increases in cytosolic Ca^{2+}, which are linked to synaptic plasticity (Parpura and Zorec, 2010). To assess the selective impact of human astrocytes on neural transmission within the host murine neural network, we compared synaptic activity in hippocampal slices prepared from human glial chimeric mice to that of both their unengrafted and allografted littermate controls. We focused on the hippocampal dentate granule layer because of the many electrophysiological and behavioral tests by which hippocampal function, learning, and LTP could be assessed (Lee and Silva, 2009). In addition, human cells typically densely engrafted this area; these included an admixture of $GFAP^+$/$hNuclei^+$ and $NG2^+$/$hNuclei^+$ cells (Figures 1B, 1F, and 2G). Stimulation of the medial perforant path (Colino and Malenka, 1993) consistently evoked a significantly steeper slope of field excitatory postsynaptic potentials (fEPSP) in the humanized chimeric mice than that in either their uninjected littermates or mouse GPC allografted controls (n = 3–40, F = 3.15, by two-way ANOVA, $p = 0.044$) (Figure 4A). The allograft controls comprised a set of mice neonatally engrafted with murine GPCs derived from EGFP transgenic mice, and they otherwise underwent the same isolation and engraftment protocols as those using human GPCs. The steeper slope of the fEPSPs in the humanized chimeras compared to that of the uninjected controls was still evident after normalization to the fiber volley amplitudes, a measure thought to reflect the number of stimulated axons (Figure S3A). Thus, slices with human glia exhibited a significant enhancement in their basal level of excitatory synaptic transmission over a wide range of stimulation intensities.

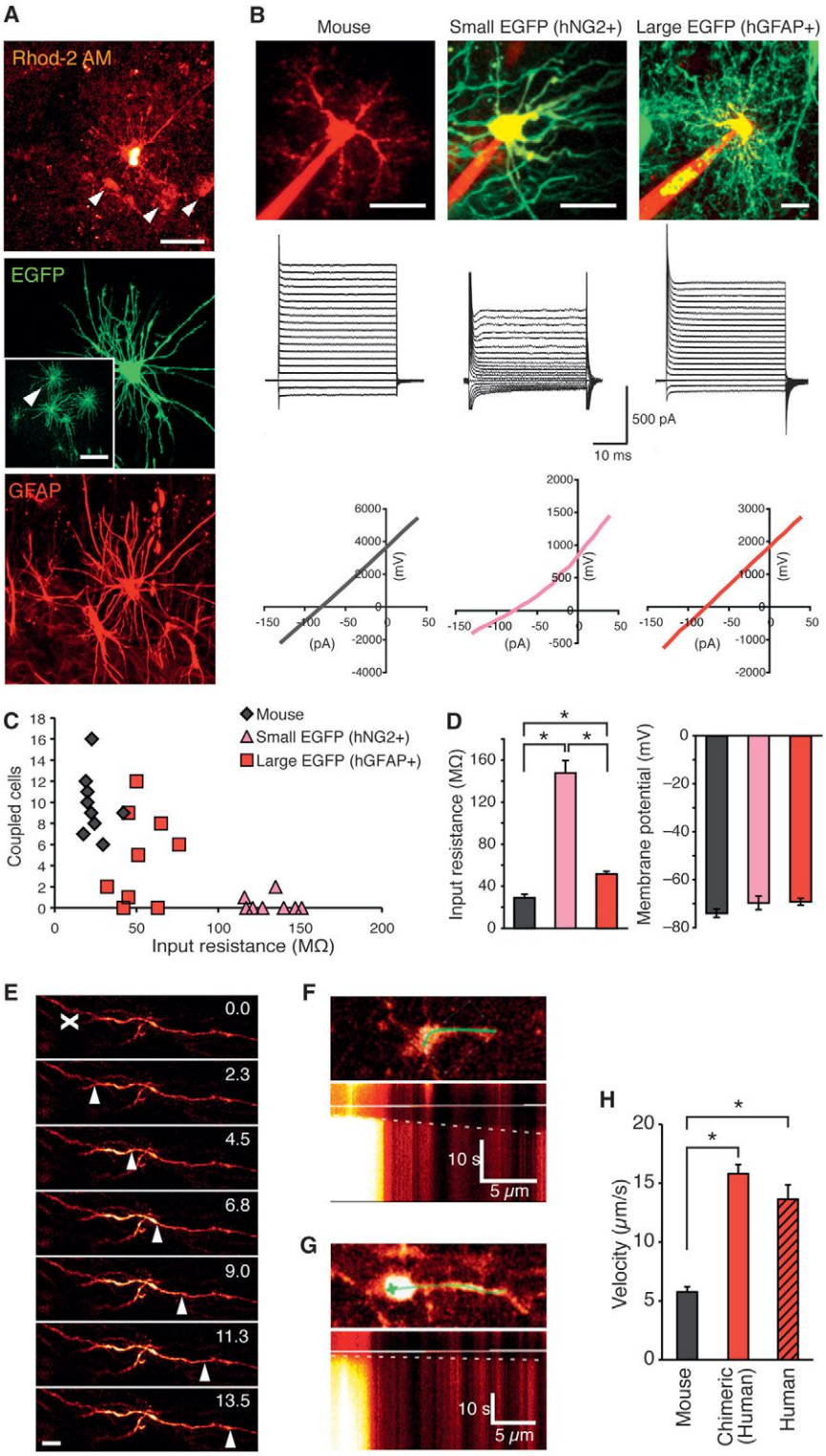

Figure 3. Functional Properties Indicate High-Density Host Engraftment by Both Human Glial Progenitors and Astrocytes

(A) Large and symmetric EGFP$^+$ cell (green) in an acute cortical slice prepared from a mouse engrafted with human EGFP$^+$ glial progenitors 4 months earlier. Inset: lower magnification of the same field. The EGFP$^+$ cell was loaded with rhod2 (red) by a patch pipette. Rhod2 diffused into several neighboring EGFP$^-$ cells (white arrows, top panel). Cell identity was verified when we immunolabeled against GFAP (red, below panel). Neighboring cells were GFAP$^+$ and their shape was characteristic of mouse astrocytes, indicating that the human EGFP$^+$/GFAP$^+$ astrocytes were coupled by functional gap junctions to host GFAP$^+$ astrocytes.

(B) I/V curves from host mouse astrocytes (n = 17); smaller, less complex EGFP$^+$ human cells, presumably glial progenitor cells (n = 14); and large and symmetric human EGFP$^+$ cells, presumably astrocytes (n = 37).

(C and D) Comparison of the input resistance and gap-junction-coupled cells detected as the number of neighboring cells labeled with Alexa 594. Mouse and large EGFP$^+$ cells (presumed human astrocytes) both manifested low input resistance and were extensively coupled by gap junctions. In contrast, small EGFP$^+$ cells—presumed human GPCs—exhibited high input resistance and were not gap junction coupled. (n = 14–37, *p < 0.05, Steel-Dwass test.) Membrane potentials were not significantly different.

(E) Photolysis of caged Ca^{2+} in an EGFP$^+$ astrocytic process. White "X" shows initiated point; white arrowhead shows Ca^{2+} propagation.

(F) Top: line scan position across the length of a mouse astrocyte filled with NP-EGTA and rhod2. Bottom: line scan image of an intra-astrocytic Ca^{2+} wave initiated by photolysis of the cell body. White dashed line indicates the velocity of the intracellular Ca^{2+} wave.

(G) Line scan image of a human astrocyte in a chimeric mouse.

(H) Comparison of velocities of intracellular Ca^{2+} waves in host murine and engrafted human EGFP$^+$ astrocytes and in human astrocytes in freshly resected surgical tissue. (n = 8–35, *p < 0.05, Steel-Dwass test.)

Scale bars: 30 μm (A); 100 μm (A, insert); 20 μm (B); and 10 μm (E). Data graphed as means ± SEM.

Human Astrocytes Enhance LTP in the Adult Murine Hippocampus

We next asked if human astrocytes might affect synaptic plasticity by assessing the effect of human glia on long-term potentiation (LTP). Two trains of high-frequency stimulation (HFS) potentiated the fEPSP slope to 151.2% ± 8.1% of baseline in chimeric mice, compared with 138.6% ± 7.6% in control littermates (n = 7 mice in both groups, 13.8 ± 1.1 versus 12.6 ± 0.4 months old, respectively, ages provided as mean ± SEM) (Figure 4B). The enhancement of fEPSP slope persisted at 60 min in humanized chimeric mice (113.6% ± 3.8%, p < 0.05), whereas fEPSP slope in unengrafted controls fell to 103.2% ± 3.9% (not significantly

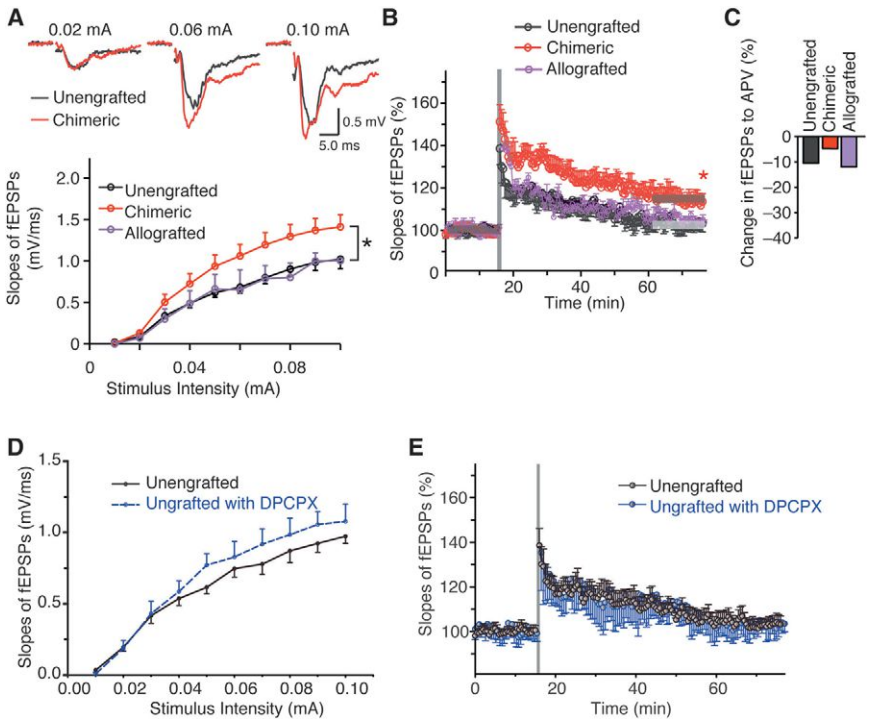

Figure 4. Strengthening of Excitatory Transmission and Synaptic Plasticity in Murine Brain by Engrafting of Human Glial Cells

(A) Comparison of field EPSPs (fEPSPs) in humanized chimeric mice and their unengrafted littermate and mouse GPC allografted controls. The slopes of fEPSP were significantly increased in human chimeric mice. (n = 3–40, F = 3.15, by two-way ANOVA with Bonferroni post hoc t test, *p < 0.05).

(B) Induction of LTP by two trains of high-frequency stimulation (each train consisted of 100 pulses at 100 Hz, with 30 s between bursts) in human chimeric mice, but not in unengrafted littermates and allografted mice. (n = 7 mice each group, *p < 0.05, t test compared between before and 60 min after the stimulation for each group.)

(C) Relative decreased percentage of fEPSP by addition of NMDA receptor antagonist APV (50 μM) in each group (n = 15–27).

(D) The adenosine A1 receptor antagonist DPCPX failed to increase the fEPSP slope in unengrafted rag2 controls (100 nM DPCPX, n = 8, p > 0.05, Bonferroni test).

(E) The adenosine A1 receptor antagonist DPCPX did not decrease the threshold for induction of LTP in unengrafted controls; the fEPSP slope returned to 101.9% ± 3.6% by 60 min after HFS, similar to the rate of extinction in untreated slices (n = 8, t test).

Data graphed as means ± SEM. See also Figure S3.

different from the fEPSP slope prior to HFS, p = 0.169). Mouse allografted controls exhibited an initial increase to 138.5% ± 2.3%, which fell to 103.8% ± 1.3% at 60 min (not significantly different from the fEPSP slope prior to HFS, n = 7, 14.0 ± 0.1 months old, p = 0.29, t test) (Figure 4B). Thus, the observed enhancement of LTP was a specific feature of human glial chimerization, and was not attributable to cell engraftment per se.

The enhancement of LTP can result from both presynaptic and postsynaptic mechanisms. An analysis of paired-pulse facilitation before and after HFS in chimeric mice suggested that postsynaptic mechanisms most likely underlie the enhancement of fEPSP slope in humanized chimeric mice (Figures S3B and S3C). To evaluate the relative contribution of AMPA- and NMDA-receptor-mediated currents to the enhancement in LTP in the chimeric mice, we analyzed the effect of NMDA receptor blockade using the NMDA receptor antagonist APV. We found that the NMDA receptor component accounted for only 4.7%–12% of fEPSP, with no significant differences across the groups analyzed, indicating that NMDA NR1 expression was not increased in the human glial chimeras. These findings suggest that NMDA receptor activation played a minor role, if any, in the enhancement of synaptic plasticity in the chimeric mice (n = 15–27) (Figure 4C). Since NMDA receptors have a higher affinity for glutamate than do AMPA receptors (Malinow and Malenka, 2002), these observations also suggest that the potentiation of fEPSPs in human glial chimeric mice was not the result of increased synaptic release of glutamate; this is consistent with the lack of enhancement of paired-pulse suppression in the chimeric mice (Figures S3B and S3C).

Neither Adenosine nor D-Serine Accounted for the Enhancement of LTP by Human Glia

Several mechanisms exist by which astrocytes can modulate excitatory transmission. Astrocytes release ATP, which, after degradation to adenosine by extracellular ectonucleotidases, can suppress both basal synaptic transmission and activity-dependent increases in synaptic strength (Pascual et al., 2005; Zhang et al., 2003). However, it seems unlikely that adenosine contributed to the enhanced synaptic strength observed in the xenografted mice. The A1 receptor antagonist 8-cyclopentyl-1,3-dipropylxanthine (DPCPX) (Grover and Teyler, 1993; Wu and Saggau, 1994) did not decrease the threshold for induction of LTP in control mice; in slices exposed to 100 nM DPCPX, the fEPSP slope returned to 101.9% ± 3.6% 60 min after HFS, similar to untreated slices (Figures 4D and 4E). Thus, it is unlikely that the reduced threshold for LTP in chimeric mice was a consequence of altered adenosine concentrations.

Astrocytes can also modulate excitatory transmission via their release of D-serine (Panatier et al., 2006; Yang et al., 2003). D-serine acts as an endogenous coagonist of NMDA receptors and facilitates NMDA receptor activation, thereby potentiating the insertion of additional AMPA receptors into the postsynaptic membrane (Panatier et al., 2006; Yang et al., 2003). We tested the effect of adding D-serine to the bath of slices prepared from control mice. D-serine had no effects on the fEPSP slopes in accordance with previous reports (p = 0.216, n = 6) (Panatier et al., 2006; Yang et al., 2003). Moreover, neither D-serine nor immunolabeling for its synthetic enzyme, serine racemase, differed between human glial chimeric and uninjected control mice (Figures S3D and S3E). These observations suggest that the lower threshold for induction of LTP in human glial chimerics

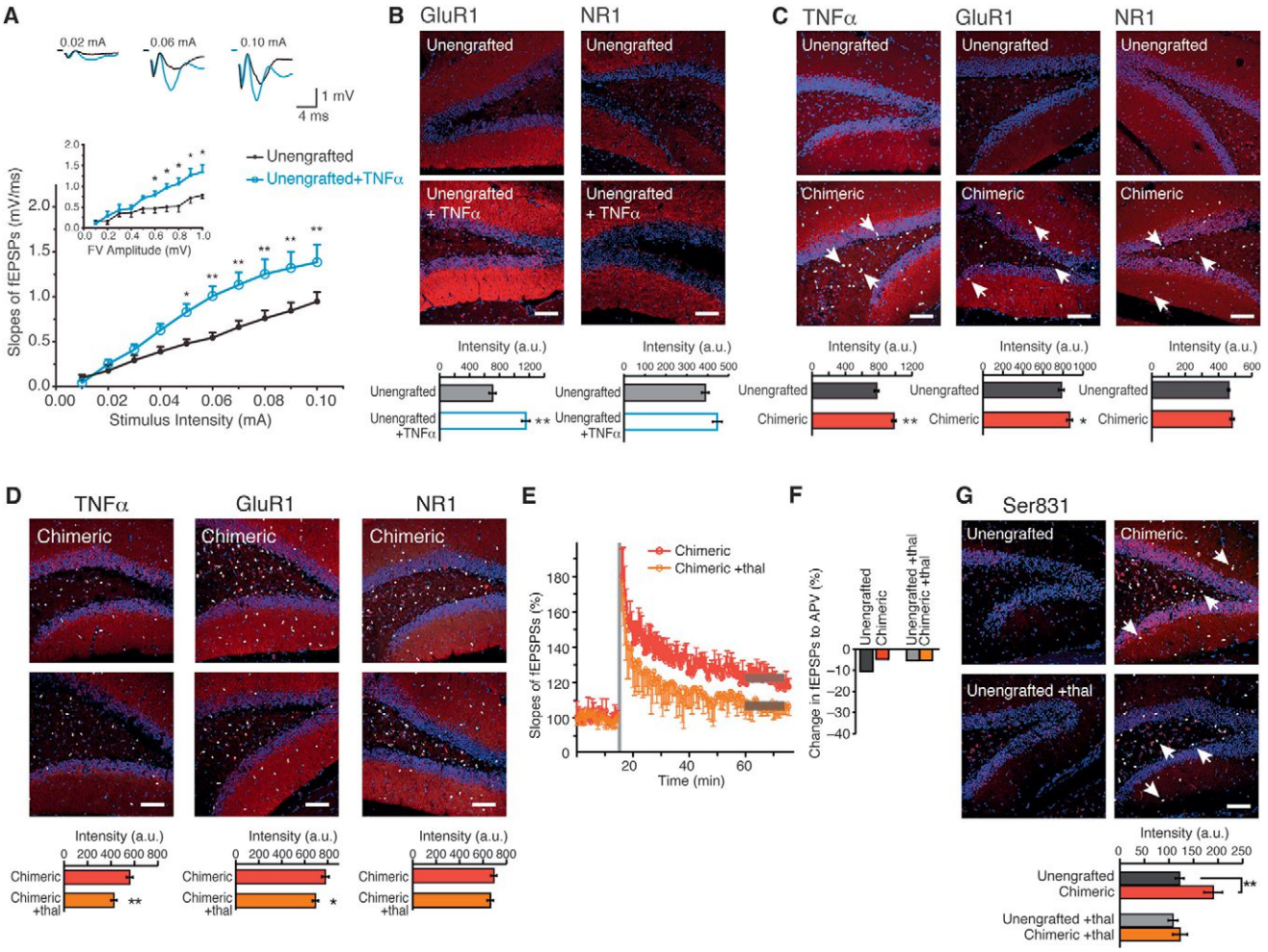

Figure 5. Astrocytic TNFα Contributes to LTP Facilitation in Chimeric Mice, which Is Attenuated by Thalidomide

(A) Hippocampal slices prepared from littermate control immunodeficient mice exhibited a potentiation of fEPSP in response to TNFα (n = 6, 12–16 months, *p < 0.05, **p < 0.01, Bonferroni post hoc t test). Inset: fEPSP slopes plotted as a function of fiber volley amplitude.

(B) Hippocampal slices exposed to TNFα (600 nM; 2–4 hr) exhibited an increase in the intensity of the GluR1 subunit of AMPA receptors as seen via immunolabeling, but not in that of the NR1 subunit of NMDA receptors (n = 5, 9–11 months, **p < 0.01, t test).

(C) Human chimeric mice exhibited a higher intensity of immunolabeling for TNFα and GluR1, but not for NR1 (n = 7, 7–20 months, *p < 0.05, **p < 0.01, t test). (hNuclei, white; representative human cells, white arrows).

(D) Thalidomide also decreased the immunolabeling of TNFα and GluR1, but not that of NR1, in chimeric mice (hNuclei, white; n = 6, 12–16 months, *p < 0.05, **p < 0.01, t test).

(E) The facilitation of LTP in chimeric mice was impaired by thalidomide (n = 6, 12.6 ± 0.3 versus 12.5 ± 0.5 months old, respectively, means ± SEM, p < 0.05, t test).

(F) Thalidomide did not change the contribution of NMDA receptor activation to fEPSP. Recordings of fEPSPs were obtained before and after addition of the NMDA receptor antagonist APV (50 μM), and the difference was calculated (n = 4).

(G) Phosphorylation of the Ser831 site of GluR1 was increased in chimeric mice compared with unengrafted littermate controls. Thalidomide attenuated the increase in phosphorylation of the Ser831 site of GluR1, but had no effect in unengrafted littermate controls, white arrows shows $hNuclei^{+}$ cells. (n = 6, 9–16 months, *p < 0.05, t test).

Scale bars: 100 μm (B, C, D, and G). All data are graphed as means ± SEM. See also Figure S4.

was not a consequence of altered adenosine tone or increased glial release of D-serine.

Human Glial TNFα Potentiates Synaptic Transmission via an Increase in GluR1 Receptors

Release of the cytokine TNFα comprises an alternative mechanism by which glia might modulate LTP. Cultured astrocytes constitutively release TNFα, which induces the addition of AMPA receptors to neuronal membranes, thereby enhancing excitatory synaptic transmission (Beattie et al., 2002; Stellwagen and Malenka, 2006). To assess the involvement of TNFα in the strengthening of excitatory transmission in the human glial chimeric mice, we first confirmed that TNFα increased both AMPA receptor current (Figure 5A) and AMPA GluR1 immunolabeling in hippocampal slices (Figure 5B). In contrast, TNFα did not affect expression of the NMDA receptor NR1 subunit in the same slices (Figure 5B). On that basis, we next asked whether chimeric mice expressed human TNFα. Using qPCR

we found that human-specific sequence encoding TNFα was indeed highly expressed in the chimeras, yet undetectable in unengrafted mice (Figure S4A). Immunolabeling confirmed that the human glial chimeras exhibited significant increases in both TNFα and GluR1, but not in NR1 (Figure 5C). We thus asked whether the inhibition of TNFα production might suppress excitatory hippocampal transmission in chimeric mice, and if so, whether TNFα inhibition might abrogate the effects of human glial chimerization on LTP.

Previous studies have analyzed the effect of TNFα on excitatory transmission in vitro by adding soluble TNFR1 receptors to scavenge free TNFα (Beattie et al., 2002; Stellwagen and Malenka, 2006). Since soluble TNFR1 would not be expected to be an efficient inhibitor in vivo, we instead administered thalidomide, a potent, BBB permeable inhibitor of TNFα production (Ryu and McLarnon, 2008). Human glial chimeric mice treated with thalidomide exhibited a significant suppression of fEPSP slopes compared to those receiving vehicle (0.5% carboxymethylcellulose) (1.41 ± 0.15 mV/ms versus 1.05 ± 0.24 mV/ms at 0.1 mA, means ± SEM, $p < 0.05$, $n = 12$). In contrast, excitatory transmission in unengrafted littermates was unaffected by thalidomide (1.02 ± 0.12 mV/ms versus 0.97 ± 0.20 mV/ms at 0.1 mA, $p = 0.32$, $n = 12$). These observations suggested that thalidomide selectively targeted the potentiation of excitatory transmission mediated by human glial TNFα. Accordingly, thalidomide also reduced the expression of both TNFα and GluR1 in the human glial chimeras, but not that of NR1 (Figure 5D). Importantly, thalidomide also prevented the facilitation of LTP in the human glial chimeras: two trains of HFS failed to trigger LTP in slices taken from chimeras pretreated with thalidomide (106.3% ± 3.9%, $n = 6$, 12.6 ± 0.3 months of age), whereas the activity-dependent potentiation of fEPSPs persisted in vehicle-treated human glial chimeras (117.6% ± 4.8%, $n = 6$, 12.5 ± 0.5 months, $p < 0.05$, t test) (Figure 5E). Thalidomide did not alter the number of NMDA receptors activated in response to medial perforant-path fiber stimulation in either chimeric or unengrafted controls, suggesting that thalidomide specifically suppressed the number of functional AMPA receptors consistent with prior publications showing that TNFα drives membrane insertion of AMPA receptors (Figure 5F) (Beattie et al., 2002; Stellwagen and Malenka, 2006). Thus, TNFα released by human glial cells (Figure S4A, Figure 5C) enhanced host neuronal fEPSPs by increasing the number of functional postsynaptic GluR1 AMPA receptors (Figure 5C), and conversely, thalidomide suppressed plasma membrane insertion of AMPA receptors, but not NMDA receptors, by inhibiting TNFα production (Figure 5D).

TNFα regulates a number of cellular processes through protein kinase C (PKC)-mediated phosphorylation (Faurschou and Gniadecki, 2008), which is thus disrupted by thalidomide. Since phosphorylation of GluR1, at sites critical for its synaptic delivery, is both necessary and sufficient for lowering the threshold for inducing LTP (Hu et al., 2007), we thus next asked if the phosphorylation state of the GluR1 subunit differed between human glial chimeric mice and their littermate controls. We focused on two phosphorylation sites, Ser845 (PKA site) and Ser831 (PKC/CaMKII site), each of which is critical for the synaptic insertion of GluR1 (Hu et al., 2007), and assessed the effects upon each of human glial chimerization and of thalidomide. Quantitative immunohistochemistry revealed that human glial chimeric mice exhibited a significant increase in Ser831 phosphorylation, the PKC-sensitive site ($n = 6$, $p = 0.008$, t test); this was significantly attenuated in human glial chimeras receiving thalidomide, but not in their unengrafted control littermates ($n = 9–10$; $p > 0.4$, t test) (Figure 5G). In contrast, phosphorylation of the Ser845 PKA site was unaffected either by the engraftment of human glia or by thalidomide ($n = 6$, $p > 0.05$, t test) (Figures S4B and S4C). Together, these results suggested that human glia facilitate synaptic insertion of the GluR1 subunit in host murine neurons through a TNFα-dependent, PKC/CaMKII-mediated pathway, which lowers the threshold for induction of LTP in human glial chimeric mice.

Enhanced Learning in Humanized Chimeric Mice

Stable, long-lasting changes in synaptic function, such as those revealed by our LTP studies, are thought to be involved in learning and memory (Lee and Silva, 2009). Since LTP was markedly enhanced in human glial chimeric mice, we next asked if these mice also exhibited improved learning. We first assessed whether auditory fear conditioning (AFC)—a task in which the mice learn to fear an innocuous tone by pairing it with foot shock (Zhou et al., 2009), and which does not require visual input (*rag2*$^{-/-}$ mice are blind)—was potentiated in the human glial chimeras. To this end, we compared the rate of acquisition of AFC in xenografted human glial chimeras to that of both allografted murine glial chimeras and unengrafted littermate controls (Figure 6A). The allografted mice—which were also generated in immunodeficient rag2 null hosts—received neonatal grafts of A2B5$^+$ cells isolated from transgenic mice with constitutive EGFP expression, which allowed us to readily identify murine donor cells. After just a single pairing of the tone with foot shock, the human glial chimeric mice exhibited a significant enhancement in learning of the tone foot shock association: they showed greater fear to the tone as measured by scoring freezing behavior (the cessation of all movement except for respiration) than did either allografted chimeras or unengrafted controls ($n = 5–20$, 9.6 ± 1.0 months old, $F = 18.9$, two-way repeated-measures ANOVA, $p < 0.001$). Moreover, after 3 continuous days of training, humanized chimeric mice also showed enhanced AFC during the 3 remaining days of testing, as manifested by their higher levels of freezing in response to the conditioned tone ($p < 0.01$, post hoc Bonferroni test). In contrast, neither murine glial chimeric mice nor unengrafted controls manifested any increase in freezing behavior during the same period, despite having been subjected to an identical fear conditioning paradigm ($p > 0.05$; Bonferroni test) (Figure 6A). Of note, no differences were observed between the human glial chimeras and their controls in the reaction to foot shock ($n = 5$, 9.6 ± 1.0 months old, $F = 0.08$ by two-way ANOVA, $p > 0.5$) (Figure S5A), suggesting that their respective nociceptive thresholds were analogous.

To specifically assess hippocampus-dependent learning, we next prepared chimeric mice using rag1 immunodeficient mice (maintained on a C57/Bl6 background), which differ from their rag2 null counterparts (on a C3h background) by having normal vision. We first compared the net engraftment of human GPCs, as well as their relative differentiation into hNG2$^+$ GPCs or GFAP$^+$ astroglia, in human glial chimeras established in rag1 null and rag2 null mice. We focused on hippocampal learning, as this region was used for our analysis of LTP (Lee and Silva,

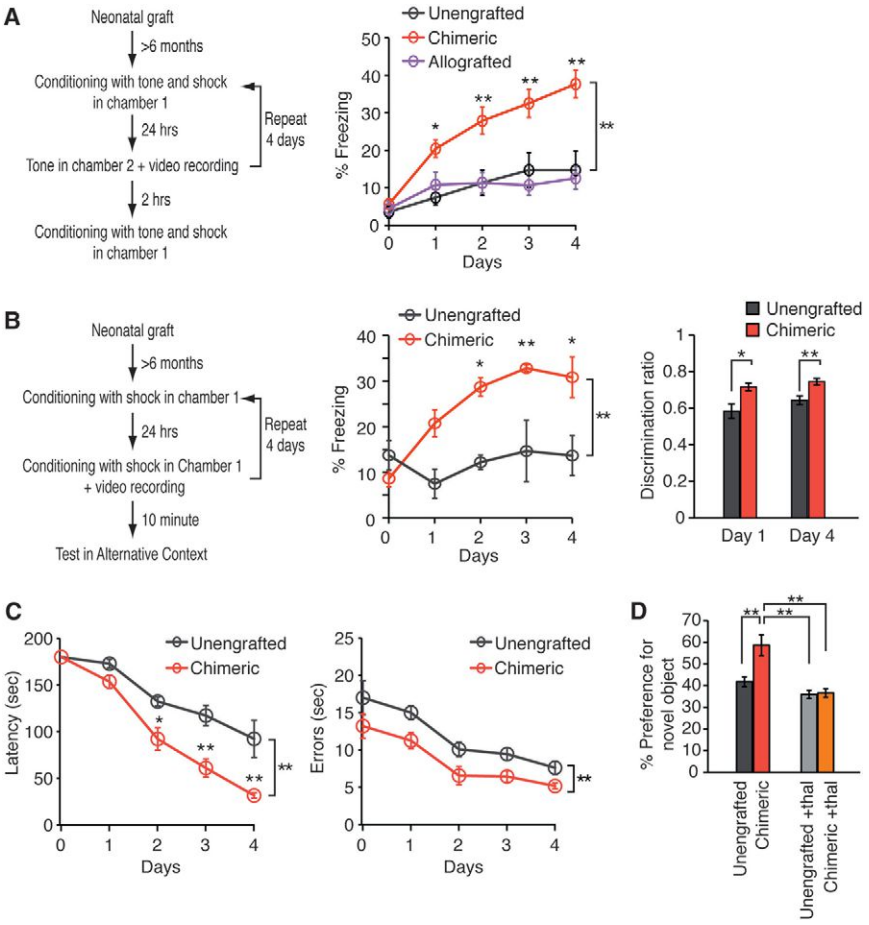

Figure 6. Humanized Chimeric Mice Learn Faster than Controls

(A) Auditory fear conditioning assessed in a cohort of human chimeric, mouse chimeric, and unengrafted control rag2 null mice. Chimeric mice exhibit prolonged freezing behavior in test chamber 2 during exposure to the tonal conditioned stimulus when compared to unengrafted mice and allografted mice (n = 5–20, *p < 0.05, **p < 0.01, two-way repeated-measures ANOVA with Bonferroni test, means ± SEM). This difference persisted throughout all 4 days.

(B) Contextual fear conditioning in human glial chimeric mice and littermate control rag1 null mice. Freezing behavior was quantified for chimeric and unengrafted littermate controls during the 2 min acclimatization period (n = 6, *p < 0.05, **p < 0.01, two-way repeated-measures ANOVA with Bonferroni test). In addition the mean discrimination ratio for each day was obtained from freezing scores in the training chamber and the alternative chamber (freezing in training chamber/total freezing time). Chimeric mice demonstrated significantly greater abilities to discriminate the chambers (n = 8–13, *p < 0.05, **p < 0.01, two-way repeated-measures ANOVA with Bonferroni test).

(C) Barnes maze testing in chimeric and unengrafted rag1 null littermate controls. Chimeric mice demonstrated a significant learning advantage, as reflected in a shorter latency and fewer errors in solving the maze (n = 6, *p < 0.05, **p < 0.01, two-way repeated-measures ANOVA with Bonferroni test).

(D) Object-Location Memory Task (OLT) in chimeric mice and their unengrafted rag1 null littermate controls demonstrated a learning advantage in chimeric mice via enhanced recognition of the novel displaced object. Thalidomide eliminated the learning advantage of chimeric mice, suggesting that the learning enhancement was TNFα mediated (n = 7, **p < 0.01, one-way ANOVA with Bonferroni test).

All data are plotted as means ± SEM. See also Figure S5.

2009; Manns and Eichenbaum, 2009). We found that both the engraftment and differentiation of human GPCs in rag1 and rag2 immunodeficient mice were indistinguishable from one another (Figures S5B and S5C). On that basis, we next assessed the effect of chimerization of rag1 null immunodeficient mice on contextual fear conditioning (CFC), a hippocampal-dependent task in which mice learn to fear a context in which they receive a foot shock (Fanselow and Poulos, 2005). The human glial-chimeric mice exhibited enhanced performance in CFC throughout all 4 days of training (Figure 6B). By just the second day, the human glial chimeric mice exhibited substantially more rapid and robust CFC than their nonchimeric littermate controls (n = 6, 6.9 ± 0.1 months of age, F = 14.8 by two-way repeated-measures ANOVA, p = 0.003), and continued to display enhanced CFC during the subsequent 2 days of CFC training (Figure 6B). To exclude the possibility that a generalized increase in freezing behavior could explain the observed differences, we also examined the context specificity of freezing responses. In these experiments, the mice were placed in a second chamber with a different floor and odor. Chimeric mice exhibited superior discrimination between the two contexts, suggesting stronger contextual learning, as opposed to a nonspecific higher level of fear (n = 8–13, 7.6 ± 0.1 months, p < 0.05, t test) (Figure 6B). No differences were observed in the reaction times to foot shock between the human glial chimeras and their rag1 null immunodeficient controls (n = 5, 9.6 ± 0.95 months, F = 0.08 by two-way ANOVA, p > 0.5) (Figure S5A). Moreover, neither thermal nor mechanical sensitivity were affected by chimerization of either rag1 or rag2 mice (Figures S5D and S5E), suggesting that their respective nociceptive thresholds were analogous.

To better assess the scope of performance enhancement in the human glial chimeras, we next assessed their performance in the Barnes maze, another hippocampal-dependent learning task. In this spatial learning task mice learn the location of a hole that leads to an escape/drop box. By just the second day of serial daily testing, the human glial chimeras made fewer errors and displayed a significantly shorter latency in finding the drop box compared to their littermate controls (n = 6, 7.4 ± 0.1 months, F = 13.4 by two-way repeated-measures ANOVA, p = 0.004) (Figure 6C). These differences persisted throughout the four-trial testing period (n = 6, 7.4 ± 0.1 months, F = 11.4, p = 0.007). With additional training, the unengrafted control mice were capable of completing the task, indicating

that they could master the task if given sufficient training (Figure S5F).

Next, we tested the mice in the Object-Location Memory Task (OLT), another hippocampal-dependent task (Manns and Eichenbaum, 2009). OLT tests the ability of the animal to recognize a familiar object in a novel location. Chimeric mice exhibited a substantially greater preference for objects in novel locations than their controls (58.6% ± 4.8% versus 41.8% ± 2.3%, means ± SEM, n = 7, 7.2 ± 0.1 months, p = 0.008, t test) (Figure 6D). Thalidomide treatment did not affect appreciably the performance of the unengrafted littermate controls on the OLT, but reduced the performance of the human glial chimeric mice to the levels of controls (n = 7, 7.8 ± 0.1 months, p = 0.82, t test) (Figure 6D). Thus, thalidomide selectively abrogated the chimerization-associated performance enhancement of the human glial chimeras.

Together, these results indicate that relative to either unengrafted mice or mice allografted with A2B5$^+$-sorted, EGFP$^+$ murine GPCs, human glial chimeric mice exhibit enhanced performance in four different learning tasks: AFC, CFC, Barnes maze, and novel object location. Moreover, the analysis of AFC indicates that alloengraftment by mouse GPCs did not affect the learning of the recipient mice, supporting the notion that the improved learning in the humanized chimeras resulted from the presence of human glia, rather than from cell engraftment per se. As an additional control, we also noted that social interactions did not differ between human chimeras generated by engraftment in rag1 mice and their littermate controls (n = 5, 6.9 ± 0.1 months, p > 0.05, t test) (Figures S5G and S5H), indicating that chimerization did not seen to affect their interactions with other mice.

DISCUSSION

Prior studies have documented that astrocytes regulate synaptic transmission and actively participate in the synaptic efficiency of neural circuits in the rodent CNS (Fields, 2004; Nedergaard and Verkhratsky, 2012; Parpura and Verkhratsky, 2012; Rusakov et al., 2011). A parallel, hitherto nonoverlapping line of work has shown that human astrocytes are larger and far more structurally complex than those of rodents (Colombo, 1996; Oberheim et al., 2009); this has led to the hypothesis that astrocytic evolution has been critical to the increased scope and capacity of central neural processing that have attended hominid evolution (Colombo, 1996; Oberheim et al., 2006, 2012). In support of this hypothesis, genomic studies have revealed that the greatest differences in brain gene expression between humans and mice are in glial transcripts (Miller et al., 2010).

In this study, we created human glial chimeric mice, in which immunodeficient but otherwise normal mice were engrafted neonatally with large numbers of human glial progenitors, resulting in the widespread integration of human glia into the mouse brain. By the time these mice reached adulthood, a large proportion of their forebrain glia were replaced by human cells. The chimerization was slowly progressive, so that extensive infiltration of cortex and hippocampus by human cells was evident by 4–12 months (Figure 1). The xenografted human cells remained as NG2-defined glial progenitor cells or differentiated as hGFAP$^+$ astrocytes; remarkably, the latter maintained their characteristic, large, and complex hominid-selective morphologies (Figure 2). In addition, some assumed the characteristic long-distance fiber extensions of interlaminar astrocytes, a domain-traversing astrocytic phenotype specific to the hominid brain (Colombo, 2001; Colombo et al., 1995; Oberheim et al., 2006). Electrophysiological analysis validated that most EGFP$^+$/hGFAP$^+$/hNuclei$^+$ human glia were protoplasmic astrocytes, based on their low input resistance, passive membrane properties, extensive gap junction coupling, and Ca^{2+} wave propagation (Figure 3).

The striking population of the recipient mouse brains by human glia raised the possibility that the engrafted human cells might significantly modulate information processing within the host murine neural networks. Indeed, the basal level of excitatory synaptic transmission was increased over a wide range of stimulation intensities. The presence of human glia also enhanced LTP in human glial chimeric hippocampal slices relative to mice that had received conspecific murine glial progenitors or vehicle injection (Figure 4). Our analysis showed that TNFα was significantly elevated in the human glial chimeric brains, consistent with the potentiation of AMPA-receptor-mediated currents (Beattie et al., 2002; Stellwagen and Malenka, 2006). Additional analysis suggested that TNFα may have directly facilitated insertion of the GluR1 subunit into the plasma membrane (Hu et al., 2007), perhaps via its increased phosphorylation at Ser831. TNFα might also potentiate astrocytic glutamate release (Ni and Parpura, 2009; Parpura and Zorec, 2010), which in turn could increase GluR1 subunit phosphorylation by NMDA-receptor-mediated activation of PKC (Figure 5) (Malinow and Malenka, 2002). Both of these pathways might have contributed to the enhancement of hippocampal LTP that we observed in the human glial chimeras, although we found no evidence of enhancement of NMDA receptor activation after engraftment (Figure 4C). Importantly, we found that thalidomide, a BBB-permeable inhibitor of TNFα, both diminished the enhancement of postsynaptic AMPA receptor current and reduced LTP in chimeric mice, yet had no such effects in unengrafted littermate controls. Behavioral analyses then revealed that human glial chimeric mice exhibited improved learning and memory in four different tasks, including AFC, CFC, the Barnes Maze, and OLT (Figure 6). As with the chimerization-associated enhancement in LTP, the enhanced learning of chimeric mice in the object location recognition assay was eliminated by thalidomide treatment (Figure 6D). Engraftment by neonatally delivered mouse GPCs did not enhance LTP, AFC, or Barnes maze performance, strongly suggesting that the potentiation of synaptic plasticity and learning afforded by glial progenitor cell chimerization was specific to human glia, and not a product of cell engraftment per se (Figures 4B and 6A).

Together, these studies demonstrate that human astrocytes generated within the mouse brain maintain their complex phenotype in a cell-autonomous fashion; they assume morphologies and Ca^{2+} wave characteristics typical of the human brain, but, to our knowledge, hitherto never observed in experimental animals. These observations strongly support the notion that the evolution of human neural processing, and hence the species-specific aspects of human cognition, in part may reflect the course of astrocytic evolution (Oberheim et al., 2006). As such, these human glial chimeric mice may present a useful

experimental model by which human glial cells, and both normative and pathological species-specific aspects of human glial biology, may now be effectively studied in the live adult brain.

EXPERIMENTAL PROCEDURES

Isolation of Human and Murine Glial Progenitor Cells

Fetal glial cell progenitors were extracted from 17- to 22-week-old human fetuses obtained at abortion. The forebrain ventricular and subventricular zones were dissected free on ice and then were dissociated using papain/DNAase as described (Windrem et al., 2004). All samples were obtained with consent under approved protocols of the University of Rochester Research Subjects Review Board. Human glial progenitor cells were isolated by magnetic activated cell sorting, as described in the Supplemental Experimental Procedures. In addition, murine A2B5$^+$ cells were identically prepared from newborn Tg(CAG-EGFP)B5Nagy/J pups (Jackson Laboratory).

Transfection and Differentiation

Human A2B5$^+$/PSA-NCAM$^-$ cells were transfected to express enhanced EGFP, and were maintained as described in the Supplemental Experimental Procedures.

Transplantation

Human glial chimeras were prepared as described, using either *rag1*$^{-/-}$ or *rag2*$^{-/-}$ immunodeficient mice (as described in Windrem et al., 2008, though using mice wild-type for myelin); see Supplemental Experimental Procedures for additional detail. All experiments were approved by the University of Rochester's Research Animal Care and Use Committee.

Quantitative Immunohistochemistry

Chimeric mice and littermate controls (ranging from 2 weeks to 20 months, depending upon experimental endpoint) were perfusion-fixed, processed histologically, and analyzed as described in the Supplemental Experimental Procedures.

Electrophysiological Characterization of Human Glia in Chimeric Mice

Patch-clamp assessment of engrafted human glia was performed in slice preparations under two-photon microscopy, as detailed in the Supplemental Experimental Procedures.

LTP

Slice preparations of both chimeric mice and their littermate controls (with an age range of 7–20 months) were used for recordings of fEPSPs and analysis of activity-dependent changes in hippocampal synaptic strength, as outlined in the Supplemental Experimental Procedures.

Ca^{2+} Imaging and Photolysis of Caged Ca^{2+}

Chimeric mice (with an age range of 4–10 months) were used for imaging intracellular Ca^{2+} in xenografted human glia. In addition, as positive controls, surgical resections of human cortex (n = 3 patients, 30.6 ± 8.8 years old) were obtained with patient consent and the approval of the University of Rochester Research Subjects Review Board; all samples were prepared for physiological assessment and analyzed as described in the Supplemental Experimental Procedures.

Detection of Human TNFα in Human Glial Chimeras

RNA isolation, PCR primer design, reverse transcription, and PCR reaction conditions and analysis were all as described in the Supplemental Experimental Procedures.

Learning Tasks and Behavioral Assessment

AFC, CFC, Barnes maze navigation, object location memory, Crawley's social interaction tasks, and both thermal and mechanical sensitivity thresholds were assessed in human glial chimeric and control mice; the latter included allografted and/or unengrafted negative controls. All tests and analyses were performed as outlined in the Supplemental Experimental Procedures.

Statistics

All data are presented and graphed as means ± SEM. The Steel-Dwass test was used to assess the relative diameters of cells, input resistances, and Ca^{2+} velocities, all variables for which normality of the data could not be assumed. For other electrophysiological data, either Student's t test for two groups or two-way ANOVA with Bonferroni post hoc t tests were used. For behavioral data, Student's t test or two-way repeated-measures ANOVA with Bonferroni post hoc test were used. Normality of the data was assessed by the Shapiro-Wilk test. $p < 0.05$ was considered significant.

SUPPLEMENTAL INFORMATION

Supplemental Information for this article includes five figures and Supplemental Experimental Procedures and can be found with this article online at http://dx.doi.org/10.1016/j.stem.2012.12.015.

ACKNOWLEDGMENTS

This work was supported by the G. Harold and Leila Y. Mathers Charitable Foundation, the Dr. Miriam and Sheldon G. Adelson Medical Research Foundation, the National Multiple Sclerosis Society, NIMH, and NINDS. We thank R. Malenka for valuable comments on the manuscript. Drs. Goldman and Windrem have a patent on the generation and use of glial chimeric mice, entitled, "Non-human animals with human glial chimeric brains," US patent no. 7,524,491. They receive no income or financial consideration from this patent.

Received: December 28, 2010
Revised: November 21, 2012
Accepted: December 19, 2012
Published: March 7, 2013

REFERENCES

Beattie, E.C., Stellwagen, D., Morishita, W., Bresnahan, J.C., Ha, B.K., Von Zastrow, M., Beattie, M.S., and Malenka, R.C. (2002). Control of synaptic strength by glial TNFalpha. Science *295*, 2282–2285.

Colino, A., and Malenka, R.C. (1993). Mechanisms underlying induction of long-term potentiation in rat medial and lateral perforant paths in vitro. J. Neurophysiol. *69*, 1150–1159.

Colombo, J.A. (1996). Interlaminar astroglial processes in the cerebral cortex of adult monkeys but not of adult rats. Acta Anat. (Basel) *155*, 57–62.

Colombo, A.J. (2001). A columnar-supporting mode of astroglial architecture in the cerebral cortex of adult primates? Neurobiology (Bp.) *9*, 1–16.

Colombo, J.A., Yáñez, A., Puissant, V., and Lipina, S. (1995). Long, interlaminar astroglial cell processes in the cortex of adult monkeys. J. Neurosci. Res. *40*, 551–556.

Cotrina, M., and Nedergaard, M. (2005). Intracellular Calcium Control Mechanisms in Glia, Second Edition (New York: Oxford University Press).

Dawitz, J., Kroon, T., Hjorth, J.J., and Meredith, R.M. (2011). Functional calcium imaging in developing cortical networks. J. Vis. Exp. *56*, pii: 3550.

Fanselow, M.S., and Poulos, A.M. (2005). The neuroscience of mammalian associative learning. Annu. Rev. Psychol. *56*, 207–234.

Faurschou, A., and Gniadecki, R. (2008). TNF-alpha stimulates Akt by a distinct aPKC-dependent pathway in premalignant keratinocytes. Exp. Dermatol. *17*, 992–997.

Fields, R.D. (2004). The other half of the brain. Sci. Am. *290*, 54–61.

Grover, L.M., and Teyler, T.J. (1993). Role of adenosine in heterosynaptic, posttetanic depression in area CA1 of hippocampus. Neurosci. Lett. *154*, 39–42.

Hu, H., Real, E., Takamiya, K., Kang, M.G., Ledoux, J., Huganir, R.L., and Malinow, R. (2007). Emotion enhances learning via norepinephrine regulation of AMPA-receptor trafficking. Cell *131*, 160–173.

Kang, S.H., Fukaya, M., Yang, J.K., Rothstein, J.D., and Bergles, D.E. (2010). NG2+ CNS glial progenitors remain committed to the oligodendrocyte lineage in postnatal life and following neurodegeneration. Neuron *68*, 668–681.

Lee, Y.-S., and Silva, A.J. (2009). The molecular and cellular biology of enhanced cognition. Nat. Rev. Neurosci. *10*, 126–140.

Malinow, R., and Malenka, R.C. (2002). AMPA receptor trafficking and synaptic plasticity. Annu. Rev. Neurosci. *25*, 103–126.

Mangin, J.M., and Gallo, V. (2011). The curious case of NG2 cells: transient trend or game changer? ASN Neuro *3*, e00052.

Manns, J.R., and Eichenbaum, H. (2009). A cognitive map for object memory in the hippocampus. Learn. Mem. *16*, 616–624.

Miller, J.A., Horvath, S., and Geschwind, D.H. (2010). Divergence of human and mouse brain transcriptome highlights Alzheimer disease pathways. Proc. Natl. Acad. Sci. USA *107*, 12698–12703.

Nedergaard, M., and Verkhratsky, A. (2012). Artifact versus reality—how astrocytes contribute to synaptic events. Glia *60*, 1013–1023.

Ni, Y., and Parpura, V. (2009). Dual regulation of Ca2+-dependent glutamate release from astrocytes: vesicular glutamate transporters and cytosolic glutamate levels. Glia *57*, 1296–1305.

Oberheim, N.A., Wang, X., Goldman, S., and Nedergaard, M. (2006). Astrocytic complexity distinguishes the human brain. Trends Neurosci. *29*, 547–553.

Oberheim, N.A., Takano, T., Han, X., He, W., Lin, J.H., Wang, F., Xu, Q., Wyatt, J.D., Pilcher, W., Ojemann, J.G., et al. (2009). Uniquely hominid features of adult human astrocytes. J. Neurosci. *29*, 3276–3287.

Oberheim, N.A., Goldman, S.A., and Nedergaard, M. (2012). Heterogeneity of astrocytic form and function. Methods Mol. Biol. *814*, 23–45.

Panatier, A., Theodosis, D.T., Mothet, J.P., Touquet, B., Pollegioni, L., Poulain, D.A., and Oliet, S.H. (2006). Glia-derived D-serine controls NMDA receptor activity and synaptic memory. Cell *125*, 775–784.

Parpura, V., and Verkhratsky, A. (2012). The astrocyte excitability brief: From receptors to gliotransmission. Neurochem. Int. *61*, 610–621.

Parpura, V., and Zorec, R. (2010). Gliotransmission: Exocytotic release from astrocytes. Brain Res. Brain Res. Rev. *63*, 83–92.

Pascual, O., Casper, K.B., Kubera, C., Zhang, J., Revilla-Sanchez, R., Sul, J.Y., Takano, H., Moss, S.J., McCarthy, K., and Haydon, P.G. (2005). Astrocytic purinergic signaling coordinates synaptic networks. Science *310*, 113–116.

Robel, S., Berninger, B., and Götz, M. (2011). The stem cell potential of glia: lessons from reactive gliosis. Nat. Rev. Neurosci. *12*, 88–104.

Rusakov, D.A., Zheng, K., and Henneberger, C. (2011). Astrocytes as regulators of synaptic function: a quest for the Ca2+ master key. Neuroscientist *17*, 513–523.

Ryu, J.K., and McLarnon, J.G. (2008). Thalidomide inhibition of perturbed vasculature and glial-derived tumor necrosis factor-alpha in an animal model of inflamed Alzheimer's disease brain. Neurobiol. Dis. *29*, 254–266.

Stellwagen, D., and Malenka, R.C. (2006). Synaptic scaling mediated by glial TNF-alpha. Nature *440*, 1054–1059.

Verkhratsky, A., Orkand, R.K., and Kettenmann, H. (1998). Glial calcium: homeostasis and signaling function. Physiol. Rev. *78*, 99–141.

Windrem, M.S., Moyle, C., Chandler-Militello, D., Han, X., Nedergaard, M., Wang, S., and Goldman, S. (2009). Neonatally-implanted human glial progenitor cells out-compete endogenous glial progenitor cells to generate fully humanized glial-chimeric mouse brains. Program No 12621/A48 Neuroscience Meeting Chicago, IL: Society for Neuroscience Online.

Windrem, M.S., Nunes, M.C., Rashbaum, W.K., Schwartz, T.H., Goodman, R.A., McKhann, G., 2nd, Roy, N.S., and Goldman, S.A. (2004). Fetal and adult human oligodendrocyte progenitor cell isolates myelinate the congenitally dysmyelinated brain. Nat. Med. *10*, 93–97.

Windrem, M.S., Schanz, S.J., Guo, M., Tian, G.F., Washco, V., Stanwood, N., Rasband, M., Roy, N.S., Nedergaard, M., Havton, L.A., et al. (2008). Neonatal chimerization with human glial progenitor cells can both remyelinate and rescue the otherwise lethally hypomyelinated shiverer mouse. Cell Stem Cell *2*, 553–565.

Wu, L.G., and Saggau, P. (1994). Adenosine inhibits evoked synaptic transmission primarily by reducing presynaptic calcium influx in area CA1 of hippocampus. Neuron *12*, 1139–1148.

Yang, Y., Ge, W., Chen, Y., Zhang, Z., Shen, W., Wu, C., Poo, M., and Duan, S. (2003). Contribution of astrocytes to hippocampal long-term potentiation through release of D-serine. Proc. Natl. Acad. Sci. USA *100*, 15194–15199.

Zhang, J.M., Wang, H.K., Ye, C.Q., Ge, W., Chen, Y., Jiang, Z.L., Wu, C.P., Poo, M.M., and Duan, S. (2003). ATP released by astrocytes mediates glutamatergic activity-dependent heterosynaptic suppression. Neuron *40*, 971–982.

Zhou, Y., Won, J., Karlsson, M.G., Zhou, M., Rogerson, T., Balaji, J., Neve, R., Poirazi, P., and Silva, A.J. (2009). CREB regulates excitability and the allocation of memory to subsets of neurons in the amygdala. Nat. Neurosci. *12*, 1438–1443.

Cell Stem Cell
Short Article

Generation of Rejuvenated Antigen-Specific T Cells by Reprogramming to Pluripotency and Redifferentiation

Toshinobu Nishimura,[1] Shin Kaneko,[1,9,*] Ai Kawana-Tachikawa,[2] Yoko Tajima,[1] Haruo Goto,[1] Dayong Zhu,[2] Kaori Nakayama-Hosoya,[2] Shoichi Iriguchi,[1] Yasushi Uemura,[6] Takafumi Shimizu,[1] Naoya Takayama,[3,10] Daisuke Yamada,[7] Ken Nishimura,[8] Manami Ohtaka,[8] Nobukazu Watanabe,[4] Satoshi Takahashi,[5] Aikichi Iwamoto,[2] Haruhiko Koseki,[7] Mahito Nakanishi,[8] Koji Eto,[3,10] and Hiromitsu Nakauchi[1,*]

[1]Division of Stem Cell Therapy, Center for Stem Cell Biology and Regenerative Medicine
[2]Division of Infectious Diseases, Advanced Clinical Research Center
[3]Stem Cell Bank, Center for Stem Cell Biology and Regenerative Medicine
[4]Laboratory of Diagnostic Medicine, Center for Stem Cell Biology and Regenerative Medicine
[5]Division of Molecular Therapy, Advanced Clinical Research Center
The Institute of Medical Science, The University of Tokyo, 4-6-1 Shirokanedai, Minato-ku, Tokyo 108-8639, Japan
[6]Division of Immunology, Aichi Cancer Center Research Institute, 1-1 Kanakoden, Chikusa-ku Nagoya, Aichi 464-8681, Japan
[7]Laboratory for Lymphocyte Development, RIKEN Center for Allergy and Immunology, 1-7-22 Suehiro-cho, Tsurumi-ku, Yokohama, Kanagawa 230-0045, Japan
[8]Research Center for Stem Cell Engineering, National Institute of Advanced Industrial Science and Technology, 1-1-1 Higashi, Central 4, Tsukuba, Ibaraki 305-8562, Japan
[9]Present address: Department of Fundamental Cell Technology, Center for iPS Cell Research and Application (CiRA), Kyoto University, 53 Kawahara-cho, Shogoin, Sakyo-ku, Kyoto 606-8507, Japan
[10]Present address: Department of Clinical Application, CiRA, Kyoto University, 53 Kawahara-cho, Shogoin, Sakyo-ku, Kyoto 606-8507, Japan
*Correspondence: kaneko.shin@cira.kyoto-u.ac.jp (S.K.), nakauchi@ims.u-tokyo.ac.jp (H.N.)
http://dx.doi.org/10.1016/j.stem.2012.11.002

SUMMARY

Adoptive immunotherapy with functional T cells is potentially an effective therapeutic strategy for combating many types of cancer and viral infection. However, exhaustion of antigen-specific T cells represents a major challenge to this type of approach. In an effort to overcome this problem, we reprogrammed clonally expanded antigen-specific CD8$^+$ T cells from an HIV-1-infected patient to pluripotency. The T cell-derived induced pluripotent stem cells were then redifferentiated into CD8$^+$ T cells that had a high proliferative capacity and elongated telomeres. These "rejuvenated" cells possessed antigen-specific killing activity and exhibited T cell receptor gene-rearrangement patterns identical to those of the original T cell clone from the patient. We also found that this method can be effective for generating specific T cells for other pathology-associated antigens. Thus, this type of approach may have broad applications in the field of adoptive immunotherapy.

INTRODUCTION

T cells play a central role in acquired immunity and the configuration of systemic immunity against pathogens. In particular, cytotoxic T lymphocytes (CTLs) are major components of this systemic response to microorganisms, viral infections, and neoplasms (Greenberg, 1991; Zhang and Bevan, 2011). T cells initiate their proliferative and effector functions upon human leukocyte antigen (HLA)-restricted recognition of specific antigen peptides via T cell receptors (TCRs). This is greatly beneficial in enabling the selective recognition and eradication of target cells, and also in long-term immunological surveillance by long-lived memory T cells (Butler et al., 2011; Jameson and Masopust, 2009; MacLeod et al., 2010). However, viruses in chronic infection or cancers often hamper or escape the T cell immunity by decreasing the expression of molecules required for T cell recognition or by inhibiting antigen presentation (Virgin et al., 2009). In addition, continuous exposure to chronically expressed viral antigens or cancer/self-antigens can drive T cells into an "exhausted" state. This is characterized by loss of effector functions and the potential for long-term survival and proliferation, ultimately leading to the depletion of antigen-responding T cell pools (Klebanoff et al., 2006; Wherry, 2011).

The infusion of ex vivo-expanded autologous antigen-specific T cells is being developed clinically for T cell immunotherapy. However, up to now, highly expanded T cells have not proven to be particularly effective (June, 2007). This is in part explained by losses of function that occur during the ex vivo manipulation of patient autologous T cells. In another instance, genetic modification of antigen receptors is an ambitious but only partially successful way to add desired antigen specificity to nonspecific T cells (Morgan et al., 2006; Porter et al., 2011). The therapeutic effect also strongly depends on the extent of functional loss that occurs during the ex vivo manipulation of T cells and on the stability of exogenous antigen receptor expression specific to target molecules in the presence of the endogenous TCR genes (Bendle et al., 2010; Brenner and Okur, 2009).

For the purpose of overcoming these obstacles, the therapeutic potential of induced pluripotent stem cells (iPSCs) is being

explored. Embryonic stem cells (ESCs) or iPSCs have the capacity for self-renewal while maintaining pluripotency (Takahashi et al., 2007) and could potentially form the basis for the unlimited induction of antigen-specific juvenile T cells. However, there are challenges to this approach as well, given that methods for the differentiation and immunological education of ESCs and iPSCs, or indeed that of intermediate hematopoietic stem and/or progenitor cells, into fully matured functional human T cells are not well established (Timmermans et al., 2009). Reprogramming the nuclei of lymphocytes was historically performed for studying whether terminally differentiated or fully matured somatic cells could revert to a pluripotent state. The first demonstration of lymphocyte reprogramming employed somatic cell nuclear transfer in murine B and T cells, proving that terminally differentiated somatic cells were reprogrammable (Hochedlinger and Jaenisch, 2002). Reprogramming murine B cells into pluripotent stem cells by iPSC technology also provided definite proof for fate reversibility in fully matured somatic cells (Hanna et al., 2008). From another point of view, nuclear reprogramming of lymphocytes is seen as having applications for regenerative medicine different than those for scientific research. The irreversible rearrangement of genes encoding immunoglobulins and TCRs was recognized solely as a genetic marker in somatic cell nuclear transfer and iPSC research. However, the preserved rearrangements in genomic DNA can also provide a blueprint of "educated" weapons for attacking cancers and pathogens in adoptive immunotherapy. Although several groups have reported the generation of T cell-derived iPSCs (T-iPSCs), their clinical applications have yet to be thoroughly explored (Brown et al., 2010; Loh et al., 2010; Seki et al., 2010; Staerk et al., 2010).

In the present study, we chose a T cell clone specific to an HIV type 1 (HIV-1) epitope of known structure to act as a generic representation of iPSC-mediated T cell regeneration. We successfully induced iPSCs from antigen-specific T cells and redifferentiated them into functional T cells. This may act as proof of concept for the application of "rejuvenated" T cells in treating various diseases. Crucial to this concept was that T-iPSCs retained the assembled "endogenous" TCR genes even after being subjected to nuclear reprogramming. Furthermore, redifferentiated T cells showed the same pattern of TCR gene arrangement as that in the original T cells. These features may therefore serve as the foundation for the reproduction of unlimited numbers of T cells that express desired TCRs conferring to antigen specificity.

RESULTS

Reprogramming an Antigen-Specific Cytotoxic T Cell Clone into Pluripotency

To establish T cell-derived iPSCs, we magnetically separated the $CD3^+$ T cell population from peripheral blood mononuclear cells (PBMCs) of healthy volunteers. The isolated $CD3^+$ T cells were stimulated with human CD3 and CD28 antibody-coated microbeads (α-CD3/28 beads) in the presence of interleukin-2 (IL-2). We then transduced the activated $CD3^+$ T cells with separate retroviral vectors that individually code for *OCT3/4*, *SOX2*, *KLF4*, and c-*MYC*. Human ESC-like colonies were obtained within 25 days of culture (Figure S1A available online).

We also isolated PBMCs from an HLA-A24-positive patient with a chronic HIV-1 infection. $CD8^+$ CTL clones specific for an antigenic peptide (amino acids [aa] 138–145) from the HIV-1 Nef protein (Nef-138-8(WT); RYPLTFGW) (Altfeld et al., 2006) were established. One of the clones, H25-#4, was stimulated using α-CD3/28 beads in the presence of IL-2 and then transduced simultaneously with six retroviral vectors encoding *OCT3/4*, *SOX2*, *KLF4*, c-*MYC*, *NANOG*, and *LIN28A*. However, we could not reprogram H25-#4 into pluripotency, possibly due to the cells being in a low infectious and exhausted state, or due to insufficient expression of the reprogramming factors. In response, we attempted to increase transduction efficiency and transgene expression by using two Sendai virus (SeV) vectors. One of them encodes tetracistronic factors (*OCT3/4*, *SOX2*, *KLF4*, and c-*MYC*) (Nishimura et al., 2011) with the miR-302 target sequence (SeVp[KOSM302L]; K.N., M.O., and M.N., data not shown), and another encodes SV40 large T antigen (SeV18[T]) (Fusaki et al., 2009). After transduction of phytohemagglutinin (PHA)-activated H25-#4 cells with the SeV vectors in the presence of IL-7 and IL-15, sufficient numbers of human ESC-like colonies appeared within 40 days of culture (Figure 1A). Use of this SeV system and optimization of transduction conditions greatly improved the reprogramming efficiency. It enabled us to reprogram several $CD8^+$ or $CD4^+$ T cell clones specific to pp65 antigen in cytomegalovirus (CMV), glutamic acid decarboxylase (GAD) antigen in type 1 diabetes, and α-GalCer (Table 1).

The resultant $CD3^+$ T cell- and H25-#4-derived ESC-like colonies (TkT3V1-7 and H254SeVT-3, respectively) exhibited alkaline phosphatase (AP) activity and expressed the pluripotent cell markers SSEA-4, Tra-1-60, and Tra-1-81 (Figures S1B–S1E and 1B–1E). H254SeVT-3 expressed HLA-A24 (Figure 1F). Both TkT3V1-7 and H254SeVT-3 also expressed human ESC-related genes (Figures S1F and 1G). The expression of exogenous reprogramming factors from the integrated provirus (TkT3V1-7) was halted (Figure S1F), and nonintegrated SeV genomic RNA was successfully removed from the cytosol by RNAi or by self-degradation caused by temperature-sensitive mutations (H254SeVT-3) (Figure 1H). Comparison of gene-expression profiles revealed that the gene-expression patterns in the ESC-like cells were similar to those in human ESCs, but differed significantly from those in peripheral blood (PB) T cells (Figure S1G). Scant methylation of the *OCT3/4* and *NANOG* promoter regions was confirmed using bisulfite PCR, thus indicating successful reprogramming (Freberg et al., 2007) (Figures S1H and 1I). In addition, when injected into nonobese diabetic severe combined immunodeficient (NOD-Scid) mice, those cells formed teratomas containing characteristic tissues derived from all three germ layers, which is indicative of pluripotency (Brivanlou et al., 2003) (Figures S3 and 2A). Therefore, those colonies were confirmed as typical human iPSCs.

T-iPSCs Carry Preassembled TCR Genes from the Original T Cell

Almost all TCRs are composed of heterodimerically associated α and β chains. *TCRA* or *TCRB* gene (encoding α chain or β chain, respectively) rearrangements are involved in normal αβ T cell development in the thymus. These rearrangements enabled us to determine retrospectively whether the iPSCs were derived from an αβ T cell. The BIOMED-2 consortium designed multiplex-PCR primers for analyzing *TCRB* gene assemblies (van Dongen et al., 2003), and we designed the primers for detecting *TCRA*

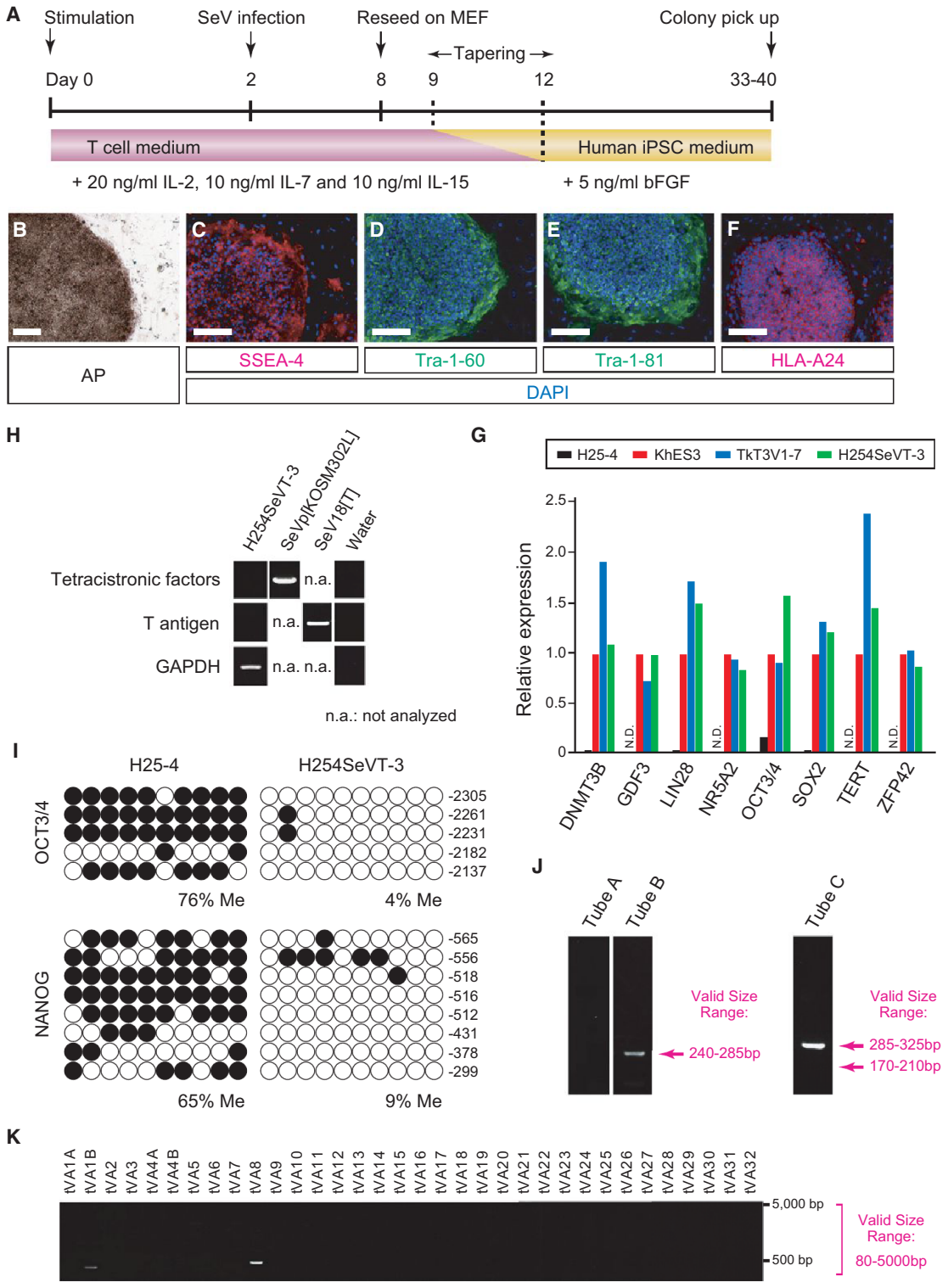

Figure 1. Generation of Human iPSCs from a CTL Clone

(A) Schematic illustration showing the generation of T-iPSCs from H25-#4 T cells using SeV vectors encoding polycistronic *OCT3/4*, *SOX2*, *KLF4,* and c-*MYC*, or SV40 large T antigen. The "tapering" indicates the gradual replacement of culture medium with human iPSC medium.

(B–F) AP activity (B) and expression of pluripotency markers (SSEA-4, C; Tra-1-60, D; and Tra-1-81, E) and HLA-A24 (F) in H254SeVT-3 cells. Nuclei were counterstained with DAPI. The scale bar represents 200 μm.

(G) Quantitative PCR for pluripotency genes in H25-#4, KhES3, TkT3V1-7, and H254SeVT-3 cells. Individual PCR reactions were normalized against 18S ribosomal RNA (rRNA).

(legend continued on next page)

Table 1. Generation of Human T-iPSCs from Various Patient-Derived T Cell Specimens

Antigen	T Cell Source	Initial Cell Number	No. of ESC-like Colonies	No. of Colonies Picked up for Establishing T-iPSC Clones	Date (MM/YYYY)
HIV-1 Nef	monoclonal T cell clone	4×10^5	7	7	05/2011
CMV pp65	polyclonal tetramer-sorted cells	~5,000	15	15	07/2011
GAD	monoclonal T cell clone	1×10^6	>100	not picked up	08/2012
		5×10^5	>100	19	08/2012
α-GalCer	FACS-sorted Vα24$^+$ cells	1×10^6	>100	not picked up	08/2012
		5×10^5	>100	7	08/2012

Sample cells were transduced with *OCT3/4*, *SOX2*, *KLF4*, *c-MYC*, and SV40 large T-antigen by using two Sendai virus (SeV) vectors (SeVp [KOSM302L] and SeV18[T]). After around 40 days, the number of embryonic stem cell (ESC)-like colonies were counted on the basis of morphology and alkaline phosphatase (AP) activity. All established T cell-derived induced pluripotent stem cell (T-iPSC) lines were free from residual SeV vectors (one example in the case of the HIV-1 Nef-specific T-iPSC clone is shown in Figure 1H). CMV, cytomegalovirus; GAD, glutamic acid decarboxylase; FACS, fluorescence-activated cell sorting.

gene assemblies (Figure S2). *TCRB* and *TCRA* gene assemblies were identified as single bands representing each allele in TkT3V1-7 and H254SeVT-3 (Figures S1H, S1I, 1J, and 1K).

We next confirmed the presence of an antigen-recognition site on the TCR that consisted of three complementarity-determining regions (CDR1, CDR2, and CDR3). CDR3 is the most diversifiable among the three because it spans the V(D)J-junction region, where several random nucleotides (N or P nucleotides) are inserted (Alt and Baltimore, 1982; Lafaille et al., 1989). We determined the CDR3 sequences of the assembled *TCRA* and *TCRB* genes in TkT3V1-7 and H254SeVT-3 and identified a set of productive *TCRA* and *TCRB* gene rearrangements (i.e., in-frame junction with no stop codon) (Table S1 and Table 2). Furthermore, the sequences of CDR3 from H254SeVT-3 and H25-#4 were completely identical at both *TCRA* and *TCRB* gene loci. These results indicated that the iPSCs established were derived from a single T cell and that the antigen specificity encoded in the genomic DNA of the T cell was conserved during reprogramming.

Redifferentiation of T-iPSCs into CD8 Single-Positive T Cells Expressing the Desired TCR

Following the application of specific in vitro differentiation protocols, iPSCs can give rise to mesoderm-derived cell types, especially hematopoietic stem and/or progenitor cells (Takayama et al., 2008; Vodyanik et al., 2005) (Figure 2B). This was applied to assess the capacity of T-iPSCs for hematopoietic differentiation by coculturing on C3H10T1/2 feeder cells in the presence of VEGF, SCF, and FLT-3L for the generation of CD34$^+$ hematopoietic stem and/or progenitor cells. On day 14 of culture, the cells were transferred onto Delta-like 1-expressing OP9 (OP9-DL1) feeder cells (Timmermans et al., 2009) and were cocultured in the presence of FLT-3L and IL-7 (Ikawa et al., 2010) (Figure 2B). After 21–28 days of culture, the hematopoietic cells differentiated into CD45$^+$, CD38$^+$, CD7$^+$, CD45RA$^+$, CD3$^+$, and TCRαβ$^+$ T lineage cells (Figure S4). As was the case with TCRαβ transgenic mice (Borgulya et al., 1992) and chimeric mice derived from ESCs produced through nuclear transplantation of T cells (Serwold et al., 2007), aberrant expression of TCRαβ was observed at the CD4/CD8 double-negative (DN) stage. Although some of these T lineage cells differentiated into the CD4/CD8 double-positive (DP) stage and the more mature CD4 or CD8 single-positive (SP) stages (Figure 2C), we could not characterize the small number of SP cells in more detail.

During thymocyte development, the CD4/CD8 DN and DP stages correspond respectively to the *TCRB*-encoded β chain and *TCRA*-encoded α chain assembly stages (von Boehmer, 2004). In the *TCRB* locus, the negative-feedback regulation of gene assembly and the capacity to deter further rearrangement are very strict (Khor and Sleckman, 2002). In the *TCRA* locus, by contrast, negative-feedback regulation is relatively loose, and further gene assembly of the preassembled gene, a phenomenon known as "receptor revision," tends to occur (Huang and Kanagawa, 2001; Krangel, 2009). In experiments using TCRα transgenic mice, the reactivation of *Rag1* and *Rag2*, genes related to recombination machinery, occurred in CD4/CD8 DP-stage thymocytes, and gene assembly of endogenous *Tcra* was observed (Padovan et al., 1993; Petrie et al., 1993). Such further gene assembly would be exceedingly undesirable for our purposes, because it would probably convert the tropism of the TCR and render the redifferentiated T cells incapable of attacking the previously targeted antigen. To determine whether such receptor revision could occur in redifferentiating T lineage cells, we collected CD1a$^-$ DN- and CD1a$^+$ DP-stage cells from among the CD45$^+$, CD3$^+$, TCRαβ$^+$, and CD5$^+$ T lineage cells and then analyzed the gene rearrangement of TCR messenger RNAs (mRNAs) (Figures S5A–S5C). Nucleotide sequences of *TCRB* mRNAs in the T lineage cells were identical to those in

(H) Detection of the remnants of SeV genomic RNAs by RT-PCR. Each column represents the template cDNA synthesized from H254SeVT-3 cells, SeVp [KOSM302L] virus solution, and SeV18[T] virus solution. cDNAs from virus solution were the positive controls.
(I) Bisulfite sequencing analyses of the *OCT3/4* and *NANOG* promoter regions in H25-#4 and H254SeVT-3 cells. White and black circles represent unmethylated and methylated (Me) CpG dinucleotides, respectively.
(J) Multiplex PCR analysis to detect *TCRB* gene rearrangements in the H254SeVT-3 genome. Tubes A and B contain Vβ-(D)Jβ assemblies; Tube C contains D-Jβ assemblies.
(K) Multiplex PCR analysis for detection of *TCRA* gene rearrangements (V-Jα assemblies).
See Figures S1, S2, and S3 for additional data.

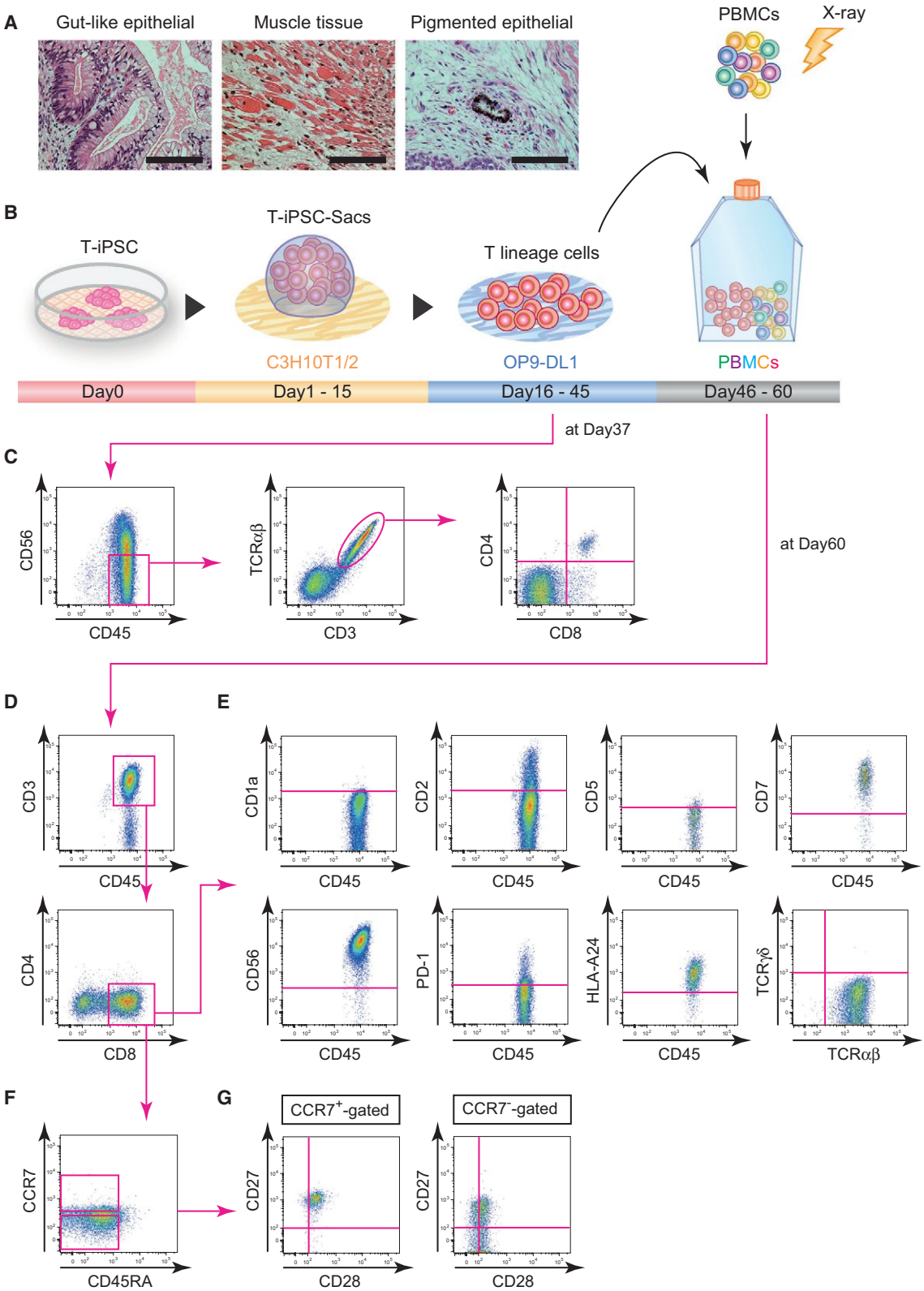

Figure 2. Redifferentiation of T-iPSCs into T Cells

(A) Representative hematoxylin- and eosin-stained sections of a teratoma formed in a NOD/ShiJic-*scid* mouse testis. H254SeVT-3 differentiated into cell lineages derived from endoderm (goblet cells in gut-like epithelial), mesoderm (smooth myocytes in muscle tissue), and ectoderm (retina cells in pigmented epithelial). The scale bar represents 100 μm.

(legend continued on next page)

the T-iPSCs at both the DN and DP stages. By contrast, some *TCRA* mRNAs at the DN and DP stages were identical to those in the T lineage cells, but others differed, and differing sequences were observed more frequently at the DP stage than the DN stage (Table S2). *RAG1* and *RAG2* expression were observed at both the DN and the DP stages, though stronger expression was observed at the DP stage (Figure S5D).

To create mature CD8 SP cells from T-iPSC-derived T lineage cells without receptor revision, we focused on TCR signaling. Turka et al. (1991) reported that TCR signaling via peptide-major histocompatibility complex (MHC) complexes during positive selection ends expression of *RAG* genes and prevents further assembly of TCR genes. They also showed that mimicking TCR signaling using CD3 antibodies had the same effect. Therefore, we tried to stimulate the TCRs of redifferentiating T lineage cells before the completion of the DN-to-DP transition (Figure 2B). For this experiment, we cultured T lineage-committed cells on OP9-DL1, stimulated them with α-CD3/28 beads or PHA (we defined this as the first stimulation) and then cocultured them with irradiated HLA-A24$^-$ PMBCs in the presence of IL-7 and IL-15, which are required for the generation of memory phenotype CD8$^+$ T cells (Kaneko et al., 2009; Prlic et al., 2002; Tan et al., 2002). After 14 days, CD8 SP cells appeared (Figure 2D). These were deemed to be derivatives of H254SeV-3 based on their expression of HLA-A24 (Figure 2E). These CD8 SP cells did not express the immature thymocyte marker CD1a, but they were positive for CD56, which is expressed on CD8$^+$ T cells cultured in vitro (Lu and Negrin, 1994). In addition, these cells expressed CD7 and some CD2, but not CD5. On the one hand, they did not express PD-1, a marker of exhausted T cells (Figure 2E). On the other hand, some of them expressed the memory T cell markers CCR7, CD27, and CD28 simultaneously, thus representing a central memory T cell phenotype (Figures 2F and 2G) (Romero et al., 2007).

To test whether the redifferentiated CD8 SP cells would recognize the same epitope on the same HLA, the entire population of redifferentiated T cells was mixed with the A24/Nef-138-8(WT) tetramer and subjected to flow-cytometric analysis (Kawana-Tachikawa et al., 2002). Most of the CD8 SP cells were stained positively by the A24/Nef-138-8(WT) tetramer, but not by the control tetramer, which represents HIV-1 envelope-derived peptides (RYLRDQQLL; Figure 3A and data not shown). We then collected the A24/Nef-138-8(WT) tetramer-reactive CD8$^+$ cells and expanded them once again using α-CD3/28 beads or PHA stimulation (defined as the second stimulation; Figure 3A). Finally, after several independent redifferentiation experiments, we obtained A24/Nef-138-8(WT) tetramer-reactive CD8 SP cells (reT-1, reT-2.1, reT-2.2, and reT-3). As expected, sequence analysis of *TCRA* and *TCRB* mRNAs in the redifferentiated CD8 SP cells revealed that the TCR gene rearrangement pattern was identical to that in the H25-#4 original T cell clone (Figure 3B and Table 1).

To determine whether the redifferentiated CD8 SP cells were of the T cell lineage, we used quantitative PCR to compare gene-expression profiles among redifferentiated CD8 SP cells, PB CD4$^+$ and CD8$^+$ T cells, and the H25-#4 original T cell clone. As shown in Figure 3C, the expression patterns of CD3, CD4, and CD8 were similar among PB CD8$^+$ T cells, redifferentiated CD8 SP cells, and the H25-#4 original T cell clone. However, the pattern differed from those in PB CD4$^+$ T cells (Figure 3C). Cytotoxic "signature" genes such as granzyme B (*GZMB*), perforin (*PRF1*), interferon-γ (IFN-γ; *IFNG*), and FAS ligand (*FASLG*) were expressed in PB CD8$^+$ T cells. These genes were also expressed relatively strongly in redifferentiated CD8 SP cells and in the H25-#4 original T cell clone; that is, in already-primed T cells (Figure 3D). The expression patterns of several factors involved in transcription or signal transduction and of cell-surface molecules were similar among PB CD8$^+$ T cells, redifferentiated CD8 SP cells, and the H25-#4 original T cell clone (Figure 3E). To exclude the possibility that the redifferentiated CD8 SP cells had acquired natural killer (NK)-like properties during their coculture with OP9-DL1 or PBMCs, we used a complementary DNA (cDNA) microarray to analyze global gene-expression profiles in redifferentiated CD8 cells, the H25-#4 original T cell clone, and PB NK cells. Correlation and cluster analyses of the gene-expression profile of the redifferentiated CD8 SP cells showed it to be similar to that of the H25-#4 original T cell clone but different from that of NK cells (Figures 3F and 3G). These data strongly suggest that T-iPSCs are able to redifferentiate into CD8$^+$ T cells that exhibit the same antigen specificity as that of the original T cell.

Generation of Highly Proliferative T Cells through T-iPSCs

Fewer than 10^5 T lineage cells were obtained from ~3 × 10^5 T-iPSCs after coculture with C3H10T1/2 and OP9-DL1 cells. However, they could be expanded to >10^8 cells with the first stimulation (data not shown). After separating A24/Nef-138-8(WT) tetramer-reactive CD8$^+$ cells, we assessed the expansion rate induced by the second stimulation and also assessed the establishment of reT-1, reT-2.2, and reT-3. We found that these cells expanded from 100-fold to 1,000-fold within 2 weeks in the presence of IL-7 and IL-15, whereas the H25-#4 original T cell clone expanded only about 20-fold (Figure 4A). Even after 100-to-1,000-fold expansions, some cells still expressed central memory T cell markers such as CCR7, CD27, and CD28 (Figure S6). Perhaps with passage through the iPSC state, wherein telomerase activity is quite high (Marion et al., 2009; Takahashi et al., 2007), re-elongation of shortened telomeres in the H25-#4 original T cell clone gives the redifferentiated T cells high replicative potential (Monteiro et al., 1996; Weng et al., 1998). In fact, the redifferentiated T cells carried longer telomeres than the original T cell clone (Figure 4B), an overall process that we call

(B) Schematic illustration of redifferentiation from T-iPSCs into T cells.
(C) Flow-cytometric analysis of the phenotypes of differentiating T lineage cells at 37 days after starting redifferentiation.
(D and E) Flow-cytometric analysis of the phenotypes of T cells at 60 days after starting redifferentiation. Fluorescence-activated cell sorting (FACS) analyses revealed CD8 single-positive maturation (D) and expression of several T cell markers (E).
(F and G) Memory phenotypes of redifferentiated CD8$^+$ T cells. There existed memory-phenotyped cells such as all positive for CCR7 (F), CD27, and CD28 (G).
Data are representative of at least three independent experiments. See Figures S3, S4, and S5 and Table S2 for additional data.

Table 2. TCR Gene Rearrangements in H25-4, H254SeVT-3, or Redifferentiated CD8$^+$ T Cells

Cell	Genome or mRNA	Productivity	Rearrangement			Sequence of Junctional Region		
			Vα		Jα	3′Vα	P(N)	5′Jα
TCRA								
H25-4	genome	productive	TRAV8-3*01		TRAJ10*01	TGTGCTGTGGGT	T	TCACGGGAGGAGGAAACAAACTC ACCTTTT
		unproductive[a]	TRAV13-1*01		TRAJ29*01	TGTGCAGCAA	TCC	TCAGGAAACACACCTCTTGTCTTT
H254SeVT-3	genome	productive	TRAV8-3*01		TRAJ10*01	TGTGCTGTGGGT	T	TCACGGGAGGAGGAAACAAACTC ACCTTTT
		unproductive[a]	TRAV13-1*01		TRAJ29*01	TGTGCAGCAA	TCC	TCAGGAAACACACCTCTTGTCTTT
reT-1	mRNA	productive	TRAV8-3*01		TRAJ10*01	TGTGCTGTGGGT	T	TCACGGGAGGAGGAAACAAACTC ACCTTTT
		unproductive[a]	TRAV13-1*01		TRAJ29*01	TGTGCAGCAA	TCC	TCAGGAAACACACCTCTTGTCTTT
reT-2.1	mRNA	productive	TRAV8-3*01		TRAJ10*01	TGTGCTGTGGGT	T	TCACGGGAGGAGGAAACAAACTC ACCTTTT
		unproductive[a]	TRAV13-1*01		TRAJ29*01	TGTGCAGCAA	TCC	TCAGGAAACACACCTCTTGTCTTT
reT-3	mRNA	productive	TRAV8-3*01		TRAJ10*01	TGTGCTGTGGGT	T	TCACGGGAGGAGGAAACAAACTC ACCTTTT
		unproductive[a]	TRAV13-1*01		TRAJ29*01	TGTGCAGCAA	TCC	TCAGGAAACACACCTCTTGTCTTT
			Vβ	Dβ	Jβ	3′Vβ	N1-Dβ-N2	5′Jβ
TCRB								
H25-4	genome	productive	TRBV7-9*01	TRBD1*01	TRBJ2-5*01	TGTGCCAGCAGCTTA	CGGGACAGGGTGCCG	GAGACCCAGTACTTC
		unproductive	germline	TRBD1*01	TRBJ2-7*01	TACAAAGCTGTAACATTGTG	GGGACAACT	CTACGAGCAGTACTTCGGGCCG
H254SeVT-3	genome	productive	TRBV7-9*01	TRBD1*01	TRBJ2-5*01	TGTGCCAGCAGCTTA	CGGGACAGGGTGCCG	GAGACCCAGTACTTC
		unproductive	germline	TRBD1*01	TRBJ2-7*01	TACAAAGCTGTAACATTGTG	GGGACAACT	CTACGAGCAGTACTTCGGGCCG
reT-1	mRNA	productive	TRBV7-9*01	TRBD1*01	TRBJ2-5*01	TGTGCCAGCAGCTTA	CGGGACAGGGTGCCG	GAGACCCAGTACTTC
reT-2.1	mRNA	productive	TRBV7-9*01	TRBD1*01	TRBJ2-5*01	TGTGCCAGCAGCTTA	CGGGACAGGGTGCCG	GAGACCCAGTACTTC
reT-3	mRNA	productive	TRBV7-9*01	TRBD1*01	TRBJ2-5*01	TGTGCCAGCAGCTTA	CGGGACAGGGTGCCG	GAGACCCAGTACTTC

PCR-amplified samples (H25-4: not shown; H254SeVT-3: shown in Figures 1J and 1K; reT-1, reT-2.1, and reT-3: shown in Figure 3B) were sequenced, then V, D, and J segment usages and junctional sequences in CDR3 were identified. Following reprogramming and redifferentiation, there were no alterations in gene rearrangement in either allele at the *TCRA* and *TCRB* gene loci. See Table S1 for additional data on another T-iPSC clone (TkT3V1-7).

[a]Out-of-frame junction (at CDR3).

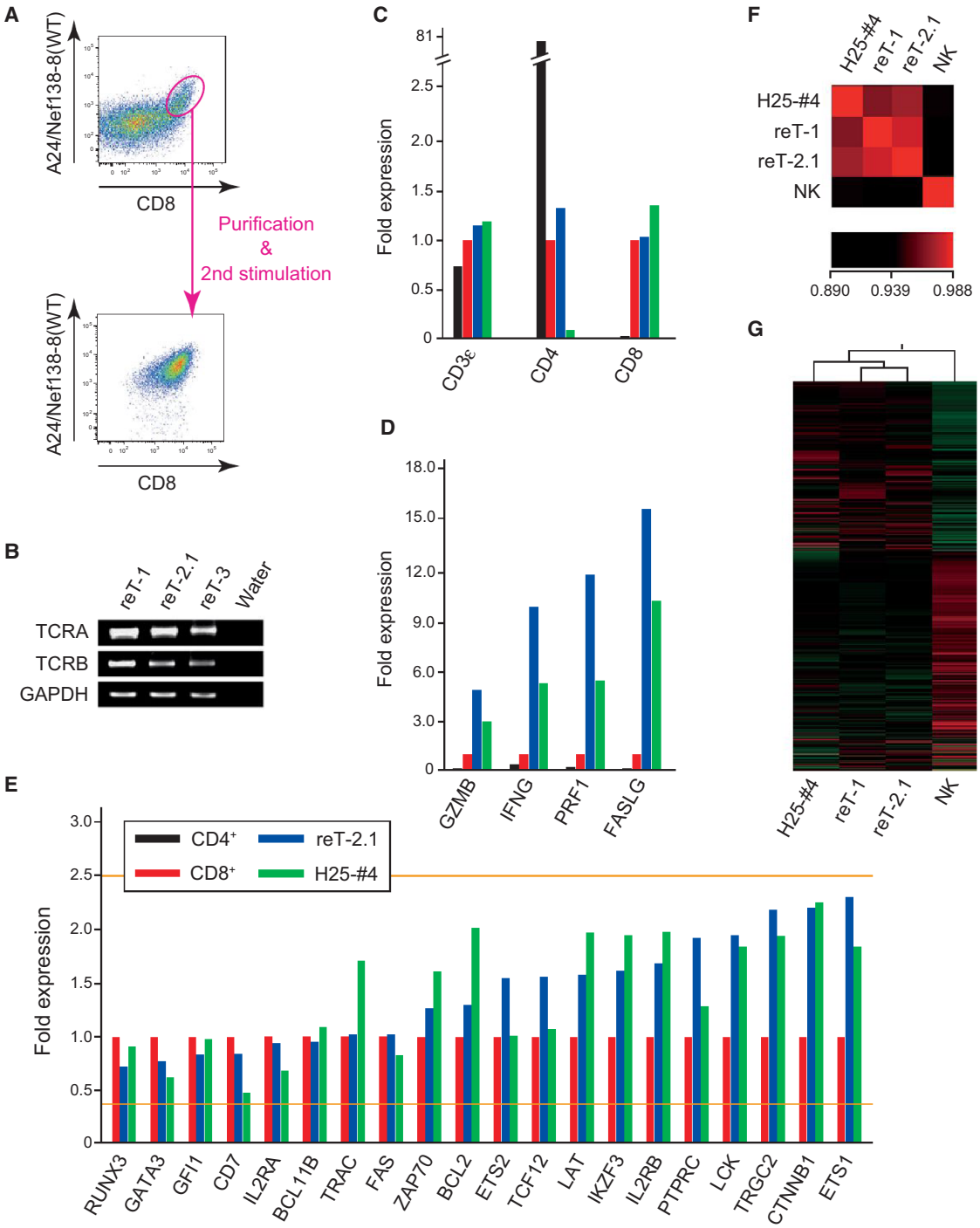

Figure 3. Characterizations of Redifferentiated T Cells as T Cells

(A) Recognition of A24/Nef-138-8(WT) tetramer at 50–60 days after starting redifferentiation, analyzed by flow cytometry (upper panel). Tetramer-positive cells were sorted by FACS or magnetically selected, then cultured for an additional 14 days, after which the expanded T cells were reanalyzed for tetramer (lower panel).

(B) TCR mRNAs were identified in a SMART-mediated cDNA library for reT-1, reT-2.1, and reT-3 cells. *GAPDH* is an internal control for PCRs.

(C–E) Quantitative PCR to compare the expression of major cell surface molecules (C), cell lytic molecules (D), and transcription factors and signal-transduction molecules (E) among PB $CD4^+$, PB $CD8^+$, reT-2.1, and H25-#4 cells. Individual PCR reactions were normalized against 18S rRNA.

(F and G) Global gene expression was analyzed using a cDNA microarray. Heat maps show the correlation coefficients between samples (F) and differential expression (>3-fold) of genes relative to NK cells (G). Red and green colorations indicate increased and decreased expression, respectively.

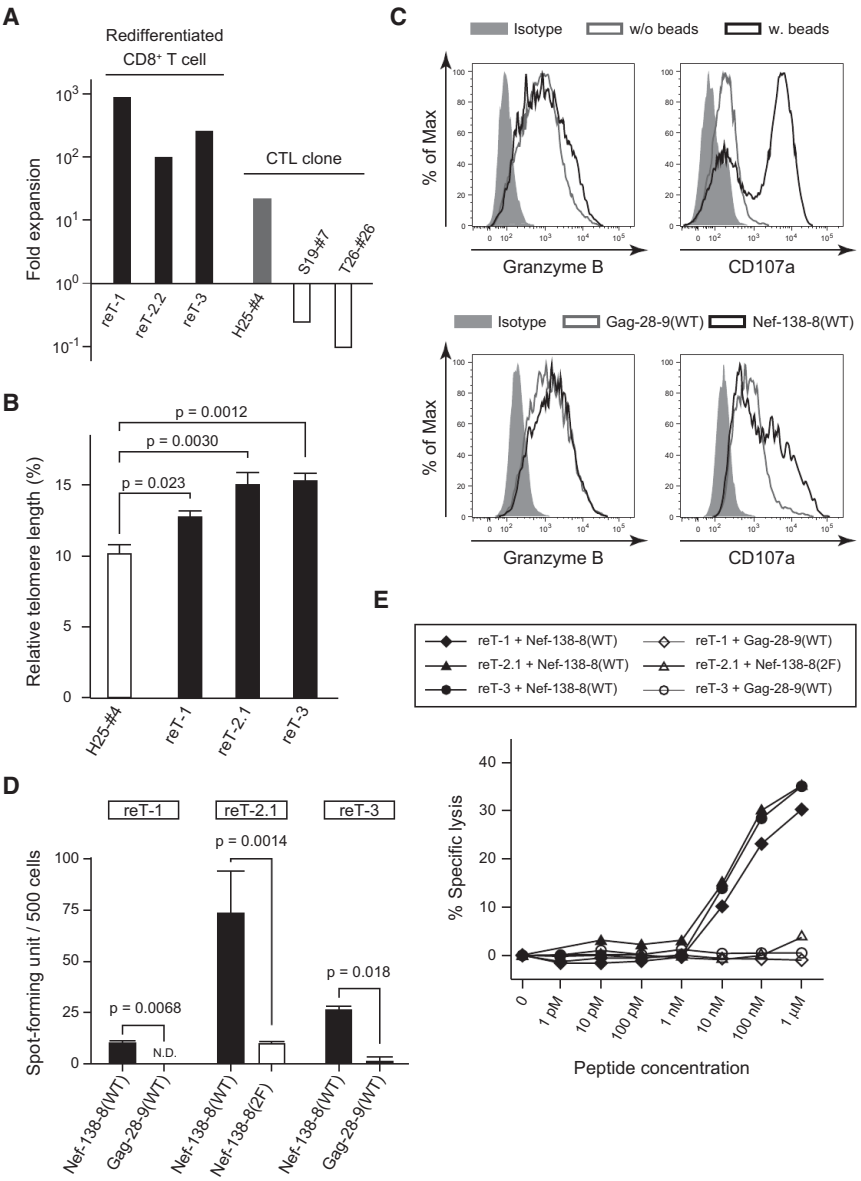

Figure 4. Redifferentiated T Cells Show T Cell Functionality and the Same Antigen Specificity as the Original CTL Clone

(A) Expansion ratios for reT-1, reT-2.2, and reT-3 cells elicited by PHA, IL-7, and IL-15 stimulation for 2 weeks. H25-#4 is the original clone. S19-#7 and T26-#26 were other Nef-138-8(WT)-specific CTL clones derived from different patients.

(B) Relative telomere length determined using flow-FISH. Data are presented as mean ± SEM.

(C) Intracellular production of granzyme B (left panel) and CD107a mobilization (right panel) induced by stimulation of reT-2.1 cells with α-CD3/CD28 beads or Nef-138-8(WT). Shaded plot: stimulated cells, isotype antibody; gray line: unstimulated cells, granzyme B or CD107a antibody; black line: stimulated cells, granzyme B or CD107a antibody.

(D) IFN-γ production in the presence of Nef-138-8(WT) measured using ELISPOT. Data are presented as mean ± SD. N.D., not determined.

(E) Standard ^{51}Cr release assay performed using the indicated concentrations of Nef-138-8(WT). Effector:target = 5:1.

See Figure S6 for additional data.

"rejuvenation." Throughout the experiments, neither autonomous cell expansion nor aberrant cell survival without cytokines as leukemia cells was observed (data not shown). Taken together, these data indicate that by passing through the T-iPSC state, cloned cytotoxic T cells can become "rejuvenated" to central memory-like T cells with excellent potential for proliferation and survival.

Redifferentiated CD8$^+$ T Cells Exhibit Antigen-Specific T Cell Functionality

To determine whether redifferentiated CD8$^+$ T cells exerted cytotoxic effects upon recognition of specific peptides in the context of an MHC, we performed functional assays using HLA-A24-positive B-LCL cells as antigen-presenting cells. Gag-28-9(WT) (KYKLKHIVW) is an antigenic peptide (aa 28–36) from the HIV-1 Gag protein (Altfeld et al., 2006), whereas Nef-138-8(2F) (RFPLTFGW) is a Tyr-to-Phe-substituted single-residue mutant form of Nef-138-8(WT). Both peptides were presented on HLA-A24 cells.

One of the major mechanisms by which CTLs induce cytotoxity is the secretion of cytolytic molecules triggered by TCR signaling. Intracellular staining revealed that the cytolytic molecule granzyme B was produced and stored in the granules of redifferentiated CD8$^+$ T cells (Figure 4C, left column). CD107a, also known as lysosomal-associated membrane protein 1 (LAMP1), is a granulocyte membrane protein that transiently appears at the cell surface and is coupled to degranulation (secretion of cytolytic molecules) of the stimulated CTLs, after which CD107a returns to the cytoplasm (Rubio et al., 2003). CD107a molecules on the cell surface were captured by a fluorochrome-conjugated antibody when redifferentiated CD8$^+$ T cells were stimulated with α-CD3/28 beads or Nef-138-8(WT) peptide, but not in the absence of the beads or Gag-28-9(WT) peptide (Figure 4C, right column). In the second experiment, we used the enzyme-linked immunosorbent spot (ELISPOT) assay to assess cytokine productivity per cell and confirmed that redifferentiated CD8$^+$ T cells produced significant levels of IFN-γ in response to stimulation by its specific antigen, Nef-138-8(WT) (Figure 4D). In a separate experiment, we used a ^{51}Cr release assay to investigate cytolytic capacity and found that redifferentiated CD8$^+$ T cells lysed ^{51}Cr-incorporated B-LCLs only when Nef-138-8(WT) was presented on B-LCLs (Figure 4E).

These results are highly indicative that redifferentiated CD8$^+$ T cells can release cytotoxic molecules and kill antigen-expressing target cells in an antigen-specific manner. Moreover,

monoclonal TCRs mediate highly precise cell targeting that should broaden the therapeutic window for antigen-specific T cell therapy by avoiding the troublesome mispairing TCRs that can occur with the commonly used exogenous TCR transfer technique for inducing antigen-specific T cells from hematopoietic stem cells or peripheral mature T cells (Bendle et al., 2010; Brenner and Okur, 2009).

DISCUSSION

Using a HIV-1-epitope-specific CTL clone as a model, we demonstrated here that the reprogramming into pluripotency of a T cell clone and the subsequent redifferentiation to mature functional $CD8^+$ T cells are possible. These redifferentiated $CD8^+$ T cells are highly proliferative naive cells with elongated telomeres, and they exert T cell functions in the same HIV-1-epitope-specific manner, permitting the inference that this process of reprogramming and redifferentiation can rejuvenate mature antigen-specific T cells.

Generation of iPSCs from T cells was initially difficult. On the basis of reports by Seki et al. (2010), we also found that SeV is suitable for the reprogramming of aged and exhausted fibroblasts, as well as of T cells. We also found that coexpression of SV40 large T antigen acted synergistically with the classic Yamanaka factors in enhancing the reprogramming efficiency of T cells. Therefore, SV40 large-T antigen introduction using the SeV vector system was also included in the protocol. Worth noting is that c-*MYC* is a known oncogene, and when it is inserted into the genomic DNA by the retroviral vector, it may become a risk for tumorigenesis in the generation of iPSCs. The same concern does not apply to SeV vector systems, given that the genomic RNA could be removed from the cytosol after reprogramming. Therefore, the utilization of SeV vectors both improved reprogramming efficiency and shielded redifferentiating cells from oncogene- or provirus-mediated tumorigenesis (Kohn et al., 2003).

In the redifferentiation experiments, mimicking TCR signaling led to CD8-linage specification without reassembly of *TCRA* genes. Preassembled TCR genes are a distinctive feature of T-iPSCs not found on other pluripotent stem cells. TCR$\alpha\beta$ is aberrantly expressed on redifferentiating CD4/CD8 DN cells, and the TCR signaling evoked results in the cessation of *RAG* expression. Serwold and colleagues reported that aberrantly early expression of TCR from preassembled *Tcra* and *Tcrb* following TCR signaling in murine thymocytes drives later lymphomagenesis (Serwold et al., 2010). They cautioned that T-iPSCs might confer risk for TCR-mediated lymphomagenesis. Therefore, the redifferentiation method will need to be further optimized and confirmed for clinical safety before application in practical treatments. This may be achieved by the use of an inducible suicide-gene system for eliminating unwanted tumors after injections (Hara et al., 2008; Veldwijk et al., 2004).

Immunological assays found that the redifferentiated $CD8^+$ T cells exerted T cell functions such as cytolytic activity, IFN-γ secretion, and degranulation in a normal manner when stimulated with their specific antigens. The most striking difference was in their proliferation capacity and elongated telomeres, which correlates with the central-memory T cell phenotype. Stem cell-like memory T cells (T_{SCM}) were recently identified as a subpopulation of T cells that has the capacity for self-renewal and that is multipotent and able to generate central memory, effector memory, and effector T cells (Gattinoni et al., 2011; Turtle et al., 2009). In a humanized mouse model, T_{SCM} cells reconstituted the T cell population more efficiently than other known memory subsets while mediating a superior antitumor response. It was found that inhibition of GSK3β enhances the generation of T_{SCM} in culture. Combining T-iPSC-mediated T cell rejuvenation with GSK3β inhibition may therefore enable efficient generation of T_{SCM} cells and permit highly effective immunotherapy along with the reconstitution of a normal T cell immune system.

Although these data suggest that rejuvenated T cells enjoy an advantage over the original T cell clone, it remains unclear whether these HIV-epitope-specific rejuvenated T cells are effective in improving the overall status of HIV infection. This is because the role of $CD8^+$ T cells in HIV infection appears to vary depending on the disease stage (Appay et al., 2000; Borrow et al., 1994; Brodie et al., 1999; Day et al., 2006; Koup et al., 1994). Evasion of the immune response through CTL escape is another important factor in HIV pathogenesis, and the escaped virus is a substantial hurdle for HIV therapies (Phillips et al., 1991). Therefore, this system may work best instead against tumors such as a melanoma, for which certain antigenic epitopes are known, or against viral infections other than HIV, for which the roles of $CD8^+$ cytotoxic T cells are more established. Nonetheless, the system described in our study will make it possible to preserve and to supply highly proliferative, functional $CD8^+$ T cells specific to a variety of HIV epitopes without worrying about exhaustion. It may also act as a valuable tool in better understanding the role of adoptive immunity in HIV infection.

Here, we have presented a proof of concept of $CD8^+$ T cell rejuvenation. The concept is not limited only to $CD8^+$ cytotoxic T cells. It may also be applied to $CD4^+$ helper or regulatory T cells to control desired or undesired immune reactions in the context of malignancies, chronic viral infections, autoimmune diseases, or transplantation-related immune disorders, if optimization of redifferentiation conditions can be achieved. Biological and technical challenges lie ahead, but the data presented in this work open new avenues toward antigen-specific T cell therapies that will supply unlimited numbers of rejuvenated T cells and will regenerate patients' immune systems.

EXPERIMENTAL PROCEDURES

Generation of Antigen-Specific CTL Clones

Nef138-8(WT)-specific CTL lines were induced from PBMCs of a patient chronically infected with HIV-1 who is positive for HLA-A24, as described (Kawana-Tachikawa et al., 2002). Each CTL line was expanded from a single-cell sorted $tetramer^+$ T cell, and the cells in every CTL line were confirmed for expression of only one kind of TCR$\alpha\beta$. For more details of CTL-clone establishment, see the Supplemental Experimental Procedures.

Generation of T-iPSCs

Human iPSCs were established from PB T cells or a CTL clone as described (Takayama et al., 2010), slightly modifying the culture conditions. In brief, T cells were stimulated by α-CD3/CD28 antibody-coated beads (Miltenyi Biotec) or by 5 μg/ml PHA-L (Sigma-Aldrich). The activated cells were transduced with reprogramming factors via retroviral or SeV vectors and were cultured in RH10 medium (RPMI-1640 supplemented with 10% human AB Serum, 2 mM L-glutamine, 100 U/ml penicillin, and 100 ng/ml streptomycin), which was

gradually replaced with human iPSC medium (Dulbecco's modified Eagle's medium/F12 FAM supplemented with 20% knockout serum replacer, 2 mM L-glutamine, 1% nonessential amino acids, 10 μM 2-mercaptoethanol, and 5 ng/ml basic fibroblast growth factor [bFGF]). The established iPSC clones were transfected with small interfering RNA L527 (Nishimura et al., 2011) using Lipofectamine RNAi Max (Invitrogen) for removal of SeV vectors from the cytoplasm.

Analysis of TCR Gene Rearrangement in Genomic DNA

Genomic DNA was extracted from approximately 5 × 10^6 cells using QIAamp DNA kits (QIAGEN) according to the manufacturer's instructions. For *TCRB* gene rearrangement analysis, PCR was performed according to BIOMED-2 protocols (van Dongen et al., 2003). For *TCRA* gene rearrangement analysis, PCR was performed using the primers shown in Figure S2 and LA Taq HS (TaKaRa). The PCR protocol entailed three amplification cycles (30 s at 95°C, 45 s at 68°C, and 6 min at 72°C); 15 amplification cycles (30 s at 95°C, 45 s at 62°C, and 6 min at 72°C); and 12 amplification cycles (15 s at 95°C, 30 s at 62°C, and 6 min at 72°C). The dominant band within the expected size range was purified using a QIAquick gel-extraction kit (QIAGEN) and was then sequenced. V, D, and J segment usages were identified by comparison to the ImMunoGeneTics (IMGT) database (http://www.imgt.org/) and by using an online tool (IMGT/V-QUEST) (Lefranc, 2003). Gene-segment nomenclature follows IMGT usage.

Analysis of TCR Gene Rearrangement in mRNA

A method based on the "switch mechanism at the 5′-end of the reverse transcript (SMART)" (Du et al., 2006) was used to synthesize double-stranded cDNAs (Super SMART cDNA synthesis kit; BD Clontech). Reverse transcription was conducted with the 3′ SMART CDS primer, SMART II A oligonucleotides (Super SMART cDNA synthesis kit), and PrimeScript Reverse Transcriptase (TaKaRa) for 90 min at 42°C. Double-stranded cDNA was then synthesized and was amplified with 5′ PCR Primer II A (Super SMART cDNA synthesis kit), and reagents were provided in an Advantage 2 PCR Kit (BD Clontech). The PCR protocol entailed 20 cycles of 5 s at 95°C, 5 s at 65°C, and 3 min at 68°C. The amplified double-stranded cDNA was used as templates in TCRA- or TCRB-specific amplification reactions. With forward primer (2^{nd}_5′-SMART) and reverse primer (3′-TRAC for *TCRA* or 3′-TRBC for *TCRB*), 25 cycles of amplification were performed (30 s at 94°C, 30 s at 55°C, and 1 min at 72°C). PCR products were cloned into pGEM-T Easy Vector (Promega) and were sequenced.

T Cell Differentiation from T-iPSCs

To differentiate human iPSCs into hematopoietic cells, we slightly modified a previously described protocol (Takayama et al., 2008). Small clumps of iPSCs (<100 cells) were transferred onto irradiated C3H10T1/2 cells and cocultured in EB medium (Iscove's modified Dulbecco's medium supplemented with 15% fetal bovine serum [FBS] and a cocktail of 10 μg/ml human insulin, 5.5 μg/ml human transferrin, 5 ng/ml sodium selenite, 2 mM L-glutamine, 0.45 mM α-monothioglycerol, and 50 μg/ml ascorbic acid) in the presence of VEGF, SCF, and FLT-3L. Hematopoietic cells contained in iPSC sacs were collected and were transferred onto irradiated OP9-DL1 cells (provided by RIKEN BRC through the National BioResource Project of the Ministry of Education, Culture, Sports, Science, and Technology [MEXT]) (Watarai et al., 2010). The hematopoietic cells underwent T lineage differentiation on OP9-DL1 cells during coculture in OP9 medium (αMEM supplemented with 15% FBS, 2 mM L-glutamine, 100 U/ml penicillin, and 100 ng/ml streptomycin) in the presence of FLT-3L and IL-7. The T lineage cells were then harvested, mixed with irradiated HLA-A24$^-$ PBMCs, and cocultured in RH10 medium in the presence of IL-7 and IL-15.

Intracellular Staining

For intracellular staining of granzyme B, T cells were stimulated by α-CD3/28 beads or peptide-loaded HLA-A24$^+$ B-LCLs. After 2 hr, brefeldin A (5 μg/ml; Invitrogen) was added, with incubation for 4 hours more. Cells were then harvested and fixed in Fixation/Permeabilization solution (BD Biosciences). Intracellular staining was performed as per the manufacturer's protocol using Perm/Wash buffer (BD Biosciences) and fluorescein isothiocyanate (FITC)-conjugated granzyme B antibody (BD Biosciences). For capturing CD107a transiently expressed on cell surfaces, T cells were incubated with α-CD3/28 beads or peptide-loaded HLA-A24$^+$ B-LCLs and were cultured with FITC-conjugated CD107a antibody (BioLegend) for 6 hr. Harvested cells were fixed and stained as described above. Data were acquired on FACSAria II equipment (BD Biosciences) and analyzed using FlowJo software (Tree Star).

Measurement of Telomere Length by Flow-FISH

Telomere length was measured using a Telomere PNA Kit/FITC (DAKO) as previously described (Neuber et al., 2003).

ELISPOT and ^{51}Cr Release Assays

The antigen-specific responses of T cells were measured using an ELISPOT assay for IFN-γ and a standard ^{51}Cr release assay as described (Kawana-Tachikawa et al., 2002; Tsunetsugu-Yokota et al., 2003). HLA-A24$^+$ B-LCLs were used as antigen-presenting cells.

Statistics

All data are presented as mean ± SD. All statistics were performed using Excel (Microsoft) and Prism (GraphPad software) programs, applying two-tailed Student's t test. Values of $p < 0.05$ were considered significant. For additional details, see the Supplemental Experimental Procedures.

ACCESSION NUMBERS

The Gene Expression Omnibus accession number for microarray data reported in this paper is GSE43136.

SUPPLEMENTAL INFORMATION

Supplemental Information includes six figures, three tables, and Supplemental Experimental Procedures and can be found with this article online at http://dx.doi.org/10.1016/j.stem.2012.11.002.

ACKNOWLEDGMENTS

We thank Yumiko Ishii and Yuji Yamazaki (The University of Tokyo) for FACS operation; Sou Nakamura, Ryoko Jono-Onishi, and Shuichi Kitayama (The University of Tokyo) for technical help; Hiroshi Kawamoto, Kyoko Masuda, and Raul Vizcardo (RIKEN Center for Allergy and Immunology) for kindly providing OP9-DL1 cells and for helpful discussions; Yasuharu Nishimura and Satoru Senju (Kumamoto University) for kindly providing T cell clones; Makoto Otsu, Akihide Kamiya, Motoo Watanabe, Ayako Kamisato, and Masataka Kasai (The University of Tokyo) and Masaki Yasukawa, Hiroshi Fujiwara, and Toshiki Ochi (Ehime University) for helpful discussions; and Alex Knisely and Huan-Ting Lin for critical reading of the manuscript. The project was supported in part by a grant from the Project for Realization of Regenerative Medicine, by a Grant-in-Aid for Scientific Research (KAKENHI) and by the Global Center of Excellence program from MEXT of Japan, by a Grant-in-Aid for scientific research from the Japan Society for the Promotion of Science, and by grants for AIDS research from the Ministry of Health, Labor, and Welfare of Japan. The experimental protocol was approved by the institutional regulation board for human ethics at the Institute of Medical Science, University of Tokyo (approval number: 20-6-0826). The entire study was conducted in accordance with the Declaration of Helsinki.

Received: May 31, 2012
Revised: September 28, 2012
Accepted: November 6, 2012
Published: January 3, 2013

REFERENCES

Alt, F.W., and Baltimore, D. (1982). Joining of immunoglobulin heavy chain gene segments: implications from a chromosome with evidence of three D-JH fusions. Proc. Natl. Acad. Sci. USA *79*, 4118–4122.

Altfeld, M., Kalife, E.T., Qi, Y., Streeck, H., Lichterfeld, M., Johnston, M.N., Burgett, N., Swartz, M.E., Yang, A., Alter, G., et al. (2006). HLA Alleles

Associated with Delayed Progression to AIDS Contribute Strongly to the Initial CD8(+) T Cell Response against HIV-1. PLoS Med. *3*, e403.

Appay, V., Nixon, D.F., Donahoe, S.M., Gillespie, G.M., Dong, T., King, A., Ogg, G.S., Spiegel, H.M., Conlon, C., Spina, C.A., et al. (2000). HIV-specific CD8(+) T cells produce antiviral cytokines but are impaired in cytolytic function. J. Exp. Med. *192*, 63–75.

Bendle, G.M., Linnemann, C., Hooijkaas, A.I., Bies, L., de Witte, M.A., Jorritsma, A., Kaiser, A.D., Pouw, N., Debets, R., Kieback, E., et al. (2010). Lethal graft-versus-host disease in mouse models of T cell receptor gene therapy. Nat. Med. *16*, 565–570, 1p following 570.

Borgulya, P., Kishi, H., Uematsu, Y., and von Boehmer, H. (1992). Exclusion and inclusion of alpha and beta T cell receptor alleles. Cell *69*, 529–537.

Borrow, P., Lewicki, H., Hahn, B.H., Shaw, G.M., and Oldstone, M.B. (1994). Virus-specific CD8+ cytotoxic T-lymphocyte activity associated with control of viremia in primary human immunodeficiency virus type 1 infection. J. Virol. *68*, 6103–6110.

Brenner, M.K., and Okur, F.V. (2009). Overview of gene therapy clinical progress including cancer treatment with gene-modified T cells. Hematology (Am. Soc. Hematol. Educ. Program), 675–681.

Brivanlou, A.H., Gage, F.H., Jaenisch, R., Jessell, T., Melton, D., and Rossant, J. (2003). Stem cells. Setting standards for human embryonic stem cells. Science *300*, 913–916.

Brodie, S.J., Lewinsohn, D.A., Patterson, B.K., Jiyamapa, D., Krieger, J., Corey, L., Greenberg, P.D., and Riddell, S.R. (1999). In vivo migration and function of transferred HIV-1-specific cytotoxic T cells. Nat. Med. *5*, 34–41.

Brown, M.E., Rondon, E., Rajesh, D., Mack, A., Lewis, R., Feng, X., Zitur, L.J., Learish, R.D., and Nuwaysir, E.F. (2010). Derivation of induced pluripotent stem cells from human peripheral blood T lymphocytes. PLoS ONE *5*, e11373.

Butler, N.S., Nolz, J.C., and Harty, J.T. (2011). Immunologic considerations for generating memory CD8 T cells through vaccination. Cell. Microbiol. *13*, 925–933.

Day, C.L., Kaufmann, D.E., Kiepiela, P., Brown, J.A., Moodley, E.S., Reddy, S., Mackey, E.W., Miller, J.D., Leslie, A.J., DePierres, C., et al. (2006). PD-1 expression on HIV-specific T cells is associated with T-cell exhaustion and disease progression. Nature *443*, 350–354.

Du, G., Qiu, L., Shen, L., Sehgal, P., Shen, Y., Huang, D., Letvin, N.L., and Chen, Z.W. (2006). Combined megaplex TCR isolation and SMART-based real-time quantitation methods for quantitating antigen-specific T cell clones in mycobacterial infection. J. Immunol. Methods *308*, 19–35.

Freberg, C.T., Dahl, J.A., Timoskainen, S., and Collas, P. (2007). Epigenetic reprogramming of OCT4 and NANOG regulatory regions by embryonal carcinoma cell extract. Mol. Biol. Cell *18*, 1543–1553.

Fusaki, N., Ban, H., Nishiyama, A., Saeki, K., and Hasegawa, M. (2009). Efficient induction of transgene-free human pluripotent stem cells using a vector based on Sendai virus, an RNA virus that does not integrate into the host genome. Proc. Jpn. Acad., Ser. B, Phys. Biol. Sci. *85*, 348–362.

Gattinoni, L., Lugli, E., Ji, Y., Pos, Z., Paulos, C.M., Quigley, M.F., Almeida, J.R., Gostick, E., Yu, Z., Carpenito, C., et al. (2011). A human memory T cell subset with stem cell-like properties. Nat. Med. *17*, 1290–1297.

Greenberg, P.D. (1991). Adoptive T cell therapy of tumors: mechanisms operative in the recognition and elimination of tumor cells. Adv. Immunol. *49*, 281–355.

Hanna, J., Markoulaki, S., Schorderet, P., Carey, B.W., Beard, C., Wernig, M., Creyghton, M.P., Steine, E.J., Cassady, J.P., Foreman, R., et al. (2008). Direct reprogramming of terminally differentiated mature B lymphocytes to pluripotency. Cell *133*, 250–264.

Hara, A., Aoki, H., Taguchi, A., Niwa, M., Yamada, Y., Kunisada, T., and Mori, H. (2008). Neuron-like differentiation and selective ablation of undifferentiated embryonic stem cells containing suicide gene with Oct-4 promoter. Stem Cells Dev. *17*, 619–627.

Hochedlinger, K., and Jaenisch, R. (2002). Monoclonal mice generated by nuclear transfer from mature B and T donor cells. Nature *415*, 1035–1038.

Huang, C., and Kanagawa, O. (2001). Ordered and coordinated rearrangement of the TCR alpha locus: role of secondary rearrangement in thymic selection. J. Immunol. *166*, 2597–2601.

Ikawa, T., Hirose, S., Masuda, K., Kakugawa, K., Satoh, R., Shibano-Satoh, A., Kominami, R., Katsura, Y., and Kawamoto, H. (2010). An essential developmental checkpoint for production of the T cell lineage. Science *329*, 93–96.

Jameson, S.C., and Masopust, D. (2009). Diversity in T cell memory: an embarrassment of riches. Immunity *31*, 859–871.

June, C.H. (2007). Adoptive T cell therapy for cancer in the clinic. J. Clin. Invest. *117*, 1466–1476.

Kaneko, S., Mastaglio, S., Bondanza, A., Ponzoni, M., Sanvito, F., Aldrighetti, L., Radrizzani, M., La Seta-Catamancio, S., Provasi, E., Mondino, A., et al. (2009). IL-7 and IL-15 allow the generation of suicide gene-modified alloreactive self-renewing central memory human T lymphocytes. Blood *113*, 1006–1015.

Kawana-Tachikawa, A., Tomizawa, M., Nunoya, J., Shioda, T., Kato, A., Nakayama, E.E., Nakamura, T., Nagai, Y., and Iwamoto, A. (2002). An efficient and versatile mammalian viral vector system for major histocompatibility complex class I/peptide complexes. J. Virol. *76*, 11982–11988.

Khor, B., and Sleckman, B.P. (2002). Allelic exclusion at the TCRbeta locus. Curr. Opin. Immunol. *14*, 230–234.

Klebanoff, C.A., Gattinoni, L., and Restifo, N.P. (2006). CD8+ T-cell memory in tumor immunology and immunotherapy. Immunol. Rev. *211*, 214–224.

Kohn, D.B., Sadelain, M., and Glorioso, J.C. (2003). Occurrence of leukaemia following gene therapy of X-linked SCID. Nat. Rev. Cancer *3*, 477–488.

Koup, R.A., Safrit, J.T., Cao, Y., Andrews, C.A., McLeod, G., Borkowsky, W., Farthing, C., and Ho, D.D. (1994). Temporal association of cellular immune responses with the initial control of viremia in primary human immunodeficiency virus type 1 syndrome. J. Virol. *68*, 4650–4655.

Krangel, M.S. (2009). Mechanics of T cell receptor gene rearrangement. Curr. Opin. Immunol. *21*, 133–139.

Lafaille, J.J., DeCloux, A., Bonneville, M., Takagaki, Y., and Tonegawa, S. (1989). Junctional sequences of T cell receptor gamma delta genes: implications for gamma delta T cell lineages and for a novel intermediate of V-(D)-J joining. Cell *59*, 859–870.

Lefranc, M.P. (2003). IMGT databases, web resources and tools for immunoglobulin and T cell receptor sequence analysis, http://imgt.cines.fr. Leukemia *17*, 260–266.

Loh, Y.H., Hartung, O., Li, H., Guo, C., Sahalie, J.M., Manos, P.D., Urbach, A., Heffner, G.C., Grskovic, M., Vigneault, F., et al. (2010). Reprogramming of T cells from human peripheral blood. Cell Stem Cell *7*, 15–19.

Lu, P.H., and Negrin, R.S. (1994). A novel population of expanded human CD3+CD56+ cells derived from T cells with potent in vivo antitumor activity in mice with severe combined immunodeficiency. J. Immunol. *153*, 1687–1696.

MacLeod, M.K., Kappler, J.W., and Marrack, P. (2010). Memory CD4 T cells: generation, reactivation and re-assignment. Immunology *130*, 10–15.

Marion, R.M., Strati, K., Li, H., Tejera, A., Schoeftner, S., Ortega, S., Serrano, M., and Blasco, M.A. (2009). Telomeres acquire embryonic stem cell characteristics in induced pluripotent stem cells. Cell Stem Cell *4*, 141–154.

Monteiro, J., Batliwalla, F., Ostrer, H., and Gregersen, P.K. (1996). Shortened telomeres in clonally expanded CD28-CD8+ T cells imply a replicative history that is distinct from their CD28+CD8+ counterparts. J. Immunol. *156*, 3587–3590.

Morgan, R.A., Dudley, M.E., Wunderlich, J.R., Hughes, M.S., Yang, J.C., Sherry, R.M., Royal, R.E., Topalian, S.L., Kammula, U.S., Restifo, N.P., et al. (2006). Cancer regression in patients after transfer of genetically engineered lymphocytes. Science *314*, 126–129.

Neuber, K., Schmidt, S., and Mensch, A. (2003). Telomere length measurement and determination of immunosenescence-related markers (CD28, CD45RO, CD45RA, interferon-gamma and interleukin-4) in skin-homing T cells expressing the cutaneous lymphocyte antigen: indication of a non-ageing T-cell subset. Immunology *109*, 24–31.

Nishimura, K., Sano, M., Ohtaka, M., Furuta, B., Umemura, Y., Nakajima, Y., Ikehara, Y., Kobayashi, T., Segawa, H., Takayasu, S., et al. (2011). Development of defective and persistent Sendai virus vector: a unique gene delivery/expression system ideal for cell reprogramming. J. Biol. Chem. *286*, 4760–4771.

Padovan, E., Casorati, G., Dellabona, P., Meyer, S., Brockhaus, M., and Lanzavecchia, A. (1993). Expression of two T cell receptor alpha chains: dual receptor T cells. Science *262*, 422–424.

Petrie, H.T., Livak, F., Schatz, D.G., Strasser, A., Crispe, I.N., and Shortman, K. (1993). Multiple rearrangements in T cell receptor alpha chain genes maximize the production of useful thymocytes. J. Exp. Med. *178*, 615–622.

Phillips, R.E., Rowland-Jones, S., Nixon, D.F., Gotch, F.M., Edwards, J.P., Ogunlesi, A.O., Elvin, J.G., Rothbard, J.A., Bangham, C.R., Rizza, C.R., et al. (1991). Human immunodeficiency virus genetic variation that can escape cytotoxic T cell recognition. Nature *354*, 453–459.

Porter, D.L., Levine, B.L., Kalos, M., Bagg, A., and June, C.H. (2011). Chimeric antigen receptor-modified T cells in chronic lymphoid leukemia. N. Engl. J. Med. *365*, 725–733.

Prlic, M., Lefrancois, L., and Jameson, S.C. (2002). Multiple choices: regulation of memory CD8 T cell generation and homeostasis by interleukin (IL)-7 and IL-15. J. Exp. Med. *195*, F49–F52.

Romero, P., Zippelius, A., Kurth, I., Pittet, M.J., Touvrey, C., Iancu, E.M., Corthesy, P., Devevre, E., Speiser, D.E., and Rufer, N. (2007). Four functionally distinct populations of human effector-memory CD8+ T lymphocytes. J. Immunol. *178*, 4112–4119.

Rubio, V., Stuge, T.B., Singh, N., Betts, M.R., Weber, J.S., Roederer, M., and Lee, P.P. (2003). Ex vivo identification, isolation and analysis of tumor-cytolytic T cells. Nat. Med. *9*, 1377–1382.

Seki, T., Yuasa, S., Oda, M., Egashira, T., Yae, K., Kusumoto, D., Nakata, H., Tohyama, S., Hashimoto, H., Kodaira, M., et al. (2010). Generation of induced pluripotent stem cells from human terminally differentiated circulating T cells. Cell Stem Cell *7*, 11–14.

Serwold, T., Hochedlinger, K., Inlay, M.A., Jaenisch, R., and Weissman, I.L. (2007). Early TCR expression and aberrant T cell development in mice with endogenous prerearranged T cell receptor genes. J. Immunol. *179*, 928–938.

Serwold, T., Hochedlinger, K., Swindle, J., Hedgpeth, J., Jaenisch, R., and Weissman, I.L. (2010). T-cell receptor-driven lymphomagenesis in mice derived from a reprogrammed T cell. Proc. Natl. Acad. Sci. USA *107*, 18939–18943.

Staerk, J., Dawlaty, M.M., Gao, Q., Maetzel, D., Hanna, J., Sommer, C.A., Mostoslavsky, G., and Jaenisch, R. (2010). Reprogramming of human peripheral blood cells to induced pluripotent stem cells. Cell Stem Cell *7*, 20–24.

Takahashi, K., Tanabe, K., Ohnuki, M., Narita, M., Ichisaka, T., Tomoda, K., and Yamanaka, S. (2007). Induction of pluripotent stem cells from adult human fibroblasts by defined factors. Cell *131*, 861–872.

Takayama, N., Nishikii, H., Usui, J., Tsukui, H., Sawaguchi, A., Hiroyama, T., Eto, K., and Nakauchi, H. (2008). Generation of functional platelets from human embryonic stem cells in vitro via ES-sacs, VEGF-promoted structures that concentrate hematopoietic progenitors. Blood *111*, 5298–5306.

Takayama, N., Nishimura, S., Nakamura, S., Shimizu, T., Ohnishi, R., Endo, H., Yamaguchi, T., Otsu, M., Nishimura, K., Nakanishi, M., et al. (2010). Transient activation of c-MYC expression is critical for efficient platelet generation from human induced pluripotent stem cells. J. Exp. Med. *207*, 2817–2830.

Tan, J.T., Ernst, B., Kieper, W.C., LeRoy, E., Sprent, J., and Surh, C.D. (2002). Interleukin (IL)-15 and IL-7 jointly regulate homeostatic proliferation of memory phenotype CD8+ cells but are not required for memory phenotype CD4+ cells. J. Exp. Med. *195*, 1523–1532.

Timmermans, F., Velghe, I., Vanwalleghem, L., De Smedt, M., Van Coppernolle, S., Taghon, T., Moore, H.D., Leclercq, G., Langerak, A.W., Kerre, T., et al. (2009). Generation of T cells from human embryonic stem cell-derived hematopoietic zones. J. Immunol. *182*, 6879–6888.

Tsunetsugu-Yokota, Y., Morikawa, Y., Isogai, M., Kawana-Tachikawa, A., Odawara, T., Nakamura, T., Grassi, F., Autran, B., and Iwamoto, A. (2003). Yeast-derived human immunodeficiency virus type 1 p55(gag) virus-like particles activate dendritic cells (DCs) and induce perforin expression in Gag-specific CD8(+) T cells by cross-presentation of DCs. J. Virol. *77*, 10250–10259.

Turka, L.A., Schatz, D.G., Oettinger, M.A., Chun, J.J., Gorka, C., Lee, K., McCormack, W.T., and Thompson, C.B. (1991). Thymocyte expression of RAG-1 and RAG-2: termination by T cell receptor cross-linking. Science *253*, 778–781.

Turtle, C.J., Swanson, H.M., Fujii, N., Estey, E.H., and Riddell, S.R. (2009). A distinct subset of self-renewing human memory CD8+ T cells survives cytotoxic chemotherapy. Immunity *31*, 834–844.

van Dongen, J.J., Langerak, A.W., Brüggemann, M., Evans, P.A., Hummel, M., Lavender, F.L., Delabesse, E., Davi, F., Schuuring, E., García-Sanz, R., et al. (2003). Design and standardization of PCR primers and protocols for detection of clonal immunoglobulin and T-cell receptor gene recombinations in suspect lymphoproliferations: report of the BIOMED-2 Concerted Action BMH4-CT98-3936. Leukemia *17*, 2257–2317.

Veldwijk, M.R., Berlinghoff, S., Laufs, S., Hengge, U.R., Zeller, W.J., Wenz, F., and Fruehauf, S. (2004). Suicide gene therapy of sarcoma cell lines using recombinant adeno-associated virus 2 vectors. Cancer Gene Ther. *11*, 577–584.

Virgin, H.W., Wherry, E.J., and Ahmed, R. (2009). Redefining chronic viral infection. Cell *138*, 30–50.

Vodyanik, M.A., Bork, J.A., Thomson, J.A., and Slukvin, I.I. (2005). Human embryonic stem cell-derived CD34+ cells: efficient production in the coculture with OP9 stromal cells and analysis of lymphohematopoietic potential. Blood *105*, 617–626.

von Boehmer, H. (2004). Selection of the T-cell repertoire: receptor-controlled checkpoints in T-cell development. Adv. Immunol. *84*, 201–238.

Watarai, H., Rybouchkin, A., Hongo, N., Nagata, Y., Sakata, S., Sekine, E., Dashtsoodol, N., Tashiro, T., Fujii, S., Shimizu, K., et al. (2010). Generation of functional NKT cells in vitro from embryonic stem cells bearing rearranged invariant Valpha14-Jalpha18 TCRalpha gene. Blood *115*, 230–237.

Weng, N.P., Hathcock, K.S., and Hodes, R.J. (1998). Regulation of telomere length and telomerase in T and B cells: a mechanism for maintaining replicative potential. Immunity *9*, 151–157.

Wherry, E.J. (2011). T cell exhaustion. Nat. Immunol. *12*, 492–499.

Zhang, N., and Bevan, M.J. (2011). CD8(+) T cells: foot soldiers of the immune system. Immunity *35*, 161–168.

Cell Stem Cell
Short Article

Modeling Alzheimer's Disease with iPSCs Reveals Stress Phenotypes Associated with Intracellular Aβ and Differential Drug Responsiveness

Takayuki Kondo,[1,2,7] Masashi Asai,[7,9,10] Kayoko Tsukita,[1,7] Yumiko Kutoku,[11] Yutaka Ohsawa,[11] Yoshihide Sunada,[11] Keiko Imamura,[1] Naohiro Egawa,[1] Naoki Yahata,[1,7] Keisuke Okita,[1] Kazutoshi Takahashi,[1] Isao Asaka,[1] Takashi Aoi,[1] Akira Watanabe,[1] Kaori Watanabe,[7,10] Chie Kadoya,[7,10] Rie Nakano,[7,10] Dai Watanabe,[3] Kei Maruyama,[9] Osamu Hori,[12] Satoshi Hibino,[13] Tominari Choshi,[13] Tatsutoshi Nakahata,[1] Hiroyuki Hioki,[4] Takeshi Kaneko,[4] Motoko Naitoh,[5] Katsuhiro Yoshikawa,[5] Satoko Yamawaki,[5] Shigehiko Suzuki,[5] Ryuji Hata,[14] Shu-ichi Ueno,[15] Tsuneyoshi Seki,[16] Kazuhiro Kobayashi,[16] Tatsushi Toda,[16] Kazuma Murakami,[6] Kazuhiro Irie,[6] William L. Klein,[17] Hiroshi Mori,[18] Takashi Asada,[19] Ryosuke Takahashi,[2] Nobuhisa Iwata,[7,10,*] Shinya Yamanaka,[1,8] and Haruhisa Inoue[1,7,8,*]
[1]Center for iPS Cell Research and Application (CiRA)
[2]Department of Neurology, Graduate School of Medicine
[3]Department of Biological Sciences, Graduate School of Medicine and Department of Molecular and Systems Biology, Graduate School of Biostudies
[4]Department of Morphological Brain Science, Graduate School of Medicine
[5]Department of Plastic and Reconstructive Surgery, Graduate School of Medicine
[6]Organic Chemistry in Life Science, Division of Food Science and Biotechnology, Graduate School of Agriculture
Kyoto University, Kyoto 606-8507, Japan
[7]Core Research for Evolutional Science and Technology (CREST)
[8]Yamanaka iPS Cell Special Project
Japan Science and Technology Agency (JST), Saitama 332-0012, Japan
[9]Department of Pharmacology, Faculty of Medicine, Saitama Medical University, Saitama 350-0495, Japan
[10]Laboratory of Molecular Biology and Biotechnology, Department of Molecular Medicinal Sciences, Graduate School of Biomedical Sciences, Nagasaki University, Nagasaki 852-8521, Japan
[11]Department of Neurology, Kawasaki Medical School, Okayama 701-0192, Japan
[12]Department of Neuroanatomy (Biotargeting), Kanazawa University Graduate School of Medical Sciences, Ishikawa 920-8640, Japan
[13]Faculty of Pharmacy and Pharmaceutical Sciences, Fukuyama University, Hiroshima 729–0292, Japan
[14]Department of Functional Histology
[15]Department of Psychiatry
Ehime University Graduate School of Medicine, Ehime 791-0295, Japan
[16]Division of Neurology/Molecular Brain Science, Kobe University Graduate School of Medicine, Kobe, Hyogo 650-0017, Japan
[17]Department of Neurobiology, Northwestern University, Evanston, IL 60208, USA
[18]Department of Neuroscience, Graduate School of Medicine, Osaka City University, Osaka 545-8585, Japan
[19]Department of Neuropsychiatry, Institute of Clinical Medicine, University of Tsukuba, Ibaraki 305-8577, Japan
*Correspondence: haruhisa@cira.kyoto-u.ac.jp (H.I.), iwata-n@nagasaki-u.ac.jp (N.I.)
http://dx.doi.org/10.1016/j.stem.2013.01.009

SUMMARY

Oligomeric forms of amyloid-β peptide (Aβ) are thought to play a pivotal role in the pathogenesis of Alzheimer's disease (AD), but the mechanism involved is still unclear. Here, we generated induced pluripotent stem cells (iPSCs) from familial and sporadic AD patients and differentiated them into neural cells. Aβ oligomers accumulated in iPSC-derived neurons and astrocytes in cells from patients with a familial amyloid precursor protein (APP)-E693Δ mutation and sporadic AD, leading to endoplasmic reticulum (ER) and oxidative stress. The accumulated Aβ oligomers were not proteolytically resistant, and docosahexaenoic acid (DHA) treatment alleviated the stress responses in the AD neural cells. Differential manifestation of ER stress and DHA responsiveness may help explain variable clinical results obtained with the use of DHA treatment and suggests that DHA may in fact be effective for a subset of patients. It also illustrates how patient-specific iPSCs can be useful for analyzing AD pathogenesis and evaluating drugs.

INTRODUCTION

Alzheimer's disease (AD) is the most prevalent neurodegenerative disorder. One of the pathological features of AD is the oligomerization and aggregation and accumulation of amyloid-β peptide (Aβ), forming amyloid plaques in the brain. Cognitive impairment observed in clinical AD is inversely well correlated with the amount of Aβ oligomers in the soluble fraction rather than the amount of Aβ fibrils (amyloid plaques) constituting the oligomers (Haass and Selkoe, 2007; Krafft and Klein, 2010). Increasing evidence has shown that Aβ oligomers extracted from AD model mice or made from synthetic peptides cause

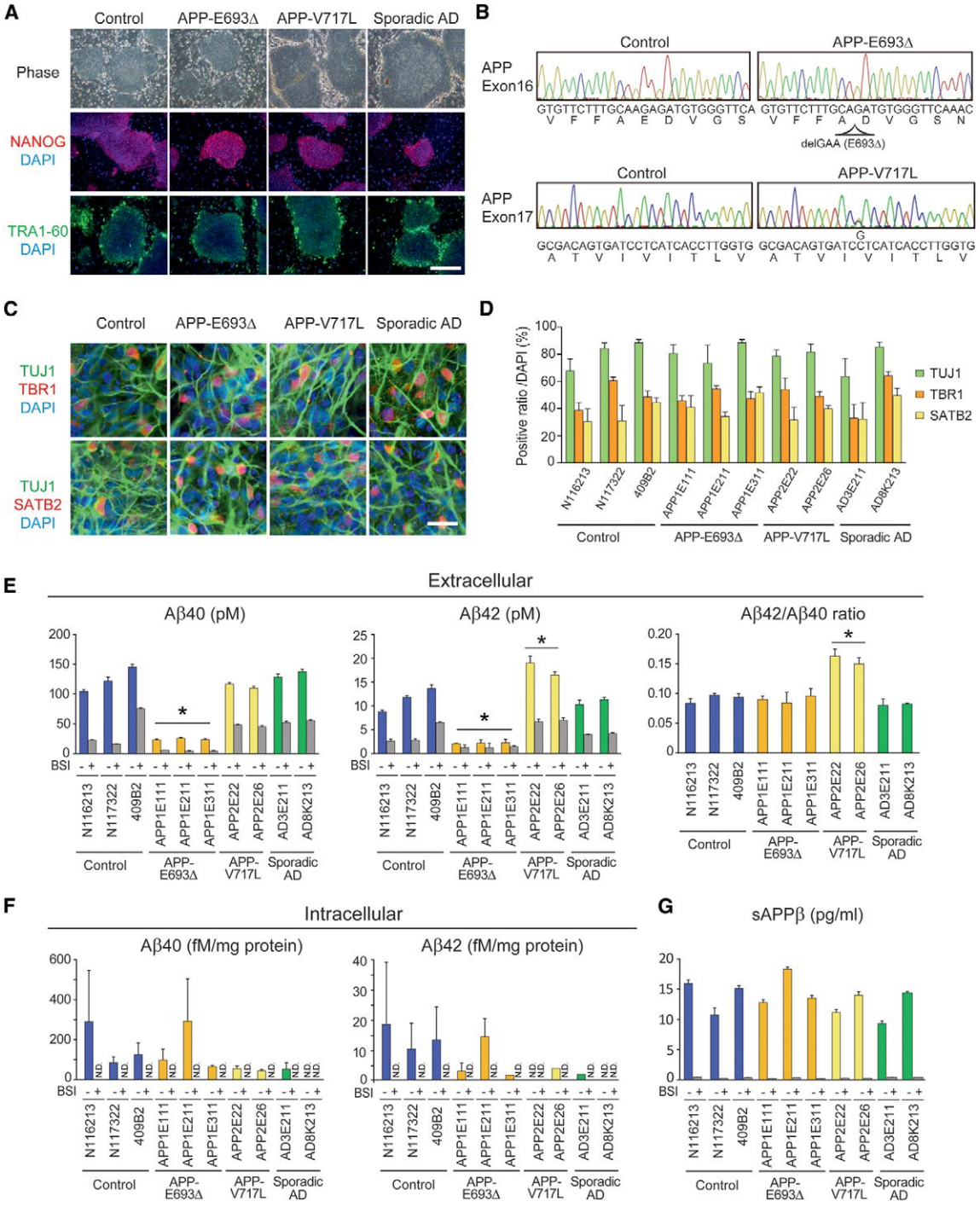

Figure 1. Establishment of Control and AD Patient-Specific iPSCs, and Derivation of Cortical Neurons Producing Aβs from iPSCs

(A) Established iPSCs from both controls and AD patients showed embryonic stem cell-like morphology (Phase) and expressed pluripotent stem cell markers NANOG (red) and TRA1-60 (green). The scale bar represents 200 μm.

(B) Genomic DNA sequences showed the presence of the homozygous genotype for E693 deletion and the heterozygous genotype for V717L mutation on the *APP* gene only in AD iPSCs.

(C) Estimation of neuronal differentiation from control and AD-iPSCs. After 2 months of differentiation, neurons were immunostained with antibodies against the neuronal marker TUJ1 and the cortical neuron markers TBR1 and SATB2. The scale bar represents 30 μm.

(D) Proportions of TUJ1-, TBR1-, and SATB2-positive cells in control and AD-iPSCs. Data represent mean ± SD (n = 3 per clone).

(E) Aβ40 and Aβ42 secreted from iPSC-derived neural cells into the medium (extracellular Aβ) were measured at 48 hr after the last medium change. Data represent mean ± SD (n = 3 per clone). Levels of Aβ40 and Aβ42 in AD(APP-E693Δ) without β-secretase inhibitor IV (BSI, 1 μM) were significantly lower than those of the others (*, $p < 0.006$), and the level of Aβ42 and the ratio of Aβ42/Aβ40 in AD(APP-V717L) without BSI were significantly higher than those of the others

(legend continued on next page)

neurotoxicity and cognitive impairments in vitro and in vivo (Walsh et al., 2002; Gong et al., 2003; Lesné et al., 2006), and this was also true in humans (Kuo et al., 1996; Shankar et al., 2008; Noguchi et al., 2009). Therefore, the formation and accumulation of Aβ oligomers has been presumed to play a central role in the pathogenesis and clinical symptoms of AD. Aβs are composed of 38–43 amino acid residues and are generated from the amyloid precursor protein (APP) by β- and γ-secretase-mediated sequential cleavages. A number of mutations linked to familial AD in the *APP* gene have been identified. Recently, an atypical early-onset familial AD, caused by an E693Δ mutation of an APP-producing variant Aβ lacking 22nd Glu was discovered in Japan (Tomiyama et al., 2008). This APP-E693Δ mutation presents rare, autosomal-recessive mutations of the *APP* gene related to familial AD. Patients with the mutation show overt early-onset symptoms of AD but lack Aβ deposition, according to positron emission tomography (PET) scan analysis with a [^{11}C] Pittsburgh compound-B (PIB) radioprobe (Tomiyama et al., 2008; Shimada et al., 2011). The 22nd Glu within the Aβ sequence has a destabilizing effect on the formation of oligomeric structures because of the electrostatic repulsion between the adjacent side chain of 22nd Glu (Kassler et al., 2010), and the deletion of the amino acid residue leads to the ready formation of Aβ oligomers in vitro (Nishitsuji et al., 2009). APP-E693Δ transgenic mice show AD-like pathology, including intracellular oligomer accumulation, but lack extracellular amyloid plaque formation (Tomiyama et al., 2010). However, it remains unclear whether Aβ oligomers are accumulated in familial and sporadic AD patient neural cells and how intracellular Aβ oligomers play a pathological role. The compound and/or drugs that might rescue the Aβ oligomer-induced pathological phenotypes are also unclear. Recent developments in induced pluripotent stem cell (iPSC) technology have facilitated the investigation of phenotypes of patient neural cells in vitro and have helped to overcome the lack of success in modeling sporadic AD.

Here, we report the derivation and neuronal and astroglial differentiation of iPSCs from a familial AD patient with an APP-E693Δ mutation, a familial case with another APP mutation, as well as other sporadic cases. Using patient neurons and astrocytes, we addressed the accumulation and possible pathological roles of intracellular Aβ oligomers in familial and sporadic AD. We found that Aβ oligomers were not proteolytically resistant and that docosahexaenoic acid (DHA) treatment attenuated cellular phenotypes of AD neural cells with intracellular Aβ oligomers in both familial and sporadic AD patients.

RESULTS

iPSC Generation and Cortical-Neuronal Differentiation

Dermal fibroblasts were reprogrammed by episomal vectors (Okita et al., 2011). Control iPSC lines from three unrelated individuals, three and two familial AD iPSC lines from patients with E693Δ[AD(APP-E693Δ)] and V717L[AD(APP-V717L)] APP mutations, respectively, and two sporadic iPSC lines (AD3E211 and AD8K213) from two unrelated patients (Figure S1A available online) were generated (Figures 1A, 1B, and S1B–S1H). To characterize cortical neurons derived from the iPSC lines, we established differentiation methods for cortical neurons by modifying previous procedures (Morizane et al., 2011) (Figure S1I). The differentiated cells expressed the cortical neuron subtype markers SATB2 and TBR1 (Figure 1C), and the differentiated neurons were functionally active (Figures S1J and S1K). There was no prominent difference in the differentiation propensity between control and AD neurons (Figures 1D and S1L).

We analyzed the amounts of extra- and intracellular Aβ40 and Aβ42 (Figures 1E and 1F). As expected, both Aβ species were strongly decreased in all cloned AD(APP-E693Δ) neural cells in comparison to those in control neural cells. In familial AD(APP-V717L) neural cells, an increase in the extracellular Aβ42 level and a corresponding decrease in the intracellular Aβ42 level were observed, and the Aβ42/Aβ40 ratio in the culture medium was increased up to 1.5-fold, suggesting that the abnormality of APP metabolism in AD is dependent on the mutation sites in *APP*. Extracellular Aβ levels in sporadic AD neural cells were not changed in comparison to those in control neural cells, but intracellular Aβ in sporadic AD8K213 neural cells apparently decreased (that is, below the detection limit). APP expression levels in the AD(APP-E693Δ) neural cells were lower than in the others, but the levels of α- and β-secretase-mediated APP processing remained unaltered in all neural cells (Figures 1G, S1M, and S1N). Soluble APPβ production was strongly inhibited by treatment with β-secretase inhibitor IV (BSI) (Figure 1G). Aβ levels in the original fibroblasts and iPSC-derived astrocytes, in which APP expression levels were relatively higher than those in neural cells (data not shown), were lower than those of the corresponding neural cells (Figures S1O and S1P).

Intracellular Accumulation of Aβ Oligomers in AD(APP-E693Δ) and in One of the Sporadic AD Neural Cells

Using an immunocytochemical method with the Aβ-oligomer-specific antibody NU1 (Lambert et al., 2007), we investigated whether AD(APP-E693Δ) neural cells harbor Aβ oligomers or not. We found that Aβ oligomers were accumulated as puncta in the neurons of AD(APP-E693Δ) and in one of the sporadic AD cases (Figure 2A). The area of Aβ-oligomer-positive puncta was significantly increased in AD(APP-E693Δ) neuronal cells relative to control neuronal cells (Figure 2B). Dot blot analysis using cell lysates revealed that Aβ oligomers were markedly elevated in the AD(APP-E693Δ) and sporadic AD8K213 neural cells (Figures 2C and 2D), whereas Aβ oligomers were not detected in the culture medium (data not shown). Another antibody against Aβ, 11A1, which detects low-molecular-weight oligomers rather than the Aβ monomer (Murakami et al., 2010), showed results similar to those observed with NU1 (Figures

(*, $p < 0.001$). There are significant differences between dimethyl sulfoxide (DMSO)-control and BSI treatment in each case (*, $p < 0.001$) except that of AD(APP-E693Δ) for Aβ42.
(F) Aβ40 and Aβ42 in cell lysates (intracellular Aβ). N.D., not detected. Data represent mean ± SD (n = 3 per clone).
(G) The amount of soluble APPβ was not altered in control and AD. Data represent mean ± SD (n = 3 per clone).
See also Figure S1.

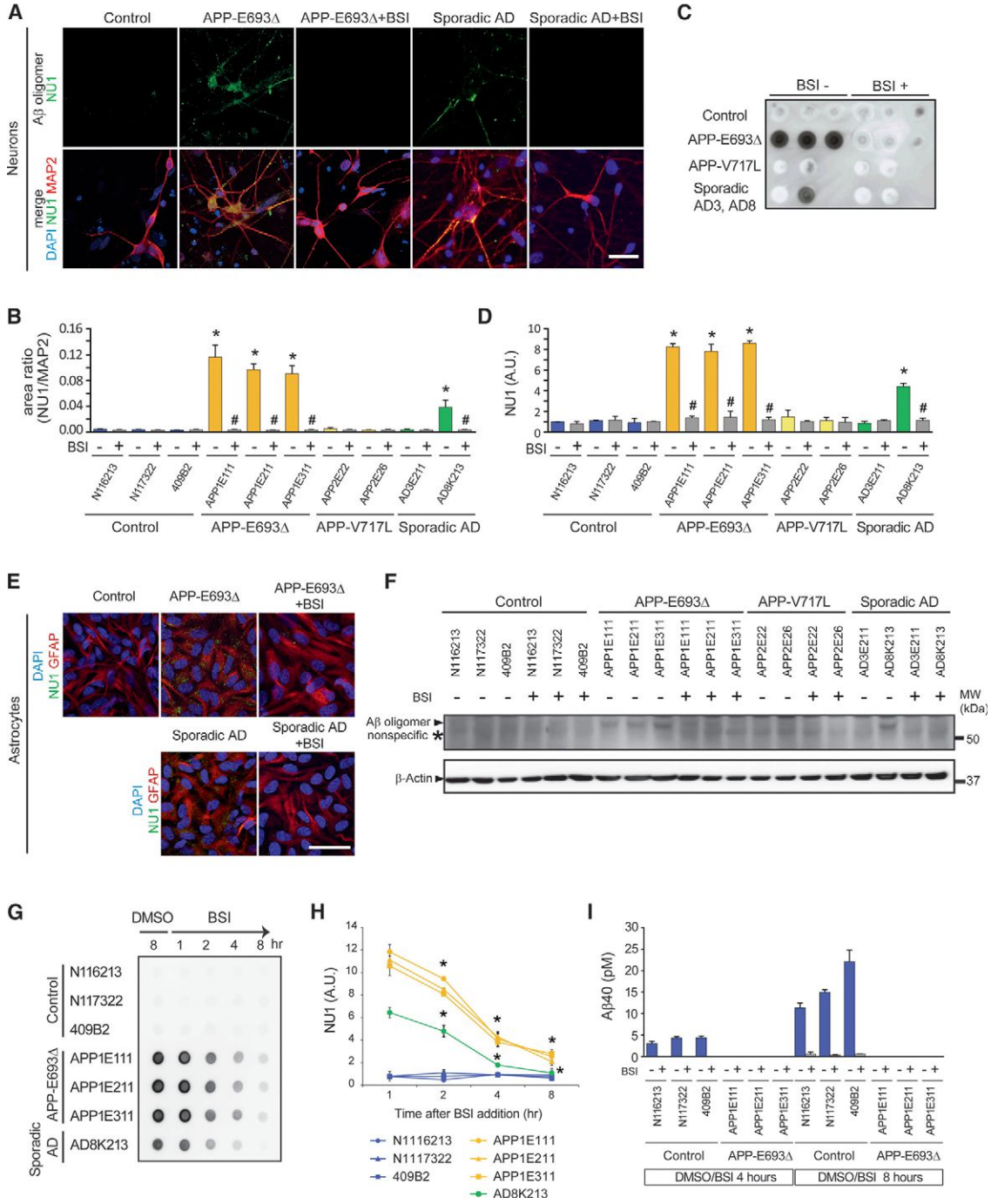

Figure 2. Familial AD(APP-E693Δ) and Sporadic AD iPSC-Derived Neurons Have Intracellular Aβ Oligomers

(A) Intracellular Aβ oligomer accumulation in iPSC-derived neurons (red, MAP2-positive cells) was detected by the Aβ-oligomer-specific monoclonal antibody NU1 (green) with a punctate pattern. Aβ oligomer accumulation was massive in AD(APP-E693Δ) and sporadic AD(AD8K213) neurons but only faint in control neurons. Treatment with 1 μM BSI decreased Aβ oligomer accumulation. DAPI, nuclear staining (blue). The scale bar represents 30 μm.

(B) Quantification of Aβ oligomer accumulation in (A); the ratio of the NU1-positive area in the MAP2-positive area was analyzed. Data represent mean ± SD (n = 3 per clone). Aβ oligomer levels in the AD(APP-E693Δ) and sporadic AD(AD8K213) neural cells without BSI were significantly different from those of other neural cells (*, $p < 0.005$) and from corresponding neural cells with BSI (#, $p < 0.005$).

(C) Dot blot analysis with the use of NU1 antibody. Control (N116213, N117322, 409B2), APP-E693Δ(APP1E111, APP1E211, APP1E211), APP-V717L (APP2E22, APP2E26), and sporadic AD (AD3E211, AD8K213) neural cells were dotted from the left. Blank is RIPA buffer only.

(D) Signals of blot in (C) were quantified. Data represent mean ± SD (n = 3 per clone). Aβ oligomer levels in AD(APP-E693Δ) and sporadic AD(AD8K213) neurons without BSI were significantly different from those of other neurons (*, $p < 0.001$) and from corresponding neurons treated with 1 μM BSI (#, $p < 0.001$).

(E) Aβ oligomer accumulation in AD astrocytes. The scale bar represents 30 μm.

(legend continued on next page)

S2A–S2D). However, Aβ oligomers were not detected in cell lysates from the fibroblasts that generate iPSC lines (Figure S2E). To confirm whether Aβ oligomers were derived from mutant APP(E693Δ), we transduced a lentiviral vector driven by an EF1α promoter to overexpress wild or mutant APP(E693Δ) in control iPSC-derived neural cells and found that Aβ oligomers emerged inside control neural cells overexpressing mutant APP(E693Δ) (Figure S2F).

To investigate the intracellular accumulation of Aβ oligomers in astrocytes derived from control and AD iPSCs, we established an astrocyte-enrichment culture by modifying the method previously reported (Krencik et al., 2011) (Figures S2G–S2J). Dot blot analysis using Aβ oligomer antibodies revealed that the astrocytes of AD(APP-E693Δ) and one of the sporadic AD iPSCs accumulated Aβ oligomers intracellularly (Figures 2E, S2K, and S2L), which was compatible with the results of neurons. On the other hand, we detected no difference in the uptake of extracellular glutamate between control and AD astrocytes (Figure S2M).

Aβ oligomers were also detected as a protein band with a molecular mass of 50∼60 kDa by western blot analysis (Figures 2F and S2N). The accumulation of Aβ oligomers was inhibited by treatment with BSI (Figures 2A–2G, S2A–S2D, and S2N). To clarify whether the E693Δ mutation results in accelerated Aβ oligomerization and/or in a proteolytically resistant and stable form of Aβ oligomers, we analyzed the levels of Aβ oligomers over a course of time after BSI treatment. Intracellular Aβ oligomers started to disappear from 2 hr after the treatment with BSI, almost reaching the control level by 8 hr (Figures 2G and 2H). Secretion of Aβ40 from control neural cells was already inhibited at 2 hr after BSI treatment, but the secretion from AD neural cells was under the detection limit in both the presence and absence of BSI (Figure 2I).

Cellular Stress Responses Caused By Intracellular Aβ Oligomers in AD iPSC-Derived Neural Cells

Extracellular Aβ deposition in patient brains carrying APP with an E693Δ mutation is predicted to be extremely low, as amyloid PET imaging with a [^{11}C] PIB probe revealed a far lower signal in the patients than those observed in sporadic AD brains (Tomiyama et al., 2008). Given that processing by β- and γ-secretases largely proceeds within vesicular endosomal compartments, it was possible that Aβ oligomers were associated with specific organelles. We characterized the Aβ oligomer-positive punctate structures in AD(APP-E693Δ) neural cells and astrocytes by coimmunostaining with antibodies for markers of vesicular compartments and subcellular organelles. Subpopulations of Aβ oligomer-positive puncta in the AD neurons showed positive immunostaining for an endoplasmic reticulum (ER) marker, binding immunoglobulin protein (BiP); an early endosomal marker, early endosome-associated antigen-1 (EEA1); and a lysosomal marker, lysosomal-associated marker protein 2 (LAMP2) (data not shown).

To uncover molecules that might be implicated in the dysfunction of AD(APP-E693Δ) neural cells, we analyzed gene expression profiles of control and AD neural cells (Figure 3A and Table S1). Gene ontology analysis revealed that oxidative-stress-related categories, including peroxiredoxin, oxidoreductase, and peroxidase activities, were upregulated in the AD, whereas glycosylation-related categories were downregulated (Figures 3B and 3C and Table S1), suggesting that ER and Golgi function might be perturbed in AD neural cells. Western blot analysis clarified that the amounts of both BiP and cleaved caspase-4 were elevated in the neurons and astrocytes of the AD(APP-E693Δ) case, and that of BiP in one of the sporadic AD cases, AD8K213, but not in fibroblasts (Figures 3D–3F and S3A–S3F). We also found that BSI treatment not only prevented the increase in Aβ oligomer-positive puncta area per cell in the context of AD(APP-E693Δ) lines but also decreased the amount of BiP and cleaved caspase-4 (Figures 3D–3F). *PRDX4*-coding antioxidant protein peroxiredoxin-4 was the most highly upregulated gene (Figure 3C). Western blot analysis confirmed that the amount of peroxiredoxin-4 was increased up to approximately 5- to 7-fold in lysates from AD(APP-E693Δ) and in one of the sporadic AD cases, AD8K213 neural cells, but not in fibroblasts, and was decreased by the BSI treatment (Figures 3D, 3G, S3A, S3D, S3G, and S3H), indicating that the antioxidant stress response was provoked by Aβ oligomer formation in AD(APP-E693Δ) and sporadic AD8K213. To identify pathogenic species evoking oxidative stress in AD(APP-E693Δ), we visualized reactive oxygen species (ROS) and found that ROS was increased in both neurons and astrocytes in AD(APP-E693Δ) and AD8K213 (Figures 3H–3J and S3I –S3L). This increase was counteracted by the BSI treatment. These results indicated that intracellular Aβ oligomers provoked both ER and oxidative stress, and the increase in ROS most likely occurred via a vicious cycle between ER and oxidative stress (Malhotra and Kaufman, 2007).

Alleviation of Intracellular Aβ Oligomer-Induced Cellular Stress by DHA

We evaluated BSI and three additional drugs that had been reported to improve ER stress or to inhibit ROS generation: (1) DHA (Begum et al., 2012), (2) dibenzoylmethane (DBM14-26) (Takano et al., 2007), and (3) NSC23766 (Lee et al., 2002) (Figures 4 and S4). DHA treatment significantly decreased the protein level of BiP, cleaved caspase-4, and peroxiredoxin-4 in AD (APP-E693Δ) neural cells (Figures 4A, 4B, S4A, and S4B), and BiP and peroxiredoxin-4 in sporadic AD8K213 (Figures S4C and S4D). Furthermore, DHA treatment also decreased the generation of ROS in AD(APP-E693Δ) neural cells (Figures 4C and 4D), whereas the amount of Aβ oligomers in cell lysates

(F) Western blot analysis of control and AD neural cells in the presence or absence of BSI. BSI treatment (1 μM) disappeared 6E10-positive ≈55 kDa protein bands in cell lysates of AD(APP-E693Δ) and sporadic AD(AD8K213) neural cells.
(G) Disappearance of Aβ oligomers after BSI treatment was analyzed by dot blot analysis with the use of the NU1 antibody. Intracellular Aβ oligomers started to disappear 2 hr after BSI treatment.
(H) Signals of blots in (G) were quantified. Data represent mean ± SD (n = 3 per clone). BSI treatment (1 μM) decreased intracellular Aβ in AD neural cells and was reduced to 16∼23% of vehicle control by 8 hr. Post hoc analysis revealed that the amounts of Aβ oligomers at 2 hr after BSI treatment were significantly decreased in comparison to those of DMSO control oligomers (*, $p < 0.005$).
(I) Changes in extracellular Aβ40 levels were analyzed in the experimental condition of (G). Data represent mean ± SD (n = 3 per clone).
See also Figure S2.

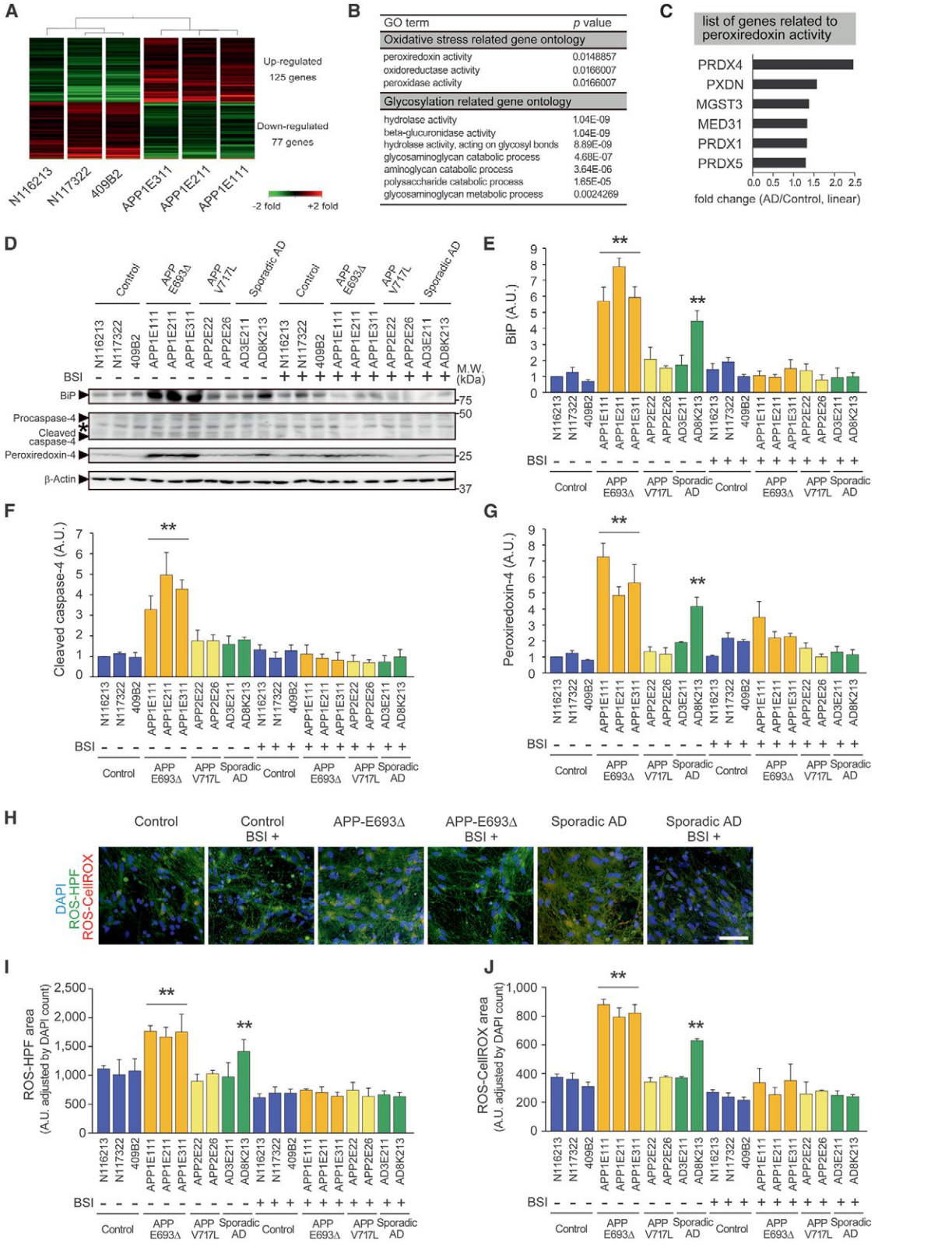

Figure 3. Cellular Stress Responses Caused by Intracellular Aβ Oligomers in Familial AD(APP-E693Δ) and Sporadic AD(AD8K213) iPSC-Derived Neural Cells

(A) Hierarchical clustering analysis of differentiated neuronal cells and a heatmap of significantly up- and downregulated genes in AD neural cells. The statistically significant cutoff p value is < 0.05.

(legend continued on next page)

was not altered (Figures S4E–S4G). In contrast, the high concentration of DHA, DBM14-26, or NSC23766 treatment increased the protein level of BiP (Figure S4B). Finally, to confirm the protective effects of DHA in short-term screening, we analyzed the effect on the survival of AD(APP-E693Δ) neural cells. Neuronal cells were labeled with a lentiviral vector expressing synapsin I-promoter-driven EGFP and cultivated in the medium depleted of neurotrophic factors and neural culture supplements mix. The real-time survival rate of AD(APP-E693Δ) neurons was lower than that of normal control neurons; however, DHA treatment for 16 days partially rescued AD(APP-E693Δ) cell viability (Figures 4E–4G). The real-time survival rate of sporadic AD(AD3E211, AD8K213) neurons for 16 days was unchanged (Figures 4E and 4F and Table S2). We confirmed these results through a lactate dehydrogenase (LDH) assay (Figure 4G). The AD(APP-E693Δ) neurons were also vulnerable to oxidative stress by hydrogen peroxide treatment (Figure S4H). Extracellular Aβ levels were not altered in the assay (Figure 4H).

DISCUSSION

The present study shows that neural cells derived from a patient carrying the pathogenic APP-E693Δ mutation and a sporadic AD patient produce intracellular Aβ oligomers, and the use of these neural cells provided an experimental system for addressing whether such oligomers would cause cellular stress and the killing of neurons and how such intracellular Aβ oligomers might contribute to the disease pathogenesis, despite only one patient carrying the E693Δ mutation being available. Our findings also suggest that the possible heterogeneity of familial and sporadic AD stems from phenotypic differences of intracellular Aβ oligomers and suggests the possibility that DHA, a drug that failed in some clinical trials of AD treatment, might be effective in a portion of AD patients.

We demonstrated that Aβ oligomers were formed and accumulated inside AD(APP-E693Δ) and sporadic AD(AD8K213) neurons by immunostaining (Figures 2A and 2B), dot blot analysis (Figures 2C and 2D), and western blot analysis (Figures 2F and S2N). In addition, intracellular accumulation of Aβ oligomers, which has been supposed to be proteolytically resistant, disappeared after treatment with BSI in both AD neurons (Figures 2G and 2H), indicating that AD(APP-E693Δ) and sporadic AD(AD8K213) neurons still seemed to retain a degrading activity toward Aβ oligomers in which proteasomes, autophagosomes, and/or lysosomes may be involved and, thereby, that the pathological property of Aβ oligomers in a part of AD might be completely abrogated. The sporadic AD(AD8K213) neurons may retain a specific cellular environment that permits the formation of Aβ oligomers. Additional studies aimed at identifying the factors causing such an environment are needed.

We observed that the accumulation of Aβ oligomers induced ER and oxidative stress both in AD(APP-E693Δ) and in sporadic AD(AD8K213) neurons, although caspase-4 activation appeared not to accompany sporadic AD, probably because of the lesser extent of ER stress in comparison to AD(APP-E693Δ). Previously, Nishitsuji et al. (2009) reported that accumulated Aβ oligomers in ER provoke ER stress. This result suggests that oligomers represent a self-aggregating state of Aβ. During this process, Aβ generates ROS, which is supported by the fact that Aβ coordinates the metal ions zinc, iron, and copper, which induce the oligomerization of Aβ. Iron and copper then cause the generation of toxic ROS and calcium dysregulation (Barnham et al., 2004), leading to membrane lipid peroxidation and the impairment of the function of a range of membrane-associated proteins (Hensley et al., 1994; Butterfield, 2003), antioxidant factors being thought to protect ER-stress-induced cellular toxicities (Malhotra and Kaufman, 2007).

We found that intracellular Aβ oligomers were accumulated not only in a case of familial AD with APP-E693Δ mutation but also in a sporadic AD case, although only three clones derived from one familial AD patient carrying an APP-E693Δ mutation and two clones from two sporadic AD patients were analyzed in this study because of the limited number of patients. In contrast, in familial AD with the APP-V717L mutation, of which only one case was available, intracellular Aβ oligomers were not detected, but the extracellular Aβ42/Aβ40 ratio, which is increased in mutant presenilin-mediated familial AD, as reported previously (Yagi et al., 2011), was increased, lending support to the notion that AD could be classified into two categories: extracellular Aβ type and intracellular Aβ type. Although it has been supposed that environmental factors and/or the aging process contribute to neurodegenerative diseases, our findings support the idea that a genetic factor might play a role in a part of sporadic AD, a finding that is compatible with a previous report (Israel et al., 2012). However, identifying the genetic factor would require a larger sample size. The sporadic AD case with intracellular Aβ oligomers might correspond to the case without extracellular Aβ40 elevation of Israel et al. (2012). Analysis of neurons

(B) The gene ontology (GO) term list, calculated from the significantly altered gene expression patterns in the microarray analysis of AD versus control neural cells.
(C) Altered expression levels of genes related to peroxidation activity detected by GO analysis. All values were significantly different from that of the control ($p < 0.05$).
(D–G) Western blot analysis of ER stress markers (BiP and casapase-4), peroxiredoxin-4, and a reference protein (β-actin) in the presence or absence of BSI. (E–G) Densitometric analysis of (D) are shown. Measured values of proteins were normalized by β-actin. Data represent mean ± SD (n = 3 per clone). Levels of BiP (E), cleaved caspase-4 (F), and peroxiredoxin-4 (G) in AD(APP-E693Δ) and sporadic AD(AD8K213) neural cells without BSI were significantly different from those of the other neural cells (**, $p < 0.005$).
(H) Typical images of reactive oxygen species (ROS) staining, detected by HPF or CellROX, in control and AD neural cells with or without BSI treatment. Scale bars represent 30 μm.
(I and J) Quantitative data of (H), ROS-HPF (I), and ROS-CellROX (J). Each value was shown as a ratio of the HPF-stained or CellROX area (average of random 25 fields per sample) adjusted with DAPI counts. Data represent mean ± SD (n = 3 per clone). ROS-generation levels in AD(APP-E693Δ) and sporadic AD(AD8K213) neural cells were significantly different from those of the others (**, $p < 0.001$). Data represent mean ± SD (n = 3 per clone).
See also Figure S3 and Table S1.

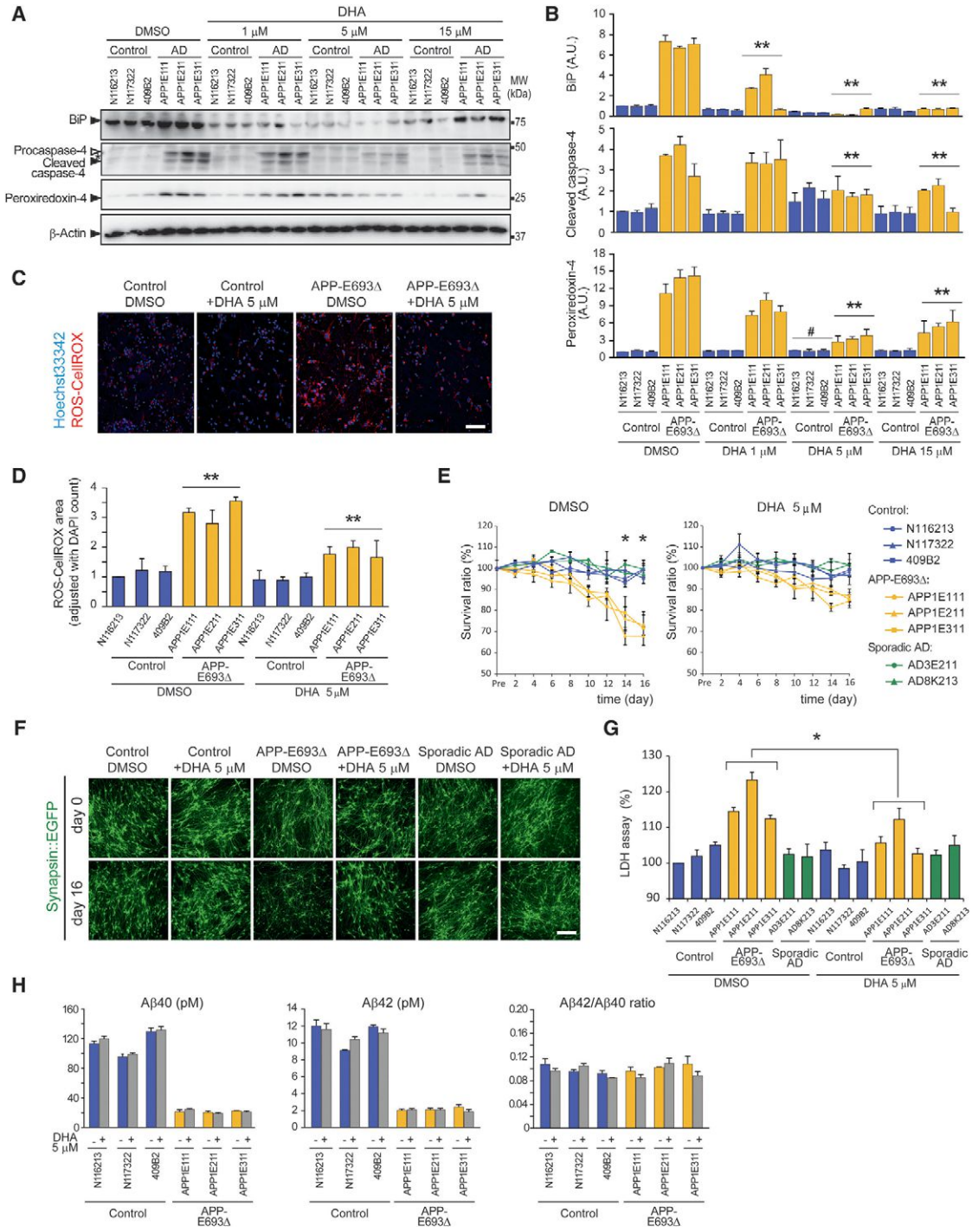

Figure 4. DHA-Alleviated Cellular Stress Caused By Intracellular Aβ Oligomers

(A) Control and AD(APP-E693Δ) neural cells at day 72 were treated with DHA for 48 hr. Then, cells were lysed and subjected to immunoblot analysis (1 μM, 5 μM, and 15 μM of docosahexaenoic acid [DHA]).

(B) Densitometric analysis of (A) is shown. Measured values were normalized by that of β-actin. Data represent mean ± SD (n = 3 per clone). Two-way analysis of variance (ANOVA) showed significant main effects of DHA treatment (BIP, $F_{[3,64]} = 136.712$, $p < 0.001$; cleaved caspase-4, $F_{[3,64]} = 50.855$, $p < 0.001$) with a significant interaction between APP mutation and DHA treatment (BIP, $F_{[3,64]} = 99.658$, $p < 0.001$; cleaved caspase-4, $F_{[3,64]} = 53.005$, $p < 0.001$). Post hoc analysis revealed significant differences between DMSO (control) and DHA treatment (1, 5, and 15 μM) in AD(APP-E693Δ) neural cells (**, $p < 0.001$). Two-way ANOVA for peroxiredoxin-4 showed significant main effects of DHA treatment ($F_{[3,64]} = 16.995$; $p < 0.001$) with a significant interaction between APP mutation and DHA treatment ($F_{[3,64]} = 32.093$; $p < 0.001$). Post hoc analysis revealed significant differences between DMSO-control and DHA treatment (5 and 15 μM) in AD(APP-E693Δ) neural cells (**, $p < 0.001$). In control neural cells, the 5 μM DHA group was significantly different from the other groups (#, $p < 0.005$).

(C) Typical images of ROS-CellROX and Hoechst33342 signals after treatment with vehicle or 5 μM DHA. The scale bar represents 50 μm.

(legend continued on next page)

and astrocytes, as we performed here, from larger numbers of patients might result in the classification of sporadic AD.

To date, the clinical effectiveness of DHA treatment is still controversial (Freund-Levi et al., 2006; Quinn et al., 2010). It is of particular interest that one of two sporadic AD neurons accumulated intracellular Aβ oligomers and showed cellular phenotypes that could respond to DHA but the other did not, and this result may explain why DHA treatment was effective for some AD patients, those with the intracellular Aβ oligomer-associated type of AD, although the timing (that is, the stage of disease development) for starting the treatment would be another critical factor. These results may suggest that patient-specific iPSCs provide a chance to re-evaluate the effect of a drug that failed in AD clinical trials, depending on the selection of the patient type. In the present study, the amount of Aβ oligomers in our culture was not affected by DHA, although it would be effective for reducing cellular stresses, and reducing the oligomerization of Aβ was also presumed to be a candidate mechanism of DHA treatment (Cole and Frautschy, 2006). These results indicate that therapy with DHA would alleviate symptoms. Furthermore, the data showing that BSI treatment leads to a reduction in ROS formation at a relatively similar level (Figure 2G) in both AD and control cells might indicate an Aβ oligomer-independent effect, in addition to an Aβ oligomer-dependent effect, of BSI.

In any event, patient-specific iPSCs would provide disease pathogenesis, irrespective of the disease being in a familial or sporadic form, as well as enable the evaluation of drug and patient classification of AD.

EXPERIMENTAL PROCEDURES

Derivation of Patient-Specific Fibroblasts

Control and AD-derived human dermal fibroblasts (HDFs) were generated from explants of 3 mm dermal biopsies. After 1–2 weeks, fibroblast outgrowths from the explants were passaged.

iPSC Generation

Human complementary DNAs for reprogramming factors were transduced in HDFs with episomal vectors (*SOX2, KLF4, OCT4, L-MYC, LIN28*, and small hairpin RNA for p53). Several days after transduction, fibroblasts were harvested and replated on an SNL feeder cell layer. On the following day, the medium was changed to a primate embryonic stem cell medium (ReproCELL, Japan) supplemented with 4 ng/ml basic FGF (Wako Pure Chemicals Industries, Japan). The medium was changed every other day. iPSC colonies were picked up 30 days after transduction.

Statistical Analysis

All data are shown as mean ± SD. For comparisons of the mean between two groups, statistical analysis was performed by applying Student's t tests after confirming equality between the variances of the groups. When the variances were unequal, Mann-Whitney U tests were performed (SigmaPlot 11.2.0, Systat Software, USA). Comparisons of the mean among three groups or more were performed by one-way, two-way, or three-way analysis of variance followed by a post hoc test with the use of Student-Newman-Keuls Method (SigmaPlot 11.2.0). p values < 0.05 were considered significant.

ACCESSION NUMBERS

The Gene Expression Omnibus accession numbers for microarray data reported in this paper are GSE43326 (gene-expression comparison between control and AD clones), GSE43382 (gene-expression change along with the astroglial differentiation), and GSE43328 (gene-expression comparison of generated iPSCs).

SUPPLEMENTAL INFORMATION

Supplemental Information contains Supplemental Experimental Procedures, four figures, and two tables and can be found with this article online at http://dx.doi.org/10.1016/j.stem.2013.01.009.

ACKNOWLEDGMENTS

We would like to express our sincere gratitude to all our coworkers and collaborators, Mari Ohnuki, Megumi Kumazaki, Mitsuyo Kawada, Fumihiko Adachi, Takako Enami, and Misato Funayama for technical assistance; Nobuya Inagaki and Norio Harada for technical advice; and Kazumi Murai for editing the manuscript. This research was funded in part by a grant from the Funding Program for World-Leading Innovative R&D on Science and Technology (FIRST Program) of the Japan Society for the Promotion of Science (JSPS) to S.Y., from the Alzheimer's Association (IIRG-09-132098) to H.M., from the JST Yamanaka iPS Cell Special Project to S.Y. and H.I., from CREST to H.I., H.M., N.I., and T.T., from a Grant-in-Aid from the Ministry of Health, Labour and Welfare of Japan to H.I., from a Grant-in-Aid for Scientific Research on Innovative Area "Foundation of Synapse and Neurocircuit Pathology" (22110007) from the Ministry of Education, Culture, Sports, Science and Technology of Japan to H.I. and N.I., and from the Japan Research Foundation for Clinical Pharmacology to H.I. H.I. conceived the project; T.K., N.I., M.A., and H.I. designed the experiments; T.K., N.I., M.A., K.W., C.K., R.N., N.E., N.Y. and K. Tsukita performed the experiments; T.K., N.I., M.A., and H.I. analyzed the data; K.O., I.A., K.M., T.N., K.I., W.L.K., O.H., S.H., and T.C. contributed

(D) Quantitative data of (C) is shown. Each value indicated the ratio of the CellROX-stained area (an average of random 25 fields per sample) adjusted with DAPI counts. Data represent mean ± SD (n = 3 per clone). Two-way ANOVA showed significant main effects of DHA treatment ($F_{[1,32]} = 43.140$; $p < 0.001$) with a significant interaction between the APP mutation and DHA treatment ($F_{[3,32]} = 23.410$; $p < 0.001$). The DHA group in AD(APP-E693Δ) neural cells was significantly different from the other groups (**, $p < 0.005$).

(E) Real-time survival rate of control and AD neural cells with and without DHA showing cell viability. The numbers of control and AD(APP-E693Δ) neurons with Synapsin I-promoter-driven EGFP were sequentially imaged (average of 25 random fields per sample) and counted to assess the survival ratio (n = 3 per clone). Data represent mean ± SD (n = 3 per clone). In the cell-survival ratio, three-way ANOVA showed significant main effects of the APP mutation ($F_{[1,256]} = 377.611$; $p < 0.001$), DHA treatment ($F_{[1,256]} = 36.117$; $p < 0.001$), and time ($F_{[7,256]} = 65.272$; $p < 0.001$), with significant interactions between the APP mutation and DHA treatment ($F_{[1,256]} = 18.315$; $p < 0.001$), between the APP mutation and time ($F_{[7,256]} = 20.023$; $p < 0.001$), between DHA treatment and time ($F_{[7,256]} = 4.534$; $p < 0.001$), and among all three factors ($F_{[7,256]} = 5.277$; $p < 0.001$). Post hoc analysis revealed that, on day 14 and day 16, AD(APP-E693Δ) neural cells were more vulnerable in the long culture than control neural cells and that DHA treatment rescued the vulnerability (*, $p < 0.001$).

(F) Typical images of Synapsin::EGFP neurons used in real-time survival assay. The scale bar represents 50 μm.

(G) Cytotoxicity in neural culture derived from control and AD iPSCs after treatment with DHA (5 μM) for 16 days. Measured fluorescent lactate dehydrogenase (LDH) release served as a measure of cytotoxicity. Data represent mean ± SD (n = 3 per clone). Two-way ANOVA showed significant main effects of DHA treatment ($F_{[1,32]} = 16.710$; $p < 0.001$) with a significant interaction between APP-E693Δ mutation and DHA treatment ($F_{[3,32]} = 9.210$; $p < 0.005$). There was a significant difference in AD(APP-E693Δ) neural cells between the DMSO-control and DHA groups (*, $p < 0.05$).

(H) Aβ40 and Aβ42 secreted from iPSC-derived neurons into medium (extracellular Aβ) at day 16 of the long-term culture were measured at 48 hr after the last medium change. Data represent mean ± SD (n = 3 per clone).

See also Figure S4 and Table S2.

reagents, materials and analysis tools; Y.K., Y.O., Y.S., M.N., K.Y., S.Y., S.S., T.A., R.H., and S.U. recruited the patients; R.T., H.M., and S.Y. provided critical reading and scientific discussions; T.S., K.K., T.T., and K. Takahashi performed microarray analysis; T.A. performed karyotyping; A.W. performed bisulfite genomic sequencing; K.I. and D.W. performed electrophysiology; K. Tsukita, T.K., and H.H. produced the lentivirus; H.I., N.I., M.A., and T.K. wrote the paper. The experimental protocols dealing with human or animal subjects were approved by the institutional review board at each institute. S.Y. is a member without salary of the scientific advisory boards of iPierian, iPS Academia Japan, Megakaryon Corporation, and Retina Institute Japan.

Received: February 27, 2012
Revised: December 22, 2012
Accepted: January 18, 2013
Published: February 21, 2013

REFERENCES

Barnham, K.J., Masters, C.L., and Bush, A.I. (2004). Neurodegenerative diseases and oxidative stress. Nat. Rev. Drug Discov. *3*, 205–214.

Begum, G., Kintner, D., Liu, Y., Cramer, S.W., and Sun, D. (2012). DHA inhibits ER Ca^{2+} release and ER stress in astrocytes following in vitro ischemia. J. Neurochem. *120*, 622–630.

Butterfield, D.A. (2003). Amyloid β-peptide [1-42]-associated free radical-induced oxidative stress and neurodegeneration in Alzheimer's disease brain: mechanisms and consequences. Curr. Med. Chem. *10*, 2651–2659.

Cole, G.M., and Frautschy, S.A. (2006). Docosahexaenoic acid protects from amyloid and dendritic pathology in an Alzheimer's disease mouse model. Nutr. Health *18*, 249–259.

Freund-Levi, Y., Eriksdotter-Jönhagen, M., Cederholm, T., Basun, H., Faxén-Irving, G., Garlind, A., Vedin, I., Vessby, B., Wahlund, L.O., and Palmblad, J. (2006). Omega-3 fatty acid treatment in 174 patients with mild to moderate Alzheimer disease: OmegAD study: a randomized double-blind trial. Arch. Neurol. *63*, 1402–1408.

Gong, Y., Chang, L., Viola, K.L., Lacor, P.N., Lambert, M.P., Finch, C.E., Krafft, G.A., and Klein, W.L. (2003). Alzheimer's disease-affected brain: presence of oligomeric A β ligands (ADDLs) suggests a molecular basis for reversible memory loss. Proc. Natl. Acad. Sci. USA *100*, 10417–10422.

Haass, C., and Selkoe, D.J. (2007). Soluble protein oligomers in neurodegeneration: lessons from the Alzheimer's amyloid β-peptide. Nat. Rev. Mol. Cell Biol. *8*, 101–112.

Hensley, K., Carney, J.M., Mattson, M.P., Aksenova, M., Harris, M., Wu, J.F., Floyd, R.A., and Butterfield, D.A. (1994). A model for β-amyloid aggregation and neurotoxicity based on free radical generation by the peptide: relevance to Alzheimer disease. Proc. Natl. Acad. Sci. USA *91*, 3270–3274.

Israel, M.A., Yuan, S.H., Bardy, C., Reyna, S.M., Mu, Y., Herrera, C., Hefferan, M.P., Van Gorp, S., Nazor, K.L., Boscolo, F.S., et al. (2012). Probing sporadic and familial Alzheimer's disease using induced pluripotent stem cells. Nature *482*, 216–220.

Kassler, K., Horn, A.H., and Sticht, H. (2010). Effect of pathogenic mutations on the structure and dynamics of Alzheimer's A β 42-amyloid oligomers. J. Mol. Model. *16*, 1011–1020.

Krafft, G.A., and Klein, W.L. (2010). ADDLs and the signaling web that leads to Alzheimer's disease. Neuropharmacology *59*, 230–242.

Krencik, R., Weick, J.P., Liu, Y., Zhang, Z.J., and Zhang, S.C. (2011). Specification of transplantable astroglial subtypes from human pluripotent stem cells. Nat. Biotechnol. *29*, 528–534.

Kuo, Y.M., Emmerling, M.R., Vigo-Pelfrey, C., Kasunic, T.C., Kirkpatrick, J.B., Murdoch, G.H., Ball, M.J., and Roher, A.E. (1996). Water-soluble Abeta (N-40, N-42) oligomers in normal and Alzheimer disease brains. J. Biol. Chem. *271*, 4077–4081.

Lambert, M.P., Velasco, P.T., Chang, L., Viola, K.L., Fernandez, S., Lacor, P.N., Khuon, D., Gong, Y., Bigio, E.H., Shaw, P., et al. (2007). Monoclonal antibodies that target pathological assemblies of Abeta. J. Neurochem. *100*, 23–35.

Lee, M., You, H.J., Cho, S.H., Woo, C.H., Yoo, M.H., Joe, E.H., and Kim, J.H. (2002). Implication of the small GTPase Rac1 in the generation of reactive oxygen species in response to β-amyloid in C6 astroglioma cells. Biochem. J. *366*, 937–943.

Lesné, S., Koh, M.T., Kotilinek, L., Kayed, R., Glabe, C.G., Yang, A., Gallagher, M., and Ashe, K.H. (2006). A specific amyloid-β protein assembly in the brain impairs memory. Nature *440*, 352–357.

Malhotra, J.D., and Kaufman, R.J. (2007). Endoplasmic reticulum stress and oxidative stress: a vicious cycle or a double-edged sword? Antioxid. Redox Signal. *9*, 2277–2293.

Morizane, A., Doi, D., Kikuchi, T., Nishimura, K., and Takahashi, J. (2011). Small-molecule inhibitors of bone morphogenic protein and activin/nodal signals promote highly efficient neural induction from human pluripotent stem cells. J. Neurosci. Res. *89*, 117–126.

Murakami, K., Horikoshi-Sakuraba, Y., Murata, N., Noda, Y., Masuda, Y., Kinoshita, N., Hatsuta, H., Murayama, S., Shirasawa, T., Shimizu, T., and Irie, K. (2010). Monoclonal antibody against the turn of the 42-residue amyloid β-protein at positions 22 and 23. ACS Chem. Neurosci. *1*, 747–756.

Nishitsuji, K., Tomiyama, T., Ishibashi, K., Ito, K., Teraoka, R., Lambert, M.P., Klein, W.L., and Mori, H. (2009). The E693Δ mutation in amyloid precursor protein increases intracellular accumulation of amyloid β oligomers and causes endoplasmic reticulum stress-induced apoptosis in cultured cells. Am. J. Pathol. *174*, 957–969.

Noguchi, A., Matsumura, S., Dezawa, M., Tada, M., Yanazawa, M., Ito, A., Akioka, M., Kikuchi, S., Sato, M., Ideno, S., et al. (2009). Isolation and characterization of patient-derived, toxic, high mass amyloid β-protein (Abeta) assembly from Alzheimer disease brains. J. Biol. Chem. *284*, 32895–32905.

Okita, K., Matsumura, Y., Sato, Y., Okada, A., Morizane, A., Okamoto, S., Hong, H., Nakagawa, M., Tanabe, K., Tezuka, K., et al. (2011). A more efficient method to generate integration-free human iPS cells. Nat. Methods *8*, 409–412.

Quinn, J.F., Raman, R., Thomas, R.G., Yurko-Mauro, K., Nelson, E.B., Van Dyck, C., Galvin, J.E., Emond, J., Jack, C.R., Jr., Weiner, M., et al. (2010). Docosahexaenoic acid supplementation and cognitive decline in Alzheimer disease: a randomized trial. JAMA *304*, 1903–1911.

Shankar, G.M., Li, S., Mehta, T.H., Garcia-Munoz, A., Shepardson, N.E., Smith, I., Brett, F.M., Farrell, M.A., Rowan, M.J., Lemere, C.A., et al. (2008). Amyloid-β protein dimers isolated directly from Alzheimer's brains impair synaptic plasticity and memory. Nat. Med. *14*, 837–842.

Shimada, H., Ataka, S., Tomiyama, T., Takechi, H., Mori, H., and Miki, T. (2011). Clinical course of patients with familial early-onset Alzheimer's disease potentially lacking senile plaques bearing the E693Δ mutation in amyloid precursor protein. Dement. Geriatr. Cogn. Disord. *32*, 45–54.

Takano, K., Kitao, Y., Tabata, Y., Miura, H., Sato, K., Takuma, K., Yamada, K., Hibino, S., Choshi, T., Iinuma, M., et al. (2007). A dibenzoylmethane derivative protects dopaminergic neurons against both oxidative stress and endoplasmic reticulum stress. Am. J. Physiol. Cell Physiol. *293*, C1884–C1894.

Tomiyama, T., Nagata, T., Shimada, H., Teraoka, R., Fukushima, A., Kanemitsu, H., Takuma, H., Kuwano, R., Imagawa, M., Ataka, S., et al. (2008). A new amyloid β variant favoring oligomerization in Alzheimer's-type dementia. Ann. Neurol. *63*, 377–387.

Tomiyama, T., Matsuyama, S., Iso, H., Umeda, T., Takuma, H., Ohnishi, K., Ishibashi, K., Teraoka, R., Sakama, N., Yamashita, T., et al. (2010). A mouse model of amyloid β oligomers: their contribution to synaptic alteration, abnormal tau phosphorylation, glial activation, and neuronal loss *in vivo*. J. Neurosci. *30*, 4845–4856.

Walsh, D.M., Klyubin, I., Fadeeva, J.V., Cullen, W.K., Anwyl, R., Wolfe, M.S., Rowan, M.J., and Selkoe, D.J. (2002). Naturally secreted oligomers of amyloid β protein potently inhibit hippocampal long-term potentiation *in vivo*. Nature *416*, 535–539.

Yagi, T., Ito, D., Okada, Y., Akamatsu, W., Nihei, Y., Yoshizaki, T., Yamanaka, S., Okano, H., and Suzuki, N. (2011). Modeling familial Alzheimer's disease with induced pluripotent stem cells. Hum. Mol. Genet. *20*, 4530–4539.

Cell Press content is widely accessible

At Cell Press we place a high priority on ensuring that all of our journal content is widely accessible and on working with the community to develop the best ways to achieve that goal.

Here are just some of those initiatives...

Open archives

We provide free access to Cell Press research journals 12 months following publication

Access for developing nations

We provide free & low-cost access through programs like Research4Life

Open access journal

We launched Cell Reports - a new Open Access journal spanning the life sciences

Funding body agreements

We work cooperatively and successfully with major funding bodies

Public access

Full-text online via ScienceDirect is also available to the public via walk in user access from any participating library

Submission to PubMed Central

Cell Press deposits accepted manuscripts on our authors' behalf for a variety of funding bodies, including NIH and HHMI, to PubMed Central (PMC)

www.cell.com/cellpress/access

Cell PRESS

Cell Stem Cell
Resource

A TALEN Genome-Editing System for Generating Human Stem Cell-Based Disease Models

Qiurong Ding,[1,10] Youn-Kyoung Lee,[1,10] Esperance A.K. Schaefer,[3,5,10] Derek T. Peters,[1,5] Adrian Veres,[1,5] Kevin Kim,[1] Nicolas Kuperwasser,[1,6] Daniel L. Motola,[3,5] Torsten B. Meissner,[1] William T. Hendriks,[1,2] Marta Trevisan,[1,2] Rajat M. Gupta,[1,5,6] Annie Moisan,[7] Eric Banks,[8] Max Friesen,[1] Robert T. Schinzel,[1] Fang Xia,[1] Alexander Tang,[1] Yulei Xia,[1] Emmanuel Figueroa,[1] Amy Wann,[1] Tim Ahfeldt,[1] Laurence Daheron,[1,2] Feng Zhang,[8,9] Lee L. Rubin,[1,2] Lee F. Peng,[3,5] Raymond T. Chung,[3,5] Kiran Musunuru,[1,2,5,6,8,11,*] and Chad A. Cowan[1,2,4,5,8,11,*]
[1]Department of Stem Cell and Regenerative Biology
[2]Harvard Stem Cell Institute
Harvard University, Cambridge, MA 02138, USA
[3]Gastrointestinal Unit, Department of Medicine
[4]Center for Regenerative Medicine
Massachusetts General Hospital, Boston, MA 02114, USA
[5]Department of Medicine, Harvard Medical School, Boston, MA 02115, USA
[6]Division of Cardiovascular Medicine, Brigham and Women's Hospital, Boston, MA 02115, USA
[7]Metabolism Discovery and Translational Area, Roche Pharmaceuticals, 4070 Basel, Switzerland
[8]Broad Institute, Cambridge, MA 02142, USA
[9]Department of Brain and Cognitive Sciences, McGovern Institute for Brain Research, Massachusetts Institute of Technology, Cambridge, MA 02139, USA
[10]These authors contributed equally to this work
[11]These authors contributed equally to this work
*Correspondence: kiranmusunuru@gmail.com (K.M.), ccowan@fas.harvard.edu (C.A.C.)
http://dx.doi.org/10.1016/j.stem.2012.11.011

SUMMARY

Transcription activator-like effector nucleases (TALENs) are a new class of engineered nucleases that are easier to design to cleave at desired sites in a genome than previous types of nucleases. We report here the use of TALENs to rapidly and efficiently generate mutant alleles of 15 genes in cultured somatic cells or human pluripotent stem cells, the latter for which we differentiated both the targeted lines and isogenic control lines into various metabolic cell types. We demonstrate cell-autonomous phenotypes directly linked to disease—dyslipidemia, insulin resistance, hypoglycemia, lipodystrophy, motor-neuron death, and hepatitis C infection. We found little evidence of TALEN off-target effects, but each clonal line nevertheless harbors a significant number of unique mutations. Given the speed and ease with which we were able to derive and characterize these cell lines, we anticipate TALEN-mediated genome editing of human cells becoming a mainstay for the investigation of human biology and disease.

INTRODUCTION

The study of human disease has been facilitated by the ability to identify the gene mutations responsible; at the same time, it has been hampered by the lack of an inexhaustible supply of easily accessible tissues from patients bearing those mutations. Another limitation is that many gene mutations that would be informative for disease biology if they could be studied in isolated cells are incompatible with human life (i.e., embryonic lethal). Classical gene-targeting technology via homologous recombination has proven to be an invaluable tool of experimental biology through its use in mouse embryonic stem cells for generating germline knockout and knockin mice; however, its use in mammalian systems has been limited primarily to studies in mice. In many cases, mice do not faithfully phenocopy human physiology and disease, e.g., cholesterol metabolism, coronary artery disease, and human hepatitis C virus (HCV) infection. The emergence of genome editing with engineered nucleases, as well as human pluripotent stem cell (hPSC) technology and differentiation protocols to obtain a variety of cell and tissue types in vitro, now make it possible to rapidly interrogate the effects of genetic modification in otherwise isogenic human model systems.

Transcription activator-like effector nucleases (TALENs) are a new class of engineered nucleases that, due to their modular domain structure, have proven more straightforward to design and construct for performing genome editing than other types of nucleases (Bogdanove and Voytas, 2011). TALENs are typically designed as a pair that binds to genomic sequences flanking a target site and generates a double-strand break, which is repaired by the cell using either homology-directed repair (HDR) or the error-prone process of nonhomologous end-joining (NHEJ) (Christian et al., 2010; Li et al., 2011; Miller et al., 2011; Hockemeyer et al., 2011). NHEJ can be exploited to introduce small insertions or deletions (indels) resulting in frameshift mutations that effectively knock out a protein-coding gene. An exogenously introduced double-stranded DNA or single-stranded DNA oligonucleotide (ssODN) can serve as a repair template for HDR to incorporate an alteration into the genome (Soldner et al., 2011). In principle, TALEN pairs can be generated de novo with standard molecular biology techniques in a matter of

days (Cermak et al., 2011; Sanjana et al., 2012). To demonstrate the utility, efficiency, and rapidity of TALEN technology in generating human cellular models with which to derive new biological insights, we created mutations in 15 genes and performed detailed phenotypic analysis of four genes for which novel roles in disease biology have emerged in recent years—*APOB*, *SORT1*, *AKT2*, and *PLIN1*.

RESULTS

Modular Assembly and Use of TALENs for Efficient and Rapid Genome Editing

The DNA-binding domain of a TALEN comprises an array of 33- to 35-amino-acid monomers that are "coded" to recognize and bind specific DNA base pairs (bp) in a 1:1 fashion (Moscou and Bogdanove, 2009; Boch et al., 2009). We built upon previously described modular Golden Gate methodologies to allow assembly of multiple DNA fragments in an ordered fashion (Li et al., 2011; Cermak et al., 2011), such that a single ligation of preassembled tetramers and trimers generates TALENs that recognize any 15 bp recognition site in the genome (Figure 1; Figure S1 available online). This assembly method requires only 1–2 days for completion and is not prone to errors that complicate methods that rely on PCR amplification of monomers. Furthermore, we have developed a set of optimized vectors and methods for the delivery of TALENs into mammalian cells and, in particular, hPSCs. In brief, we transfect or electroporate TALEN pairs into cells and then subject them to fluorescence-activated cell sorting (FACS) 48 hr posttransfection based on fluorescent-marker expression. We replate the sorted cells at low density and allow them to recover and grow for 1 week, resulting in the formation of distinct single colonies. Colonies are expanded, genomic DNA purified, and mutations analyzed by PCR, agarose-gel screening, and Sanger sequencing (Figure 1 and Figure S1). The entire process from start to finish can be completed in less than one month.

Utilizing these methods, we generated TALEN pairs to target 16 distinct sites in 15 genes in human somatic cell lines, human embryonic stem cell (hESC) lines, or human induced pluripotent stem cell (iPSC) lines; the alterations included a variety of knockout mutations as well as a knockin missense mutation and a functional frameshift mutation (Table 1). We observed that the efficiency of mutation varied by genomic location as well as among different cell lines, with indels from NHEJ occurring in roughly 2% to 34% of clones screened and the efficiency of knockin by HDR occurring at a frequency of 1.6%. We then proceeded to perform detailed phenotypic analyses of cells harboring mutations in four human disease-related genes—*APOB*, *SORT1*, *AKT2*, and *PLIN1*.

APOB Is Required for HCV Replication

APOB, which encodes apolipoprotein B, the core protein of very-low-density lipoprotein and low-density lipoprotein (LDL) particles that transport cholesterol and triglycerides from the liver to other tissues via the bloodstream, has been suggested as playing a critical role in HCV infection. In HCV models using cultured human HuH-7 hepatoma cells, RNA interference resulting in partial knockdown of *APOB* expression has been reported to reduce HCV secretion, albeit not HCV replication (Huang et al., 2007; Nahmias et al., 2008); however, another report has suggested that apolipoprotein E, but not apolipoprotein B, is necessary for HCV production (Jiang and Luo, 2009). Thus, the importance of *APOB* and precise points of interaction with the HCV lifecycle remain to be determined. We sought to address this question by generating *APOB* knockout HuH-7 cells.

The human *APOB* gene encodes a 512 kDa protein termed apoB-100. We designed a TALEN pair targeting a site in exon 13 (Figure 2A); frameshift mutations at the site would generate truncated proteins about 12.5% of the size of apoB-100 (apoB-12.5). We transfected a clonal line of HuH-7 with high expression of CD81 (a coreceptor for HCV entry, HuH-7 [CD81^{hi}]) with the *APOB* TALEN pair. Following FACS with a cotranslated fluorescent marker, replating of sorted cells at a limiting dilution, and expansion of single clones, we found that of 126 screened clones, indels were present in nine clones (Figure S2A), of which four had exon 13 frameshift mutations in both alleles (Figure 2A). Compared to wild-type controls from the same set of screened clones, *APOB* knockout cells had no detectable intracellular apoB protein, no secreted apoB mass in the media, and <3% *APOB* messenger RNA (mRNA) expression, consistent with nonsense-mediated mRNA decay (Figures 2B, 2C, and 2D).

We infected *APOB*$^{-/-}$ and wild-type cells with the tissue-culture-infectious HCV strain JFH-1. The *APOB*$^{-/-}$ cells had significantly lower intracellular HCV RNA levels (74% reduction, $p = 0.006$), with minimal detectable HCV core protein (Figures 2B and 2E). Reintroduction of apoB-100 protein into the *APOB*$^{-/-}$ cells by adding LDL particles to the media, allowing for cellular LDL uptake, resulted in partial restoration of HCV core protein levels, arguing that the HCV replication defect was the result of loss of *APOB* function rather than an off-target effect of the TALENs (i.e., mutagenesis at other sites in the genome) (Figure 2B). Together, these data suggest that apoB-100 is integral to the HCV viral life cycle and that *APOB*-targeting therapeutics (e.g., mipomersen) may have efficacy in treating HCV-infected patients.

Isogenic Disease Models in hPSCs

We found that the karyotype of the HuH-7 cells was severely abnormal (Figure S2B)—fortuitously, it harbored two *APOB* alleles, in contrast to *SORT1*, with at least five alleles—highlighting the disadvantages of cultured tumor cell lines for rigorous genetic studies. hPSCs offer several advantages: they can maintain stable genomes with normal karyotypes while propagated in culture (Figure S2B), preserving correct gene dosage; they can be differentiated into a variety of cell types, extending studies beyond a single cell type; and they can yield human cell types that are not available as cultured cell lines, e.g., adipocytes and motor neurons.

These advantages are mitigated by the significant variability in differentiation capacity and phenotypic characteristics among different hPSC lines, particularly among iPSC lines. This variability is attributed to differences in genetic background, in epigenetic state, and in derivation of the cell lines and adaptation to culture, among other factors. In this variability lies the potential for confounding of any phenotypic differences observed among differentiated cell lines generated to serve as disease models or controls—a significant weakness of studies in which a few iPSC lines from patients are compared with a few iPSC lines from healthy individuals, as has been the case with most published

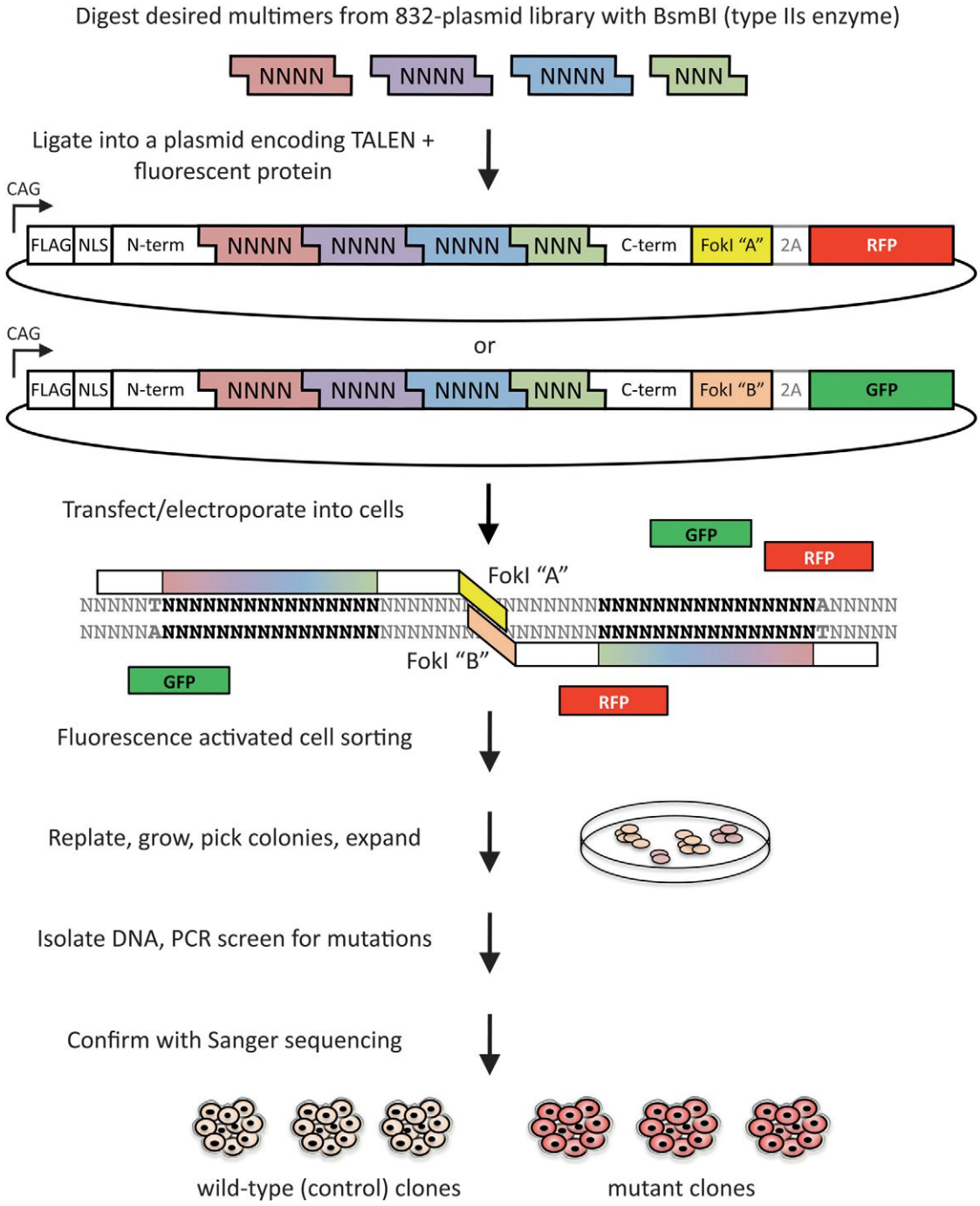

Figure 1. Schematic of System for Efficient and Rapid Genome Editing with TALENs

GFP, green fluorescent protein; RFP, red fluorescent protein; NLS, nuclear localization signal; N-term; N-terminal doman; C-term, C-terminal domain. See also Figure S1.

studies to date, because any observed differences cannot be reliably attributed to the effects of disease mutations. We demonstrated this cell line-to-cell line variability by differentiating two hESC lines, HUES 1 and HUES 9, into hepatocyte-like cells (HLCs) using an adapted protocol (Si-Tayeb et al., 2010) (Figure S3). We found that there were significant differences in the amounts of apoB and albumin secreted by the two cell lines and retained in the media (Figure S4A); when apoB mass was normalized to albumin mass, there was a 2-fold difference between the two lines ($p = 0.0001$).

Using genome editing to generate isogenic cell lines that differ only with respect to a single mutation of interest provides a superior study design, because the cell lines have the same origin and would thus be matched in genetic background, epigenetic state,

Table 1. Targeting Efficiency of TALENs at 16 Loci in 15 Genes in Various Cell Types

Gene	Target Sequence (Flanked by Underlined TALEN Binding Sites)	Cell Line[a]	Number of Clones Screened	Number of Mutants	Efficiency of Mutation
AKT2	TCCCTTCCTGCCTCATTTCAGGTGAATACATCAAGACCTGGAGGCCA	HUES 9	192	17	8.9%
AKT2 E17K	TCCCTTCCTGCCTCATTTCAGGTGAATACATCAAGACCTGGAGGCCA	HUES 9	192	3[b]	1.6%
ANGPTL3	TCAAAACTTGAAAGCCTCCTAGAAGAAAAAATTCTACTTCAACAAAA	HUES 9	424	84	19.8%
APOB	TAAGCGACTGGCTGCCTATCTTATGTTGATGAGGAGTCCTTCACA	HuH-7	126	9	7.1%
ATGL	TTGCTGGCGTTGCCCCCCGCCCGCCCCCACGGCCCAGAGGACAAGGA	HUES 9	192	28	14.6%
C6orf106	TGGAGGGCATGGACGTAGACCTGGACCCGGAGCTGATGCAGAAGTTCA	HUES 9	216	13	6.0%
CIITA	TAACAGCGATGCTGACCCCCTGTGCCTCTACCACTTCTATGACCAGA	BJRiPS	292	37	12.7%
CELSR2	TGCTGGCTCGGCTGCCCTGAGGTTGCTCAATCAAGCACAGGTTTCAA	HUES 1	506	18	3.5%
CFTR	TGGAATCACACTGAGTGGAGGTCAACGAGCAAGAATTTCTTTAGCA	CF-RiPS	140	3	2.1%
GLUT4	TGGTCCTTGCTGTGTTCTCTGCGGTGCTTGGCTCCCTGCAGTTTGGGTA	HUES9	155	52	33.5%
LINC00116	TCAGAGAGGACACTGCAGTTGTCCGTGCTAGTAGCCTTCGCTTCTGGA	HUES 9	88	26	29.5%
NLRC5	TGGAGCTGTCTTGTGAGGCTGCTCACCAAAGACCCAGAATGGCTGAA	BJ-RiPS	83	6	7.2%
PLIN1	TGACAACGTGGTGGACACAGTGGTGCATTACGTGCCGGTGAGTACCA	HUES 9	293	70	23.8%
PLIN1	TGACAACGTGGTGGACACAGTGGTGCATTACGTGCCGGTGAGTACCA	BJ-RiPS	439	29	6.6%
SORT1 (exon 2)	TGATGATCTCAGAGGCTCAGTATCCTTGTCCTGGGTTGGAGATAGCA	HUES 1	576	128	22.2%
SORT1 (exon 3)	TGGTAATTATGACTTTTGGACAGTCCAAGCTATATCGAAGGTGAGATCA	HUES 9	192	21	10.9%
TRIB1	TCTTCAAGCAGATTGTCTCCGCCGTCGCCCACTGCCACCAGTCAGCCA	HUES 9	169	41	24.2%
TTN	TTGAGGCTCCTTAATGATGACAGAAGAGAAGGCTTCTCTGGGTTCA	BJ-RiPS	250	17	6.8%

TALENs, transcription activator-like effector nucleases.
[a]HUES 1 and HUES 9 are human embryonic stem cell lines (Cowan et al., 2004); BJ-RiPS and CF-RiPS are induced pluripotent stem cell lines (Warren et al., 2010); and HuH-7 cells are cultured human hepatocellular carcinoma cells.
[b]Successfully inserted E17K knockin mutation using single-stranded DNA oligonucleotide.

differentiation capacity, derivation and adaptation to culture, etc. This would minimize confounding of the experiment and allow for more confidence in concluding that any phenotypic differences are secondary to the mutation. For these reasons, our subsequent studies were all performed in genome-edited hESCs.

SORT1 Mediates Diverse Cellular Functions in Hepatocytes, Adipocytes, and Neurons

SORT1 (encoding sortilin) was recently discovered through genome-wide association studies to regulate human blood LDL cholesterol levels and risk for coronary artery disease, via the modulation of the hepatic secretion of apoB-100-containing particles into the bloodstream; however, conflicting studies in humans and mice disagree about the direction of the effect of sortilin on apoB secretion (Musunuru et al., 2010; Kjolby et al., 2010). Human genetic studies have found that SNPs associated with increased hepatic *SORT1* expression are also associated with decreased blood LDL cholesterol levels (Musunuru et al., 2010). Knockdown and overexpression of *Sort1* in mouse liver suggested that sortilin functions to decrease hepatocyte apoB secretion (Musunuru et al., 2010). In contrast, a study of *Sort1* knockout mice suggested that sortilin *increases* hepatocyte apoB secretion (Kjolby et al., 2010).

We targeted exon 2 in the hESC line HUES 1 and, in a single round of TALEN targeting, generated three clones that were compound heterozygous for frameshift mutations (out of 576 clones screened) and confirmed that they lacked sortilin protein (Figures 3A and 3B). In parallel, we targeted exon 3 in the hESC line HUES 9 and obtained two knockout clones (out of 192 clones screened). We differentiated two *SORT1*$^{-/-}$ and two wild-type HUES 1 clones or two *SORT1*$^{-/-}$ and two wild-type HUES 9 clones into HLCs using an adapted protocol (Si-Tayeb et al., 2010) (Figure S3). Measuring the levels of apoB as well as albumin and apoA-I (reference controls) secreted from the HLCs and retained in the media, we found that knockout cells had significantly increased apoB mass (HUES 1: 117% increase in apoB/albumin ratio, $p = 0.04$; HUES 9: 65% increase in apoB/albumin ratio, $p = 0.05$) (Figure 3C and Figure S4B). We infected knockout HUES 1 HLCs or HUES 9 HLCs with a lentivirus expressing the *SORT1* complementary DNA (cDNA) or a control lentivirus and found that reconstitution of *SORT1* to the levels observed in wild-type HUES 1 or HUES 9 HLCs resulted in normalization of the apoB mass (Figure 3D and Figure S4C), confirming that the observed differences in apoB mass are specific to *SORT1* function and not the result of off-target effects. We found that secreted levels of additional hepatic proteins—ANGPTL4, ANGPTL6, HGF, and FGF-19—did not differ among the various experimental conditions (Figure S4D), nor did mRNA levels of *APOB* and other lipid-related genes such as *HMGCR*, *LDLR*, and *SREBP1* (Figure S4E). Our data suggest that, in humans, sortilin acts in hepatocytes to reduce apoB-containing particle levels in the blood, resulting in lower cholesterol levels and reduced risk of coronary artery disease—consistent with human genetic studies (Musunuru et al., 2010) and, notably,

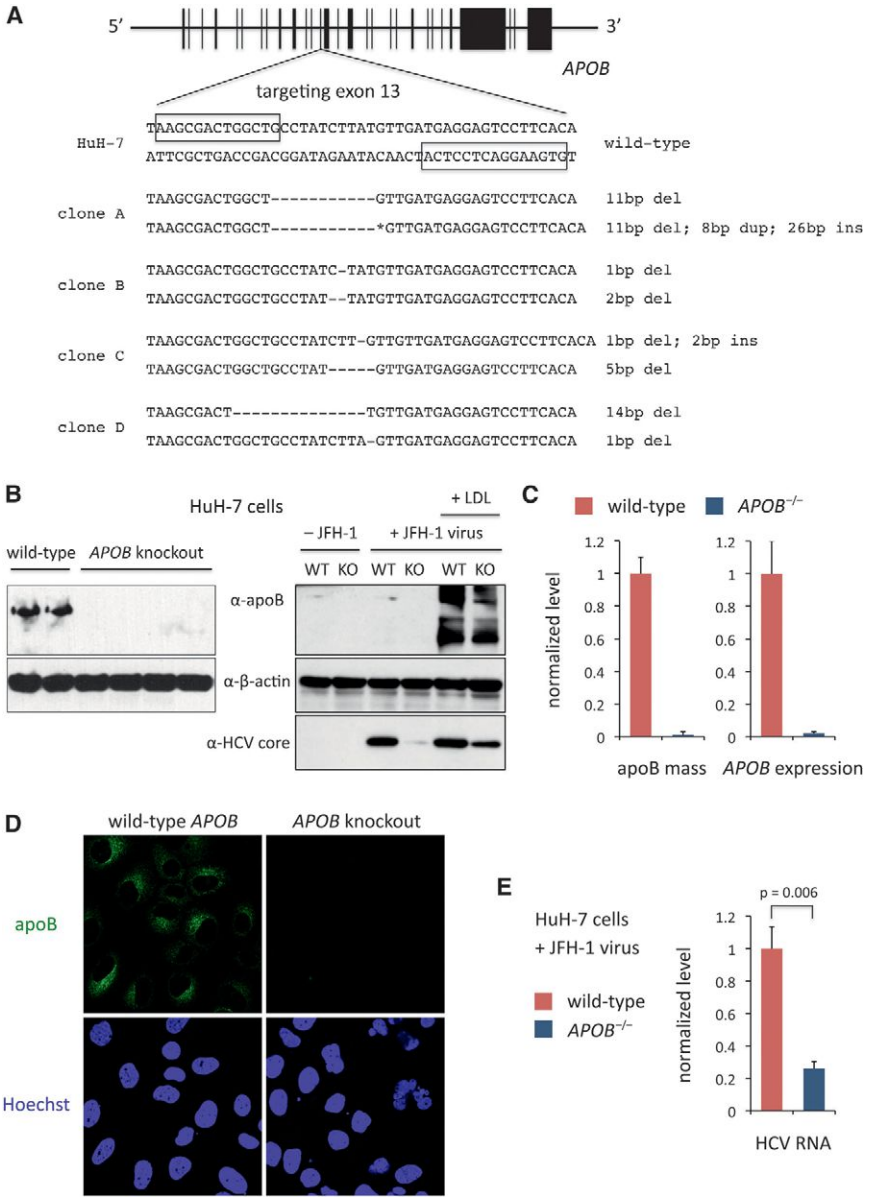

Figure 2. *APOB* Is Important for HCV Replication

(A) Generation of *APOB* knockout HuH-7 clones with TALENs targeting exon 13. Boxes indicate the TALEN binding sites. Deletions, insertions, and duplications in the two alleles of each clone are indicated. The 26 bp insertion and 8 bp duplication (asterisk) in clone A are 5′-GAGTCGCTTCT CCGGGAGATAAGTCA-3′ and 5′-GACTGGCT-3′, respectively.

(B) Left panel, western blot using whole-cell lysates from two wild-type (WT) and four knockout (KO) HuH-7 cell lines (clones A–D). Right panel, western blot from a wild-type clone and a knockout clone (clone A) infected with or without JFH-1 virus and incubated with or without LDL particles. The same wild-type clone and knockout clone (clone A) were used for all subsequent experiments.

(C) Left panel, apoB ELISAs performed on conditioned media from cells; values are normalized to the level in the wild-type clone. Right panel, *APOB* mRNA expression by qRT-PCR from whole-cell lysates; expression is indicated as the fold change of $2^{-\Delta\Delta Ct}$ with reference to 18S ribosomal RNA (rRNA), normalized to the level in the wild-type clone.

(D) Immunocytochemistry for apoB.

(E) HCV RNA levels by qRT-PCR from clones infected with JFH-1 virus; expression is indicated as the fold change of $2^{-\Delta\Delta Ct}$ with reference to *GAPDH*, normalized to the level in the wild-type clone.

The error bars show SEM from experiments with biological replicates, N = 3. p values were calculated with an unpaired t test. See also Figure S2.

contradicting the results reported from *Sort1* knockout mice (Kjolby et al., 2010).

SORT1 has also been suggested as playing an important role in regulating blood glucose levels by modulating insulin-dependent translocation of the fat- and muscle-specific glucose transporter, Glut4, to the plasma membrane via the formation and transport of Glut4 storage vesicles, based on studies in cultured mouse 3T3-L1 cells (Shi and Kandror, 2005). We differentiated two *SORT1*$^{-/-}$ and two wild-type HUES 1 clones into white adipocytes using a recently published protocol (Ahfeldt et al., 2012), and we observed a substantial increase in glucose uptake in wild-type adipocytes upon treatment with insulin (63% increase, p = 0.009), but not in *SORT1*$^{-/-}$ adipocytes (Figure S5A). We infected the knockout adipocytes with a *SORT1* or control lentivirus and found that reconstitution of *SORT1* restored insulin-responsive glucose uptake (60% increase, p = 0.002), confirming that the loss of insulin response in the knockout adipocytes was specific to *SORT1* function and not the result of off-target effects (Figure 3E and Figure S5B). Thus, *SORT1* appears to be critical for insulin-responsive glucose uptake in human adipocytes and may play a role in insulin sensitivity in humans.

Finally, *SORT1* has also been implicated in the viability and function of neurons (Nykjaer and Willnow, 2012). In motor neurons, sortilin has been found to regulate neuronal survival during a temporally and spatially specific period of programmed cell death. Specifically, induction of motor-neuron cell death by the proform of brain-derived neurotrophic factor (proBDNF) has been reported to be dependent on the presence of sortilin (Teng et al., 2005; Taylor et al., 2012). We differentiated two *SORT1*$^{-/-}$ and two wild-type HUES 9 clones into TUJ1^{+} ISL-1^{+} motor neurons using an adapted protocol (Di Giorgio et al., 2008; Chambers et al., 2009) and observed that although both *SORT1*$^{-/-}$ and wild-type hPSCs generated similar numbers of motor neurons (Figure S5C), wild-type motor neurons exhibited a substantial reduction after 3 days of proBDNF treatment (23% reduction, p = 0.004), whereas *SORT1*$^{-/-}$ motor neurons were unaffected (Figures 3F and 3G).

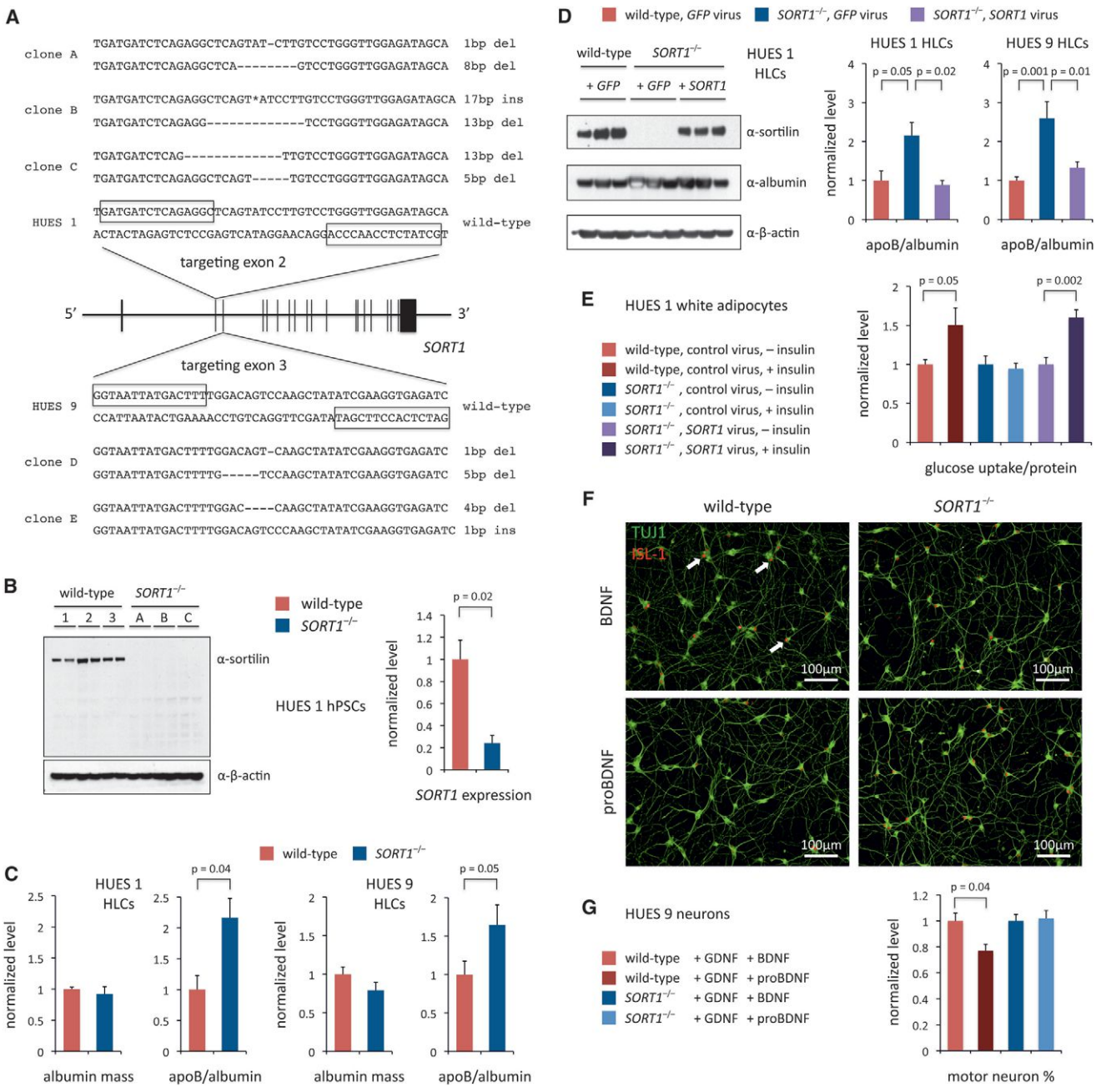

Figure 3. *SORT1* Reduces Hepatocyte-Secreted ApoB Mass, Is Important for Insulin-Responsive Glucose Transport in Adipocytes, and Mediates proBDNF-Induced Motor-Neuron Death

(A) Generation of *SORT1* knockout hPSC clones with TALENs targeting exon 2 or exon 3. Boxes indicate the TALEN binding sites. Deletions and insertions in the two alleles of each clone are indicated. The 17 bp insertion (asterisk) in clone B is 5′-TGCTATCTCCAACCAGG-3′.

(B) Western blot for sortilin and qRT-PCR for *SORT1* mRNA in wild-type and knockout HUES 1 clones (clones A–C); mRNA expression is indicated as the fold change of $2^{-\Delta\Delta Ct}$ with reference to 18S rRNA, normalized to the mean level in the wild-type clones.

(C) Albumin and apoB mass measured by ELISA in media collected from wild-type and knockout HLCs (two clones each; A and B for HUES 1, D and E for HUES 9), normalized to mean levels in wild-type HLCs. N = 3 for HUES 1, N = 6 for HUES 9.

(D) Western blots of lysates and ELISAs in media from wild-type and knockout HLCs (one clone each, A for HUES 1; two clones each, D and E for HUES 9) infected with *SORT1*- or *GFP*-expressing lentivirus, normalized to mean levels in wild-type HLCs. N = 2 for HUES 1, N = 6 for HUES 9.

(E) Ratios of glucose uptake to total protein content in wild-type and knockout HUES 1 adipocytes (one clone each; clone A) infected with *SORT1*-expressing or control lentivirus and treated with or without insulin, all normalized to the mean ratio in wild-type adipocytes without insulin. N = 6.

(F) Immunocytochemistry for TUJ1 and ISL-1 in wild-type and knockout HUES 9 motor neurons. Arrows indicate representative double-positive cells.

(G) Counts of wild-type and knockout HUES 9 (two clones each, D and E) motor neurons (TUJ1 and ISL-1 double-positive cells) treated with BDNF versus proBDNF. N = 12. GDNF, glial cell-derived neurotrophic factor.

The error bars show SEM from experiments with biological replicates. p values were calculated with an unpaired t test. See also Figures S3, S4, and S5.

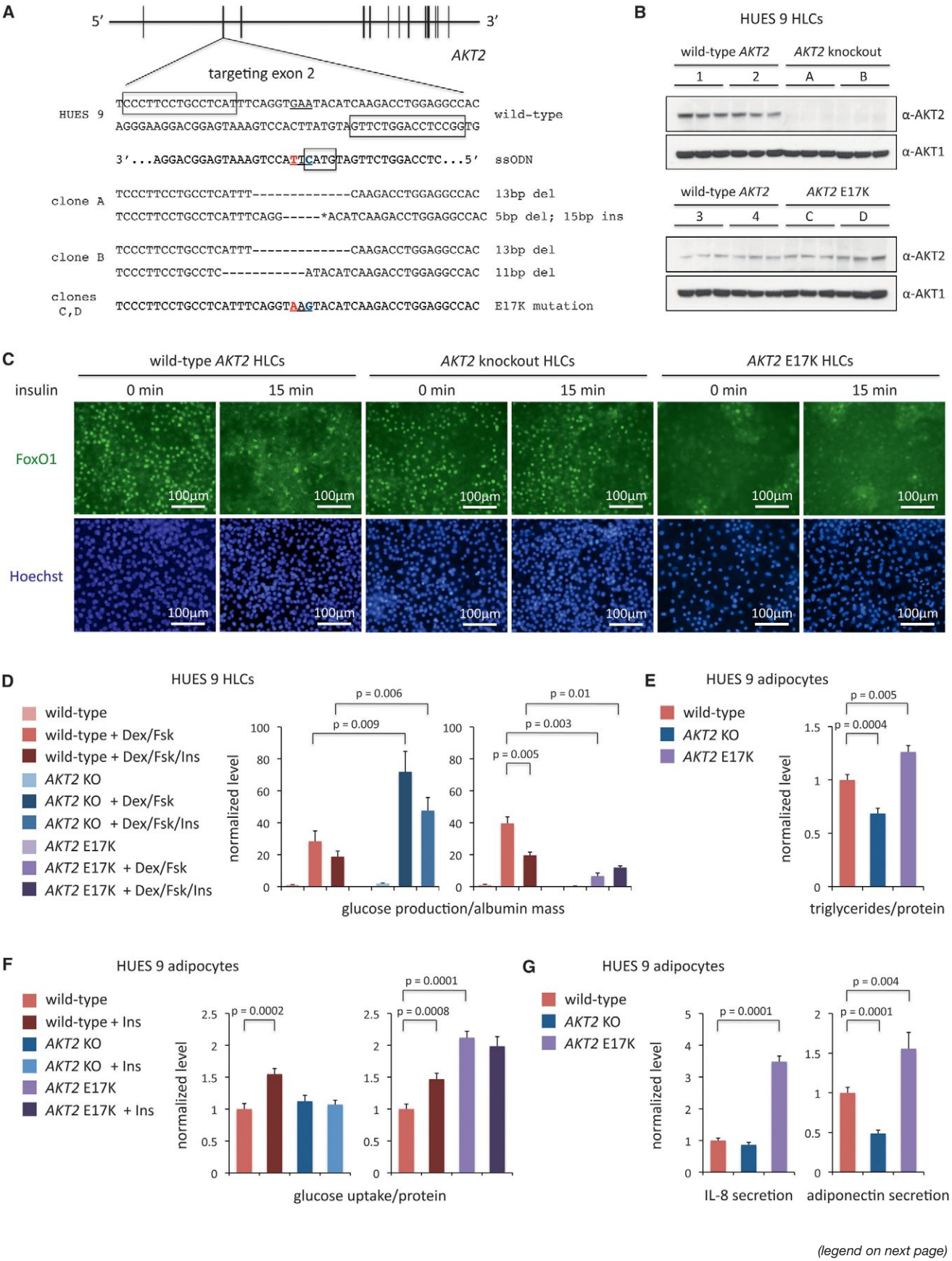

(legend on next page)

These data agree with the reported requirement of *SORT1* for proBDNF-induced programmed cell death in human motor neurons.

AKT2 Regulates Insulin Signaling and Glucose Metabolism in Hepatocytes and Adipocytes

The human *AKT2* gene (encoding RAC-β serine/threonine-protein kinase, also known as AKT2 or PKBβ) has also been implicated in the regulation of insulin sensitivity. Loss of function of *AKT2* in humans has been reported to result in severe insulin resistance, as well as decreased body fat and partial lipodystrophy, attributed to reduced adipocyte differentiation (George et al., 2004; Agarwal and Garg, 2006); also, *Akt2* knockout mice are resistant to the effects of insulin on glucose metabolism in liver and muscle, and they manifest lipoatrophy (Cho et al., 2001; Garofalo et al., 2003). Recently, three patients with severe hypoglycemia, hypoinsulinemia, and increased body fat were reported to bear a missense mutation in *AKT2*, p.Glu17Lys (E17K) (Hussain et al., 2011). Although the function of the mutant AKT2 E17K protein was assessed by heterologous overexpression studies in cultured cell lines (HeLa and 3T3-L1) and interpreted as being activated, the inability to study a physiologically relevant phenotype (e.g., glucose metabolism) in physiologically relevant tissues (e.g., human liver) precluded the conclusion that the *AKT2* mutation was causal for the metabolic disorder in the patients.

We sought to unequivocally establish a dominant, activated function of the AKT2 E17K mutant on glucose metabolism by generating an allelic series of isogenic hPSC lines with wild-type *AKT2*, knockout of *AKT2*, or a single $AKT2^{E17K}$ allele. We designed TALENs to target the site of the E17K mutation in the second coding exon (Figure 4A). In one round of targeting of HUES 9 cells with the TALEN pair alone, we obtained 17 clones with indels (out of 192 clones screened), none of which was compound heterozygous for frameshift mutations. A second round of TALEN targeting with a clone with one frameshift allele yielded two clones compound heterozygous for frameshift mutations (out of 96 clones screened). In parallel, we coelectroporated wild-type HUES 9 cells with the TALEN pair and a 67 nt antisense ssODN harboring the E17K missense variant, yielding three $AKT2^{E17K}$ heterozygous clones (out of 192 clones screened) (Figure S6A).

We differentiated the allelic series of hPSC clones (two clones each) into HLCs. No AKT2 protein was apparent in the knockout cells, with comparable levels of AKT2 observed in the wild-type and E17K cells (Figure 4B). We assessed the regulation of the FoxO1 transcription factor, an AKT2 substrate that upon phosphorylation is translocated from the nucleus to the cytoplasm. In wild-type HLCs, FoxO1 was predominantly nuclear at baseline and cytoplasmic after insulin stimulation; in $AKT2^{-/-}$ HLCs, it was predominantly nuclear both at baseline and after stimulation; and in $AKT2^{E17K}$ HLCs, it was predominantly cytoplasmic both at baseline and after stimulation (Figure 4C). We assessed glucose production in the allelic series of HLCs and found that with all three genotypes, addition of dexamethasone and forskolin to the media dramatically increased glucose production; the further addition of insulin decreased glucose production in the wild-type HLCs, but not in the mutant HLCs (Figure 4D). In all media conditions, glucose production was significantly higher in $AKT2^{-/-}$ HLCs and lower in $AKT2^{E17K}$ HLCs compared to wild-type HLCs. Similar trends were observed in the mRNA expression levels of two genes involved in gluconeogenesis, *G6PC* and *PCK1* (Figure S6B).

We also differentiated the *AKT2* allelic series of hPSC clones into white adipocytes and found that $AKT2^{-/-}$ adipocytes had significantly decreased triglyceride content (32% reduction, $p = 0.0004$) and $AKT2^{E17K}$ adipocytes had significantly increased triglyceride content (26% increase, $p = 0.005$) (Figure 4E), consistent with the fat-related phenotypes observed in patients with *AKT2* mutations. We observed a substantial increase in glucose uptake in wild-type adipocytes upon treatment with insulin (~50% increase in two different experiments) but, as with $SORT1^{-/-}$ adipocytes, we observed no significant change in glucose uptake in $AKT2^{-/-}$ adipocytes with insulin (Figure 4F). In contrast, $AKT2^{E17K}$ adipocytes displayed higher levels of glucose uptake at baseline compared to wild-type adipocytes (111% increase, $p = 0.0001$); upon treatment with insulin, there was no further increase in glucose uptake, presumably because the cells were in a constitutively active state with respect to insulin signaling (Figure 4F). In the same vein, $AKT2^{E17K}$ adipocytes displayed substantially increased secretion of inflammatory adipokines such as interleukin-18 (IL-8) (Figure 4G), MCP1, and PAI-1 (Figure S6C). Finally, $AKT2^{-/-}$ and $AKT2^{E17K}$

Figure 4. *AKT2* E17K Is a Dominant, Activating Mutation

(A) Generation of *AKT2* knockout and E17K knockin hPSC clones with TALENs targeting exon 2. The underline indicates the codon encoding the E17K change. Boxes in the wild-type sequence indicate the TALEN binding sites. The box in the ssODN sequence indicates the RsaI restriction site created by the synonymous mutation in blue; the nucleotide in red indicates the missense mutation for E17K. Deletions and insertions in the two alleles of each clone are indicated. The 15 bp insertion (asterisk) in clone A is 5′-GACCTCCAGGTCCTG-3′.

(B) Western blot for AKT2 and AKT1 in wild-type, knockout, and E17K HUES 9 HLCs (A and B for knockout; C and D for E17K).

(C) Immunocytochemistry for FoxO1 in HLCs (clones A and C) at baseline and after 15 min of insulin stimulation.

(D) Ratios of glucose production to secreted albumin mass (ELISA) in wild-type, knockout, and E17K HUES 9 HLCs (two clones each; A and B for knockout; C and D for E17K) treated with or without dexamethasone (Dex) and forskolin (Fsk) with or without insulin (Ins), all normalized to the mean ratios in wild-type HLCs without additives. Left panel, N = 4; right panel, N = 2.

(E) Ratios of triglyceride content to total protein content in wild-type, knockout, and E17K HUES 9 adipocytes (two clones each; A and B for knockout; C and D for E17K), normalized to the mean ratio in wild-type adipocytes. N = 5.

(F) Ratios of glucose uptake to total protein content in wild-type, knockout, and E17K HUES 9 adipocytes (two clones each; A and B for knockout; C and D for E17K) treated with or without insulin, all normalized to the mean ratio in wild-type adipocytes without insulin. N = 6.

(G) IL-8 and adiponectin mass measured by ELISA in media collected from wild-type, knockout, and E17K HUES 9 adipocytes (two clones each; A and B for knockout; C and D for E17K), normalized to mean levels from wild-type adipocytes. N = 4.

The error bars show SEM from experiments with biological replicates. p values were calculated with an unpaired t test. See also Figures S3 and S6.

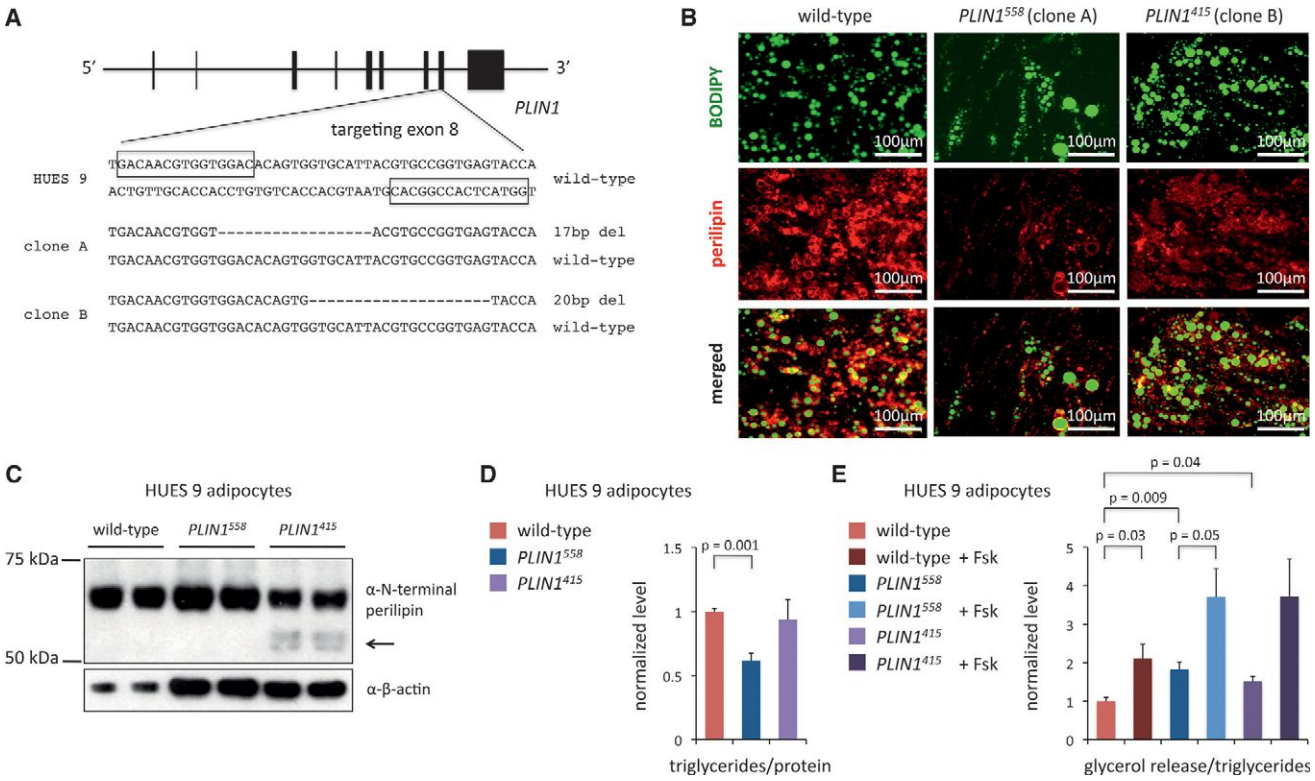

Figure 5. *PLIN1* Frameshift Mutations Produce Dominant-Acting and Truncated Proteins

(A) Generation of *PLIN1* frameshift mutant hPSC clones with TALENs targeting exon 8. Boxes indicate the TALEN binding sites. Deletions in the one allele of each clone are indicated.

(B) Immunocytochemistry for perilipin and BODIPY in wild-type, *PLIN1*^{558} (clone A), and *PLIN1*^{415} (clone B) adipocytes.

(C) Western blot for the N terminus of perilipin in wild-type, *PLIN1*^{558}, and *PLIN1*^{415} adipocytes; the arrow indicates a truncated protein.

(D) Ratios of triglyceride content to total protein content in wild-type, *PLIN1*^{558}, and *PLIN1*^{415} adipocytes. N = 3.

(E) Ratios of lipolysis activity (as measured by glycerol release) to total triglyceride content in wild-type, *PLIN1*^{558}, and *PLIN1*^{415} adipocytes treated with or without 10 μM forskolin. N = 4.

The error bars show SEM from experiments with biological replicates. p values were calculated with an unpaired t test. See also Figure S7.

adipocytes showed decreased and increased secretion of adiponectin, respectively (Figure 4G).

The opposing effects of the knockout and *AKT2*^{E17K} alleles, in addition to indicating that the effects were specific to *AKT2* function and not the result of off-target effects, establish that E17K is indeed a dominant, activating mutation in *AKT2* and causal for the hypoglycemia and increased body fat observed in the three patients.

PLIN1 Frameshift Mutations Dominantly Alter Lipolysis in Adipocytes

PLIN1 encodes the protein perilipin, the most abundant protein coating lipid droplets in adipocytes, where it is required for droplet formation and maturation, optimal triglyceride storage, and the release of free fatty acids from the droplet (Brasaemle et al., 2009). Frameshift mutations in *PLIN1* have recently been identified in patients with a novel autosomal-dominant subtype of partial lipodystrophy (Gandotra et al., 2011). The frameshift mutations found in patients result in a C-terminal elongation of perilipin, with a significantly altered amino acid sequence. Mice lacking *Plin1* exhibit elevated levels of basal lipolysis in adipocytes (Tansey et al., 2001; Zhai et al., 2010), which has been suggested as the mechanism by which patients harboring the frameshift mutations develop lipodystrophy (Gandotra et al., 2011). Mechanistic studies of these disease-causing mutations have been limited to the overexpression of mutant and wild-type human cDNAs in mouse 3T3-L1-derived adipocytes, with the conclusion being that wild-type *PLIN1*, but not mutant *PLIN1*, is able to inhibit basal lipolysis (Gandotra et al., 2011).

We designed TALENs to target the site of one of the naturally occurring patient-specific mutations (Val398fs) in the eighth coding exon of *PLIN1* (Figure 5A). In a single round of targeting of HUES 9 cells we identified 70 mutant clones (out of 293 clones screened). We characterized two mutant clones, one of which harbors a frameshift mutation that elongates perilipin to a length of 558 amino acids (designated *PLIN1*^{558}; wild-type perilipin has 522 amino acids)—very similar to the effect of the naturally occurring Val398fs mutation—and the other of which has a frameshift resulting in a C-terminal truncation of the protein (415 amino acids; designated *PLIN1*^{415}) (Figure S7A).

We differentiated the allelic series of hPSCs—wild-type, *PLIN1*^{558}, and *PLIN1*^{415}—into white adipocytes and observed a substantial reduction in the number of lipid-droplet-containing cells, as well as smaller lipid droplets in *PLIN1*^{558} adipocytes

compared to either wild-type or *PLIN1*^{415} cell lines (Figure 5B and Figure S7B). We confirmed the presence of perilipin protein in the adipocytes via western blot analysis (Figure 5C and Figure S7C). We found that the *PLIN1*^{558} adipocytes had significantly reduced triglyceride content (38% reduction compared to wild-type adipocytes, p = 0.0009), whereas the *PLIN1*^{415} adipocytes had similar triglyceride content to wild-type adipocytes (Figure 5D). We also measured basal and forskolin-stimulated lipolysis and found that both *PLIN1*^{558} and *PLIN1*^{415} adipocytes had increased basal lipolysis compared to wild-type adipocytes (83% increase, p = 0.008, and 52% increase, p = 0.04, respectively) (Figure 5E). Interestingly, both the *PLIN1*^{558} and *PLIN1*^{415} mutations resulted in increased lipolysis, though the effect was more marked with the *PLIN1*^{558} mutation; furthermore, there were significant differences in the expression levels of adipocyte-specific genes between the *PLIN1*^{558} and *PLIN1*^{415} cells, underscoring that the two different frameshifts (one leading to elongation of perilipin, the other to truncation) have distinct functional consequences (Figure S7D). Together, these data point to the C-terminal elongated form of perilipin, via a frameshift similar to naturally occurring mutations in lipodystrophy patients, acting in a dominant fashion to alter lipolysis and reduce triglyceride storage and lipid-droplet formation in human adipocytes.

TALENs Exhibit Minimal Off-Target Effects, but Sequence Variants Abound

Because the extent of off-target effects of TALENs (i.e., mutagenesis at other sites in the genome) in hPSCs remains to be defined, we performed exome sequencing of six cell lines: the parental HUES 1 cell line (clone X); the three *SORT1* knockout HUES 1 clones (clones A–C in Figure 3A); a control HUES 1 clone that had been grown in parallel with the *SORT1* knockout clones (i.e., had been exposed to the *SORT1* exon 2 TALEN pair but retained two wild-type alleles; clone W); and a clone that had been targeted in the *CELSR2* gene with a different TALEN pair (clone Y). It should be noted that TALENs virtually always induce indels by NHEJ rather than single-nucleotide variants (SNVs). Restricting our analysis to novel DNA sequence variants not found in the parental HUES 1 cell line, we identified the known on-target indels in *SORT1* in clones A–C; otherwise, we identified just two indels in the exome, a 4 bp deletion in clone C in the coding sequence of *LARP6*, resulting in a predicted frameshift mutation, and a 1 bp deletion in clone Y in an intron near an exon-intron boundary of *LUC7L3* (Table 2). Neither of these sites is flanked by sequences resembling predicted TALEN binding sites, arguing against (but not ruling out) the indels being TALEN-mediated off-target effects. More noteworthy were the 35 Sanger-sequencing-confirmed SNVs we discovered across the five experimental and control clones (Table 2). None of these SNVs lay near predicted off-target TALEN binding sites (see next paragraph). It is more likely that these SNVs represent intrinsic and perhaps unavoidable heterogeneity among single-cell clones of the original pool of HUES 1 cells. Arguing in favor of this interpretation, several of the SNVs were shared by both experimental and control clones, implying a common clonal origin within the original pool of HUES 1 cells. The functional significance of these SNVs is unclear, but the majority resulted in missense mutations, and at least one lay in a well-established disease gene (*DMD*, responsible for Duchenne muscular dystrophy).

We also performed whole-genome sequencing of the same six cell lines. Because the sequencing was performed at low coverage (6–12× coverage on average), it was not possible to perform de novo genome assembly and ascertain all sequence variation among the genomes. Instead, we used the sequencing data to interrogate the sites in the genome at which one or the other TALEN of the *SORT1* exon 2 TALEN pair would be most likely to bind based on a weighted TAL monomer-nucleotide association probability matrix developed by Doyle et al. (2012), and would thus be most likely to induce an off-target sequence change. About 100,000 potential off-target genomic sites were identified; we screened all of these sites for evidence of nearby indels. Besides the known *SORT1* indels in clones A–C, we identified no indels meeting our criteria.

Thus, although we are not able to completely rule out TALEN off-target effects, we conclude that off-target indels rarely occur based on the results of the exome and whole-genome sequence analyses. However, extrapolating to the entire genome, we expect that each clonal cell line harbors hundreds of SNVs that distinguish it from other cell lines derived from the same pool of parental cells. Thus, it may be virtually impossible to derive truly isogenic cell lines, even with the minimized manipulation of cells entailed by our genome-editing system.

DISCUSSION

In our studies we have used human model systems to generate strong evidence that apoB-100 is critical for HCV replication in human hepatocytes; that sortilin reduces apoB secretion by human hepatocytes, facilitates insulin-mediated glucose uptake by human adipocytes, and is necessary for proBDNF-mediated motor-neuron apoptosis; that *AKT2* E17K is a gain-of-function mutation that leads to reduced glucose production in human hepatocytes and increased triglyceride content in human adipocytes; and that *PLIN1* frameshift mutations increase basal lipolysis in human adipocytes. More generally, these findings highlight the various types of studies to which genome editing in human cells may be applied for obtaining novel biological insights.

We note that genome-editing technology is rapidly advancing, and we anticipate that improvements in the engineering of TALENs will continue to make genome editing more rapid and efficient. Indeed, since we established our system, high-throughput automated assembly methods have been reported (Reyon et al., 2012; Briggs et al., 2012), as well as the characterization of TAL monomers with improved nucleotide-binding specificity (Streubel et al., 2012; Cong et al., 2012). Although our specific TALEN assembly platform does not incorporate these latest advancements, in principle any up-to-date assembly platform that is paired to a delivery methodology similar to ours should be able to achieve efficient genome editing on a timescale of less than a month.

Whatever the assembly platform, our studies suggest that TALENs incur a low burden of off-target effects but that there is nevertheless significant clone-to-clone genetic variation in the form of SNVs; even if not secondary to TALEN use, they cannot be ignored. The ease and rapidity of TALEN-mediated

Table 2. Clonal Sequence Variants Detected by Exome Sequencing and Their Predicted Effects on Protein Products

Chr	Pos	Ref	Alt[a]	Gene	Clone A[b]	Clone B	Clone C	Clone W	Clone Y
1	21014224	G	T	*KIF17*	–	–	S432Y	–	–
1	90178297	G	A	*LRRC8C*	–	–	–	P56P	–
1	149921554	C	T	*OTUD7B*	–	–	–	–	Q367Q
2	109347284	T	C	*RANBP2*	–	–	–	F39F	–
2	113820048	C	A	*IL36RN*	–	–	–	–	L88I
2	173330424	C	T	*ITGA6*	–	intronic	–	–	–
3	132319348	T	C	*CCRL1*	–	–	–	–	V36A
3	193002674	G	T	*ATP13A5*	intronic	–	intronic	intronic	–
4	113568377	GAAGA	G	*LARP7*	–	–	frameshift[c]	–	–
6	152652970	C	A	*SYNE1*	–	–	–	–	A4284S
7	2260574	C	T	*MAD1L1*	–	–	–	–	G47D
7	22179660	G	C	*RAPGEF5*	L601V	–	–	–	–
8	15508246	C	T	*TUSC3*	–	–	R117C	–	–
9	33354142	G	A	*NFX1*	E130K	–	–	–	–
10	75541848	C	T	*CHCHD1*	–	S5S	–	–	–
11	124095534	G	A	*OR8G2*	–	–	G46E	–	–
12	80752469	G	T	*OTOGL*	–	C2026F	–	–	–
12	101750754	G	T	*UTP20*	R1862I	–	R1862I	R1862I	–
12	105445861	G	T	*ALDH1L2*	–	intronic	–	–	–
14	21967435	C	A	*METTL3*	–	intronic	–	–	–
15	43827249	G	T	*PPIP5K1*	–	–	P1071T	–	–
15	48805891	C	A	*FBN1*	–	–	intronic	–	–
15	90631649	C	A	*IDH2*	–	–	–	–	W155L
16	20043135	C	A	*GPR139*	–	S328S	–	–	–
17	11998899	G	A	*MAP24K4*	R145Q	–	R145Q	R145Q	–
17	48817653	AT	A	*LUC7L3*	–	–	–	–	intronic[d]
17	73567174	G	T	*LLGL2*	–	L712L	–	–	–
17	79226178	C	A	*SLC38A10*	–	–	–	A588S	–
18	30992086	G	T	*C18orf34*	–	–	–	–	intronic
19	9028296	G	T	*MUC16*	–	–	–	–	L12166M
19	56552245	G	T	*NLRP5*	intronic	–	intronic	intronic	–
20	60498685	G	T	*CDH44*	–	E425D	–	–	–
22	37325592	C	A	*CSF2RB*	D100E	–	D100E	D100E	–
22	39078278	A	T	*TOMM22*	–	intronic	–	–	–
X	32328257	G	T	*DMD*	–	A1897D	–	–	–
X	48558634	C	T	*SUV39H1*	–	–	T106T	–	–
X	135956509	C	A	*RBMX*	–	–	–	–	S323I

Chr, chromosome; Pos, position; Ref, reference allele; Alt, alternate allele.

[a]Alternate allele compared to reference allele in parental HUES 1 cell line (clone X), confirmed by Sanger sequencing.

[b]Clones A, B, and C are *SORT1*$^{-/-}$ clones in HUES 1; clone W is a wild-type (*SORT1*$^{+/+}$) clone in HUES 1 that was exposed to *SORT1* transcription activator-like effector nucleases (TALENs), from the same pool as clones A–C; clone Y is a wild-type (*SORT1*$^{+/+}$) clone that was exposed to a different set of TALENs (targeting *CELSR2*).

[c]The surrounding sequence is CAGAA GAGAA GAAAA AGAAA AAGAA **GAAGA** AAGGC CGAAT GAAAA AGGAA GACAA.

[d]The surrounding sequence is ATAAT CACAG ATAAT TTATA CAATT AT**AT**T TTTTC CCCCA GGTCC GTGTG AAAAA.

genome editing allows for rigorous study designs that can alleviate any concerns about off-target effects or other potential confounding by clonal sequence variation. As we have demonstrated with *SORT1*, it is straightforward to (1) generate multiple distinct mutant cell lines with each TALEN pair, (2) use distinct TALEN pairs to target different sites in a gene, (3) generate mutant clones in different cell lines with different genetic backgrounds, and (4) perform reconstitution experiments in knockout clones. Having used all of these approaches, we are able to conclude with great confidence that the observed cellular phenotypes are indeed related to *SORT1* function. We suggest that using at least one of these approaches should become *de rigeur* for future genetic studies in order to minimize confounding by clonal sequence variation.

Given the ability to use TALENs to readily insert specific gene variants into cells, the current enthusiasm for the generation and comparison of "disease" iPSC lines from patients with genetic disorders and "control" iPSC lines from unmatched healthy individuals should shift to the use of genome editing to engineer isogenic cell lines with and without disease mutations. The time required to recruit a patient for the donation of tissue from which to make iPSCs (assuming such a patient is readily accessible, which may not be the case for rare disorders), to perform reprogramming for deriving iPSC clones, to perform quality control for identifying clones that are pluripotent and that will readily differentiate into the desired cell type, and then to undertake differentiation and phenotypic studies—in the absence of isogenic control cell lines—is a minimum of six months and usually longer. Within a shorter time frame, we have found it to be quite feasible to use TALENs to edit a well-characterized and prevalidated (with respect to differentiation capacity) hPSC line and yield both mutant cell lines and isogenic control cell lines, allowing for a more rigorous study design, and to undertake differentiation and phenotypic studies, without any need for patient contact.

The potential advantages offered by prevalidated wild-type cell lines notwithstanding, there are many disorders for which the genetic background (i.e., modifier genes) plays a significant role in determining whether disease mutations result in clinical phenotypes. In these cases, it will be important to use iPSC lines from patients with clinically apparent diseases in order to have cell lines with the correct genetic backgrounds for complete disease penetrance (whereas wild-type cell lines may have nonpermissive genetic backgrounds). Genome editing with TALENs could be readily applied to patient-specific iPSC lines to "cure" disease mutations and generate appropriate isogenic control lines. Indeed, the most robust study design possible may be to assess both the effect of inserting a disease mutation into a wild-type cell line, thereby testing the sufficiency of the mutation for disease, and the effect of removing a disease mutation from a patient-specific iPSC line, thereby testing the necessity of the mutation for disease. Certainly the rapidity and efficiency of genome editing with TALENs should make it feasible to test the effects of a disease mutation in a variety of genetic backgrounds.

Finally, genome editing potentially allows for the interrogation of a large number of DNA sequence variants, such as those now emerging from next-generation sequencing studies of human populations, on a single genetic background. Creating a robust allelic series of isogenic cell lines represents an approach that hitherto has only been possible in nonmammalian organisms. Such studies will represent a significant advance in our ability to dissect genotype-phenotype relationships and thereby better elucidate human biology and disease.

EXPERIMENTAL PROCEDURES

TALEN Construction

TALEN genomic binding sites were chosen to be 15 bp in length or, in a few cases, 13 bp in length such that the target sequence between the two binding sites was between 14 and 18 bp in length; each binding site was anchored by a preceding T base in position "0" as has been shown to be optimal for naturally occurring TAL proteins (Moscou and Bogdanove, 2009; Boch et al., 2009). A library of 832 tetramer or trimer TAL repeats was constructed using methods based on the PCR-based protocol of Zhang et al. (2011); these multimers were designed to have complementary sticky ends when digested out of library plasmids with the type IIs restriction enzyme BsmBI. As outlined in Figure 1, multimers were assembled into an array and subcloned into a full-length TALEN harboring, in order, an N-terminal FLAG tag, a nuclear localization signal, the N-terminal portion of the TALE PthXo1 from the rice pathogen *X. oryzae* pv. oryzae (a kind gift of Dr. Daniel Voytas, University of Minnesota) lacking the first 176 amino acids (after Miller et al., 2011), the engineered TAL repeat array, the following 63 amino acids from the corresponding C-terminal portion of PthXo1 (after Miller et al., 2011), and one of two enhanced FokI domains. The FokI domains used were obligate heterodimers with both the Sharkey (Guo et al., 2010) and ELD:KKR (Doyon et al., 2011) mutations for enhancing cleavage activity, engineered by PCR. Each TALEN was in a plasmid with the CAG promoter for optimal expression in hPSCs, with the TALEN being coexpressed with a fluorescent marker (enhanced green fluorescent protein, mCherry [Clontech], or turbo red fluorescent protein [Evrogen]) via an intervening viral 2A sequence. The generic TALEN protein sequences are shown in Figure S1A. All reagents, protocols, and plasmid sequences needed for generating TALENs and performing genome editing by the methods described in this manuscript will be available to academic researchers through Addgene (http://www.addgene.org/TALEN_genome_editing_collection).

Cell Culture, Transfection or Electroporation, and Sorting

HuH-7 ($CD81^{hi}$) cells were grown in adherent culture in Dulbecco's modified Eagle's medium High Glucose containing glutamine and pyruvate (Invitrogen) and supplemented with 10% fetal bovine serum, penicillin, and streptomycin. Transfection of the plasmids expressing the *APOB* TALEN pair into HuH-7 cells was performed using FuGENE 6 (Roche) in 10 cm tissue-culture plates according to manufacturer instructions. HUES 1 and HUES 9 cells (Cowan et al., 2004) were grown in feeder-free adherent culture in chemically defined mTeSR1 (STEMCELL Technologies) supplemented with penicillin and streptomycin on plates precoated with Geltrex matrix (Invitrogen). The cells were dissociated into single cells with Accutase (Invitrogen), and 10 million cells were electroporated with 50 μg of the TALEN pair (25 μg of each plasmid), or with a mix of 30 μg of the TALEN pair (15 μg of each plasmid) and 30 μg of the ssODN (5′-CAGGA AGTAC CGTGG CCTCC AGGTC TTGAT GTACT TACCT GAAAT GAGGC AGGAA GGGAG GGAGA GA-3′) in a single cuvette and replated as previously described (Schinzel et al., 2011). The cells were collected from the culture plates 48 hr posttransfection or postelectroporation by trypsin or Accutase treatment, respectively, and resuspended in PBS. Cells expressing green and/or red fluorescent markers were collected by FACS (FACSAria II; BD Biosciences) and replated on 10 cm tissue-culture plates at 15,000 cells/plate to allow for recovery in growth media.

Isolation of Targeted Clonal Cell Populations

Post-FACS, the cells were allowed to recover for 7–10 days, after which single colonies were manually picked, dispersed, and replated individually to wells of 96-well plates. Colonies were allowed to grow to near confluence over the next 7 days, at which point they were split using trypsin (for HuH-7 cells) or Accutase (for hESCs) and replica-plated for the creation of a working stock and a frozen stock. The working stock was grown to confluence. Genomic DNA was extracted in 96-well format from working stocks in lysis buffer (10 mM Tris [pH 7.5], 10 mM EDTA, 10 mM NaCl, 0.5% Sarcosyl) containing proteinase K at 56°C overnight in a humidified chamber. Genomic DNA was precipitated by the addition of 95% ethanol containing 75 mM NaCl for 1 hr at room temperature. The DNA was then washed two times in 70% ethanol, allowed to dry at room temperature, and then resuspended in nuclease-free water.

Genotyping at the TALEN target site was then performed for each sample by PCR amplication (94°C, 30 s; 56°C, 30 s; 68°C, 30 s) using FastStart Taq (Roche) and a primer pair designed to yield small amplicons (~150–200 bp) around the target site. Amplicons were subjected to electrophoresis on 2.5% agarose gels to discriminate clones with indels, with positive clones having a band or bands visibly shifted in size from the baseline (see Figures S1B and S6A for examples); for *AKT2* E17K candidate clones, the amplicons were digested with RsaI for 1 hr and subjected to electrophoresis, with positive clones displaying cleavage products (Figure S6A). For a subset of the potentially positive clones, PCR amplicons were subcloned using the TOPO TA Cloning Kit (Invitrogen) and subjected to numerous sequence reads for confirmation of the presence of mutant alleles; in a similar fashion, a subset of the

potentially negative clones were confirmed to be wild-type. Clones with confirmed compound heterozygous mutant alleles (or the *AKT2* E17K mutation) or confirmed to be wild-type were retrieved from the frozen stocks and expanded for further experiments. When no compound heterozygous clones were identified, a heterozygous clone with one mutant allele was expanded and subjected to a second round of TALEN targeting.

Differentiation of hPSCs into HLCs, White Adipoctyes, and Motor Neurons

Differentiation was performed following the protocols of Si-Tayeb et al. (2010), Ahfeldt et al. (2012), and Di Giorgio et al. (2008) and Chambers et al. (2009). Details are given in Supplemental Experimental Procedures.

ELISAs, Immunocytochemistry, and Western Blot Analysis

These procedures were performed using standard methods. Details are given in Supplemental Experimental Procedures.

Glucose Production, Glucose Uptake, Triglyceride Content, and Lipolysis Assays

Glucose production and glucose uptake were measured using protocols adapted from Hagiwara et al. (2012) and Ahfeldt et al. (2012), respectively. Details of the various procedures are given in Supplemental Experimental Procedures.

Quantitative RT-PCR

Quantitative RT-PCR (qRT-PCR) was performed using standard methods. Details and oligonucleotide sequences are given in Supplemental Experimental Procedures.

HCV Infection of HuH-7 Cells

Details are given in Supplemental Experimental Procedures.

Exome and Whole-Genome Sequence Analyses

Exome sequencing and whole-genome sequencing were performed as previously described (Gnirke et al., 2009; Stransky et al., 2011). Procedural and analytical details are given in Supplemental Experimental Procedures.

SUPPLEMENTAL INFORMATION

Supplemental Information includes seven figures and Supplemental Experimental Procedures and can be found with this article online at http://dx.doi.org/10.1016/j.stem.2012.11.011.

ACKNOWLEDGMENTS

This work was supported in part by a Roche Postdoctoral Fellowship (Q.D.); the Sternlicht Director's Fund Award for Graduate Students from the Harvard Stem Cell Institute (D.T.P.); the Harvard Presidential Scholars Fund of the Harvard Medical School MD/PhD Program (A.V.); grants T32-DK007191 (E.A.K.S. and D.L.M.), T32-HL007604 (R.M.G.), K08-DK088951 (L.F.P.), K24-DK078772 (R.T.C.), P01-NS066888 (L.L.R.), R00-HL098364 (K.M.), U01-HL107440 (C.A.C.), and R01-DK097768 (F.Z., K.M., and C.A.C.) from the United States National Institutes of Health; the New York Stem Cell Foundation (L.L.R.); the Broad Institute's Lawrence H. Summers Fellowship and the Carlos Slim Foundation (K.M.); the Harvard Stem Cell Institute (T.B.M., L.L.R., K.M., and C.A.C.); and Harvard University (L.L.R., K.M., and C.A.C.). A.M. is a full-time employee of Roche Pharmaceuticals. We thank David Altshuler, Noel Burtt, Guillermo del Angel, Mark DePristo, Stacey Gabriel, Namrata Gupta, J. Keith Joung, Adam Kaplan, Ami Levy-Moonshine, Heng Li, Elyse Macksoud, Khalid Shakir, Alanna Strong, Kristin Thompson, Jayaraj Rajagopal, Stephanie Regan, Jennifer Shay, and the staffs of the HSCRB-HSCI Flow Cytometry Core and the Broad Institute's Genomics Platform for assistance and suggestions.

Received: August 24, 2012
Revised: October 19, 2012
Accepted: November 12, 2012
Published: December 13, 2012

REFERENCES

Agarwal, A.K., and Garg, A. (2006). Genetic disorders of adipose tissue development, differentiation, and death. Annu. Rev. Genomics Hum. Genet. *7*, 175–199.

Ahfeldt, T., Schinzel, R.T., Lee, Y.K., Hendrickson, D., Kaplan, A., Lum, D.H., Camahort, R., Xia, F., Shay, J., Rhee, E.P., et al. (2012). Programming human pluripotent stem cells into white and brown adipocytes. Nat. Cell Biol. *14*, 209–219.

Boch, J., Scholze, H., Schornack, S., Landgraf, A., Hahn, S., Kay, S., Lahaye, T., Nickstadt, A., and Bonas, U. (2009). Breaking the code of DNA binding specificity of TAL-type III effectors. Science *326*, 1509–1512.

Bogdanove, A.J., and Voytas, D.F. (2011). TAL effectors: customizable proteins for DNA targeting. Science *333*, 1843–1846.

Brasaemle, D.L., Subramanian, V., Garcia, A., Marcinkiewicz, A., and Rothenberg, A. (2009). Perilipin A and the control of triacylglycerol metabolism. Mol. Cell. Biochem. *326*, 15–21.

Briggs, A.W., Rios, X., Chari, R., Yang, L., Zhang, F., Mali, P., and Church, G.M. (2012). Iterative capped assembly: rapid and scalable synthesis of repeat-module DNA such as TAL effectors from individual monomers. Nucleic Acids Res. *40*, e117.

Cermak, T., Doyle, E.L., Christian, M., Wang, L., Zhang, Y., Schmidt, C., Baller, J.A., Somia, N.V., Bogdanove, A.J., and Voytas, D.F. (2011). Efficient design and assembly of custom TALEN and other TAL effector-based constructs for DNA targeting. Nucleic Acids Res. *39*, e82.

Chambers, S.M., Fasano, C.A., Papapetrou, E.P., Tomishima, M., Sadelain, M., and Studer, L. (2009). Highly efficient neural conversion of human ES and iPS cells by dual inhibition of SMAD signaling. Nat. Biotechnol. *27*, 275–280.

Cho, H., Mu, J., Kim, J.K., Thorvaldsen, J.L., Chu, Q., Crenshaw, E.B., 3rd, Kaestner, K.H., Bartolomei, M.S., Shulman, G.I., and Birnbaum, M.J. (2001). Insulin resistance and a diabetes mellitus-like syndrome in mice lacking the protein kinase Akt2 (PKB beta). Science *292*, 1728–1731.

Christian, M., Cermak, T., Doyle, E.L., Schmidt, C., Zhang, F., Hummel, A., Bogdanove, A.J., and Voytas, D.F. (2010). Targeting DNA double-strand breaks with TAL effector nucleases. Genetics *186*, 757–761.

Cong, L., Zhou, R., Kuo, Y.C., Cunniff, M., and Zhang, F. (2012). Comprehensive interrogation of natural TALE DNA-binding modules and transcriptional repressor domains. Nat. Commun. *3*, 968.

Cowan, C.A., Klimanskaya, I., McMahon, J., Atienza, J., Witmyer, J., Zucker, J.P., Wang, S., Morton, C.C., McMahon, A.P., Powers, D., and Melton, D.A. (2004). Derivation of embryonic stem-cell lines from human blastocysts. N. Engl. J. Med. *350*, 1353–1356.

Di Giorgio, F.P., Boulting, G.L., Bobrowicz, S., and Eggan, K.C. (2008). Human embryonic stem cell-derived motor neurons are sensitive to the toxic effect of glial cells carrying an ALS-causing mutation. Cell Stem Cell *3*, 637–648.

Doyle, E.L., Booher, N.J., Standage, D.S., Voytas, D.F., Brendel, V.P., Vandyk, J.K., and Bogdanove, A.J. (2012). TAL Effector-Nucleotide Targeter (TALE-NT) 2.0: tools for TAL effector design and target prediction. Nucleic Acids Res. *40* (Web Server issue), W117–W122.

Doyon, Y., Vo, T.D., Mendel, M.C., Greenberg, S.G., Wang, J., Xia, D.F., Miller, J.C., Urnov, F.D., Gregory, P.D., and Holmes, M.C. (2011). Enhancing zinc-finger-nuclease activity with improved obligate heterodimeric architectures. Nat. Methods *8*, 74–79.

Gandotra, S., Le Dour, C., Bottomley, W., Cervera, P., Giral, P., Reznik, Y., Charpentier, G., Auclair, M., Delépine, M., Barroso, I., et al. (2011). Perilipin deficiency and autosomal dominant partial lipodystrophy. N. Engl. J. Med. *364*, 740–748.

Garofalo, R.S., Orena, S.J., Rafidi, K., Torchia, A.J., Stock, J.L., Hildebrandt, A.L., Coskran, T., Black, S.C., Brees, D.J., Wicks, J.R., et al. (2003). Severe diabetes, age-dependent loss of adipose tissue, and mild growth deficiency in mice lacking Akt2/PKB beta. J. Clin. Invest. *112*, 197–208.

George, S., Rochford, J.J., Wolfrum, C., Gray, S.L., Schinner, S., Wilson, J.C., Soos, M.A., Murgatroyd, P.R., Williams, R.M., Acerini, C.L., et al. (2004). A

family with severe insulin resistance and diabetes due to a mutation in AKT2. Science *304*, 1325–1328.

Gnirke, A., Melnikov, A., Maguire, J., Rogov, P., LeProust, E.M., Brockman, W., Fennell, T., Giannoukos, G., Fisher, S., Russ, C., et al. (2009). Solution hybrid selection with ultra-long oligonucleotides for massively parallel targeted sequencing. Nat. Biotechnol. *27*, 182–189.

Guo, J., Gaj, T., and Barbas, C.F., 3rd. (2010). Directed evolution of an enhanced and highly efficient FokI cleavage domain for zinc finger nucleases. J. Mol. Biol. *400*, 96–107.

Hagiwara, A., Cornu, M., Cybulski, N., Polak, P., Betz, C., Trapani, F., Terracciano, L., Heim, M.H., Rüegg, M.A., and Hall, M.N. (2012). Hepatic mTORC2 activates glycolysis and lipogenesis through Akt, glucokinase, and SREBP1c. Cell Metab. *15*, 725–738.

Hockemeyer, D., Wang, H., Kiani, S., Lai, C.S., Gao, Q., Cassady, J.P., Cost, G.J., Zhang, L., Santiago, Y., Miller, J.C., et al. (2011). Genetic engineering of human pluripotent cells using TALE nucleases. Nat. Biotechnol. *29*, 731–734.

Huang, H., Sun, F., Owen, D.M., Li, W., Chen, Y., Gale, M., Jr., and Ye, J. (2007). Hepatitis C virus production by human hepatocytes dependent on assembly and secretion of very low-density lipoproteins. Proc. Natl. Acad. Sci. USA *104*, 5848–5853.

Hussain, K., Challis, B., Rocha, N., Payne, F., Minic, M., Thompson, A., Daly, A., Scott, C., Harris, J., Smillie, B.J., et al. (2011). An activating mutation of AKT2 and human hypoglycemia. Science *334*, 474.

Jiang, J., and Luo, G. (2009). Apolipoprotein E but not B is required for the formation of infectious hepatitis C virus particles. J. Virol. *83*, 12680–12691.

Kjolby, M., Andersen, O.M., Breiderhoff, T., Fjorback, A.W., Pedersen, K.M., Madsen, P., Jansen, P., Heeren, J., Willnow, T.E., and Nykjaer, A. (2010). Sort1, encoded by the cardiovascular risk locus 1p13.3, is a regulator of hepatic lipoprotein export. Cell Metab. *12*, 213–223.

Li, T., Huang, S., Jiang, W.Z., Wright, D., Spalding, M.H., Weeks, D.P., and Yang, B. (2011). TAL nucleases (TALNs): hybrid proteins composed of TAL effectors and FokI DNA-cleavage domain. Nucleic Acids Res. *39*, 359–372.

Miller, J.C., Tan, S., Qiao, G., Barlow, K.A., Wang, J., Xia, D.F., Meng, X., Paschon, D.E., Leung, E., Hinkley, S.J., et al. (2011). A TALE nuclease architecture for efficient genome editing. Nat. Biotechnol. *29*, 143–148.

Moscou, M.J., and Bogdanove, A.J. (2009). A simple cipher governs DNA recognition by TAL effectors. Science *326*, 1501.

Musunuru, K., Strong, A., Frank-Kamenetsky, M., Lee, N.E., Ahfeldt, T., Sachs, K.V., Li, X., Li, H., Kuperwasser, N., Ruda, V.M., et al. (2010). From noncoding variant to phenotype via SORT1 at the 1p13 cholesterol locus. Nature *466*, 714–719.

Nahmias, Y., Goldwasser, J., Casali, M., van Poll, D., Wakita, T., Chung, R.T., and Yarmush, M.L. (2008). Apolipoprotein B-dependent hepatitis C virus secretion is inhibited by the grapefruit flavonoid naringenin. Hepatology *47*, 1437–1445.

Nykjaer, A., and Willnow, T.E. (2012). Sortilin: a receptor to regulate neuronal viability and function. Trends Neurosci. *35*, 261–270.

Reyon, D., Tsai, S.Q., Khayter, C., Foden, J.A., Sander, J.D., and Joung, J.K. (2012). FLASH assembly of TALENs for high-throughput genome editing. Nat. Biotechnol. *30*, 460–465.

Sanjana, N.E., Cong, L., Zhou, Y., Cunniff, M.M., Feng, G., and Zhang, F. (2012). A transcription activator-like effector toolbox for genome engineering. Nat. Protoc. *7*, 171–192.

Schinzel, R.T., Ahfeldt, T., Lau, F.H., Lee, Y.K., Cowley, A., Shen, T., Peters, D., Lum, D.H., and Cowan, C.A. (2011). Efficient culturing and genetic manipulation of human pluripotent stem cells. PLoS ONE *6*, e27495.

Shi, J., and Kandror, K.V. (2005). Sortilin is essential and sufficient for the formation of Glut4 storage vesicles in 3T3-L1 adipocytes. Dev. Cell *9*, 99–108.

Si-Tayeb, K., Noto, F.K., Nagaoka, M., Li, J., Battle, M.A., Duris, C., North, P.E., Dalton, S., and Duncan, S.A. (2010). Highly efficient generation of human hepatocyte-like cells from induced pluripotent stem cells. Hepatology *51*, 297–305.

Soldner, F., Laganière, J., Cheng, A.W., Hockemeyer, D., Gao, Q., Alagappan, R., Khurana, V., Golbe, L.I., Myers, R.H., Lindquist, S., et al. (2011). Generation of isogenic pluripotent stem cells differing exclusively at two early onset Parkinson point mutations. Cell *146*, 318–331.

Stransky, N., Egloff, A.M., Tward, A.D., Kostic, A.D., Cibulskis, K., Sivachenko, A., Kryukov, G.V., Lawrence, M.S., Sougnez, C., McKenna, A., et al. (2011). The mutational landscape of head and neck squamous cell carcinoma. Science *333*, 1157–1160.

Streubel, J., Blücher, C., Landgraf, A., and Boch, J. (2012). TAL effector RVD specificities and efficiencies. Nat. Biotechnol. *30*, 593–595.

Tansey, J.T., Sztalryd, C., Gruia-Gray, J., Roush, D.L., Zee, J.V., Gavrilova, O., Reitman, M.L., Deng, C.X., Li, C., Kimmel, A.R., and Londos, C. (2001). Perilipin ablation results in a lean mouse with aberrant adipocyte lipolysis, enhanced leptin production, and resistance to diet-induced obesity. Proc. Natl. Acad. Sci. USA *98*, 6494–6499.

Taylor, A.R., Gifondorwa, D.J., Robinson, M.B., Strupe, J.L., Prevette, D., Johnson, J.E., Hempstead, B., Oppenheim, R.W., and Milligan, C.E. (2012). Motoneuron programmed cell death in response to proBDNF. Dev. Neurobiol. *72*, 699–712.

Teng, H.K., Teng, K.K., Lee, R., Wright, S., Tevar, S., Almeida, R.D., Kermani, P., Torkin, R., Chen, Z.Y., Lee, F.S., et al. (2005). ProBDNF induces neuronal apoptosis via activation of a receptor complex of p75NTR and sortilin. J. Neurosci. *25*, 5455–5463.

Warren, L., Manos, P.D., Ahfeldt, T., Loh, Y.H., Li, H., Lau, F., Ebina, W., Mandal, P.K., Smith, Z.D., Meissner, A., et al. (2010). Highly efficient reprogramming to pluripotency and directed differentiation of human cells with synthetic modified mRNA. Cell Stem Cell *7*, 618–630.

Zhai, W., Xu, C., Ling, Y., Liu, S., Deng, J., Qi, Y., Londos, C., and Xu, G. (2010). Increased lipolysis in adipose tissues is associated with elevation of systemic free fatty acids and insulin resistance in perilipin null mice. Horm. Metab. Res. *42*, 247–253.

Zhang, F., Cong, L., Lodato, S., Kosuri, S., Church, G.M., and Arlotta, P. (2011). Efficient construction of sequence-specific TAL effectors for modulating mammalian transcription. Nat. Biotechnol. *29*, 149–153.

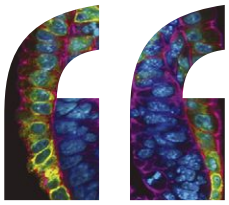

We are tough but fair.

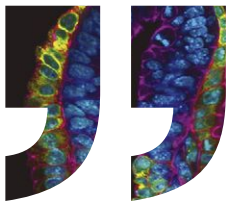

Whether your paper is accepted or rejected, we'll make sure that the feedback you get is appropriate, balanced and respectful.

When you choose Cell Press you get the attention you deserve.

For more information visit: www.cell.com/values

Your **work** is our **life**

Cell PRESS

affymetrix
eBioscience

See cells differently

Multi-dimensional Flow Cytometry

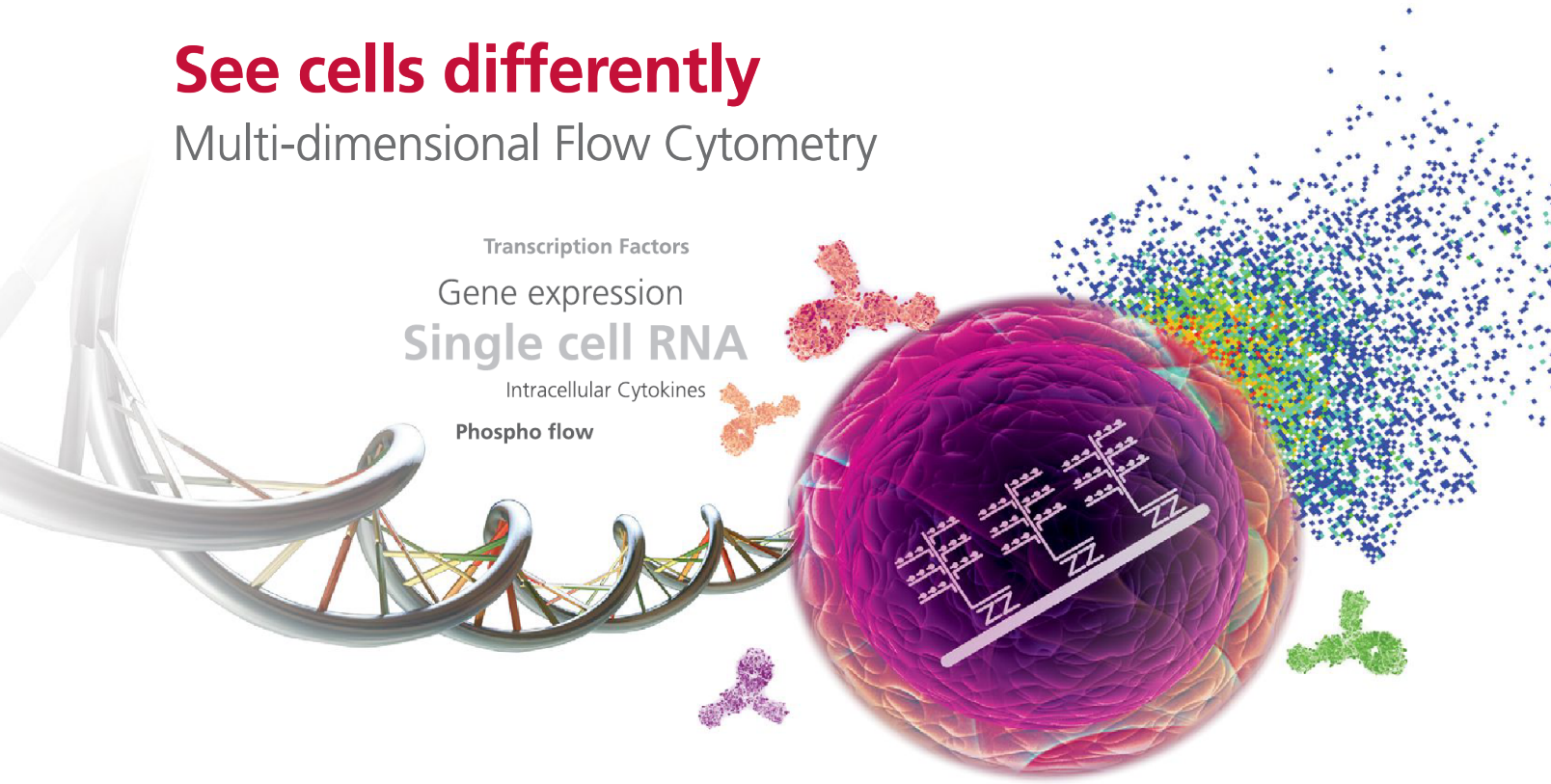

What dimension is missing in your cell's signature?

Gain insight into single cell analysis with the QuantiGene® FlowRNA Assay,
a novel multiplex RNA hybridization protocol using a standard flow cytometer. Choose from a catalog of more than 4,000 probes or request a custom set at no additional charge.

Show Me Data

Download scientific poster at **ebioscience.com/FlowRNA_stemcell**

eBioscience, an Affymetrix company, provides innovative solutions to researchers and clinicians worldwide looking to answer questions driving today's life science community.

Biology for a better world.

NORTH AMERICA: 888.999.1371 ▪ EUROPE: +43 1 796 40 40-304 ▪ JAPAN: +81 (0)3 6430 4020 ▪ INQUIRIES: info@ebioscience.com

eBioscience GeneChip USB

Molecules That Count®

Gene Expression • miRNA Expression • Epigenomics • Copy Number Variation • Single Cell

www.nanostring.com

nCounter® *for* Stem Cell Research

www.nanostring.com/technology

A New Way to Look At
Stem Cell Differentiation

Scientists worldwide are turning to the nCounter® Analysis System to address some of their most challenging research questions. With the capability to generate digital results for **up to 800 targets in a single reaction**, the nCounter System offers **a simple and sensitive way to profile mRNA, miRNA and DNA.**

- **Measure changes in gene expression for key pluripotency & differentiation markers**
- **Research pathway effects of small molecules used for programming**
- **Wide dynamic range enables profiling of heterogenous populations through differentiation**
- **Analyze important differences in your cell populations with our Single Cell Application**

nCounter® Analysis System

Direct Digital Quantification of Nucleic Acids

nanoString® TECHNOLOGIES

www.nanostring.com | info@nanostring.com | 1 888 358 6266